به نام خدا

مرکز دانلود رایگان
مهندسی متالورژی و مواد

www.Iran-mavad.com

Techniques for corrosion monitoring

Related titles:

Creep-resistant steels
(ISBN 978-1-84569-178-3)
Creep-resistant steels must be reliable over very long periods of time, at high temperatures and in severe environments. Their microstructures have to be very stable, in both the wrought and the welded states. Creep, especially long-term creep behaviour of these materials is a vital property and it is necessary to evaluate and estimate long-term creep strength accurately for safe operation of plant and equipment. The first part of the book describes the specifications and manufacture of creep-resistant steels. Part II covers the behaviour of creep-resistant steels and a final group of chapters analyses applications.

The cold spray materials deposition process
(ISBN 978-1 84569-181-3)
The cold spray process produces extremely dense, oxide-free coatings that make it ideal in diverse applications such as metal repair, electronics and the control of corrosion and wear. This important book reviews both the principles of the process and its practical uses. The first part of the book reviews its advantages and disdavantages compared with thermal spray coating. Part II discusses the role of parameters such as powders, nozzle design, particle temperature and velocity and particle-substrate interaction. The final part of the book analyses applications in such areas as improved wear and corrosion protection as well as repair of components and shielding from electromagnetic interference.

Innovative pre-treatment techniques to prevent corrosion of metallic surfaces
(ISBN 978-1-84569-365-7)
There has long been a need for effective pre-treatment techniques to prevent corrosion of metallic surfaces. This important volume discusses coating and preparation methods for aluminium alloys such as silane films, sol–gel coatings and magnesium-rich primers. It also reviews pre-treatments for steel, copper, zinc and magnesium alloys. Other chapters consider electrochemical and other techniques to monitor the effectiveness of pre-treatments in preventing corrosion together with methods for monitoring dissolution–precipitation mechanisms of a range of pre-treatments.

Details of these and other Woodhead Publishing books, as well as books from Maney Publishing, can be obtained by:

- visiting www.woodheadpublishing.com
- contacting Customer Services (e-mail: sales@woodhead-publishing.com; fax: +44 (0) 1223 893694; tel.: +44 (0) 1223 891358 ext. 130; address: Woodhead Publishing Ltd, Abington Hall, Abington, Cambridge CB21 6AH, England)

If you would like to receive information on forthcoming titles, please send your address details to: Francis Dodds (address, tel. and fax as above; e-mail: francisd@woodhead-publishing.com). Please confirm which subject areas you are interested in.

Maney currently publishes 16 peer-reviewed materials science and engineering journals. For further information visit www.maney.co.uk/journals.

Techniques for corrosion monitoring

Edited by
Lietai Yang

SOUTHWEST RESEARCH INSTITUTE®

Woodhead Publishing and Maney Publishing
on behalf of
The Institute of Materials, Minerals & Mining

CRC Press
Boca Raton Boston New York Washington, DC

WOODHEAD PUBLISHING LIMITED
Cambridge England

Woodhead Publishing Limited and Maney Publishing Limited on behalf of
The Institute of Materials, Minerals & Mining

Woodhead Publishing Limited, Abington Hall, Abington
Cambridge CB21 6AH, England
www.woodheadpublishing.com

Published in North America by CRC Press LLC, 6000 Broken Sound Parkway,
NW, Suite 300, Boca Raton, FL 33487, USA

First published 2008, Woodhead Publishing Limited and CRC Press LLC

British Library Cataloguing in Publication Data
A catalogue record for this book is available from the British Library.

Library of Congress Cataloging in Publication Data
A catalog record for this book is available from the Library of Congress.

Woodhead Publishing ISBN 978-1-84569-187-5 (book)
Woodhead Publishing ISBN 978-1-84569-405-0 (e-book)
CRC Press ISBN 978-1-4200-7089-7
CRC Press order number WP7089

The publishers' policy is to use permanent paper from mills that operate a sustainable forestry policy, and which has been manufactured from pulp which is processed using acid-free and elementary chlorine-free practices. Furthermore, the publishers ensure that the text paper and cover board used have met acceptable environmental accreditation standards.

Typeset by SNP Best-set Typesetter Ltd., Hong Kong
Printed by TJ International Limited, Padstow, Cornwall, England

Contents

Contributor contact details

(* = main contact)

Editor, Chapters 1 and 8

Dr Lietai Yang
Department of Earth, Material, and Planetary Sciences
Southwest Research Institute®
6220 Culebra Rd
San Antonio
Texas 78238
USA

E-mail: ltyang@swri.org

Chapter 2

Dr Gustavo A. Cragnolino
Southwest Research Institute
15662 Dove Meadow
San Antonio
Texas 78248
USA

E-mail: gcragnolino@satx.rr.com

Chapters 3 and 14

Dr Sankara Papavinasam
CANMET Materials Technology Laboratory
Natural Resources Canada
568 Booth Street
Ottawa
Ontario
Canada
K1A 0G1

E-mail: spapavin@nrcan.gc.ca

Chapter 4

Dr Robert A. Cottis
University of Manchester
Institute of Science and Technology
PO Box 88
Manchester
M60 1QD
UK

E-mail: Bob.cottis@umist.ac.uk

Chapter 5

Dr R. D. Klassen* and Dr P. R. Roberge
Dept of Chemistry and Chemical Engineering
Royal Military College of Canada
PO Box 17000
Stn Forces
Kingston
Ontario
Canada
K7K 7B4

E-mail: klassen@rmc.ca

Chapters 6 and 23

Dr Bo Yang, PhD
Ridgefield
CT 06877
USA

Honeywell
69 Eagle Road
Danbury
CT 06810
USA

E-mail: bo.yang@honeywell.com

Chapter 7

Dr Pavan Shukla
Center for Nuclear Waste Regulatory Analyses
Southwest Research Institute
San Antonio
Texas
USA

E-mail: pshukla@swri.edu

Chapter 9

Dr Kuang-Tsan Ken Chiang* and Dr Todd Mintz
Southwest Research Institute
6220 Culebra Road
San Antonio
Texas
USA

E-mail: kchiang@swri.edu

Chapter 10

Douglas C. Eberle
Engine Design and Development
Southwest Research Institute
PO Drawer 28510
San Antonio
TX 78228
USA

E-mail: deberle@swri.org

Chapter 11

Dr C. Sean Brossia
CC Technologies
Dublin
OH
USA

E-mail: sbrossia@cctechnologies.com

Chapter 12

Dr Glenn Light
Southwest Research Institute
6220 Culebra Road
PO Box 28510
San Antonio
Texas
USA

E-mail: glight@swri.org

Chapter 13

Dr Frank Dean
Ion Science Ltd
Lake House
Market Hill
Royston
Hertfordshire
SG8 9JN
UK

E-mail: frank.dean@ionscience.com

Chapter 15

Pierangela Cristiani
Cesiricerca SPA
Environment and Sustainable Development
V. Rubattino 54
20134
Milan
Italy

E-mail: cristiani@cesiricerca.it

Chapter 16

Dr Peter Schießl
Technical University of Munich
Institute of Building Materials
Baumbachstraße 7
81245 Muenchen
Germany

E-mail: schiessl@cbm.bv.tum.de

Dr.-Ing C. Dauberschmidt
S&R Sensortec GmbH
Landsbergerstraße 370
80687 Muenchen
Germany

E-mail: dauberschmidt@ib-schiessl.de

Engineering office
Schießl Gehlen Sodeikat GmbH
Landsbergerstraße 370
80687 Muenchen
Germany

Chapter 17

N. Khan
Saudi Aramco
E-6665
Engineering Bldg.
Dhahran
31311
Saudi Arabia

E-mail: naeem.khan@aramco.com; nakhandh@yahoo.com

Chapter 18

Dr Feng Gui and Dr C. Sean Brossia
CC Technologies
Dublin
Ohio
USA

E-mail: feng.gui@dnv.com; sbrossia@cctechnologies.com

Chapter 19

Allen Carlile
Kinder Morgan
One Allen Center
500 Dallas St, Suite 1000
Houston, Texas 770022

E-mail: allen_carlile@kindermorgan.com

Chapter 20

Rich Smalling* and Lee Blankenstein
American Innovations
12112 Technology Blvd
Austin
TX 78727
USA

E-mail: Lee.Blankenstein@amerinnovations.com; Rich.Smalling@amerinnovations.com

Chapter 21

Dr Narasi Sridhar
Det Norske Veritas
5777 Frantz Road
Dublin
OH 43017-1386
USA

E-mail: Narasi.Sridhar@dnv.com

Chapter 22

Dr Michael D. Kass
Oak Ridge National Laboratory
NTRC
2360 Cherahala Blvd.
Knoxville
TN 37932
USA

E-mail: kassmd@ornl.gov

Chapter 24

Dr Facundo Almeraya Calderón
Advanced Materials Research Center
CIMAV
Materials Physics Department
Miguel de Cervantes No. 120
Complejo Industrial Chihuahua
CP 31109
Chihuahua
Chih.
Mexico

E-mail: facundo.almeraya@cimav.edu.mx

Chapter 25

Dr Masazumi Miyazawa
Mitsubishi Chemical Corporation
Mizushima Plant
3-10 Ushiodori
Kurashiki
Okayama
712-8054
Japan

E-mail: 2604681@cc.m-kagaku.co.jp

Chapter 26

Xiaodong Sun, P. Eng.
Corr Instruments LLC
303 Clarence Tinker Drive
San Antonio
TX 78226
USA

E-mail: dawnsun@corrinstruments.com

Chapter 27

Dr Qingdong Zhong
School of Materials Science and Engineering
Shanghai University
China

E-mail: qdzhong69@sina.com; qdzhong@hotmail.com

Chapter 28

Nguyen N. Bich, P.Eng.
Pangea Solutions Inc
Building B1, Suite 101,
2451 Dieppe Avenue SW
Calgary, Alberta
Canada
T3E 7K1

E-mail: nbich@pangeasolutions.com

1
Introduction

LIETAI YANG, Department of Earth, Material and Planetary Sciences, Southwest Research Institute, San Antonio, Texas, USA

1.1 Definition of corrosion

Corrosion is the deterioration process of a material due to reactions with its surroundings. As defined in the *Random House Unabridged Dictionary*: 'Corrosion is the act or process of eating or wearing away gradually as if by gnawing, especially by a chemical action.' The materials that are subject to corrosion include metals, ceramics, polymers, and even our own teeth. To most corrosion engineers, however, corrosion refers to the oxidation of metals by chemical and/or electrochemical processes. The most common example of metal corrosion relates to its reaction with oxygen or water. Rusting of steel due to exposure to water or humid air is a well-known example of electrochemical corrosion. In this process, the metal reacts with water or oxygen and forms iron oxides, eventually causing damage to the steel. The following sections describe the importance of corrosion monitoring and the scope of this book.

1.2 Corrosion cost

Corrosion is a costly worldwide problem. According to a recent systematic study commissioned by the United States Federal Highway Administration (FHWA), the annual direct cost of corrosion in the United States was $276 billion in 1998, or 3.1% of the gross domestic product (GDP).[1] Corrosion cost studies were also conducted in other countries, such as the United Kingdom, Japan, Australia and Kuwait. Even though the level of effort varies greatly among these studies, all of them estimated the total annual cost of corrosion as ranging between 1% and 5% of each country's gross national product (GNP).[1]

In addition to the huge cost in economic terms, corrosion is also blamed for many of the disasters that cause loss of life and devastating pollution to the environment. For instance, in April 1992, in Mexico, the Guadalajara Sewer Explosion took the lives of 215 people and caused injury to another

1500 people. The financial loss was estimated at $75 million. The accident was traced to the corrosion of a gas line that caused a leak of the gas into a nearby sewage main.[2] Another example involved the sinking of a tanker, Erika, off the coast of Brittany in France, on 12 December 1999. In this accident, approximately 19000 tons of heavy oil was spilled, equal to the total amount of oil spilled worldwide in 1998. Corrosion caused the sinking of the Erika.[2]

Because corrosion takes place in many different forms, some of them cannot be eliminated, but others are avoidable by simply applying appropriate corrosion prevention/mitigation technologies. In the report commissioned by the FHWA, it was estimated that 25% to 30% of the annual corrosion costs in the United States could be eliminated, if optimum corrosion management practices were employed.[3] Other studies estimated that from 10% to 40% of the total corrosion cost could be avoided.[3] Knowing this, it seems prudent for worldwide industries to use appropriate corrosion prevention and control methods; taking such pre-emptive measures will not only avert huge economic losses (potentially close to one hundred billion dollars annually in the US alone), but also protect the environment and public safety.

1.3 Corrosion monitoring and its importance in corrosion prevention and control

Corrosion monitoring is the practice of acquiring information on the progress of corrosion-induced damage to a material or on the corrosivity of the environment surrounding the material. Corrosion inspection is usually a survey of the material condition at any given time, while corrosion monitoring consists of a series of surveys in a given time period. While test coupons are one of the most widely used and most reliable methods, corrosion monitoring usually relies on the use of electronic corrosion sensors or probes that are exposed to an environment of interest, such as outdoor air or seawater, or inserted into the inner space of a containment system, such as a vessel or a pipe in which a liquid or a gas flows or is contained. On a continuous or semi-continuous basis, the electronic corrosion sensors or probes emit information relating to the corrosion of a metal system.

The study commissioned by the FHWA further pointed out three preventive strategies in technical areas, to lessen or avoid unnecessary corrosion costs and to protect public safety and the environment. They are:

- advance design practices for better corrosion management;
- advance life prediction and performance assessment methods; and
- advance corrosion technology through research, development and implementation.

These strategies are inter-related. For example, advance design requires better life prediction and performance assessment methods, and better prediction and performance assessment methods require advancement in corrosion technology.

Corrosion monitoring is part of corrosion technology. In today's electronic age, many of the industrial process parameters – such as temperature, pH and flow – are controlled by automated feedback controllers. Only after the introduction of these controllers and the associated reliable sensors for these parameters was it possible to precisely manage them and to either improve the product quality or to produce original products. Unfortunately, the control of corrosion in many industries is still in its 'stone age' stage. According to the FHWA study, the annual use of corrosion inhibitors in the United States came to over a billion dollars; the annual cost may be over $4 billion worldwide, if the usage of inhibitors is assumed to be proportional to the GDP in each country. It is rather alarming to realize that nearly all of these inhibitors were added into the controlled systems based on parameters that are not the direct measures of corrosion (indirect parameters) or based on historical results acquired from the test coupons that were exposed in the controlled systems several months earlier. Examples of the indirect parameters include the concentration of the inhibitors and the concentration of dissolved oxygen in the controlled systems. Because of the complexity of corrosion, some concentrations of corrosion inhibitor that are shown to be effective under certain conditions may not be effective under others. In addition, the concentration of the inhibitor sampled from the bulk phase may not represent the actual concentration on the metal surface where corrosion takes place.

With the advancement of corrosion monitoring techniques, corrosion sensors may be used in the feedback controllers – as in the control systems for pH, temperature and other process parameters – to automatically control the addition of corrosion inhibitors. When such a system is implemented, it will not only provide an adequate control of corrosion – which means a better performance and a longer life for the equipment – but it will also create tremendous savings in the inhibitor costs by avoiding overdosing. This, in turn, produces a significant risk reduction for our environment, because many corrosion inhibitors are toxic.

Corrosion monitoring also provides performance data and a basis for life prediction; corrosion monitoring is one of the most important components in corrosion prevention and corrosion control.

1.4 Organization of the book

This book is organized into 28 chapters. Chapter 2 presents an overview of corrosion fundamentals and evaluation techniques. It includes detailed

discussions on the different forms of corrosion and their electrochemical characteristics.

Chapter 2 is followed by in-depth discussions on the various methods that can be used for corrosion monitoring (i.e., to measure the corrosion damage to metals or the corrosivity of a surrounding environment with an adequate response time so that the measurements can be made at desired time intervals). The response time is relative to the purpose of monitoring. For example, if a corrosion monitor is interfaced with a corrosion inhibitor dosing-controller and the dosing-controller completes the addition of an inhibitor to a system in a few minutes, the response time of the corrosion monitor should be less than one minute. However, if the purpose is to monitor the long term corrosion damage to a metallic structure in the air near a pollution source, one month may be considered a sufficient response time.

Chapters 3 through 8 discuss the electrochemical techniques for corrosion monitoring. These techniques include electrochemical polarization techniques (Chapter 3), electrochemical noise methods and harmonic analyses (Chapter 4), zero resistance ammetry and galvanic sensors (Chapter 5), differential flow through cell technique (Chapter 6), potentiometric methods for measuring localized corrosion (Chapter 7) and multielectrode systems (Chapter 8).

Chapters 9 through 14 describe the gravimetric, electrical, and other physical or chemical methods. These methods include gravimetric techniques (Chapter 9), radioactivity methods (Chapter 10), electrical resistance techniques (Chapter 11), nondestructive evaluation methods for corrosion monitoring (Chapter 12), hydrogen permeation methods (Chapter 13) and rotating cage and jet impingement techniques (Chapter 14).

Although some of the methods discussed above in Chapter 12 are primarily used as corrosion inspection tools, they are included in this book because the technology serves as a basis for nondestructive monitoring systems when used with fixed sensors, advanced data acquisition, and remote communication technologies to provide integrity status from metallic systems at regular time intervals. As advancements in these technologies continue, these inspection tools will most likely be used more and more as monitoring tools.

Corrosion is an extremely complicated process involving at least two phases, solid and liquid; solid and gas; solid, liquid and gas; or even solid, first liquid and second liquid. Corrosion monitoring is a multidisciplinary task. Very often, two or more methods are needed to adequately address the monitoring needs in a given system. In addition, different systems require different methods or a combination of different methods. Chapters 15 through 19 provide detailed discussions regarding the specific monitoring needs in selected environments, or under particular conditions. The

topics discussed in these chapters include corrosion monitoring in microbial environments (Chapter 15), corrosion monitoring in concrete (Chapter 16), corrosion monitoring in soil (Chapter 17), corrosion monitoring under coatings (Chapter 18), and corrosion monitoring under cathodic protection conditions (Chapter 19).

Data management is a vital, integral part of corrosion monitoring, and the prediction of system performance based on a finite number of available data is a vital component of an integrated system health management program. Chapters 20 and 21 provide detailed discussions on remote monitoring, and an in-depth discussion on model predictions, respectively.

Finally, Chapters 22 through 28 present applications of corrosion monitoring techniques in specific systems and case studies. These chapters provide readers with quick answers, when they have a need in a particular area or for a specific method. The topics in these chapters include corrosion monitoring in engine exhaust systems (Chapter 22), corrosion monitoring in cooling water systems, using a differential flow through cell (Chapter 23), corrosion monitoring in the pulp and paper industries (Chapter 24), corrosion monitoring in chemical plants using an electrochemical noise method (Chapter 25), corrosion monitoring under cathodic protection conditions using multielectrode sensor techniques (Chapter 26), measuring corrosion beneath organic coatings using wire beam electrodes (Chapter 27) and corrosion monitoring in piplines using the field signature method (FSM) (Chapter 28).

This suite of in depth overviews, systematic technique descriptions, and case studies provides a state-of-the-art coverage for corrosion monitoring. Researchers, engineers/operators and students alike should find this book to be an invaluable resource in meeting their corrosion monitoring needs or advancing research related to corrosion monitoring.

1.5 References

1 G. H. Koch, M. P. H. Brongers, N. H. Thompson, Y. P. Virmani, and J. H. Payer, 'Corrosion Cost and Preventive Strategies in the United States,' FHWA-RD-01-156 (Springfield, VA: National Technical Information Service, 2001).
2 P. R. Roberge, 'Corrosion Inspection and Monitoring,' Chapters 1 and 2 (Hoboken NJ: John Wiley & Sons, Inc., 2007).
3 MP editorial, 'Corrosion – A Natural but Controllable Process,' Supplement to Materials Performance, July 2002, pp. 3–3, 2002.

2

Corrosion fundamentals and characterization techniques

GUSTAVO A. CRAGNOLINO, Southwest Research Institute, San Antonio, Texas, USA

2.1 Introduction

Corrosion is defined as the chemical or electrochemical reaction between a material, usually a metal or alloy, and its environment that produces a deterioration of the material and its properties. According to the characteristics of the environment, corrosion processes are classified as chemical or electrochemical.

Chemical corrosion processes are those in which the metal reacts with a non-electrolyte (e.g., oxidation in high temperature air, dissolution in liquid metals or dissolution in a carbon tetrachloride solution containing iodine). Electrochemical corrosion processes are those in which the metal dissolves in an electrolyte forming metal cations which implies the transfer of electric charge across the metal/environment interface. Electrochemical corrosion occurs in the large variety of electrolytes found in natural environments and industrial applications ranging from groundwater to molten salts and acids dissolved in organic polar solvents (e.g., hydrochloric acid in methanol).

For practical reasons corrosion in different natural environments, such as corrosion in soils, atmospheric corrosion, fresh water corrosion, sea water corrosion, etc., are usually considered separately as is also the case for corrosion in different industries (i.e., chemical processing, oil and gas production, power generation, etc.) (Cramer and Covino, 2006). However, besides the specificity of the environments and the materials involved, these corrosion processes have fundamental aspects in common related to the thermodynamics and kinetics of the electrochemical reactions at the metal/electrolyte solution interface and the transport of chemical species in a liquid phase to and from the metallic surface (Bard and Faulkner, 1980). Several recently published books and handbooks are useful sources for general information on corrosion and its electrochemical basis (Cramer and Covino, 2003; Revie, 2000; Shreir *et al.*, 1994; Marcus, 2002). The electrochemical techniques commonly used in corrosion studies are well presented in Kelly *et al.* (2003) and corrosion tests and standards for materials in a

variety of environments and industrial applications are covered in detail in Baboian (2005).

According to the morphology of corrosive attack, different modes of corrosion can be identified through visual observation, requiring in many cases sufficiently enlarged magnification by the use of optical or electronic microscopes. The different modes of corrosion will be presented in the following sections and the most common techniques used to study and characterize corroded metal surfaces and corrosion products will be briefly introduced.

2.2 General corrosion

General corrosion is the most common and benign form of corrosion because it is characterized by a corrosive attack that extends almost uniformly over the whole exposed surface or at least over a large area. Even though the term uniform corrosion is commonly used synonymously with general corrosion, this form of corrosion is seldom completely uniform and the morphology of the corroded surface always exhibits some sort of waviness and roughness. Nevertheless, the average penetration of the attack is practically the same at each point of the corroded surface. Any corrosion process involves at least one anodic (oxidation) reaction and one cathodic (reduction) reaction.

Because charge accumulation cannot occur, the electrons generated by the oxidation reactions must be consumed by the cathodic reactions and, therefore, the total anodic current should be equal to the total cathodic current with the electrical potential at an anodic site equal to that at a cathodic site. This fundamental concept of coupled anodic and cathodic processes was proposed by Wagner and Traud (1938). The hypothesis leads to the definition of the corrosion potential as a mixed potential because the anodic reaction is the dissolution of the metal coupled to the cathodic reaction which could be the reduction of dissolved oxygen molecules, hydrogen ions or any other reducible species in solution (e.g., Fe^{3+} ions), instead of the reduction of the dissolved metal cations. From an electrochemical point of view, the main characteristic of general corrosion is the fact that metal dissolution takes place without physical separation, even at the microscopic scale, of anodic and cathodic sites.

General corrosion causes by far the largest amount of material losses as a result of corrosion, mostly due to atmospheric corrosion. Leaving aside the costs involved, general corrosion is not of great concern because the corrosion rate and, hence, the expected life of equipment or structures can be accurately estimated by means of relatively simple corrosion tests. The most critical aspect of testing is, however, the correct definition of the environment in which the component will operate and its unexpected

variations during operation. Such tests can be immersion tests, in which gravimetric methods are used for measuring the weight loss of a material specimen during a specific testing time to calculate the corrosion rate (ASTM, 2006a).

Alternatively, electrochemical tests can be used to determine the corrosion rate (CR), expressed as rate of uniform penetration for metals and alloys, from the measured current density by using Faraday laws, according to Equation [2.1]:

$$CR = i\ E_w/F\ \rho \qquad [2.1]$$

where i is the current density, E_w is the equivalent weight, F is the Faraday constant, equal to 96485 C/g-equivalent, and ρ is the density of the metal. E_w can be computed using the following expression

$$E_w = 1/\sum(z_j f_j/A_j) \qquad [2.1a]$$

where z_j is the oxidation state of the element j in the alloy, f_j is its weight fraction, and A_j is its atomic weight.

In order to calculate the corrosion rate in mm/yr, Equation [2.1] can be expressed as

$$CR = 3.27 \times 10^{-3}\ i\ E_w/\rho \qquad [2.2]$$

with i in μA/cm^2, E_w in g, and ρ in g/cm^3. The corrosion rate is also commonly given in mils per year (mpy) or in units of weight change per unit area per unit time (e.g., mg/cm^2·s) (ASTM 2006b). Values of E_w for many metals and alloys taking into account the various possible oxidation states are also provided in the same standard (see Chapter 3).

The advantage of electrochemical methods over gravimetric methods is that the instantaneous rather than the average corrosion rate can be measured. The linear polarization resistance (LPR) method (see Chapter 3) and electrochemical impedance spectroscopy (EIS) techniques (Kelly *et al.*, 2003; Baboian, 2005) are widely used to obtain real time information on corrosion rates. Corrosion rates at potentials differing from the corrosion potential can be calculated from current density measurements using potentiostatic methods when interferences from cathodic reactions (e.g., cathodic current associated with the oxygen reduction reaction due to the dissolved oxygen in solutions in equilibrium with air) are carefully eliminated.

As noted above, atmospheric corrosion which is the corrosion of materials exposed to air and its pollutants, such as sulfur compounds and NaCl, occurs mostly in the form of general corrosion. The corrosion rate is extremely dependent on relative humidity and the concentration of pollutants in the air which leads to the distinction of rural, industrial, and sea

coastal atmospheres. Prompted by the spectacular development of the electronic industry, the field of atmospheric corrosion has been extended during the last 30 years to include indoor atmospheres to deal with the corrosion problems of electronic devices. Carbon steels, weathering steels, stainless steels (SS), Cu, and certain Cu alloys are typical materials subject to outdoor atmospheric corrosion in the form of general corrosion as a result of their extensive application as structural and architectural materials (Cramer and Covino, 2005; 2006).

The fundamentals of atmospheric corrosion, as well as substantive discussions on outdoor and indoor atmospheric corrosion, are well covered by Leygraf and Graedel (2000). These authors distinguish three stages of atmospheric corrosion. The initial stage corresponds to the adsorption of molecules of water vapor on the oxide/hydroxide-covered metal surface by surface hydroxylation followed by the formation of several molecular layers. Above 50% relative humidity the number of water monolayers increases abruptly from two to more than five. The intermediate stages involve the absorption and dissolution of gases (i.e., O_2, CO_2, SO_2, HCl, H_2S) or salts as particulates (i.e., NaCl, $(NH_4)_2SO_4$, $(NH_4)HSO_4$, $(NH_4)Cl$, Na_2SO_4) in the adsorbed water layers followed by chemical reactions and subsequent electrochemical processes of proton and ligand-induced metal dissolution with the nucleation of corrosion products. The final stages are the coalescence, aging and thickening of corrosion products.

General corrosion is a common occurrence in many industrial applications. In the chemical processing industries in which more corrosion resistant materials are generally used, the environments include inorganic and organic acids, and also a large number of chemical species, over wide ranges of concentrations and temperatures. A large body of information is usually collected for each chemical (e.g., H_2SO_4, HNO_3, HCl, HF, organic acids, etc.) as isocorrosion maps which are temperature vs. concentration plots bound by the respective boiling point curve of the chemical defining regions with different values of the uniform corrosion rate for each alloy of interest (Shreir *et al*., 1994; Cramer and Covino, 2005; 2006). Well established monitoring techniques are commonly used in these applications (Labine and Moran, 1986; Roberge and Klassen, 2003).

2.3 Passivity and localized corrosion

A metal surface is considered passive when, although it is exposed to an environment under conditions such that dissolution of the metal could be expected from thermodynamic considerations, it remains essentially unchanged with time. The phenomenon of passivity and the breakdown of passivity can be illustrated by considering the schematic anodic polarization curve of metals in an aqueous environment obtained under deaerated

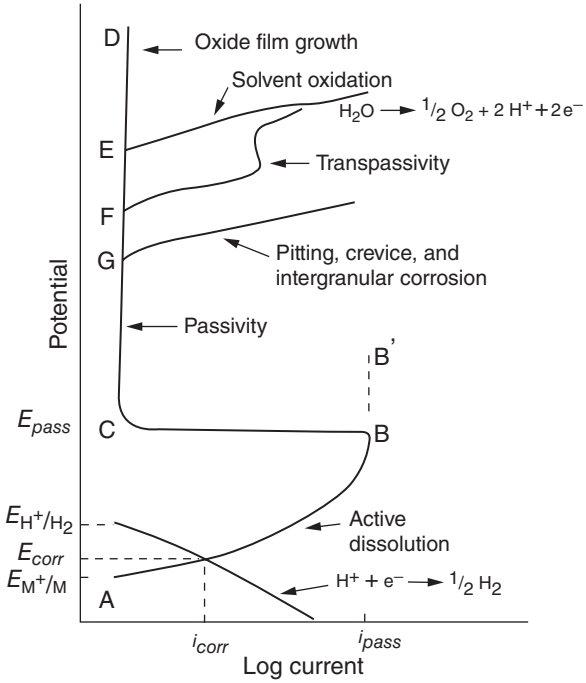

2.1 Schematic polarization curve indicating possible variations of the anodic behavior of metals in aqueous solutions.

conditions, as shown in Fig. 2.1, in which the cathodic reaction is assumed to be the reduction of hydrogen ions.

If the potential is increased in the positive direction from the corrosion potential, E_{corr}, the current will increase initially following a linear relation between the logarithm of the current and the potential (Tafel region) until an approximately constant current is reached due to diffusion limitations or formation of a surface layer of corrosion products. The curve from A to B (only accessible from E_{corr}) is characteristic of the active dissolution of the metal. If the potential is increased further the current may remain constant and high (B to B′) or decrease significantly by several orders of magnitude (B to C), due to the formation of a passive layer, usually a very thin and protective oxide film. The potential at which this process occurs is called passivation potential, E_{pass}, and the current at B passivation current, i_{pass}. By increasing the potential to even higher values the thickness of the oxide film will increase but the current in the passive range, the passive current i_p, will remain essentially constant. If the film is a poor electronic conductor (e.g., Al, Zr and Ta) very high potentials can be reached, as shown by the curve C to D. If the oxide film is a good electronic conductor (e.g.,

Fe and Ni), a significant current increase will occur at a certain potential (E) associated with the electrochemical decomposition of the solvent, which in aqueous systems corresponds to the evolution of O_2 as a result of water oxidation. However, if the oxide film is composed by cations which can be oxidized to a higher oxidation state forming soluble products (e.g., Cr, Mo or alloys such as stainless steels) a current increase may occur at lower anodic potentials (F), accompanied by the dissolution of the metal as a result of transpassivity, in some cases followed by a region of secondary passivity.

Because most of the metals and alloys of industrial importance corrode under passive conditions, the preservation of the passive film in aggressive environments is critical to the life of industrial equipment and components. Under natural corroding conditions the E_{corr} may vary up to values lower than E as a result of the presence of reducible species in solution, mainly dissolved O_2 in naturally aerated systems. Only in specific, highly oxidizing environments, E_{corr} values as high as F can be attained (e.g., SS in concentrated HNO_3) and transpassive dissolution occurs. In certain applications, the passive condition can be obtained by imposing a potential within the passive range (C to G) through potentiostatic polarization and anodic protection is attained.

For many metals and alloys exhibiting a passive behavior, the passive film becomes locally unstable above a critical potential in solutions containing halide anions, in particular chloride. In the polarization curve shown in Fig. 2.1, a sudden increase in the current is observed above G corresponding to the breakdown of passivity which may lead to various forms of localized corrosion. Depending upon the factors involved in the passivity breakdown and the morphology of the subsequent attack, localized corrosion can be classified as pitting or crevice corrosion if a chemical micro- or macro-heterogeneity is developed at the metal/solution interface. If a chemical micro-heterogeneity exists in the metal, intergranular attack or selective dissolution can occur. Stress corrosion cracking or corrosion fatigue can occur at such potential if dynamic mechanical factors are involved in the passivity breakdown. From an electrochemical point of view, the main characteristic of localized corrosion is the physical separation of anodic and cathodic areas. Under natural corroding conditions, the kinetics of the cathodic reaction on the remaining passive surface, the conductivity of the solution, and the size of the cathodic area are the factors limiting the rate of the localized attack.

Although passivity has been attributed to the formation of an adsorbed layer of dissociated O_2 molecules or to electronic modification of the metal surface, nowadays there is a general agreement that passivity is caused by the formation of a three-dimensional oxide film. Passivity is initiated in certain circumstances by isolated oxide nuclei which grow and spread

laterally. Numerous models have been proposed for the growth of passive films. Two of the most well known models are those developed by Cabrera and Mott (1948–9) and, more recently, the point-defect model (Macdonald, 1992). Nevertheless, despite significant experimental progress in recent years, there is still considerable controversy regarding the nature, composition, structure and long-term stability of passive films in many alloy/environments systems.

2.3.1 Galvanic corrosion

Galvanic corrosion (GC) occurs when two or more metallic materials having different reversible electrode potentials are coupled together and exposed to a corrosive solution or the atmosphere. Due to the metallic contact and the ionic conduction in the electrolyte a current flows from one metal to the other resulting in GC of the anodic (negative) member of the couple. Although in many cases GC is morphologically uniform, the most damaging situations occur when it is localized to a limited area. A large cathodic area in contact with a small anodic area is particularly detrimental in promoting this specific form of localized corrosion. In addition to its treatment in corrosion textbooks, important aspects of GC have been reviewed in recent publications by Zhang (2000) and Hack (2005).

The following factors determine the extent of corrosion experienced by the anodic member of the couple: (a) the E_{corr} of the metals forming the galvanic couple; (b) the nature and kinetics of the cathodic reactions (e.g., O_2 and H^+ reductions) on the more positive metal and the anodic dissolution reactions on the more negative metal; (c) geometrical factors such as the relative areas and spatial positions of the dissimilar metals; (d) the electrolyte solution properties, including concentration of ionic species, pH, temperature, and particularly conductivity.

In many circumstances the polarity of galvanic couples is different from that expected from the reversible electrode potentials because the corrosion potentials are mixed potentials determined by the kinetics of the anodic and cathodic reactions in the specific environment. In addition, there is more than one anodic oxidation reaction that takes place in the case of alloys. As a result, a specific galvanic series including metals and alloys should exist for each environment instead of the overextended, and sometimes erroneous, use of the galvanic series in sea water for other environments, even though such series can be used with certain confidence in environments similar to sea water.

As illustrated in Fig. 2.2, the following expression provides the relationship between the driving force of the galvanic couple and the galvanic current, I_g

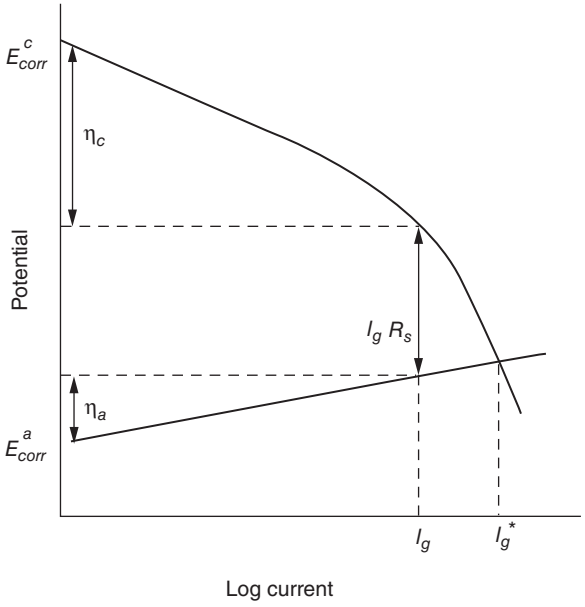

2.2 Schematic plot showing the effects of the anodic and cathodic polarization of the members of a galvanic couple and the solution resistance on the galvanic current.

$$(E^c_{corr} - \eta_c) - (E^a_{corr} + \eta_a) = I_g R_s \qquad [2.3]$$

where E^c_{corr} and E^a_{corr} are the corrosion potentials, and η_c and η_a, the polarization of the cathodic and anodic members of the couple, respectively, and R_s is the resistance of the electrolyte solution in the galvanic circuit. It should be noted that the magnitude of both η_c and η_a, depends on the cathodic and anodic polarization curves and on the value of R_s. If R_s decreases, I_g increases until a limiting I_g^* is reached when R_s tends to zero. Obviously, the anodic and polarization curves depend on the kinetics of the electrochemical reactions on each metal in the solution, and hence are functions of the solution composition, pH and temperature, as well as on the surface conditions of the metals.

When the cathode exhibits strong polarization (large η_c) and the anode does not, the couple is under cathodic control. On the other hand, the couple is under anodic control when the anode displays strong polarization (large η_a). If the resistance controls the current flow, the couple is under resistance control but most commonly all these three factors affect I_g and hence mixed control prevails.

According to Faraday laws, I_g is directly proportional to the corrosion rate of the anode in the galvanic couple. Physical contact between the

members of the couple prevents the direct measurement of I_g. However, the I_g can be measured using two isolated specimens of the galvanic couple exposed to the environment of interest and connected through a zero resistance ammeter (ASTM, 2006c). Other methods to evaluate GC are discussed by Hack (2005).

The galvanic action between two metals is governed by the potential distribution across each electrode surface from which the galvanic current distribution can be calculated. Even though the potential distribution can be obtained by experimental methods (e.g., scanning a reference electrode over the surface of the metallic couple), in most situations this approach is not practical due to the complex configuration of the system. A semi-quantitative approach to characterize the current distribution for a given metal/electrolyte combination was proposed by Wagner (1951) using a polarization parameter defined as

$$W_p = \sigma\,[\mathrm{d}\eta_i/\mathrm{d}i_i\,] \qquad [2.4]$$

where σ is the conductivity of the solution, and η_i is the overpotential of the cathode or the anode, and i_i is the current density and therefore W_p has dimensions of length. To scale-up a system, either for modeling or experimental simulations, the ratio of W_p to a characteristic length of the system, named the Wagner number, W_n, should be kept constant. Currently, the prevailing approach is based on the development of numerical models for different galvanic couples and geometries, as summarized by Zhang (2000). These models are used to evaluate galvanic corrosion but also to predict the effect of cathodic protection using sacrificial anodes.

2.3.2 Pitting corrosion

Pitting corrosion (PC) is a form of localized attack morphologically characterized by the development of small cavities usually on openly exposed surfaces of a metal. The surface diameter of these cavities is about the same or less than the depth in most cases, but different pit shapes can be observed depending on the metal or alloy and the environment. Changes in the hydrodynamic conditions or different orientations of the metal surface can alter significantly the pit morphology. The typical appearance of a pit is shown in Fig. 2.3. Under certain conditions the bottom of the pits may exhibit crystallographic facets whereas in other cases round electropolished bottoms are observed, generally covered with precipitated corrosion products.

PC occurs by the action of aggressive anions on metals and alloys exhibiting a passive behavior when exposed to environments ranging from slightly acidic to alkaline. Cl^- is the anionic species most commonly associated with PC, in part due to its wide distribution in natural waters. Other anions such

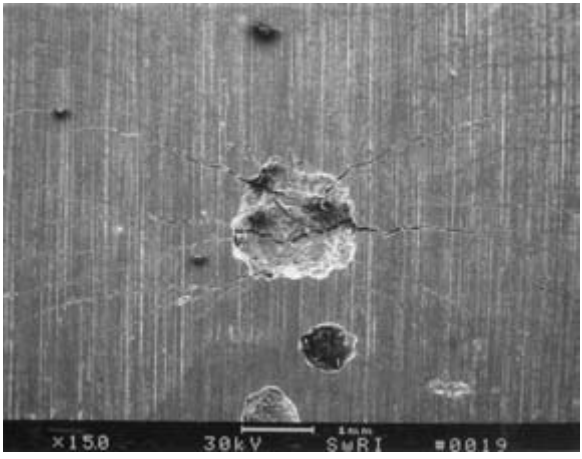

2.3 Micrograph showing the appearance of a typical pit of AISI 316L stainless steel exposed to a hot chloride solution. Cracks are emanating from the pit due to the presence of stress.

as Br^-, I^-, SO_4^{2-}, and ClO_4^- can also promote PC. Equipment failures due to perforation by PC occur without significant weight loss of the entire structure or component because the rate of dissolution in a pit can be 10^4 to 10^6 times faster than that on the rest of the surface (Galvele, 1978).

There are numerous papers in the literature and recent conferences in which phenomenological observations as well as mechanistic interpretations of PC have been thoroughly discussed (Frankel, 1998; Frankel and Newman, 1992; Natishan *et al*., 1996; Kelly *et al*., 1999). A revised second edition of a book mostly devoted to this subject has been published recently (Szklarska-Smialowska, 2005).

It has been demonstrated that stable pit growth only occurs above a certain critical potential which depends on the particular metal/anion system. The presence of an aggressive anion in the environment is a necessary but not a sufficient condition for the occurrence of PC, as clearly demonstrated by experiments in which the passive film is mechanically disrupted by scratching or straining at potentials below the critical potential and repassivation occurs. Within such anodic range metastable pits can be generated but they do not grow to become stable pits and rapidly die. Only at potentials above the critical potential do metastable pits become stable. It should be noted, however, that pit generation is a stochastic process and therefore a distribution of potentials exist above a minimum value that can be considered the 'true' pitting potential. This lower potential usually coincides with the protection potential or repassivation potential, which is the potential at which pit growth is arrested.

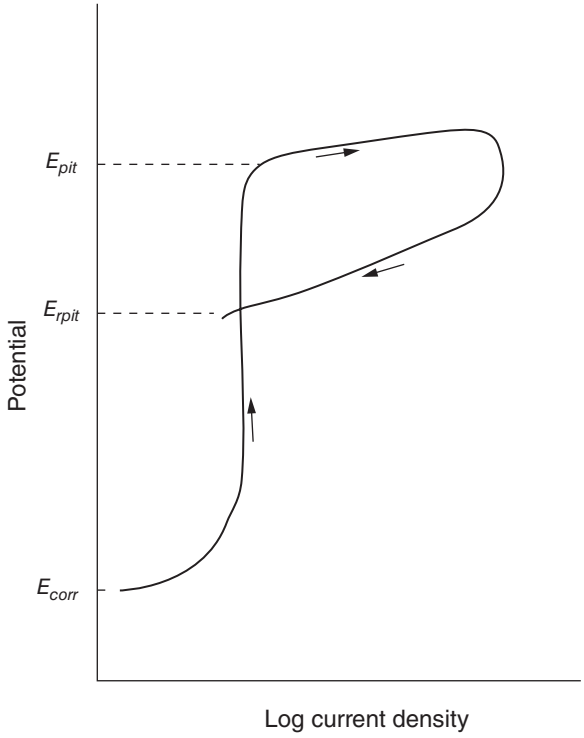

2.4 Schematic cyclic potentiodynamic anodic polarization curve showing the pitting initiation potential, E_{pit}, and the pitting repassivation potential, E_{rpit}.

The pitting initiation potential, E_{pit}, is usually measured potentiodynamically by scanning the potential upward from the corrosion potential or potentiostatically by stepping the potential until a steady state current is attained at each step (ASTM, 2006d). E_{pit} corresponds to an abrupt increase in the current density, as illustrated in the schematic anodic polarization curve shown in Fig. 2.4. When the potential is scanned or stepped backward there is usually an abrupt decrease in the current density corresponding to the arrest of the pit growth at the pitting repassivation potential, E_{rpit}, as also shown in Fig. 2.4.

Under natural corroding conditions PC occurs when E_{corr} is higher than the 'true' E_{pit}. In many metals and alloys (e.g., Al and its alloys), this occurs when the oxidant in the aqueous environment is O_2 in equilibrium with air. In more corrosion-resistant materials, oxidizing cations such as Fe^{+3} are required to attain sufficiently high E_{corr}. Indeed, Fe_3Cl solutions are used in a standard test to evaluate the susceptibility of stainless steel and related alloys to PC (ASTM, 2006e).

The E_{pit} depends, in addition to the material composition, heat treatment and surface condition, on the solution composition and temperature. For many metals and alloys the following relationship exists between the E_{pit} and the concentration of aggressive anions (e.g., Cl^-, Br^-, I^-) and inhibiting anions (e.g., CO_3^{2-}, $B_4O_7^{2-}$, PO_4^{3-})

$$E_{pit} = E^0_{pit} - B \log [X^-] + C \log [A^-] \quad [2.5]$$

where E^0_{pit}, B, and C are constants, which depend on the metal/solution system and X^- and A^- are the aggressive and inhibiting anions respectively. A similar expression exists for E_{rpit} but with different values for E^0_{rpit}, B and C.

Some basic aspects of the PC mechanism are well established. Under natural corroding conditions, rapid anodic dissolution occurs at a pit nucleus while O_2 reduction takes place on the adjacent passive surface providing the driving force for the anodic reaction. The metal cations react with water forming hydroxo-complexes and H^+ ions, thereby promoting localized acidification inside the pit. The excess of positive charge is counterbalanced by the migration of Cl^- ions creating a very aggressive environment which stimulates further the local dissolution of the metal in a rather autocatalytic fashion. Other reducible species (i.e., Fe^{3+}, Cu^{2+}, and H_2O_2) can play the same role as O_2.

The lack of dependence of E_{pit} with pH can be explained because the pH inside the pits is strongly acidic, regardless of the bulk pH. In addition PC inhibitors which are usually the salt of a weak acid or the OH^- anion will increase E_{pit} by consuming H^+ ions and thereby reducing the localized acidification inside the pit, according to the following reaction

$$H^+ + A^- \rightarrow HA \quad [2.6]$$

Galvele (1976) developed a mechanistic model based on these concepts and concluded that E_{pit} can be calculated by using the following equation:

$$E_{pit} = E^*_{corr} + \eta + \Phi + E_{inh} \quad [2.7]$$

where E^*_{corr} is the corrosion potential measured in an acidified pit-like solution, η is the overpotential necessary to attain the current density required to maintain the acidic pH inside the pit (which is characteristic of each metal or alloy), Φ is the ohmic drop inside the pit and E_{inh} the increase in E_{pit} due to the action of the inhibitor (the last term in Equation 2.5). The current density necessary to maintain the pit actively growing multiplied by the depth of the pit ($i \cdot x$) must be higher than a certain value characteristic of each metal/solution system and the value of η is calculated by assuming Tafel behavior in the pit-like solution. Laycock and Newman (1997) developed a rather similar expression (without the last term in Equation 2.7) for the transition potential between metastable and stable pits by introducing

the concept of diffusion-controlled (salt-covered) pit growth. This transition potential is conceived as a 'true' E_{pit}.

2.3.3 Crevice corrosion

Crevice corrosion (CC) is a form of localized corrosion that occurs within crevices and other shielded areas where a small volume of a stagnant solution is present. Such crevices can be formed at metal/metal or metal/nonmetal junctions, such as those associated with gaskets, valve seats, rivet and bolt heads and lap joints, as well as under surface deposits (i.e., corrosion products, sand and dirt) or marine biofouling. Crevice corrosion is mainly observed on passive metals and alloys covered with protective oxide films, such as stainless steels, Ti alloys, and Ni-base alloys immersed in aerated aqueous environments containing Cl^- ions (e.g., sea and brackish water).

The morphology of the attack inside the crevice could vary from pitting to a more uniform corrosion. The geometrical dimensions of the crevice are critical, particularly the crevice gap, because the gap must be wide enough to allow entry of the solution but sufficiently narrow to maintain an occluded environment inside the crevice. In addition, the depth and the exterior/interior area ratio are important factors in determining the severity of the attack. The typical appearance of crevice corrosion is shown in Fig. 2.5.

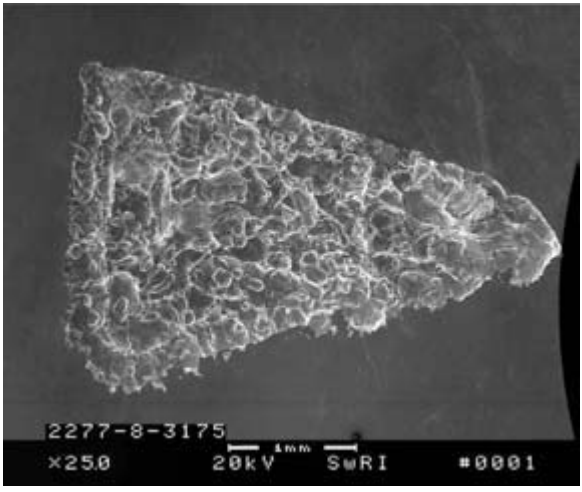

2.5 Micrograph showing an example of crevice corrosion. Attack on alloy C-22 under the feet of a crevice former exposed to a hot chloride solution.

There are valuable reviews on CC (Combrade, 2002; Szklarska-Smialowska, 2005) where experimental observations and fundamental concepts are discussed. The development of alloys more resistant to PC led in recent years to place more emphasis in the study of CC. This phenomenon occurs when the local environment inside the crevice becomes sufficiently aggressive to induce passivity breakdown, either by the generation of pits or a more generalized depassivation. In the occluded environment where mass transport by diffusion and convection is severely limited, hydrolysis of the dissolved metal cations coupled with the buildup of the Cl^- concentration required to maintain electroneutrality lead to the formation of a solution with a critical composition in terms of Cl^- concentration and pH. As soon as the metal in the crevice becomes active the E_{corr} inside the crevice decreases. This activation is accompanied by a substantial ohmic drop, equal to the product of the current by the solution resistance, due to the difference between E_{corr} inside and outside the crevice. From a mechanistic point of view there are many similarities between PC and CC and, therefore, the condition for a crevice to be active is that the current density multiplied by the depth of the crevice reaches a certain critical value (Sridhar *et al*., 2001; Kehler *et al*., 2001), as originally proposed by Galvele (1976).

A thorough review of tests developed to evaluate the CC resistance of alloys was presented by Sridhar *et al*. (2005). Standard tests in Fe_3Cl solutions in which an oxidizing species (i.e., Fe^{3+} ions) is used in addition to Cl^- to accelerate the initiation of CC are reviewed, as well as electrochemical tests conducted under either open circuit or constant applied potentials. The use of critical potentials and critical temperatures for the initiation of CC as tools for the evaluation and ranking of different alloys is discussed in some detail (Sridhar *et al*., 2005).

Similarly to PC, a critical potential for the initiation of CC, E_{crev}, exists, but its value exhibits an ill-defined dependence on crevice geometry. As in the case of PC, a distribution of potentials is observed. The most reliable parameter to assess the resistance to CC of passive alloys, particularly SS or Ni-Cr-Mo alloys, in a variety of aggressive environments containing Cl^- anions is the repassivation potential for crevice corrosion, E_{rcrev}, because it is independent of crevice depth (Dunn *et al*., 1996; 2000).

Dunn *et al*. (2005; 2006) found that for a given alloy with a specific heat treatment, E_{rcrev} can be expressed as:

$$E_{rcrev} = A_1 + A_2\, T + (B_1 + B_2 T)\, \log[Cl^-] \qquad [2.8]$$

where the coefficients A_1, A_2, B_1, and B_2 are independent of the temperature T. Even though the expression and the coefficients were determined for Alloy 22, similar expressions with the corresponding coefficients can be obtained for other alloys. The expression has been extended to include effect of inhibitors, such as NO_3^-, SO_4^{2-} and CO_3^{2-}. A semi-empirical model

has recently been developed by Anderko *et al.* (2005) to account for the effect of Cl^- concentration on E_{rcrev} in the presence of complexing species in solution.

2.3.4 Dealloying

Dealloying is the selective removal by electrochemical dissolution of the most active metal from an alloy under specific environmental conditions. It may occur either as localized corrosion accompanied by perforation (plug type) or as a more uniform attack (layer type). One of the oldest cases reported, the removal of Zn from the brasses (Cu-Zn alloys) is known as dezincification. The phenomenon is also termed selective leaching or parting. Many examples have been reported, such as the removal of Ni from Cu-Ni alloys, Al from Al-bronzes, Sn from Cu-Sn alloys, and Cu from Cu-Au alloys among others. Dealloying has been extensively studied and there are recent reviews covering the subject such as those by Corcoran (2003) and Van Orden (2005) in which many alloy/environment systems are discussed.

As noted by Corcoran (2003), dealloying can occur in principle in any system where a large difference exists between the reversible electrode potentials of the alloy elements. Fig. 2.6 is a schematic polarization curve for a binary A_pB_{1-p} alloy in which a passivity range is indicated, followed by a substantial increase in the current density at the critical potential for dealloying, E_{crit}. At this potential, selective dissolution of A, the most active element of the alloy, occurs. It should be noted that E_{crit}, even though it is essentially determined by the composition of both the alloy and the electrolyte solution, is affected by the potential scan rate and the prior history of the alloy surface. Above E_{crit} the morphology of the dealloyed metal surface is characterized by a porous structure (sponge) enriched in the more noble alloying element. The structure consists of metal–void phases with a pore spacing of few nanometers which can be coarsened by annealing at higher temperatures.

Originally there were two mechanisms proposed to explain dealloying. The first mechanism – the dissolution-redeposition mechanism – suggested that both elements of the alloy dissolve and the more noble elements redeposit on the surface. The second mechanism postulated that only the active element is selectively dissolved from the alloy. A fundamental issue in this case relates to the process by which dealloying is sustained over more than a few atomic layers. Some authors suggested that dealloying is supported by solid-state diffusion of both atoms in the alloy to assure the necessary supply of electroactive solute atoms at the reactive layer. Others proposed that enhanced surface diffusion of the noble metal ad-atoms and surface restructuring allow continuous dissolution of the most active metal through a porous layer that progress in depth. A recent extension of this last

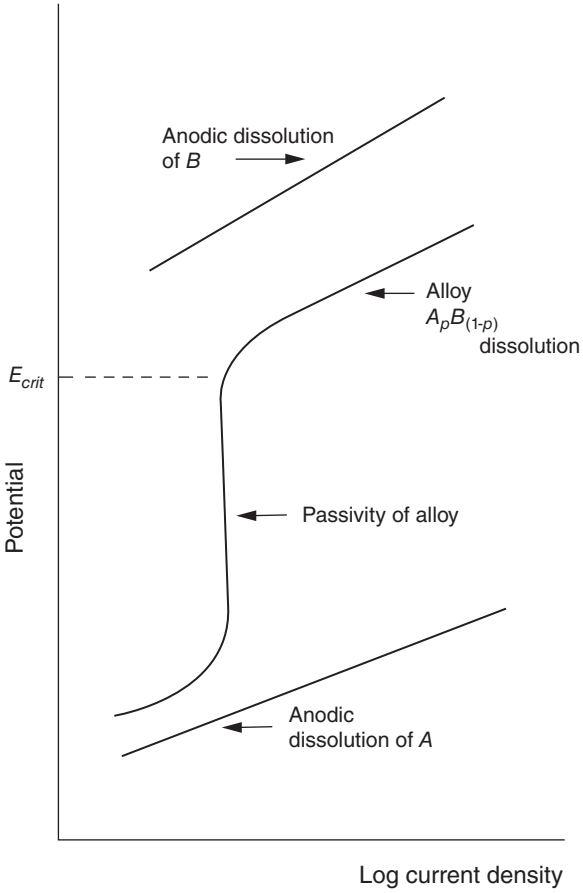

2.6 Schematic anodic polarization curve of a binary alloy A_pB_{1-p}, where *B* is the more noble alloy element, showing the range of passivity and the critical potential for dealloying, E_{crit}.

mechanism is the percolation model which accounts for preexisting interconnected paths in the binary alloy in order to explain that an alloy compositional threshold exists below which dealloying will not occur for a given alloy system. Van Orden (2005) has discussed some techniques used to study and evaluate dealloying indicating that there are no standards as have been developed for other localized corrosion processes.

2.3.5 Intergranular corrosion

Intergranular corrosion (IGC) is a form of localized corrosion characterized by preferential corrosion at grain boundaries or areas adjacent to

them, with little or negligible attack on the grains. Similarly to other forms of localized corrosion, it mainly occurs on passive alloys exposed to specific corrodents. IGC of commercial alloys is generally caused by enrichment or depletion of alloying elements in the area adjacent to the grain boundaries, by intergranular precipitation of second-phase particles or by the presence of alloy impurities segregated at the grain boundaries.

Most alloys, after being submitted to specific heat treatments or as a result of fabrication processes, experience IGC when exposed to an appropriate environment. A large number of cases involve Fe-Ni-Cr alloys, either Fe-based or Ni-based, particularly austenitic stainless steels (SS) due to their widespread use in many industrial applications. Austenitic SSs, such as AISI 304 (UNS S30400), after being slowly cooled through the temperature range of 850 to 550 °C, might become susceptible to IGC in relatively benign environments. The phenomenon is called 'sensitization' to indicate that the alloy is sensitive to grain boundary attack. Sensitization may occur as a result of various situations: (a) slow cooling from the annealing temperature, which could be the case in heavy section components; (b) stress relieving in the sensitization range, which is possible when ferritic steels that require such treatment are welded to austenitic steel parts that become sensitized; (c) welding operations, which is by far the most common cause of sensitization. The failure of AISI 304 and 316 (UNS S31600) SS components due to IGC in the heat-affected zone (HAZ) of the weld, the so-called weld decay, has been a problem in many industrial applications.

Sensitization of austenitic Fe-Cr-Ni alloys is caused by precipitation of Cr-rich carbides at grain boundaries, accompanied by Cr depletion of the regions adjacent to the carbides to levels below those required for passivation. Within the temperature range of sensitization, C diffuses toward the grain boundaries quite readily whereas the bulk diffusion of Cr from the austenitic matrix to the depleted region is too slow to allow replenishment. Since at least 12 wt % Cr is necessary to preserve passivity in an acidic medium, depletion of Cr below such level leads to IGC. However, if a sensitized austenitic SS is held long enough at the sensitization temperature it becomes desensitized because Cr diffusion from the bulk replenishes the Cr-depleted region, even though the carbides are still precipitated. Austenitic SSs become less susceptible to sensitization, and hence intergranular corrosion, by decreasing the C content or by adding alloying elements such as Ti or Nb which are stronger carbide formers than Cr.

Ferritic and duplex SSs are also subject to sensitization but their susceptibility is quite different. Ferritic SSs are sensitized at temperatures above 925 °C by Cr depletion of the matrix in the vicinity of precipitated carbides and nitrides at grain boundaries. Even though the rate of sensitization is faster than that of the austenitic SSs, ferritic SSs are easily desensitized at about 650 °C because the diffusion of Cr and C are faster than that in the

austenitic phase. Duplex SSs, which contain austenite and ferrite as constituent phases, are far less susceptible to sensitization because typically the C content is lower than 0.03 wt %. These alloys are more prone to exhibit precipitation of intermetallic phases, such as σ and χ, by slow cooling through the 900 to 700 °C range due to their relatively high Cr and Mo content. However, the effect of these intermetallic precipitates is more pronounced in terms of impact properties than on corrosion. If the C content is higher, preferential precipitation of carbides at ferrite/austenite boundaries make the duplex SS less prone to IGC because the depleted zone in the austenite phase can be easily replenished.

In terms of IGC, Ni-based alloys can be divided into two groups: Ni-Cr-Fe alloys such as Alloys 600 (UNS N06600) and 800 (UNS N08800) and Ni-Cr-Mo alloys such as C-276 (UNS N10276) and C-22 (UNS N06022). The first group is also prone to IGC as a result of sensitization. Even though the C content is usually lower (0.02 to 0.05 wt %) than in the AISI 304 or 316 SS, the solubility of C is also lower in the Ni-base alloys and shorter heat treatments induce sensitization and therefore IGC in acidic environments. In the case of Ni-Cr-Mo alloys such as C-22 preferential precipitation of intermetallic phases (μ and P) occurs upon heat treatment at temperatures around 600 °C. These intermetallics, rich in Cr and Mo, promote the depletion of both alloying elements in the region around them and facilitate IGC in acidic environments. An example of IGC of Alloy 22 is shown in Fig. 2.7. IGC occurred in this case inside a crevice in which strongly acidic conditions prevailed.

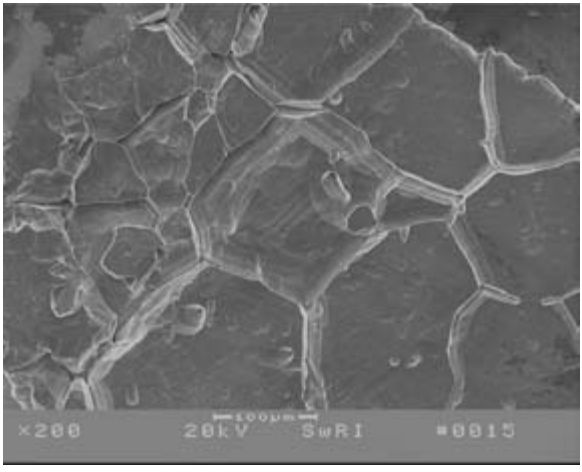

2.7 Micrographs showing an example of intergranular corrosion. Attack on alloy C-22 observed inside a crevice where acidified and concentrated chloride solutions exist.

Segregation of impurities such as S or P to grain boundaries is also the cause of IGC. The IGC of austenitic SS in hot concentrated HNO_3 has been attributed to the segregation of P to grain boundaries whereas the segregation of S to the grain boundaries of Ni is the cause of IGC in H_2SO_4 solutions, in both cases at high oxidizing potentials. Among others, models of sensitization and segregation for Fe-Ni-Cr alloys and steels that account for the most important experimental observations have been developed by Bruemmer (1990) and Gutman and McLean (1979) respectively.

Aluminum alloys are also susceptible to IGC in Cl^- solutions as a result of certain thermal aging treatments that promote precipitation of intermetallic phases along grain boundaries. The associated depletion of noble alloying elements (e.g., Cu) or the enrichment of the active ones (e.g., Zn) facilitates the preferential dissolution of the depleted area or the intermetallic phases respectively at potentials above the E_{pit} of each specific phase.

There are many standard chemical and electrochemical tests for evaluating the susceptibility of alloys to IGC. A good review of the standards and test methods for Fe-Cr-Ni alloys is presented by Streicher (2005). Standards also exist for heat-treatable Al alloys (ASTM, 2006f; 2006g).

2.4 Microbially influenced corrosion

Corrosion processes mediated by the action of microbes and their metabolic products are defined as microbially influenced corrosion (MIC). Whereas it is widely recognized that many types of aerobic and anaerobic bacteria are involved in MIC, their action is essentially related to the alteration of the local environmental and surface conditions facilitating the electrochemical reactions responsible for corrosion. Bacteria and other microorganisms, such as algae and fungi, are present in virtually all natural aqueous environments, as well as in industrial fluids and waste waters.

There is abundant literature on the deterioration of metallic materials since the anaerobic corrosion of cast iron by sulfate reducing bacteria was reported more than 70 years ago (Von Wolzogen Kuhr and Van der Vlugt, 1934). Among recent books, conference proceedings and handbook chapters, the following ones by Geesey *et al*. (1994), Borenstein (1994), Angell *et al*. (1995), Videla (1996), Little *et al*. (1997), Gu *et al*. (2000) and Dexter (2003) deserve to be mentioned. In recent years it has been recognized that there are types of bacteria that under certain conditions can inhibit corrosion (Dexter, 2005).

The initial stage of MIC is the formation of a biofilm on the metallic surface exposed to an aqueous environment. Biofilms are complex assemblages of physiologically distinct microbial species that interact to maximize their survival in that environment. A matrix of extracellular polymeric

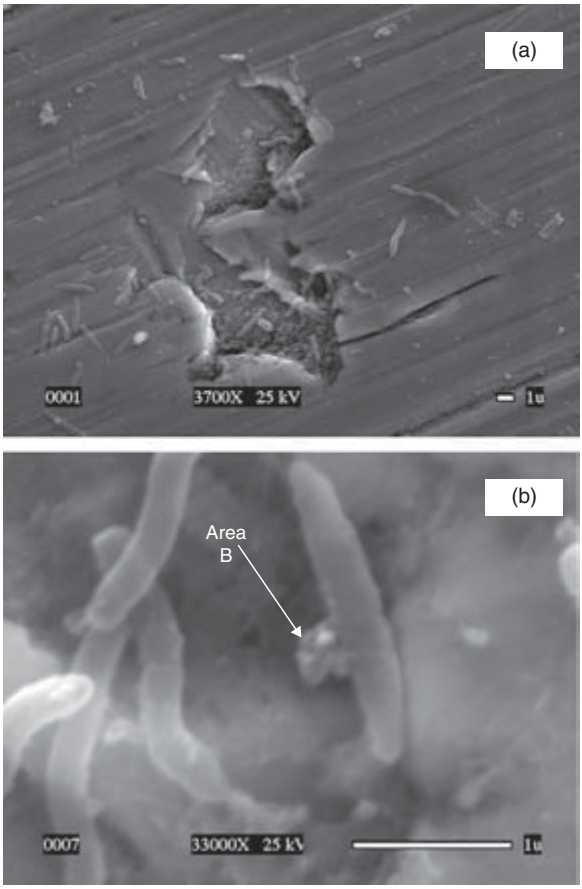

2.8 Micrographs showing: (a) typical pitting corrosion of AISI 304L stainless steel promoted by sulfate reducing bacteria; and (b) bacteria cells in a close up view of the lower pit.

substances (EPS) excreted by the bacteria anchor them to the substratum trapping essential nutrients and buffering any fluctuations in pH, toxic metals, biocides, etc. that may affect the viability and activity of the bacterial colony.

The presence of biofilms and their related heterogeneity creates microenvironments on the exposed surface, thereby affecting the mode and rate of corrosion that in most MIC cases becomes localized. An example of PC promoted by bacteria is shown in Fig. 2.8. According to Dexter (2003), bacterial actions promoting MIC comprise: (a) production of organic and inorganic acids as metabolic products; (b) production of sulfur reduced species (e.g., sulfides) under anaerobic conditions;

(c) introduction of new redox reactions; and (d) production of oxygen or generation of concentration cells.

It is beyond the scope of this chapter to discuss the specific aspects of all these actions and the type of bacteria involved. The publications listed above provide sufficient information. Nevertheless, it is important to emphasize the role of sulfate reducing bacteria which are able to promote localized corrosion of steels and other alloys under anaerobic conditions even though the bulk environment could be aerobic because microenvironments depleted of oxygen can exist under biodeposits of anaerobic microorganisms. This example illustrates the complexities of monitoring environmental conditions that may lead to MIC. The use of different techniques for this purpose has been discussed (Tuovinen and Cragnolino, 1986). The application of electrochemical methods and tests to investigate MIC has recently been reviewed by Little and Wagner (2001) and by Dexter (2005).

2.5 Flow-assisted corrosion and erosion corrosion

These two forms of corrosion are discussed in this section because they are closely related due to the preponderance of hydrodynamic factors on their occurrence. Whereas in some publications (Cramer and Covino, 2003; Baboian, 2005), no clear distinction is established between these two phenomena and both are considered as erosion corrosion, other authors (e.g., Efird, 2000) emphasize their differences. According to Efird, flow-assisted corrosion (FAC) or flow-influenced corrosion refers to corrosion significantly enhanced by the fast movement of a single-phase fluid. Erosion corrosion (EC) is described as the additional effect exercised by the presence of entrained second phase particles in a moving fluid, like liquid droplets entrained in a gas or solid particles suspended in a liquid or gas.

In this chapter, both phenomena are considered jointly and the specific differences will be noted. As shown schematically in Fig. 2.9, the rate of corrosion within the FAC regime is accelerated by fluid flow by increasing the rate of mass transport of reactive species to the metal surface or the rate of removal of corrosion products from such surface. At a critical flow velocity, sometimes called the breakaway or erosional velocity, a significant increase in the corrosion rate occurs well beyond the transition from laminar to turbulent flow. The critical flow velocity, V_c, for the occurrence of EC depends on the corrosion behavior of the material in the environment and the hydrodynamic parameters. It should be noted, however, that for many alloy/environment systems the boundary between both types of phenomenon is not as well defined as suggested by Fig. 2.9.

Below V_c, the corrosion rate increases slowly due to the increase in the rate of transport of electroactive species. The limiting current density,

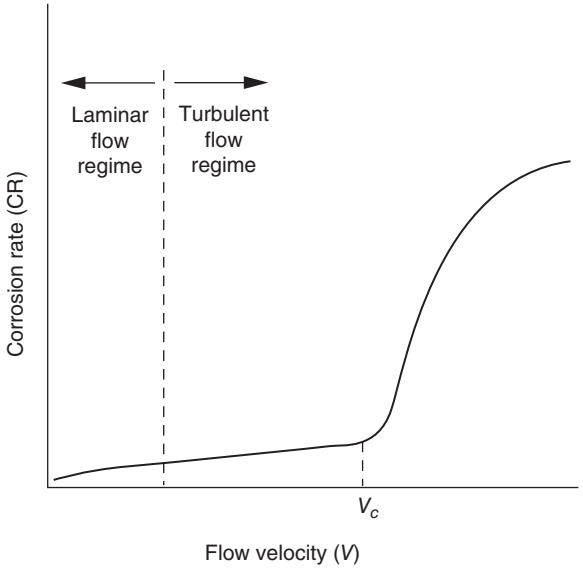

2.9 Schematic plot showing the effect of flow velocity on corrosion rate and its significant increase above the critical velocity, V_c, for erosion corrosion.

directly related to the corrosion rate by the Faraday laws, is given by the following general expression

$$i_L = Y Sc^a Re^b \quad [2.9]$$

where Y, a and b are constants, and Sc and Re are the Schmidt and Reynolds number respectively, as given by

$$Sc = D/v \quad [2.10]$$

$$Re = dV/v \quad [2.11]$$

where D is the diffusion coefficient, v is the kinematic viscosity, d the characteristic dimension and V the fluid velocity. Equation [2.9] is valid for many geometrical configurations (e.g., tubular, annular, rotating disk, rotating cylinder, etc.) under laminar, transitional, and turbulent flow conditions. The values of Y, a, and b for such geometries and conditions are available. The limiting current and hence the corrosion rate below V_c usually increases with increasing V according to V^b with $0.33 < b < 0.5$, exhibiting the largest b value in the turbulent regime.

If V is sufficiently high the shear force at the interface may become sufficiently large to mechanically remove any protective film from the surface leading to the accelerated corrosion depicted in Fig. 2.9 (i.e., the exponent

b becomes higher than 1.0). Although the attack could be localized in regions of high turbulence where reverse flow and eddying occur, corrosion is less localized than in PC and CC which are corrosion processes typical of stagnant fluids.

In addition to the hydrodynamic variables discussed above, the properties of the environment and the composition of the materials have an important influence on FAC and EC. A decrease in pH from neutral values can accelerate significantly the FAC rate whereas O_2 can have opposite effects. If FAC is under cathodic control and dominated by O_2 reduction, the corrosion rate can be accelerated by increasing the O_2 content. However, an increase in the O_2 content may displace the E_{corr} to a regime in which more protective films can be formed and the corrosion rate will decrease. Very protective passive films, such as those formed on SSs or Ti alloys, are resistant to mechanical disruption even at very high shear forces and therefore these materials do not exhibit the abrupt increase in corrosion rate shown in Fig. 2.9, unless the abrasive effects due to the presence of solid particles in the fluid play a role at very high energy transfer rates.

EC should be distinguished from other forms of erosive action such as solid particle and liquid droplet impingement damage and cavitation (Postlethwaite and Nesic, 2000) which can be considered essentially as mechanical forms of metal deterioration because the contribution of corrosion is minimal. Tests to evaluate the effect of these phenomena are discussed by Glaeser (2005) whereas Roberge (2004) has reviewed test methods for FAC and EC.

2.6 Stress corrosion cracking

Stress corrosion cracking (SCC) is a process by which cracks propagate in a metal or alloy by the concurrent action of a tensile stress (residual and/or applied) and a specific corrosive environment. Depending upon the alloy/environment system, cracks could propagate with velocities ranging from 10^{-12} to 10^{-3} m/s in alloys which do not exhibit significant general corrosion because they are covered with a protective film. For these reasons SCC is one of the more insidious forms of alloy failure in industrial applications and therefore the subject is one of the most researched areas of corrosion science and engineering. Among many books and conferences covering a wide range of alloys, environments, and applications, those by Gangloff and Ives (1988), Jones (1992, 2001), Kane (2000) and Shipilov *et al*. (2007a, b) are the most recent ones.

There are two distinctive modes of crack propagation according to the path followed by the cracks. Cracks are intergranular when they propagate along grain boundaries and are transgranular if they run across the grains,

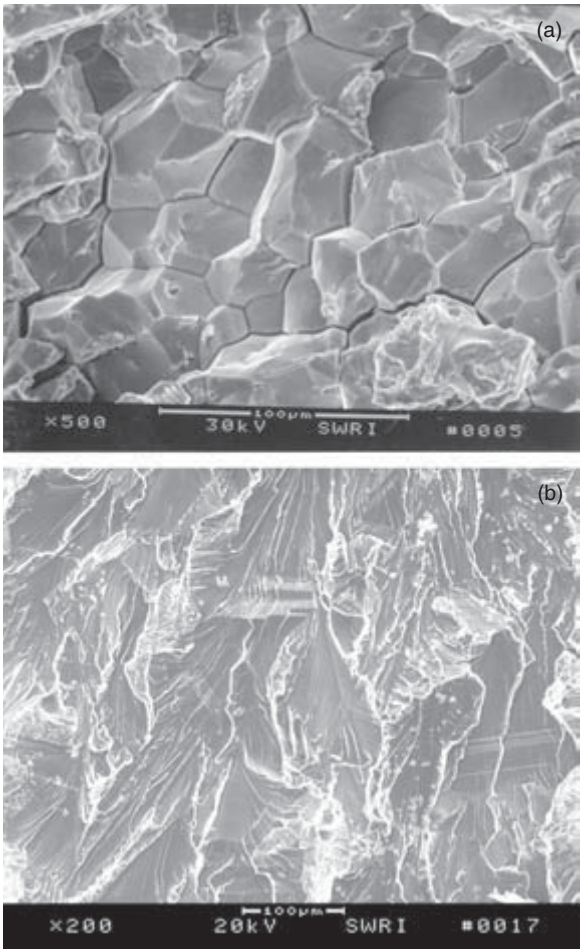

2.10 Fractographs showing the typical appearance of: (a) intergranular stress corrosion cracking; and (b) transgranular stress corrosion cracking. Both crack propagation modes were observed on AISI 316L strained in a hot $MgCl_2$ solution.

in some cases following preferential crystallographic planes (cleavage planes), as illustrated in the fractographs shown in Fig. 2.10. Depending upon the alloy/environment system, either mode of propagation can be observed, but in many cases both modes can occur simultaneously or consecutively. A transition in the mode of propagation could arise from minor changes in the composition of the corrodent (e.g., pH, or concentration of ionic species), the potential, or the composition and microstructure of the alloy.

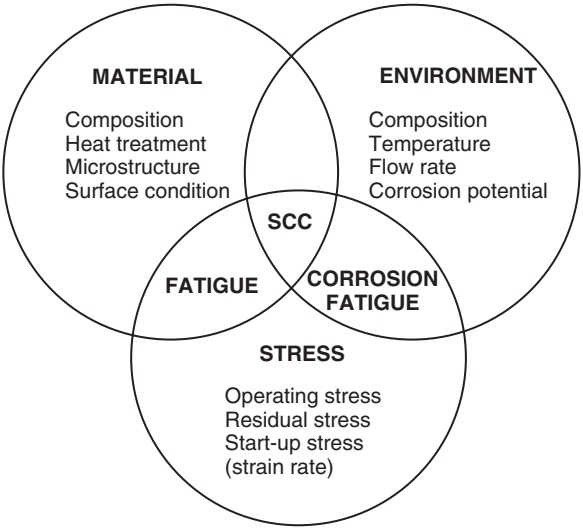

2.11 Schematic diagram showing the interplay of the three major influential factors on stress corrosion cracking of metallic materials.

The three groups of major factors affecting SCC susceptibility are schematically represented in Fig. 2.11. Material variables are uniquely important in determining SCC resistance. Compositional differences even within a class of alloys (e.g. austenitic Ni-Cr-Fe alloys) could have a remarkable effect. Microstructural modifications introduced by heat treatment can alter substantially the SCC resistance (e.g., sensitization of austenitic SS renders them susceptible to intergranular SCC in relatively innocuous environments). Even though variations in surface conditions may not alter substantially the SCC behavior, the initiation time that precedes crack propagation could be affected significantly.

Stress is another major factor required for SCC and various sources of stress are summarized in Fig. 2.11. The time of failure caused by the propagation of cracks under constant load conditions tends to increase with decreasing stress until a threshold stress, σ_{th}, is reached, usually lower than that required for macroscopic yielding as expressed by the yield strength, σ_y, of the material. The effect of applied stress, however, is better represented through the stress intensity factor, K_I, defined by fracture mechanics concepts as

$$K_I = Y\sigma\ (\pi\ a)^{1/2} \qquad [2.9]$$

where Y is a geometrical factor, σ is the applied stress, and a is the crack length. Crack propagation only occurs above a threshold stress intensity

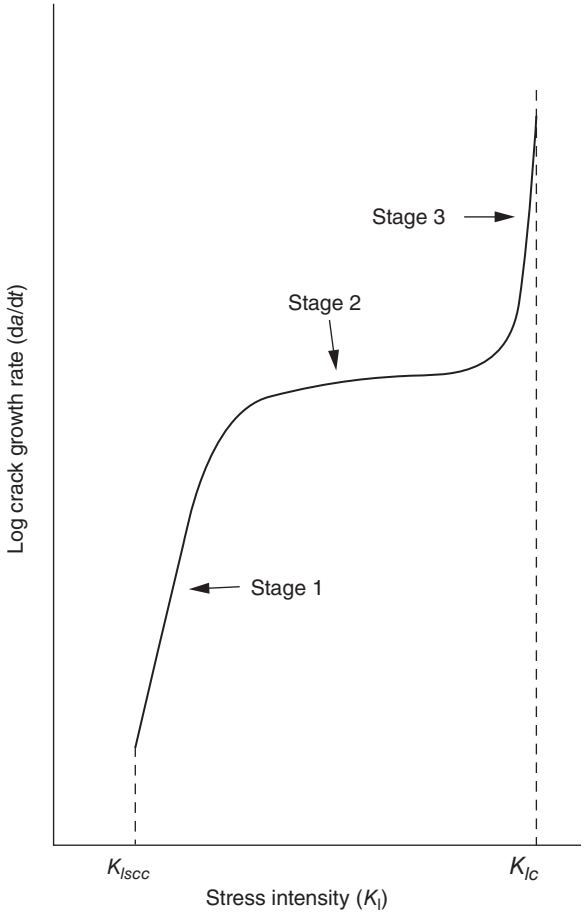

2.12 Schematic plot of the logarithm of the crack growth rate, d*a*/d*t*, as a function of stress intensity, K_I, showing the typical three stages of crack propagation at K_I values above the threshold stress intensity for stress corrosion cracking, K_{Iscc}. The critical stress intensity, K_{Ic}, for fast fracture in air is also indicated.

defined as $K_{Iscc.}$ Usually crack growth rate increases rapidly with increasing K_I above K_{Iscc} (Stage 1), until a plateau is reached at which the crack growth rate becomes independent of K_I (Stage 2), as shown schematically in Fig. 2.12.

In many cases of service failures, residual stresses caused by manufacturing processes, such as welding, become critical factors, in addition to the effect of stresses due to sustained mechanical loads or dynamic straining during start-up operations (i.e. slow strain rate conditions).

The third major factor influencing SCC is related to the properties of the environment, including variables such as chemical composition, pH, temperature, flow rate, etc. The concept of a very specific environment required to promote SCC of a given alloy (e.g. NH_3 causing SCC of α-brass) does not hold any more due to the multiplicity of chemical species able to promote SCC under an appropriate set of environmental conditions. In this regard, the potential is recognized as a critical factor because minor modifications of E_{corr} by the presence of reducible species (e.g., O_2, H_2O_2, Fe^{3+}, Cu^{2+}) may promote SCC by displacing the E_{corr} of the metal or alloy to a 'window' of susceptibility. For an alloy exposed to the appropriate environment in which anodic dissolution is the predominant crack advance mechanism, the current density at the crack tip should be far faster than the current density at the exposed surface, otherwise general dissolution will occur. Moreover, if the current density at the crack walls is comparable to that at the crack tip, PC will occur instead of SCC. A critical balance must exist between anodic activity at the crack tip and passivity of the overall exposed surface to maintain the high aspect ratio of a crack. A complete passive behavior precludes SCC because any incipient crack nucleus will be soon repassivated.

Parkins (1972) proposed that a continuous spectrum of mechanisms can account for the SCC observed in a large variety of alloys and environments and Macdonald and Cragnolino (1989) extended such a concept to alloy/environment systems prevailing in the power generating industry. The mechanisms may range from: (a) intergranular SCC (e.g., ferritic steels in caustic solutions); promoted by anodic dissolution along preexisting active paths (i.e., depleted or segregated grain boundaries); (b) transgranular SCC (e.g., austenitic SS in hot chloride solutions), initiated by mechano-chemical passivity breakdown in the form of incipient pits just above E_{pit} or E_{rpit} (see Fig. 2.4) and propagated along strain generated paths; and (c) mixed intergranular and transgranular SCC (e.g. high strength steels in water or steam) induced by absorption of atomic hydrogen and decohesion. Newman (2002) proposed that a brittle film on the metal surface, such as a dealloyed layer, can trigger a fast short-life cleavage promoting discontinuous transgranular crack propagation. On the other hand, Galvele (1995) after reviewing all the postulated models for SCC has developed a model based on surface mobility. Ionic species in the environments can create a contaminated layer where accelerated self-diffusion of ad-atoms induces the generation of vacancies at the stressed crack tip as the crack advance mechanism. Proposed SCC mechanisms and models have been reviewed and discussed by Jones (2003). The existence of a critical potential for the transgranular SCC of austenitic SSs in hot chloride solutions, E_{SCC}, coincident with E_{rcrev} has been discussed by Cragnolino *et al.* (2001), whereas other authors (Andresen *et al.*, 2001) dispute the existence of such

critical potentials on the basis of research conducted in environments such as high temperature water.

The most important parameter for monitoring SCC is the crack growth rate which has been measured in compact tension specimens by using potential drop methods, instrumented loading bolts and more recently Micro-Electro-Mechanical Systems (MEMS). Techniques for evaluating SCC are described by Sedriks (1990) and Phull (2003a). Sensors to measure stress and strain or strain rate are necessary as well as those required for monitoring environmental parameters which are common to other localized corrosion processes, including E_{corr}.

2.7 Corrosion fatigue

Corrosion fatigue (CF) occurs when a metallic component exposed to a corrosive environment is subjected to cyclic stresses. It is distinguished from fatigue (see Fig. 2.11), which takes place in the absence of a corrosive environment (i.e., dry inert gas or vacuum). CF is closely related to SCC and usually jointly considered as environmentally assisted cracking (EAC). However, the effect of the environment is far less specific in CF. As suggested by the lack of superposition with the materials circle in the diagram of Fig. 2.11, almost all metals and alloys, either under active or passive conditions, experience CF in an aqueous environment because their fatigue life is reduced with respect to that in an inert environment. Even humid air is an aggressive environment for many metals and alloys. In alloys exhibiting passive behavior (e.g., ferritic SSs used in turbine blades) transgranular cracks typical of CF – which do not exhibit the branching features characteristic of transgranular SCC – are initiated from pits. Comprehensive reviews of CF can be found in many books, handbook chapters and conference proceedings. Among those recently published, Magnin (2002) and Gangloff (2005) provide valuable reviews.

Gangloff (2005) describes four successive stages of CF with increasing number of load cycles: (a) cyclic plastic deformation; (b) microcrack initiation; (c) small crack growth to linkup and coalescence; and (d) macrocrack propagation. The initial stages are the subject of high-cycle fatigue (HCF) which is characterized by cyclic loads that lead to small scale yielding. HCF is studied by using smooth or notched cylindrical specimens and test results are plotted showing the applied cyclic stress amplitude, σ_a, vs. the number of cycles to failure, N. The value of σ_a decreases with N until a limiting value named the fatigue strength or endurance limit is reached at $N \approx 5 \times 10^6$ cycles. In an inert environment this parameter is well defined and represents the fatigue resistance of the material. In a corrosive environment, however, σ_a tends to decrease continuously with increasing N and the

CF strength is usually defined at an arbitrary value of N (e.g. 10^7 cycles). The CF life, as assessed by the σ_a vs. N curves, is dominated by microcrack initiation, as evidenced by the fact that notched specimens, where crack initiation is facilitated, fail at substantially lower N than smooth specimens when subjected to the same σ_a values.

Macrocrack propagation is evaluated using fracture mechanics techniques. The CF crack growth rate per cycle, da/dN, is plotted as a function of the stress intensity range, $\Delta K = K_{max} - K_{min}$ as shown in Fig. 2.13a. In vacuum or dry air, a threshold stress intensity range, ΔK_{th}, exists below which da/dN becomes negligible. Above ΔK_{th}, and at intermediate ΔK values, the following Paris relationship is valid

$$da/dN = C\,(\Delta K)^n \qquad [2.10]$$

where C and n are empirical constants. In a corrosive environment, da/dN usually exhibits a more complex dependency with ΔK, $R = K_{min}/K_{max}$ and frequency, f, and the changes in behavior schematically illustrated in Fig. 2.13b–d can be observed. In the first case (Fig. 2.13b), there is a synergism between cyclic loading and the corrosion reactions at the crack tip leading to what is termed 'true corrosion fatigue'. As a result, da/dN increases with decreasing frequency below 1 Hz because the environment has more time to interact with the crack tip during the rising part of the load cycle. The second case (Fig. 2.13c) is observed in materials/environment systems in which SCC occurs above K_{Iscc} (e.g., high strength steels in NaCl solution). In this case the environment has a strong effect on da/dN only within the $K_{Iscc} < K_{max} < K_c$ range. Also, da/dN increases with decreasing frequency and with increasing $K_{mean} = (K_{max} + K_{min})/2$. The third case (Fig. 2.13d) represents a combination of the two previous

2.13 (a) Schematic plot of the logarithm of the cyclic crack growth rate, da/dN, as a function of the logarithm of the stress intensity range, ΔK, showing the threshold stress intensity range, ΔK_{th}, for fatigue and the critical stress intensity, K_{Ic}, for fast fracture in an inert environment. (b) Schematic plot of the logarithm of the cyclic crack growth rate, da/dN, as a function of the logarithm of the maximum stress intensity, K_{max}, showing the effect of a corrosive environment on 'true' corrosion fatigue. (c) Schematic plot of the logarithm of the cyclic crack growth rate, da/dN, as a function of the logarithm of the maximum stress intensity, K_{max}, showing the effect of a corrosive environment only above the threshold stress intensity for stress corrosion cracking, K_{Iscc}. (d) Schematic plot of the logarithm of the cyclic crack growth rate, da/dN, as a function of the logarithm of the maximum stress intensity, K_{max}, showing the effect of a corrosive environment on 'true corrosion fatigue' below K_{Iscc} and the superposition of corrosion fatigue and stress corrosion cracking above K_{Iscc}.

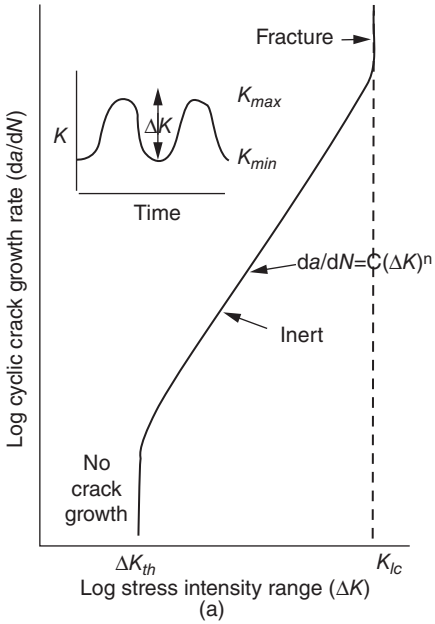

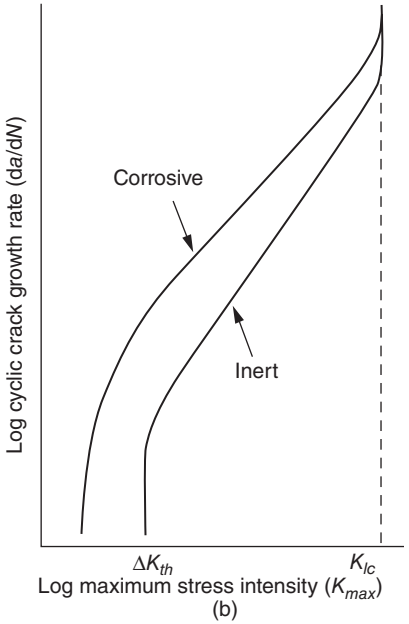

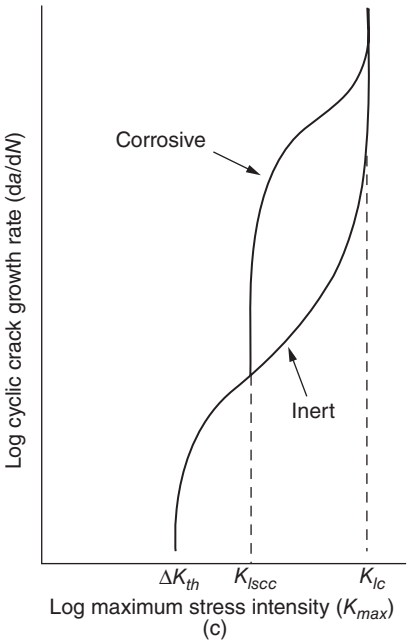

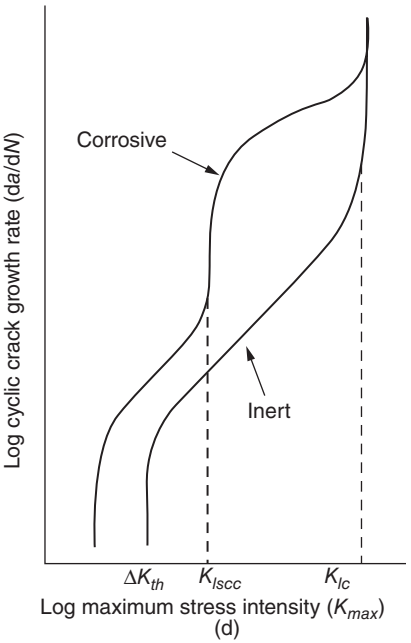

behaviors (e.g., α/β Ti alloys in NaCl solution), 'true corrosion fatigue' below K_{Iscc} and superposition of CF and SCC above K_{Iscc}. This behavior leads to an expression of the crack growth rate for EAC on a time basis given by:

$$(\mathrm{d}a/\mathrm{d}t)_{EAC} = f\,(\mathrm{d}a/\mathrm{d}N)_{TCF} + (\mathrm{d}a/\mathrm{d}t)_{SCC} \qquad [2.11]$$

As indicated in Fig. 2.11, environmental variables play an important role on CF. Although their influence is less specific than in SCC, the localized environment inside the crack which is, among other factors, controlled by the potential, determines the rate at which corrosion reactions occur and hence affect the CF crack growth rate. Finally, it should be emphasized that the CF behavior is strongly affected by metallurgical variables, among them alloy composition and microstructure, and in particular mechanical propertie such as tensile strength and fracture toughness. Comprehensive reviews of CF testing are presented by Phull (2003b) and Gangloff (2005).

2.8 Hydrogen embrittlement

There is a tendency to consider hydrogen embrittlement (HE) as a form of EAC. In this section, however, it is defined separately, taking into account the almost unique physicochemical properties of hydrogen and its specific interaction with metals. Hirth and Johnson (1976) in their phenomenological classification of such interaction in nine categories separated three forms of HE from other forms of hydrogen damage. The mode of hydrogen entry in a metal lattice distinguishes hydrogen stress cracking (HSC) from hydrogen environment embrittlement (HEE), both characterized by a loss of tensile stress due to the subcritical growth of cracks at tensile stresses below the yield strength, whereas loss in tensile ductility corresponds to the decrease in elongation or reduction in area in a tensile test. There are many comprehensive books, handbooks and conference proceedings dealing with HE of different classes of alloys, particularly steels due to their technological significance (e.g., Oriani *et al.*, 1985; Turnbull, 1995; Thompson and Moody, 1996; Moody *et al.*, 2003).

The process of greatest interest is HSC because hydrogen entry is caused by a corrosion process in aqueous media whereas the usual source of hydrogen in HEE is gaseous. The cathodic reduction of H^+ ions by either the chemical desorption mechanism or the electrochemical desorption mechanism leads to the chemical adsorption of atomic hydrogen on the metal surface, according to the following reaction step:

$$M + H_3O^+ + e^- \rightarrow MH_{ad} + H_2O \qquad [2.12]$$

The hydrogen atom can diffuse into the metal lattice, particularly in body-centered cubic (bcc) metals in which the diffusion coefficient is high ($D \approx 10^{-4}$ cm^2/s). The entry of the hydrogen atoms in the lattice is strongly favored by the presence of species in the environment, such as H_2S and other volatile hydrides (e.g. H_2Se, PH_3, AsH_3 and SbH_3), which act as poisons for the recombination of adsorbed hydrogen atoms, limiting the desorption of H_2 molecules and hence increasing the available concentration of hydrogen atoms on the metal surface.

There are a large number of atomic, microscopic and macroscopic defects, where hydrogen atoms may accumulate in a metallic structure. These traps include interstitial and substitutional solute atoms, lattice vacancies, inclusions, voids and pores. This trapped hydrogen can lead to crack propagation and failure in the presence of a tensile stress of sufficient magnitude. HSC is commonly associated with brittle failure, either in the form of intergranular cracking or transgranular cracking with a quasi-cleavage appearance, even though in some cases ductile fracture occurs. For steels the fracture mode depends on the value of K_I. The fracture mode may change from intergranular cracking at low K_I, to transgranular tearing with quasi-cleavage facets at intermediate K_I, and microvoid coalescence, typical of ductile failure at high K_I.

The crack growth rate for a variety of medium- and high-strength steels in environments promoting HE depends on K_I, exhibiting a dependence similar to that shown in Fig. 2.12. above a threshold value defined as K_{IEH}. The crack growth rate in Stage 2 increases with increasing cathodic potentials suggesting that SCC of high-strength steels in aqueous environments is caused by HE. The crack growth rate also increases in NaCl solutions at anodic potentials above E_{pit} because atomic hydrogen is generated inside the pits as a result of localized acidification and the subsequent reduction of H^+ ions. Test methods for evaluating HE are discussed by Phull (2003c) and Interrante and Raymond (2005).

2.9 Characterization techniques

Techniques used to characterize and analyze corroded and fractured surfaces and features like pits and cracks, as well as corrosion products, are presented and discussed in many papers, books and other publications. A useful series of articles written by different specialists were published as Surface Analysis Series in many issues of Volumes 41, 42, and 43 of *Corrosion Engineering* (the English translation of Boshoku Gijutsu). Marcus and Mansfeld (2005) have recently edited a book in which surface analysis and electrochemical techniques are discussed in some detail. In the following sections, brief descriptions of the different techniques are presented.

Table 2.1 Surface sensitive analytical techniques, principles and applications (adapted from Shah, 2003, with minor modifications)

Analytical technique	Principle	Target information
Surface morphology		
Optical microscopy	Reflected light is used to generate a magnified image.	Macroscopic surface structure details
Scanning electron microscopy (SEM)	Incident electron beam generates a secondary electron emission that is used to generate the surface image.	Microscopic imaging of the surface structure
Atomic force microscopy (AFM)	Microscopic force sensor (cantilever) is used to sense the force between a sharp tip and the sample surface as the sample is scanned to generate an image.	Imaging of insulated surface structure at atomic resolution
Scanning tunneling microscopy (STM)	Tunneling current is motivated as the probe tip is scanned over a surface of interest in the *x-y* plane to generate an image.	Imaging of conducting surface structure at atomic resolution
Chemical identification and composition		
Energy dispersive x-ray spectroscopy (EDS)	Incident electron beam generates emission of x-rays characteristic of element present at the surface.	Elemental identification of the surface species
X-ray diffraction (XRD)	Diffraction of the incident x-ray beam from various plans of crystal lattice create a diffraction pattern characteristic of the sample.	Elemental and phase identity and composition of inorganic corrosion product
Auger electron spectroscopy (AES)	Incident electron beam initiates a multistep process to facilitate the ejection of an outer shell electron. The energy of this ejected electron is characteristic of the surface atoms.	Elemental identity and composition of the surface species and the depth profile

2.9.1 Surface characterization

Several techniques are used to examine and characterize topological features of corroded metal and fracture surfaces. They include traditional optical microscopy and electron microscopy. Table 2.1 adopted from Shah (2003) summarizes the techniques used to examine the surface topological structure and those to obtain the chemical identity and composition of surface films and layers as well as corrosion products by examining the atomic and molecular structure. More detailed information is available on materials characterization in Volume 10 of the *ASM Handbook*.

Table 2.1 Continued

Analytical technique	Principle	Target information
X-ray photoelectron spectroscopy (XPS)	Incident x-rays on the surface eject photoelectrons. The energy of the photoelectrons is characteristic of the surface atoms.	Elemental identity and composition of the surface species, the electronic structure, chemical bonding, and elemental depth profile
Glow discharge optical emission spectrometry (GDS)	Gas discharge with inert gas (Ar) at 1–10 Torr generate plasma and sputtered atoms excited in the plasma will emit light with characteristic wave length.	Elemental identity and composition of surface species and the depth profile
Ion scattering spectroscopy (ISS)	The energy of scattered primary ions from the surface allows identification of surface atoms.	Chemical composition of the surface films at atomic and a molecular level
Secondary ion mass spectrometry (SIMS)	Incident ion beam ejects the surface atoms as ions, and mass of these secondary ions is measured.	Chemical composition of the surface adsorbed species
Extended x-ray absorption fine structure (EXAFS)	The x-ray absorption generates the interference effects between emitted photoelectron waves and backscattering waves characteristic of the local structure.	Composition of adsorbed species, number, and separation distances of surface atoms
Fourier transform infrared absorption spectroscopy (FTIR)	The absorption of the infrared photons results in vibrational excitation that is characteristic of the surface molecules and the environment.	Vibrational structure of molecules and bonding interactions with the surface and the surroundings
Raman and surface enhanced Raman spectroscopy (Raman, SERS)	Energy shifts of the scattered photons are characteristic of the molecular identity.	Vibrational structure of adsorbed molecules on the surface

Energy dispersive X-ray analysis (EDS) is routinely used in conjunction with scanning electron microscopy (SEM) to examine and analyze corroded and fractured surfaces, whereas it is combined with scanning transmission electron microscopy (STEM) to analyze at much higher magnification concentration profiles around precipitates, pits or cracks, intermetallic compositions, etc. X-ray photoelectron spectroscopy (XPS), Auger electron spectroscopy (AES) and glow discharge optical emission spectrometry

(GDS) are commonly used in combination with ion milling or sputtering to study in-depth composition of surface layers or passive films.

Ellipsometry is an optical method used to characterize the optical properties of surface and surface layers using the reflection of polarized light. It has been extensively used to determine the thickness of passive films among other applications.

2.9.2 Corrosion products characterization

Many of the techniques used to characterize and analyze deposited, suspended or dissolved corrosion products, including ionic species in solution are listed in Table 2.1. These techniques include among others, SEM combined with EDS, X-ray diffraction (XRD), Fourier transform infrared absorption spectroscopy (FTIR), laser Raman spectroscopy, and inductively coupled plasma mass spectrometry, as well as traditional methods such as atomic absorption spectroscopy for the analysis of species in solution.

2.10 References

Anderko A, Sridhar N, and Dunn D S (2004), 'A general model for the repassivation potential as a function of multiple aqueous solution species', *Corrosion Science*, 46, 1583–1612.

Andresen P L, Angeliu T M, and Young L M (2001), 'Immunity, thresholds, and other SCC fiction', in *Chemistry and Electrochemistry of Corrosion and Stress Corrosion Cracking: A Symposium Honoring the Contributions of R. W. Staehle,* Jones R H, Ed., Warrendale, PA: The Minerals, Metals, and Materials Society, 65–82.

Angell P, Borenstein S W, Buchanan R A, Dexter S C, Dowling N J E, Little B J, Lundi C D, McNeil M B, Pope D H, Tatnall R E, White D C and Ziegenfuss H G, Ed. (1995), *International Conference on Microbially Influenced Corrosion,* Houston, TX: NACE International.

ASTM (2006a) G–1 'Standard Practice for Preparing, Cleaning and Evaluating Corrosion Tests Specimens', West Conshohocken, PA: ASTM International.

ASTM (2006b) G–102 'Standard Practice for Calculation of Corrosion Rates and Related Information from Electrochemical Measurements', West Conshohocken, PA: ASTM International.

ASTM (2006c) G–71 'Standard Guide for Conducting and Evaluating Galvanic Corrosion Tests in Electrolytes', West Conshohocken, PA: ASTM International.

ASTM (2006d) G–61 'Standard Test Method for Conducting Cyclic Potentiodynamic Polarization Measurements for Localized Corrosion Susceptibility of Iron-, Nickel-, or Cobalt-Based Alloys', West Conshohocken, PA: ASTM International.

ASTM (2006e) G–48 'Standard Test Methods for Pitting and Crevice Corrosion Resistance of Stainless Steels and Related Alloys by Use of Ferric Chloride Solution', West Conshohocken, PA: ASTM International.

ASTM (2006f), G–110 'Practice for Evaluating Intergranular Corrosion Resistance of Heat Treatable Aluminum Alloys by Immersion in Sodium Chloride + Hydrogen Peroxide Solution', West Conshohocken, PA: ASTM International.

ASTM (2006g) G–67 'Test Method for Determining the Susceptibility to Intergranular Corrosion of 5XXXX Series of Aluminum Alloys by Mass Loss after Exposure to Nitric Acid (NAMLT Test)', West Conshohocken, PA: ASTM International.

Baboian R, Ed. (2005), *Corrosion Tests and Standards: Application and Interpretation, 2nd edition*, West Conshohocken, PA: ASTM International.

Bard A J and Faulkner L R (1980), *Electrochemical Methods: Fundamentals and Applications*, New York, NY: J. Wiley & Sons, Inc.

Borenstein S W (1994), *Microbiologically Influenced Corrosion Handbook*, New York: Industrial Press Inc.

Bruemmer S M (1990), 'Quantitative modeling of sensitization development in austenitic stainless steel', *Corrosion* 46, 698–709.

Cabrera N and Mott N F (1948–1949), 'Theory of oxidation of metals', *Reports on Progress in Physics*, 12, 163–184.

Combrade P (2002), 'Crevice corrosion of metallic materials', in *Corrosion Mechanisms in Theory and Practice, Second Edition, Revised and Expanded*, Marcus P, Ed, New York, Marcel Dekker, Inc, 349–397.

Corcoran S (2003), 'Effect of metallurgical variables on dealloying corrosion', in *ASM Handbook, Vol. 13A, Corrosion: Fundamentals, Testing and Protection*, Cramer S D and Covino Jr. B S, Eds, Materials Park, OH: ASM International, 287–293.

Cragnolino G A, Dunn D S, Pan Y M and Sridhar N (2001), 'The critical potential for the stress corrosion cracking of Fe-Cr-Ni alloys and its mechanistic implications', in *Chemistry and Electrochemistry of Corrosion and Stress Corrosion Cracking: A Symposium Honoring the Contributions of R. W. Staehle*, Jones R H, Ed, Warrendale, PA: The Minerals, Metals, and Materials Society, 83–104.

Cramer S D and Covino Jr. B S, Eds. (2003), *ASM Handbook, Vol. 13A, Corrosion: Fundamentals, Testing and Protection*, Materials Park, OH: ASM International.

Cramer S D and Covino Jr. B S, Eds. (2005), *ASM Handbook, Vol. 13B, Corrosion: Materials*, Materials Park, OH: ASM International.

Cramer S D and Covino Jr. B S, Eds. (2006), *ASM Handbook, Vol. 13C, Corrosion: Environments and Industries*, Materials Park, OH: ASM International.

Dexter S C (2003), 'Microbiologically influenced corrosion', in *ASM Handbook, Vol. 13A, Corrosion: Fundamentals, Testing and Protection*, Cramer S D and Covino, Jr. B S, Eds, Materials Park, OH: ASM International.

Dexter S C (2005), 'Microbiological effects', in *Corrosion Tests and Standards: Application and Interpretation, 2nd edition*, Baboian R, Ed., West Conshohocken, PA: ASTM International, 509–522.

Dunn D S, Pan Y M, Yang L and Cragnolino G A (2006), 'Localized corrosion susceptibility of alloy 22 in chloride solutions. II- Effects of fabrication processes', *Corrosion*, 62, 3–12.

Dunn D S, Cragnolino G A and Sridhar N (2000), 'An electrochemical approach to predicting long-term localized corrosion of corrosion-resistant high-level waste container materials', *Corrosion*, 56, 90–104.

Dunn D S, Pan Y M, Yang L and Cragnolino G A (2005), 'Localized corrosion susceptibility of alloy 22 in chloride solutions. I- Mill-annealed condition', *Corrosion*, 61, 1078–1085.

Dunn D S, Sridhar N, and Cragnolino G A (1996), 'Long-term prediction of localized corrosion of alloy 825 in high-level nuclear waste repository environments', *Corrosion*, 52, 115–124.

Efird K D (2000), 'Flow-induced corrosion', in *Uhlig's Corrosion Handbook, 2nd edition*, Revie R W, Ed., New York, NY: J. Wiley & Sons, Inc, 233–248.

Frankel G S (1998), 'Pitting corrosion of metals. A review of the critical factors', *Journal of the Electrochemical Society*, 145, 2186–2198.

Frankel G S and Newman R C, Eds. (1992), *Critical Factors in Localized Corrosion,* Proceedings Vol 92-9, Pennington, NJ, The Electrochemical Society.

Galvele J R (1976), 'Transport processes and the mechanism of pitting of metals', *Journal of the Electrochemical Society*, 123, 464–474.

Galvele, J R (1978), 'Present state of understanding of the breakdown of passivity and repassivation', in *Passivity of Metals*, Princeton, NJ: The Electrochemical Society, 285–327.

Galvele J R (1995), 'Electrochemical aspects of stress corrosion cracking', in *Modern Aspects of Electrochemistry*, Vol. 27, Vayenas C G, White R E and Gamboa-Adelco, M E, Eds, New York, NY: Plenum Press, 233–358.

Gangloff R P (2005), 'Environmental cracking – Corrosion fatigue', in *Corrosion Tests and Standards: Application and Interpretation, 2nd edition,* Baboian R, Ed., West Conshohocken, PA: ASTM International, 302–321.

Gangloff R P and Ives M B, Eds. (1988), *Environment Induced Cracking of Metals*, Houston, TX: NACE International.

Geesey G G, Lewandowski Z and Flemming H C (1994), *Biofouling and Biocorrosion in Industrial Waters*. Boca Raton, FL: CRC Press, Inc.

Glaeser W A (2005), 'Erosion, cavitation, and fretting', in *Corrosion Tests and Standards: Application and Interpretation, 2nd edition*, Baboian R, Ed., West Conshohocken, PA: ASTM International, 273–277.

Gu J D, Ford T E and Mitchell R (2000), 'Microbiological corrosion of metals', in *Uhlig's Corrosion Handbook, 2nd edition*, Revie R W, Ed., New York, NY: J. Wiley & Sons, Inc., 915–927.

Guttman M and McLean D (1979), 'Grain boundary segregation in multicomponents systems', in *Interfacial Segregation*, Johnson W C and Blakely J M, Eds, Materials Park, OH: ASM International, 261–350.

Hack H P (2005), 'Galvanic', in *Corrosion Tests and Standards: Application and Interpretation, 2nd edition*, Baboian R Ed., West Conshohocken, PA: ASTM International, 233–243.

Hirth J P and Johnson H H (1976), 'Hydrogen problems in energy related technology', *Corrosion*, 32, 3–16.

Interrante C G and Raymond L (2005), 'Hydrogen damage' in *Corrosion Tests and Standards: Application and Interpretation, 2nd edition*, Baboian R, Ed., West Conshohocken, PA: ASTM International, 322–340.

Jones R H, Ed. (1992), *Stress-Corrosion Cracking. Materials Performance and Evaluation.* Materials Park, OH: ASM International.

Jones R H, Ed. (2001), *Chemistry and Electrochemistry of Corrosion and Stress Corrosion Cracking: A Symposium Honoring the Contributions of R. W. Staehle,* Warrendale, PA: The Minerals, Metals, and Materials Society.

Kane R D, Ed. (2000), *Environmentally Assisted Cracking: Predictive Methods for Risk Assessment and Evaluation of Materials, Equipment, and Structures,* ASTM STP 1401, West Conshohocken, PA: ASTM International.

Kehler B A, Ilevbare G O and Scully J R (2001), 'Crevice corrosion behavior of Ni-Cr-Mo alloys: Comparison of alloys 625 and 22', *Proceedings of the CORROSION 2001 Research Topical Symposium on Localized Corrosion,* Frankel G S and Scully J R, Eds, Houston, TX: NACE International, 30–64.

Kelly R G, Frankel G S, Natishan P M and Newman R C, Eds. (1999), *Critical Factors in Localized Corrosion III*, Proceedings Vol 98-17, Pennington, NJ: The Electrochemical Society.

Kelly R G, Scully J R, Shoesmith D W and Buchheit R G (2003), *Electrochemical Techniques in Corrosion Science and Engineering*, New York: Marcel Dekker, Inc.

Labine P and Moran G C (1986), *Monitoring in Industrial Plants Using Nondestructive Testing and Electrochemical Methods*, ASTM STP 908, West Conshohocken, PA: ASTM International.

Laycock N J and Newman R C (1997), 'Localized dissolution, kinetics, salt films, and pitting potentials', *Corrosion Science*, 39, 1771–1790.

Leygraf C and Graedel T (2000), *Atmospheric Corrosion,* New York, NY: J. Wiley & Sons, Inc.

Little B J and Wagner P A (2001), 'Application of electrochemical techniques to the study of MIC', in *Modern Aspects of Electrochemistry*, Vol. 34, Chapter 5. Bockris J O, Conway B E and White R E, Eds, New York: Kluwer Academic/Plenum Publishers.

Little B J, Mansfeld F, Arps P J and Earthman J C (2003), 'Microbiologically influenced corrosion testing', in *ASM Handbook, Vol. 13A, Corrosion: Fundamentals, Testing and Protection*, Cramer S D and Covino, Jr. B S, Eds, Materials Park, OH: ASM International, 478–486.

Little B J, Wagner P A and Mansfeld F (1997), *Microbiologically Influenced Corrosion. Corrosion Testing Made Easy, Vol 5*, Houston, TX: NACE International.

Macdonald D D and Cragnolino G A (1989), 'Corrosion of steam cycle materials', in *The ASME Handbook on Water Technology for Thermal Power Systems*, Cohen P, Ed., New York: The American Society of Mechanical Engineers, 673–1033.

Macdonald, D D (1992), 'The point defect model for the passive state', *Journal of the Electrochemical Society*, 139, 3434–3449.

Magnin T (2002), 'Corrosion fatigue mechanisms in metallic materials', in *Corrosion Mechanisms in Theory and Practice, Second Edition*, *Revised and Expanded,* Marcus P, Ed., New York: Marcel Dekker, Inc., 451–478.

Marcus P, Ed. (2002), *Corrosion Mechanisms in Theory and Practice, Second Edition*, *Revised and Expanded*, New York: Marcel Dekker, Inc.

Marcus P and Mansfeld F (2005), *Analytical Methods in Corrosion Science and Engineering*, Boca Raton, FL: CRC Press Inc.

Moody R N, Thompson A W, Ricker R E and Was G S, Ed. (2003), *Hydrogen Effects on Material Behavior and Corrosion Deformation Interactions*, Warrendale, PA: The Minerals, Metals, and Materials Society.

Natishan P M, Kelly R G, Frankel G S and Newman R C, Eds. (1996), *Critical Factors in Localized Corrosion II*, Proceedings Vol. 95–15, Pennington, NJ: The Electrochemical Society.

Newman R C (2002), 'Stress-corrosion cracking mechanisms', in *Corrosion Mechanisms in Theory and Practice, Second Edition*, *Revised and Expanded*, Marcus P, Ed., New York: Marcel Dekker, Inc, 399–450.

Oriani R A, Hirth J P and Smialowski M, Eds (1985), *Hydrogen Degradation of Ferrous Alloys*, Park Ridge, NJ: Noyes Publications.

Parkins R N (1972), 'Stress corrosion spectrum', *British Corrosion Journal*, 7, 15–28.

Phull B (2003a), 'Evaluating stress-corrosion cracking', in *ASM Handbook, Vol. 13A, Corrosion: Fundamentals, Testing and Protection*, Cramer S D and Covino Jr. B S, Eds, Materials Park, OH: ASM International, 575–616.

Phull B (2003b), 'Evaluating corrosion fatigue', in *ASM Handbook, Vol. 13A, Corrosion: Fundamentals, Testing and Protection*, Cramer S D and Covino, Jr. B S, Eds, Materials Park, OH: ASM International, 625–638.

Phull B (2003c), 'Evaluating hydrogen embrittlement', in *ASM Handbook, Vol. 13A, Corrosion: Fundamentals, Testing and Protection*, Cramer S D and Covino, Jr. B S, Eds, Materials Park, OH: ASM International, 617–624.

Postlethwaite J and Nesic S (2000), 'Erosion-corrosion in single and multiphase flow', in *Uhlig's Corrosion Handbook, 2nd edition*, Revie R W, Ed., New York: J. Wiley & Sons, Inc, 249–272.

Revie R W, Ed. (2000), *Uhlig's Corrosion Handbook, 2nd edition*, New York: J. Wiley & Sons, Inc.

Roberge P (2004), *Erosion-Corrosion, Corrosion Testing Made Easy, Vol 8*, Houston, TX: NACE International.

Roberge P R and Klassen R D (2003), 'Corrosion monitoring techniques', in *ASM Handbook, Vol. 13A, Corrosion: Fundamentals, Testing and Protection*, Cramer S D and Covino Jr. B S, Eds, Materials Park, OH: ASM International, 514–518.

Sedriks A J (1990), *Stress Corrosion Test Methods, Corrosion Testing Made Easy*, Houston, TX: NACE International.

Shah S (2003), 'Application of modern analytical instruments in corrosion', in *ASM Handbook, Vol. 13A, Corrosion: Fundamentals, Testing and Protection*, Cramer S D and Covino, Jr. B S, Eds, Materials Park, OH: ASM International, 992–998.

Shipilov S A, Jones R H, Olive J M and Rebak R B, Eds (2007a), *Environment-Induced Cracking of Metals: Chemistry, Mechanics and Mechanisms*, Oxford: Elsevier Science.

Shipilov S A, Jones R H, Olive J M and Rebak R B, Eds (2007b), *Environment-Induced Cracking of Materials: Prediction, Industrial Developments and Evaluation*, Oxford: Elsevier Science.

Shreir L L, Jarman R A and Burstein G T, Eds (1994), *Corrosion, 3rd edition*, London: Butterworth/Heinemann.

Sridhar N, Dunn D S, Brossia C S and Cragnolino G A (2001), 'Stabilization and repassivation of localized corrosion', *Proceedings of the CORROSION 2001 Research Topical Symposium on Localized Corrosion*, Frankel G S and Scully J R, Eds, Houston, TX: NACE International, 1–29.

Streicher M A (2005), 'Intergranular', in *Corrosion Tests and Standards: Application and Interpretation, 2nd edition*, Baboian R, Ed., West Conshohocken, PA: ASTM International, 244–265.

Szklarska-Smialowska Z (2005), *Pitting and Crevice Corrosion*, Houston, TX: NACE International.

Thompson A W and Moody R N, Eds (1996), *Hydrogen Effects on Materials,* Warrendale, PA: The Minerals, Metals, and Materials Society.

Tuovinen O H and Cragnolino G A (1986), 'A review of microbiological and electrochemical techniques in the study of corrosion induced by sulfate-reducing bacteria', in *Corrosion Monitoring in Industrial Plants Using Non-destructive Testing and Electrochemical Methods*, ASTM STP 908, Labine P and Moran G C, Eds, West Conshohocken, PA: ASTM International, 413–432.

Turnbull A, Ed. (1995), *Hydrogen Transport and Cracking of Metals*, London: The Institute of Materials.

Van Orden A C (2205), 'Dealloying', in *Corrosion Tests and Standards: Application and Interpretation, 2nd edition*, Baboian R, Ed., West Conshohocken, PA: ASTM International, 278–288.

Videla H A (1996), *Manual of Biocorrosion*, Boca Raton, FL: CRC Press Inc.

Von Wolzogen Kuhr C A H and Van der Vlugt I S (1934), 'Graphitization of cast iron as an electro-biochemical process in anaerobic soils' (English translation), *Water* (The Hague), 18 (16), 147–165.

Wagner C (1951), 'Theoretical analysis of the current density distributions in electrolytic cells', *Journal of the Electrochemical Society*, 98, 116–128.

Wagner C and Traud W (1938), 'The interpretation of corrosion phenomena by superposition of electrochemical partial reactions and the formation of potentials of mixed electrodes' (English Translation), *Z Elektrochem*, 44, 391.

Zhang X G (2000), 'Galvanic corrosion', in *Uhlig's Corrosion Handbook, 2nd edition*, Revie R W, Ed., New York, NY: J. Wiley & Sons, Inc. 137–164.

Part I

Electrochemical techniques for corrosion monitoring

3

Electrochemical polarization techniques for corrosion monitoring

SANKARA PAPAVINASAM, CANMET Materials Technology Laboratory, Natural Resources Canada, Ottawa, Ontario, Canada

3.1 Introduction

The mechanism of corrosion taking place in aqueous phase is electrochemical. Therefore a broad range of electrochemical techniques have been developed. The main advantages of electrochemical techniques include sensitivity to low corrosion rates, short experimental duration, and well-established theoretical understanding. During electrochemical experiments specimens are polarized to accelerate the corrosion measurement process and the measurements are made within minutes or hours. Electrochemical measurements are used both in the laboratory and in the field. Commonly used electrochemical polarization techniques include polarization resistance methods, Tafel extrapolation methods, cyclic potentiodynamic methods, potentiostatic methods, galvanostatic methods, and galvanic current methods. The electrochemical polarization methods are used to monitor quantitatively general corrosion and galvanic corrosion. They can also be used qualitatively to monitor localized corrosion (pitting and crevice). In this chapter fundamental aspects, procedures to use, advantages and limitations of electrochemical techniques for monitoring corrosion are presented. Several standards are developed by various standardization organizations. Where applicable, suitable standards are referenced in this chapter.

3.2 Electrochemical nature of corrosion

Corrosion of metals and alloys in aqueous solution or in any other ionically conducting medium takes place by an electrochemical mechanism. The electrochemical corrosion reaction requires four elements (ACME) (Fig. 3.1): anode (A), cathode (C), metallic conductor (M) and electrolytic conductor (E).

At the anode metallic ions leave the metal surface and go into solution. In this process it leaves electrons behind on the metal surface. Therefore

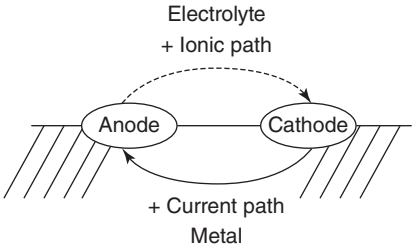

3.1 Four elements of a corrosion process.

the metal is oxidized (loss of electrons) at the anode (A). This process is corrosion. The anodic (corrosion) reaction can be written as Equation [3.1]:

$$M \rightarrow M^{n+} + ne^{-} \qquad [3.1]$$

The metallic ions, or other reactive species or ions are carried from the anode to the cathode by the ionically-conducting electrolyte (E). Electrolytes are mostly liquids, but they may also be solids. If the electrolyte has more ions then it has higher conductivity and hence it is a better electrolyte.

There are two types of ions: anions and cations. Anions are negatively charged and they move towards the anode. Cations are positively charged and they move towards the cathode. The electrolyte may contain several species that could undergo reduction. The most commonly occurring reduction reactions at the cathode are: hydrogen ion reduction (Equation [3.2]) or oxygen reduction (Equation [3.3]):

$$2H^{+} + 2e^{-} \rightarrow H_2 \qquad [3.2]$$

$$O_2 + 2H_2O + 4e^{-} \rightarrow 4OH^{-} \qquad [3.3]$$

The electrons left by the metal ions at the anode site are carried to the cathodic site by the metallic conductor (M).

In order for electrochemical corrosion to take place all four processes should occur simultaneously. Absence of any one of the four elements prevents corrosion from taking place. In the presence of all four elements a balance is established, so that the rate of anodic reaction (oxidation) is equal to that of cathodic reaction (reduction). Electrochemical polarization measurements are used to determine the rate of anodic or cathodic reactions individually or collectively.

3.3 Energy–potential–current relationship

3.3.1 Energy

When you drop a ball (or a bucket of water) it rolls to the lowest point where it ultimately settles. It does so because it seeks a state of lowest energy. This tendency is given by Gibb's free energy change (ΔG). If this energy change is negative as a result of a process or reaction then the result of the process or product of the reaction is one of lower energy than the starting material. Therefore the product is more stable and, hence, the process is energetically possible. If the free-energy change is positive then the reaction does not take place spontaneously.

3.3.2 Potential

The free energy change related to the potential is shown in Equation [3.4]

$$E = -\frac{\Delta G}{nF} \qquad [3.4]$$

where E is the potential, n is the number of electrons transferred and F is the Faraday constant.

Therefore the potential is a measure of the reaction (corrosion) tendency. Positive potential (E) corresponds to negative ΔG and hence to spontaneous reaction.

The arrangement of metals based on standard potentials is known as the Standard Oxidation-Reduction (redox) Potential or Standard Equilibrium Reduction Potential or Standard Potential or Electro-Motive Force (EMF) Series or Standard Reversible Potential. The standard potential series of metals is given in Table 3.1.[1] Standard potential is the potential of a metal in contact with its own ions at a concentration equal to unit activity. In this series the potential is presented as reduction reaction. (The same series can be developed based on oxidation reaction, in which case the values will be the same but the 'signs' will be reversed.)

The standard redox potentials can be used to understand the corrosion tendency of metals. For example, let us see what happens when copper and zinc pieces each immersed separately into their own ions (Fig. 3.2) are electrically connected (commonly called short-circuited).[2] From Table 3.1, the standard redox potential of copper is +0.337 V and that of zinc is –0.763 V, so that:

1. Copper reduction is spontaneous +0.337 V
2. Copper oxidation is non-spontaneous –0.337 V

Table 3.1 Redox potential series. Used with permission from Uhlig and Revie[1]

Electrode reaction	Standard potential $\phi°$ (in volts) at 25°C
$Au^{3+} + 3e^- = Au$	1.50
$Pt^{2+} + 2e^- = Pt$	ca. 1.2
$Pd^{2+} + 2e^- = Pd$	0.987
$Hg^{2+} + 2e^- = Hg$	0.854
$Ag^+ + e^- = Ag$	0.800
$Hg_2^{2+} + 2e^- = 2Hg$	0.789
$Cu^+ + e^- = Cu$	0.521
$Cu^{2+} + 2e^- = Cu$	0.337
$2H^+ + 2e^- = H_2$	0.000
$Pb^{2+} + 2e^- = Pb$	–0.126
$Sn^{2+} + 2e^- = Sn$	–0.136
$Mo^{3+} + 3e^- = Mo$	ca. –0.2
$Ni^{2+} + 2e^- = Ni$	–0.250
$Co^{2+} + 2e^- = Co$	–0.277
$T1^+ + e^- = T1$	–0.336
$In^{3+} + 3e^- = In$	–0.342
$Cd^{2+} + 2e^- = Cd$	–0.403
$Fe^{2+} + 2e^- = Fe$	–0.440
$Ga^{3+} + 3e^- = Ga$	–0.53
$Cr^{3+} + 3e^- = Cr$	–0.74
$Cr^{2+} + 2e^- = Cr$	–0.91
$Zn^{2+} + 2e^- = Zn$	–0.763
$Nb^{3+} + 3e^- = Nb$	ca. –1.1
$Mn^{2+} + 2e^- = Mn$	–1.18
$Zr^{4+} + 4e^- = Zr$	–1.53
$Ti^{2+} + 2e^- = Ti$	–1.63
$Al^{3+} + 3e^- = Al$	–1.66
$Hf^{4+} + 4e^- = Hf$	–1.70
$U^{3+} + 3e^- = U$	–1.80
$Be^{2+} + 2e^- = Be$	–1.85
$Mg^{2+} + 2e^- = Mg$	–2.37
$Na^+ + e^- = Na$	–2.71
$Ca^{2+} + 2e^- = Ca$	–2.87
$K^+ + e^- = K$	–2.93
$Li^+ + e^- = Li$	–3.05

3. Zinc reduction is non-spontaneous –0.763 V
4. Zinc oxidation is spontaneous +0.763 V

Therefore when an ACME setup shown in Fig. 3.2 is established, a potential of 1.1 V is created and zinc undergoes anodic oxidation (corrosion) while copper ion undergoes cathodic reduction at the copper cathode. Thus the series helps to determine the corrosion tendency of metals quickly and easily.

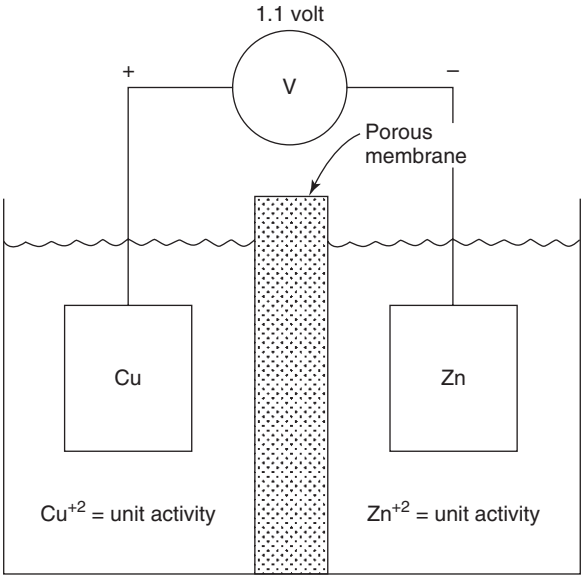

3.2 Reversible cell containing copper and zinc electrodes in equilibrium with their ions. Used with permission from Fontana and Greene.[2]

To determine the potential of a metal in which the reactants are not at unit activity, Nernst derived an equation as shown in Equation [3.5].

$$E = E_o + 2.303\frac{RT}{nF}\log\frac{a_{oxid}}{a_{red}} \qquad [3.5]$$

Where E is the potential, E_o is the standard redox potential, R is the gas constant, T is the absolute temperature, n is the number of electrons transferred, F is the Faraday constant and a_{oxid} and a_{red} are the activities (concentrations) of oxidized and reduced species. As indicated in Equation [3.5] potential becomes more and more positive as the amount of oxidized species increases. For each tenfold increase in the oxidized reactant, the half-cell potential increased by 59 mV for a single electron reaction, i.e., $n = 1$, at 25 °C.

In order for corrosion to occur no metals need to be in contact with their own ions. In practice both anode and cathode can exist on the same metal sample (Fig. 3.3), which can also act as metallic conductor (i.e., A, C, and M can exist on the metal sample). When a piece of metal is immersed into an electrolyte and all four elements (ACME) are established, a potential is developed and corrosion starts to occur. This potential is called corrosion potential or mixed potential (different from 'standard equilibrium potential').

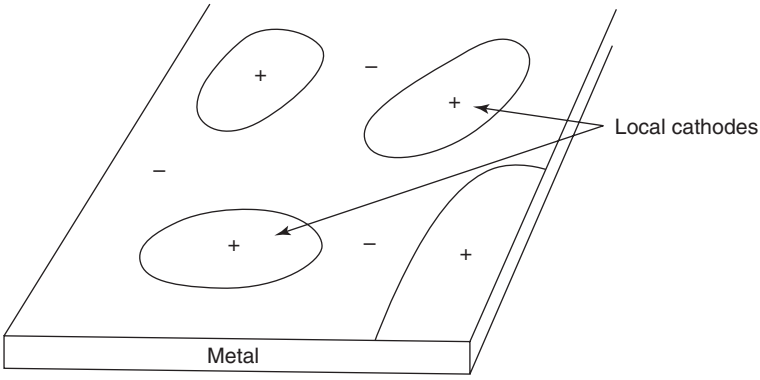

3.3 Anodes and cathodes co-exist on the same metal.

The measurement of the corrosion potential is the fundamental primary step for understanding the corrosion tendency of metals or alloys in an electrolyte. However, the potential of a single electrode cannot be directly measured; only the difference between potentials of two electrodes can be measured. For this reason the corrosion potential of an electrode is measured using another electrode called a 'reference electrode'. Therefore the corrosion potential should always be reported with respect to a particular reference electrode. Some commonly used standard reference electrodes are: the saturated calomel electrode (SCE); the silver/silver chloride (Ag/AgCl) electrode; and the copper/copper sulphate (CCS) electrode. The corrosion potential measured against one reference electrode can be converted against another reference electrode. Table 3.2 presents correction factor to convert the corrosion potential from one reference electrode to another.[3]

Metals and alloys can be arranged based on their corrosion potentials in a given environment (electrolyte). Such arrangement of metals and alloys is called a 'galvanic series'. The tendency of metals or alloys to act as an anode or cathode in a given electrolyte can be distinguished from the galvanic series. The differences between galvanic and EMF series are presented in Table 3.3.

3.3.3 Current

Potential provides an indication of the tendency of metals to corrode, but it does not provide information on the rate of corrosion reaction. The rate of corrosion is proportional to the rate of electrons transferred between the electrode and the electrolyte. The rate of electron transfer is represented as current (I). The amount of current (I) per unit surface area (A) is current density (i).

Table 3.2 Potentials of standard reference electrodes and conversion factors to convert potentials against one standard reference electrode to another. Used with permission from Treseder *et al.*[5]

Electrode	Potential (V) at 25°C		Thermal temperature coefficient[a] (mV/°C)
	E'[b]	E''[c]	
$(Pt)/H_2(\alpha = 1)/H^+(\alpha = 1)$ (SHE)	0.000	–	+0.87
Ag/AgCl/1 M KCl	+0.235	–	+0.25
Ag/AgCl/0.6 M Cl^- (seawater)	+0.25	–	–
Ag/AgCl/0.1 M Cl^-	+0.288	–	+0.22
Hg/Hg_2Cl_2/sat KCl (SCE)	+0.241	+0.244	+0.22
Hg/Hg_2Cl_2/1 M KCl	+0.280	+0.283	+0.59
Hg/Hg_2Cl_2/0.1 M KCl	+0.334	+0.336	+0.79
$Cu/CuSO_4$ sat	+0.30	–	+0.90
$Hg/Hg_2SO_4/H_2SO_4$[d]	+0.616	–	–

[a] To convert from thermal to isothermal temperature coefficients, subtract 0.87 mV/°C. Thus the isothermal temperature coefficient for Ag-AgCl is –0.62 mV/°C.
[b] E' is the standard potential for the half cell corrected for the concentration of the ions.
[c] E'' also includes the liquid junction potentials for a saturated KCl salt bridge. To convert from one scale to another, add the value indicated.
[d] Potential given is for a range of H_2SO_4 molalities as discussed in Ref (10).

From (E')	To SHE scale	To SCE scale (E')
H_2/H^+	–	–0.241
Ag/AgCl/1 M KCl	+0.235	–0.006
Ag/AgCl/0.6 M Cl (seawater)	+0.25	+0.009
Ag/AgCl/0.1 M Cl	+0.288	+0.047
$Hg/Hg_2/Cl_2$/sat KCl (SCE)	+0.241	–
Hg/Hg_2Cl_2, 1 M	+0.280	+0.039
Hg/Hg_2Cl_2, 0.1 M	+0.334	+0.093
$Cu/CuSO_4$ sat	+0.30	+0.06
$Hg/Hg_2SO_4/H_2SO_4$	+0.616	–

Example:
An electrode potential of +1.000 V versus SCE would be (1.000 + 0.241) = +1.241 V versus SHE. An electrode potential of –1.000 V versus SCE would give (–1.000 + 0.241) = –0.759 V versus SHE.

If a metal (e.g., zinc) is in equilibrium with its ions at unity it would be at the standard redox potential (as given in Table 3.1) and the redox potential of the zinc ($E_{Zn^{n+}/Zn}$) at other concentrations of its ions can be calculated from Nernst Equation [3.5]. The rate of exchange of electrons under this condition is known as exchange current density ($i_{Zn^{n+}/Zn}$).

Table 3.3 Galvanic series vs. EMF series

Galvanic series	EMF series
List of metals and alloys	List of metals ONLY
Tendency of corrosion of metals and alloys in a given environment (e.g., sea water)	Tendency of corrosion of metals in solution of its own ions at unit activity
Several galvanic series can be developed to represent corrosion tendency of metals and alloys in various environments	Only one series
Associated with 'corrosion potential'	Associated with equilibrium 'redox potential' or 'reversible potential'

Note: There has been some confusion in the corrosion literature on the use of term 'open-circuit potential'. Some references use the term 'open-circuit potential' to represent 'corrosion potential' or others to represent 'equilibrium potential'.

Similarly if we consider the hydrogen electrode in equilibrium with H^+ ions, it would be at the redox potential ($E_{H^+/H}$) and a corresponding exchange current density ($i_{H^+/H}$). What will happen if we combine these two systems?

If the zinc is immersed into a solution containing H^+ ions (e.g., hydrochloric acid), the potential of the metal will not be at the redox potential of either the zinc or the hydrogen, but the potential will stabilize at the mixed or corrosion potential (E_{corr}). At E_{corr} the rate of zinc dissolution is equal to the rate of hydrogen evolution and charge conservation is maintained. The current at E_{corr} is known as I_{corr}, which is the rate at which the zinc will corrode when it is immersed in hydrochloric acid. Fig. 3.4 explains how the system moves from reversible potentials of zinc and hydrogen towards the corrosion potential.

The relationship between potential and current is given by Equation [3.6] for activation controlled processes:

$$E - E_{corr} = \eta = \pm\beta \log \frac{I}{I_{corr}} \qquad [3.6]$$

Where E is the potential, η is commonly known as the overpotential, β is a constant known as the Tafel constant, I is the rate of oxidation or reduction in terms of current. Determination of I_{corr}, E_{corr}, and I–E relationship is the underlying fundamental principle in calculating the corrosion rate by electrochemical polarization techniques.

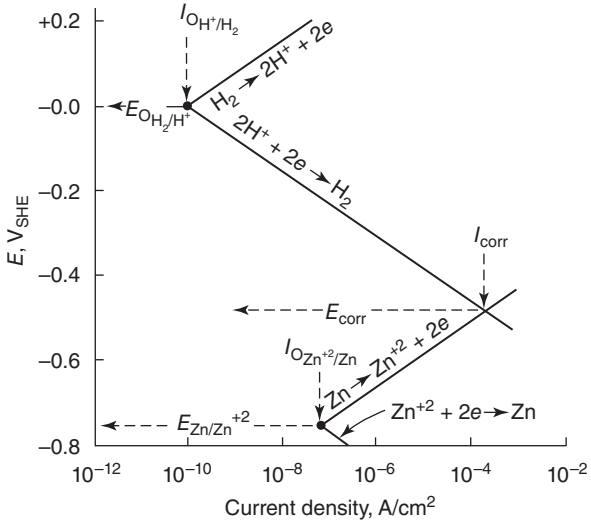

3.4 Electrode kinetic behaviour of zinc in acid solution – schematic. Used with permission from Fontana and Greene.[2]

3.4 Electrochemical polarization techniques for determining corrosion rates

There are several methods by which the *I–E* relationship is established. These involve application of an electrochemical excitation to an electrode and measure the response of the electrode to that excitation. When the excitation is given, because the electrode moves away from the corrosion potential, the electrode is said to be polarized and hence these methods are called polarization methods of determining corrosion rates.

If the potential of an electrode is controlled and the response of current is monitored then the method is called potentiostatic. If the potential of the electrode is varied at a constant rate and the response of the current is continuously monitored then the method is called potentiodynamic. On the other hand, if the current of an electrode is controlled and the response of the potential is monitored then the method is called galvanostatic. If the current of the electrode is varied at a constant rate and the response of the potential is continuously recorded then the method is called galvanodynamic.

Most electrochemical measurements are conducted by controlling the potential (potentiostatic or potentiodynamic) rather than by controlling the current (galvanostatic or galvanodynamic), because of the theoretical relationship between potential and energy. The most common electrochem-

Table 3.4 Characteristics of different electrochemical polarization techniques

Polarization method	Typical measurement	Information obtained	Type of corrosion studied	Relevant standards
Polarization resistance	Application of ± 30 mV (typically ± 10 mV) around corrosion potential	Corrosion current (I_{corr})	General corrosion	ASTM G3, ASTM G5, ASTM G59, ASTM G102
Tafel extrapolation	Application of an overpotential of +500 mV both in anodic and cathodic directions, from corrosion potential	Corrosion current (I_{corr}), and Tafel slopes (anodic and cathodic)	General corrosion	ASTM G5, ASTM G102
Cyclic potentiodynamic polarization	Application of overpotential from corrosion potential towards noble direction to a potential at which current is 5 mA, where the potential is reversed and scanned until hysteresis loop is completed or until corrosion potential is reached	Critical pitting potential, passive current, transpassive region	Pitting corrosion	ASTM G5, ASTM G61 ASTM G102

ical methods for determining general corrosion rates are polarization resistance (R_p) and Tafel extrapolation. In some studies very high values of potentials are applied and also the direction of the potential is reversed to study localized corrosion (cyclic potentiodynamic polarization). Characteristics of different electrochemical polarization techniques are presented in Table 3.4.

3.4.1 Polarization resistance method

About 50 years ago, Stern and Geary[4] found that the slope of current–potential plot around the corrosion potential is essentially linear; the slope

Table 3.4 Continued

Polarization method	Typical measurement	Information obtained	Type of corrosion studied	Relevant standards
Cyclic galvanostatic polarization	Application of current steps (typically in 20 μA/cm^2 increments between 0 to 120 μA) both in anodic and cathodic directions	Protection potential (E_{prot}) and breakpoint potential (E_b)	Pitting corrosion	ASTM G100
Potentiostatic polarization	Application of one potential step (typically to 700 mV vs SCE)	Change of current with a variable e.g., temperature (determination of critical pitting temperature)	Pitting corrosion	ASTM G150
	Application of potential step to a more positive potential (above E_b), and stepping it down to a less positive potential (below E_b)	Protection potential and breakpoint potential	Pitting corrosion	ASTM F746
Galvanic corrosion rate	Immersion of two dissimilar metals in an electrolyte and electrically connecting them using zero-resistance ammeter	Galvanic current	Galvanic corrosion	ASTM G71 and ASTM G82

of which is called polarization resistance (R_p). R_p is defined mathematically as Equation [3.7]:

$$R_p = \left(\frac{\Delta V}{\Delta I} \right)_{E_{corr}} \qquad [3.7]$$

R_p is related to corrosion current (I_{corr}) as in Equation [3.8]:

$$I_{corr} = \frac{B}{R_p} \qquad [3.8]$$

The constant B is defined in Equation [3.9]:

$$B = \frac{\beta_a \cdot \beta_c}{2.303(\beta_a + \beta_c)} \quad [3.9]$$

where β_a and β_c are anodic and cathodic Tafel constants.

By combining Equations [3.7]–[3.9], we obtain Equation [3.10]:

$$I_{corr} = \frac{1}{R_P}\left(\frac{\beta_a \cdot \beta_c}{2.303(\beta_a + \beta_c)}\right) \quad [3.10]$$

If β_a and β_c values are known the corrosion rate can be calculated from R_p.

Because only a very small perturbation potential (less than ±30 mV, typically ±10 mV) is applied, this technique does not interfere with corrosion reactions. A typical polarization resistance plot is presented in Fig. 3.5.[3] From the slope, R_p (in ohms/cm^2 if the current density is plotted or in ohms if the current is plotted) is calculated.

It should be noted that the i–E curve around corrosion potential may not be linear. Also, the curve in the anodic and cathodic regions may or may not be symmetrical. The symmetrical i–E curve is obtained only when both β_a and β_c are equal.

β_a and β_c values that are required to calculate corrosion current could either be determined by the Tafel extrapolation method (discussed in Section 3.4.2) or could be assumed. Typical values of B, β_a, and β_c are presented in Table 3.5.[5] For majority of cases the values of β fall between

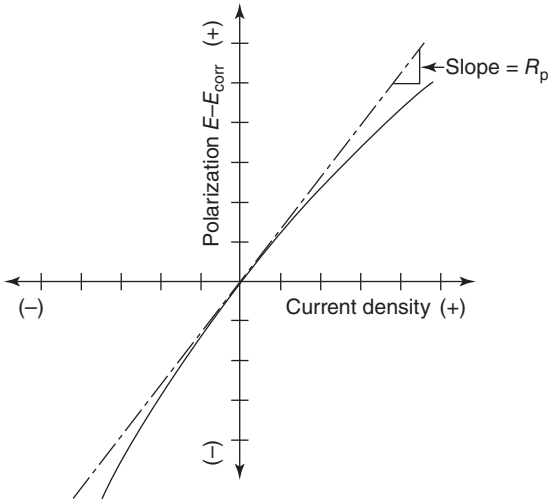

3.5 Hypothetical linear polarization resistance plot. Used with permission from ASTM G3.[3]

Table 3.5 Values of constant '*B*' for the polarization resistance method. Used with permission from Treseder *et al.*[5]

Corroding system	β_a, mV	β_c, mV	*B*, mV
Theoretical	30	30	6.5
(Values of *B* calculated from arbitrary β_a	30	60	9
and β_c values using formula on	30	120	10
previous page; β_a and β_c values can be	30	180	11
interchanged).	30	x	26
	60	60	13
	60	90	16
	60	120	17
	60	180	20
	60	x	26
	90	90	20
	90	120	22
	90	180	26
	90	x	39
	120	120	26
	90	x	39
	120	120	26
	120	x	52
	180	180	39
	180	x	78
Iron, 4% NaCl, pH 1.5	–	–	17
Iron, 0.5 N H_2SO_4, 30 °C	–	–	17
Iron, 1 N H_2SO_4	–	–	10–20
Iron, 1 N HCl	–	–	18–23
Iron, 0.02 M citric acid, pH 2.6, 35 °C	–	–	12
Carbon steel, seawater	57	x	25
Carbon steel, 1N Na_2SO_4, H_2, pH 6.3, 30 °C	–	–	19
304 L SS, 1 N H_2SO_4, O_2	Inf.	50	22
304 SS, lithiated water, 288 °C	85	160	24
304 SS, 3% NaC1, 90 °C	Inf.	50	22
430 SS 1 N H_2SO_4, H_2, 30 °C	–	–	20
600 alloy, lithiated water, 288 °C	82	160	24
Al 1199, 1 N NaC1, pH 2, 30 °C	–	–	44
Aluminium, seawater	45	600	18
Zircaloy 2, lithiated water, 288 °C	Inf.	186	81
OFHC Copper, 1 N NaC1, H_2, pH 6.2, 30 °C	–	–	26

60 and 120 mV. Therefore in many instances a value of 120 mV is assumed for both β_a and β_c. Consequently Equation [3.10] may reduce to Equation [3.11]:

$$I_{corr} = \frac{26}{R_p} \qquad [3.11]$$

The error in determining corrosion current using Equation [3.11] is presented in Fig. 3.6. In Fig. 3.6 negative error values indicate that the actual

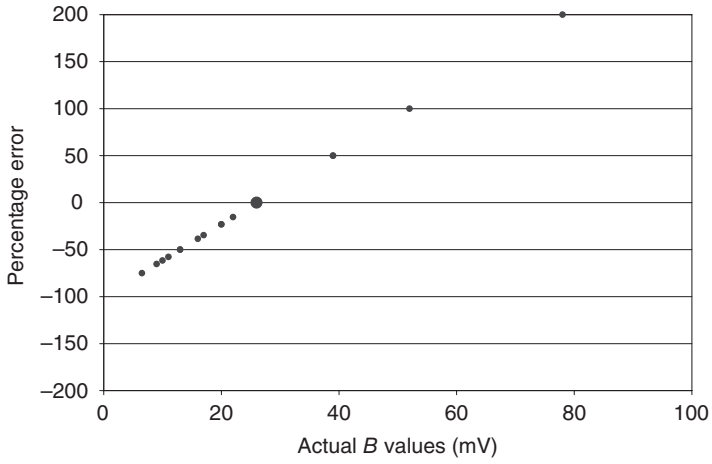

3.6 Percentage error in calculating i_{corr} assuming a *B* value of 26.

corrosion rate is *higher* than the one determined by polarization resistance method and positive error values indicate that actual corrosion rate is *lower* than the one determined by polarization method. Equation [3.11] may not be very accurate but it provides a rapid method of determining corrosion current.

R_p measurements can be obtained by the potentiodynamic method or by the step-wise potentiostatic polarization method. In both methods the corrosion potential is first measured, typically for one hour (during which time corrosion potentials of most electrodes are stabilized) or until it is stabilized. After that, a potential step, at increments of ±5 or ±10 or ±20 mV, is applied (potential-step method) or the potential is scanned at a constant rate (typically 60 mV/h) (potentiodynamic method). In both methods, the experiment is started at the negative potential, moving on to the positive potential through the corrosion potential. From the slope of the plot of the potential–current, R_p is determined.

The advantages of the polarization resistance method include:

- The corrosion current is measured rapidly, typically within a few minutes and hence this technique can be used as an online monitoring technique.
- Only very small amounts of potential are applied (less than ±30 mV, typically less than ±10 mV), hence the corrosion rate is not affected due to measurements.
- This technique can be used to measure low corrosion rates (less than 0.1 mil/yr (2.5μm/yr)).
- Measurements can be taken repeatedly.

ASTM G3[3] provides a convention for reporting and displaying electrochemical corrosion data. ASTM G5[6] provides details of instruments and materials and ASTM G59[7] describes an experimental procedure required to carry out polarization resistance measurement.

3.4.2 Tafel extrapolation method

About 100 years ago, Tafel found that a linear relationship between E and log I exists if an electrode is polarized to sufficiently large potentials, both in anodic and cathodic directions.[8] The regions in which such relationships exist are known as Tafel regions. Mathematically this relationship is given as Equation [3.12]:

$$I = I_{\text{corr}}\left[\exp\left\{\frac{2.303(E-E_{\text{corr}})}{\beta_{\text{a}}}\right\} - \exp\left\{-\frac{2.303(E-E_{\text{corr}})}{\beta_{\text{c}}}\right\}\right] \qquad [3.12]$$

Where I is the current, I_{corr} is the current at corrosion potential E_{corr}, E is the applied potential, E_{corr} is the corrosion potential, β_{a} and β_{c} are Tafel constants which are anodic and cathodic slopes of E-log I plots in the Tafel regions. Corroding metals that show Tafel behaviour when polarized will exhibit a plot similar to the one shown in Fig. 3.7.[3]

The difference between E and E_{corr} is called overpotential, η. At sufficiently larger values of η (typically between 100 and 500 mV), in the anodic direction, i.e., η_{a}, Equation [3.12] becomes Equation [3.13]:

$$\eta_{\text{a}} = \beta_{\text{a}}\log\frac{I}{I_{\text{corr}}} \qquad [3.13]$$

Similarly at sufficiently large η_{c} (in the cathodic direction), Equation [3.12] becomes Equation [3.14]:

$$\eta_{\text{c}} = -\beta_{\text{c}}\log\frac{I}{I_{\text{corr}}} \qquad [3.14]$$

In cases where Tafel regions are observed, I_{corr} can be determined by the extrapolation of either anodic or cathodic or both Tafel regions to E_{corr}, as illustrated in Fig. 3.7.

Tafel extrapolation measurements can be performed either by the potentiodynamic method or by the step-wise potentiostatic polarization method. As in R_{p} measurements, in both methods corrosion potential is first measured, typically for one hour (during which time corrosion potentials of most electrodes are stabilized) or until it stabilizes. After that, the potential step – at increments of ±25 or ±50 or ±100 mV, every 5 minutes, recording the current at the end of each 5-minute period – is applied (potential-step method) or the potential is scanned at a constant rate (typically 0.6 V/h)

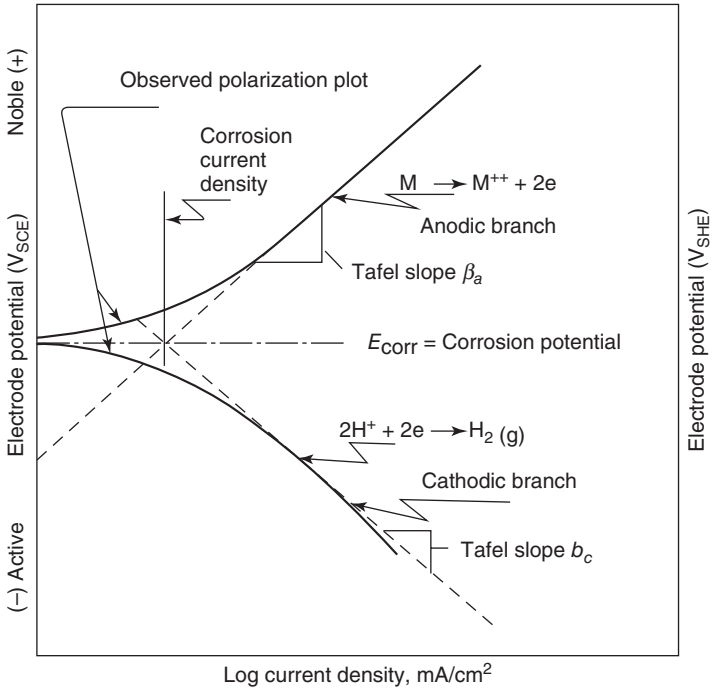

3.7 Hypothetical cathodic and anodic Tafel polarization diagram. Used with permission from ASTM G3.[3]

(potentiodynamic method). In both methods, the experiment is started at the corrosion potential and the cathodic polarization is first conducted by applying an overpotential of approximately 500 mV or until gas (e.g., hydrogen) evaluation occurs at the electrode, at a constant rate of 0.6 V/h. After that the corrosion potential is measured again (typically for an hour), and then anodic polarization is conducted by applying an overpotential so that the potential at the end of the anodic polarization is +1.6 V vs SCE. Tafel plots are generated by plotting both anodic and cathodic data in a semi-log paper as E–log I. From the plot, three values are determined: the anodic Tafel slope, the cathodic Tafel slope and I_{corr} (from back-extrapolation of both anodic and cathode curves to E_{corr}). The main advantage of this method is that it provides a simple, straightforward method to determine Tafel constants.

This method applies a large overpotential to the metal surface therefore it is considered as destructive. This is particularly true during anodic polarization during which the metal surface may be permanently changed/damaged. For this reason it is not used as a monitoring technique in the field. However, ASTM G5 provides a procedure to construct an anodic

polarization plot. It does not provide a procedure to construct a cathodic polarization plot nor a procedure to determine I_{corr} by the Tafel extrapolation method.[6]

3.4.3 Cyclic potentiodynamic polarization

The cyclic potentiodynamic polarization method is used qualitatively to understand the pitting corrosion tendency of metals and alloys. In this method the potential is scanned in the noble direction, monitoring the current continuously until it reaches 5 mA, at which point, the scan direction is reversed (i.e., scanned in the active direction), until the hysteresis loop closes or until the corrosion potential is reached. The results are plotted as E–log I, as in the Tafel extrapolation method. A plot of representative polarization curve generated by this method is shown in Fig. 3.8.

Initiation of localized corrosion is determined by the potential at which the anodic current increases rapidly. The more noble this potential, the less susceptible is the alloy to initiation of localized corrosion. In general, once initiated, localized corrosion can propagate at some potential more electropositive than that at which the hysteresis loop is completed. The potential at which the hysteresis loop is completed is determined at a fixed scan rate. The more electropositive the potential at which the

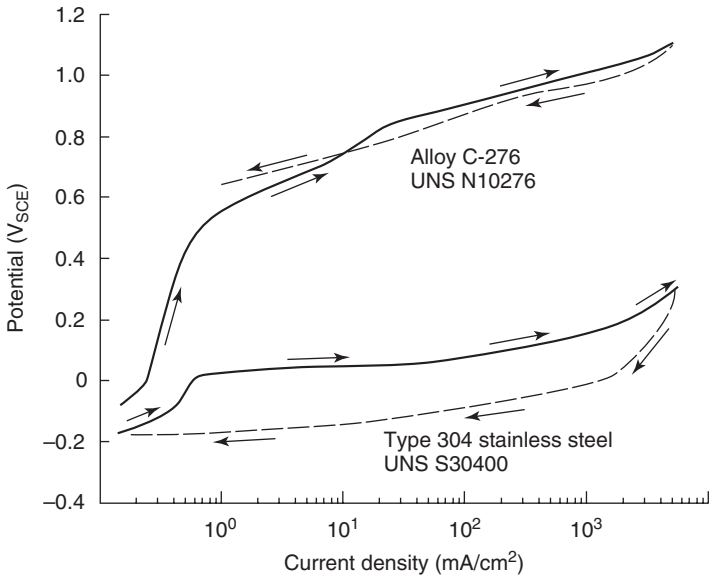

3.8 Representative cyclic potentiodynamic polarization curves. Used with permission from ASTM G61.[9]

hysteresis loop is completed the less likely it is that localized corrosion will occur.

The polarization curves shown in Fig. 3.8 indicate that initiation and propagation of localized corrosion occurs at potentials more electronegative than the oxygen evolution potential on sample S30400. The curve for sample N10276 does not show any hyteresis indicating localized corrosion does not occur on this sample, but uniform corrosion in the transpassive or oxygen evolution region may occur. Assuming that the corrosion potentials of both metals are similar, these curves indicate that sample N10276 is more resistant to initiation and propagation of localized corrosion than sample S30400.

Some other parameters that can be determined from the potentiodynamic polarization curves (Fig. 3.9) are the primary passivation potential (E_{pp}, potential positive to which passive surface layers are formed), the critical current density (I_{cc}, minimum current required before surface layers are formed), the breakdown potential (E_b, potential positive to which passive surface layer is destroyed and transpassive region starts), the protection potential (E_{prot}, potential at which passive layers are stable and protective), passive current (I_p, current of the electrode in E_{prot}) and the area of the hysteresis loop. Many of these parameters determined are based on empirical observations. As with any empirical method, it is beset with many questions about the extent of its validity. The results obtained by this

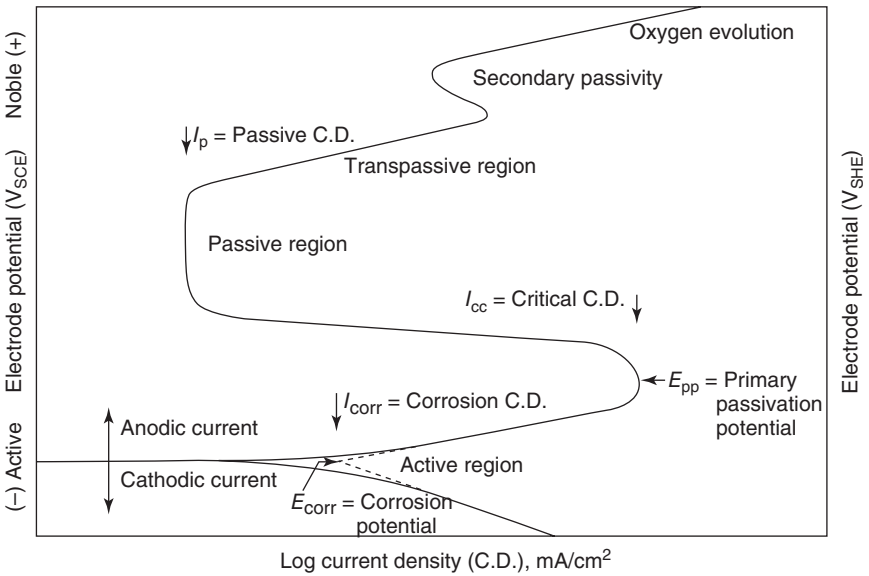

3.9 Hypothetical cathodic and anodic polarization plot for determining localized corrosion parameters. Used with permission from ASTM G3.[3]

method can be function of scan rate, pit size or depth, polarization curve shape and specimen geometry. Therefore the results should be considered as qualitative rather than quantitative.

ASTM G61 provides a procedure for conducting cyclic potentiodynamic polarization measurements.[9]

3.4.4 Cyclic galvano-staircase polarization

Susceptibility to localized corrosion of metals is indicated by a protection potential (E_{prot}), which can be determined by cyclic galvano-staircase polarization (CGSP). The more noble the E_{prot} is, the less susceptible is the metal or alloy to initiation of localized corrosion. When the applied potential is more negative than E_{prot}, no pits are initiated and when the applied potential is more positive than E_{prot} pits are initiated even when the applied potential is less than E_b.

In this method a current staircase signal from 0 to 120 μA/cm^2 is applied using a step height of 20 μA/cm^2 and step duration of 2 min and then the current-step is reversed and stepped back to 0-current, at the same step-increments (i.e., 20 μA/cm^2) (Fig. 3.10). The current staircase may be generated manually, but use of a computer controlled commercial potentiostat increases accuracy. The potential transients are recorded at every current-step. The step-up points are extrapolated to zero current to obtain E_b. Similarly the step-down points are extrapolated to zero current to obtain E_{prot}.

The advantage of the method is that it provides a quick way to determine susceptibility to initiation of pit initiation. However this technique does not provide information on pit propagation. The technique can only be used as qualitative technique. Because sensitive instrumentation is required to conduct the experiment, it cannot be routinely used for all alloys.

A procedure for conducting CGSP to determine susceptibility to localized corrosion is provided in ASTM G100.[10] This test method also describes a procedure that can be used to check for one's experimental technique and instrumentation. In the round robin experiment conducted (to develop ASTM G100) using aluminium alloy 303-H14 (UNS A93003), it was found that E_b (–636 mV vs SCE) is more electropositive than E_{prot} (–652 mV vs SCE).

3.4.5 Potentiostatic polarization

There are several ways in which potentiostatic polarization experiments are conducted. In one method only one potential step is applied and the variation of current is monitored. For instance, in a procedure to evaluate resistance of stainless steel and related alloys to pitting corrosion, the potential

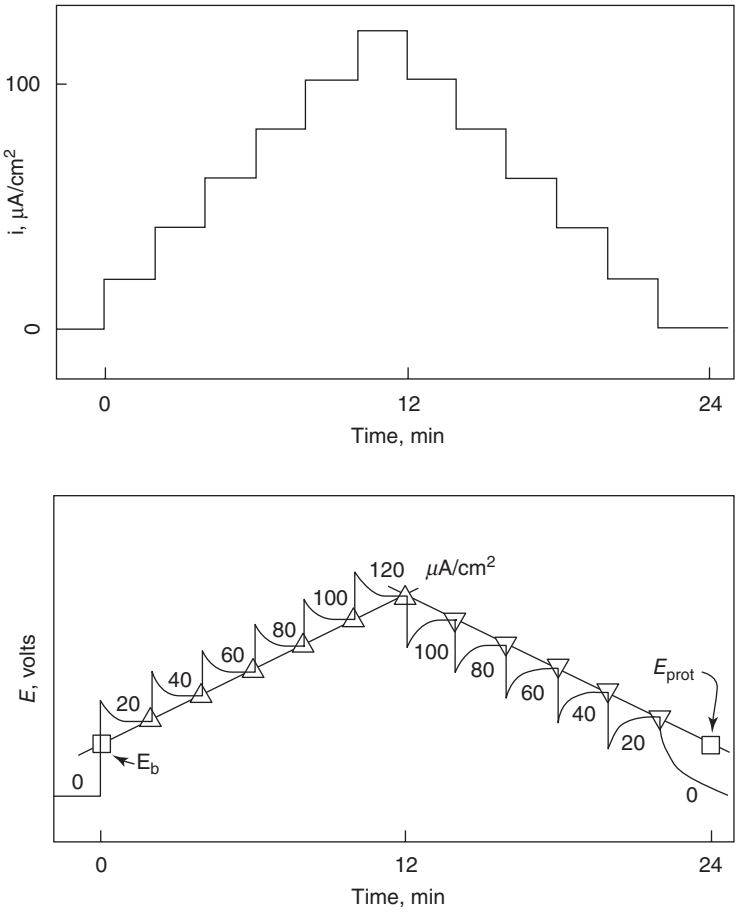

3.10 Relationship of a schematic CGSP curve (lower) to the current staircase signal (upper). Used with permission from ASTM G100.[10]

is stepped and held constant at 700 mV (or other suitable potential) and the variation of current is monitored as a function of other changes (e.g., temperature variation). ASTM G150 covers a procedure for the evaluation of the resistance of stainless steel and related alloys to pitting corrosion, using this method to determine critical pitting temperature.[11]

In another procedure the potential is first stepped to a higher value and the current is monitored (this potential is set at a high enough value to induce and grow stable pits). The potential is then stepped down and the current monitoring continued. In this method, in order to induce pits, the initial potential should be stepped more electropositively than E_b so that the second potential applied is above E_{prot}, and pit propagation is

sustained. For this reason the technique cannot be used independently without results from other techniques and prior knowledge of the alloy and metal behaviour. ASTM F746 provides a test procedure for this type of measurement.[12]

3.4.6 Galvanic corrosion rate

When two dissimilar metals in electrical contact are exposed to a common electrolyte, one of the metals can undergo increased corrosion while the other can undergo decreased corrosion. This type of corrosion is known as galvanic corrosion.

A simple method of determining the galvanic corrosion rate involves immersing two dissimilar metals in an electrolyte and electrically connecting the materials together using a zero-ammeter to measure the resulting current as a function of time. ASTM G71 provides a guide for conducting and evaluating galvanic corrosion tests both in the laboratory as well as in the field.[13] ASTM G82 covers the development of a galvanic series and its subsequent use as a method of predicting the effect that one metal can have upon another metal when they are in electrical contact while immersed in an electrolyte.[14]

3.5 Conversion of I_{corr} into the corrosion rate

Corrosion current values obtained from galvanic current measurement, polarization resistance and Tafel extrapolation methods should be converted into the corrosion rate. For this reason it should be assumed that the current distribution is uniform across the area used in the calculation. With this assumption the current value is divided by the surface area as shown in Equation [3.15]:

$$i_{corr} = \frac{I_{corr}}{A} \qquad [3.15]$$

where i_{corr} is the current density (μA/cm^2), I_{corr} is the current (μA), and A is the exposed specimen area, cm^2. Other commonly used units for current are mA and A. Based on Faraday's law the corrosion rate (CR) Equation [3.16] or mass loss rate (MR) Equation [3.17] can be calculated as:

$$CR = K_1 \left(\frac{\rho_{corr}}{\rho} \right) EW \qquad [3.16]$$

$$MR = K_2 \cdot i_{corr} \cdot EW \qquad [3.17]$$

where CR is given in mm/y, i_{corr} in μA/cm^2, K_1 is 3.27 × 10^{-3} and has units of mm g/μA cm y, ρ is the density g/cm^3. MR is given in g/m^2, K_2

Table 3.6 Constants to convert corrosion current into penetration rate and mass loss rate. Used with permission from ASTM G102[15]

A				
Penetration rate unit (CR)	I_{corr} unit	ρ unit	K_t	Units of K_1[a]
mpy	μA/cm^2	g/cm^3	0.1288	mpy g/μA cm
mm/yr[b]	A/m^{2b}	kg/m^{3b}	327.2	mm kg/A m y
mm/yr[b]	μA/cm^2	g/cm^3	3.27×10^{-3}	mm g/μA cm y

B			
Mass loss rate unit	I_{corr} unit	K_2	Units of K_2[a]
g/m^{2}d[b]	A/m^{2b}	0.8953	g/Ad
mg/dm^{2}d (mdd)	μA/cm^2	0.0895	mg cm^2/μA dm^2 d
mg/dm^{2}d (mdd)	A/m^{2b}	8.953×10^{-3}	mg m^2/A dm^2 d

[a] EW is assumed to be dimensionless.
[b] SI unit.

is 8.954×10^{-3} g cm^2/μA m^2 d and EW is the equivalent weight. Other values for K_1 are given in Table 3.6.[15]

Equivalent weight EW is the mass in grams that will be oxidized by the passage of one Faraday (96 489 C (amp-sec)) of electric charge. For pure elements EW is given as Equation [3.18]:

$$\mathrm{EW} = \frac{W}{n} \qquad [3.18]$$

Where W is the atomic weight of the element and n is the number of electrons required to oxidize an atom of the element in the corrosion process, i.e., the valence of the element. To calculate EW of alloy the following formula is used:

$$\mathrm{EW} = \frac{1}{\sum \frac{n_i f_i}{w_i}} \qquad [3.19]$$

Where n_i is the valence of the ith element of the alloy; w_i is the atomic weight of the ith element of the alloy, and f_i is the mass fraction of the ith element of the alloy.

Calculation of EW of alloys may create two problems:

- It is assumed that the process of oxidation (corrosion) is uniform and does not occur selectively for any component of the alloy. If this is not true then the calculation should be adjusted.

- Valance assignments for elements that exhibit multiple valences can create uncertainty. It is best if an independent technique is used to establish the proper valence for each alloying element.

ASTM G102 provides details of calculating corrosion rate from corrosion current determined by polarization techniques.[15]

3.6 Measurement of corrosion rate by polarization methods in the laboratory

Measuring the corrosion rate in the laboratory requires two basic components: a laboratory methodology, to simulate corrosive conditions and a monitoring technique to measure the corrosion rate simulated by the laboratory methodologies. The monitoring techniques by themselves do not (and more importantly should not) alter the corrosion rate. One of the greatest advantages of using electrochemical polarization experiments is that they provide quick, easy and relatively straightforward results in a short period of time.[18–30]

Various laboratory methodologies in which electrochemical polarization techniques are used as monitoring technique are listed in Table 3.7.[18,30] The list of laboratory methodologies in Table 3.7 is not extensive, but is

Table 3.7 Laboratory methodologies in which electrochemical polarization method is used as the monitoring technique

Laboratory methodology	Variables simulated in the laboratory methodologies	Relevant standards
Electrochemical polarization cell (Fig. 3.11).	Composition (of material and environment) and temperature	ASTM G5
Kettle or bubble test	Composition (of material and environment) and temperature	NACE 1D196[16]
Rotating disk electrode (RDE)	Composition (of material and environment), temperature, and velocity	NACE 5A195[17]
Rotating cylinder electrode (RCE)	Composition (of material and environment), temperature, and velocity	NACE 5A195,[17] ASTM G170, ASTM G185
Jet impingement (JI)	Composition (of material and environment), temperature, and velocity	NACE 5A195,[17] ASTM G170
High-pressure versions of RDE, RCE and JI	Composition (of material and environment), temperature, pressure and velocity	ASTM G170, ASTM G184, ASTM G185

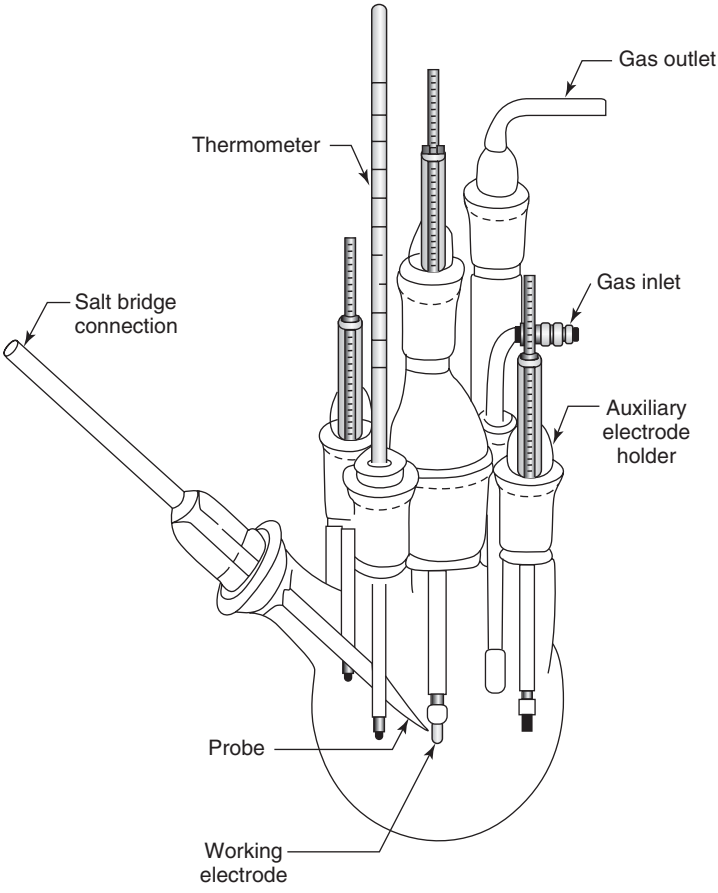

3.11 Schematic diagram of a laboratory experimental setup in which an electrochemical polarization method is used as the monitoring technique. Used with permission from ASTM G5.[6]

provided only for illustration. A basic laboratory methodology in which the electrochemical polarization technique is used as monitoring technique is given in Fig. 3.11.[6] In addition to accessories required to build the laboratory methodology, other accessories to perform electrochemical polarization techniques include: working electrode (metal whose corrosion rate to be determined), counter electrode, reference electrode, conducting electrolyte (i.e., environment), potentiostat, potential-measuring instrument, current-measuring instrument and Luggin capillary with salt bridge connection to reference electrode. Before proceeding to understand these components we should understand why we need three different electrodes to conduct electrochemical polarization measurement.

Recollect that potential of a single electrode cannot be measured; only the difference between two electrodes can be measured. Therefore we need at least two electrodes to conduct electrochemical polarization measurement. During polarization measurement a potential or current is impressed on these electrodes, and as a consequence the potentials of both the electrodes move from their respective corrosion potentials. The potential difference measured between these two electrodes (working electrode and reference electrode) then includes the value of the two overpotentials. But we are interested in the polarization of only one electrode (working electrode). To resolve this issue another electrode, auxiliary or counter electrode is used. During electrochemical measurements, this counter electrode gets polarized in the opposite direction to the working electrode, i.e., if the working electrode is polarized in the noble direction, the counter electrode is polarized in the active direction. A standard reference electrode (Table 4.1) is connected to the working electrode through a high-impedance voltmeter. This arrangement prevents any current passing through the reference electrode. Therefore the reference electrode is not polarized.

3.6.1 Working electrode

This is the primary electrode whose corrosion rate is being measured. Care should be taken that this electrode is properly prepared and mounted (without any crevice). A simple method in which the working electrode is mounted is shown in Fig. 3.12. A leak-proof assembly is obtained by the proper compression fit between the electrode and an insulator gasket.

3.6.2 Counter electrode

Auxiliary or counter electrode is usually made up of inert materials, e.g., platinum or graphite. Generally two auxiliary electrodes or one large sheet of one auxiliary electrode is used. The auxiliary electrode is mounted in the same way as that of the working electrode.

3.6.3 Reference electrode

Reference electrodes should have stable and reproducible potential. Reference electrodes used are preferably reversible type electrodes. In a reversible electrode a small cathodic current produces the reduction reaction, while a small anodic current produces the oxidation reaction. Several commonly used reference electrodes and their reversible potential relationships are provided in Table 3.2. An SCE reference electrode with a controlled rate of leakage (about 3 μL/h) is recommended by ASTM G5 standard. This type of electrode is durable, reliable and commercially available. The

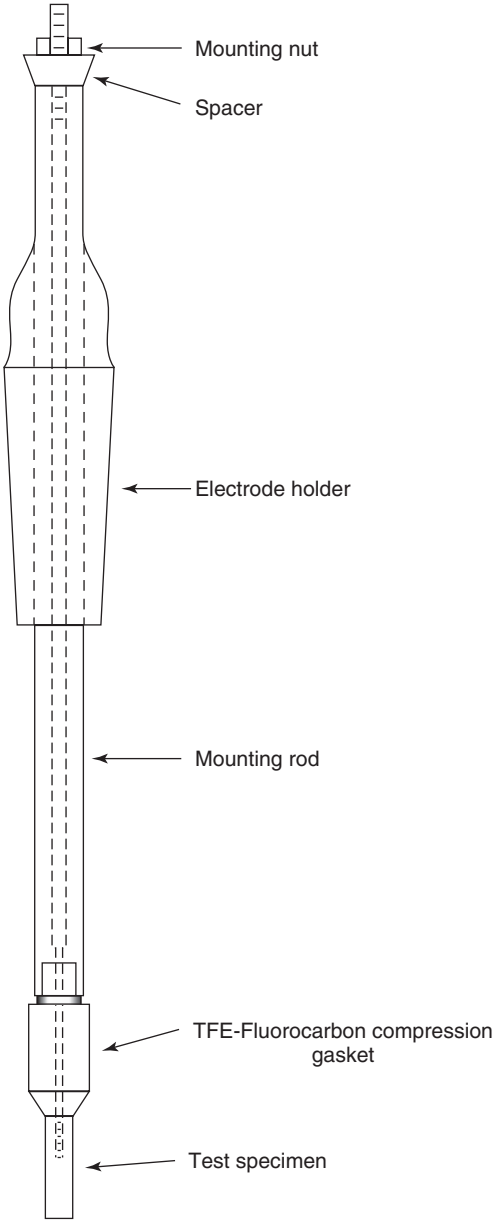

3.12 Schematic diagram of an electrochemical specimen mounted on a holder. Used with permission from ASTM G5.[6]

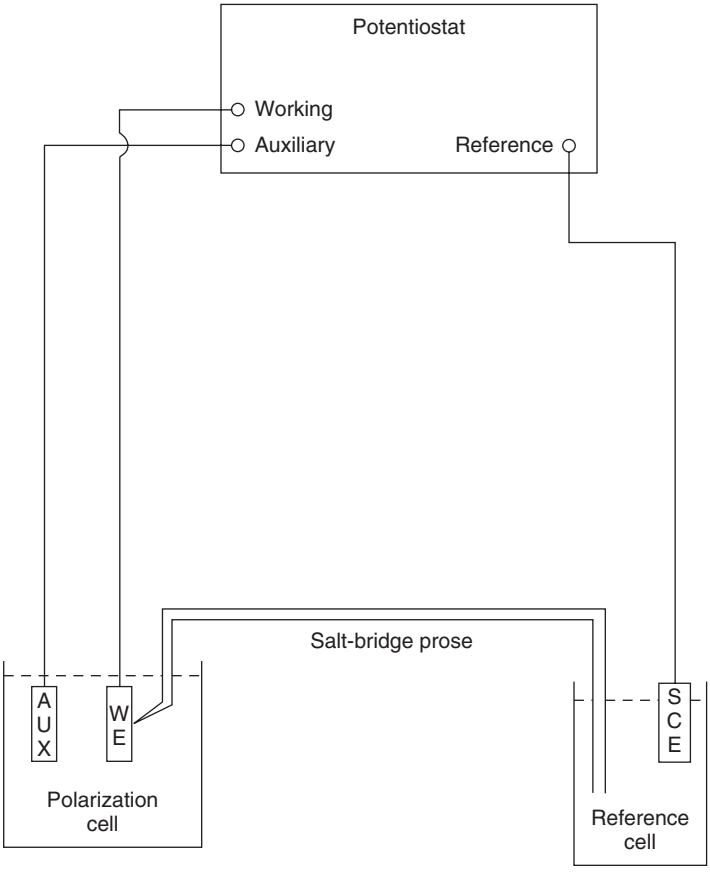

3.13 Schematic diagram of a setup to connect a reference electrode to an electrochemical cell through a salt-bridge.

potential of reference electrode should be checked at periodic intervals to ensure the accuracy of the reference electrode.

Sometimes the reference electrode is placed in a separate vessel and is connected to the working electrode through the Luggin capillary with a salt bridge. This arrangement minimizes contamination of the reference electrode from the products of corrosion reactions (Fig. 3.13). This arrangement requires special care and precaution.

3.6.4 Electrolyte

The basic requirement of any electrochemical measurement is a reasonably conducting (low-resistivity) electrolyte. Electrolytes with low-conductivity

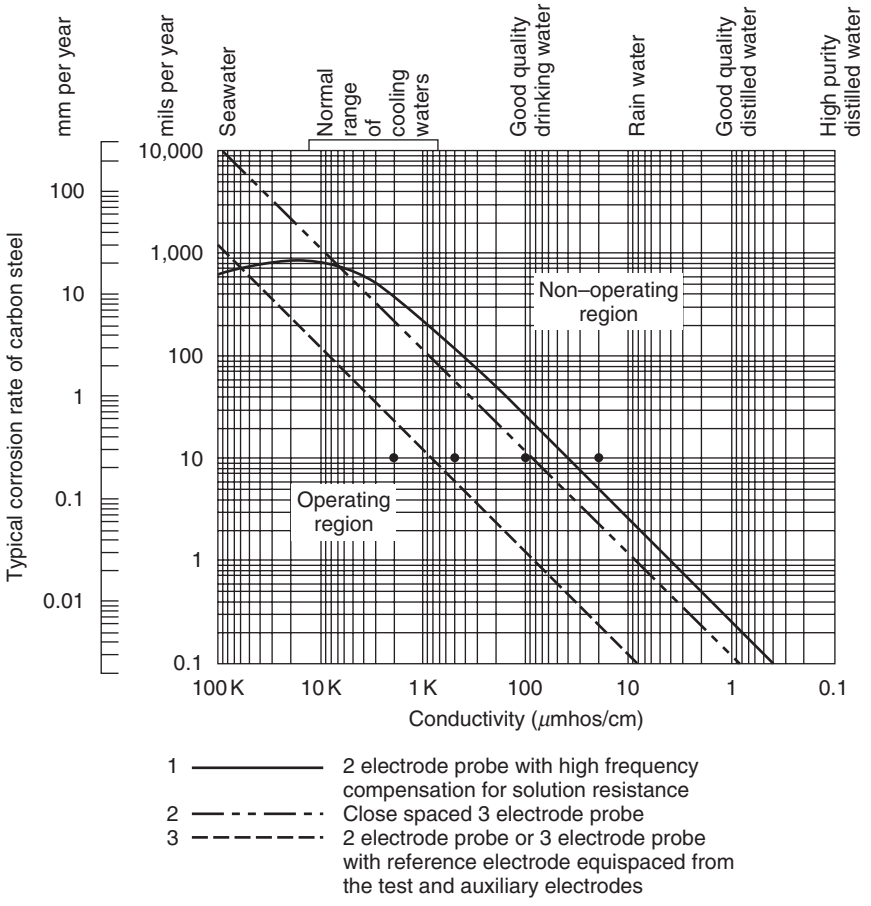

3.14 Guidelines on the operating range for polarization resistance. Used with permission from ASTM G96.

produce erroneously low corrosion rate, because their resistance (solution resistance, R_s) is added to the polarization resistance (R_p) during measurement. If in doubt the resistivity or conductivity of the electrolyte should be determined. ASTM D1125 describes test methods for electrical conductivity and resistivity of water.[19] Guidelines on the operating range of solution conductivity in which the electrochemical polarization (R_p) method can be conducted is provided in Fig. 3.14.

3.6.5 Potentiostat

This is the instrument that maintains the potential of the working electrode. Most of the corrosion reactions occur between –2 to +2 V potential

range and between 1 to 10^6 μA current range. Therefore the instrument should have a sufficient range of potential and current to supply them on a standard electrode type and shape. Modern computer-controlled potentiostats, with user-friendly software, have multiple functions, including applying potential, monitoring current, storing data, analysing data and producing trend.

3.7 Measurement of corrosion rate by polarization methods in the field

Because polarization resistance method has the advantage of providing corrosion rate measurement within minutes and it does not affect the ongoing corrosion rates, this method is the most widely used in the field. All other polarization methods are invariably used only in the laboratory.

When compared with conducting polarization measurements in the laboratory, using polarization resistance method in the field requires several changes. Table 3.8 compares the main differences.

Several configurations of probes are used. Modern methods of introducing and retrieving probes under pressure and temperature are available. Some commonly used probe designs are presented in Figs. 3.15 and 3.16.[20–23] It is necessary to place the probes in the most corrosive spot in the system. For instance, referring to Fig. 3.16, measurements using probes 5 and 6 are not relevant, as they may be in the oil or gas phase. Placing the probes in those locations is relatively easy from the operational standpoint, but the results obtained from those probes are irrelevant or erroneous. Recording R_p measurements using probes 1 and 2 is most relevant because the probes

Table 3.8 Main differences in using polarization resistance method in the laboratory and in the field

R_p parameter	Laboratory	Field
Auxiliary electrode	Platinum or graphite – two electrodes	Normally made of the same material as that of working electrode
Reference electrode	Standard reference electrode (reversible). See Table 3.1	Normally made of the same material as that of working electrode
Tafel constants	Determined by Tafel extrapolation method	Normally assumed
Luggin capillary	Used	Not used
Corrosion potential	Measured and reported against standard reference electrode	Only stable values are noted.

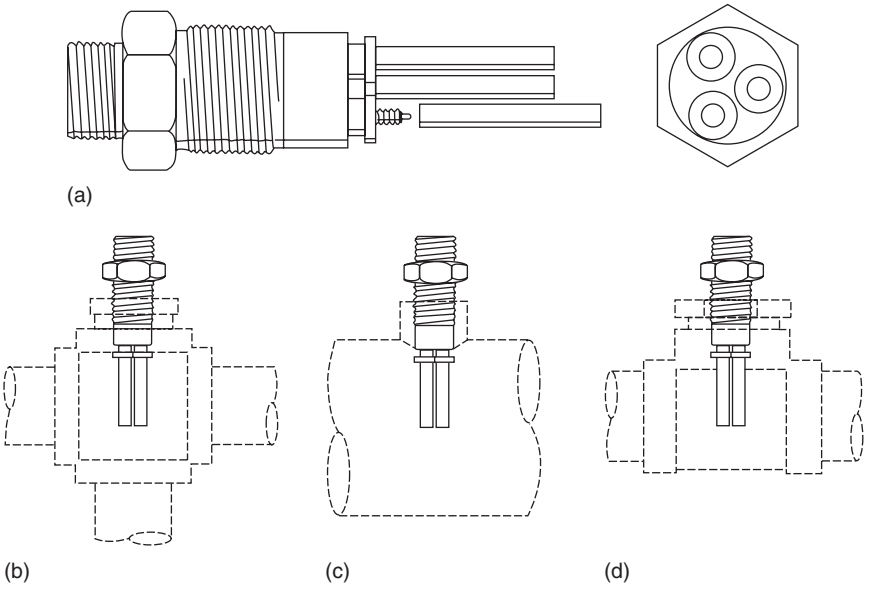

3.15 Schematic diagram of a typical three-electrode polarization resistance probe (a) for determining the corrosion rate in the field and installation of such a probe in pipe fitting (b), in weld line (c), and in pipe tee (d). Used with permission from *ASTM Handbook*.[20]

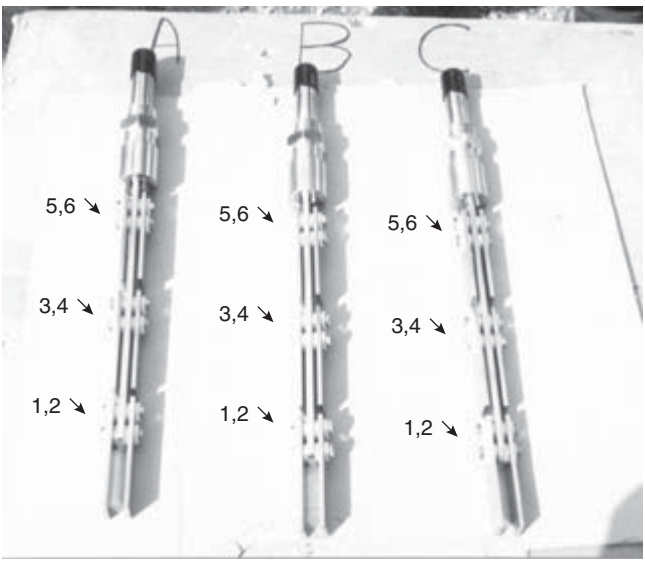

3.16 Photo of a 3-tree holder to mount a 6-coupon assembly in an operating field. Note: the numbers shown in the figure are the coupon identification numbers.

are in the brine solution (high conductivity). When probes 3 and 4 are used, one should make sure that they are indeed in the conducting brine phase during the entire time that the R_p measurements are conducted.

One other precaution that should be considered in using the probes in the field is the ability to directly make electrical connections from the probes to the measuring instrument. These connections must be insulated; sometimes installation of such a system may be costly.

3.8 General limitations of polarization methods of determining the corrosion rate

As with any other techniques electrochemical polarization techniques also have advantages and disadvantages. In this section the shortcomings of electrochemical techniques, methods to overcome the shortcomings and caution that should be exercised when the shortcomings are unable to be addressed, are discussed.[24–26]

3.8.1 Solution resistance

The data obtained during electrochemical measurements should be directly relevant to corrosion. In all electrochemical polarization methods, either the current is applied and potential monitored or the potential applied and the current monitored. From these measurements polarization of the electrode to the signal is determined (e.g., polarization resistance and Tafel slopes). In all the calculations the resultant resistance (R) is assumed to be related to corrosion. However the measured R is made up of two components: R_s and R_p. It is assumed that the R_s, i.e. the solution resistance, is low (highly conducting solution), so that the measured $R \sim R_p$. If the R_s value is appreciable that the measured corrosion rate will be underestimated (because R_p is inversely proportional to corrosion rate, higher values of R_s exhibit a higher value of R). The error due to R_s in the R_p measurement is normally significant in systems with high corrosion rates and low conductivity.

3.8.2 Scan rate

The electrode (i.e., corroding element) can be considered as a capacitor. A capacitor is an electrical device that can store energy in the electric field. When voltage or potential is applied to the capacitor, it builds up an electric charge. The amount of charge stored in a capacitor is measured in terms of capacitance. When a potential is applied at a higher rate, the electrode's charge build-up is higher. Thus the measured current will have a higher

component of capacitance current rather than a current resulting from the corrosion process. The current associated with the corrosion process is known as the Faraday current. The relationship between the measured current, capacitance current and the Faraday current (i.e., corrosion current) is given in Equation 3.20:

$$I_{\text{total}} = I_{\text{F}} + C\frac{\mathrm{d}V}{\mathrm{d}t} \qquad [3.20]$$

Where I_{total} is the total current measured, I_{F} is the Faradaic current associated with corrosion rate, C is the electrode capacitance, $\mathrm{d}V/\mathrm{d}t$ is the scan rate (i.e., rate of change of potential as a function of time). From Equation [3.20], the error due to capacitance increases as the scan rate increases. As a result of this error the corrosion rate is overestimated. To minimize the error due to capacitance current, polarization experiments are conducted at lower scan-rate (typically 0.6 V/h).

3.8.3 Electrode-bridging

This error occurs mostly in the field-monitoring probes when the products of corrosion reactions electrically connect the electrodes. This usually happens when the conductivity of the corrosion products are higher (e.g., FeS). As a result, component 'E' of the ACME is lost. This system behaves as an electric circuit rather than as an electrochemical corrosion system. When this problem is suspected the distances between the electrodes should be increased (see Fig. 3.16).

3.8.4 Presence of oxidation-reduction species

As a result of electrochemical excitation (either potential or current), if electrochemically active species are present in the electrolyte they prefer to undergo a reaction rather than a corrosion reaction. Under this condition measurement of corrosion rates from electrochemical techniques has no meaning.

3.8.5 Variation of corrosion potential

If the corrosion potential varies during electrochemical measurements, the results obtained are not meaningful. Therefore before conducting any electrochemical measurement, the corrosion potential of the system should be monitored for a sufficiently longer duration to establish that it is stable. If the corrosion potential does not stabilize then electrochemical techniques may not be used.

3.8.6 Diffusion-controlled condition

In order to use electrochemical techniques for measuring corrosion, the reaction should be charge-controlled, i.e., the rate of the reaction is proportional to the rate at which electron transfer occurs at the electrode–electrolyte interface. If the charge-transfer rate is high, a situation is developed – usually near the cathode – when the reduction species is quickly depleted. At this stage the reaction rate is controlled by the rate of diffusion of species on to the cathode, i.e., diffusion-controlled corrosion, under which conditions the results from polarization methods are not accurate.

3.8.7 General corrosion only

Most electrochemical polarization parameters measured are related to the general corrosion rate only. Initiation and propagation of localized corrosion complicates the response of polarization measurements. Localized corrosion alters the chemistry of the solution locally. It also alters the electrode geometry and the surface area – all of which results in a change in polarization response which is difficult to quantify. Qualitatively these effects are determined to some extent by cyclic potentiodynamic polarization (section 3.4.3) or by CGSP (section 3.4.4) methods.

3.9 Applications of polarization methods in the field

The polarization resistance method is the only electrochemical technique widely used as an online monitoring technique in the field. This method has been used in various fields for online monitoring including the oil and gas field (for determining the corrosion inhibitor), pipelines (for determining the effect of cathodic protection), chemical processing plants (for monitoring process changes), aircraft (for monitoring crevice corrosion and pipes), pulp and paper (for monitoring liquor composition effect on corrosion), and water handling systems (for identifying corrosion upsets).

The electrochemical polarization technique is used in many standard tests. For example in cathodic disbondment tests, to understand the compatibility between protective polymeric coatings and cathodic protection, the electrode sample is polarized, typically to –1.5 V vs SCE, and the resultant current is monitored.[30]

3.10 Future trends

Computers and computer-based information systems have revolutionized many fields. The growth of computer software and hardware technologies,

communication technologies, and the Internet have been phenomena for over a decade. Electrochemical techniques have also benefited from the application of computer-based systems and tools promoting automatic data collection, analysis and problem solving. Currently almost all electrochemical monitoring instruments are computer controlled. Graphical user-friendly interfaces (GUI) and software packages enable electrochemical measurements to be made easily and quickly as well as instantaneous analysis of results. Many constants, e.g., Tafel slope, equivalent weight of metals, surface area and conversions of corrosion current density to corrosion rate, can now be selected by the click of a button from a preloaded database. These advances currently make it possible to conduct electrochemical polarization methods repeatedly and continuously. As a result there are now systems available to conduct online, real-time measurements.

In the future, the electrochemical polarization probes will increasingly be used as online sensors in the field, in addition to their traditional rule as laboratory monitoring tools. The advancements in information technology and web-based knowledge sharing will make the amount of data collected using one sensor phenomena. The data collected will be integrated in the decision-making process online. It is anticipated that the decision-making centres will in future be used to perform four functions:

1. Interpret the data based on the signal provided from electrochemical polarization sensors.
2. Predict future behaviour of the system in question.
3. Trigger an action (the action triggered may include taking corrosion control measurement, e.g., addition of a corrosion inhibitor if the corrosion rate is high or adjusting the operating parameter, e.g., varying temperature, pressure, or shutting down the system where necessary).
4. Store the data in a suitable form and place for future reference.

Thus electrochemical sensors will function as the front-end of an intelligent system to monitor, model, mitigate, maintain and manage corrosion online and in real time. In the future the sensors will thus play a key rule in the Supervisory Control And Data Acquisition (SCADA) systems.

All automotive and fast systems have shortcomings. Caution should be exercised in using electrochemical polarization techniques; their advantages and limitations should be understood before they are used as sensors. When using the techniques it will serve best to the corrosion professionals to use at least two or more independent measurement techniques, preferably one electrochemical and one non-electrochemical, so that the limitations of one technique are compensated by the other.

3.11 Further information

The purpose of this chapter is to provide an overview of the types of electrochemical polarization techniques that might be used to understand corrosion. The discussions provided are not exhaustive. They are meant to provide a flavour of types of techniques available, how to use them, and what information can be obtained.

Several advances have been made in the field of monitoring and new standards are developed every day. Most of the advances are published in corrosion journals (including those published by NACE *Corrosion Journal*, NACE *Materials Performance*, *The Journal of the Electrochemical Society*, *British Corrosion Journal*, and *Corrosion Science*), symposia (including those organized by ASTM, NACE, European Federation of Corrosion (EFC), books (including those published by ASTM, ASM, NACE and EFC), and standards (including those developed by ASTM G01 committee and NACE STG 62 committees).

3.12 References

1 H.H. Uhlig and R.W. Revie, *Corrosion and Corrosion Control*, An introduction to Corrosion Science and Engineering, 3rd Edition, John Wiley and Sons, Hoboken, NJ, 1985, p. 28. Table 2 Electromotive Force Series, used with permission.

2 M.G. Fontana and N.D. Greene, *Corrosion Engineering*, McGraw-Hill Series in Materials Science and Engineering, 2nd Edition, McGraw-Hill Book Company, Columbus, OH, 1967, p. 299. Figs 9.3 and 9.17 used with permission.

3 ASTM G3, 'Standard Practice for Conventions Applicable to Electrochemical Measurements in Corrosion Testing', *Annual Book of ASTM Standards*, Vol. 03.02, ASTM, West Conshohocken, PA. Figs 2, 3 and 4 used with permission.

4 M. Stern and A.L. Geary, 'Electrochemical Polarization', *Journal of the Electrochemical Society*, 104 (1957), p. 56.

5 NACE *Corrosion Engineer's Reference Book*, Eds, R.S. Treseder, R. Baboian and C.G. Munger, p. 66, NACE International, Houston, TX. Table (Values of the constant B for the polarization resistance method) uesd with permission.

6 ASTM G5, 'Standard Reference Test Method for Making Potentiostatic and Potentiodynamic Anodic Polarization Measurements', *Annual Book of ASTM Standards*, Vol. 03.02, ASTM, West Conshohocken, PA. Figs 3 and 5 used with permission.

7 ASTM G59, 'Standard Test Method for Conducting Potentiodynamic Polarization Resistance Measurements', *Annual Book of ASTM Standards*, Vol. 03.02, ASTM, West Conshohocken, PA.

8 Z. Tafel, *Phys. Chem.* 50, 1904, p. 641.

9 ASTM G61, 'Standard Test Method for Conducting Cyclic Potentiodynamic Polarization Measurements for Localized Corrosion Susceptibility of Iron-, Nickel-, or Cobalt-based Alloys', *Annual Book of ASTM Standards*, Vol. 03.02, ASTM, West Conshohocken, PA. Fig. 2 used with permission.

10 ASTM G100, 'Standard Test Method for Conducting Cyclic Galvanostaircase Polarization', *Annual Book of ASTM Standards*, Vol. 03.02, ASTM, West Conshohocken, PA. Fig. 3 used with permission.
11 ASTM G150, 'Standard Test Method for Electrochemical Critical Pitting Temperature Testing of Stainless Steel', *Annual Book of ASTM Standards*, Vol. 03.02, ASTM, West Conshohocken, PA.
12 ASTM F746, 'Standard Test Method for Pitting or Crevice Corrosion of Metallic Surgical Implant Materials', *Annual Book of ASTM Standards*, Vol. 13.01, ASTM, West Conshohocken, PA.
13 ASTM G71, 'Standard Guide for Conducting and Evaluating Galvanic Corrosion Tests in Electrolytes', *Annual Book of ASTM Standards*, Vol. 03.02, ASTM, West Conshohocken, PA.
14 ASTM G82, 'Standard Guide for Development and Use of a Galvanic Series for Predicting Galvanic Corrosion Performance', *Annual Book of ASTM Standards*, Vol. 03.02, ASTM, West Conshohocken, PA.
15 ASTM G102, 'Standard Practice for Calculation of Corrosion Rates and Related Information from Electrochemical Measurements', *Annual Book of ASTM Standards*, Vol. 03.02, ASTM, West Conshohocken, PA. Table 2 used with permission.
16 NACE Task Group T-1D-34 Technical Committee Report, *Laboratory Test Methods for Evaluating Oilfield Corrosion Inhibitors*, NACE Publication 1D196, December 1996, NACE International, Houston, TX.
17 NACE Task Group T-5A-31 Technical Committee Report, *State-of-the-art Report on Controlled-Flow Laboratory Corrosion Tests*, NACE Publication 5A195, December 1995, NACE International, Houston, TX.
18 S. Papavinasam, R.W. Revie, M. Attard, A. Demoz and K. Michaelian, 'Comparison of Laboratory Methodologies to Evaluate Corrosion Inhibitors for Oil and Gas Pipelines', *Corrosion*, 59 (10), 897, 2003.
19 ASTM D1125, 'Standard Test Methods for Electrical Conductivity and Resistivity of Water' *Annual Book of ASTM Standards*, Vol. 11.01, ASTM, West Conshohocken, PA.
20 S.W. Dean, 'In-Service Monitoring', *ASM Handbook, Volume 13: Corrosion*, ASM International, Materials Park, OH, 1996, p. 197. Fig. 3.15 used with permission.
21 S. Papavinasam, R.W. Revie, M. Attard, A. Demoz and K. Michaelian, 'Comparison of Techniques for Monitoring Corrosion Inhibitors in Oil and Gas Pipelines', *Corrosion*, 59 (12), 1096, 2003.
22 D.C. Silverman, Chapter 68: 'Practical Corrosion Prediction Using Electrochemical Techniques', in *Uhlig's Corrosion Handbook*, Second Edition, Ed. R.W. Revie, 2000, John Wiley and Sons, New York, p. 1179.
23 J.R. Scully, 'Methods for Determining Aqueous Corrosion Reaction Rates', in *ASM Handbook, Volume 13A, Corrosion: Fundamentals, Testing, and Protection*, ASM International, Materials Park, OH, 2003, p. 68.
24 F. Mansfeld, 'Electrochemical Methods of Corrosion Testing', in *ASM Handbook, Volume 13A, Corrosion: Fundamentals, Testing, and Protection*, ASM International, Materials Park, OH, 2003, p. 446.
25 J.R. Scully, 'Electrochemical Tests', in *ASTM Corrosion Tests and Standards: Application and Interpretation*, 2nd Edition, Ed. R. Baboin, ASTM, West Conshohocken, PA.

26 N.G. Thompson and J.H. Payer, 'DC Electrochemical Test Methods', *Corrosion Testing Made Easy*, Volume 6, 1998, NACE, Houston, TX.
27 D.A. Jones, *Principles and Prevention of Corrosion*, Prentice-Hall, Upper Saddle River, NJ, 1996, ISBN-0-13-359993-0.
28 R. Baboian and S.W. Dean, Eds., 1989, *Corrosion Testing and Evaluation, ASTM STP 1000*, ASTM, West Conshohocken, PA, ISBN. 0-8031-1406-0.
29 J.R. Scully, 'Polarization Resistance Methods for Determination of Instantaneous Corrosion Rates', *Corrosion*, 56 (2000), 218.
30 S. Papavinasam, Chapter 67, 'Evaluation and Selection of Corrosion Inhibitors', in *Uhlig's Corrosion Handbook*, Ed. R.W. Revie, John Wiley and Sons, Inc., New York, 2000, p. 1169, ISBN 0-471-15777-5.
31 S. Papavinasam, M. Attard and R.W. Revie, 'Modified Cathodic Disbondment Testing of External Polymeric Pipeline Coatings', Paper #7021, NACE CORROSION 2007, Houston, TX (2007).

4

Electrochemical noise for corrosion monitoring

ROBERT A. COTTIS, University of Manchester, Institute of Science and Technology, Manchester, UK

4.1 Introduction to electrochemical noise

4.1.1 What is electrochemical noise?

Electrochemical noise (EN) is a generic term used to describe the fluctuations in potential and current that occur on a corroding electrode. EN is produced by the processes causing the corrosion (or other electrochemical reactions), and it has been a hope of corrosion researchers that its interpretation would provide an understanding of the corrosion process that cannot be obtained by other means. So far this hope has not been completely realised, but some progress has been made, and the method has been used for corrosion monitoring. This chapter will review the development of our current understanding of EN, and the methods that have been used in corrosion monitoring.

4.1.2 History of EN measurement

Any measurement of the potential of a corroding electrode or of the current to an electrode at a controlled potential will implicitly measure EN, in addition to whatever is being measured deliberately. However, it was only in 1968 that noise was seen as a possible source of information, rather than an 'error' in the measurement. The first deliberate measurement of EN for a corrosion system was made by Iverson,[1] who recorded the electrochemical potential noise (EPN), and concluded '*Investigations of these voltage fluctuations appear to offer much promise for the detection and study of the corrosion process and for the study of corrosion inhibitors*'. At about the same time Tyagai[2] examined EN from an electrochemical engineering perspective, and presented a relatively advanced interpretation of the expected characteristics of the noise. While it was not generally described as EN at the time, several workers, including Stewart *et al.*,[3] recorded the fluctuations in current associated with the

phenomenon of metastable pitting. This was thus probably the first measurement of electrochemical current noise (ECN). The next major advance came when Eden *et al.*[4] realised that three electrodes could be used to make a simultaneous measurement of potential and current noise. By dividing the potential noise by the current noise (as the standard deviations) a parameter with units of resistance, and consequently termed the electrochemical noise resistance, and commonly referred to as R_n, was obtained. The details of the derivation of this parameter and its significance are discussed further below. The three-electrode measurement configuration has become the standard for EN measurements, although a number of attempts have been made to try to make an EN measurement on a single electrode, and thereby avoid some of the compromises that are inherent in the analysis of the conventional measurement. These are discussed further below.

4.2 Measurement of EN

At first sight the measurement of EN is simple, and this has been promoted as an advantage of the method. However, considerable care is needed to obtain reliable measurements (early results should be viewed with some suspicion, as they were often seriously contaminated with noise from other than electrochemical sources).

4.2.1 Electrochemical potential noise

The measurement of EPN can be made either by recording the potential difference between a corroding electrode and a low-noise reference electrode or the potential difference between two corroding electrodes. The latter technique has advantages for practical corrosion monitoring, although the results may be slightly more difficult to interpret as it is not possible to determine unequivocally which of the two electrodes is the source of the noise.

4.2.2 Electrochemical current noise

The measurement of ECN is normally made by measuring the current between two nominally identical electrodes. Alternatively it can be made by measuring the current drawn by a single electrode held at a fixed potential. The first method is simpler, as it avoids the requirement for a low-noise reference electrode and potentiostat, and it avoids questions about the effect of holding the working electrode at a fixed potential, rather than allowing it to vary naturally.

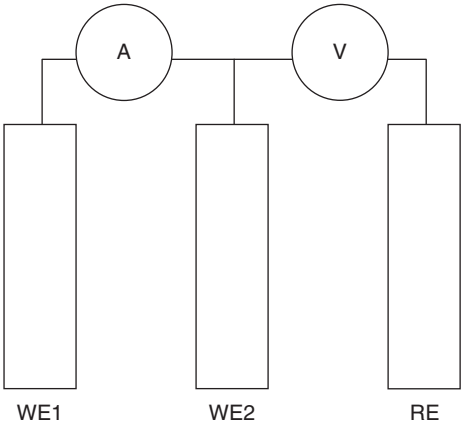

4.1 Three-electrode method of EN measurement.

4.2.3 Simultaneous measurement of potential and current noise

If the ECN is measured as the current between two nominally identical working electrodes, the potential of this coupled working electrode pair can be measured with respect to a reference electrode or a third working electrode. This permits the measurement of R_n as the standard deviation of potential divided by the standard deviation of current, and has become the conventional method of measurement of EN (see Fig. 4.1). There are differences between the method using a reference electrode or a third working electrode; the former method is scientifically somewhat better, since it avoids complications associated with uncertainty as to whether the noise emanates from the reference electrode, but it requires a reliable reference electrode, which may be problematic in practical monitoring applications. Thus two working electrodes and a reference electrode are normally used in the laboratory, whereas the three similar electrode method is more common in corrosion monitoring.

4.2.4 Instrumental requirements

It is beyond the scope of this chapter to present a detailed description of the instrumentation aspects of the measurement of EN (see reference 5 for further information), but it is important that users are familiar with the requirements of reliable measurements, as there are many artefacts that can lead to erroneous results.

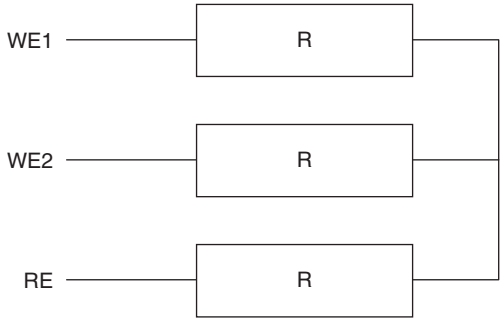

4.2 Dummy cell for measurement of instrument noise levels – all resistor values can be the same, and should be comparable to the impedance of the source being measured.

Potential measurement

Most electrical measuring devices are designed to measure voltage, and at first sight the measurement of EPN is simple. However, the amplitude of EPN is typically relatively low (less than 1 mV), and if a true reference electrode is used the average potential may be several hundred mV. Thus the measuring system should have a high sensitivity, and it may be beneficial to offset the average dc level, either by subtracting a pre-defined value or by using a very low frequency high-pass filter to remove the dc. Any real voltage amplifier (whether the input of the voltage measuring system or the input of a signal conditioning circuit used before the voltage measurement) will have a number of error and noise sources. The influence of these on the measurement will depend on the source impedance of the system being measured, and it is recommended that the performance of the measuring system should be checked using a dummy cell with properties similar to those expected for the real measurement (see Fig. 4.2).

Current measurement

In general current is measured as the voltage across a resistor. This resistor can be placed directly in the current path, but for the conventional ECN measurement this will inevitably lead to a voltage difference between the two working electrodes. While the resistor, and hence the voltage drop can be kept small, this in turn leads to difficulties in the measurement of the voltage. Therefore it is normal to use a current amplifier that produces a voltage output that is proportional to a current input, with (nominally) no voltage drop between the input terminals. Because of the latter property the device is normally called a *zero resistance amplifier* (ZRA) in the cor-

rosion community. As with the voltage amplifier, a real ZRA has a number of error sources, and the performance of the system should be checked using a dummy cell.

Filtering

EN is almost invariably analysed using computing techniques (though for monitoring application the computer may be embedded in the measuring instrument). Consequently it is necessary to sample the continuous, analogue signal before digitising it to produce a sequence of numbers that can be handled by the computer. It is beneficial to remove some signal frequencies before the analogue signal is sampled. A low-pass filter (one that allows frequencies below a specified value, known as the cut-off frequency, to pass, while removing higher frequencies) should normally be used to remove frequencies above the Nyquist frequency (half the sampling frequency, the maximum frequency that can be represented by the digitised output) to avoid the problem of aliasing. A high-pass filter (one that allows frequencies above a specified value to pass, while removing lower frequencies) can be used to remove the dc component of a signal and low frequency drift, although it is important to be aware that a high-pass filter with a low cut-off frequency can take a very long time to respond to step changes in the input, so a long settling time is needed after the filter is first connected to a signal source.

Error sources

As well as the noise and other error sources associated with the potential and current amplifiers, additional errors may arise as a result of artefacts in the signal-conditioning or digitisation process.

Aliasing

Aliasing occurs when the input signal contains frequencies above the Nyquist frequency for the analogue-to-digital converter. Once the signal has been sampled, it is impossible to distinguish components produced by aliasing of higher frequencies from real lower frequency information, so it is important to prevent aliasing from occurring by appropriate filtering or by the use of a digitisation method that automatically removes higher frequencies. The most common problem with aliasing that can be easily detected is due to power-line interference, which will manifest itself as a peak in the power spectrum. However, the more insidious result of aliasing is erroneous, but apparently ‘normal’ data.

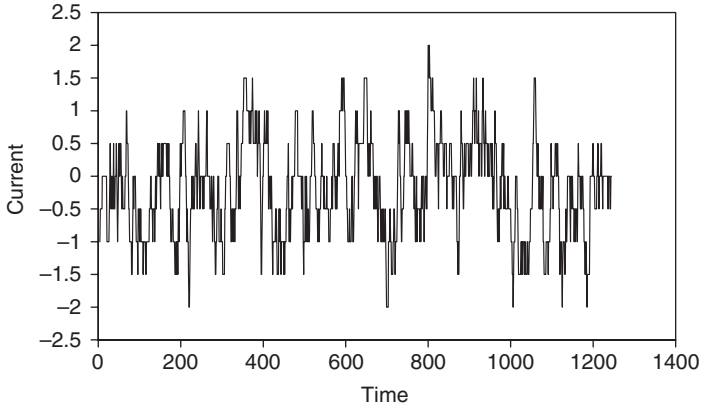

4.3 Simulated time record showing quantisation noise with a quantization step size of 0.5.

Quantisation

Quantisation is the inevitable result of representing a value as a number with a fixed number of decimal places. This leads to a step between successive possible values, producing a form of noise. Quantisation noise is apparent in a plot of the time record as a set of clear discrete steps in the data (see Fig. 4.3). Quantisation noise is not too serious if the steps are small compared with the overall signal, but if the digital signal consists of only a few steps, then the resolution of the data acquisition system needs to be improved.

Interference

Interference is a result of voltages or currents produced by the coupling of electromagnetic radiation with the measuring circuit. Much interference will be induced by power cables, and will therefore consist of a sine wave (often quite distorted and hence containing higher harmonics) at the power line frequency (normally 50 or 60 Hz). Other sources of interference include inductive spikes due to switching of large currents (refrigerator on-off cycling is a common source in laboratories), and high frequency ac interference due to radio frequency induction heaters and the like. Interference typically has a higher frequency than the regions of interest for EN measurements, and it can therefore often be removed by filtering. However, it is best minimized by shielding the measurement system (e.g. by using a Faraday cage), by paying careful attention to the layout of signal cables and by avoiding ground loops.

4.3 Alternative EN measurement methods

While the conventional three-electrode method is widely used, a number of modifications of this method have been proposed. All too often these methods have been developed on an ad-hoc basis, with no analysis of the underlying theory.

4.3.1 Methods using asymmetric electrodes

One class of method uses asymmetric electrodes, either through necessity (e.g. when making measurements on a straining electrode during stress corrosion cracking studies), accident (as when studying painted samples, where it is almost inevitable that the samples will differ somewhat) or design.

The theoretical analysis of EN generation with asymmetric electrodes had been reported by Bautista *et al.*[6] A key conclusion of this analysis is that it is not possible to determine all of the properties of the working electrodes (the impedance and current noise of each of the electrodes), as there are four unknowns and only two measured parameters. The solution to this problem is to arrange for the properties of one electrode to be known, so that the properties of the other electrode can be determined. However, this still does not provide a complete solution, as it tends to be difficult to measure both properties of the 'unknown' electrode. Thus one variant of the method uses a working electrode coupled to a low noise electrode that is nominally used to sense the current noise. In practice the sensing electrode is polarised by the potential noise of the working electrode and the resultant current provides a measure of the impedance of the sensing electrode, and the impedance of the working electrode cannot be determined.

Benish *et al.*[7] used working electrodes that were nominally identical, but they were maintained with a potential difference between them using a modified ZRA. This was intended as a method of ensuring that all anodic transients emanated from one electrode in order to simplify the analysis. The method may achieve this, but a more important potential advantage may be the tendency to encourage pitting corrosion on the more positive electrode, thereby providing an early warning of possible problems.

Another method using deliberately asymmetric electrodes is that of Chen and Bogaerts.[8] This uses a single working electrode, coupled to a platinum 'microcathode', with the potential of the coupled electrode pair being measured against a conventional reference electrode. An analysis of the system appears to show that this configuration can measure both the impedance and current noise of the working electrode, but it has been shown[9] that the analysis is flawed, and the configuration is not recommended.

A similar method has been used by Klassen and Roberge,[10] who used a graphite electrode coupled to nickel aluminium bronze. This work uses a heuristic analysis to estimate the polarization resistance; based on the work of Bautista *et al.*,[6] it is expected that the majority of the current noise will be produced on the metal electrode, and consequently the potential noise will be similar to that for the uncoupled metal electrode, but modified by the galvanic connection to graphite, while the current noise will be the result of the potential noise acting on the impedance of the graphite electrode. Thus the measured polarization resistance should be that of the graphite, and the net result is that the coupling to graphite serves only to degrade the potential measurement, without providing information of any relevance to the corrosion of the metal.

4.3.2 Switching methods

A problem with the conventional three-electrode method is the need to assume that the two working electrodes are similar. A number of workers have attempted to make near-simultaneous measurements of current and potential noise by switching between a current and a potential measuring configuration. These attempts have often been flawed by the treatment of the corroding metal electrode as a pure resistor, without taking capacitive and diffusional effects into account. Thus initial attempts switched rapidly between current and potential control. In this configuration the current-measuring part of the cycle, which necessarily imposes a controlled potential on the working electrode, effectively swamps any potential fluctuations. Subsequent attempts have recognised this problem and switch more slowly (of the order of minutes per cycle or longer). In the latter case the measurements are valid (providing a sufficient settling time is allowed following the switch in the measurement configuration), but there is a question about the stationarity of the system, especially in the presence of significant changes in the connection of the system.

Two implementations of switching systems have been used commercially:

- The CorrElNoise method[11] was first reported in about 1996. It uses rapid switching (the actual switching frequency is unclear from the manufacturer's web site, but appears to be of the order of 10 Hz) between current and potential measurement between two nominally identical electrodes. The analysis presented is based on the treatment of the corroding system as a voltage noise source in series with a purely resistive impedance, with no account taken of the capacitive character of the electrodes. Based on the analysis above, it seems questionable whether the measured potential noise is of any value.

- In 2005 a method of switching between current noise and potential noise measurement was patented by Gill *et al.*[12] This uses a relatively long switching cycle (of the order of 30 minutes), with an EPN time record for a single electrode first being monitored in open-circuit conditions, and then switched to potentiostatic control at the free corrosion potential (at the time of switching – this will include a contribution of the potential noise) to measure an ECN time record. The method appears sound from a theoretical viewpoint, although the current and potential noise will not be correlated in time, so it is difficult to see that it offers a major advantage over the conventional method.

4.3.3 Combined noise and impedance measurement

An alternative approach to the problem of making noise measurements on a single electrode is to recognise that the only reason for measuring both current and potential noise is to permit the estimation of the impedance of the electrode. Consequently an alternative approach is to measure just the potential noise (which will provide an indication of the nature of the corrosion, or the current noise can be inferred from the potential noise and the impedance), but at the same time to measure the impedance of the electrode at a single frequency by applying a low frequency current signal. This method was patented by Cottis,[13] but has yet to be used in practical corrosion monitoring.

4.3.4 Testing EN instrumentation

In most cases EN instrumentation will be purchased from a commercial supplier, and should be of a high quality. However, there is a relatively complex relationship between the source of the noise and the errors induced by the measuring instrument, and this cannot easily be deduced from instrument specifications (and it is rare for the specification to give sufficient information). Thus it is recommended that EN-measuring instrumentation should be tested to determine the level of instrument noise. This should be done using a dummy cell with impedance comparable to that expected in the real measurement. Even resistors produce a certain amount of thermal or Johnson noise – the dummy cell will produce a potential noise power spectral density (see below) of $4kTR$ V^2/Hz (where k is Boltzmann's constant, T the temperature in K, and R the resistance) and a thermal current noise power spectral density of $4kT/R$ A^2/Hz. These are the lowest levels of noise that can be detected – good instruments should be able to achieve these noise levels for high source impedances, but will probably not be able to do it for low source impedance. Most electronic devices also exhibit $1/f$ noise at low frequencies (typically below 1 Hz), so the instrument noise

usually also becomes more of a problem at the low frequencies that are often of interest for the interpretation of EN.

4.4 Interpretation of EN

4.4.1 Introduction

The fluctuations that are measured as EN have been produced by the corrosion process without any external influence, and it might therefore be supposed that it would be possible to obtain a lot of information about the corrosion process from the EN data. There have been many attempts to extract useful information from EN data. These have been successful in part, and it is usually possible to get a reasonably good indication of the rate of corrosion. A more challenging objective is to determine the type of corrosion occurring; some progress has been made in this, with parameters that give a reasonable indication of the tendency to localised corrosion having been developed, but only very limited success has been obtained in discriminating between different types of localised corrosion – see reference 14 for further information.

This section will present the various methods that have been used, with an emphasis on the techniques that are sufficiently mature, and sufficiently simple to interpret, for use in practical corrosion monitoring.

4.4.2 Direct examination of time records

The simplest method of interpretation of EN data (at least in terms of computational complexity) is direct examination of the potential and current time record. A number of properties can be derived from this:

- Metastable pitting will show as transients in potential and current. If the measurement uses a true reference electrode, all of the transients will be produced on one or other of the working electrodes, so the transients in current may go in either direction (depending on which working electrode the pit occurs), but the potential transient will always go in the negative direction, since the anodic transient from the pit will polarize the cathodic reaction of the two working electrodes. Every current transient should be matched by a potential transient (if not, then the transient may be due to interference rather than being true EN). If the three working electrode method is used, then the behaviour is a little more complex. Pits on one or other of the two working electrodes should give a corresponding negative-going potential transient with a corresponding current transient. Pits on the electrode used as a reference electrode will give a positive-going potential transient, but no current transient.

- The initiation period of crevice corrosion will give similar behaviour to metastable pitting (indeed it can be argued that it is metastable pitting). Stable crevice corrosion will typically lead to a significant drop in the potential of the electrode with the crevice, and consequently a relatively large coupling current if the electrode is one of the current-measuring electrodes. Little work has been done on stable pitting corrosion, but this might reasonably be expected to exhibit similar behaviour.
- The initiation of stress corrosion cracks also gives transient events in current and potential, but these tend to diminish in amplitude as the cracks become longer and hence more effective at shielding the crack tip.

While direct examination of time records provides a relatively simple interpretation of the behaviour for systems showing clear independent transients, it becomes much less effective as the frequency of the corrosion events increases and transient events start to overlap. It is also dependent on interpretation by a skilled human, which makes it impractical for routine use in corrosion monitoring. However, it is commonly the primary method used to validate computational methods of interpretation. This may be considered as a weakness of most work on EN, in that it is rare for EN interpretation methods to be compared with anything other than other EN interpretation methods, notably direct examination of the time record. While unfortunate, this weakness is understandable, in that there are currently few alternative methods that provide the necessary sensitivity for the instantaneous detection of localized corrosion.

4.4.3 Statistical methods

A large class of methods (and almost all that are currently used in practical corrosion monitoring) are based on statistical analysis of the EN data. These methods treat the potential and current noise data as an unordered sample of values from a population. Note the word unordered, which means that the position of a particular value in a time record is not given any significance, and nor is the correlation between the potential and current measured at a given time. It might be expected that the loss of the information present in the ordering of the data would limit the capability of these methods, but this is compensated for by the very effective data reduction (usually to only a few values), which makes subsequent interpretation relatively easy.

Mean current and potential

It is a moot point whether or not the mean potential or current can truly be regarded as EN, and some measurement methods explicitly remove this

by the use of a high-pass filter. However, the mean potential and current are usually measured, and they may contain useful information. Thus the mean potential of steel in concrete can provide an indication of whether or not corrosion is likely, and a mean current with a large absolute amplitude can be used as an indication that one electrode of a coupled pair is suffering from stable crevice or pitting corrosion.

Standard deviation of current and potential

The standard deviation is a direct indication of the amplitude of the fluctuations associated with the noise, and it is by far the most common parameter used in EN applications for corrosion monitoring, at least as the first step in the analysis process.

A number of features of the standard deviation need to be appreciated:

- The magnitude of the standard deviation is dependent on the range of frequencies included in the measurement (usually described in terms of the bandwidth), with a larger bandwidth leading to a larger standard deviation. The exact dependence will be influenced by the shape of the power spectrum.
- Drift in the time record will also contribute to the standard deviation, and it may be appropriate to remove this, either by high pass filtering before sampling, or by digital filtering or linear trend removal applied to the digital time record.
- The standard deviation of current is normally expected to be proportional to the square root of the specimen area, while the standard deviation of potential is expected to be inversely proportional to the square root of the specimen area. These relationships are not guaranteed to be correct, however, and it is recommended that the specimen area should be quoted, but no normalisation for the area should be performed. This is not usually a significant issue for corrosion monitoring, where the probe area is generally fixed.

Noise resistance

Eden *et al.*[4] proposed the division of the standard deviation of potential times the specimen area by the standard deviation of current to obtain a parameter with units of resistance times area, and known as the electrochemical noise resistance, R_n:

$$R_n = \frac{\sigma_E A}{\sigma_I}$$

where σ_E and σ_I are the standard deviations of potential and current respectively, and A the area of the sample. Several series of experiments have shown that R_n is comparable with linear polarisation resistance, R_p. This can also be demonstrated theoretically, providing it is assumed that the response of the metal-solution interface to the noise current can be described by R_p.

Accepting the equivalence of R_p and R_n, it is possible to determine the corrosion current density from the Stern–Geary equation:

$$i_{corr} = \frac{B}{R_n}$$

where B is the Stern–Geary coefficient. This method is arguably the only established EN method, and it has been widely used in corrosion monitoring.

Skewness of current and potential

The skew or skewness is an indicator of the extent to which the distribution of values is skewed in one direction or another. It is normalised with respect to the standard deviation, and so is dimensionless. An unskewed distribution has a skew of 0. A time record exhibiting a moderate number of transients in one direction can be expected to have a non-zero skew, and the skew has been used as an indicator of metastable pitting events. However, bidirectional transients will tend to give a skew of zero, so this parameter can be expected to be less useful for corrosion monitoring using three similar electrodes.

Kurtosis of current and potential

The kurtosis is an indicator of the 'peakedness' of the distribution of values. As conventionally defined the kurtosis of a normal distribution is 3, and it is always positive. It is common to subtract 3 from the measured value, in which case it is recommended by this author to use the term 'normalised kurtosis' to avoid confusion, although this is not always done. A distribution showing a moderate number of bidirectional transients can be expected to have a kurtosis that is greater than 3, and this has been used as an indicator of localised corrosion.[22]

Coefficient of variation

The coefficient of variation is the standard deviation divided by the mean. It clearly only makes sense for the current, as the mean potential will vary

according to the reference electrode used. The coefficient of variation is an indicator of the relative scatter of the values, and it was initially suggested that a large value would indicate localised corrosion. However, it is now recognised that it has a major problem; since the mean current can be zero (indeed the expected value is zero), the value of the coefficient of variation may go to infinity (in principle it can also go to minus infinity, as the mean may be positive or negative, but the absolute value is normally taken). This problem is a manifestation of a more fundamental difficulty of the coefficient of variation, as it is only meaningful for a one-sided distribution (one where all values are either all positive or all negative). For this reason the coefficient of variation of current is not now in common use.

Localisation index

The localisation index was developed as a replacement for the coefficient of variation in order to avoid the problem of the possibility of very large values. It is defined as the standard deviation of current divided by the root mean square (rms) current. Since the rms is necessarily greater than the mean, the value can never exceed 1. Unfortunately, it can readily be shown that the localization index is a simple transformation of the coefficient of variation, and it suffers exactly the same fundamental limitation.

Pitting factor

The fundamental problem with the coefficient of variation and the localisation index is that the measured mean current is actually the difference between the currents from the two working electrodes, whereas the standard deviation of current will be derived from the sum of the individual standard deviations (strictly the variances add). An indication of the sum of the currents is often available as the estimated corrosion current, and a better parameter can therefore be obtained by dividing the standard deviation of current by the corrosion current. This method has been developed by Kane *et al.*,[15] and is used in commercial monitoring systems. In this implementation, the corrosion current is obtained from an independent measurement using harmonic analysis. There is a dimensional problem with the parameter, in that the standard deviation of current (which is expected to be proportional to the square root of area) is divided by the corrosion current density (which will be independent of area) times the area, so the pitting factor is inversely proportional to the square root of the area. However, this is not significant in corrosion monitoring, where the probe size will remain constant. A similar parameter, termed the true coefficient of variation may also be computed using I_{corr} derived from R_n, in which case

it can be shown[16] that the true coefficient of variation is the standard deviation of potential divided by the Stern–Geary coefficient:

$$\text{True coefficient of variation} = \frac{\sigma_I}{I_{corr}} = \frac{R_n \sigma_I}{B} = \frac{\sigma_E}{B}$$

Thus the standard deviation of potential provides a simple indicator of the tendency to localised corrosion.

Shot noise parameters

Many of the parameters used in the interpretation of EN data are heuristic, which essentially means that they seem to work, but don't have a theoretical basis. This is a rather disappointing aspect of the use of EN in corrosion studies, as there are relatively simple theoretical analyses available for noise processes. One of the simplest approaches is based on the theory developed originally by Shottky[17] for noise in vacuum electronic devices, and known as shot noise.

The basic assumptions of the shot noise theory are:

- The current is comprised exclusively of packets of charge of a fixed size. In the case of electronic noise, the packet of charge is the electron.
- The passage of individual packets of charge is independent of other packets; that is to say that the probability of a packet passing in a particular time interval is not influenced by when a packet last passed.
- The packets of charge pass instantaneously (this implies an infinite current, but passing for an infinitesimal time). This is known as a Dirac delta function, a transient of zero width, but finite area.

With these assumptions, it can be shown that the standard deviation of the current will be given by

$$\sigma_I = \sqrt{2qIb}$$

where q is the charge in each packet, I is the average current and b is the bandwidth of the measurement.

This theory can be applied to corrosion processes if it is assumed that the corrosion is produced by a series of 'events' of short duration and constant charge. The basic theory assumes a Dirac delta function for the packets of charge, but if the measurement bandwidth is restricted to low enough frequencies that the events are short compared with the period of the highest frequencies considered, this requirement is effectively met. If it is also assumed that only one of the anodic or cathodic processes is producing noise, and all of that current is produced as packets of charge, then the current I will be the corrosion current, while the charge q will be the charge

produced by each event. Hence the standard deviation of current can be calculated.

If it is further assumed that the corrosion current can be derived from R_n, then is it possible to estimate both I_{corr} and q:

$$I_{corr} = \frac{B}{R_n} = \frac{B\sigma_I}{\sigma_E}$$

$$q = \frac{\sigma_I \sigma_E}{Bb}$$

where B is the Stern–Geary coefficient.

Note that q and I_{corr} are, respectively, the charge and the current resulting from the passage of packets of charge q. Thus it is also possible to calculate the average frequency of the corrosion events, f_n (termed the characteristic frequency):

$$f_n = \frac{I_{corr}}{q} = \frac{B^2 b}{\sigma_E^2}$$

As it is reasonable to assume that the corrosion current and the frequency of events are proportional to the sample area, it is reasonable to normalise these by dividing by area.

Note that f_n is similar in character to the pitting factor, although it provides a better normalisation with respect to area, while q should be independent of area. Also, note that the shot noise theory depends on the frequencies included in the measurement of standard deviation being low enough to include many complete transient events. A better way of making this measurement is to use the power spectral density (PSD) at a given, low frequency, but the standard deviation forms are given here as these are probably simpler for corrosion monitoring applications (the PSD form can be obtained by using the relationship PSD $\equiv \sigma^2/b$).

Coulomb counting

The 'coulomb counting' or CoulCount method was developed by Schmitt *et al*.[18] as a heuristic method, although the underlying theory is reasonably accessible.[19] It depends on the recording of the current noise only. The signal is filtered with a high-pass filter with a cut-off frequency of 0.01 Hz. The filter may be either analogue (although the implementation of a good-quality 0.01 Hz analogue filter is difficult) or digital. The absolute value of the measured current samples is then summed over time. A steep slope is taken as an indication of rapid corrosion, although it is not possible to calibrate this in terms of an estimated corrosion rate.

It can be shown that this method is similar to integrating the standard deviation of current over time.[19] The use of the integrating plot provides a form of low pass filtering that may make it easier to see trends, but this can also be accomplished by digital filtering. The use of only the current noise restricts the value of the technique, as it does not allow for the estimation of the noise resistance (and hence the corrosion rate), and it is difficult to see what real advantages the method has over the conventional three-electrode method, although the use of integrating plots may be of value.

4.4.4 Spectral methods

In spectral methods the noise data are transformed from the time domain (i.e. potential or current versus time) into the frequency domain, in which the power present at different frequencies is plotted as a function of frequency. The power is normally plotted as V^2/Hz or A^2/Hz, termed the power spectral density (PSD), and the plot of PSD against frequency is known as a power spectrum (usually plotted on log–log axes). The process of transforming from the time to the frequency domain is known as spectral estimation. Two methods are commonly used, the Fast Fourier Transform (FFT) and the Maximum Entropy Method (MEM).[20] It should be appreciated that there is a close relationship between the variance (the square of the standard deviation) and the power spectral density. In effect the PSD can be thought of as the variance measured over a narrow frequency range and normalized to a bandwidth of 1 Hz. The integral of the PSD over the full frequency range included in the measurement is equal to the variance.

Spectral methods generally produce an output that is too complex for use in monitoring, but they may be useful in research. They also provide improved parameters compared with statistical measures for the calculation of noise resistance, pitting factor and f_n, since the most appropriate frequency range can be chosen, rather than using the arbitrary collection of frequencies present in the standard deviation. One potentially useful extension of spectral methods is the computation of the electrochemical noise impedance by dividing the PSD of potential by the PSD of current and then taking the square root (the calculation being performed at each frequency). The result is also known as the spectral noise resistance, on the basis that only the modulus of the impedance can be obtained, with no phase information.

4.4.5 Wavelet methods

Wavelet methods may be regarded as a form of spectral method, in that wavelets of finite duration are fitted to the time record, rather than a series

of continuous sine waves. A nominal advantage of the use of wavelet methods is the avoidance of assumptions about stationarity of the system. However, they are complex to interpret, and while they are of theoretical interest, and the subject of ongoing study, they are, as yet, inappropriate for corrosion monitoring.

4.4.6 Chaos methods

The methods of analysis of chaotic systems are concerned with the detection of deterministic behaviour in apparently random signals. There is some evidence that localised corrosion processes have a chaotic character, but the analysis methods are not yet appropriate for corrosion monitoring.

4.4.7 Neural network methods

In essence neural networks provide a mechanism for the fitting of complex functions to measured data, without the need for any knowledge about the functional relationship between the input and output variables [see[21] for a review of the use of neural network methods in corrosion]. In the case of EN, neural network methods have been used to construct a model of the relationship between the statistical properties of potential and current noise and the type of corrosion.[22] As the type of corrosion was assessed by the examination of the EN data by a human expert, the neural network was effectively being used to emulate a human. This is potentially a viable approach to the production of simple outputs that are suitable for corrosion monitoring, and it merits further investigation, especially if combined with some of the more effective conventional analysis methods, such as R_n and pitting factor or f_n.

4.5 Comparison of EN and polarization resistance for the estimation of corrosion rate

Both R_n and R_p can be used to estimate the corrosion rate using the Stern–Geary equation, and both can be applied reasonably easily in a corrosion monitoring situation. Relatively few detailed comparisons of the merits of the two methods have been reported, although several workers have demonstrated a reasonable correlation between them. Even fewer have tested the ‘correct’ corrosion rate by gravimetric methods, so it difficult to say which of the two methods is better in respect of the accuracy of measurement. However, we can compare a number of claimed advantages of EN.

4.5.1 Claimed advantages of noise resistance

- It is often suggested that R_n is simpler to measure than R_p. This is rather questionable, especially when considering dedicated instruments for corrosion monitoring; the electronic requirements of the two methods are very similar, and the major difference between the two measurements is liable to be the program in the control microprocessor, rather than the electronic hardware. Furthermore, R_n typically requires a more sensitive measurement and is more easily contaminated by interference.
- The measurement of R_n is claimed not to perturb the system being measured. This can be demonstrated by the thought experiment of considering the two working electrodes in the conventional measurement as being two halves of the same piece of metal. Some workers have been concerned about the 'alien' influence of the ZRA used to measure the current, but providing this is well-designed it is difficult to see how it can influence the behaviour of the two electrodes. A more difficult question is whether the measurement of R_p affects the behaviour of the electrodes. Another thought experiment is to record the potential noise of a corroding electrode, and then use this as a control signal to measure the properties of a new working electrode – this would effectively measure the impedance of the working electrode, and hence R_p; is this then any different from an R_n measurement? Thus it is arguable that measurements of R_p can be made in such a way that they do not influence the behaviour of the electrodes any more than an R_n measurement (although this is not the case for conventional LPR or impedance measurements).
- In some early work it was suggested that R_n was not affected by the solution resistance. This is now known to be incorrect, and R_n has just the same dependence on solution resistance as R_p. Similarly, R_n and R_p both measure the properties of the most rapid electrochemical reactions, which may not be the corrosion reactions; they both assume that the reactions are far from equilibrium, and they both depend on at least one of the reactions being activation controlled.

At present it is reasonable to say that the jury is still out on the relative merits of the two methods, but it seems that R_p is rather less noisy and possibly a little more reliable.

4.5.2 Use of EN for the identification of the type of corrosion

Where EN really has a 'unique selling point' is in its potential ability to give an indication of the type of corrosion. For corrosion monitoring the method

used for identification must be relatively simple, ideally just providing a uniform/localised green-amber-red indication. However, the best method of obtaining this information remains to be determined; some of the methods that have been proposed are:

- The coefficient of variation of current was proposed in early work. It does tend to have a larger value when localised corrosion is occurring, but it is also very sensitive to the value of the mean current, and it is therefore little used now. The Localization Index is similar.
- The Pitting Factor is used in commercial systems. It has some theoretical justification, other than its rather questionable dimensions, and the performance in service seems to be relatively reliable.
- The characteristic frequency, f_n, derived from a shot-noise analysis has also been found to correlate reasonably well with the occurrence of localised corrosion. It is similar to the pitting factor, but with the minor advantage of a well-defined area dependence. Note that f_n is a function of the standard deviation of potential, and the latter could also be used directly (and very simply) as an indicator. A method of presentation that may be useful is to present the measurements on a map of R_n against f_n,[23] which should map different types of corrosion to different parts of the map.
- The slope of the frequency-dependent part of the power spectrum has been suggested as being indicative of the type of corrosion. However, while this may be valid for a small set of experiments, comparison of a wider range gives conflicting results,[20] and the method is probably not appropriate for corrosion monitoring.

While the measurement of R_n is relatively insensitive to other sources of noise, such as flow fluctuation, it should be appreciated that the parameters used to identify the type of corrosion are generally very sensitive to such interference. Thus, in work that used a peristaltic pump to change the corrosive solution, it was found that the measured characteristic frequency dropped by several orders of magnitude to approximately the pump pulsation frequency when the pump was switched on.[24] In contrast the measurement of R_n was hardly affected.

4.6 Practical applications

A number of practical applications of EN to corrosion monitoring have been reported, many at the regular Symposium on Electrochemical Noise that is held at the Annual NACE Corrosion Conference (see www.nace.org for past conference papers).

One application that has been thoroughly reported is the use of EN in the monitoring of the nuclear waste storage tanks at the Hanford site.

This is a difficult monitoring problem. As a result of the required safety assessments and decontamination procedures, the installation of probes is extremely expensive, the composition of the solutions stored in the tanks is not known exactly (and they tend to be inhomogeneous due to precipitation of salts), and there is no way of obtaining an independent check on the validity of the measurements. The solutions stored in the tanks are designed to passivate the tanks, so the rate of general corrosion is low, and the main concern is the possibility of localised corrosion. For this reason the use of EN provides the only realistic option for corrosion monitoring, despite uncertainties over the optimum interpretation of the data. As far as it is possible to judge, the programme has been successful.[25]

4.7 Harmonic distortion analysis

Any methods that use the Stern–Geary equation to estimate corrosion rate, including the use of electrochemical noise resistance, depend on the value of the Stern–Geary coefficient. This is not a constant, and presents an element of uncertainty in the estimation of corrosion rate. There are a number of solutions available for this problem, including the use of an arbitrary value (usually of the order of 25 mV), calibration against corrosion rate measured by another method for the system in question, or measurement of Tafel slopes in a separate polarisation experiment. None of these solutions are guaranteed to provide a correct value, since the behaviour of the real system is obviously not known exactly (otherwise there would be no need to monitor it), and the method of harmonic distortion analysis (often termed just harmonic analysis) provides the only method of directly measuring the Stern–Geary coefficient on the actual system being monitored. The method relies on the determination of the Tafel coefficients by analysis of the distortion of a sine wave applied to a corroding probe (see reference 26 for more details of the method). The distortion leads to the production of harmonics of the original sine wave, and the amplitudes of the harmonics can be used to estimate the value of the Stern–Geary coefficient. This is illustrated in Figure 4.4, which shows the response of a simulated metal–solution interface to an applied potential sine wave. For this simulation the anodic Tafel slope was set at 60 mV/decade, while the cathodic Tafel slope was set at 1 V/decade (simulating a mass-transport limited reaction). The peak to peak amplitude of the potential sine wave was the 60 mV, and this gives a severely distorted signal. Figure 4.5 shows the power spectrum calculated for this signal. At the same time the amplitude of the response at the fundamental frequency provides a measure of the linear polarisation resistance (although it is implicitly measured in somewhat non-linear conditions). Thus harmonic distortion analysis should provide a more

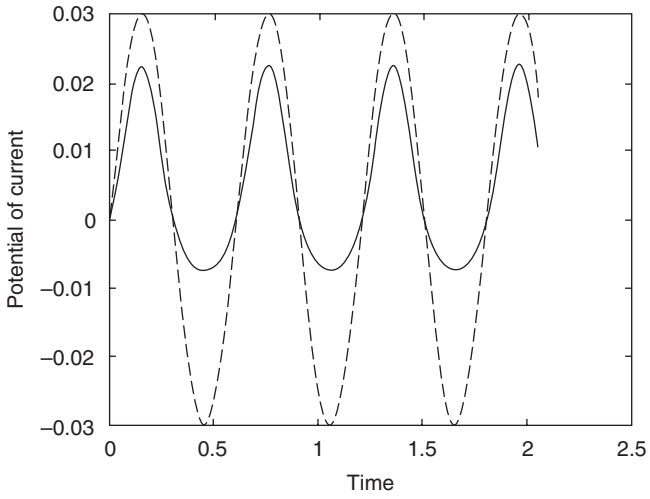

4.4 Simulated potential (--) and current (–) signals for a non-linear metal–solution interface (arbitrary units).

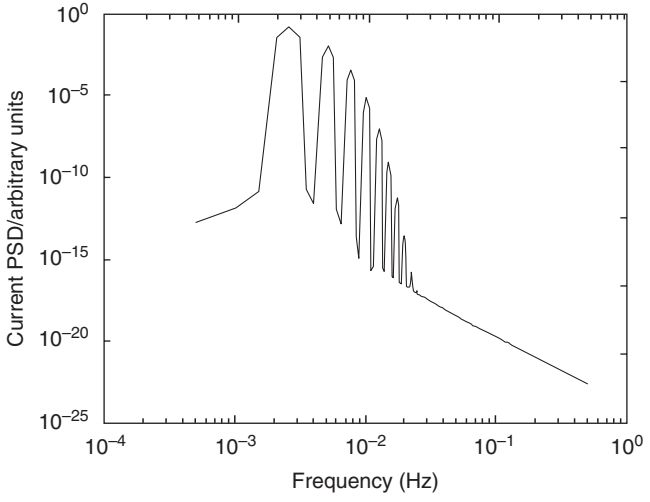

4.5 Power spectrum corresponding to the current signal in Fig. 4.4.

reliable estimate of the corrosion rate than other methods that have to use a less direct measure of the Stern–Geary coefficient. Note, however, that the analysis makes similar assumptions to those used in the derivation of the Stern–Geary equation, and it is not guaranteed that these assumptions will be valid in all cases:

1. It is assumed that both the anodic and the cathodic reactions follow Tafel's Law. This is only true if the reactions are activation controlled; while this is often the case for rapid corrosion processes, such as active metals corroding in acid, it is by no means certain that it is valid for real corroding systems, where factors such as mass-transport limitation and solution/film resistance effects may be important.
2. It is assumed that both anodic and cathodic reactions are far from equilibrium, so that the rates of the reverse reactions can be ignored. While this is often true, there are situations where it is not. Thus in hydrogenated water systems, such as are used in the primary circuit of pressurised water reactors, the hydrogen–water reaction is essentially in equilibrium, and electrochemical measurements essentially just measure the exchange current density of that reaction. Similarly, for copper corrosion processes it is likely that copper will be close to equilibrium with copper ions in the solution.
3. It is assumed that the frequency of measurement is low enough for capacitive currents to be ignored. This implies a very low frequency of measurement, and in some systems it is questionable whether a valid measurement can be achieved. Thus iron sulphide deposits formed in sour (H_2S-containing) environments can be electronically conductive and have a very large surface area by virtue of their porosity, such that the apparent capacitance is many mF/cm^2, leading to great difficulty in making valid measurements.

Despite these potential problems, harmonic distortion analysis has proved commercially successful. It has been used in conjunction with electrochemical noise measurement to provide an indicator of localised corrosion in the form of the pitting factor (see above).

4.8 Electrochemical frequency modulation

A further extension of the harmonic distortion method uses two simultaneous sine waves. When applied to a nonlinear corroding interface these interact to produce sum and difference frequencies. The method has been termed electrochemical frequency modulation by the developers[27] (the process is known as 'intermodulation' in electrical engineering). Analysis of these components also allows determination of the Stern–Geary coefficient, and additionally allows the production of two 'quality indicators' which can be used to check that the measurement is valid. As far as the author is aware, the method has not been used in commercial corrosion monitoring, although it may have promise for the future.

4.9 References

1 W.P. Iverson, 'Transient Voltage Changes Produced in Corroding Metals', *Journal of the Electrochemical Society*, 115, pp. 617–618 (1968).
2 V.A. Tyagai, 'Faradaic Noise of Complex Electrochemical Reactions', *Electrochimica Acta*, 16, pp. 1647–1654 (1971).
3 J. Stewart and D.E. Williams, 'The Initiation of Pitting Corrosion on Austenitic Stainless Steel: On The Role and Importance of Sulphide Inclusions', *Corrosion Science*, 33, pp. 457–474 (1992).
4 D.A. Eden, D.G. John and J.L. Dawson, 'Corrosion Monitoring', UK Patent 8611518 (1986), US Patent 5139627 (filed 1987, granted 1992).
5 S. Turgoose and R.A. Cottis, 'Corrosion Testing Made Easy: Electrochemical Impedance and Noise', NACE Houston, TX (2000).
6 A. Bautista, U. Bertocci and F. Huet, 'Noise Resistance Applied to Corrosion Measurements: V. Influence of Electrode Asymmetry', *Journal of the Electrochemical Society*, 148 (10), pp. B412–B418 (2001).
7 M.L. Benish, J. Sikora, B. Shaw, S. Sikora, M. Yaffe, A. Krebs and G. Martinchek, 'A New Electrochemical Noise Technique For Monitoring the Localized Corrosion of 304 Stainless Steel in Chloride-containing Solutions', *Corrosion* 98, Paper 370 (1998).
8 J.F. Chen and W.F. Bogaerts, 'Electrochemical Emission Spectroscopy for Monitoring Uniform and Localized Corrosion', *Corrosion*, 52 (10), pp. 753–759 (1996).
9 R.A. Cottis, 'The Significance of Electrochemical Noise Measurements on Asymmetric Electrodes', *Electrochimica Acta*, 52 (27), pp. 7585–7589 (2007) (available online from Jan 2007).
10 R.D. Klassen and P.R. Roberge, 'Self Linear Polarization Resistance', *Corrosion*/2002; NACE, Paper 02 (2002).
11 B. Röseler and C.A. Schiller, 'Strom-Potential-korrelierte Rauschmessung (CorrElNoise) – Ein neues Verfahren zur elektrochemischen Rauschanalyse', *Materials and Corrosion*, 52 (6), pp. 413–417 (2001).
12 R.P. Gill, V. Jovancicevic, W.Y. Mok, P. Hammonds, 'Quantitative, Real Time Measurements of Localized Corrosion Events', US Patent publication number 20060144719 (filed 31 October 2005, published 6 July 2006).
13 R.A. Cottis, "Method and Apparatus for monitoring Corrosion', GB2407169 (filed 6 June 2003, granted 16 November 2005).
14 R.A. Cottis, 'Sources of Electrochemical Noise in Corroding Systems', *Russian Journal of Electrochemistry*, 42 (5), pp. 497–505 (May 2006).
15 R.D. Kane, D.C. Eden and D.A. Eden, 'Evaluation of Potable Water Corrosivity using Real Time Monitoring Methods', *Corrosion*/2003, Paper 03271 (2003).
16 R.A. Cottis, 'Parameters for the Identification of Localized Corrosion: Theoretical Analysis', *Electrochemical Society Proceedings* PV 2001-22, pp. 254–263 (2001).
17 W. Schottky, 'Über spontane Stromschwankungen in verschiedenen Elektrizitätsleitern', *Annals of Physics*, 362 (23), pp. 541–567 (1918).
18 G. Schmitt, K. Moeller and P. Plagemann, 'A new service oriented method for evaluation of electrochemical noise data for online monitoring of crevice corrosion', *Corrosion*/2004, Paper 04454 (2004).

19 R.A. Cotta and R.A. Cottis, 'Methods for the Visualisation of Electrochemical Noise Data', *Corrosion*/2007, Paper 07363 (2007).
20 R.A. Cottis, 'The Interpretation of Electrochemical Noise Data', *Corrosion*, 27 (3), 265–285 (2001).
21 R.A. Cottis, Li Qing, G. Owen, S.J. Gartland, I.A. Helliwell and M. Turega, 'Neural Networks for Corrosion Data Reduction', *Materials and Design*, 20 (4), 169–178 (1999).
22 S. Reid, G.E.D. Bell and G.L. Edgemon, 'The use of Skewness, Kurtosis and Neural Networks for Determining Corrosion Mechanism from Electrochemical Noise Data', *Corrosion* 98, Paper 176, NACE (1998).
23 H. Al-Mazeedi and R.A. Cottis, 'Parameter Maps for the Assessment of Corrosion Type from Electrochemical Noise Data', NACE *Corrosion*/2004, Paper 04460, 2004.
24 R.A. Cottis, H.A. Al-Mazeedi and S. Turgoose, 'Measures for the Identification of Localized Corrosion from Electrochemical Noise Measurements', NACE *Corrosion*/2002, Paper 02329 (2002).
25 G.L. Edgemon 'Design and Performance of Electrochemical Noise Corrosion Monitoring Systems at the Hanford Site', NACE *Corrosion* 2004, Paper 04448 (2004).
26 C. Gabrielli, M. Keddam, and H. Takenouti, 'An Assessment of Large Amplitude Harmonic Analysis in Corrosion Studies', *Materials Science Forum*, 8, pp. 417–427 (1986).
27 R.W. Bosch, J. Hubrecht, W.F. Bogaerts and B.C. Syrett, 'Electrochemical Frequency Modulation: A New Electrochemical Technique for Online Corrosion Monitoring', *Corrosion* (USA), 57 (1), pp. 60–70 (2001).

5

Zero resistance ammetry and galvanic sensors

R. D. KLASSEN and P. R. ROBERGE, Department of Chemistry and Chemical Engineering, Royal Military College of Canada, Kingston, Ontario, Canada

5.1 Introduction

In the mid-1780s, anatomist Luigi Galvani in Bologna, Italy, was studying the effects of lightning. One day, in his garden, he fastened brass hooks between the spinal cord of a dissected frog and an iron railing. To his amazement the frog's legs twitched wildly, not only when lightning flashed, but also when the sky was calm. Galvani incorrectly interpreted his results in terms of animal electricity and proclaimed that the muscle retained a 'nerveo-electrical' fluid similar to that of an electric eel. While his papers on the subject ignited research among scientists of Europe, the most significant consequence of Galvani's discovery was the concept of Galvanism, which refers to the production of electrical current from the contact of two metals in a moist environment. Actually, the frog's legs provided an electrolyte pathway to permit galvanic current to pass between the brass and iron.

When dissimilar metals are immersed in a conductive solution, a potential difference develops between them. This difference is the driving force for galvanic current. The more corrosion prone of the two metals corrodes and releases electrons and the less corrosion prone metal provides the site for cathodic reactions, where electrons are consumed. Cathodic reactions include oxygen reduction and hydrogen evolution, neither of which consumes metal. An electrode that is corroding and consuming metal is termed the anode. The galvanic series is a relative ranking of about three dozen metals and alloys in seawater (Fontana, 1986, p. 43).

Ordinary ammeters indicate current by measuring the voltage across a known resistance and then converting the voltage reading into current by Ohm's law. However, this method can interfere with the phenomenon being measured by reducing the overall potential driving force. A zero resistance ammeter (ZRA) measures current by changing current to voltage, but uses a feedback loop to bring the voltage drop between the input terminals to 'zero' and therefore bypasses this limitation.

5.2 Galvanic current

In terms of mixed potential theory, the potential difference between the equilibrium potentials at anodic and cathodic sites is the sum of the following components: (a) anodic overpotential; (b) *iR* drop between the anodic and cathodic sites; (c) cathodic overpotential; and (d) cathodic concentration overpotential. The sites could be on the same electrode or on different electrodes. Galvanic current occurs when the sites are on different metals. The *iR* drop is due to the ionic conduction of charge between anodic and cathodic sites. The summation of relevant potential terms is:

$$E_{eq,c} - E_{eq,a} = iR_s + \beta_a \log \frac{i}{I_{o,a}} + \beta_c \log \frac{i}{I_{o,c}} + \eta_{conc} \quad [5.1]$$

where

$E_{eq,c}$ = equilibrium potential at the cathodic site, *V*
$E_{eq,a}$ = equilibrium potential at the anodic site, V
i = galvanic current, A
$I_{o,c}$ = exchange current at the cathodic site, A
$I_{o,a}$ = exchange current at the anodic site, A
β_a = Tafel slope for anodic branch, V/decade
β_c = Tafel slope for cathodic branch, V/decade
R_s = solution resistance
η_{conc} = cathodic concentration overpotential

The exchange current is the product of the exchange current density (A/cm^2) and the appropriate site area (cm^2). The cathodic concentration overpotential term in the case where oxygen diffusion is rate-limiting is

$$\eta_{conc} = \frac{2.303RT}{nF} \log_{10}\left(1 - \frac{i}{i_L}\right) \quad [5.2]$$

where T is the temperature, n is the number of electrons involved in the reaction, F is the Faraday constant and i_L is the current at which oxygen diffusion controls the corrosion rate.

According to Equation [5.1], the magnitude of galvanic current primarily depends on the magnitude of the potential difference of the electrodes in a common electrolyte and the anodic and cathodic kinetics. However, it is also affected by solution resistance and oxygen availability if the cathodic reaction is oxygen reduction. Both of these factors can reduce galvanic current to zero (Klassen and Roberge, 2003, 2006). Another consideration is the probability of a difference in solution resistance in between electrodes and that on top of each electrode. When the solution resistance between electrodes is much greater than that between anodic and cathodic sites on each electrode, the coupling current remains within each electrode and

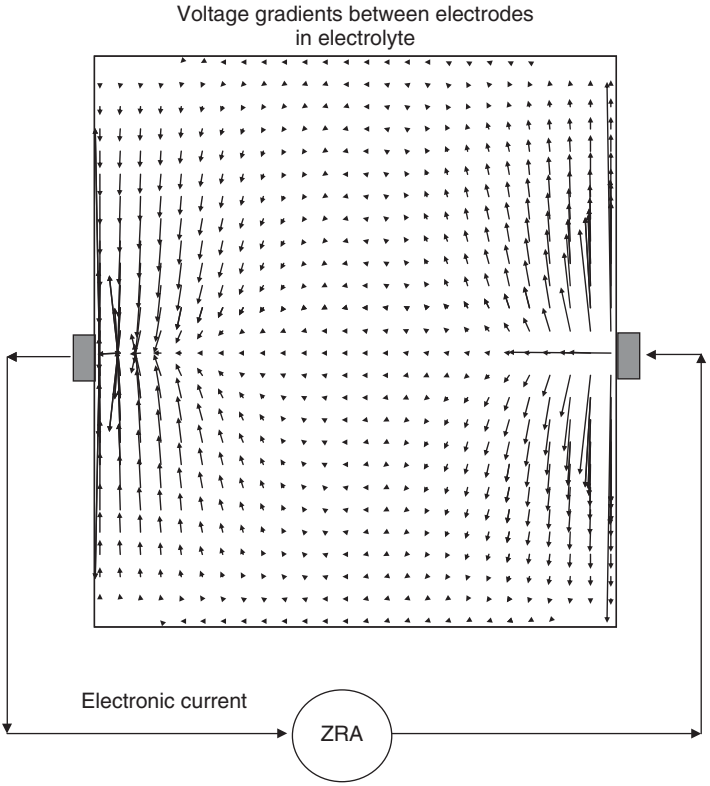

5.1 Schematic of voltage gradients between facing electrodes through an electrolyte and an external ZRA circuit.

by-passes a ZRA circuit. In this case, the anode will corrode undetected electronically.

A schematic of a circuit measuring current between two electrodes using a ZRA is shown in Fig. 5.1. The measured electronic current is balanced by the ionic current between the electrodes through the electrolyte. The voltage in the electrolyte between electrodes follows Laplace's equation,

$$\nabla^2 V = 0 \qquad [5.3]$$

The pattern of voltage gradient depends on the geometry between electrodes, with the magnitude of voltage gradients depending on the magnitude of the overall voltage difference. The current density, at any point, depends on the electrolyte resistivity, ρ, and voltage gradient,

$$i = -\frac{1}{\rho}\nabla V \qquad [5.4]$$

The current flow pattern, media resistivity and effective solution resistance are related. For current flowing in parallel through a length, dl, and cross-sectional area, dA, the solution resistance is

$$dR_s = \rho \frac{dl}{dA} \quad [5.5]$$

and

$$R_s = \rho \int \frac{dl}{dA} \quad [5.6]$$

For the case of current flowing along a wire, the resistance is the wire resistivity times the wire length divided by the wire cross-sectional area. However, R_s between facing electrodes is slightly greater than that for a wire because most of the current follows a longer path than a straight line. Although the direct distance between electrodes is L, the effective path length is between L and $(\pi/2)$.

5.3 ZRA measurement circuitry

Probably the simplest ZRA circuit ever was described by Baboian and Prew (1993). Besides a power supply and voltmeter, the only two electronic components are an op-amp and a resistor. A schematic of the circuit is shown in Fig. 5.2. The input terminals are held at zero potential difference

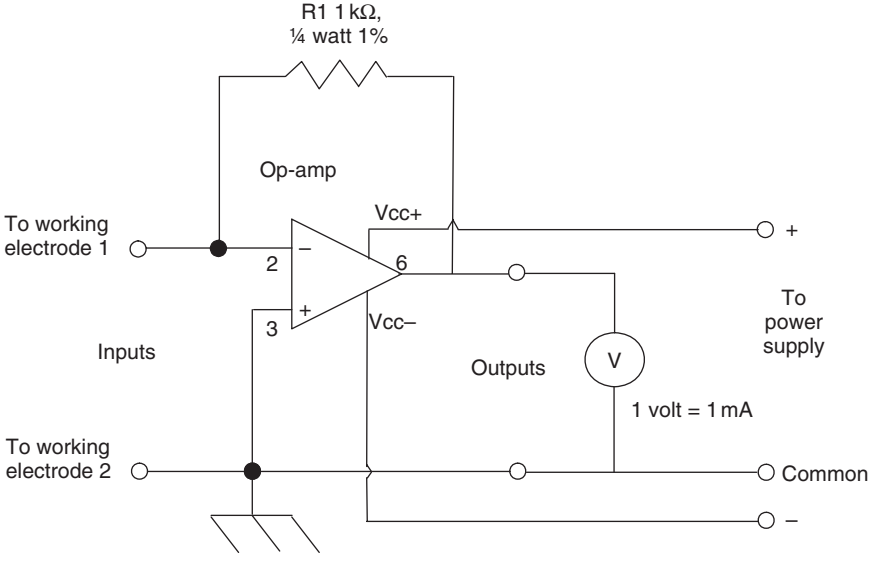

5.2 Schematic of ZRA using an op-amp and a resistor (adapted from Baboian and Prew, 1993). The op-amp suggested was TL081B.

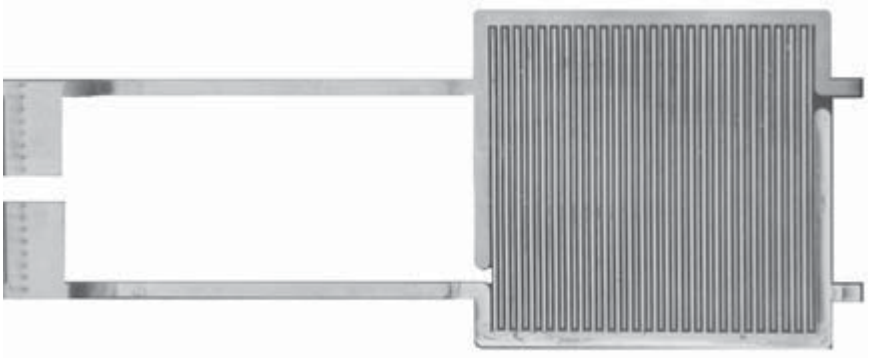

5.3 Photo of the galvanic element of a ZRA probe used for monitoring atmospheric corrosivity (Agarwala, 1996). The interdigitized sensor elements were cadmium and gold. Photo taken by Pierre R. Roberge.

and the current required to do this is proportional to the voltage between the outputs. With a resistor of 1 kΩ, 1 mA of galvanic current corresponds to 1 volt between the output terminals. More sophisticated circuits provide auto-ranging of the voltage output according to the magnitude of the current input. The simplicity of the ZRA circuitry makes the electronic part of the sensor very low cost. Frequently, the major cost is the sensor itself. Figure 5.3 shows a photo of a thin-film galvanic sensor used for monitoring atmospheric corrosion (Agarwala, 1996). The interdigitized fingers of cadmium and gold were plated onto Kapton after applying the initial pattern with copper. Cadmium functioned as the anode and gold as the cathode.

5.4 Applications

5.4.1 Atmosphere

The first attempt to quantify atmospheric corrosivity with a galvanic sensor was made in the late 1950s by measuring the current between a platinum foil and a zinc panel (Sereda, 1958). A later design was a miniature galvanic sensor consisting of interlaced elements of copper or zinc and gold (Sereda, 1982). Periods of time when the galvanic current was higher than a critical minimum (0.2 V across a shunt resistor) were interpreted as being 'wet' enough to promote corrosion. Variations in the response of these sensors over time and between locations indicated that the variables behind atmospheric corrosion are complex.

A common characteristic of galvanic sensors measuring atmospheric corrosivity is that the signal underestimates corrosivity. In a study comparing the mass loss of steel coupons and the cumulative current from steel galvanic sensors, it was found that the cumulative current only accounted for about 20% of the mass loss for the copper/steel couples (Mansfeld, 1982; Mansfield *et al.*, 1982). It was proposed that the unaccounted for current was due to local cell action on the individual plate of a sensor without current flow in the external measuring circuit. Another group found that the number of coulombs measured by a galvanic sensor was much less than the equivalent number of coulombs corroded by steel plates, i.e. 4.6 C/cm^2 for the sensor steel versus 183 C/cm^2 for a flat plate (White and Leidheiser, 1990). In another study with a thin-film galvanic sensor (Agarwala, 1996), the number of coulombs passed was compared with the mass loss of coupons of aluminum (Types A97075 and A96061) and steel at ten outdoor locations for periods of up to six months (Abbott, 2002). The ratio of coulombs corresponding to coupon mass loss to the number of coulombs registered by the galvanic sensor was quite variable, ranging from near unity to 2000.

Another observation was that galvanic current decreased slowly over time in an atmosphere of constant relative humidity (Klassen and Roberge, 2006). This was probably due to oxygen diffusion across the film becoming the rate limiting factor.

In summary, the ability of galvanic sensors to monitor atmospheric corrosivity seems to be mixed. Although they respond to severely corrosive conditions they do not seem to correlate well with the mass loss of coupons over a range of conditions. One solution is to measure solution resistance independently such as the impedance at high frequency (Klassen and Roberge, 2006). Then solution resistance effects can be separated from corrosion processes.

5.4.2 Cooling water

Localized corrosion is the main limiting factor in determining the service life of equipment (such as carbon steel heat exchangers) in industrial water systems. Chapters 6 and 23 (this volume), describe a sensor system designed to monitor the tendency of cooling water to promote localized corrosion based on the galvanically-coupled differential flow cell concept (Yang, 1995, 2000). One electrode is given a small area and a slow flow to promote anodic-only reactions and the other is given a large area and kept in a fast flow environment to promote cathodic-only reactions. Figure 5.4 shows a schematic of a differential flow cell: FE = fast flow electrode, SE1 = slow flow electrode 1, SE2 = slow flow electrode 2, RE = reference electrode. There are two electrodes in the slow flow leg. The ZRA current can be

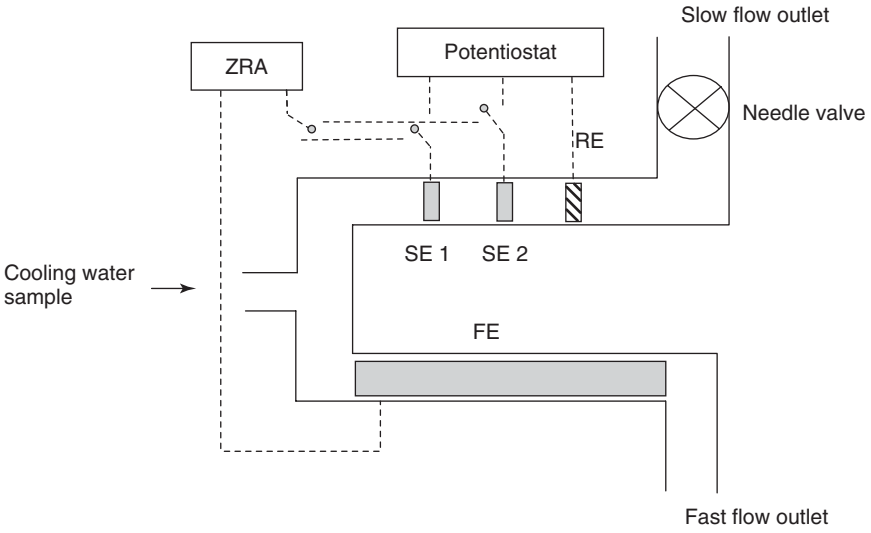

5.4 Schematic of differential flow cell. FE = fast flow electrode, SE1 = slow flow electrode 1, SE2 = slow flow electrode 2, RE = reference electrode (adapted from Yang, 1995).

read from one or the other slow flow electrode relative to the fast flow electrode. A potentiostat measures the uniform corrosion rate by a measurement of linear polarization resistance (LPR) (see Chapter 3) on one or the other slow flow electrodes when disconnected from the ZRA circuit. The degree of localized corrosion is considered as the sum of the ZRA current and the equivalent current based on measuring the uniform corrosion rate of each SE. However, a better measure of localized corrosion would seem to be the ratio of ZRA current to uniform corrosion current rather than the sum.

5.4.3 Soil

The external corrosion of water distribution systems leads to two major problems for water utilities. The first problem is the failure of the pipes. The second is the contamination of water as soil contaminants are transported into the distribution system. In a series of papers, Choi *et al.* (2005, 2006; Choi and Kim, 2006) described tests with galvanic sensors in groundwater, tapwater and soil. In synthetic groundwater over a period of 100 days, there was a linear relationship between the number of coulombs of galvanic current passed between electrodes of steel and copper and the mass loss of pipe-grade steel. Similar results were obtained in synthetic tap water and soil using LPR and electrochemical impedance spectros-

copy (EIS) as primary corrosion rate measurements. In another series of tests, a galvanic sensor was placed near a lab-scale pipe that was under cathodic protection. The galvanic sensor responded to the cathodic protection current even though it was not electrically connected. Since the direction of sensor current reflected the flow of current from the cathodic protection system (i.e. stray current), it was concluded that the galvanic sensor was an effective tool for monitoring the effectiveness of cathodic protection.

5.4.4 Crevice

Intensive localized corrosion frequently occurs within crevices and other shielded areas on metal surfaces exposed to corrosives. This type of attack is usually associated with small volumes of stagnant solution caused by holes, gasket surfaces, lap joints, surface deposits and crevices under bolt and rivet heads. It is understood that oxygen depletion is the first step in the development of crevice corrosion. This occurs where the rate of oxygen consumption, as the cathodic reaction, is much higher than the rate of oxygen transport by convection and diffusion. A zone of oxygen depletion then causes imbalances in metal ion, pH and chloride concentrations, which then accelerate the anodic reactions.

The study of crevice corrosion has been conducted using three approaches. One is a qualitative method consisting of a multi-crevice former applied to the surface of a sample using a set torque (ASTM G48). Specimens are immersed in a standardized solution over a long period of time. Alloys susceptible to crevice corrosion are compared by determining the number of sites that initiated under a multiple crevice former. The other is an electrochemical approach involving measuring the critical initiation and passivation potentials. Unfortunately, the current density is not homogeneous over the crevice area and the exact crevice area is unknown. Therefore, the crevice corrosion initiation position, growth of breakdown sites and their propagation rates are uncertain. A third approach is to measure the current between a sample in a 'crevice' and a sample outside a crevice. The 'crevice' can be a solution simulating the interior of a crevice (i.e. low pH, high chloride and metal concentration) or an electrode under a stagnated volume of electrolyte. Differences in electrochemical reaction (anodic versus cathodic) and chemical concentrations cause differences in potential.

A variant of the third approach is to orient the crevice cover perpendicular to the specimen surface instead of parallel to the specimen surface in a gap fashion (Klassen *et al.*, 2001). This can be accomplished by placing an inert cover (of Perspex) with a hole over the specimen under compression as shown in Fig. 5.5. Sealant was also placed on the outside of the

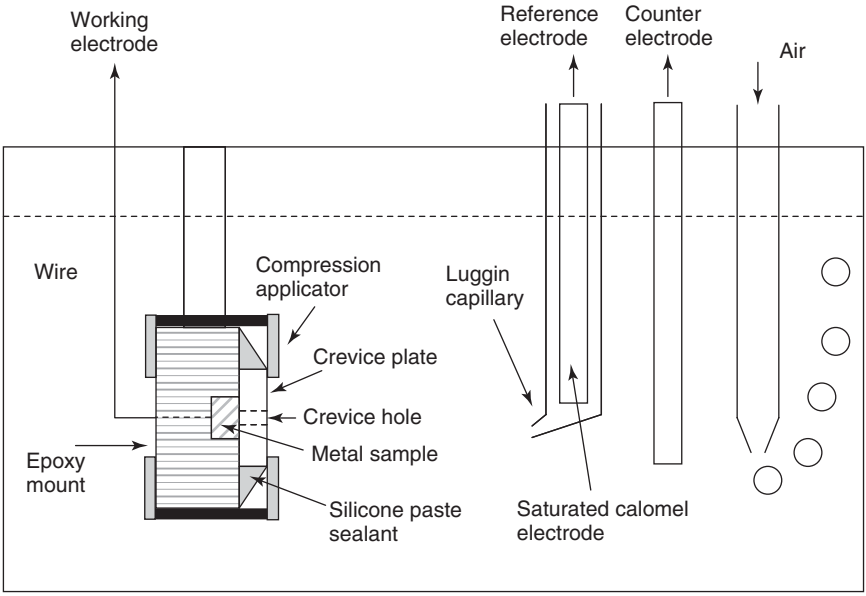

5.5 Schematic of the experimental apparatus for a perpendicular crevice (adapted from Klassen *et al.*, 2001).

cover. Because the current and transport phenomenon in the electrolyte are both normal to the specimen surface, the current can be normalized over the specimen surface area as current density. The intensity of transport resistance can be varied by changing the height of the crevice cover. The greater the cover height, the longer the diffusion path. The current between the specimen and a counter electrode can be measured with a zero resistance ammeter and the potential between the coupled electrodes versus a reference electrode can be measured. The ratio of creviced area to cathodic area can be controlled by the size of the counter electrode. A scanning electron micrograph (SEM) of a nickel aluminum bronze sample after 24 hours is shown in Fig. 5.6. The corrosive effect of the crevice environment is in clear contrast to the unaffected metal outside of the crevice hole, which was dry. Figure 5.7 shows the de-trended current density of two samples of nickel aluminum bronze in aerated 3.5% sodium chloride solution. De-trending was done by subtracting out the average current as obtained by linear regression. Each sample was coupled with a porous graphite counter electrode (0.9 cm dia. and 7 cm long). The exposed area was the same for both (0.18 mm dia.). The depth of the crevice former for the covered sample was 6 mm. As shown, the de-trended current density from the creviced sample was much more erratic compared to the

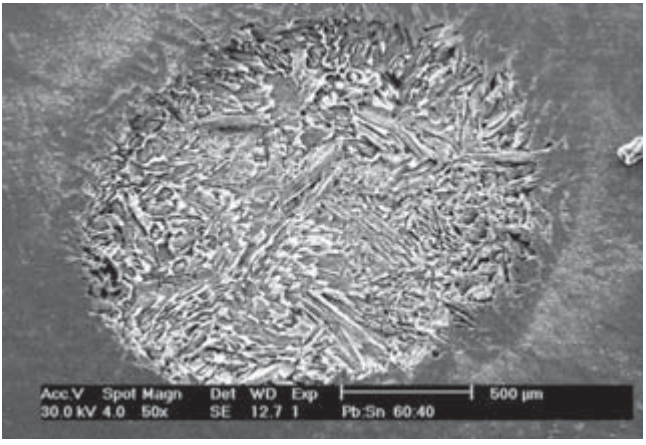

5.6 SEM micrograph of nickel aluminum bronze specimen after 24 hours (50× mag.) with a crevice cover depth of 6 mm and hole diameter of 1.8 mm (adapted from Klassen *et al.*, 2001).

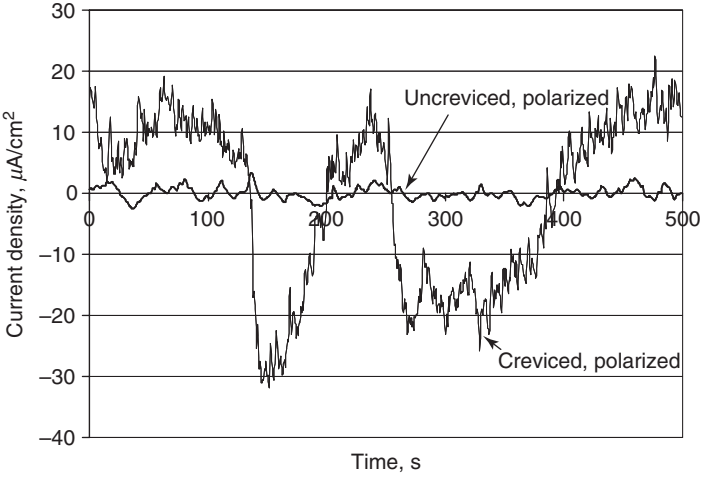

5.7 De-trended current density from nickel aluminum bronze samples. Each was coupled to a graphite counter electrode, one uncovered and the other covered with a 6 mm deep hole (1.8 mm dia.) (adapted from Klassen *et al.*, 2001). The overall current indicated a net anodic current from both samples.

uncreviced sample. As current fluctuations are often associated with localized corrosion events, the crevice environment apparently promoted localized corrosion.

Another variant of the third approach is an application of multi-electrode arrays (MEA). A version of a MEA using the voltage drop

across resistors to measure current was described by Yang *et al.* (2002). Budiansky *et al.* (2006) used a ZRA-coupled MEA to monitor corrosion phenomena along a line perpendicular to the crevice mouth. Figure 5.7 is a schematic showing the relative position of a crevice former, solution and MEA.

Using a MEA to study crevice corrosion requires rescaling of the crevice. It is possible to relate the crevice gap width to the position of maximum attack using a geometric scaling factor (Lee *et al.*, 2004). The scaling factors, or scaling laws, describe the effect of crevice geometry on the corrosion behavior inside the crevice. Two factors are usually used, X/G or X^2/G with X being either the length of the crevice or the distance from the crevice mouth and G being the crevice gap. Using these scaling laws, a rescaled creviced array can be used to monitor the spatial evolution of the current during the initiation of crevice corrosion.

Figure 5.8 shows a planar view of the MEA electrode assembly with an array of micro-electrodes (5 × 20) embedded in epoxy-filled groove. A drilled and tapped hole was used to hold down the crevice former. The stainless steel encasing becomes part of the crevice, albeit not instrumented. For a crevice gap of 1 µm, inclusion of this surface allowed the metal area to crevice volume to be $10^4\,cm^{-1}$, which is the same as that for a conventional crevice sample (ASTM G48).

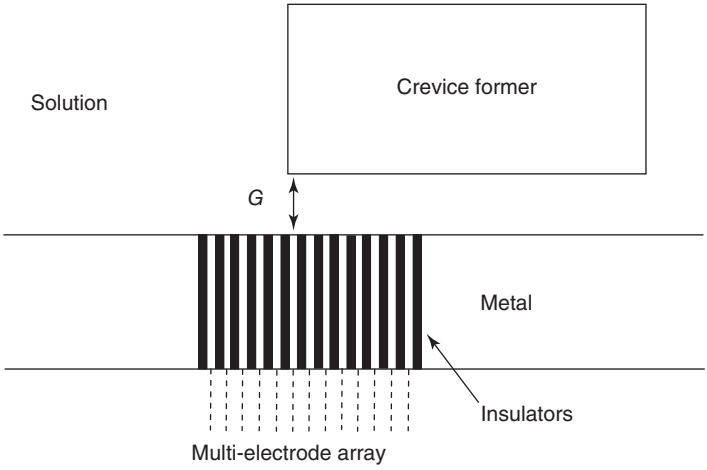

5.8 Schematic of MEA with crevice former: *G* is the gap distance (adapted from Budiansky, 2006).

5.4.5 Concrete

Gonzalez *et al.* (1995) compared the ability of surface potential and galvanic current to distinguish zones of actively corroding and passive sections of rebar in concrete. The experimental setup is shown in Fig. 5.9. A counter electrode and reference electrode were connected with a wet pad to the concrete block. The working electrode was the rebar. Part of the rebar was actively corroding by chloride and part was kept passive. In Fig. 5.10(a), the rebar was contiguous between these sections and in Fig. 5.10(b) these sections were separate. Both surface potential and galvanic current were able to clearly distinguish between the active and passive sections when these rebar sections were separate. However, neither was able to clearly distinguish the active and passive sections when the rebar was contiguous as is normally the case in working installations.

The lifetime of a concrete structure can be considered to be the sum of the time required to initiate corrosion and the time required for corrosion propagation to develop enough to cause concrete cracking (Budiansky, 2006). One solution is to use rebar alloys with more cor-

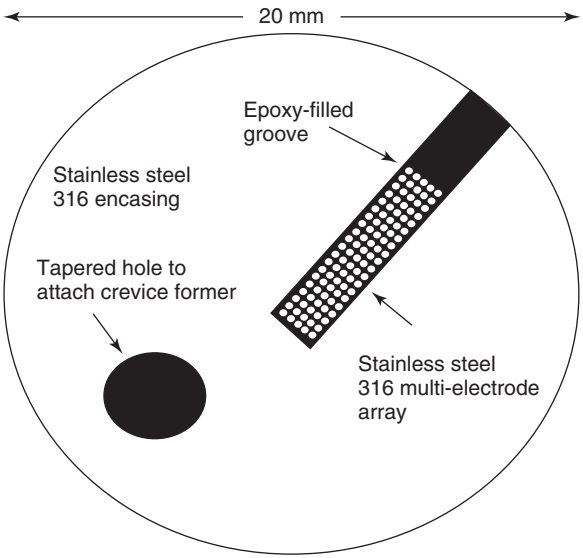

5.9 Planar view of MEA used in crevice experiments. The solid metal encasing was grooved to allow the MEA to be mounted in the center of the encasing. Additionally, the threaded hole for the crevice former attachment is shown. Adapted from Budiansky (2006).

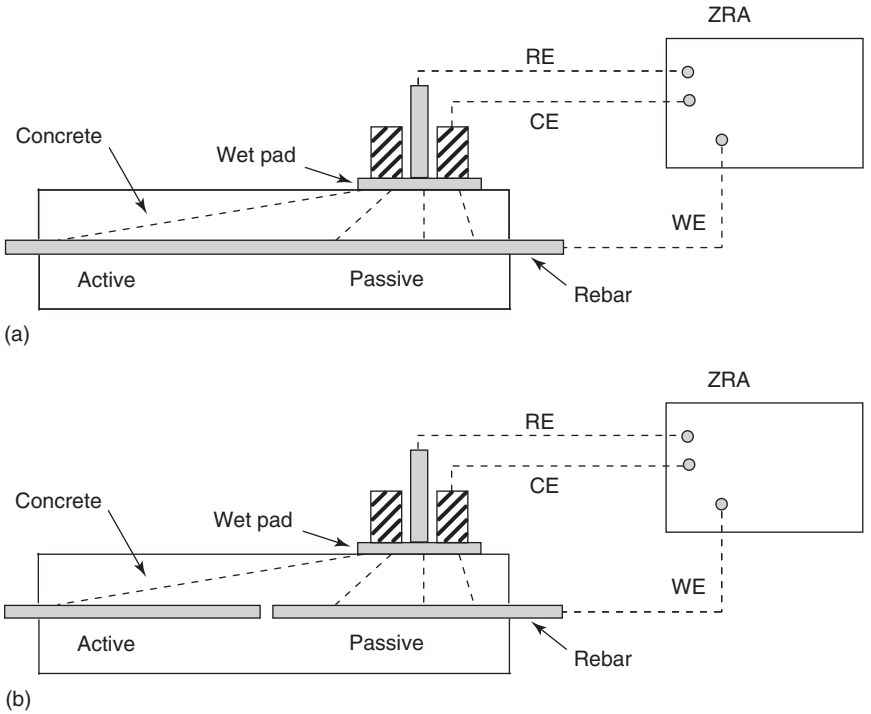

5.10 Concrete ZRA probe over active and passive sections of rebar. In (a) these sections are contiguous whereas in (b) they were separate (adapted from Gonzalez *et al.,* 1995).

rosion resistance than conventional carbon steel rebar at both initiation and propagation. To qualify new rebar materials, the chloride threshold for corrosion initiation, radial and lateral propagation rates, and the Pilling-Bedworth ratios (ratio of the relative volume of an oxide and its parent metal) must be determined. MEAs provided a technique to examine the lateral corrosion spreading behavior of new candidate rebar alloys when embedded in concrete. Early measurements clearly distinguished differences in corrosion propagation between carbon steel and AISI 316L stainless steel (UNS S31603) with 100 wire MEAs. Carbon steel held at $0.2V_{SCE}$ displayed active corrosion that initiated quickly and spread rapidly over the entire MEA surface in less than 2000 seconds. However, 316L stainless steel showed no corrosion spreading from preferentially active sites (held at $1V_{SCE}$) on to surrounding electrodes (held at $0.2V_{SCE}$) despite a considerably more aggressive testing environment.

5.5 Future trends

Assuming we want more information than seeing frog's legs twitch wildly, a key question is whether the unvarnished galvanic sensor is an adequate way of quantifying corrosion processes. A limitation to measuring only galvanic current is that changes in ionic resistance between electrodes can confound indications of corrosion activity. A way around this is to measure ionic resistance independently from galvanic current. Since this can be done by measuring the impedance at high frequency, one must ask why not use the same electronics for a full frequency scan and measure corrosion rate as an EIS sensor? For example, Davis *et al.* (2005) have described an EIS sensor that is under development for measuring atmospheric corrosivity and coating integrity.

The answer to the question of how or if a galvanic sensor can be utilized depends on the time frame of interest, the nature of the electrolyte and the relative importance of geometry. An EIS scan with sufficient low-frequency measurements to obtain a reasonably accurate measure of corrosion rate (via polarization resistance) takes about 30 minutes. The factors that drive atmosphere, soil and concrete are slow moving compared to this time frame. Therefore, EIS may be the best approach for these applications. Localized corrosion events, on the other hand, can occur over a time frame of seconds. If localized corrosion is the phenomenon of interest and if the electrolyte resistance is consistently low compared to the corrosion resistance, then a galvanic sensor is probably the best option. Electrochemical noise (EN), which is described in Chapter 4, utilizes this approach. In a cooling water system then, an EN probe in the pipe of interest is probably preferable to the split electrode system described in Section 5.4.2. This is because the corrosivity in the slow flow leg may not be representative of the conditions in the cooling water and there are many subtleties in the analysis of EN data that would be missed with simply observing the overall galvanic current. In the study of crevice corrosion, the perpendicular crevice with a galvanic circuit, described in Section 5.4.4, seems to be a reasonable way to study certain crevice parameters. In a gap crevice, where the corrosion process is very sensitive to geometry with respect to the crevice former, MEAs seem to be the best option since they are designed to provide spatial resolution. The addition of EIS capability to each electrode in an MEA adds even more value to this application (Cooper *et al.*, 2006).

5.6 References

Abbott WH (2002), 'Field Experience in Evaluation of a Wireless Corrosion Sensor', 5th International Aircraft Corrosion Workshop, sponsored by the Naval Air

Systems Command and the Office of Naval Research, Solomons, Maryland (August).
Agarwala VS (1996), 'In-situ Corrosivity Monitoring of Military Hardware Environments', *Corrosion* 1996, Paper No. 632, NACE International.
ASTM (n.d) ASTM G48, Standard Test Method for Pitting and Crevice Resistance of Stainless Steels and Related Alloys by Use of Ferric Chloride Solution, American Society for Testing and Materials.
Baboian R and Prew P (1993), 'Low-Cost Electronic Devices for Corrosion Measurements', *Materials Performance*, (July) p. 58.
Budiansky ND, Bocher F, Cong H, Hurley MF and Scully JR (2006), 'Use of Coupled Multi-Elecrode Arrays to Advance the Understanding of Selected Corrosion Phenomenon', NACE International, San Diego, CA, Paper 06677.
Choi YS, Kim J-G and Yang SJ (2006), 'A Galvanic Sensor for Monitoring the Corrosion Damage of Buried Pipelines: Part 2 – Correlation of Sensor Output to Actual Corrosion Damage of Pipeline in Soil and Tap Water Environments', *Corrosion*, (June) pp. 522–32.
Choi YS and Kim J-G (2006), 'A Galvanic Sensor for Monitoring the Corrosion Damage of Buried Pipelines: Part IV. Electrochemcial Tests to Determine the Correlation of Probe Current to Cathodic Protection Conditions', NACE International, San Diego, March, Paper No. 06324.
Choi YS and Kim J-G (2005), 'A Galvanic Sensor for Monitoring the Corrosion Damage of Buried Pipelines: Part 1 – Electrochemical Tests to Determine the Correlation of Probe Current to Actual Corrosion Damage in Synthetic Groundwater', *Corrosion*, 61(3), pp. 293–301.
Cooper KR, Smith M, Scully JR and Budiansky ND (2006), 'Development of a Multielectrode Array Impedance Analyzer for Corrosion Science and Sensors', NACE International, paper No. 06674, San Diego, CA.
Davis GD, Raghu S, Carkhuff BG, Garra F, Srinivasan R and Phillips TE (2005), 'Corrosion Health Monitor for Ground Vehicles', Tri-Service Corrosion Conference, 14–18 November, Orlando, FL.
Fontana MG (1986), *Corrosion Engineering*, New York: McGraw Hill.
Gonzalez JA, Benito M, Feliu S, Rodriguez P and Andrade C (1995), 'Suitability of Assessment Methods for Identifying Active and Passive Zones in Reinforced Concrete', *Corrosion*, 51(2), pp. 145–52.
Klassen RD and Roberge PR (2003), 'Role of Solution Resistance in Measurements from Atmospheric Corrosivity Sensors', *Corrosion* 2003, NACE International, Houston, Paper No. 3427.
Klassen RD and Roberge PR (2006), 'Technical Note: Measuring Corrosiveness with a Dual Galvanic/Surface Film Resistance Sensor', *Corrosion*, 62(3), p. 195.
Klassen RD, Roberge PR and Hyatt CV (2001), 'A Novel Approach to Characterizing Localized Corrosion Within a Crevice', *Electrochimica Acta*, 46(24–25), pp. 3705–13.
Lee JS, Reed ML and Kelly RG (2004), 'Combining Rigorously Controlled Crevice Geometry and Computational Modeling for Study of Crevice Corrosion Scaling Factors', *Journal of the Electrochemical Society*, 143(8), pp. B423–B433.
Mansfeld F (1982), 'Electrochemical Methods for Atmospheric Corrosion Studies', Chapter 9 in *Atmospheric Corrosion*, Ed., WH Ailor, New York: John Wiley & Sons, p. 139.

Mansfeld F, Tsai S, Jeanjaquet S, Meyer E, Fertig K and Ogden C (1982), 'Reproducibility of Electrochemical Measurements of Atmospheric Corrosion Phenomena', in *Atmospheric Corrosion of Metals*, ASTM STP 767, SW Dean, Jr, and EC Rhea, Eds., American Society for Testing and Materials, pp. 309–38.

Sereda PJ (1958), *American Society for Testing and Materials Bulletin* No. 228 (February), pp. 53–5.

Sereda PJ, Croll SG and Slade HF (1982), 'Measurement of the Time-of-Wetness by Moisture Sensors and Their Calibration', Atmospheric Corrosion of Metals, ASTM STP 767, SW Dean, Jr, and EC Rhea, Eds., West Conshohocken, PA: American Society for Testing and Materials, pp. 267–85.

White ML and Leidheiser Jr H (1990), 'The Corrosion Coulometer – A New Corrosion Monitor for Steel Structures', *Corrosion*, 46(8), p. 653.

Yang B (1995), 'Method for On-Line Determination of Underdeposit Corrosion Rates in Cooling Water Systems', *Corrosion*, 51(2), pp. 153–65.

Yang B (2000), 'Real-Time Localized Corrosion Monitoring in Industrial Cooling Water Systems', *Corrosion*, 56(7), pp. 743–56.

Yang L, Sridhar N, Pensado O and Dunn DS (2002), 'An In-Situ Galvanically Coupled Multielectrode Array Sensor for Localized Corrosion', *Corrosion*, December, pp. 1004–1014.

6

Differential flow through cell technique

BO YANG, Honeywell, Ridgefield, Connecticut, USA

6.1 Introduction

In this chapter, a corrosion measurement technique, i.e., the differential flow cell method, designed for on-line and real-time determination of the rates of localized corrosion (such as pitting, crevice/under-deposit corrosion, microbiologically influenced corrosion or MIC and galvanic corrosion) of metals used in cooling water systems is described. The chapter begins with a detailed discussion of the operating principles of the method. The localized corrosion rate calculation methods, typical flow cell and monitoring instrument design, verification of the results by other known reliable measurement methods, and guidance on data interpretation are provided. The usefulness of the methods is also discussed. The chapter ends by pointing out future developmental needs of the method to broaden its application potential. Examples of laboratory and field applications of the methods are described in Chapter 23.

6.2 Principles of the differential flow cell (DFC) method

6.2.1 The problem the method was designed to solve

Because of differences in system design, water temperature, flow rate, metal alloy composition, water chemistry, chemical treatment and operation variations, cooling water systems suffer many different forms of corrosion. Commonly observed forms of corrosion in cooling water systems include general (or uniform) corrosion, pitting, crevice/under-deposit corrosion, galvanic corrosion, microbiologically influenced corrosion, stress-corrosion cracking, erosion-corrosion, corrosion fatigue, cavitation damage, and selective dissolution (or de-alloying) corrosion. Except for general (or uniform) corrosion, all of these forms of corrosion can be classified as localized corrosion, since the corrosion damage does

not occur uniformly on the whole surface of the exposed metallic component (see Chapter 2).

Based on field survey results and industrial experience,[1–4] the most commonly observed forms of localized corrosion for components made of carbon steel, cast iron, galvanized steel and aluminum in cooling water systems are pitting, crevice/under-deposit corrosion, and microbiologically influenced corrosion. For stainless steel components, stress corrosion cracking is the predominant cause of corrosion failures.[3–7] Pitting and under-deposit corrosion, often associated with microbial activity, are also frequently observed. Furthermore, pitting and under-deposit corrosion on stainless steel components (e.g., heat exchangers) often become the initiation sites leading to the subsequent stress corrosion cracking failures. For components made of copper and copper alloys, corrosion failures are often attributed to under-deposit corrosion, microbiologically influenced corrosion, selective dissolution (e.g., dezincification), ammonia corrosion and erosion-corrosion.[4,8]

Ferrous metals such as carbon steel, cast iron and galvanized steel are among the most widely used structure materials in industrial cooling water systems. Transfer lines or pipes, heat exchanger shells, tubes, baffles and water boxes, pump components, valves, screens, plumbing fixtures and cooling tower basins and other tower components are often made of these ferrous metals. Localized corrosion, such as pitting, crevice/under-deposit corrosion and microbiologically influenced corrosion is usually the main limiting factor in determining their service life in cooling water systems.[1–3] The complex and dynamic nature of industrial operations, combined with the lack of effective monitoring tools, mean little is known about the impact of variations in process conditions and water chemistry on localized corrosion. As a result, premature equipment failures occur, in spite of the use of relatively large design safety factors. A recent survey of the Japanese petrochemical industry shows that more than 70% of cooling water failures of carbon steel heat exchangers are due to localized corrosion.[1–2] In addition, 59% of industrial heat exchangers have lifetimes of less than 10 years. Obviously, reduction of localized corrosion will lead to the extension of equipment service life. Hence, the ability to reliably monitor and control localized corrosion is a major industrial need.

Many direct or indirect measurement techniques are available for corrosion assessment.[9–10] Indirect measurement techniques, such as pH, conductivity, corrosive ion or corrosion product ion concentrations (e.g., chloride or ferrous ions), temperature and flow rate measurements, measure parameters that may greatly influence, or are influenced by, the extent of corrosion. While these indirect measurement methods are generally useful for predicting or assessing the potential risk of corrosion and may also be useful

for process control, they do not yield quantitative corrosion rate results. To obtain quantitative corrosion information, direct corrosion measurement techniques are used.

The commonly used methods that measure the extent of corrosion directly in industrial water systems include weight (mass) loss methods such as coupons (see Chapter 9), polarization resistance-based methods (see Chapter 3), electrical resistance-based methods (see Chapter 11), and plant equipment inspection or failure analysis.[1,9,11–13] Although both coupons and plant equipment inspection or failure analysis can provide useful information about corrosion, obtaining quantitative corrosion rate data (especially localized corrosion data, such as maximum pit depth) from these methods is often time-consuming and costly. They usually require equipment shutdown or sample extraction. Furthermore, these two methods only yield the average corrosion rate over the period of exposure, typically ranging from several months to several years. Since many important factors influencing corrosion (e.g., temperature, flow rate, solution composition, inhibitor and/or chemical treatment dosages, and pH, etc.) in an industrial or commercial system are time-dependent variables, it is usually very difficult (if not nearly impossible) to identify clearly the root causes for the observed high corrosion rate based on equipment inspection and/or coupon analysis results. In addition, equipment inspection methods do not permit remedial measures to be taken before significant damage to the system components has occurred. On the other hand, polarization resistance- and electrical resistance-based methods cannot be used to determine the localized corrosion rate because the corrosion rate obtained is averaged over the whole surface area of the test probe that is generally not corroded uniformly.

To obtain more timely information about localized corrosion, several techniques, including the polarization resistance-based general corrosion monitor pitting index (or imbalance technique, similar to electrochemical noise), electrochemical noise techniques (see Chapter 4), scanning vibrating electrode techniques, and zero resistance ammeter-based occluded cell techniques, have been used to monitor or study localized corrosion.[9–11] However, none of these techniques can be used to obtain an accurate quantitative localized corrosion rate under normal corrosion conditions because the anodic corrosion and cathodic corrosion reactions do not occur at well-separated sites and times. They remain largely qualitative in measuring localized corrosion.

To overcome these limitations, the differential flow cell (DFC) method was developed recently for the real-time, on-line and reliable measurement of localized corrosion rates (e.g., pitting, crevice/under-deposit corrosion, microbiologically influenced corrosion, and galvanic corrosion) of metals in industrial water systems.[1,11–16] In the rest of the chapter, the term localized

corrosion is narrowly defined to include only pitting, crevice/under-deposit corrosion, microbiologically influenced corrosion, and galvanic corrosion.

6.2.2 The physical model

The DFC method was initially developed for measuring pitting, and crevice or under-deposit corrosion of carbon steel in cooling water systems.[13] In cooling water systems, propagating pitting and crevice or under-deposit corrosion on carbon steel has similar characteristics. They can all be considered as a form of 'concentration cell' corrosion. Concentration cell corrosion occurs when metal surfaces encounter very different physical and chemical conditions within the same water system. These differences predispose specific surface sites to localized corrosion. At these sites, an increase in the corrosive nature of the process conditions or water chemistry can lead to the formation of a localized corrosion cell (a pit). Examples of metal surfaces that are predisposed to pitting corrosion are:

- A surface beneath a deposited particle (mineral scale, corrosion product, silt).
- A surface beneath a biofilm deposit.
- A surface between rifled tube grooves.
- A surface immediately after a weld or flange.
- A surface behind a baffle, within a 'dead-leg', or other low flow areas.
- A surface that is touching the surface of a different material.
- A surface with microstructure defects or impurities (e.g., sulfide inclusion).

These metal surface differences allow for the creation of anodes and cathodes (regions differing in electrochemical potential) that are localized within a micro-environment. Differences in dissolved ion (or other chemical) concentration, such as hydroxyl ion, oxygen, chloride and sulfate, eventually develop between predisposed and nearby regions. In this way, localized corrosion cells are established. The predisposed sites become anodic, resulting in loss of metal to the solution ($Fe \rightarrow Fe^{2+} + 2e^-$). The nearby 'open' sites become cathodic, causing oxygen reduction to form hydroxide ($H_2O + 1/2O_2 + 2e^- \rightarrow 2OH^-$). The predominant cathodic reaction in the corrosion of carbon steel or copper alloys is normally oxygen reduction in cooling water systems with a pH value typically between 6.5 and 9.5. Hydrogen evolution occurring in pits or under-deposit corrosion sites generally contributes only a small part to the overall cathodic corrosion current.[1] It should be noted that when low pH upset operating conditions (e.g., acid overfeed, acid cleaning or excessive growth of acid-producing bacteria) are present in the system, hydrogen evolution reaction may become the major contributor to the corrosion processes. Similarly, halogen

reduction reaction may become the major contributor to the corrosion processes when overfeed of an oxidizing biocide occurs. The generation of hydroxide results in highly alkaline localized surface conditions, which can result in the formation of a mixed deposit, containing corrosion products and mineral scales (e.g., $Fe(OH)_2$, $Fe(OH)_3$, $FePO_4$, $Mg(OH)_2$, $Ca_3(PO_4)_2$, and $Zn(OH)_2$, etc.). The intense localized attack at the site leads to the formation of a deposit layer that is porous and not as protective as the inhibited deposit layer formed at other parts of the surface. The presence of relatively high concentrations of corrosion product metallic ions (such as Fe^{2+}, Fe^{3+}, Cu^{2+} and Al^{3+}) near the corrosion sites is generally known to have a significant negative effect on the performance of scale inhibition and particle dispersing ability of dispersant polymers typically included in cooling water treatments and would be one of the contributing factors in forming the porous, loosely attached and less protective deposit layers on the corrosion sites.

As localized corrosion proceeds, a crust (called a 'tubercle') can form over the top of the localized corrosion site, creating an under-deposit localized corrosion environment. Biofilm or biofouling may also start to accumulate around the deposits covering the localized corrosion site (the pit) under suitable conditions.

Systematic investigation carried out by Yang and coworkers[1,11–13,16–17] shows that the anodic and cathodic current distribution around a localized corrosion (e.g., pitting, crevice or under-deposit corrosion) site can be represented by a model shown in Fig. 6.1. In other words, the mixed potential corrosion theory is found to be applicable to the typical localized corrosion conditions. According to this model, the anodic reaction and cathodic

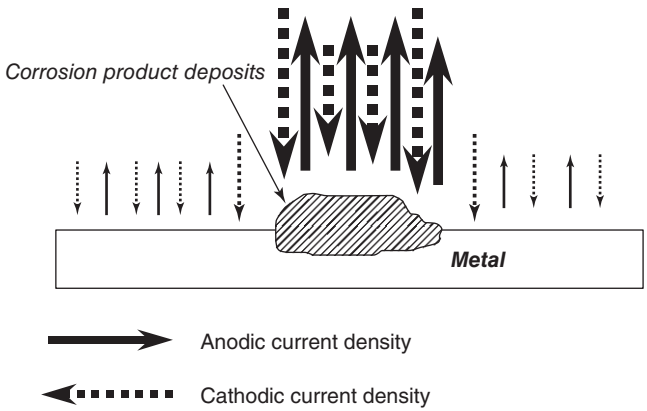

6.1 Physical model for the DFC method – distribution of anodic and cathodic currents around a localized corrosion site.

reaction of the corrosion process can occur at the same surface location at the same time around a localized corrosion site.

The anodic current density is proportional to the rate of metal dissolution partial reaction in the corrosion process. The cathodic current density is proportional to the cathodic partial reactions in the corrosion process. In cooling water systems, the cathodic partial reactions are commonly comprised of oxygen reduction, halogen (commonly used as oxidizing biocide) reduction and hydrogen evolution (e.g., inside the localized corrosion sites for carbon steel, other ferrous metals, and aluminum alloys, etc.). Experimental studies demonstrate that the model depicted in Fig. 6.1 can be used to describe the localized corrosion processes of carbon steel, admiralty brass, aluminum alloys and magnesium alloys in aqueous fluids,[1,16–17] such as cooling water, process water in a paper mill and food processing plant, boiler steam condensate, vehicle engine coolant[16] and oil-field production stream.[18]

6.2.3 The DFC method to obtain localized corrosion rate

The DFC method uses an electrolytic cell assembly to simulate the localized corrosion conditions of interest and an electrical instrument/data acquisition system to measure the localized corrosion rate in real-time from the simulation cell.[11,13,14] A unique combination of linear polarization resistance (LPR) and zero resistance measurements (ZRA) is usually used to obtain the rate of localized corrosion (such as pitting, crevice/under-deposit, microbiologically influenced corrosion, and galvanic corrosion) for metals in aqueous solutions from the simulation electrolytic cell.

Typical electrolytic cell assembly

Several methods have been used to configure the electrolytic cell assembly to simulate the localized corrosion conditions.[1,13,16,19] In a typical application in cooling water systems, the electrolytic cell assembly has a differential flow cell configured to simulate the essential features of the propagating localized corrosion process. The flow cell generally contains two small anodes commonly placed in a slow flow condition and one large cathode placed in a faster flow condition. The anodes are used to simulate the preferential or localized attack areas of the metal in a system. The large cathode simulates the non-preferential attack area of the metal. To simulate faithfully the localized corrosion conditions, the anodes and the cathode are normally connected electrically together via a zero-resistance ammeter (ZRA) in the electrical instrument assembly to allow the occurrence of galvanic interaction among them. Fig. 6.2 shows a flow cell design for use in field applications in commercial or industrial cooling water systems.

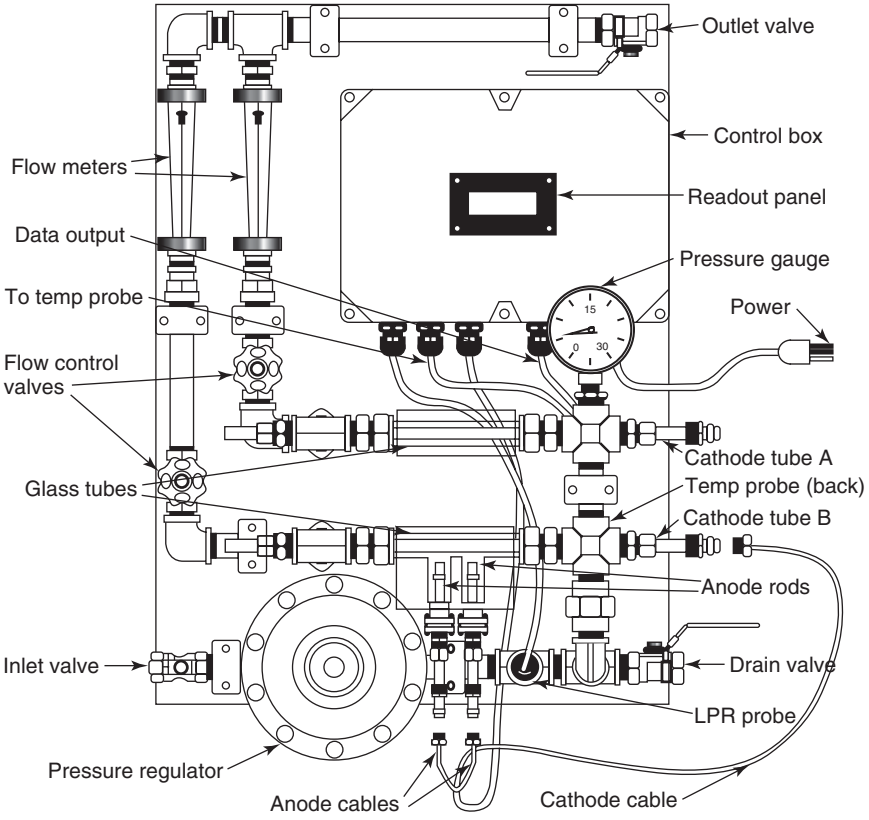

(a)

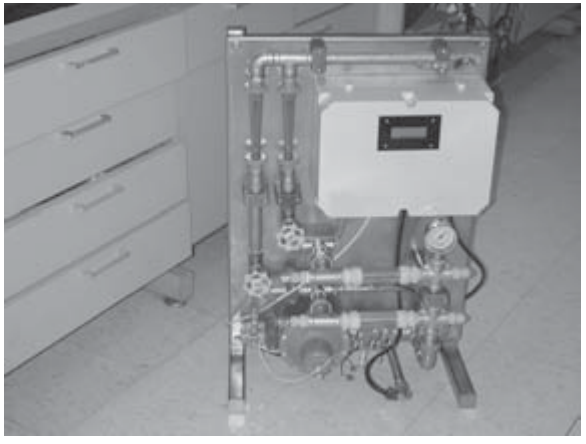

(b)

6.2 (a) Schematics of a localized corrosion monitor (LCM) based on the DFC method for use in cooling water systems; (b) photo of the DFC-based localized corrosion monitor (LCM) with optional stand.

The flow cell shown in Fig. 6.2 can be used to simulate the localized corrosion conditions found in tube side heat exchanger and pipeline, or shell side heat exchanger flow conditions. When the flow cell is used to simulate localized corrosion in a shell side heat exchanger, the cathode tube A placed in the upper glass tube is used as the cathode and the flow rate in the cathode flow channel is set at a higher flow rate than the one at the lower flow channel where the anodes are located. When the flow cell is used to simulate localized corrosion conditions in a tube side heat exchanger or in a pipeline, the cathode tube B placed in the lower glass tube is used. In this case, the anodes are usually recessed into the ports to create a slower flow condition than the one experienced at the cathode tube surface. The flow rates in the two flow channels and the distance between anodes and cathode tube B may be adjusted to better simulate the localized corrosion conditions in the cooling water system of interest. The flow rates used in the type of set-up shown in Fig. 6.2 were typically between 45 to 1130 L/h or about 0.04 to 2.3 m/s. More information about using tube A or tube B will be described in Chapter 23 where the application examples of the method are provided.

A number of other different designs of the electrolytic cell were also used, including the use of various occluded cells (e.g., lead-in-pencil type set-up commonly used in many pitting and crevice corrosion studies) designs, anode or cathode or both under different heat-rejection conditions and various anode/cathode configuration designs for studying galvanic corrosion. Wide ranges of exposed anode and cathode surface areas can be selected to simulate the application conditions. Exposed anode surface areas used in the DFC method were often between 0.07 to 2 cm^2. The cathode/anode surface area ratio was typically between 1 and 1000. In practice, one should choose the most appropriate design to simulate realistically the localized corrosion process under study.

Electrical instrument assembly

The electrical instrument assembly typically consists of a zero resistance ammeter (ZRA), a polarization resistance (or LPR) based general corrosion monitor with IR-drop compensation capability, instrument control and data acquisition system. In addition, relay switches, a display or read-out panel, data output (e.g., as 4–20 mA signals), power source conditional circuit and instrument enclosure, etc. may also be included in the instrument assembly. In the design shown in Fig. 6.2, the electrical instrument assembly is housed in the control box. The ZRA, LPR, relay switches, data acquisition and control and data analog outputs are all integrated in a circuit board placed inside the control box. The control box also has an enclosure (rated NEMA (National Electrical Manufacturers' Association)

12X) to protect against circulating dust, falling dirt and dripping non-corrosive liquids. The monitor design shown in Fig. 6.2 also has a probe to measure the general corrosion rate, and a sensor to measure the temperature of the test fluid. Sensors to detect other parameters (e.g., pH, flow rate, conductivity, corrosion and scale inhibitor concentrations, biocide concentration and corrosive ion or corrosion product concentrations, such as Cl^- and Fe^{3+}, etc.) important to the corrosion process may also be included in the assembly.

Methods to obtain localized corrosion rates

Three methods can be used to determine the localized corrosion rates from a DFC cell.[11,13,19] One method is based on the Tafel extrapolation of the anodic polarization curve of the anode (or the slow flow electrode) to the corrosion potential of the DFC cell (i.e., the corrosion potential recorded when the anodes and cathode are connected together). The second method is based on measuring the polarization resistance of the anodes and cathode connecting together, and the polarization resistance of the cathode when it is temporarily disconnected from the anode. A detailed description of these two methods is given in previous publications.[13,19] In theory, the Tafel extrapolation should have yielded the most accurate localized corrosion rate. The second method (polarization resistances only) would have underestimated the localized corrosion rate if the corrosion potential of the cathode alone was more positive than the corrosion potential of anodes and cathode connected together. It should be noted that the Tafel extrapolation method is generally not suitable for use to monitor the localized corrosion rate as a function of time, because it is considered a destructive method and the surface conditions of the anode generally change irreversibly after the measurement.

The third method of determining localized corrosion rates is commonly used to determine localized corrosion rates from a DFC-based localized corrosion monitor (e.g., a typical design is shown in Fig. 6.2). The localized corrosion current density ($I_{\text{localized corrosion}}$) of the anode is calculated according to the following equation:[11,13,19]

$$I_{\text{localized corrosion}} = I_{\text{ZRA}} + I_{\text{LPR}} \qquad [6.1]$$

where I_{ZRA} represents the galvanic coupling current density measured between the anode and the cathode from the differential flow cell; I_{LPR} represents the LPR (or linear polarization resistance) corrosion current density measured from the anode alone when the anode is temporarily disconnected from the cathode. (Note: To obtain a more accurate result, a solution ohmic decrease-compensated instrument should be used to measure the polarization resistance.) The Stern–Geary constant for the

metal used for the anode is calculated from either the Tafel slopes measured experimentally or the Tafel slopes recommended in the literature or obtained in previous studies under similar corrosion conditions. The localized corrosion rate of the anode is calculated from the localized corrosion current density, Faraday constant, equivalent weight, and density of the anode. I_{LPR} reflects the contribution of cathodic reactions (e.g., oxygen reduction, hydrogen evolution and halogen reduction, etc.) occurring on the anodes toward their own corrosion. I_{ZRA} reflects the contribution of cathodic reactions occurring on the cathode toward the corrosion of anodes or it reflects the contribution of the galvanic interaction among the anodes and cathode toward corrosion of the anodes.

In a DFC cell design shown in Fig. 6.2, two localized corrosion rates may be obtained as a function of time from the cell according to Equation [6.1]. In some earlier designs of DFC method-based localized corrosion monitor, both localized corrosion rates from the two anodes were reported. In a newer design, only the maximum value of the two readings from the two anodes at a given time was reported. In addition, the time average of the localized corrosion rate and the general corrosion rate (the rate averaged over the surface area of the electrodes of the linear polarization resistance (or LPR) probe) are also saved and displayed in the DFC design shown in Fig. 6.2.

In theory, Equation [6.1] or the third method yields an approximate localized corrosion rate. It was deduced under two assumptions: the corrosion attack at the anodes was uniform and the corrosion potential (E_{corr}) of the anodes alone was not much different from the E_{corr} of anodes and cathode connected together. For electrodes made of carbon steel, the first assumption can be met in most cases. It has been observed in >20 field applications of the DFC-based localized corrosion monitor that the corrosion attack on the anodes was quite uniform, especially after exposure longer than several days since the anodes usually were covered completely by corrosion products and other deposits. It should also be noted that in several laboratory tests using aluminum alloys as the anode in engine coolants, the corrosion attack on the anode was also uniform based on post-test visual examination. In bench-top tests using two rotators to create the differential flow conditions, the E_{corr} of the anode alone was generally more negative than the E_{corr} when the anode and cathode were connected together. Depending on the difference in the extent of corrosion on the carbon steel anode and the carbon steel cathode, the difference in E_{corr} values was as much as 50 mV to 60 mV several minutes after disconnecting the anode from the cathode. In theory, this means that Equation [6.1] would have tended to overestimate the localized corrosion rates. However, as shown in previous studies, the overestimation was not significant. The differences between localized corrosion rates determined using Equation [6.1] and the

rate determined from Tafel extrapolation of the anode-only anodic polarization curve to the E_{corr} of the anode and cathode connected together were <20%. The high cathodic Tafel slope values typically observed in cooling water system applications and the fact that the main cathodic reaction (i.e., oxygen reduction) in the anode corrosion process is often close to diffusion control in the observed E_{corr} region may be the likely reasons for the relatively small errors observed. The potential errors of using Equation [6.1] in DFC-based localized corrosion monitors (e.g., Fig. 6.2) due to the differences in E_{corr} appeared to be fewer than the bench-top differential flow cell set-up using two rotators. One reason is that the cathode/anode surface area ratio in the DFC-based field localized corrosion monitors (i.e., >250) shown in Fig. 6.2 was much greater than the one in the bench-top set-up (i.e., 20). Another reason is that the low-flow entrance and exit regions in the field DFC localized corrosion monitor cathode also will corrode preferentially. These factors ensure that there would be many more corrosion sites on the field localized corrosion monitor than on the bench-top set-up. Thus, the relatively high corrosion rates of the anodes tended to have less of an effect on the E_{corr} in the DFC-based field localized corrosion monitor set-up than in the bench-top set-up.

In cases where the corrosion attack on the anode is not uniform, a surface area correction factor should be used in Equation [6.1] to account for the percentage of actual surface suffering corrosion attack. One alternative solution is to change the design of the electrolytic cell used to simulate the localized corrosion. Experiments showed that the use of occluded cell type designs (in this case, the anodes are located in an occluded site similar to the ones found in a crevice; the flow velocity in the anode, or slow flow electrode, can be considered to be negligibly small or close to zero) would be helpful to ensure that the corrosion attack on the anode remain largely uniform.

Another factor to consider is the separation distance between anodes and cathode in an electrolytic cell shown in Fig. 6.2. When the DFC set-up shown in Fig. 6.2 is used to simulate shell-side heat exchanger localized corrosion, the cathode is located in the top flow channel. In this case, the anodes and cathode could be separated by a relatively large distance (e.g., ~10 cm). In cooling water with relatively high conductivity, the additional solution ohmic drop introduced by the separation is not expected to affect the measured corrosion rate substantially after the corrosion sites in the electrodes are covered with a layer of corrosion products. In bench-top experiments using two rotators to create the differential flow conditions, the solution ohmic decreases in the anode corrosion products were 10 times higher than the ones in the solution, even with a solution conductivity as low as 80 μS/cm. Nevertheless, in the absence of corrosion product deposits (e.g., in the initial stage of immersion of a sandpaper-polished anode), the

localized corrosion rate obtained from the lab set-up was reduced by the separation of anode and cathode, especially in cases where the solution conductivity was low (e.g., <200 μS/cm). No systematic investigation has been conducted to study the effect.

6.2.4 Validation of the technique

Similar to other commonly used electrochemical techniques for measuring corrosion, the DFC technique is a simulation measurement method. The advantage is that the DFC-based localized corrosion monitor is an electrochemical measurement device providing a time-averaged localized corrosion rate that is quantitative to that measured independently on the same anodes used in the instrument. In Fig. 6.3, the time-averaged and steady-state localized corrosion rates determined by the DFC-based localized corrosion monitor (LCM) are compared to the results of penetration depth measurements on the DFC anode surfaces.[13] In principle, only the time-averaged corrosion rates should be directly comparable to the corrosion rates determined from penetration depth measurements. However, under well-controlled steady-state conditions, the instantaneous corrosion rates closely approximate the time-averaged rates.

In addition, the localized corrosion rates of carbon steel, admiralty brass and aluminum alloys determined from Equation [6.1] were also shown to

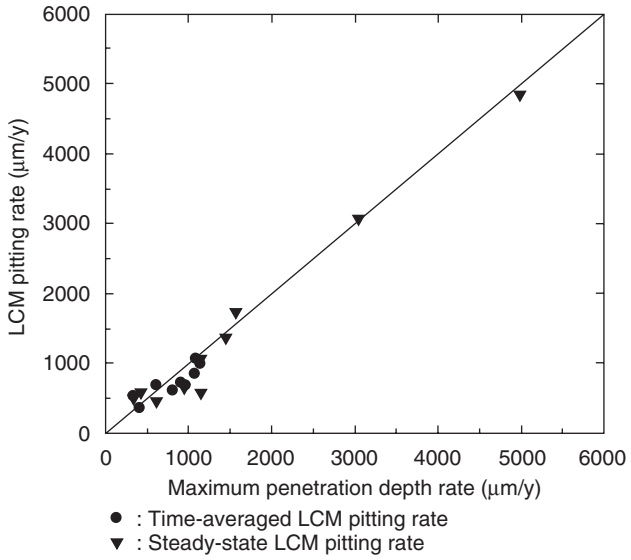

6.3 Comparison of localized corrosion rates obtained from penetration depth measurements and DFC-based LCM readings.

be in agreement with those determined by the Tafel extrapolation of the anodic polarization curves of the anodes, providing further confirmation of the validity of the method.[13,16] Under properly chosen simulation conditions, the corrosion rate results (both localized and general rates) obtained from the DFC-based localized corrosion monitor in the field applications were also in agreement with independent physical measurement (i.e., coupons) and heat exchanger inspection (e.g., ultrasonic inspection) or operation results (e.g., service life or leakage frequency) obtained under comparable conditions.[1,11,14,17]

6.2.5 How to use a DFC-based localized corrosion monitor (LCM) for field applications

Because of its ability to obtain a quantitative, reliable and real-time localized corrosion rate, the DFC method offers great potential for use in localized corrosion research, and localized corrosion monitoring and control in industrial systems. The extensive use of this method in the laboratory and in field applications has been very fruitful for developing new insights into the localized corrosion process, for aiding troubleshooting and failure analysis of cooling water system corrosion-related problems, for developing novel, highly effective, environmentally friendly cooling water corrosion inhibitors, for performance-based optimization and control of chemical treatments (i.e., corrosion inhibitors, scale inhibitors and biocides) in industrial and commercial cooling water systems.[1,11–18,20–30] In the past, the effective use of the method for performance-based optimization and control of chemical treatments in field applications has been the most challenging, because it not only requires substantial corrosion training and knowledge, but it also requires in-depth understanding of modern cooling water chemical treatment technology, as well as detailed knowledge about the operation of the cooling water systems. Thus, guidance is provided below to help a potential user to obtain greater benefits of applying the technique.

The DFC-based LCM (shown in Fig. 6.2) measures the localized corrosion rate, general corrosion rate and water temperature in real-time. The readings are updated every 10–15 minutes. The lower the localized corrosion rate and general corrosion rate, the better corrosion protection the treatment is providing to the system.

Most importantly, one should be less concerned about the localized corrosion rate reading if the general corrosion rate is unacceptably high. In this case, the large amount of corrosion product generated by the high general corrosion rate is likely to result in widespread under-deposit corrosion and scaling problems in other parts of the system. Thus, one should first perform program optimization practices to reduce the general

corrosion rate to an acceptable level. Then, further program optimization can be performed to address any localized corrosion issues.

Corrosion in an industrial system is often non-uniform and is a function of time and location. Thus, one usually observes that corrosion failure in a plant occurs individually at a specific time. For this reason, one should never expect to be able to equate one single corrosion rate reading obtained at a specific location to all the observable corrosion rates in a plant or even within a single heat exchanger. This is true for direct corrosion measurement methods and for side-stream simulation devices.

Therefore, even though the LCM has many distinguished capabilities in measuring localized corrosion, the readings obtained from it do not yield all the corrosion rates occurring throughout an industrial water system. There is only one way to obtain all the actual corrosion rates of a system – to measure them directly from every location in the system. Obviously, this is not an economically sensible approach. The next preferred solution is to install as many LCMs as needed, with each unit set up to obtain localized and general corrosion rate information from well-simulated conditions at each specific location. It is likely that one may need tens or hundreds of LCMs for simulating the different operating environments in a chemical processing plant, paper mill, utility, office building or refinery. Thus, this approach may also not be economically feasible.

Often only one or a few LCMs can be made available for a given plant, leaving two primary options:

1. Simulate a specific plant condition at a particular location of concern. Then, monitor and optimize the treatment for that specific location and condition (for instance, a critical heat exchanger previously known to have corrosion problems).
2. Choose a typical system condition. Then, monitor and optimize the treatment for that specific condition (for instance, water from the cooling water return line).

Based on well-established engineering principles, one can assume that when corrosion under the chosen condition is under good control, other parts of the system are also most likely to be under good control – unless the conditions differ drastically. The benefit of option 1 is that by selecting a critical, highly-stressed system condition, by minimizing localized corrosion at this location, it is very likely that localized corrosion at all other locations will be similarly improved. The challenge of option 1 is that it may be logistically very difficult to plumb-in the LCM sufficiently close to the actual plant equipment of interest (for instance, a critical heat exchanger located 30 m above the ground in the middle of a refinery).

Checking corrosion control at various parts of the system from time to time and making required changes would ensure the success of these

approaches. In this way, the LCM can be used to monitor changes in the corrosivity of the water or the effectiveness of the treatment program to control the propagation of pitting and general corrosion. The data obtained will be most effective in program selection, optimization, control and diagnosis of failure mechanisms.

One should always remember that LCM is a simulation device. It is not a substitution for plant equipment inspection. It does provide new capability in the battle against corrosion. The more techniques one can afford to use to monitor or measure the extent of corrosion, the greater the confidence one will have on the results obtained, and the greater the chance one will be able to keep corrosion under control in an industrial system.

6.3 Data interpretation and use

6.3.1 General considerations for effective carbon steel corrosion control

In order to interpret the LCM localized corrosion data correctly, one must first understand that many factors that influence corrosion are time dependent variables.

Some of the factors known to have a major effect on corrosion are listed below.

Mechanical factors

(a) Composition of the alloy
(b) Structure of the alloy (single phase, multiple phases, and presence of precipitates)
(c) Mechanical state of the alloy (degree of cold work, presence of defects)
(d) Equipment design features (stagnant regions, galvanic contact, etc.).

Operational factors

(a) Upset conditions (e.g., process leaks, extended shut-down, etc.)
(b) Chemical treatments (type and dosages)
(c) Improper treatment program selection or application
(d) Poor control of water chemistry and operating parameters
(e) Economic or environmental restrictions on chemical use or proper dosages
(f) Presence of mechanical stresses
(g) Debris blockage.

Chemical/environmental factors

(a) Water chemistry (O_2, pH, Cl^-, SO_4^{2-}, HCO_3^-, Ca^{2+}, $Fe^{2+/3+}$, PO_4^{3-}, SiO_2, etc.)
(b) Temperature
(c) Flow velocity
(d) Bacteria
(e) Coating.

Owners of an industrial system generally expect a chemical treatment vendor to provide the most cost-effective and reliable solutions to their cooling water system operation problems. One of the problems that chemical treatment needs to provide solutions for is carbon steel corrosion control. Many methods are available for controlling corrosion:

- switch to a more corrosion resistant material
- apply an inert barrier or coating
- use cathodic protection (e.g., sacrificial anodes, such as Zn, Mg alloy or Al)
- use anodic protection (e.g., H_2SO_4 production plant)
- adjust water chemistry
- use corrosion inhibitors.

Use of corrosion inhibitors in the form of a cooling water treatment program is often the most cost-effective solution.

6.3.2 How corrosion inhibitors work

Based on inhibition mechanisms, corrosion inhibitors may be classified into three types: oxidation, deposition, and adsorption inhibitors. Chromate (CrO_4^{2-}) and nitrite (NO_2^-) are oxidation inhibitors, which inhibit corrosion by oxidizing the metal surface, promoting the formation of a protective passive film on the metal surface. Tolyltriazole, benzotriazole, and many organic corrosion inhibitors used in iron oxide cleaning treatments, such as thiourea and acetylenic alcohols, may be considered adsorption inhibitors. Adsorption inhibitors reduce corrosion by forming a thin adsorbed layer on the metal surface. Zn^{2+}, phosphates, pyrophosphate, and phosphonates (e.g., AMP (aminotrimethylene phosphonic acid), HEDP (1-hydroxy ethylidene-1,1-diphosphonic acid), etc.) may be considered as deposition inhibitors. Deposition inhibitors function by forming a compact deposit layer on the metal surface with Ca^{2+} in the solution, Fe^{2+}/Fe^{3+} generated from the corrosion (metal dissolution) process (for phosphates or phosphonates) or OH^- (for Zn^{2+}) generated from the corrosion process (oxygen reduction). Usually, the protective layers formed by deposition inhibitors are thicker than the ones formed by either oxidation or adsorption inhibitors.

Table 6.1 Components in modern cooling water chemical treatments

Classification	Typical active components	Use
All organic	Phosphonates, acrylate based copolymer or terpolymer, azole	Open recirculating systems
Low Zn	Zn^{2+}, phosphate, phosphonate, acrylate based copolymer or terpolymer, azole	Open recirculating systems
Stabilized phosphate	Phosphate, phosphonate or phosphinate, acrylate based copolymer or terpolymer, azole	Open recirculating systems
Alkaline stabilized phosphate	Phosphate, phosphonate or phosphinate, acrylate based copolymer or terpolymer, azole	Open recirculating systems
Zn – phosphonate	Zn^{2+}, phosphonate, acrylate based copolymer or terpolymer, azole	Open recirculating systems
Molybdate	Molybdate, phosphonate, acrylate based copolymer or terpolymer, azole	Open recirculating systems
Silicate – molybdate	Silicate, molybdate, acrylate based polymer, azole	Open recirculating or closed systems
Nitrite – molybdate	Nitrite, molybdate, azole, polymer dispersant	Closed systems
Silicate – nitrite	Silicate, nitrite, borate, azole, polymer dispersant	Closed systems

Deposition corrosion inhibitors are most commonly used for mild steel corrosion protection in open-recirculating industrial cooling systems. Major types and the typical components of the most widely used modern cooling water treatments for corrosion and scale control are shown in Table 6.1.[13,17,25,30–35]

Water soluble inorganic phosphates such as orthophosphates and pyrophosphates are commonly used as the phosphate components in the treatments. Phosphonates typically used in the treatments include PBTC (2-butane phosphono-1,2,4-tricarboxylic acid), HEDP, AMP, HPA (2-hydroxy phosphono acetic acid), and PCAM (phosphono carboxylate acid mixture, or Bricorr 288, a mixture of sodium salts of organophosphonic acid, H-[CH(COONa)CH(COONa)]$_n$-PO_3Na_2, where $n < 5$ and $n_{mean} = 1.4$). The phosphinate used in the chemical treatments is PSO

(phosphinic acid oligomers) which is a mixture of mono, bis and oligomeric phosphinosuccinic acid adduct described in a recent US patent.[31] Acrylate based polymers frequently used include Good-Rite® K797 and K798 (both are acrylate/sodium styrene sulfonate/2-acrylamido-2-methylpropane sulfonic acid terpolymers) from Noveon (OH, USA), Aquatreat® AR-540 (an acrylic acid/2-propenoic acid, 2-methyl, methyl ester/benzenesulfonic acid, 4-[2-methyl-2-propenyl)oxy]-, sodium salt/2-propene-1-sulfonic acid, 2-methyl-, sodium salt quad-polymer) and AR-545 (an acrylic acid/2-acrylamido-2-methylpropane sulfonic acid copolymer) from Alco Chemical (TN, USA), Acumer® 2000 (an acrylic acid/2-acrylamido-2-methylpropane sulfonic acid copolymer), and Acumer® 3100 (an acrylic acid/t-butyl acrylamide/2-acrylamido-2-methylpropane sulfonic acid terpolymer) from Rohm and Haas (PA, USA); acrylic acid/acrylamide/acrylamidomethanesufonic acid terpolymers, acrylate/hydroxypropyl acrylate copolymers, acrylic acid/allyloxy-2-hydroxypropylsulfonic acid copolymers and acrylic acid/allyloxy-2-hydroxypropylsulfonic acid/polyethyleneglycol allyl ether terpolymers.

Azole compounds suitable for use include benzotriazole and tolytriazole. Polymer dispersants suitable for use are generally polyacrylate, or acrylate based polymers. In some cases, PESA, a polyepoxysuccinic acid acting mainly as a calcium carbonate scale inhibitor, is used to substitute the phosphonate or phosphinate used in the phosphate- or zinc-containing chemical treatments listed in Table 6.1. The benefits of using PESA instead of some common phosphonates such as HEDP, PBTC or AMP may include the reduction of polymer demand and in some cases, an enhancement of halogen stability of the treatments if the phosphonate being replaced is not halogen stable. In addition to the corrosion and scale control treatments, a biocide treatment (using either an oxidizing biocide or a non-oxidizing biocide or both) is also generally required for microbial growth control in a cooling water system.[33,35]

The formation of a compact and protective layer on a metal surface using a deposition type corrosion inhibition chemical treatment depends on a number of factors. The important factors include Ca^{2+}, phosphate, Zn^{2+}, calcium carbonate scale inhibitors (e.g., phosphonates, PSO or PESA), and dispersant polymer concentrations, pH and/or alkalinity concentration, water temperature, corrosive ion (e.g., Fe^{3+}, Cu^{2+}, Cl^{-} and SO_4^{2-}) concentrations, flow rate and microbial activity level in the system. Generally, the chemical treatment dosages have to be selected based on the water chemistry and system operating conditions. In order to make correct treatment program optimization decisions, one needs to measure the water chemistry, product feed rates and residual active concentrations and relate to the system's operational and corrosion performance information.

6.3.3 Performance issues in cooling water treatments

Corrosion control, scale control, and microbial control (or biofouling control) are the main performance parameters used to judge whether the application of a cooling water program is meeting the system needs.[1] In addition, compliance of applicable regulations and discharge limits are also the required performance parameters. As in all engineering applications, a safety margin needs to be included in the selection and application of cooling water treatment chemicals and their use dosages. In this regard, past application experience and treatment active monitoring are essential in ensuring the operation of the system in the safe region without excessive chemical feeds. These factors and the cost of the treatment program are then used to establish the cost vs. performance relationships. The cost vs. performance relationships can be used as the objective criteria for choosing a particular treatment for a given system.

Generally, determining whether a chosen treatment program will meet the requirements of applicable regulations and discharge limits is relatively easy to accomplish. It typically requires one to choose the appropriate treatments and/or their dosages to avoid or limit the use of some specified restricted chemicals. In some cases, the effluent can be treated to remove the harmful substances before discharge to the environment. For example, in utilities industry, Na_2SO_3 may be used to react with the residual NaOCl or NaOBr in the blowdown water before discharging it to the river. In this case, only periodical monitoring of NaOCl or NaOBr in the blowdown water to control the Na_2SO_3 feed may be needed.

Controlling scale formation can be easily accomplished via pH control, cycle control, effective use of scale inhibitors and a combination of these methods. Monitoring of scale formation on equipment such as exchangers can also be accomplished with well-established temperature, flow and/or pressure drop measurements. In fact, many chemical processing plants, refineries and power plants are already conducting real time total (including the effects of both water side and process side) heat transfer efficiency measurements on their critical exchangers and/or reactors. Prediction of the likelihood of scale formation under specified conditions based on water analysis results, temperature and flow rate data is also well established, e.g., Langelier Saturation Index[33] and French Creek WaterCycle® software from French Creek Software (PA, USA). Addition of biocides, biodispersants and side-stream filtration to remove nutrients are the proven methods to control excessive microbiological growth and biofouling. In addition, the damaging effects of scaling and biofouling can often be reversed via cleaning. In contrast, the only options of reversing a corrosion failure, e.g., perforation of an exchanger tube, is to replace it with a new tube or cease usage via plugging.

Generally, cooling chemical treatments and their application control parameters are developed based on the general corrosion control performance obtained from laboratory tests and a small number of controlled field tests. In a typical application of the chemical treatments in a cooling water system, general corrosion control performance is also often monitored by periodic testing of corrosion product concentrations, such as Fe^{3+} and Cu^{2+}, in the water. In addition, corrosion coupons are also often used in many systems. Thus, chemical treatment technologies and their application methods to control general (average) corrosion rate to an acceptable level, e.g., <3 mpy (75 μm/y) are generally well developed and widely practiced in many cooling water systems. However, localized corrosion remains unpredictable. Often, the extent of localized corrosion under a given application condition has been the key remaining unknown in the cost vs. performance relationships.[1,17]

6.3.4 Integrated solutions needed to improve cooling water treatment performance

Controlling corrosion, scale formation and biofouling (or microbiological growth) are required for the effective operation of cooling water systems. The problems caused by corrosion, scale formation and biofouling are inter-related (see Fig. 6.4) and can present serious challenges for the normal operation of cooling water systems.

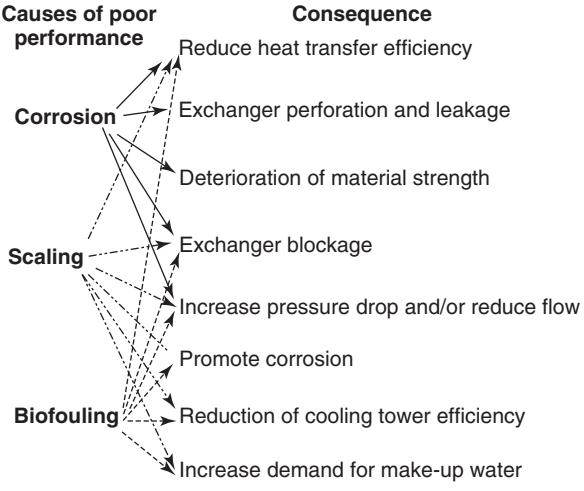

6.4 Problems caused by corrosion, scaling and biofouling in cooling water systems.

The primary function of a cooling water system is to satisfy the heat transfer needs of the plant. Thus, preventing and/or controlling scale and biofouling to ensure adequate heat transfer efficiency is one of the primary requirements a chemical treatment program must fulfill. However, although scaling and biofouling may be controlled to provide effective process cooling needs, they may still pose a serious threat to localized corrosion control. For instance, the tendency of stress corrosion cracking of a stainless steel heat exchanger in a CPI (or chemical processing industry) plant usually increases as scaling and fouling increase. One reason for the need of controlling general corrosion to an acceptable level is to prevent the deposition of corrosion products downstream on other equipment, which may initiate new concerns about reduction of heat transfer efficiency and promotion of further corrosion damage. Under cooling water conditions, a high carbon steel localized corrosion rate is usually observed when the metal is partially protected and/or there is high microbial activity.

Following the operating guidelines provided by the chemical treatment supplier, the carbon steel localized corrosion rate (or pitting rate) in a synthetic plant water containing 450 ppm $CaCl_2$ as $CaCO_3$ was found to vary according to the following chemical program sequence in bench-top tests:[13]

$$\text{Stabilized Phosphate} = \text{Low Zinc} < \text{Alkaline Stabilized Phosphate} < \text{All Organic}$$

While all of these programs can be optimized to give low localized corrosion rates, the treatments that operate at the higher pHs require more attention due to the greater likelihood of under-deposit corrosion, by deposition of calcium carbonate and calcium phosphate in isolated regions of heat exchanger surfaces.

Under the same make-up water chemistry conditions, the recommended operating pH in the recirculating cooling water for the treatment programs typically have the following sequence:

$$\text{Stabilized Phosphate} < \text{Low Zinc} < \text{Alkaline Stabilized Phosphate} < \text{All Organic}$$

Depending on the operating conditions, the following have been shown to be effective in reducing the carbon steel localized corrosion rate:[1,17]

- Adjusting the corrosion inhibitor feed
- Adjusting dispersant polymer feed
- Adjusting the pH
- Feeding a more effective biocide or a more proper biocide dosage
- Increase the blowdown rate.

Examples of using these methods to reduce pitting and general rates are discussed in the case study sections.

6.3.5 Factors to consider on interpreting LCM readings

Time dependence of corrosion rate measurements

A carbon steel corrosion rate is time dependent even under constant conditions (e.g., water flow, water temperature, chemical treatment type and dosages, cycle of concentration, absence of process leaks, absence of biofouling, etc.). This can be attributed most to the effect of corrosion product and inhibitor film build-up on the metal surface, creating a barrier to restrict mass transfer and increase solution resistance. For this reason, a minimum exposure time is recommended in order to report steady-state corrosion rate values. The following equation is recommended by ASTM to obtain consistent general corrosion rate information using coupons.[36]

$$\text{Minimum coupon exposure time (hour)} = 2000/(\text{expected general corrosion rate, mpy or } 25.4\,\mu\text{m/y})$$

For the LPR general corrosion rate reading obtained from the LCM, the steady state value under constant operating conditions should be reached in at most ~1/10 of the time needed for the coupon general rate measurements:[1,14,17,20,24–25,27–28]

$$\text{Minimum LCM (LPR) exposure time (hour)} = 200/(\text{expected general corrosion rate, mpy or } 25.4\,\mu\text{m/y})$$

In field applications, the time needed to reach the steady-state general corrosion rate value is often shorter than the time given by the above equation, assuming an error of ~15% is allowed.

Like the general corrosion rate, the localized corrosion rate requires time to reach a steady-state condition. Meanwhile, changes in corrosivity may be reliably monitored even before the steady-state condition is reached. Because the LCM is sensitive to even slight changes in system corrosivity, such as the swings in the daily water temperature from night-time to day-time, reliable detection of variations in localized corrosion is possible prior to reaching the steady-state localized corrosion value. In this way, the LCM is quite different from a device that only monitors the general corrosion rate.

One critical phenomenon needs to occur in order for the LCM to become fully reliable. This involves the formation of a tubercle over each anode surface. In some cases, during the first week of operation, considerable fluctuations in the localized corrosion rate may be observed which are specifically due to partial formation of a tubercle, followed by partial sloughing off of the tubercle. In some cases, little or no signal fluctuations are

observed during the first week. Once a stable tubercle covering has developed over each anode, any further fluctuations in the localized corrosion rate can be attributed to actual corrosivity events in the cooling water system.

Because of the time required for tubercle growth to develop and the presence of complete corrosion product deposits on the localized corrosion sites, the time-dependence of the localized rate is different from that of the general rate. Depending on the corrosivity of the water, it normally takes about 2–3 weeks for the localized corrosion rate to reach a quasi-steady-state value. It should be noted that even after the initial 2–3-week period, the localized corrosion rate would continue to decrease if the system conditions remain largely the same.

For example, in Great Lakes of United States drinking water, the maximum carbon steel pitting rate was found to be given by the following equation.[33]

$$\text{Max. pitting rate (mpy)} = \text{constant} * t^{-2/3}$$

where t is time in years, or

$$\text{Max. pitting depth} = \text{constant} * t^{1/3}$$

The constant is a function of water temperature and Ryznar Index.[33] It should be pointed out that these equations are obtained in the absence of chemical treatments except bleach. It should be used as a rough indicator for trends only.

Based on these expected time-dependence of localized and general corrosion rates, the time-averaged localized and general corrosion rates are expected to decrease continuously with time, assuming other conditions, e.g., temperature, flow, chemical treatments, biocide treatments and water chemistry remain largely the same.

If there is an interruption in this general trend, then it indicates that a major corrosivity change in the system has occurred.

Effect of water temperature

The rate of corrosion is dependent on temperature, as are the rates of most other chemical reactions. In the absence of an insulating, non-porous layer of scale on the metal surface, the corrosion rate will increase with increasing temperature. Since the LCM measures the water temperature as well as the corrosion rates, the effect of temperature on general and localized corrosion can be easily observed and evaluated. Figure 6.5 clearly shows the sensitivity of the localized corrosion rate compared to the general corrosion rate, with respect to temperature fluctuations. In this Figure, each temperature increase, followed by decrease, corresponds to

the daily temperature fluctuation in the cooling system. As can be seen, in this system, a 5 °F (2.8 °C) change causes a 5 mpy (127 μm/y) change in the localized corrosion rate. Little or very slight correlation can be seen in the general corrosion rate readings. In addition to temperature, other factors (e.g., conductivity, as shown in Fig. 6.5) can also influence corrosion rates.

Attributing causes of corrosion rate variations and treatment optimization strategy

After the initial tubercle growth and pre-steady-state corrosion period has passed (2–3 weeks), if the LCM localized corrosion rates continue to decrease, it indicates either:

- Water temperature decrease
- Blowdown rate increase
- Better corrosion control due to the following
  - adjustment to a more appropriate pH set-point
  - use of a more effective corrosion inhibitor (or more appropriate inhibitor dosage)
  - use of a more effective polymer (or more appropriate polymer dosage)
  - use of a more appropriate biocide or increase of biocide feed if there is an existing MIC problem
- Formation of a large amount of non-conducting scales (e.g., $Ca_3(PO_4)_2$, $CaCO_3$).

If the LCM localized corrosion rate is increasing, it indicates that one or more of the following events may be happening:

- Water temperature increase
- Increase in cycles of concentration (or increase of total dissolved solid concentration)
- Poor pH control (e.g., acid overfeed, or incorrect pH set-point)
- Insufficient corrosion inhibitor feed
- Overfeed corrosion inhibitor (ortho-PO_4, pyro-PO_4, phosphonate, and/or Zn)
- Insufficient polymer feed
- Oxidizing biocide overfeed
- Biocide underfeed, causing MIC problems
- Process leaks
- Instrument malfunctions: Need to check flow and/or electronics.

Since a typical LCM measures water temperature at the same time as the corrosion rates, the effects of temperature changes should be the easiest

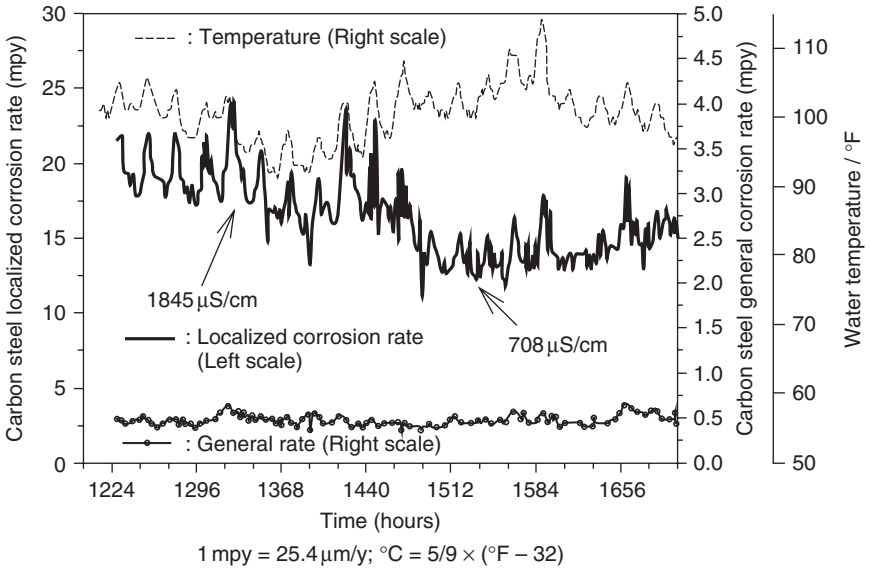

6.5 Effects of water temperature and conductivity on carbon steel corrosion rates.

to check first before considering other factors as the possible cause of corrosion rate changes. The localized corrosion rate is usually more sensitiveto all corrosivity changes than the general rate. Therefore, the localized corrosion rate may show significant increasing or decreasing trends while the general corrosion rate may remain unchanged.

An example is shown in Fig. 6.5. The effect of cycle change can be clearly distinguished from the daily water temperature variation (due to daily change of sunlight and/or atmospheric weather conditions).[11] In this cooling system, a decrease in conductivity from 1845 to 708 µS/cm resulted in a decrease in the localized corrosion rate from 15–20 to 10–15 mpy (381–508 to 254–381 µm/y). Meanwhile, the general corrosion rate fluctuated between 0.4 and 0.6 mpy (10 and 15 µm/y) during this study, and did not show a correlation with the conductivity change.

In general, all of the major changes in LCM readings can be correlated to one or a combination of the events listed above. However, developing reliable correlation may not be an effort-free task. Reliable correlation can generally be developed by comparing the corrosion rate trends to other readily measured parameters, like water temperature, conductivity, pH, halogen feed rate or ORP (oxidation-reduction potential) readings, changes in biocide feed strategies, process operating conditions, changes in program feed rates, changes in the chemical program, changes in the residual

program activity levels, microbial activity changes and the changing quality of the make-up water. Additionally, one needs to check that the flow rates for the water passing through the LCM and other side-stream monitoring devices are maintained and the equipment is properly calibrated. Although many changes can occur in the actual cooling water system, rarely do all or several of them occur simultaneously or within a relatively short time period, e.g., 1–2 hours. Because of the capability of the LCM to provide reliable, sensitive, real time and continuous measurement of corrosion rates and water temperature, using it to establish correlation between localized corrosion changes and process variations has become possible. It should be stressed that the more one knows about the system operating conditions, water chemistry parameters, and chemical treatment residuals, the easier it will be to establish meaningful correlation of localized corrosion rate changes with the events occurring in the system. One should also be aware that since many of the system changes listed above can be controlled and easily repeated at will, a correlation that may not be established with high confidence at its first occurrence can be easily repeated and confirmed.

Maximum localized corrosion rate versus length of localized corrosion events

To provide true cost-effective solutions to industrial cooling water treatment problems, one must have a sense of proportion. For instance, the actual corrosion damage done to a cooling system depends not only on how high the instantaneous corrosion rate is, but more importantly on how long a high corrosion rate event lasts. For example, a localized corrosion rate of 200 mpy (5.08 mm/yr) lasting one-day will only produce a penetration depth of 0.54 mils (13.7 μm). This amount of attack by itself is not significant in reducing the service life of a carbon steel exchanger with a thickness of 1/8 inch (3.18 mm), assuming that the localized corrosion rate is reduced to an acceptable level soon afterwards. On the other hand, one should be more concerned if the localized corrosion rate increases from 10 to 50 mpy (from 254 to 1270 μm/yr) for one year since 40% of the tube thickness could be penetrated. Thus, in general, one needs to worry more about sustained and prolonged corrosivity changes than short-life, transient spikes of corrosion rates.

Some process variations in cooling water systems are unavoidable, such as cycle changes due to fluctuating make-up water quality, daily or seasonal temperature fluctuations, pH variations due to poor acid feed control, occasional process leaks, etc. One objective of using the LCM is to optimize the chemical treatment (both in terms of dosage and application methodology) so that the damaging effects of these process variations can be minimized.

6.4 Applications

The DFC based LCM technology has been used in many cooling water systems (the author had been involved in about 30 field applications), including once-through, open-recirculating, and closed-loop cooling water systems in petroleum refineries, nuclear and fossil fuel power plants, chemical processing industry plants, pulp and paper mills, and food processing plants. Several examples of the applications of this technique in cooling water systems are described in Chapter 23. The DFC-based LCM was demonstrated to be very useful for localized corrosion monitoring, for failure cause analysis, and for the performance-based optimization and control of chemical treatments (i.e., corrosion inhibitors, scale inhibitors, polymer dispersants and biocides) and their application methodologies in these systems.[1,11–15,17,20–25,27–30] The LCM technology has also been adapted for use to study localized corrosion in oil-field systems,[18] the iron-oxide cleaning process,[26] boiler condensate corrosion and aluminum corrosion in engine coolants.[16] Interested readers may consult the references provided at the end of this chapter.

6.5 Future trends and additional information

To the author's knowledge, the DFC-based LCM technology is the first real-time localized corrosion monitoring method based on the mixed potential theory of corrosion initially developed by Wagner and Traud.[37] Although the mixed potential theory has been widely accepted for use to interpret general corrosion, previously the more phenomenological local cell theory has been commonly assumed to be valid for localized corrosion. Before the development of DFC-based LCM technology, the local cell theory has been universally used as the theoretical basis for various real-time localized corrosion monitoring technologies, including the more widely used methods based on electrochemical noise measurements, and various ZRA-based occluded cell methods. The success of the DFC-based LCM technology in cooling water applications suggests that the mixed potential theory may also be generally applicable to localized corrosion processes in other environments. New real-time methods based on the mixed potential theory for localized corrosion are expected to be developed in the future to allow a more accurate and reliable measurement of localized corrosion in these environments.

6.6 References

1 Bo Yang, 'Minimizing Localized Corrosion via New Chemical Treatments and Performance Based Treatment Optimization and Control', NACE Corrosion/99, 1999, Paper no. 307.

2 *Field Usage Data on Soft-Steel Heat Exchangers in Cooling Water Environments*, edited by Corrosion Subcommittee of Chemical Equipment Materials Committee, Japanese Society of Chemical Engineers, October 1990.
3 *Heat Exchanger Management and Residual Life Prediction*, Edited by the Task Group for Heat Exchanger Residual Life Prediction, Corrosion and Anticorrosion Subcommittee, Japanese Material Society, September 1996.
4 *Handbook of Corrosion and Corrosion Protection – Corrosion and Protection of Production Equipments of Chemical Industry*, Edited by Research Institute of Chemical Engineering Machinery, P.R. China, Chemical Industry Publishing House, Beijing (1991).
5 D. R. McIntyre, MTI Publication No. 27, *Experience Survey Stress Corrosion Cracking of Austenitic Stainless Steels in Water*, 1987, Materials Technology Institute of the Chemical Process Industries, St Louis, MO.
6 S. Hayruyama, 'Stress Corrosion Cracking by Cooling Water of Stainless Steel Shell and Tube Heat Exchangers', *Materials Performance*, March, 1982, pp 14–19.
7 *Results of Second Field Survey on Stress Corrosion Cracking in Multi-tube Stainless Steel Heat Exchangers and Life Analysis*, Japanese Society of Chemical Engineers, (1984).
8 M. O. Speidel and A. Atrens (Eds), *Corrosion in Power Generating Equipment*, Plenum Press, New York (1984).
9 NACE Publication #T199, 'Techniques for Monitoring Corrosion and Related Parameters in Field Applications,' 1999, NACE, Houston, TX.
10 Baboian, R. (Ed.), *Corrosion Tests and Standards: Application and Interpretation*, 2005, ASTM International, West Conshohocken, PA.
11 B. Yang, 'Real-time Localized Corrosion Monitoring in Industrial Cooling Water Systems', *Corrosion*, 56, 743 (2000).
12 B. Yang, 'Localized Corrosion Monitoring in Cooling Water Systems', *Corrosion/95*, Paper no. 541, NACE, Houston, TX (1995).
13 B. Yang, 'Method for On-line Determination of Underdeposit Corrosion Rates in Cooling Water Systems', *Corrosion*, 51, 153 (1995).
14 B. Yang, 'Advances in Localized Corrosion Control in Cooling Water Systems', *PowerPlant Chemistry GmbH*, 2 (6), 321 (2000).
15 M. Enzien and B. Yang, 'Effective Use of Monitoring Techniques for Use in Detecting and Controlling MIC in Cooling Water Systems', *Biofouling*, 17 (1), 47 (2001).
16 B. Yang, F. J. Marinho, and A.V. Gershun, 'New Electrochemical Methods for the Evaluation of Localized Corrosion in Engine Coolants,' *Journal of ASTM International*, 4 (1), (2007), available online at www.astm.org.
17 B. Yang, 'Corrosion Control in Industrial Water Systems', Presented at NACE Central Area Conference, Corpus Christi, TX, 7–10 October, 2001.
18 S.L. Fu, A.M. Griffin, J.G. Garcia and B. Yang, 'A New Localized Corrosion Monitoring Technique for the Evaluation of Oilfield Inhibitors', *Corrosion/96*, Paper No. 346, NACE, Houston, TX (1996).
19 B. Yang, 'Method and Apparatus for Measuring Underdeposit Localized Corrosion Rate or Metal Corrosion Rate under Tubercles in Cooling Water Systems', US5,275,704.
20 B. Yang, 'Real Time Localized Corrosion Monitoring in Industrial Cooling Water Systems', *Corrosion Review*, 19 (3–4), 315 (2001).

21 M. Enzien and B. Yang, 'On-line Performance Monitoring of Treatment Programs for MIC Control', *Corrosion/2001*, paper no. 279, NACE, Houston, TX (2001).
22 B. Yang, 'Advances in Localized Corrosion Control in Cooling Water Systems', Proceedings of 9th European Symposium on Corrosion Inhibitors, 2, 821, University of Ferrara, Ferrara, Italy (2000).
23 M. Enzien and B. Yang, 'Effective Use of Biocide for MIC Control in Cooling Water Systems', *Corrosion/2000*, paper no. 384, NACE, Houston, TX (2000).
24 E.R. Hale, B. Yang and M.V. Enzien, 'Corrosion Control in Cooling Water Systems: Recent Experience Using a New Corrosion Monitor', Proceedings of AIM 2000, Venice, Italy (2000).
25 D.A. Meier, E.B. Smyk, and B. Yang, 'Advances in Zinc Free Alkaline Cooling Water Treatment', *Corrosion/99*, paper no. 304, NACE, Houston, TX (1999).
26 K. Sotoudeh and B. Yang, 'On-Line Cleaning of Year-Round Building HAVC Loops', *Corrosion/99*, paper no. 102, NACE, Houston, TX (1999).
27 E. Hale and B. Yang, 'Real-time, On-line Localized Corrosion Rate Measurements for Monitoring and Control of Cooling Water Corrosion', EPRI Corrosion and Degradation Conference, 12–13 June, (1999), St Pete Beach, FL.
28 E. Hale and B. Yang, 'Evaluation of Various Application Regimes to Control Mild Steel Corrosion in a Nuclear Power Service Water System Using a Localized Corrosion Monitor', EPRI Service Water System Reliability Improvement Seminar, 13 July (1999), Biloxi, MS.
29 B. Yang, 'Real Time Localized Corrosion Monitoring in Refinery Cooling Water Systems', *Corrosion/98*, paper no. 595, NACE, Houston, TX (1998).
30 B. Yang, 'A Novel Method for On-line Determination of Underdeposit Corrosion Rates in Cooling Water Systems', *Corrosion/94*, Paper No. 335, NACE, Houston, TX (1994).
31 B. Yang, P.E. Reed, and J.D. Morris, 'Corrosion Inhibitors for Aqueous Systems', US6,572,789B1.
32 B. Yang and J. Tang, 'Hydroxyimino Alkylene Phosphonic Acids for Preventing Corrosion and Scale in Aqueous Systems', US5,788,857A1.
33 R.W. Lane, *Control of Scale and Corrosion in Building Water Systems*, McGraw-Hill, New York (1993).
34 B. Yang and W. Chen, 'Water Treatment Chemicals and Addition Method thereof', CN1,483,684.
35 K.D. Demadis, B. Yang, P.R. Young, D.L. Kouznetsov, and D.G. Kelley, 'Rational Development of New Cooling Water Chemical Treatment Programs for Scale and Microbial Control', in *Advances in Crystal Growth Inhibition Technologies*, Z. Amjad (Ed.), Kluwer Academic/Plenum Publishers, New York, (2000), p. 215.
36 ASTM Standard G4-01, 'Standard Guide for Conducting Corrosion Tests in Field Applications', *ASTM Standards on Disc*, Vol. 03.02, ASTM International, West Conshohochen, PA (2003).
37 C. Wagner and W. Traud, 'On the Interpretation of Corrosion Processes Through the Superposition of Electrochemical Partial Processes and on the Potential of Mixed Electrodes', *Z. Elektrochem.*, 44, 391 (1938); English Translation by M.O. Friedman, *Corrosion*, 62, 844 (2006).

7

Thermodynamics of corrosion and potentiometric methods for measuring localized corrosion

PAVAN SHUKLA, Center for Nuclear Waste Regulatory Analyses, Southwest Research Institute, San Antonio, Texas, USA

7.1 Introduction

Potentiometric methods are used to measure the electrochemical potentials of a metallic structure in a given environment. These potential values act as a corrosion susceptibility indicator. This chapter describes the underlying thermodynamic concepts of different potential values measured in the field. The concepts of electrochemical potential, standard electrode potential, and corrosion potential are discussed. The mixed potential theory is used to elaborate the concept of corrosion potential.

The concepts of localized corrosion susceptibility indicators such as repassivation and breakdown potential are discussed. The fundamentals of localized corrosion and the concept of passivity are also described. In addition, the potentiometric methods used for measuring localized corrosion susceptibility indicators are discussed.

7.2 Thermodynamics of corrosion

Most electrochemical processes are the result of heterogeneous reactions that involve generation or consumption of electrons and various ionic species. In aqueous corrosion processes, the electrochemical reaction takes place at the interface of metal and solution. This process is initiated if the thermodynamics of the electron transfer reaction are favorable. Thermodynamics determine whether a reaction can occur spontaneously (i.e., without the input of an external driving force or the need for an external energy source). If the thermodynamic criterion does not favor metal dissolution in a given aqueous environment, corrosion will not occur. It is for this reason that noble metals such as gold and platinum do not corrode in pure water. The use of thermodynamics allows one to understand the corrosion tendencies of metals in a given environment. Corrosion tendencies are measured in terms of electrochemical potential or its variations. These measurements act as thermodynamic indicators, and provide information on corrosion

tendencies. This chapter discusses different potential terms that are used to measure the tendencies of localized corrosion processes. The next four subsections discuss the concepts of chemical potential, electrochemical potential, electrode potential, change in Gibbs free energy, Nernst's Equation, and mixed potential theory.

7.2.1 Chemical and electrochemical potential

The concept of electrochemical potential is closely tied to the chemical potential; therefore, for the sake of completeness the chemical potential is described first. To define chemical potential, it is helpful to start with an aqueous system that consists of several dissolved species. If the chemical species in the system are at equilibrium and the system is in mechanical and thermal equilibrium with its surrounding environment, the Gibbs free energy (denoted by G) of the system will attain a minimum value (i.e., no chemical reaction would take place). If an infinitesimal quantity of a given species is added to the system, the chemical potential of that species is defined as the ratio of change in Gibbs free energy to the added molar quantity of the species. This definition can be expressed by the following equation

$$\mu_i = \left(\frac{\partial G}{\partial n_i}\right)_{T,P,n_j} \qquad [7.1]$$

where

μ_i = chemical potential
∂G = change in Gibbs free energy
∂n_i = added moles of species i
T, P = temperature and pressure of the system
n_j = denotes other chemical species present in the system

The chemical potential can also be specified in terms of changes in Helmholtz free energy, internal energy, and entropy.

The chemical potential of a species is measured in terms of the difference between two thermodynamic states and never in terms of absolute value in a particular state. However, the absolute value of chemical potential at one thermodynamic state can be obtained by carefully assigning a value to chemical potential at another state. For example, the chemical potential of species i can be estimated with respect to a reference state by assigning a value of chemical potential at the reference state. The equation below represents the difference in chemical potential of species i as a function of temperature and activity of the chemical species

$$\mu_i - \mu_i^0 = \mathrm{RT} \ln\left(\frac{a_i}{a_i^0}\right) \qquad [7.2]$$

where

μ_i = chemical potential
μ_i^0 = chemical potential of species i in the reference state
a_i = activity of species i
a_i^0 = activity of species i in the reference state

The concept of chemical potential helps explain the equilibrium between two phases. For example, if two phases are in equilibrium, the chemical potential of species present in both phases will be equal at the interface of the two phases. Figure 7.1 shows phases α and β in contact with each other with both phases containing species A. The chemical potential of species A in α, i.e., μ_A^α will be equal to μ_A^β at equilibrium. If a gradient of chemical potential exists between two phases, species A will move in the direction of chemical potential gradient. If μ_A^α is greater than μ_A^β, species A will spontaneously flow to phase β. Using Equation [7.2] and by assigning the same reference state for species A in both phases, the difference in the chemical potential of species A can be expressed by the following equation

$$\mu_A^\alpha - \mu_A^\beta = \mathrm{RT} \ln\left(\frac{a_A^\alpha}{a_A^\beta}\right) \qquad [7.3]$$

Guggenheim (1929) first introduced the concept of the electrochemical potential. The electrochemical potential of a species is the sum of its chemical potential and electrostatic potential. It is a function of temperature, pressure, chemical composition, and electrical state of the phases. For charged ionic species i in phase α, the electrochemical potential is defined by

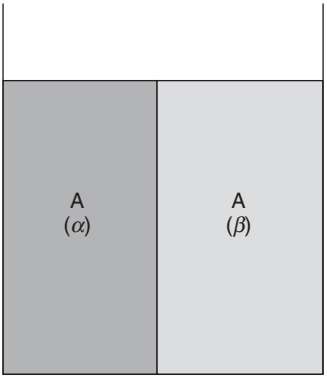

7.1 Illustration of two phases, α and β, containing chemical species A in equilibrium with each other.

$$\bar{\mu}_i^{\alpha} = \mu_i^{\alpha} + z_i F \Phi^{\alpha} \quad [7.4]$$

where

$\bar{\mu}_i^{\alpha}$ = electrochemical potential of species i
μ_i^{α} = chemical potential of species i
z_i = electrostatic charge on species i
F = Faraday's constant
Φ^{α} = electrostatic potential

Similar to chemical potential, the electrochemical equilibrium is attained when the difference in electrochemical potential of a charged species between two phases is zero. The gradient of electrochemical potential will result in transport of the ionic species. For identical chemical composition of phase α and β, the work done to transfer one mole of a species at constant pressure and temperature is given by

$$w = \bar{\mu}_i^{\alpha} - \bar{\mu}_i^{\beta} = z_i F(\Phi^{\alpha} - \Phi^{\beta}) \quad [7.5]$$

The positive electrochemical potential gradient will favor the transport of the charged species. However, unlike the uncharged chemical species, the sign of the charge (i.e., either positive or negative) of the species determines its flow direction. The positive ions will flow from high potential to low potential, whereas negative ions will flow in the opposite direction.

7.2.2 Electrode potential

In an active corrosion process, the metal immersed in an aqueous environment spontaneously dissolves. The corrosion process will proceed naturally if the electrochemical potential of the metallic ions in the metal is higher than in solution. Electrode potential of a metal in a given solution is the difference between its electrochemical potential in a pure metal state and in solution. The term electrode potential refers to the potential drop for a reaction across the metal/solution interface. The standard electrode potential of an electron transfer reaction refers to the equilibrium potential when a metal is in 1 M solution of its salt at 298 K and 1 atmosphere with all reactants and products being at unit activity. For electrochemical reaction in a dilute aqueous environment, the activity and concentration are used interchangeably. Table 3.1 of Chapter 3 lists standard electrode potential of various electrochemical reactions of interest. The concepts of electrode potential, and Gibbs free energy are briefly described in Chapter 3; however, for the sake of completeness, these topics are discussed in detail in this chapter.

The standard electrode potential is also called standard reduction potential because reported values are listed for reduction of metallic ions. The oxidation reaction is obtained by reversing the direction of the arrow in the

reduction reaction, and the corresponding standard potentials for the oxidation reaction can be obtained by reversing the sign of the standard potential of the reduction reaction.

The standard electrode potential of the hydrogen reduction reactions is arbitrarily assigned as zero. This acts as a reference state for measuring the standard electrode potential. The standard electrode potentials of metal dissolution reactions are experimentally determined by coupling the metal with the standard hydrogen electrode. The experimental electrochemical cell consists of metal immersed in its 1 M salt solution and hydrogen reference electrode. For example, to measure the standard electrode potential of an iron metal electrode, an electrochemical cell is constructed with the anode compartment containing iron metal electrode in 1 M iron chloride ($FeCl_2$) solution. The reaction occurring at the metal surface in the equilibrium state is expressed as

$$Fe = Fe^{2+} + 2e^- \qquad [7.6]$$

The electrons produced by the oxidation reactions are consumed by the reduction of hydrogen in the equilibrium state, which is expressed as

$$2H^+ + 2e^- = H_2 \qquad [7.7]$$

The following line notation can represent the electrochemical cell where the iron oxidation reaction (Equation [7.6]) and hydrogen reduction reaction (Equation [7.7]) are taking place:

$$Fe(s)|Fe^{2+}(aq),\ 1M||H^+(aq),\ 1M|Pt(H_2(1\,atm)) \qquad [7.8]$$

The single vertical line represents the boundary between two phases, whereas double vertical lines represent the liquid junction between two half-cells. The two ends of the electrochemical cells (in the example represented by Equation [7.8], the iron metal and platinum wire) are connected to a voltmeter. The reading on the voltmeter corresponds to the potential of the iron metal with respect to the standard hydrogen electrode. Because the half-cell standard electrode potential of the hydrogen reduction reaction is arbitrarily set to zero, the reading of the voltmeter is the standard potential of the iron oxidation reaction (Equation [7.6]). The standard potential for the reduction reaction is deduced by reversing the sign of the voltmeter reading. The use of the standard potential of a reduction reaction is the International Union of Pure and Applied Chemistry (IUPAC) standard.

7.2.3 Gibbs free energy

The standard electrode potential is related to changes in Gibbs free energy by the following equation

$$\Delta G^0 = -n\mathrm{F}\mathrm{E}^0 \quad [7.9]$$

where ΔG^0 is the change in standard Gibbs free energy of the reaction, and n is the number of electrons participating in the reduction reaction. The standard electrode potentials for reduction reactions are tabulated in increasing order in Table 3.1 of Chapter 3. When the standard electrode potential of the metal is less than zero, the metal naturally oxidizes (dissolves) in the solution where the metal ion concentration is less than 1 M. However, the reduction process is not always governed by the standard electrode potential. For spontaneous corrosion of a metal in a given environment, the reduction (cathodic) and oxidation (anodic) reactions must occur simultaneously, and the change in Gibbs free energy of the combined system must be less than zero. For example, when a zinc (Zn) metal plate is immersed in the hydrochloric acid (HCl) solution, zinc ions spontaneously dissolve and hydrogen gas evolves. This process can be represented by the following reaction

$$\mathrm{Zn} + 2\mathrm{HCl} \rightarrow \mathrm{ZnCl_2} + \mathrm{H_2} \quad [7.10]$$

where zinc ions in the hydrochloric solution combine with chloride ions and form zinc chloride ($\mathrm{ZnCl_2}$). The reaction can be reduced into a simple ionic reaction by the following equation

$$\mathrm{Zn} + 2\mathrm{H}^+ \rightarrow \mathrm{Zn}^{2+} + \mathrm{H_2} \quad [7.11]$$

The reaction can be further divided into partial half-cell reactions:

$$\mathrm{Zn} \rightarrow \mathrm{Zn}^{2+} + 2\mathrm{e}^- \text{ (anodic)} \quad [7.12]$$

and

$$2\mathrm{H}^+ + 2\mathrm{e}^- \rightarrow \mathrm{H_2} \text{ (cathodic)} \quad [7.7]$$

The dissolution of zinc metal in hydrochloric acid will occur spontaneously if standard potential of the zinc oxidation reaction (Equation 9.12) is higher than standard electrode potential for hydrogen evolution reaction (Equation [7.7]). The addition of these two quantities yields the electrode potential for the reaction couple

$$E = E^{\mathrm{a}} + E^{\mathrm{c}} \quad [7.13]$$

The electrode potential of the reaction couple (Equation [7.11]), E, is associated with change in Gibbs free energy, ΔG, by the following relationship

$$\Delta G = -n\mathrm{FE} \quad [7.14]$$

where n is the number of electrons involved in the reaction, and F is the Faraday constant (96 500 coulombs per equivalent).

Another example illustrates the use of the standard electrode potentials list (see Table 3.1, Chapter 3) to determine the feasibility of the corrosion process. Consider iron metal immersed in 1 M $FeSO_4$ solution that is saturated with dissolved oxygen. For spontaneous corrosion of iron, the anodic dissolution (oxidation) of iron

$$Fe \rightarrow Fe^{2+} + 2e^{-} \quad \text{(anodic)} \qquad [7.6]$$

must take place along with the oxygen reduction reaction.

$$O_2(aq) + 2H_2O + 4e^{-} \rightarrow 4OH^{-}(aq) \quad \text{(cathodic)} \qquad [7.15]$$

The standard electrode potential for the iron oxidation is 0.44 volts and for the oxygen reduction reaction is 0.4 volts in neutral-to-alkaline solution. To balance the number of electrons produced by the cathodic reaction, the standard electrode potential of the iron oxidation reaction is doubled. The net potential of the reaction couple is equal to

$$E_{cell} = 2E^{0}_{Fe/Fe^{2+}} + E^{0}_{O_2(aq)/OH^{-}(aq)} \qquad [7.16]$$

The calculated value of the cell potential is equal to 1.28 volts, and the change in Gibbs free energy is –49.4 kilo-joules/mole, indicating that this reaction system is thermodynamically favorable. As a result, iron will corrode naturally in the aerated 1 M $FeSO_4$. When system conditions are nonstandard, exercise caution in using the standard electrode potential table. In such a situation, the temperature and concentration effects of the solution on the reduction potential must be accounted for by using the Nernst equation. The following section discusses using the Nernst equation to determine the electrode potential in nonstandard conditions.

7.2.4 Electrode potential in nonstandard conditions

Table 3.1 in Chapter 3 lists the values of standard potentials for various reduction reactions only when all reactants and products are at unit activity. However, this condition is not likely to exist for most environments where corrosion of a metal is taking place. The Nernst equation provides a mean to calculate the electrode potential under nonstandard conditions. The Nernst equation can be derived using the Gibbs free energy principle for electrochemical reactions (Milazzo and Caroli, 1978; Bard and Faulkner, 1980).

A general electrochemical reaction in the equilibrium state can be expressed as

$$aA + bB = cC + dD \qquad [7.17]$$

where a moles of reactant A react with b moles of reactant B to produce c moles of product C and d moles of product D. The corresponding change

in Gibbs free energy for reaction under the standard conditions is represented by the following equation:

$$\Delta G^0 = (cG_C^0 + dG_D^0) - (aG_A^0 + bG_B^0) \quad [7.18]$$

where superscript 0 denotes the standard conditions (i.e., unit activity for products and reactants at 25 °C). For nonstandard conditions, Equation [7.18] can be expressed as

$$\Delta G = (cG_C + dG_D) - (aG_A + bG_B) \quad [7.19]$$

Algebraic subtraction of Equation [7.19] from Equation [7.18] yields

$$\Delta G - \Delta G^0 = c(G_C - cG_C^0) + d(G_D - dG_D^0) - a(G_A - G_A^0) - b(G_B - G_B^0) \quad [7.20]$$

Each term on the right-hand side of Equation [7.20] can be expressed in terms of activity for estimating the change in Gibbs free energy with respect to the standard state. For example, the change in the Gibbs free energy of reactant A, is given by

$$a(G_A - G_A^0) = a\mathrm{RT}\ln[\mathrm{A}] \quad [7.21]$$

In this expression, the activity of the species A has been replaced by its concentration [A] by assuming that reaction occurs in a dilute solution – a condition applicable for most corrosion environments. Substitution of Equation [7.21] and equivalent expressions for other reactants and products in Equation [7.20] yields

$$\Delta G - \Delta G^0 = \mathrm{RT}\ln\frac{[\mathrm{C}]^c[\mathrm{D}]^d}{[\mathrm{A}]^a[\mathrm{B}]^b} \quad [7.22]$$

Using the relationship between changes in Gibbs free energy and electrode potential (i.e., $\Delta G^0 = -n\mathrm{F}E^0$ and $\Delta G = -n\mathrm{F}E$) yields

$$E = E^0 - \frac{\mathrm{RT}}{n\mathrm{F}}\ln\frac{[\mathrm{C}]^c[\mathrm{D}]^d}{[\mathrm{A}]^a[\mathrm{B}]^b} \quad [7.23]$$

Equation [7.23] is the general form of Nernst's equation. For convenience, the natural logarithmic function in this equation is transformed to the logarithmic function of base 10, which yields

$$E = E^0 - \frac{2.303\mathrm{RT}}{n\mathrm{F}}\log\frac{[\mathrm{C}]^c[\mathrm{D}]^d}{[\mathrm{A}]^a[\mathrm{B}]^b} \quad [7.24]$$

Equation [7.24] can be applied to determine the electrode potential at nonstandard conditions. This representation of Nernst's equation is convenient

to use because the concentration and pH of aqueous environments are often represented as 10^x where x is a real number.

To illustrate the use of Nernst's equation, the electrode potential of the hydrogen reduction reaction is considered. The electrode potential for the hydrogen reduction reaction, represented by Equation [7.7], is obtained using Equation [7.24]

$$E_{H^+/H_2} = E^0_{H^+/H_2} - \frac{2.303RT}{2F}\log\frac{[H_2]}{[H^+]} \qquad [7.25]$$

Assuming $[H_2] = pH_2$ equal to 1 atmospheric pressure, Equation [7.25] yields

$$E_{H^+/H_2} = E^0_{H^+/H_2} - \frac{2.303RT}{2F}(-\log[H^+]) = E^0_{H^+/H_2} - \frac{2.303RT}{2F}pH \qquad [7.26]$$

At 25 °C, the electrode potential for the hydrogen reduction reaction as a function of pH of the solution can be represented by

$$E_{H^+/H_2} = 0.059\ pH \qquad [7.27]$$

Similarly, an expression for electrode potential of the oxygen reduction reaction, represented by Equation [7.15], is also obtained using Equation [7.24]

$$E_{O_2/OH^-} = E^0_{O_2/OH^-} - \frac{2.303RT}{2F}\log\frac{[OH^-]^4}{pO_2} \qquad [7.28]$$

where pO_2 represents the partial pressure of oxygen. These two examples show that even though the Nernst equation is a convenient tool for determining the electrode potential under nonstandard conditions, additional information on the chemical environment is needed to use the equation effectively. However, in many situations, the precise chemical environmental conditions, and potential electrochemical reactions that could occur are not available. In such cases, several potentiometric methods can be used to obtain insight on thermodynamic viability of various corrosion processes.

7.2.5 Corrosion potential and mixed potential theory

The corrosion potential is the potential difference across the metal/solution interface when a metal is immersed in an aqueous solution, and it is measured against a reference electrode (e.g., the standard hydrogen electrode). The sum of currents associated with the anodic dissolution reactions must be equal to the sum of the cathodic reactions at the corrosion potential. At

the corrosion potential, the oxidation of the metal and the reduction of a species in solution occur simultaneously at the metal/electrolyte interface. The corrosion potential lies between the reduction potential of the reduction reaction and reduction potential of the oxidation reaction (see Figure 3.4 in Chapter 3). The net measurable current is zero, and the corroding metal is charge neutral at corrosion potential. This condition can be represented by the following expression

$$I_A + I_C = 0 \quad [7.29]$$

where

I_A = total anodic current generated by anodic reactions
I_C = total cathodic current generated by cathodic reactions

In corrosion processes, the anodic current is usually assigned the positive sign and cathodic the negative sign. While anodic reactions are dependent on the metal composition, the dominant cathodic reactions in the aerated aqueous solution with neutral to alkaline pH are oxygen reduction and water reduction reactions

$$O_2 + 2H_2O + 4e^- \rightarrow 4OH^- \quad [7.15]$$

$$2H_2O + 2e^- \rightarrow H_2 + 2OH^- \quad [7.30]$$

The oxygen reduction is the dominant reaction for most corroding systems in an alkaline environment. The water reduction reaction is very slow, and it only contributes significantly at very low values of corrosion potential. The standard electrode potential for water reduction reaction is –0.827 volts versus the standard hydrogen reference electrode in the alkaline environment (also represented as –0.827 V_{SHE} where V denotes the unit of volt, and subscript SHE is acronym for standard hydrogen reference electrode). Therefore, this reaction will not dominate at corrosion potentials higher than –0.827 V_{SHE}.

In acidic solution, the dominant cathodic reactions are hydrogen evolution and oxygen reduction reactions, expressed as

$$2H^+ + 2e^- \rightarrow H_2 \quad [7.7]$$

$$O_2 + 4H^+ + 4e^- \rightarrow 2H_2O \quad [7.31]$$

In acidic solutions, hydrogen gas evolves at the cathode due to hydrogen reduction reaction, and the oxygen reduction reaction produces water. The oxygen reduction reaction is more likely in the acidic environment if the corrosion potential is higher than 0.0 V_{SHE}. However, if the corrosion potential is less than 0.0 V_{SHE}, then both reduction reactions will be dominant in the cathodic region. The relative amount of current produced by each reaction depends upon individual kinetic rate.

Corrosion potential is relatively easy to measure. It can either be measured while conducting the polarization measurements or by using a reference electrode and a voltmeter in field studies. To measure the corrosion potential of a metallic structure in field studies, the metal structure and reference electrode are connected to a high impedance voltmeter. Under ideal conditions, no net current should flow between the reference and working electrode. However, a small current is necessary to measure the potential drop. The reading of the voltmeter is the corrosion potential of the electrode with respect to the reference electrode. The measured potential contains 'IR' drop error. This error originates because of a very small quantity of current that flows between reference and working electrode. The 'IR' drop error can be higher when electrolyte conductivity is low. Therefore, to reduce the 'IR' drop, it is recommended that the reference electrode be placed close to the electrode surface. A reference electrode placed far from the working electrode will introduce a larger error in corrosion potential drop. When measuring the potential of a polarized structure such as a buried pipeline subject to cathodic protection, the potential measured against a reference electrode will contain a significant 'IR' drop error. This error arises from the resistance of soil placed between the pipeline and the reference electrode. The current can be interrupted instantaneously during a potential measurement to correct for 'IR' effect.

By definition, corrosion potentials usually refer to open circuit (no current flow) measurements. These two terms – open circuit potential and corrosion potential – are used interchangeably in corrosion literature. The net current at the electrode is zero at the open circuit and the corrosion potential. However, a distinction is made between these two terms in this chapter. The open circuit potential is the measured potential with respect to the reference electrode when the electrode is connected to the potentiostat. The corrosion potential is the point of transition between the cathodic and anodic region in the potentiodynamic polarization curve (see Chapter 3 for further details on the potentiodynamic polarization method). The measured value of corrosion and open circuit potential should be the same. However, a difference of several millivolts may be observed. This difference arises from the presence of an oxide layer at the electrode surface. In the measurement of the polarization curve, the electrode is first polarized to a cathodic value. This action results in removal of the oxide layer present at the electrode surface. Then, the potential is incrementally changed in the anodic direction. The transition between the cathodic and anodic curve is marked by a sharp dip in measured current. The corrosion potential is recorded at this transition point.

Polarization experiments are widely used in corrosion studies. These experiments provide useful information such as corrosion potential, pitting potential and repassivation potential. Polarization experiments are

conducted in aerated and deaerated solutions. Polarization experiments also provide information on kinetics of anodic and cathodic reactions taking place on the metal/solution interface. The polarization curve can be decomposed using the theory of mixed potential to understand the kinetics of different electrochemical reactions taking place at the electrode surface. The premise of the mixed potential theory is that each electrochemical reaction taking place at the metal/solution interface can be treated independently (Davis, 2000). The mixed potential diagrams are also called Evans diagrams. In the mixed potential theory, any electrochemical reaction can be algebraically divided into separate oxidation and reduction reactions. An Evans diagram for zinc metal in hydrochloric acid is presented in Figure 3.4 of Chapter 3. The figure depicts the Evans diagram of the dissolution reaction of zinc metal, given by

$$Zn \rightarrow Zn^{2+} + 2e^{-} \qquad [7.12]$$

and the Evans diagram of hydrogen reduction reaction, given by

$$2H^{+} + 2e^{-} \rightarrow H_2 \qquad [7.7]$$

Both half-cell reactions occur at the same metal surface. The reduction reactions help sustain the anodic dissolution of zinc by consuming the electrons produced by metal oxidation. Both reactions have half-cell electrode potential and corresponding exchange current density, as illustrated in Figure 3.4 of Chapter 3. Since both half-cell reactions must coexist at the same metal surface, each reaction must polarize to a common intermediate potential value. This value is called corrosion potential, denoted by E_{corr} in Figure 3.4 of Chapter 3. The corrosion potential is also referred to as mixed potential because it is a result of dynamic equilibrium between oxidation and reduction reactions at the electrode surface. In aerated electrolytes, E_{corr} is also a function of the oxygen content and transport characteristics of dissolved oxygen. When the level of oxygen is low, a more negative corrosion potential is seen, which can be attributed to a lower corrosion rate. If there are several cathodic reactions, the corrosion potential is determined when the sum of the cathodic current curve intersects the anodic current curve in the Evans diagram. An example of the mixed potential theory for iron corrosion is presented in this chapter. This example also shows the effect of more than one cathodic reaction on corrosion potential.

For freely corroding iron in the neutral to alkaline solution, the anodic corrosion reaction

$$Fe \rightarrow Fe^{2+} + 2e^{-} \qquad [7.6]$$

must be balanced by the oxygen reduction reaction

$$O_2 + 2H_2O + 4e^{-} \rightarrow 4OH^{-} \qquad [7.15]$$

If the potential is sufficiently low, the water reduction reaction will also proceed along with the oxygen reduction reaction.

$$2H_2O + 2e^- \rightarrow H_2 + 2OH^- \quad [7.30]$$

The anodic current density generated by the iron oxidation reaction can be expressed as

$$i_{a,Fe} = 10^{\left[\frac{V-E_{a,Fe}}{\beta_{a,Fe}}\right]} - 10^{-\left[\frac{V-E_{c,Fe}}{\beta_{c,Fe}}\right]} \quad [7.32]$$

where

$i_{a,Fe}$ = current density due to iron dissolution reaction (Ampere/cm^2)
V = potential drop across metal/solution interface (Volts)
$E_{a,Fe}$ = effective anodic equilibrium potential (Volts)
$E_{c,Fe}$ = effective cathodic equilibrium potential (Volts)
$\beta_{a,Fe}$ = anodic Tafel slope (Volts/decade)
$\beta_{c,Fe}$ = cathodic Tafel slope (Volts/decade)

Both anodic and cathodic Tafel slopes are computed from a polarization plot where current is plotted on logarithmic scale (see Chapter 3 for additional details). The current density expression represented by Equation [7.32] is a variation of the Butler–Volmer equation (Bard *et al.*, 1989) which is widely used in the electrochemistry literature. A general representation of the Butler–Volmer equation has four parameters that are experimentally determined: 1. exchange current density; 2. equilibrium potential; 3. anodic charge transfer coefficient; and 4. cathodic charge transfer coefficient. Similarly, the current density represented by Equation [7.32] also contains four parameters ($E_{a,Fe}$, $E_{c,Fe}$, $\beta_{a,Fe}$, $\beta_{c,Fe}$) that are determined experimentally. The first term on the right-hand side of Equation [7.32] represents the current density due to anodic reaction and the second term is due to the reverse or cathodic reaction. In modeling the kinetics of iron dissolution, the second term can be neglected because the cathodic contribution will be negligibly small in the anodic region. Therefore, the current density due to the corrosion reaction is then given by

$$i_{a,Fe} = 10^{(V-E_{Fe})/\beta_{Fe}} \quad [7.33]$$

where $E_{a,Fe}$ and $\beta_{a,Fe}$ (see Equation [7.32] are replaced by E_{Fe} and β_{Fe}, respectively.

The cathodic current generated due to oxygen reduction reaction is given by

$$i_{c,O_2} = 10^{\left[\frac{V-E_{a,O_2}}{\beta_{a,O_2}}\right]} - 10^{\left[\frac{V-E_{c,O_2}}{\beta_{c,O_2}}\right]} \quad [7.34]$$

where

i_{c,O_2} = current density due to oxygen reduction reaction (Ampere/cm^2)
V = potential drop across metal/solution interface (Volts)
E_{a,O_2} = effective anodic equilibrium potential (Volts)
E_{c,O_2} = effective cathodic equilibrium potential (Volts)
β_{a,O_2} = anodic Tafel slope (Volts/decade)
β_{c,O_2} = cathodic Tafel slope (Volts/decade)

The first term of Equation [7.34] can be neglected because anodic contribution in the cathodic region will be negligibly small for the oxygen reduction reaction. Hence, the current generated by the oxygen reduction reaction is give by

$$i_{c,O_2} = -10^{(V-E_{O_2})/\beta_{O_2}} \quad [7.35]$$

where E_{c,O_2} is replaced by E_{O_2}, and β_{c,O_2} is replaced by β_{O_2}. The polarization plot for cathodic portion of the oxygen reduction reaction is shown in Fig. 7.2. This polarization plot can be sectioned into two parts. The first part, where the potential drop across the metal/solution interface is the driving force for the reaction, is called the activation controlled region of the polarization curve. In the second part of the polarization curve, the diffusion of

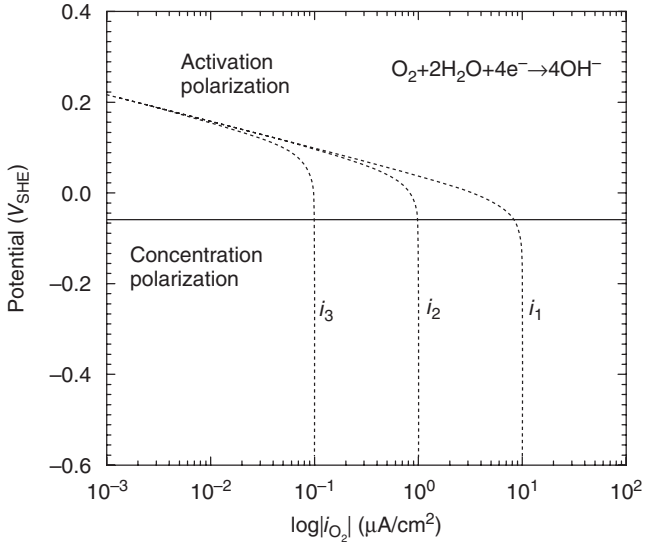

7.2 Polarization plots of oxygen reduction reaction in neutral and alkaline solution for three values of mass transfer limited current designated as i_1, i_2 and i_3 where $i_1 > i_2 > i_3$. The horizontal line demarcates the activation and concentration parts of the polarization curve. In the activation regions, the three plots superimpose for the part of the range of the interfacial potential.

dissolved oxygen to the metal surface controls the current at the metal/solution interface. In this region, the oxygen reduction reaction rate is fast compared to the diffusion of dissolved oxygen. In other words, as soon as oxygen molecules reach the metal surface, they react with available electrons at the metal surface to produce the hydroxyl ions. For this reason, this portion of the curve is called the concentration polarization. The current density due to the oxygen reduction reaction is controlled by the mass-transfer of oxygen to the electrode surface, and the corresponding measured current is the mass-transfer-limited current. In the concentration polarization region, the oxygen reduction current density does not change with potential. The expression for oxygen reduction current density is modified according to the following equation to account for mass-transfer-limited current in kinetic rate expression (Nisancioglu, 1987)

$$i_{c,O_2} = -\left(\frac{1}{i_{lim,O_2}} - 10^{(V-E_{O_2})/\beta_{O_2}} \right)^{-1} \quad [7.36]$$

where i_{lim,O_2} denotes the mass-transfer-limited current.

In neutral to alkaline solutions, the oxygen reduction reaction can also produce hydrogen peroxide H_2O_2 (Jones, 1992). However, an experimental study conducted by Jovancicevic *et al.* (1986) indicates that the oxygen reduction reaction primarily proceeds via four electron pathways with a little H_2O_2 as an intermediate species on the bare iron.

If the corrosion potential is low enough, the water reduction reaction will also proceed along with the oxygen reduction reaction. The mechanism of the water reduction reaction is a topic of research (Jerkiewicz, 1998; Chialvo and Chialvo, 2000). The cathodic current due to water reduction is given by

$$i_{c,H_2} = 10^{\left[\frac{V-E_{a,H_2}}{\beta_{a,H_2}}\right]} - 10^{\left[\frac{V-E_{c,H_2}}{\beta_{c,H_2}}\right]} \quad [7.37]$$

where

i_{c,H_2} = current density due to water reduction reaction (Ampere/cm^2)
V = potential drop across metal/solution interface (Volts)
E_{a,H_2} = effective anodic equilibrium potential (Volts)
E_{c,H_2} = effective cathodic equilibrium potential (Volts)
β_{a,H_2} = anodic Tafel slope (Volts/decade)
β_{c,H_2} = cathodic Tafel slope (Volts/decade)

The first term on the right-hand side of Equation [7.37] can be neglected in the cathodic region which yields

$$i_{c,H_2} = -10^{(V-E_{H_2})/\beta_{H_2}} \quad [7.38]$$

where E_{c,H_2} is replaced by E_{H_2}, and β_{c,H_2} is replaced by β_{H_2}.

The net current density due to i_{net} for iron corrosion is given by the sum of current densities due to the individual electrochemical reactions

$$i_{net} = i_{a,Fe} + i_{c,H_2} + i_{c,O_2} \quad [7.39]$$

The Evans diagram for iron corrosion, hydrogen evolution and oxygen reduction reactions is presented in Fig. 7.3. The calculated polarization plot representing the net current versus potential is also shown in Fig. 7.3. The parameters used in Equations [7.33], [7.36] and [7.38] are given in Table 7.1. The intersection point of i_{c,O_2} and $i_{a,Fe}$ determine the corrosion potential of the freely corroding iron. The water reduction reaction has a negligible effect on the corrosion potential in this example because cathodic current due to this reaction is negligible. However, in a deaerated solution, the corrosion potential would be determined by the intersection of i_{c,H_2} and $i_{a,Fe}$.

For potential more positive than E_{corr}, the net current density is anodic. In the anodic region, the iron corrosion reaction dominates the water and oxygen reduction reactions, and $i_{net} \approx i_{a,Fe}$. At potentials less than E_{corr}, the net current is dominated by the cathodic reactions. In the potential range of $E_{corr} > V > -0.1$, there was a large change in the absolute

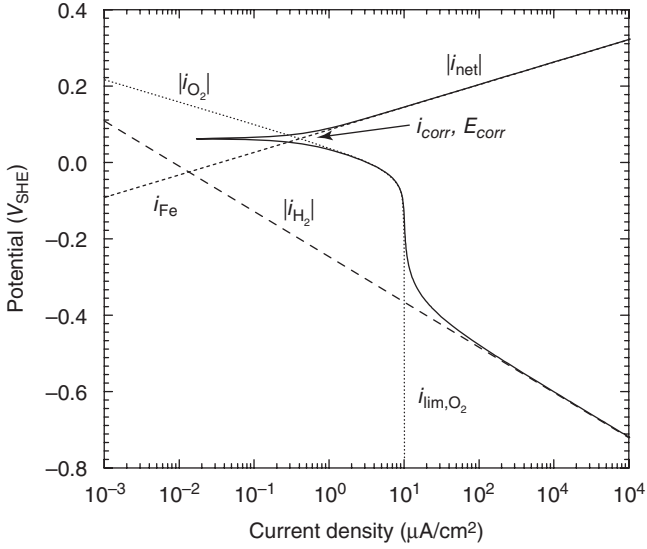

7.3 Polarization plot for corroding iron showing the interfacial potential versus current densities for anodic dissolution of iron i_{Fe}, hydrogen evolution i_{H_2}, and oxygen reduction i_{O_2} and net current density.

Table 7.1 Parameter values used in Equations [7.33], [7.36] and [7.38] for calculating current versus potential diagram for iron oxidation, oxygen reduction and water reduction reactions

Reaction	β, *V*/decade	*E* (Volts versus standard hydrogen reference electrode)
$Fe \rightarrow Fe^{2+} + 2e^-$	0.0626	–0.475
$O_2 + 2H_2O + 4e^- \rightarrow 4OH^-$	0.0665	–0.500
$2H_2O + 2e^- \rightarrow H_2 + 2OH^-$	0.132	–0.800

value of i_{net} with applied potential. At $V > -0.1\ V_{SHE}$, the change of current density with applied potential was significantly reduced as i_{lim,O_2} was reached. For $V < -0.2\ V_{SHE}$, the change in current density with applied potential was resumed as the hydrogen evolution reaction became more favorable. For $V < -1\ V_{SHE}$, the plots for the absolute value of i_{c,H_2} and i_{net} are superimposed.

This example shows that given sufficient information about the electrochemical reaction, the mixed potential theory can be used to calculate the corrosion potential and corrosion current. However, in practice, very limited data is available to generate the Evans diagram with confidence. In general, experimental techniques such as polarization methods are used to determine the polarization plot, which is then interpreted using the mixed potential theory.

7.3 Galvanic series of alloys

Because alloys consist of more than one metal element, the standard electrode potential of these systems cannot be defined by the electrode potential of pure metal. Moreover, the conditions affecting the corrosion potential of the solid alloys in a given environment are not well understood. For this reason, the galvanic series has been developed by experimentally measuring the corrosion potential of alloys in a given environment.

A galvanic series has been compiled from experimentally collected data for corrosion potential of metals and alloys in aerated flowing seawater, which indicates their relative nobility. The relative position of the materials can change in other environments. The further apart the materials are in this series, the higher the risk of galvanic corrosion, which occurs when two dissimilar metals are in electrical contact with each other. In galvanic corrosion, a less noble alloy corrodes faster than a nobler alloy. For example, if zinc and steel are electrically connected in a saltwater solution, the zinc will corrode, whereas steel will not. This is due to fact that zinc is more

active than steel. Therefore, a thermodynamically viable electrochemical cell will set up between the two metals.

The relative position of an alloy with respect to other alloys is a useful tool for selecting metals to be joined. The closer positioned alloys have a lesser tendency to interact galvanically, and the further apart the materials are in the galvanic series, the higher the risk of galvanic corrosion (ASTM, 1984). As a result, the more active alloys corrode at enhanced rates. The galvanic series does not provide any information on the rate of corrosion. It serves only as a basic qualitative guide. The galvanic series must be used with caution. If the environment is different from aerated seawater, the corrosion potential measurements must be independently performed.

The corrosion potentials of various alloys in flowing aerated seawater are listed in Table 7.2. This list is compiled from the graphical data presented in several sources (Kelly *et al.*, 2003; Uhlig and Revie, 1984; Treseder *et al.*, 1991). Therefore, exact values reported in the table must be used with caution. Many of these alloys have dual surface behavior and can become active after exhibiting passivity, particularly in low-velocity or poorly

Table 7.2 Measured corrosion potentials of alloys in flowing seawater

Alloy	E_{corr} (Volts vs. Saturated Calomel Reference Electrode)
Graphite	0.3 to 0.2
Hastelloy C-276	0.1 to –0.04
Titanium and titanium alloys	0.06 to –0.05
Alloy 825	0.04 to –0.02
Inconel 625	0.1 to –0.04
Nickel 200	–0.1 to –0.2
Stainless steel – Type 316, 317	0.0 to –0.15 (–0.36 to –0.46 in poorly aerated solution, crevice areas, or when covered with slimed film of bacteria)
Stainless steel – Type 302, 304, 321, 347	–0.07 to –0.12 (–0.46 to –0.57 in poorly aerated solution, crevice areas, or when covered with slimed film of bacteria)
90–10 copper nickel	–0.21 to –0.28
Pb-Sn solder (50/50)	–0.26 to –0.35
Aluminum bronze	–0.3 to –0.4
Naval brass, tin brass, red brass	–0.3 to –0.4
Nickel-chromium alloy 600	–0.38 to –0.47
Cast irons	–0.6 to –0.72
Mild steel	–0.6 to –0.72
Aluminum alloy	–0.7 to –0.9

aerated water and at shielded areas. To develop the galvanic series of various alloys, use the ASTM standard procedure (ASTM, 1984).

7.4 Potentiometric methods for measuring localized corrosion

Localized corrosion is a term used for accelerated loss of material due to electrochemical reactions at selective sites of a metal's surface. In localized corrosion, the discrete sites at a metal surface corrode at an accelerated rate compared to the rest of the metal surface. In Chapter 2, the fundamental concepts of localized corrosion and passivity are described. Nonetheless, additional material on localized corrosion is covered in this chapter to complete the discussion on these topics. In Chapter 3, various potentiometric methods that are used to evaluate corrosion processes are described. In this section, the use of potentiometric methods for measuring the localized corrosion susceptibility of a given structure submersed in a chemical solution is discussed. Examples are presented to highlight key points.

There are different forms of localized corrosion such as pitting and crevice corrosion. In general, the localized corrosion sites at a given metal surface experience accelerated anodic reactions. The anodic reactions at selected sites are supported by cathodic reactions at the rest of the metal surface. The occurrence of localized corrosion proves that the anodic surface area can be much smaller than the cathodic area. Therefore, a sufficient cathodic area is necessary to support the anodic reaction. The ratio of anodic to cathodic area can be an important factor for localized corrosion whereas in the general corrosion process both anodic and cathodic sites are assumed to occupy equal area. Corrosive microenvironments, which tend to be very different from the bulk environment, often play a critical role in the initiation and propagation of corrosion pits or crevice sites (Day *et al.*, 2003). The localized corrosion could result in perforation or other failure, thus reducing the service lifetime of the structure in use. To understand the localized corrosion, we first briefly explore the concept of passivity.

7.4.1 Passivity

As discussed in Chapter 2, passivity plays an important role in corrosion resistant alloys. Thermodynamically, a metal surface may have a large driving force for its dissolution in an aqueous environment. However, corrosion-resistant alloys are covered with a protective passive film, which reduces the rate of corrosion of the metal in the solution (Uhlig, 1978; Wagner, 1965).

In a series of experiments, Faraday (1965) observed that iron dissolves rapidly in dilute nitric acid solution. However, in concentrated nitric acid

solution, the iron does not react with nitric acid, and the same iron sample showed corrosion-resistant properties when immersed in the dilute nitric acid solution. The sample also started to corrode at an elevated rate when scratched. Schöenbien (1836) termed this phenomenon as passivity. He suggested that in the concentrated nitric acid, the iron surface develops a passive film, which retards its dissolution. However, once a scratch damages the passive film, the metal dissolved at an accelerated rate in the dilute nitric acid solution.

The potentiodynamic polarization measurements can be used to determine whether a metal will exhibit passive corrosion or active corrosion. These measurements can be conducted using a cyclic potentiodynamic polarization test. The polarization plot of a metal exhibiting the passive behavior is presented in Fig. 3.9 of Chapter 3. The figure shows that when metal potential is increased to a more positive value, the rate of metal dissolution increases. The rate of dissolution reaches a maximum value when applied potential is at the primary passive potential, denoted by E_{pp} in the figure. The corresponding current, termed as critical anodic dissolution current density, is denoted by i_{crit}. When applied potential is more positive to E_{crit}, the metal dissolution current decreases with applied potential. The region of the polarization curve where the dissolution current remains high is called the active region. As the potential is increased to a more positive value than E_{crit}, the dissolution current becomes constant with applied potential in the passive region. This behavior of the metal surface is called passive dissolution, and the associated region of the curve is labeled the passive region. If the corrosion potential of the metal/solution system lies in the passive region, the metal will corrode at the rate of passive current density, denoted by i_{pass}. In the passive region, a large potential increase of the metal does not cause significant increases in dissolution rates. As the metal potential increases to a more positive value, passive film would break down. As a result, the current increases rapidly with the applied potential, which indicates that the passive film is no longer able to protect the metal surface.

Passivity behavior is attributed to passive film on the metal surface. The passive film acts as a barrier between the metal surface and the corrosive environment. Such films can block the oxygen transport and cause the corrosion potential to change. For example, Alloy 22 passivates in chloride solution due to the formation of chromium oxide film (Mon *et al.*, 2005). Similarly, steel pipes may passivate in alkaline solutions due to formation of an $Fe(OH)_2$ film on the pipe surface (Jones, 1992).

The stability of passive film on a metal surface in a given environment can be determined by examining its polarization plot and location of the corrosion potential in the polarization curve (Fontana, 1978). An aniodic polarization of the metal in a given solution is presented in Fig. 7.4. This

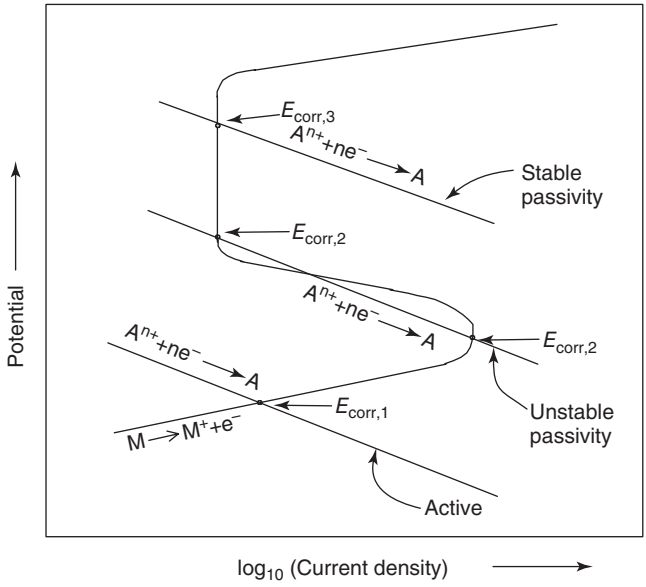

7.4 Hypothetical polarization plot of a passive metal. The metal exhibits the stable passive behavior when corrosion potential lies in the passive region.

hypothetical anodic polarization curve represents the condition when little or no oxidizing species (such as dissolved oxygen in aerated solution) are present in the solution. In this Figure, the cathodic polarization curves for three different conditions are also presented. In the first conditions (starting from a lower potential cathodic curve), the corrosion potential, denoted by $E_{corr,1}$ lies in the active region. As a result, the passive film will not form and metal will corrode at an elevated rate. The second cathodic curve intersects the anodic curve at two positions: the first intersection point lies in the passive region and the second one in the active region. The corresponding corrosion potential is $E_{corr,2}$ at the locations of intersection. In this case, the passive film is unstable because the metal will come to the stable state where maximum current is achieved. In the third case, the cathodic current curve intersects the anodic current curve in the passive region, and the corrosion potential at the point of intersection is denoted by $E_{corr,3}$. The passive film will remain stable at $E_{corr,3}$, and slow passive dissolution of metal will take place.

The long-term stability of the passive film is still not completely understood (Baker, 1986). If the passive film becomes unstable, the metal surface will corrode at the higher rate. The US Department of Energy has proposed using a 2 cm thick Alloy 22 outer container for the permanent disposal of

high-level waste in the potential repository at Yucca Mountain (Bechtel SAIC Company, 2004). Alloy 22 is a highly corrosion-resistant material that depends on a passive layer only nanometers-thick for its corrosion resistance (Estill *et al.*, 2003). The measurement of the corrosion rate of passive Alloy 22 has been determined to less than 0.1 μm/year in the potential Yucca Mountain repository environment (in both alkaline and acidic solutions) at temperatures below 95 °C. Technical experience with Alloy 22 is only a few decades long, whereas service lifetime of 10 000 years or more is expected of these containers in the proposed repository. Technical advances in determining the long-term stability of passive film could help determine the service lifetime of metal containers for high-level nuclear waste disposal.

7.4.2 Localized corrosion susceptibility indicators

The initiation and development of the localized corrosion can be judged by measuring the potential drop across metal/solution interface under various conditions. As discussed in Chapter 2, the crevice and pitting corrosion are two possible modes of localized corrosion (Farmer and McCright, 1998). The schematic diagrams of crevice and pitting corrosions are presented in Fig. 7.5a and b, respectively.

In pitting corrosion, cavities or holes appear on the exposed metal surface. The anodic metal dissolution reactions proceed with an accelerated rate in these cavities. The large cathodic areas surrounding the cavities and holes support the anodic area. In the crevice corrosion, the metal dissolution reactions take place in the occluded regions. In both modes of localized corrosion, a local chemical environment develops in the anodic sites (Tsujikawa *et al.*, 1987; Tsujikawa and Okayama, 1990; Newman *et al.*, 1987). In most cases of localized corrosion, the local environment in the pits and crevices is more acidic than the cathodic region. For crevice corrosion, the occluded regions tend to occur in shielded areas (crevices) such as those formed under gaskets, washers, insulation material, fastener heads, surface deposits, disbonded coatings, threads, lap joints and clamps. Crevice corrosion is initiated by changes in local chemistry within the crevice. The changes in chemistry could occur due to depletion of oxygen, buildup of aggressive ionic species such as chloride ions, or depletion of inhibiting species (Walton *et al.*, 1996).

The threshold of chemical, environmental, electrochemical and metallurgical conditions to initiate pitting corrosion is generally higher than conditions necessary for crevice corrosion initiation (Frankel, 1998). For example, Alloy 22 is expected to have a very low propensity to pitting corrosion in the potential Yucca Mountain repository environment; however, sufficient evidence exists that crevice corrosion could be induced in the

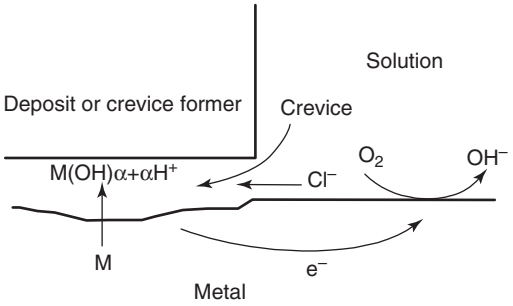

7.5a Schematic diagrams of the crevice corrosion.

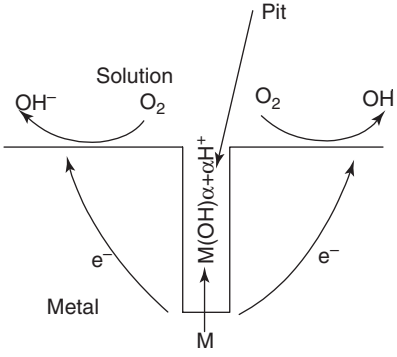

7.5b Schematic diagrams of the pitting corrosion.

repository environment, which would be a combination of high-concentration chloride salts and high temperatures (Gdowski, 1991; Cragnolino *et al.*, 1999; Dunn *et al.*, 2003).

The repassivation potential, E_{rp}, has been proposed as an indicator for long-term initiation of localized corrosion by several investigators (Tsujikawa and Hisamatsu, 1984; Tsujikawa and Kojima, 1991; Dunn *et al.*, 1995). If the corrosion potential, E_{corr}, of the metal exceeds E_{rp}, then localized corrosion can initiate. Pourbaix *et al.* (1963) also proposed the use of the E_{rp} (also called the protection potential) as localized corrosion susceptibility indicator. However, later studies (Wilde, 1974; Rosenfeld *et al.*, 1978) indicated that the E_{rp} decreases with an increasing extent of prior corrosion; therefore, to be a useful parameter for predicting long-term localized corrosion, a lower bound value for E_{rp} must be established.

The breakdown potential, denoted by E_{bd}, is the potential above which pits are initiated, while pits repassivate below the repassivation potential.

The crevice corrosion is initiated above the repassivation potential E_{rp}. The corrosion potential E_{corr} of the metal/solution interface must exceed the E_{bd} for the initiation of pitting corrosion and E_{rp} for the initiation of crevice corrosion. Thus, the higher the value of E_{bd}, the more resistant is the metal to the initiation of pitting corrosion. The higher E_{rp}, the more easily the metal can repassivate. At potentials between E_{rp} and E_{bd}, crevice or pitting sites that have initiated can propagate.

7.4.3 Measurement of localized corrosion susceptibility indicators

The localized corrosion will initiate and propagate if the corrosion potential, E_{corr}, is greater than the repassivation potential, E_{rp}. Pits will initiate and propagate if corrosion potential is greater than breakdown potential, E_{bd}, whereas crevices will undergo localized corrosion when corrosion potential is greater than the repassivation potential, E_{rp}.

E_{bd} and E_{rp} are determined by conducting the cyclic potentiodynamic polarization in the deaerated test solutions. The use of deaerated solution is important; otherwise, the oxygen reduction reaction will interfere with anodic dissolution reactions of the metal. A standard procedure for cyclic potentiodynamic polarization measurements is outlined in ASTM standard G61-86 (ASTM, 2003). In this test method, the potential of the metal surface is scanned starting from the corrosion potential to an anodic value. The electrode potential is scanned at a fixed rate. The ASTM standard procedure recommends a scan rate of 0.6 volts/hour. The electrochemical cell to conduct this test can be similar to that shown in Fig. 3.11 of Chapter 3. The test solution must be sufficiently purged to remove oxygen before specimen immersion. The electrochemical cell contains the working electrode (i.e., metal being studied), a reference electrode, and a counter electrode usually made of platinum. The cell has a gas bubbler to control the quantity of dissolved gases in the solution. The electrolyte can be deaerated by bubbling the pure argon or nitrogen to purge the dissolved oxygen from the solution. Similarly, if necessary, the electrolyte can be saturated with pure oxygen by bubbling it with air for studying the oxygen reduction reaction. As a standard practice, the potential is scanned in the positive direction beginning at the corrosion potential (E_{corr}) at a scan rate of 0.6 volts/hour. The current is continuously recoded by the potentiostat. The breakdown potential marking the onset of localized corrosion is where a rapid increase in current is observed at potentials below the oxygen-evolution potential. When the current reaches 5 milliampere, the potential scan direction is reversed, and applied potential is decreased until the hysteresis loop closes or until the corrosion potential is reached.

A generic polarization of a metal that exhibits passivity (no passive film breakdown) between the corrosion potential and the breakdown potential is presented in Fig. 2.4 of Chapter 2, where E_{rp} is labeled as E_{rpit} and E_{bd} is labeled as E_{pit}. If no breakdown of passive film is seen in the polarization plot at high enough anodic potentials, then breakdown potential is observed when oxygen evolution reaction begins. At the breakdown potential, the current rapidly increases with applied potential. After reaching a high current value (5 mA is recommended by the ASTM Procedure (2003)), the potential scan direction is reversed. As a result, the current starts to decrease. The reverse scan intersects the forward scan at E_{rp} where measured current density is to the level of intact passive film current density in the forward scan. E_{rp} provides a measure of crevice corrosion susceptibility for evaluating the passive alloys. A large amount of experimental data has confirmed this observation. In general, once initiated, localized corrosion can propagate at a potential more electropositive than the repassivation potential. For high-level spent fuel waste packages, the repassivation potential is selected by the US Department of Energy as the lowest potential at which crevice corrosion can initiate in extremely long exposures (Hua *et al*., 2004, Dunn *et al*., 2000a, b).

Two representative cyclic potentiodynamic polarization plots for Alloy 22 in 5.0 M $CaCl_2$ solution and in 5.0 M $CaCl_2$ plus 0.5 M $Ca(NO_3)_2$ solution are presented in Fig. 7.6 (Bechtel SAIC Company, LLC, 2003). These experiments were conducted for the multiple crevice assembly sample in two separate solutions. In the first cyclic potentiodynamic polarization plot of Alloy 22 in 5.0 M $CaCl_2$ solution, the reverse scan intersects the forward scan at 0.1 V_{SSC} (SSC is the acronym for the saturated silver–silver chloride reference electrode), whereas the point of intersection is lowered to the value of –0.18 V_{SSC} with addition of 0.5 M $Ca(NO_3)_2$, as shown in the second polarization plot. The repassivation potential is lowered by approximately 0.3 volts with the addition of nitrate ions in the test solutions. This result demonstrates a strong inhibitory effect of nitrate anion on initiation of localized corrosion.

If the reverse polarization scan does not intersect the forward scan, the repassivation potential can be estimated using a threshold current density (Bechtel SAIC Company, LLC, 2003). Such a cyclic potentiodynamic polarization plot is presented in Fig. 7.7 where current values of reverse scan potentials are less than forward scan. For this system, the repassivation potential is determined where the threshold current density of 1 μA/cm^2 is attained in the reverse polarization curve.

The repassivation potentials obtained from the cyclic potentiodynamic polarization tests are conservative measures of the critical potential for localized corrosion initiation, and information on processes such as localized corrosion initiation time (i.e., initial local passive film breakdown),

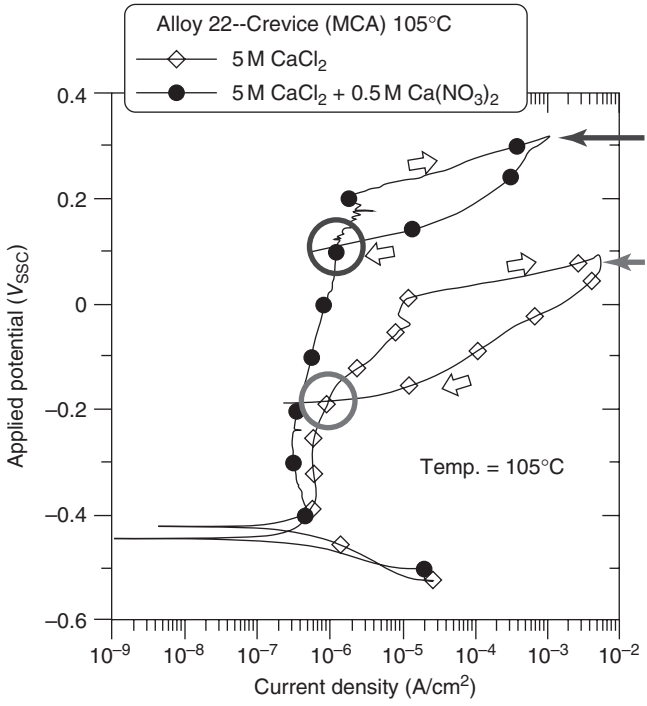

7.6 Cyclic potentiodynamic polarization of Alloy 22 multiple crevice assembly in 5 M $CaCl_2$ Brine at 105 °C, with and without inhibition by NO_3.

stabilization, and propagation cannot be obtained from cyclic potentiodynamic polarization tests. A more realistic measure of the critical potentials can be obtained using the potentiostatic polarization method. Pitting and crevice corrosion initiation times can be measured by polarizing a test specimen to potentials above and below the E_{rp} measured in cyclic potentiodynamic polarization tests. This method can be used to validate the repassivation potential as a parameter for determining long-term performance. In this technique, the sample is potentiostatically held at a potential and monitored for the corrosion current. The procedure for this test has been outlined in Chapter 3. In localized corrosion studies, a test sample is polarized at a given potential, and variation of current is recorded as a function of time. This test is conducted in an aerated solution.

When a metal is polarized at a constant potential, the measured current may decrease with time until a steady state is reached. If steady-state current density is equal to or less than passive current density, the localized

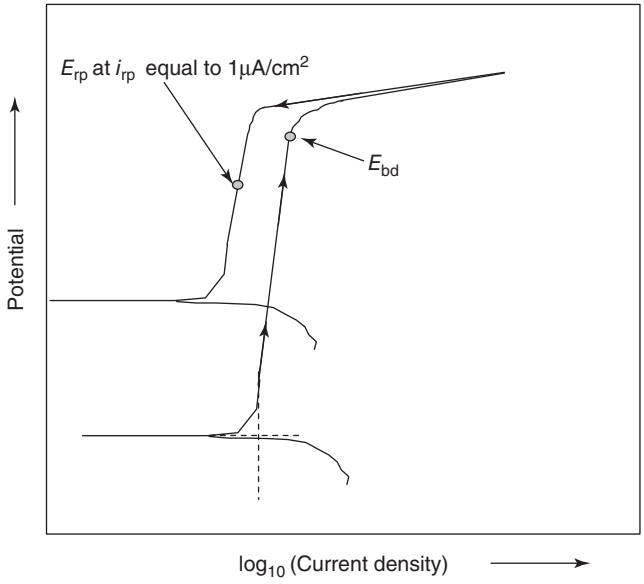

7.7 A schematic of a cyclic potentiodynamic polarization plot for a passivating metal where reverse scan does not intersect with forward scan. The repassivation potential is determined where current density at the reverse scan reaches 1 μA/cm^2.

corrosion would not initiate; otherwise, the localized corrosion penetration rate can be estimated from potentiostatic measurements. For Alloy 22, potentiostatic tests have been used to determine the evolution of the crevice corrosion penetration depth as a function of time (Bechtel SAIC Company, LLC, 2003). The measured current densities from the potentiostatic tests were used to determine the localized corrosion penetration rates under various conditions. However, steady state may not be achieved in laboratory tests. Furthermore, the measured current density may not accurately represent anodic dissolution reactions. For example, in the presence of dissolved oxygen, the reduction of oxygen to water may consume electrons, short-circuiting the flow of current to the counter electrode. Thus, the actual passive current density for metal dissolution may be higher than the measured one. The magnitude of this underestimation of the passive current will depend on the system and the value of the applied potential.

7.5 Summary

Although the use of repassivation potential as a localized corrosion susceptibility indicator is still debated, it is widely used for this purpose for

extremely corrosion-resistant materials such as Alloy 22. The repassivation potentials obtained from the cyclic potentiodynamic polarization in deaerated solutions are conservative measures of the critical potentials for localized corrosion initiation. Both crevice and localized corrosion could propagate when corrosion potential, measured in aerated solution, is higher than repassivation potential. However, the threshold of chemical, environmental, electrochemical and metallurgical conditions necessary to initiate pitting corrosion is generally higher than conditions necessary for crevice corrosion initiation. The breakdown potential, denoted by E_{bd}, is the potential above which pits are initiated, while pits repassivate below the repassivation potential, denoted by E_{rp}. The corrosion potential, E_{corr}, of the metal/solution interface must exceed E_{bd} or initiate pitting corrosion and E_{rp} to initiate crevice corrosion. In addition, existing pits are likely to propagate above the repassivation potential. Thus, the higher the value of E_{bd}, the more resistant is the metal to the initiation of pitting corrosion. The higher E_{rp}, the more easily the metal can repassivate. At potentials between E_{rp} and E_{bd}, crevice or pitting sites that have initiated can propagate.

7.6 References

1 Guggenheim, E.A., 'The Conceptions of Electrochemical Potential Different Between Two Phases and Individual Activities of Ions,' *Journal of Physical Chemistry*, 33, 842–849, 1929.
2 Milazzo, G. and S. Caroli, *Tables of Standard Electrode Potentials,* John Wiley and Sons, New York, 1978.
3 Bard, A.J. and L.R. Faulkner, *Electrochemical Methods*, John Wiley and Sons, New York 1980.
4 American Society for Testing Materials (ASTM), *Standard Reference Test Method for Making Potentiostatic and Potentiodynamic Anodic Polarization Measurements*, ASTM Designation: G5-94, Philadelphia, PA, 2004.
5 Davis, J.R., editor, *Corrosion: Understanding the Basics*, ASM International, Materials Park, OH 2000.
6 Nisancioglu, K., 'Predicting the Time Dependence of Polarization on Cathodically Protected Steel in Seawater,' *Corrosion*, 43, 100–111, 1987.
7 Jones, D., *Corrosion*, 2nd edition, Prentice Hall, Upper Saddle River, NJ, 1992.
8 Jovancicevic, V. and J.O.M. Bockris, 'The Mechanism of Oxygen Reduction on Iron in Neutral Solution', *Journal of the Electrochemical Society*, 133, 1789–1807, 1986.
9 Jerkiewicz, G., 'Hydrogen Sorption AT/IN Electrodes', *Progress in Surface Science*, 57, 137–186, 1998.
10 Chialvo, M. de, and A. Chialvo, 'Existence of Two Sets of Kinetic Parameters in the Correlation of the Hydrogen Electrode Reaction', *Journal of the Electrochemical Society*, 147, 1619–1622, 2000.

11 American Society for Testing Materials (ASTM), *Standard Guide for Development and Use of a Galvanic Series for Predicting Galvanic Corrosion Performance*, ASTM Designate: G 82–83, Race Street, Philadelphia, PA, 1984.
12 Kelly, R.G., J.R. Scully, D.V. Shoesmith and R.G. Buckheit, *Electrochemical Techniques in Corrosion Science and Engineering*, Marcel Dekker Inc., New York, 2003.
13 Uhlig, H.H. and R.W. Revie, *Corrosion and Corrosion Control: An Introduction to Corrosion Science and Engineering*, 3rd edition, John Wiley and Sons, New York, 1984.
14 Treseder, R., R. Baboian and C.G. Munger, *NACE Corrosion Engineer's Reference Book*, NACE International, Houston, TX, 1991.
15 Day, S.D., K.J. Evans and G.O. Ilevbare, in *Critical Factors in Localized Corrosion IV*, PV 2002–24, p. 534, The Electrochemical Society, Pennington, NJ, 2003.
16 Uhlig, H., 'History of Passivity, Experiments, and Theories', in *Passivity of Metals, Proceedings of the Fourth Symposium on Passivity*, edited by R. Frankenthal and J. Krugger, Electrochemical Society, Princeton, NJ, 1978.
17 Wagner, C., 'Passivity and inhibition during the oxidation of metals at elevated temperatures', *Corrosion Science*, 5, 751–764, 1965.
18 Faraday, F., *Experimental Researches in Electricity*, Vol. II, Dover, New York, 1965.
19 C. Schöenbien, *Pogg. Ann.*, 390, Vol. 37, 1836.
20 Mon, K.G., P. Pasupathi, A. Yilmaz and R.B. Rebak, 'Stifling of Crevice Corrosion in Alloy 22 During Constant Potential Tests', ASME Pressure Vessels & Piping Division Conference, Denver, CO, July 2005.
21 Fontana, M.G. and N.D. Greene, *Corrosion Engineering*, McGraw-Hill, New York, 1978.
22 Baker, E.A., 1988. 'Long-Term Corrosion Behavior of Materials in the Marine Atmosphere', Degradation of Metals in the Atmosphere, Proceedings of the Symposium on Corrosion of Metals, Philadelphia, Pennsylvania, 12–13 May 1986.
23 Bechtel SAIC Company, LLC, 'General Corrosion and Localized Corrosion of Waste Package Outer Barrier', Rev. 02, Las Vegas, NV, 2004.
24 Estill, J.C., G.A. Hust and R.B. Rebak, 'Long Term Corrosion Potential Behavior of Alloy 22', Proceedings of the CORROSION 2003 Conference, Paper No. 03688, NACE International, Houston, TX, 2003.
25 Farmer, J.C. and D. McCright, 'Crevice Corrosion and Pitting of High-Level Waste Containers: Integration of Deterministic and Probabilistic Models', Proceedings of the CORROSION 1998 Conference, NACE International, Houston, TX, 1998.
26 Tsujikawa, S., Y. Sone and Y. Hisamatsu, In: *Corrosion Chemistry Within Pits, Crevices and Cracks*, A. Turnbull, ed., Her Majesty Stationery Office, London, 171, 1987.
27 Tsujikawa, S. and S. Okayama, 'Repassivation Method to Determine Critical Conditions in Terms of Electrode Potential, Temperature and NaCl Concentration to Predict Crevice Corrosion Resistance of Stainless Steels', *Corrosion Science*, 31, 441–446, 1990.
28 Newman, R.C., K. Sieradzki, J. Woodward, *Corrosion Chemistry Within Pits, Crevices and Cracks*, A. Turnbull, ed., HMSO, 203, 1987.

29 Walton, J.C., G. Cragnolino and S.K. Kalandros, 'A Numerical Model of Crevice Corrosion for Passive and Active Metals', *Corrosion Science*, 38, 1–18, 1996.
30 Frankel, G.S., 'Pitting Corrosion of Metals, A Review of the Critical Factors', *Journal of the Electrochemical Society*, 145(6), 2186–2198, 1998.
31 Gdowski, G.E., *Survey of Degradation Modes of Four Nickel-Chromium-Molybdenum Alloys*, Lawrence Livermore National Laboratory, Livermore, CA, 1991.
32 Cragnolino, G.A., D.S. Dunn, C.S. Brossia, V. Jain and K.S. Chan, *Assessment of Performance Issues Related to Alternate Engineered Barrier System Materials and Design Options*, Center for Nuclear Waste Regulatory Analyses, CNWRA 99-003. San Antonio, TX, 1999.
33 Dunn, D.S., L. Yang, Y-M. Pan and G.A. Cragnolino, 'Localized Corrosion Susceptibility of Alloy 22', Proceedings of the CORROSION 2003 Conference, Paper No. 03697, NACE International, Houston, TX, 2003.
34 Tsujikawa, S. and Y. Hisamatsu, 'Repassivation Potential as a Crevice Corrosion Characteristic for Austenitic and Ferritic Stainless Steels', in *Improvement of Corrosion Resistance of Structural Materials in Aggressive Media*, Ya. M. Koloyrkin, ed., Nauka Publishers, Moscow, Russia, 1984.
35 Tsujikawa S. and Y. Kojima, 'Repassivation Method to Predict Long-Term Integrity of Low-Alloy Titanium for Nuclear Waste Package', *Scientific Basis for Nuclear Waste Management XIV*, T. Abrajano and L.H. Johnson, eds., Pittsburgh, PA: Materials Research Society: Symposium Proceedings 212: pp 261–268, 1991.
36 Dunn, D.S., N. Sridhar and G.A. Cragnolino, 'Effects of Surface Chromium Depletion on Localized Corrosion of Alloy 825 as a High Level Nuclear Waste Container Material', *Corrosion*, 51(8), 618–624, 1995.
37 Pourbaix, M., L. Klimzack-Mathieu, J. Meunier, C. Vanleugenhaghe, L. Munck, J. Laureys, L. Neelemans and M. Warzee, 'Potentiokinetic and Corrosimetric Investigations of the Corrosion Behaviour of Alloy Steels', *Corrosion Science*, 3, 239–259, 1963.
38 Wilde, B.E., 'On Pitting and Protection Potentials: Their Use and Possible Misuses for Predicting Localized Corrosion Resistance of Stainless Alloys in Halide Media', in *Localized Corrosion*, R.W. Staehle, B.F. Brown, J. Kruger and A. Agarwal eds. 342–352. 1974.
39 Rosenfeld, I.L., I.S. Danilov and R.N. Oranskaya, 'Breakdown of the Passive State and Repassivation of Stainless Steels', *Journal of the Electrochemical Society*, 125(11), 729–735, 1978.
40 American Society for Testing Materials (ASTM), *Standard Test Method for Conducting Cyclic Potentiodynamic Polarization Measurements for Localized Corrosion Susceptibility of Iron-, Nickel-, or Cobalt-Based Alloys*, ASTM Designation # G61-86, Race Street, Philadelphia, 2003.
41 Hua, F., J. Sarver, J. Jevec and G. Gordon, 'Corrosion Behavior of Alloy 22 and Ti Grade 7 in a Nuclear Waste Repository Environment', *Corrosion*, 60(8), 764–777, NACE International, Houston, TX, 2004.
42 Dunn, D.S., Y-M. Pan and G.A. Cragnolino, 'Stress Corrosion Cracking, Passive, and Localized Corrosion of Alloy 22 High Level Radioactive Waste Containers',

Proceedings of the CORROSION 2000 Conference, Paper No. 00206, NACE International, Houston, TX, 2000a.
43 Dunn, D.S., G.A. Cragnolino and N. Sridhar, 'An Electrochemical Approach to Predicting Long-Term Localized Corrosion of Corrosion-Resistant High-Level Waste Container Materials', *Corrosion*, 56(1), 90–104, 2000b.
44 Bechtel SAIC Company, LLC., Technical Basis Document No. 6: Waste Package and Drip Shield Corrosion. Las Vegas, NV, 2003.

8

Multielectrode systems

LIETAI YANG, Department of Earth, Material and Planetary Sciences, Southwest Research Institute, San Antonio, Texas, USA

8.1 Introduction

Multielectrode systems have been used for electrochemical and corrosion studies for at least three decades. Coupled multielectrode systems, in which the multiple electrodes are connected together through an external circuit and all electrodes are essentially at the same potential, were first used as high throughput devices for the measurements of the stochastic behavior of pitting corrosion in 1977. Similar concepts were reported for corrosion detection in concrete in 1991, and for crevice corrosion measurements in 1993.

Multielectrode arrays, in which the multiple electrodes are arranged in a given pattern and each electrode is addressable, have been used since 1984. The early work on the multielectrode arrays appears to have been for the development of electronic devices. The concept of multielectrode arrays for corrosion studies, in the uncoupled form, was first reported in 1991. The first coupled multielectrode array that was used to simulate a one-piece metal for studying the spatiotemporal electrochemical behaviors and corrosion processes of iron in sulfuric acid solutions was published in 1996. Because the electrodes in a multielectrode array can be arranged in any given pattern and each of the electrodes is addressable, the coupled multielectrode arrays have been widely used by researchers to study the corrosion processes, especially the localized corrosion processes, of metals.

Recently, coupled multielectrode arrays have been used as sensors (called coupled multielectrode array sensors (CMASs)) for online and real-time monitoring of corrosion in laboratories and industrial fields. Because a CMAS does not require the presence of bulk electrolytes, CMAS probes have been used to quantitatively measure the localized corrosion of metals not only in aqueous solutions, but also in wet gases, oil/water mixtures, salt deposits, biodeposits, soil, concrete and undercoatings. CMAS probes were also used for real-time monitoring of the performance of cathodic

protection systems. In addition to the real-time measurement of the quantitative rate of localized corrosion, such as pitting and crevice corrosion, CMAS probes have also been used to measure the average corrosion rates. This chapter presents a review for the development of the coupled multielectrode array systems for corrosion monitoring.

8.2 Earlier multielectrode systems for high throughput corrosion studies

The first published use of a multielectrode system appears to have been by Shibata and Takeyama[1] concerning the evaluation of the stochastic behavior of pitting corrosion. Figure 8.1 shows the schematic diagram of the multielectrode system. Twelve stainless steel specimens were assembled onto a specimen holder and each of them was individually connected, through independent ammeters and relays, to a common joint which was in turn connected to a potentiostat. The potential of the specimens was increased at a given constant rate (mV per second) in the anodic direction by the potentiostat. A timer was used for each specimen to trigger the

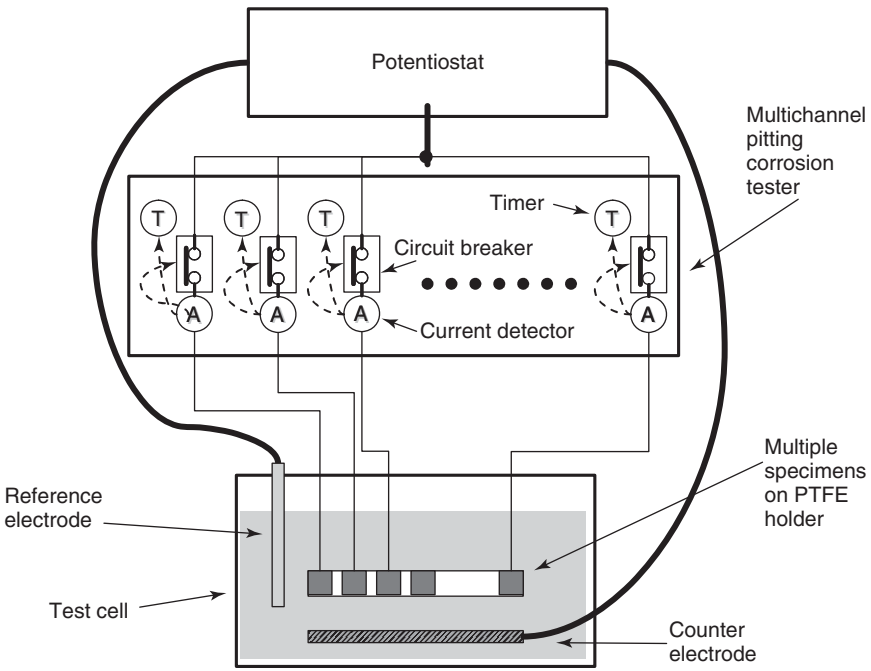

8.1 Schematic diagram of a multielectrode system for high throughput pitting potential measurements.[1]

opening of the relay if the current from that specimen exceeded a given value, which indicated the initiation of pitting corrosion for that specimen. Because the potential was increased linearly from a known value, the potential at which each relay was triggered was known from the timer. In this way, the authors were able to obtain 12 pit initiation potentials in one experiment, which greatly increased the efficiency of the pitting potential measurements, and enabled them to study the stochastic behavior of the pitting corrosion of stainless steel.

Because the multiple electrodes were connected to one common joint and all the electrodes were at the same electrode potential during the test (before the trigger was initiated by the timer), this system can also be categorized as a coupled multielectrode system. The current through each electrode was also individually measured.

Similar high-throughput measurements were also reported by Tan and Xu in 1987 in the evaluation of coating performance on steel.[2] Multiple specimens coated with different corrosion-prevention oils were assembled in an electrochemical cell and connected to a common joint through individual manual switches (Fig. 8.2). This was the same as Shibata and

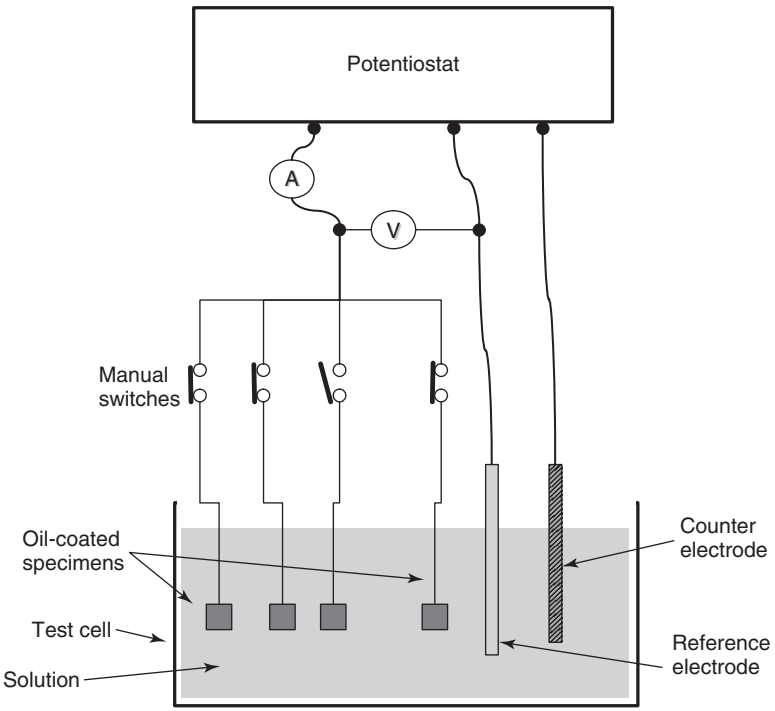

8.2 Schematic diagram of a multielectrode system for high throughput evaluation of coatings.[2]

Takeyama's approach. The common joint was connected to a potentiostat; an ammeter and a voltmeter were used to measure the total current flowing through all the specimens (electrodes) and the potential of the electrodes (at the common joint), respectively. During the measurements, a constant anodic current was applied to the multiple specimens (measured as the total current as compared with the individual current in the study by Shibata and Takeyama). Because the specimens with poor coatings allowed the anodic current to pass easily and the specimens with high-quality coatings did not allow the current to flow, the authors were able to identify the quality of the different coatings by interrogating the switches. For example, if the potential changed significantly only after opening the switch connected to the first specimen, the coating quality on the first specimen was poor. On the other hand, if the potential did not change before and after opening the first switch, the quality of the coating on the first specimen was at least not worse than one of the others that were connected to the common joint.

8.3 Uncoupled multielectrode arrays

The first published multielectrode array appears to be the multiple gold microelectrode system on a single-crystal silica substrate developed by the group at Massachusetts Institute of Technology (USA)[3–5] using microfabrication techniques. In one example,[4] the array was comprised of eight individually addressable gold microelectrodes, each being about 0.12 μm thick, 3 μm wide, and 140 μm long, and separated from each other by a distance of 1.4 μm (Fig. 8.3). The authors coated electroactive polymers on

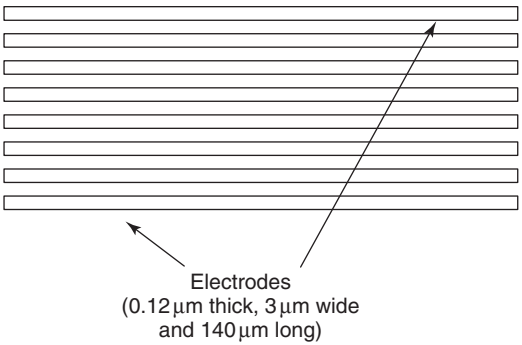

8.3 Schematic diagram of a micro multielectrode array device.[4]

the microelectrode arrays and electrochemically characterized the semiconducting properties of the arrays as molecule-based electronic devices such as diodes. A similar microelectrode array was also used by Wang to study the electrochemical behavior of the high-resistance lubricant by coating the closely packed electrodes with ionically conducting polyethylene oxide film.[6]

The first published uncoupled multielectrode array for corrosion studies (also called wire beam electrode, WBE) appears to be the one described by Tan[7] and Tan and Yu[8] in 1991 for measuring the corrosion behavior of carbon steel under oil-based coatings. Later, similar multielectrode arrays were used to study nonuniform corrosion under protective coatings and salt deposits.[9–16] In a typical uncoupled multielectrode array, a large number of wires (0.5 to 2 mm in diameter) are flush-mounted in epoxy and arranged in a square configuration with the cross-section exposed to an electrolyte. The spatial behavior of corrosion or the electrochemical heterogeneity is characterized by the measurement of the open-circuit potential map from each electrode, and by the measurement of the current map or electrical resistance map between pairs of selected wires. Readers are encouraged to read Chapter 27 for more on this topic.

8.4 Coupled multielectrode systems for corrosion detection

One of the devices described by Schiessl in a US patent[17] issued in 1991, and in a patent application[18] initially filed in Germany in 1988 appeared to be the first coupled multielectrode system for corrosion monitoring (Figure 8.4). This coupled multielectrode system consisted of multiple steel anodes that were composed of materials similar to the reinforcement material and a corrosion-resistance cathode. Both the anodes and the cathode were embedded in a concrete structure. The steel anodes were separated from each other at different distances from the external surface of the concrete structure, and each electrode was independently connected (coupled) to the cathode through a resistor. The coupling current from each anode to the cathode as a result of corrosion was measured by a voltage-measuring system that was connected to both ends of the resistor to establish the temporal course of the penetration of substances (e.g., chloride) that were capable of damaging the reinforcement. Similar applications in concrete were reported later in other publications by Schiessl and coworkers and by other investigators.[19–24]

In 1993, Steinsmo and coworkers reported on similar galvanically coupled multielectrode systems used to study the crevice corrosion of stainless steel materials in seawater.[25–28] Figure 8.5 shows the galvanically coupled multielectrode system used by Steinsmo and coworkers. In this system, several

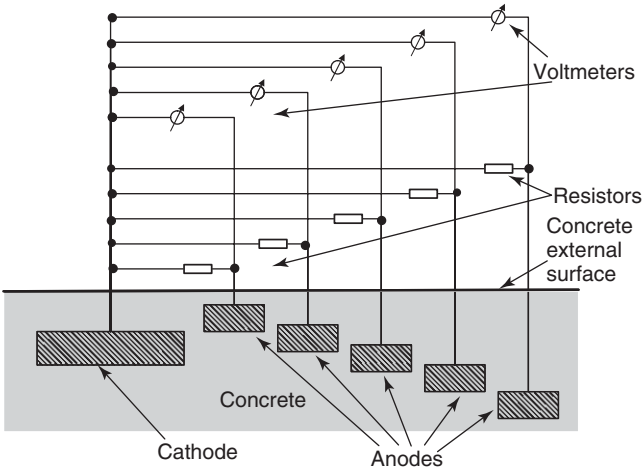

8.4 Schematic diagram of a galvanically coupled multielectrode system used to detect the onset of corrosion of carbon steel reinforcing materials at different locations. Note: The anodes were made of carbon steels similar to the reinforcing material; the cathode was made of special steels or alloys.[17]

creviced stainless steel specimens were independently coupled to a large non-creviced specimen (similar to the creviced specimens in composition) through resistors. The corrosion process taking place in the crevices made the electrode potential of the creviced specimen more negative (or anodic) than the large non-creviced specimen (cathode) and produced a coupling current from the large non-creviced specimen to the creviced specimen. The coupling current was measured across its associated resistor and used to indicate the degree of crevice corrosion. The reference electrode in Fig. 8.5 was used to measure the potential of the coupled multielectrode system.

Figure 8.6 shows typical results obtained with the coupled multielectrode system by Steinsmo *et al*.[27] The measurement was conducted in a seawater test loop at 15 °C, a condition under which the specimen is normally not subject to crevice corrosion. The purpose of this measurement was to study the effect of temporary upset conditions on crevice corrosion of a welded UNS S31254 material in seawater. Prior to the start of the measurement in Fig. 8.6, the crevice specimens were temporarily aged at high temperatures and high electrochemical potentials to initiate crevice corrosion. Figure 8.6 shows that the corrosion attack continued to propagate at 15 °C for 10 to 20 days before repassivation took place.

The use of resistors between the coupling joint and each electrode in Figs 8.4 and 8.5 might cause potential variations among the different electrodes.

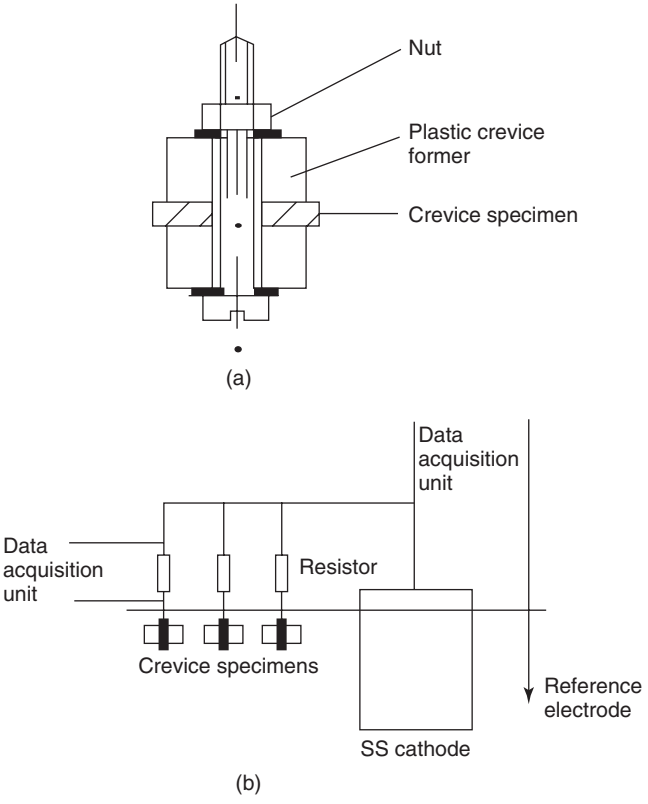

8.5 Schematic diagram of a galvanically coupled crevice cell system. (a) Crevice assembly and (b) galvanic coupling of crevice assemblies and stainless steel cathode.[27] © NACE International 1997.

As long as the currents flowing through the individual electrodes were low, or the resistors were small, such variations would not be significant compared with the potential changes required to cause significant current changes on a typical polarization curve. Therefore, Figs 8.4 and 8.5 may be considered as the coupled multielectrode systems according to the definition at the beginning of this chapter (all electrodes are essentially at the same potential).

The multielectrode technique shown in Figs 8.4 and 8.5 requires only straightforward voltage measurements and yet is capable of detecting the onset of general and localized corrosion under service conditions. Depending on its accuracy and resolution, the voltage-monitoring instrument may be able to detect corrosion in the early stages of degradation. The disadvantage of this technique is that it cannot be used to determine the true

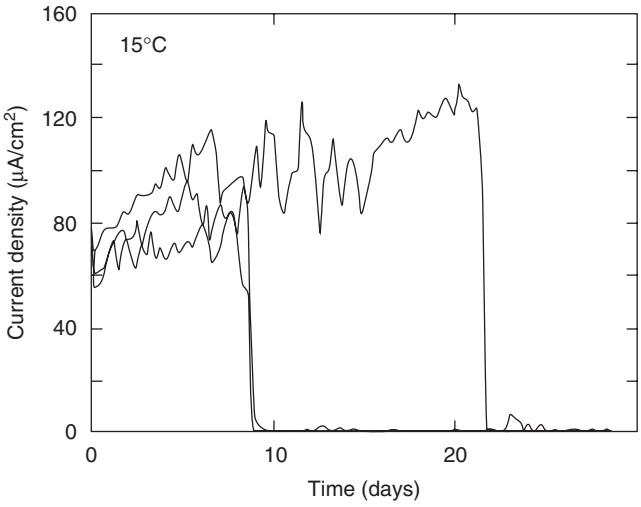

8.6 Galvanic current densities between three creviced specimens of welded UNS S31254 and a cathode as a function of time in seawater at 15 °C.[27] © NACE International 1997.

rate of general or localized corrosion because of the large surface area of the crevice (5.5 cm^2 in Fig. 8.5).

8.5 Coupled multielectrode arrays for spatiotemporal corrosion and electrochemical studies

The first published coupled multielectrode array for corrosion and electrochemical studies appears to be the one described by Fei *et al*. in 1996.[29] The coupled multielectrode array was used to simulate a one-piece metal electrode for the study of the spatiotemporal electrochemical behavior of iron metal in a sulfuric acid solution. The electrode arrays consisted of 16 (a 2 × 8 rectangle or a 4 × 4 square) or 61 (a hexagonal shaped-bundle) electrodes (cross-section of 0.5 mm diameter wires) embedded in epoxy (Fig. 8.7).[29–30] The individual wires were coupled to a common joint using a multichannel zero-resistance ammeter (ZRA) box and the current flowing through each individual electrode was independently measured. The common coupling joint was connected to the working electrode jack of a potentiostat so that the electrode array could be polarized to study the electrochemical spatiotemporal pattern of the electrode array at different potentials. With the 61-electrode array, it was shown (Fig. 8.8)

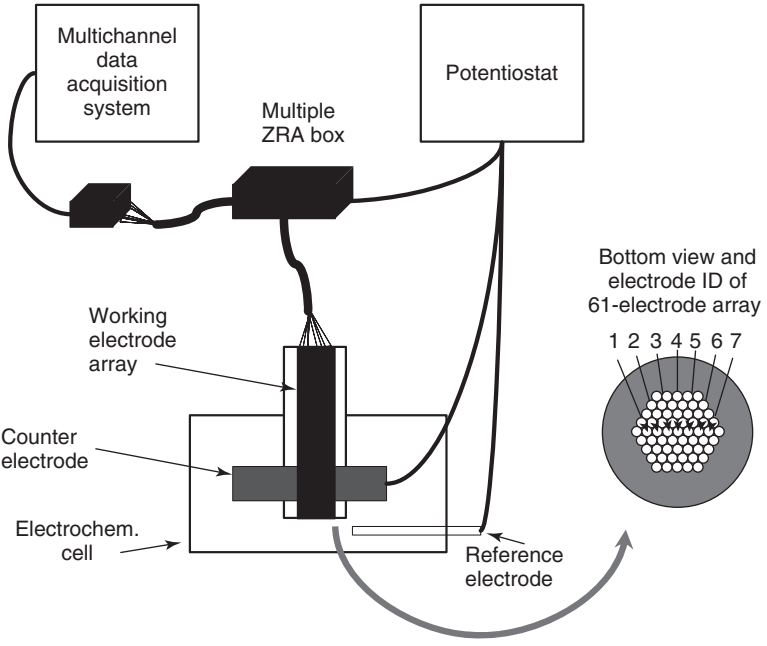

8.7 Schematic diagram of a coupled multielectrode array system used to study the spatiotemporal pattern of the nonuniform corrosion of iron in sulfuric acid solution. Modified according to Ref. 30, with permission from Z. Fei and J.L. Hudson.

that: (a) the activation (corrosion) of metal started at the center electrodes and propagated from the center to the edge; and (b) the passivation started from the edge electrodes and propagated in the opposite direction (from the edge to the center). By comparing the behavior of the total current from the electrode array with the behavior of the current from a one-piece electrode, the authors concluded that the array of electrodes behaved similarly to a one-piece electrode of the same shape and total area. Thus, the electrochemical spatial patterns observed with the electrode array are representative of patterns on a one-piece metal electrode. By using the coupled multielectrode array, the authors were able directly to determine the spatial pattern of the active-passive electrochemical oscillations and how the oscillation wave front travels on a large iron electrode. Hudson and coworkers conducted extensive studies in this area, and the results were reported in a large number of publications.[31–44] Similar coupled multielectrode arrays were also used extensively by others to study the corrosion mechanism and spatial interactions among the

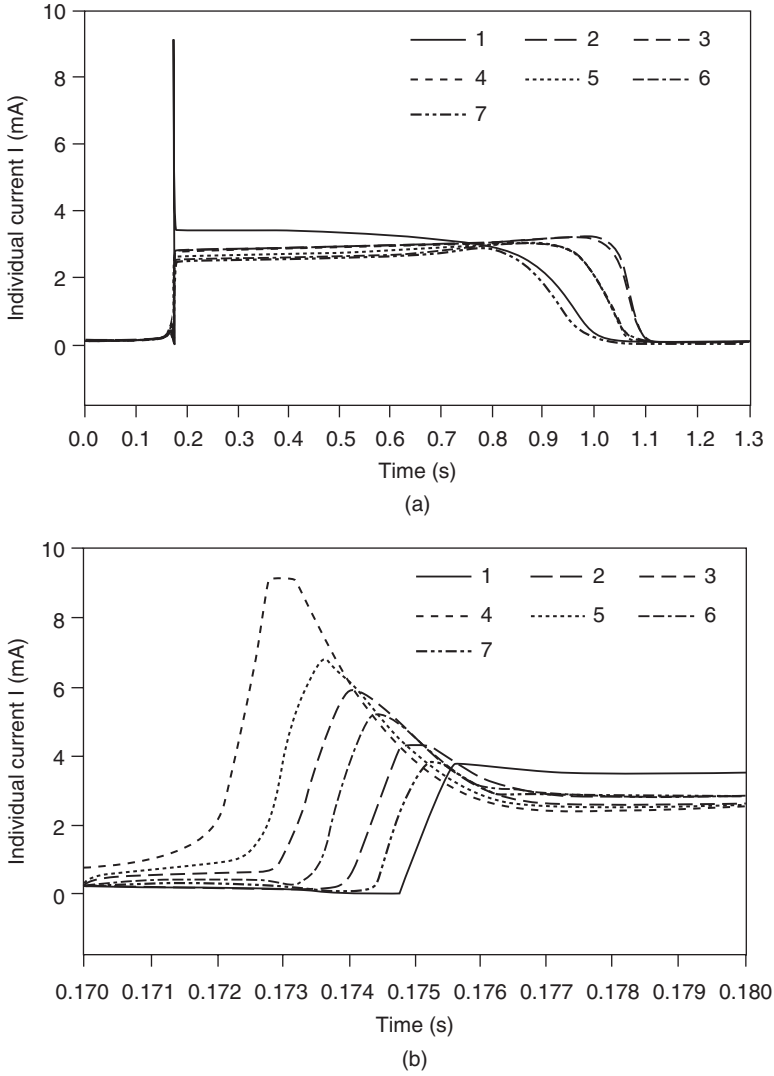

8.8 Currents of individual electrodes on the 61-electrode array, as shown in Fig. 8.7 during (a) activation and (b) passivation. Note: The electrode numbers are shown in Fig. 8.7. Source: Ref. 30, with permission from the American Chemical Society.

localized corrosion sites on different metals,[45–53] and the localized corrosion behavior of aluminum alloys,[54–60] copper alloy,[61] nickel,[62] the characteristics of chromate coatings[63] and atmospheric corrosion.[61,64] Coupled multielectrode systems were also used to study the deposition of metals.[65–66]

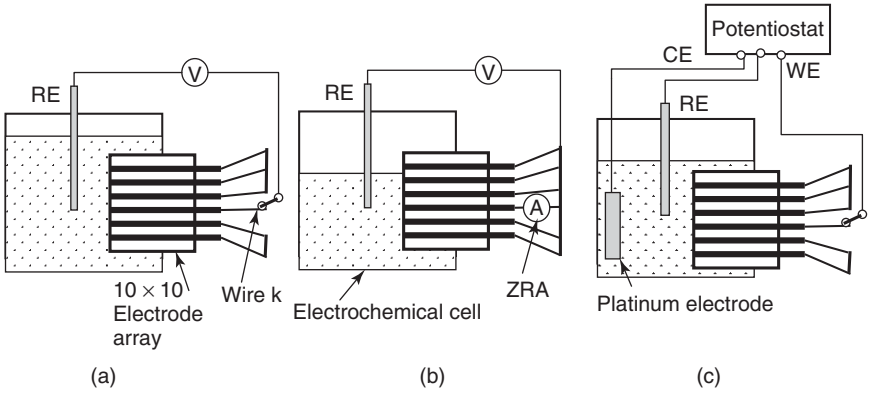

8.9 Schematic diagram of the coupled multielectrode array system for measurement of: (a) open-circuit potentials of individual wires; (b) galvanic currents between individual wires and the system; and (c) Tafel slopes of individual wires.[68] © NACE International 1998.

8.6 Coupled multielectrode arrays for spatiotemporal corrosion measurements

Coupled multielectrode arrays (also called WBE) were used by Tan *et al.*, to study the spatiotemporal patterns of the localized corrosion current and potential on carbon steel electrodes.[67–78] Their work with the coupled multielectrode arrays was first published in 1997.[67] Figs 8.9a and b show the multielectrode array used in their studies.[68] In Figs 8.9a and b, multiple electrodes were directly connected to a common joint. The current flowing through each electrode was measured by momentarily decoupling the electrode from the common joint and inserting a ZRA between the electrode and the common joint. The potential of the individual electrodes and the coupling joint was measured with a voltmeter (V) and a reference electrode (RE). Because the potential of each electrode was measured under open-circuit conditions, this system was not operating under truly coupled conditions. The decoupling of electrodes for the measurement of the open-circuit potential may have affected the ability of this system to simulate the behavior of a one-piece metal.

In a localized corrosion environment, each mini-electrode was considered to corrode uniformly and behave as an ideal electrochemical system because of the small size (three to four orders of magnitude smaller than the electrode in a typical conventional corrosion probe such as a linear polarization resistance probe). Therefore, the following formulae were derived on the basis of the Butler–Volmer equation to calculate the corrosion current on each electrode:[68]

$$I_{ka} = I_{kcouple}/\{1 - \exp[-(2.3/b_{ka} + 2.3/b_{kc})\ (E_{coup} - E_{kopen})]\} \quad [8.1]$$

where I_{ka} is the anodic current (or corrosion current) from electrode k; $I_{kcouple}$ is the coupling current from electrode k measured with the ZRA; E_{kopen} is the open-circuit potential of electrode k; E_{coup} is the coupling potential of all the electrodes; and b_{ka} and b_{kc} are the anodic and the cathodic Tafel slopes, respectively. It was proposed to use a separate *RE* to measure the values for E_{kopen}, when electrode k is disconnected from the coupling joint, and E_{coup}. Linear polarization measurements were conducted to obtain the Tafel slopes.

It was hypothesized that if the value of $E_{coup} - E_{kopen}$ for an electrode is greater than 100 mV, the exponential term in Equation [8.1] will vanish, and the corrosion current from electrode k could be estimated by the coupling current from the electrode:

$$I_{ka} = I_{kcouple} \quad [8.2]$$

A system used to experimentally measure the coupling currents, coupling potential, open-circuit potential, and Tafel slopes is shown in Figs 8.9a, b, and c.

This method has been applied to mapping the localized corrosion behavior (coupled currents) of carbon steel materials in aqueous solutions,[67] crevice,[74] water/gas interface[75] and soil.[77] In localized corrosion conditions, electrode kinetics of actively pitting electrodes are often diffusion-controlled and the kinetics of the passive electrodes are controlled by a thin oxide film. Because the Butler–Volmer equation applies to activation controlled processes, the application of Equation [8.1] to localized corrosion conditions should be evaluated. In addition, the decoupling of individual electrodes for the measurement of the open-circuit potential or Tafel slope may alter the localized corrosion processes.

Tan and coworkers also used the multielectrode arrays in conjunction with the electrochemical noise technique to measure the localized corrosion rate distributions.[71,78] With this approach, the electrochemical noise resistances between paired electrodes in the multielectrode array were measured, and the localized corrosion rate for each electrode was calculated based on the electrochemical noise theory. Because the noise resistance was measured in pairs, the multielectrode array that operated under this mode was not a coupled multielectrode array.

8.7 Coupled multielectrode array sensors with simple output parameters for corrosion monitoring

The coupled multielectrode array systems have been used as sensors (called coupled multielectrode array sensors or CMAS) for real-time monitoring

the rate of corrosion, particularly localized corrosion.[79–121] As described in Sections 8.4 through 8.6, coupled multielectrode systems can provide not only temporal, but also spatial information on corrosion, especially localized corrosion in two dimensions. It is an excellent tool for the studies of corrosion phenomena in laboratories. However, the data from a multielectrode system are often huge and incomprehensible by ordinary plant or facility operators. The data must be greatly reduced to one or to a few simple parameters so that the multielectrode systems can be used as a sensor to provide real-time data for the operation of a plant or facility in the field. This section describes the working principle of the coupled multielectrode array sensors that are suitable for corrosion monitoring and the methods used to derive the simple parameters.

8.7.1 Principle of coupled multielectrode array sensors for corrosion monitoring

Figure 8.10 shows the schematic diagram of a typical CMAS.[85,104,109] A coupling resistor was used between each electrode and the common coupling point. Electrons from a corroding (or a relatively more corroding) electrode (or an anodic half-cell) flow through the resistor connected to the electrode and produce a small potential drop. This potential drop is measured by a high-resolution voltage-measuring instrument and used to derive the current. It should be noted that for the multiple electrodes in the CMAS probe to simulate the behavior of a one-piece large metal, the potentials of the electrodes must be substantially the same. Variable coupling resistors whose value can be automatically changed by a controller during the measurements have been used to minimize the potential differences across the coupling resistors.[114]

The CMAS probes can be made in many configurations and sizes, depending on the applications. They may be used for high temperature and high pressure applications if the electrodes are properly sealed and insulated with high temperature insulators. Figure 8.11 shows a typical commercial CMAS monitor (nanoCorr™) and some typical commercial probes for real-time corrosion monitoring in plants or in fields. (nanoCorr is the trade name of Corr Instruments, LLC, San Antonio, TX, USA.)

Figure 8.12 shows the principle of a CMAS probe, assuming that one electrode on the probe is anodic and all the other electrodes are cathodic. Because localized corrosion often involves small areas of corroded anodic sites accompanied by large areas of cathodic sites, such assumption is often reasonable under many environments. The thin solid curves represent the dissolution and reduction polarization behaviors on the anodic electrode. The thick solid curves represent the combined dissolution and reduction polarization behaviors on the rest of the electrodes (the cathodic

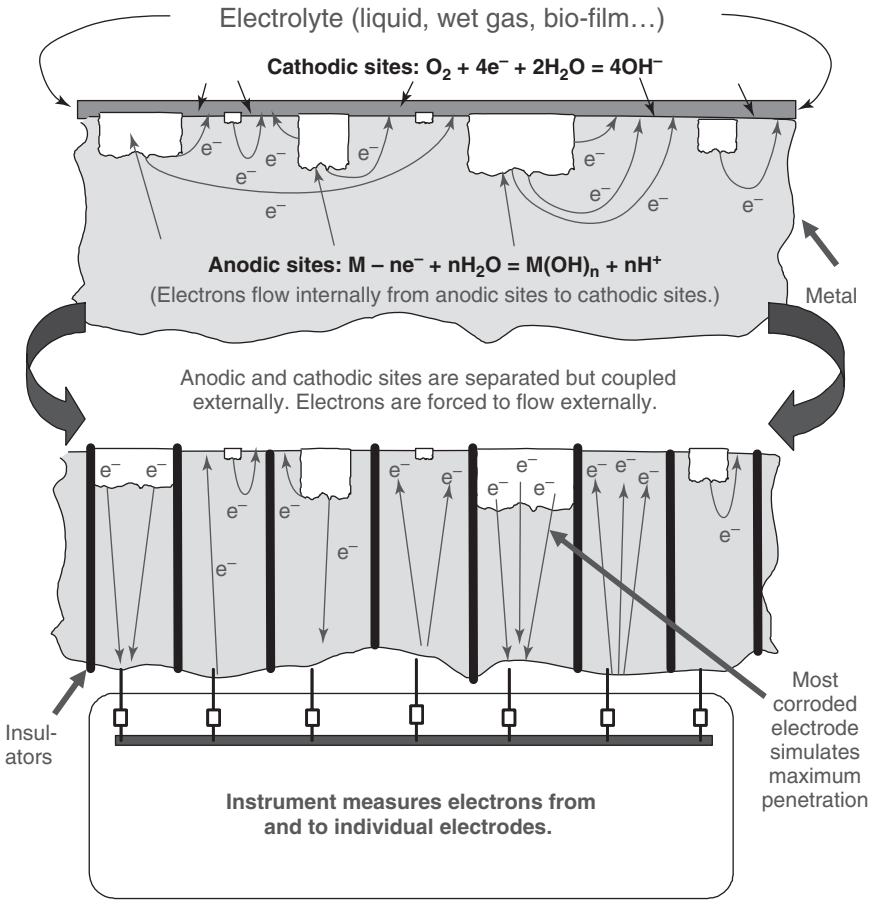

8.10 Schematic diagram showing the principle of coupled multielectrode array sensors for localized corrosion monitoring.[104] © NACE International 2006.

electrodes) if these cathodic electrodes are coupled as a single electrode. The thick dashed lines represent the reduction curve for all electrodes, or the dissolution behavior for all electrodes on the CMAS probe. For a passive metal, in the cathodic area (or the cathodic electrodes in a CMAS probe) where no localized corrosion has been initiated, the anodic current is usually extremely low due to the protective layer of the oxide formed on the metal (see Chapter 2) and the corrosion potential for the cathodic electrodes, E^c_{corr}, is high (or noble). For the anodic electrode where localized corrosion has been initiated and the protective layer has been compromised, however, the anodic current is usually high and the corrosion

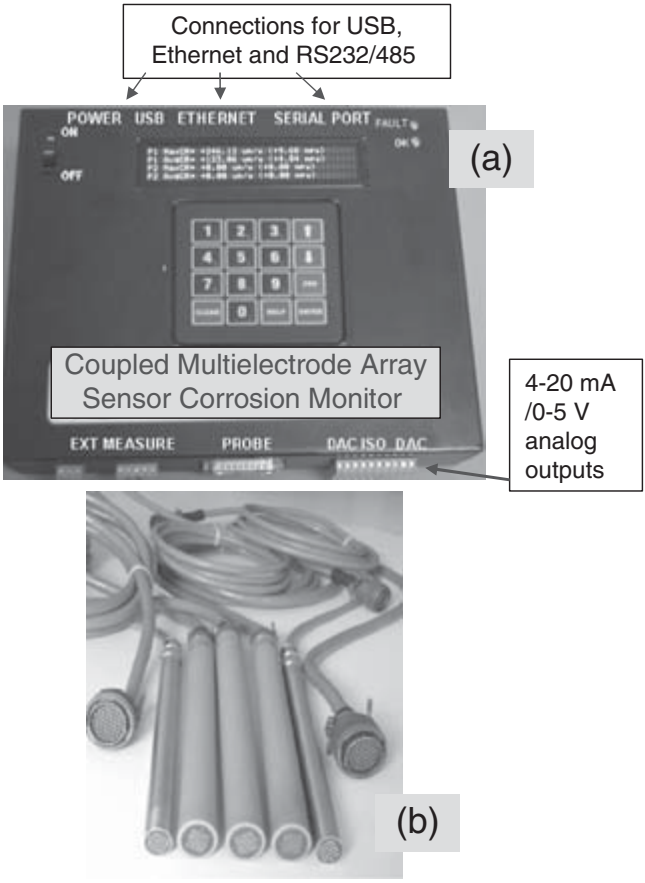

8.11 (a) A typical commercial CMAS monitor and (b) typical commercial CMAS probes for real time corrosion monitoring in plants or fields. Courtesy of Corr Instruments, LLC.

potential for the anodic electrode, E^{a}_{corr}, is low (or active). Note in Fig. 8.12, the cathodic current on the combined cathodic electrodes is significantly higher than that on the anodic electrode. This is because we have assumed that the surface area on the anodic electrode is significantly smaller than that of the cathodic electrodes (one anodic electrode versus many cathodic electrodes). In addition, the cathodic reactions deep in an anodic pit on the anodic electrode require more effort for the reactants (O_2 or H^+) to overcome the mass transfer barrier.

When the anodic electrode and the combined cathodic electrodes are coupled, the corrosion potential changes to a new value, E_{coup} (or E_{corr} for all

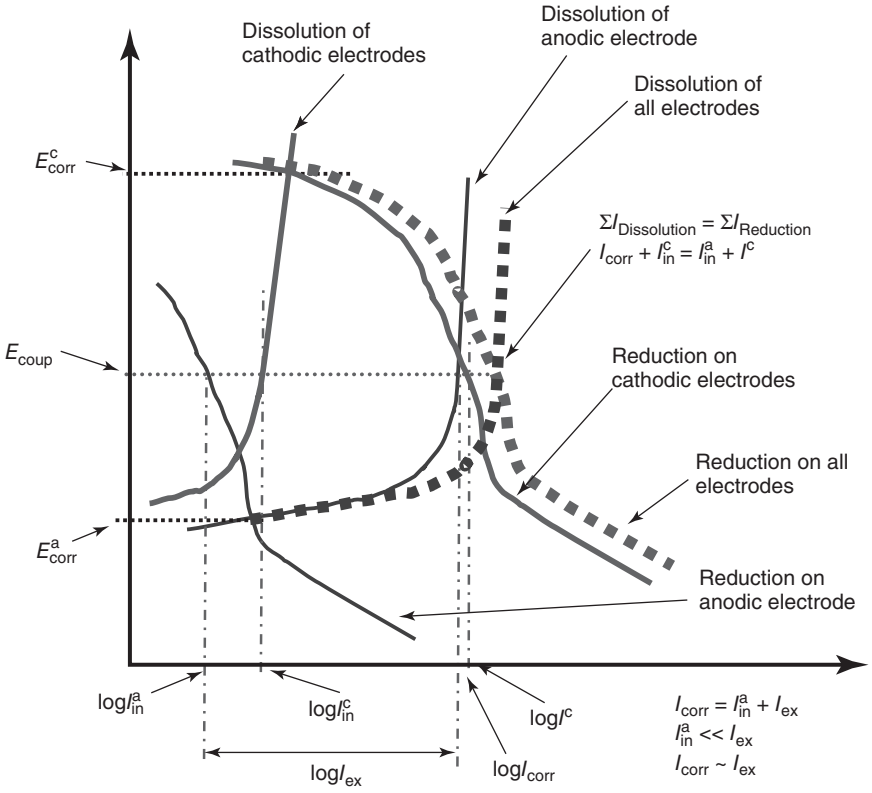

8.12 Schematic diagram for the polarization curves on one anodic electrode and several cathodic electrodes that are connected together on a coupled multielectrode sensor.

coupled electrodes), and the total anodic dissolution currents equal the total cathodic reduction currents (see the thick dashed lines in Figure 8.12):

$$I_{corr} + I^c_{in} = I^a_{in} + I^c \qquad [8.3]$$

Where I_{corr} is the corrosion current (total dissolution current) on the anodic electrode, I^c_{in} is the internal dissolution (anodic) current on all the cathodic electrodes (anodic current that flows within all the cathodes), I^a_{in} is the internal reduction current on the anode (the cathodic current that flows within the anode) and I^c the cathodic current on the combined cathodes.

On the anodic electrode, the corrosion current (total dissolution current), I_{corr}, is equal to the sum of the externally flowing anodic currents, I_{ex}, and the internally flowing anodic currents which is equal to the internally flowing cathodic currents (or the internal reduction current), I^a_{in}. Therefore,

$$I_{corr} = I_{ex} + I_{in}^{a} \quad [8.4]$$

Because the I_{in}^{a} for the anodic electrode, especially when the anodic electrode is the most anodic electrode of the CMAS probe (see Section 8.7.2), is often much smaller than its I_{ex} at the coupling potential in a localized corrosion environment, the externally flowing current from such anodic electrode of the probe can often be directly used to estimate the localized corrosion current:

$$I_{corr} \approx I_{ex} \quad [8.5]$$

In a less corrosive environment or with a more corrosion-resistant alloy, however, there would be less separation between the anodic electrodes and the cathodic electrodes. The behavior of even the most anodic electrode may be similar to the other electrodes in the CMAS probe. In this case, the I_{in}^{a} for the anodic electrode would be close to I_{ex}, and I_{in}^{c} would be close to the I^{c}. The most anodic electrode may still have significant cathodic sites available, and the electrons from the anodic sites would flow internally to the cathodic sites within the same electrode. Therefore, I_{in}^{a} in Equation [8.4] cannot be ignored in the calculation of the corrosion current.

Equation [8.4] may also be represented as:[80,85,99]

$$I_{ex} = \varepsilon I_{corr} \quad [8.6]$$

where ε is a current distribution factor that represents the fraction of electrons resulting from corrosion that flows through the external circuit. The value of ε may vary between 0 and 1, depending on parameters such as surface heterogeneities on the metal, the environment, the electrode size, and the number of sensing electrodes. If an electrode is severely corroded and significantly more anodic than the other electrodes in the probe, the ε value for this corroding electrode would be close to 1 ($I_{in}^{a} = 0$), and the measured external current would be equal to the localized corrosion current.[80,85] More discussion of ε is given in Section 8.8.1.

8.7.2 Maximum localized corrosion rate

In a corrosion management program for engineering structures, field facilities or plant equipment, the most important parameter is the remaining life (often the remaining wall thickness) of the systems. If localized corrosion is a concern, the remaining wall thickness in the most corroded area or site is often used to evaluate the remaining life. Therefore, the corrosion depth (the corrosion-induced wall thinning) or the maximum localized corrosion depth (the corrosion-induced wall thinning at the most corroded area) for localized corrosion is often the most important parameter in an operator's mind. Because the corrosion depth is a parameter that takes a long time

(often many years) to accumulate, the corresponding parameter that is important to the day-to-day operation would be the corrosion rate or the maximum localized corrosion rate if localized corrosion is a concern. Because the anodic electrodes in a CMAS probe simulate the anodic sites on a metal surface, the maximum anodic current (the current from the most anodic electrode) may be considered as the corrosion current from the most corroding site on the metal. Therefore, the maximum anodic current should be used as one of the most import parameters for the CMAS probes.[80,85]

The value, based on three times the standard deviation of currents from a CMAS probe, was sometimes used to represent the maximum anodic current.[80,85] Because the number of electrodes in a CMAS probe is always limited and usually far fewer than the number of corroding sites on the surface of a metal coupon, the use of the value based on the statistical parameter, such as three times the standard deviation of current, to represent the maximum anodic current, may sometimes be a better choice than the true maximum anodic current.[80,85] The standard deviation value may be derived from the anodic currents or from both the anodic and the cathodic currents.[80,101]

Accordingly, the maximum localized corrosion rate (or maximum localized corrosion penetration rate) may be derived from the maximum anodic current.[80,85] The following equation has been used to calculate the maximum localized corrosion rate:

$$CR_{max} = (1/\varepsilon) I_{max} W_e/(F\rho A) \qquad [8.7]$$

where CR_{max} is the calculated maximum penetration rate (cm/s), I_{max} is the maximum anodic current, or the most anodic current, F is the Faraday constant (96 485 C/mol), A is the surface area of the electrode (cm^2), ρ is the density of the alloy or electrode (g/cm^3), W_e is the equivalent weight (g/mol) (see Chapter 3 for details). Equation [8.7] assumes that corrosion on the most corroded electrode is uniform over the entire surface. Because the electrode surface area is usually between 0.01 and 0.0003 cm^2, which is approximately two to four orders of magnitude less than that of a typical linear polarization resistance (LPR) probe or a typical electrochemical noise (EN) probe, the prediction of penetration rate or localized corrosion rate by assuming uniform corrosion on the small electrode is realistic in most applications.[80,85]

The corrosion depth or penetration is related to the total damage accumulated in a given time period. The corrosion depth of the ith electrode may be derived from the cumulative charge that can be obtained by integrating the corrosion current through the electrode from time zero to time t:

$$Q_i = \int I_i(t)\mathrm{d}t \qquad [8.8]$$

where Q_i is the cumulative charge of the ith electrode. Similar to the maximum localized corrosion rate, the following equation has been used to calculate the maximum cumulative localized corrosion depth or penetration (cm):

$$CD_{max} = (l/\varepsilon)Q_{max}W_e/(F\rho A) \quad [8.9]$$

where Q_{max} is the maximum of the cumulative charges (coulomb) from all the electrodes. The cumulative charge of each electrode is calculated individually using Equation [8.8].

Figure 8.13a shows typical responses of the standard deviation of the currents measured from a 25-electrode probe made of Type 304 stainless steel (UNS S30400).[80,85] The following order of increasing corrosiveness was observed: deionized water < saturated KCl < 0.0025 M $FeCl_3$ < 0.25 M $FeCl_3$. Figure 8.13a also shows that $NaNO_3$ is an effective corrosion inhibitor for stainless steel in $FeCl_3$ solution.

Figure 8.13b shows typical responses of the maximum localized corrosion rate (derived from the most anodic current) of a low carbon steel CMAS probe measured by a commercial instrument.[108] The maximum localized corrosion rate in air was close to the instrument theoretical detection limit (10 nm/y). The initial maximum localized corrosion rate was 10 μm/yr in distilled water. The maximum localized corrosion rate in simulated seawater was approximately 1 mm/y. When 10 mM H_2O_2 was added to the simulated seawater, the corrosion rate was 10 mm/y. It was later verified that the corrosion of the electrode in the distilled water and in the simulated seawater was mainly in the form of pitting corrosion.[104] Therefore, the maximum corrosion rate in Figure 8.13b represents the maximum pitting rate.

8.7.3 Estimation of general corrosion rate using coupled multielectrode array sensors and localized corrosion rate factor

The maximum localized penetration rate and cumulative maximum localized penetration depth are, no doubt, the two most important parameters for the assessment of localized corrosion. However, the maximum penetration rate data for alloys are rarely available, and the measured localized corrosion rates by the CMAS probes cannot be easily compared with the general corrosion rates commonly reported in literature. In addition, maximum penetration rate is difficult to measure, whereas general corrosion rate can be measured by many methods, such as the LPR and ER probes, or weight loss methods.

In most cases, localized corrosion is associated with some degree of general corrosion. When a metal is undergoing corrosion, the corroding

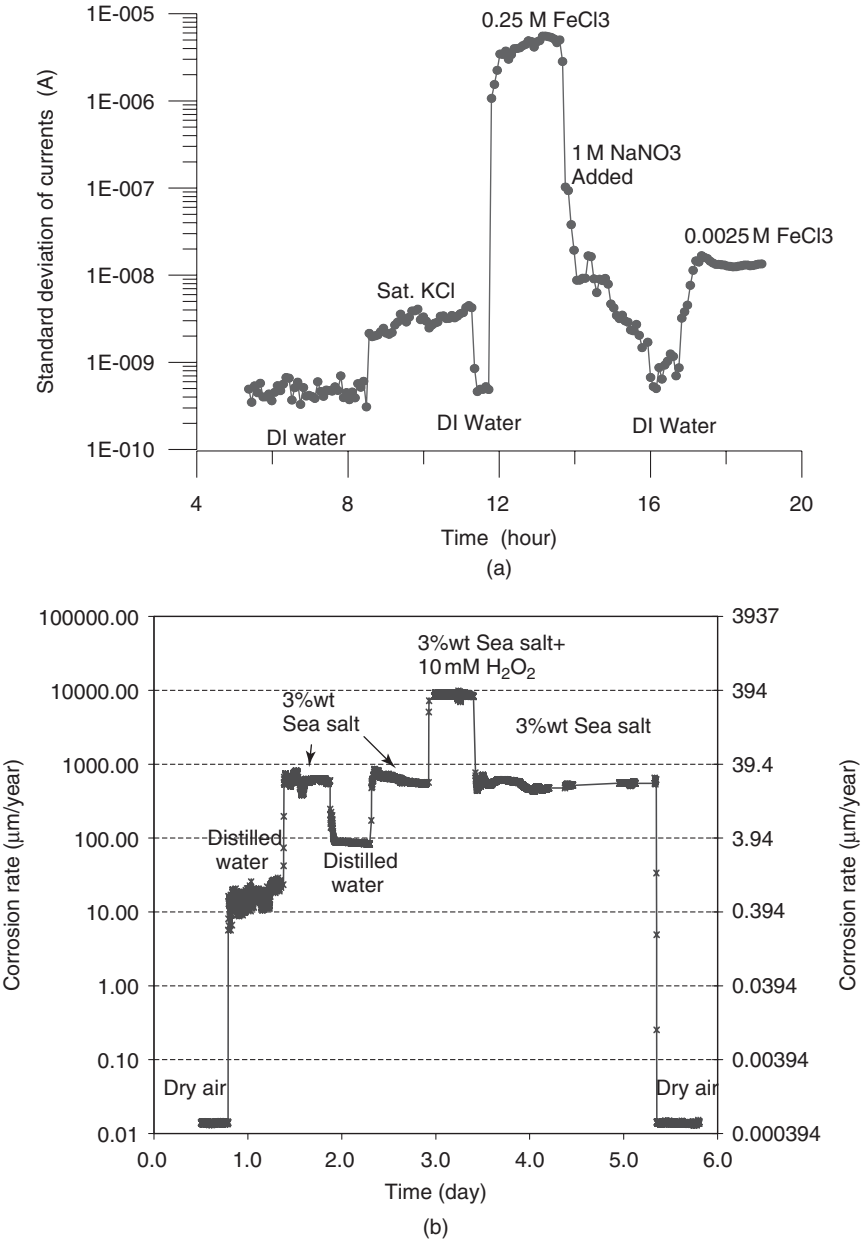

8.13 Typical response of standard deviation of the current signals from (a) a 25-electrode Type 304 stainless steel probe and (b) maximum localized corrosion rate from a 16-electrode carbon steel probe to the changes in solution chemistry.[85,108] © NACE International 2003/2004.

metal is usually at an electrochemical potential (corrosion potential) that is significantly higher than the metal's deposition potential. Thus, the cathodic currents do not directly contribute to the metal loss or the metal gain (electroplating), and therefore can be ignored in the corrosion rate calculation. For this reason, the average corrosion penetration rate may be calculated using the average value of the anodic currents from the CMAS probe.[103]

$$I_{\text{avg}} = (\sum I_i^{\text{a}})/n, \; i \text{ from 1 to } n \qquad [8.10]$$

where I_i^{a} is the anodic current from the ith electrode, n is the number of electrodes in the probe, and I_{avg} is the average of the anodic currents. If I_i^a is cathodic, it is set to zero in the summation. Figure 8.14 shows the current from each electrode, the maximum anodic current, and the average of the anodic currents from a typical 16-electrode stainless steel probe in simulated seawater.[118]

Thus, the average corrosion rate, CR_{avg}, may be calculated by[103]

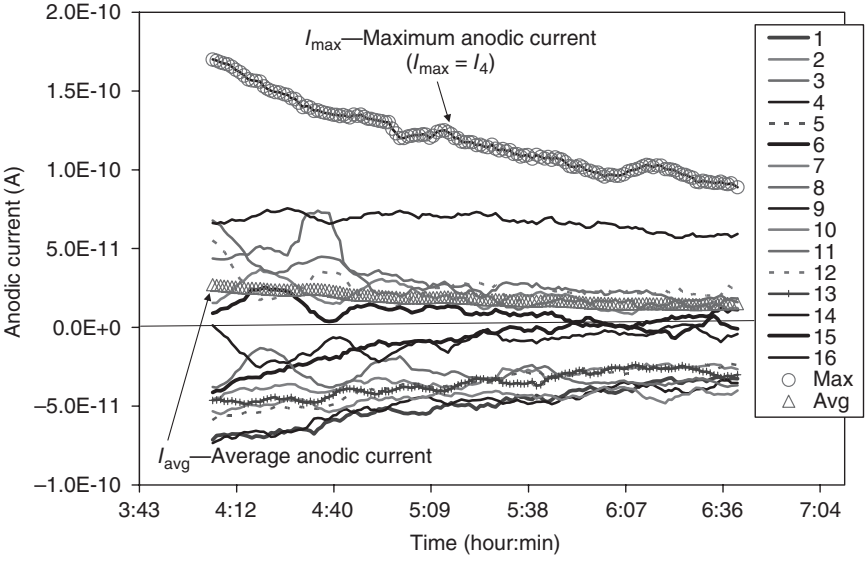

8.14 Typical currents measured from a stainless steel coupled multielectrode array sensor probe in simulated seawater. Maximum anodic current was due to one electrode (Electrode #4) throughout the measurement period. Note: the numbers in the key indicate the ID of the sensor electrodes; a negative value of the anodic current means that the current is actually cathodic.[118] © NACE International 2007.

$$CR_{avg} = (1/\varepsilon)I_{avg}W_e/(F\rho A) \quad [8.11]$$

The general corrosion penetration rate obtained using the weight loss method or by an electrochemical method using relatively large electrodes is essentially the corrosion rate averaged over the sample surface area. Therefore, Equation [8.11] may be used to estimate the general corrosion rate. It should be noted that the general corrosion rate estimated with Equation [8.11] should be used with caution because some of the corrosion currents on the corroding electrodes flow internally (see Sections 8.7.1 and 8.8.1), especially on those that are not corroding more significantly than the others (in contrast to the most corroding electrode). The general corrosion rate estimated using Equation [8.11] may be lower than the true general corrosion rate.

The localized corrosion rate factor, f_{rate}, was defined as the ratio of the maximum localized corrosion rate to the average corrosion penetration rate. It can be expressed by[103]

$$f_{rate} = CR_{max}/CR_{avg} \quad [8.12]$$

The localized corrosion rate factor indicates how much higher the localized corrosion rate (e.g., the penetration rate of the fastest growing pit on the surface of a coupon in the case of pitting corrosion) is than the average corrosion rate (e.g., the average penetration rate on the surface of a coupon). It should be noted that the maximum localized corrosion rate may not always be found on one electrode. In a CMAS probe, one electrode may have the highest corrosion rate at one time, but another electrode may corrode at the highest rate at another time (see Section 8.7.5). Figure 8.15 shows the maximum localized corrosion rate, the general corrosion rate calculated using Equation [8.11], and localized corrosion rate factor for a typical freshly polished Type 1008 carbon steel (UNS G10080) probe in simulated seawater at room temperature. The data were obtained by the author using a probe with 16 electrodes (1 mm in diameter) and the equipment described by Sun and Yang.[103]

8.7.4 Estimation of general corrosion depth using coupled multielectrode array sensors and localized corrosion depth factor

Similar to the average corrosion rate, the average anodic charge, Q^a_{avg}, may be calculated by[103]

$$Q^a_{avg} = (\sum Q^a_i)/n, i \text{ from 1 to } n \quad [8.13]$$

where Q^a_i is the anodic charge from the ith electrode, and n is the number of electrodes in the coupled multielectrode probe. If the value of Q^a_i is

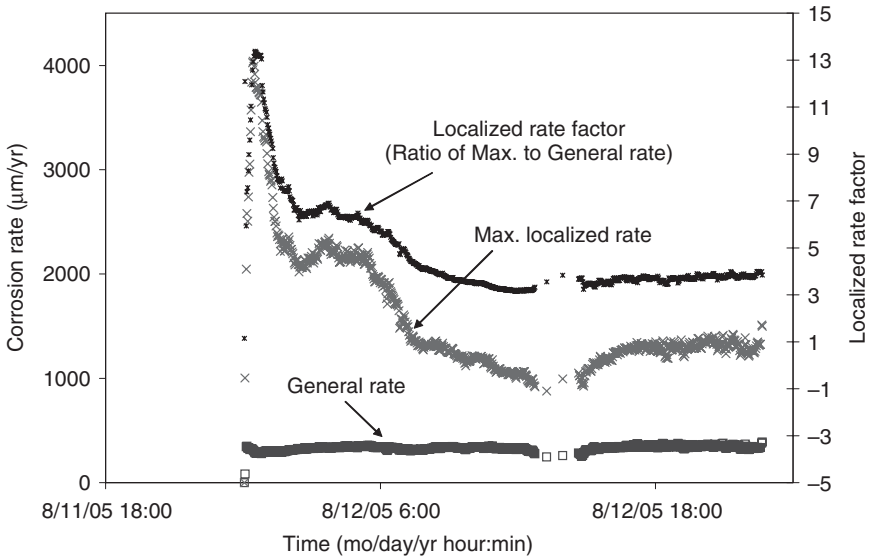

8.15 Maximum localized corrosion rate, average corrosion rate and localized corrosion rate factor for a typical freshly polished Type 1008 carbon steel probe in simulated seawater at room temperature. Note: Number of electrode: 16; electrode diameter: 1 mm.

cathodic, it is set to zero in the summation. Figure 8.16 shows the charge from each electrode, the maximum anodic charge, and the average of the anodic charge for the data shown in Fig. 8.14.[118]

Thus, the average corrosion penetration depth, $CD_{avg,}$ may be calculated by[103]

$$CD_{avg} = (1/\varepsilon)(Q^{a}_{avg})W_e/(F\rho A) \quad [8.14]$$

Similar to the average corrosion rate, Equation [8.14] may be used to estimate the general corrosion penetration depth. It should be noted, however, that the general corrosion depth estimated with Equation [8.14] may be lower than the true general corrosion depth because some of the corrosion currents on the corroding electrodes flow internally (see Sections 8.7.1 and 8.8.1), especially those electrodes that are not corroding more significantly than the others (in contrast to the most corroding electrodes).

The localized penetration depth factor, f_{depth}, may be defined as the ratio of the maximum localized penetration depth to the average corrosion penetration depth[103]

$$f_{depth} = CD_{max}/CD_{avg} \quad [8.15]$$

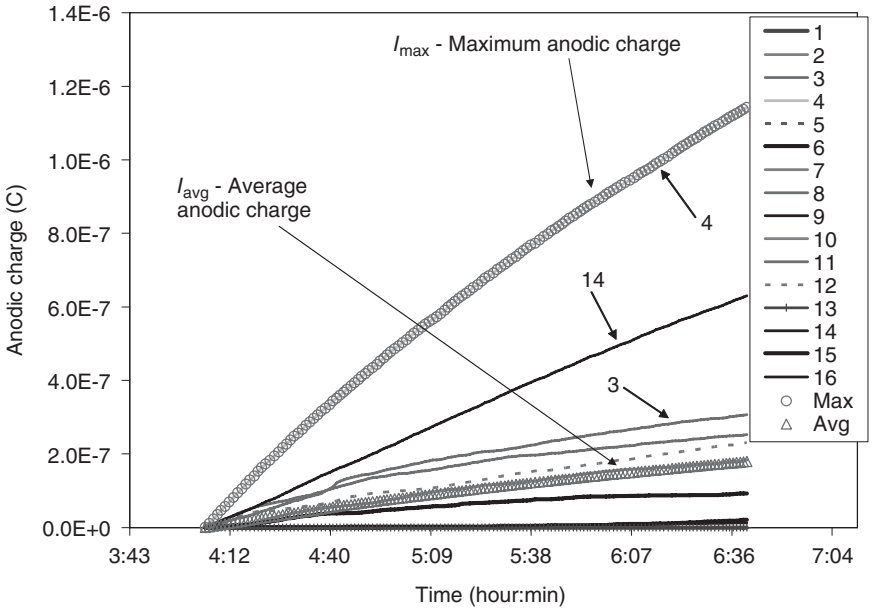

8.16 Anodic charges corresponding to Fig. 8.14. Maximum charge is the integration of the current from one electrode (Electrode #4).[118]

The localized corrosion penetration depth factor indicates the severity of localized corrosion depth (e.g., the deepest penetration of the most corroded pit on the surface of a coupon in the case of pitting corrosion) compared to the general corrosion penetration or the average corrosion penetration (e.g., the average loss in thickness on the surface of a coupon). Similar to the localized corrosion rate, the maximum penetration may not always be found on the same electrode. It also might not be found on the electrode that has the highest penetration rate at a given time. Instead, the electrode that has the highest cumulative penetration has the maximum penetration depth (see Section 8.7.5 for details). Figure 8.17 shows the maximum localized corrosion depth, average corrosion depth and localized corrosion depth factor for the data shown in Fig. 8.15. Even though localized corrosion depth factor was high initially (close to 11), it decreased quickly to 6 in about 3 hours, and reached 4 in about another 7 hours. If the trend continued, the ultimate results would be general corrosion. This result is consistent with the general observations for carbon steel in seawater – general corrosion is the main mode of attack in most cases.

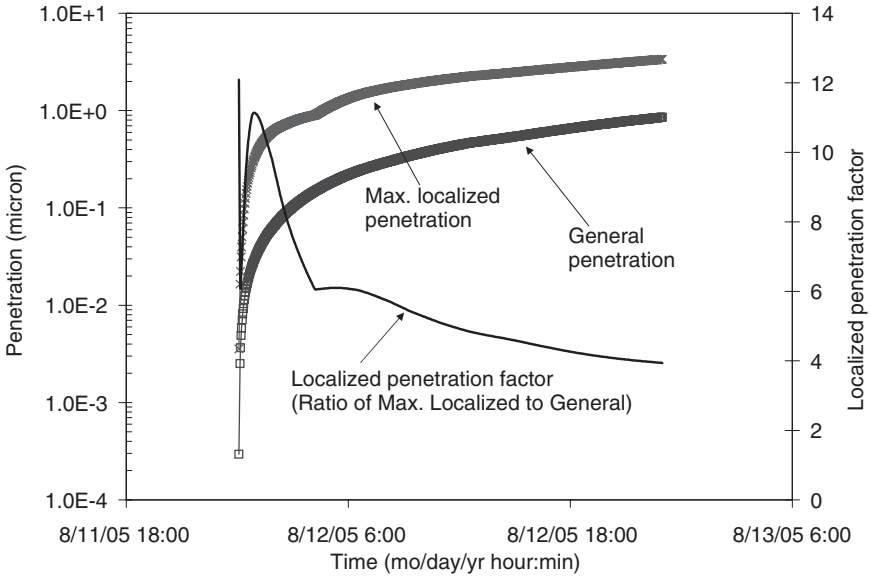

8.17 Maximum localized corrosion depth, average corrosion and localized corrosion depth factor for the data derived from the same experiment for Fig. 8.15.

8.7.5 Cumulative maximum localized corrosion rate

As shown in Fig. 8.14, the maximum anodic current was due to the current from a single electrode (Electrode #4). By applying Equations [8.7] through [8.9] to the data shown in Figs 8.14 and 8.16, and assuming $\varepsilon = 1$, the maximum localized corrosion rate and maximum corrosion depth were obtained and shown in Fig. 8.18. In Fig. 8.18, the maximum localized corrosion depth curve is the integration of the maximum localized corrosion rate curve. Because the maximum localized corrosion rate curve in Fig. 8.18 was from one electrode, the maximum localized corrosion rate curve and the maximum localized corrosion depth curve are directly related to each other.

Figure 8.19 shows typical currents measured from an aluminum coupled multielectrode array sensor probe in simulated seawater.[118] The aluminum probe had 16 electrodes made of annealed Type 3003 (UNS A93003) aluminum wire. In Fig. 8.19, the maximum anodic current was from different electrodes (Electrodes #5, #13, #12 and #16) at different times. The anodic charges corresponding to Fig. 8.19 are shown in Fig. 8.20. By applying Equations [8.7] through [8.9] to the data shown in Figs 8.19 and 8.20, the maximum localized corrosion rate and the maximum localized corrosion

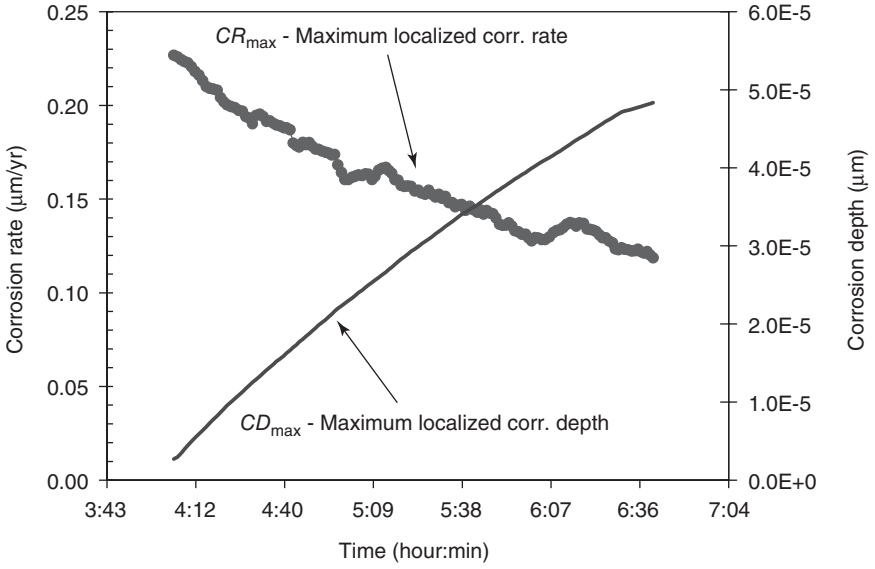

8.18 Maximum localized corrosion rate and maximum localized corrosion depth (penetration) for the data shown in Figs 8.14 and 8.16. The maximum localized corrosion depth is a direct integration of the maximum localized corrosion rate.[118] © NACE International 2007.

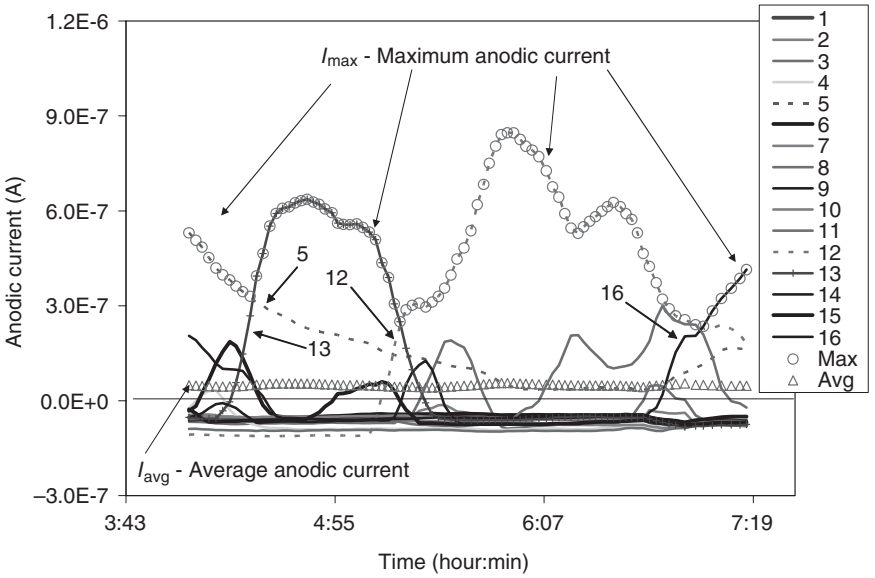

8.19 Typical currents measured from an aluminum coupled multielectrode array sensor probe in simulated seawater. Maximum anodic current was due to different electrodes (Electrodes #5, #13, #12 and #16) at different times.[118] Note: the numbers in the legend and figure indicates the ID of the sensor electrodes; a negative value of the anodic current means that the current is actually cathodic. © NACE International 2007.

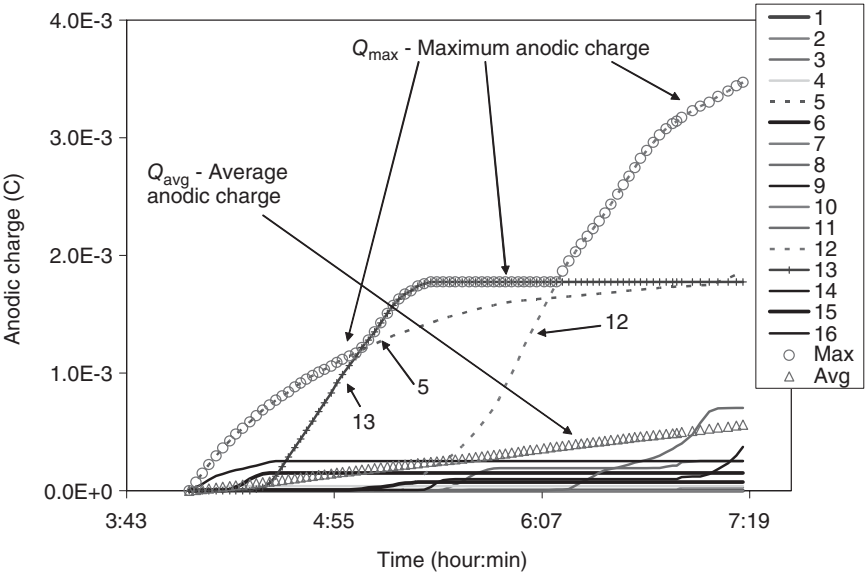

8.20 Anodic charges corresponding to Fig. 8.19. Maximum charge is the integration of the currents from different electrodes (Electrode #5, #13 and #12).[118] © NACE International 2007.

depth were obtained and are shown in Fig. 8.21. Unlike Fig. 8.18, the maximum localized corrosion depth curve is not the direct integration of the maximum localized corrosion rate curve in Fig. 8.21. The integration of the maximum localized corrosion curves would produce a much higher depth than the true maximum localized corrosion penetration depth as shown in Fig. 8.21 (dashed line). Therefore, there is no direct relationship between the maximum localized corrosion rate and the maximum localized corrosion penetration depth.

To solve the problem of discrepancy between the maximum localized corrosion rate and maximum localized corrosion depth, as shown in Fig. 8.21, a new parameter called cumulative maximum localized corrosion rate, CR_{cmax}, was introduced.[118] It was defined as the derivative of the maximum localized corrosion depth curve:

$$CR_{cmax}(t) = \mathrm{d}[CD_{max}(t)]/\mathrm{d}t \qquad [8.16]$$

The maximum localized corrosion depth, $CD_{max}(t)$, is proportional to the maximum anodic charge, Q_{max}, as shown in Fig. 8.20 (see Equation [8.9]). The maximum anodic charge in Fig. 8.20 was obtained by integrating the currents from the electrodes that had the maximum anodic charge since time zero (or had been corroded the most at time t). Therefore, the

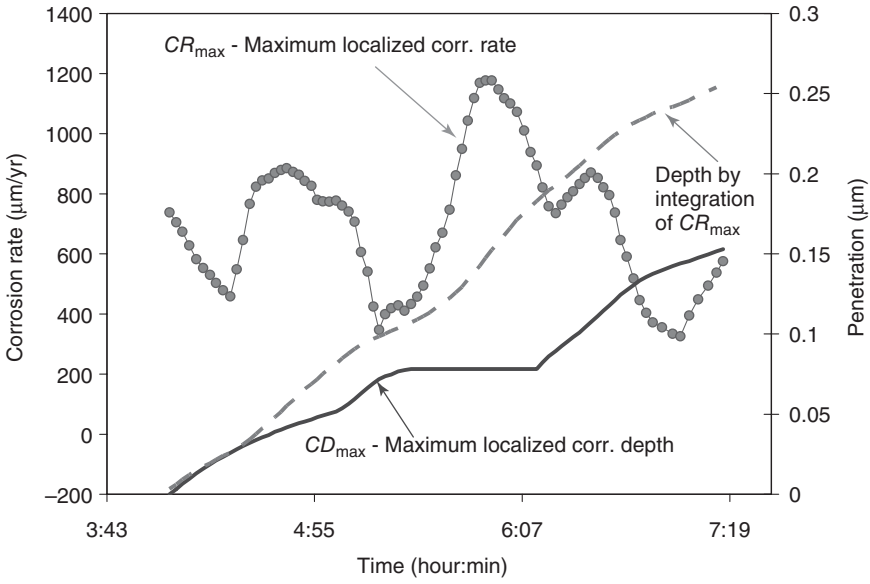

8.21 Maximum corrosion rate and maximum localized corrosion depth for the data shown in Figs 8.19 and 8.20. The dashed line was obtained by the integration of the maximum localized corrosion rate, CR_{max}, and is much higher than the actual maximum localized corrosion depth, CD_{max}.[118] © NACE International 2007.

derivative of $CD_{max}(t)$ is simply a function of the current from the electrode that has the highest anodic charge at time t, I_{max_charge}:

$$CR_{max}(t) = (1/\varepsilon)I_{max\_charge}W_e/(F\rho A) \quad [8.17]$$

The CR_{cmax} values for the data shown in Figs 8.19 and 8.20 are calculated and shown in Fig. 8.22. The maximum localized corrosion depth, CD_{max}, and the calculated corrosion rates for the electrodes that exhibited the highest corrosion currents at certain times during the test (see Fig. 8.19) are also plotted in Fig. 8.22. In the specified three time periods, the maximum localized corrosion depth was the value measured from Electrodes #5, #13 and #12, respectively (see Fig. 8.20). Therefore, the cumulative maximum localized corrosion rate, CR_{cmax}, was equal to the corrosion rates of these three electrodes during the different corresponding time intervals. Another way to look at the cumulative maximum localized corrosion rate is that it is the corrosion rate of the cumulatively most corroded electrode at any given time (or the electrode with the deepest pit, if the mode of localized corrosion is pitting corrosion). Because of the nature of localized corrosion, the deepest pit may be repassivated under certain conditions and the

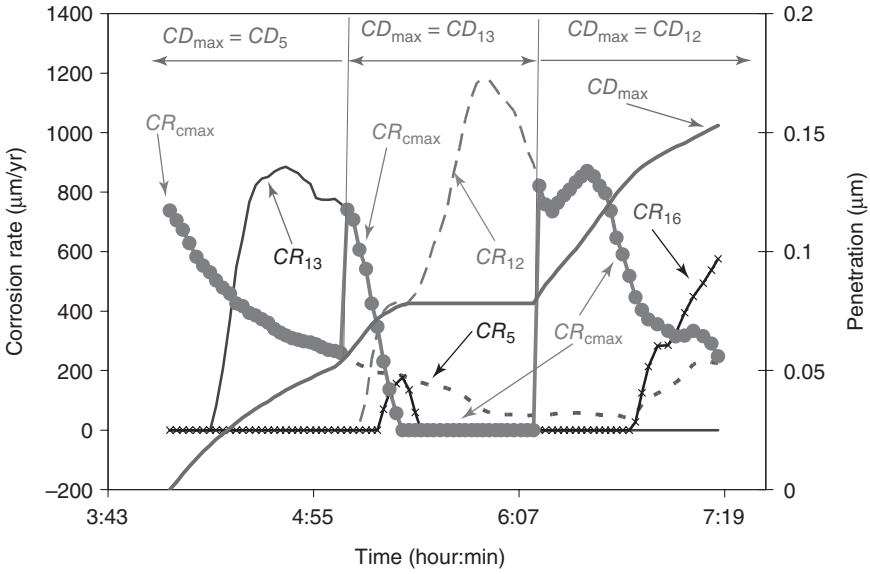

8.22 Cumulative maximum localized corrosion rate, corrosion rates of selected electrodes and maximum localized corrosion depth for the data shown in Figs 8.19 and 8.20. Note, in the specified three time periods, the maximum localized corrosion depth was due to the corrosion of Electrodes #5, #13 and #12, respectively (see Fig. 8.20).

corrosion rate in this pit may drop to zero. The zero value of CR_{cmax} in the second time interval indicates that the most corroded electrode (Electrode #13) was repassivated, and the corrosion on it was stopped from approximately 5:20 to 6:20 a.m. (Fig. 8.22).

Because the cumulative maximum localized corrosion rate is simply the corrosion rate of the electrode that passed the maximum amount of charge, a sorting algorithm may be built into a real-time corrosion monitoring software to track the most corroded electrode and obtain the cumulative maximum localized corrosion rate. The software may give the maximum localized corrosion rate, the cumulative maximum localized corrosion rate and the average corrosion rate, CR_{avg}, which is calculated from the average of the anodic currents. The average corrosion rate may be used to represent the general corrosion rate.[103] Figure 8.23 shows the maximum localized corrosion rate, cumulative localized corrosion rate and average corrosion rate from a commercial software, CorrVisual. (CorrVisual is a trade name of Corr Instruments, LLC, San Antonio, TX, USA.)

Because the cumulative maximum localized corrosion rate is defined as the derivative of the maximum localized corrosion depth, the CR_{cmax} and

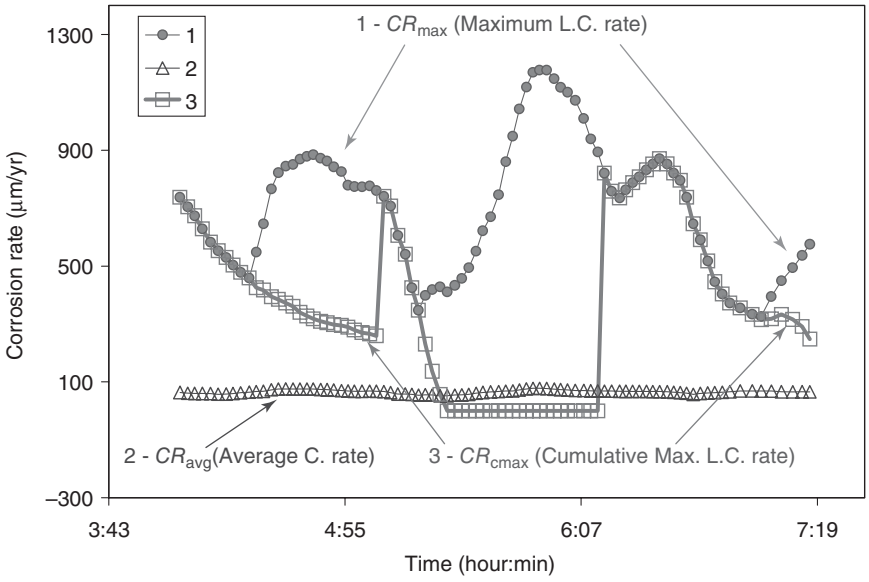

8.23 Maximum localized corrosion rate, cumulative maximum localized corrosion rate, and average corrosion rate for the data shown in Fig. 8.19.[118] © NACE International 2007.

CD_{max} values are directly related to each other. One can solve for CR_{cmax} from CD_{max} by differentiation, or solve for CD_{max} from CR_{cmax} by integration. Unlike the maximum localized corrosion rate, CR_{max}, whose integration would produce an imaginary number that may be higher than the actual maximum localized corrosion depth, the integration of the cumulative maximum localized corrosion rate would produce exactly the maximum localized corrosion depth.

Maximum localized corrosion rate is a measure of localized corrosion rate at a given moment of time. Cumulative localized corrosion rate is a measure that relates to the cumulative damage of localized corrosion to a metal. If the maximum localized corrosion rate is high, but the cumulative maximum localized corrosion rate is low, the corrosion rate at one electrode is high at one time, but remains low at other times and there is always one electrode that has a high corrosion rate. The cumulative effect of this kind of high maximum localized corrosion rate in a given time period is a high general corrosion rate (i.e., every electrode is significantly corroded after a given period of time). When the maximum localized corrosion rate is significantly different from the cumulative maximum localized corrosion rate, the cumulative maximum localized corrosion rate should be used to evaluate the persistence of localized corrosion.

Because the cumulative maximum localized corrosion rate is the corrosion rate on the most corroded electrode and the corrosion rate on the most corroded electrode may be lower than the corrosion rate taking place on the most corroding electrode (the maximum localized corrosion rate) at certain times, the cumulative maximum localized corrosion rate is always lower than or equal to the maximum localized corrosion rate.

Therefore, for process control applications (i.e., inhibitor dose control), the maximum localized corrosion rate, CR_{max}, should be used. However, for the evaluation of the effect of localized corrosion on the cumulative damage to a metal component, the cumulative maximum localized corrosion rate should be used. It should be noted that at a given time in a certain environment, the cumulative maximum localized corrosion rate may be very low, even zero, but the maximum localized corrosion rate may still be very high. This means that the localized corrosion on the most corroded electrode has stopped, but the localized corrosion on the other electrodes is still high.

8.8 Minimizing effects of internal currents, electronic-conducting deposits and crevices on performance of CMAS probes

8.8.1 Minimization of internal current effects on localized corrosion rate measurement using coupled multielectrode array sensors

As discussed in Section 8.7.1, in a less localized corrosive environment or with a more corrosion-resistant alloy, there would be a lower degree of separation between the anodic electrodes and the cathodic electrodes. Fig. 8.24 shows the electron flow paths on the different kinds of electrodes in a CMAS probe.[99] If the most anodic electrode on a probe in a given environment is a partially corroded electrode (Fig. 8.24b) rather than a totally corroded active electrode (Fig. 8.24a), it is more likely that the electrode still has the cathodic sites to accept electrons from the neighboring anodic sites on the same anode,[80,85] and the I^{a}_{in} in Equation [8.4] or the ε in Equation [8.6] cannot be ignored when calculating the corrosion current, $I_{corr.}$

In Fig. 8.24a, the electrode is totally active and fully covered by the corrosion products. Because the corrosion products may act as a diffusion layer for O_2 or H^+ to reach the metal surface; the I^{a}_{in} (also see Fig. 8.12) on this electrode is expected to be small. If the other electrodes on the CMAS probe are not corroded, all or most of the corrosion electrons from this totally corroded electrode would flow to the other electrodes through the external circuit and the corresponding ε in Equation [8.6] would be equal or close to unity. On the other hand, in Fig. 8.24b, the electrode is only

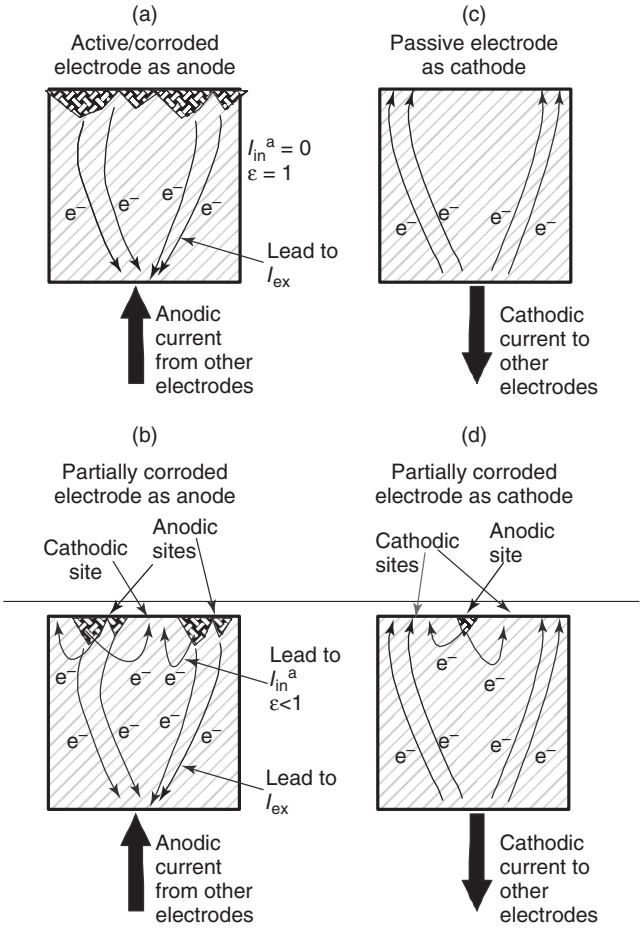

8.24 Flow of electrons on (a) a totally corroded active electrode as anode, (b) a partially corroded electrode as anode, (c) a passive electrode as cathode, and (d) a partially corroded electrode as cathode in a CMAS probe.[99] © NACE International 2005.

partially corroded; it is likely a portion of its corrosion electrons would flow to the local cathodic sites, and the corresponding ε is less than 1. Therefore, in the case of Fig. 8.24b, there is a large uncertainty in localized corrosion rate measurements using the CMAS probe if ε is assumed to be unity (Equation [8.7]).

To represent the case as depicted in Fig. 8.24b, Fig. 8.12 is modified into Fig. 8.25. In Fig. 8.25, the anodic and cathodic behaviors are only shown for two electrodes: one is the most anodic electrode, the other is the most cathodic electrode (rather than for many cathodic electrodes as shown in

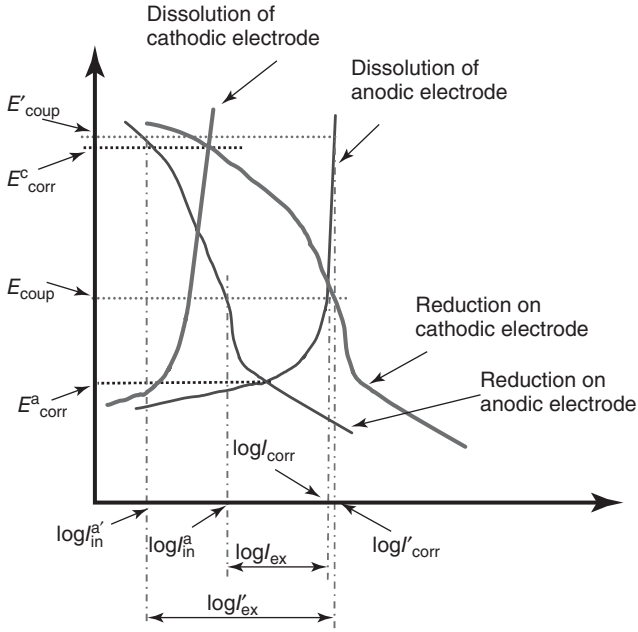

8.25 Schematic diagram for the polarization curves on one anodic electrode and one cathodic electrode of a coupled multielectrode sensor.

Fig. 8.12 because there may not be many cathodic electrodes for one anodic electrode in the case as shown in Fig. 8.24b). In addition, the cathodic curve on the most anodic electrode is deliberately shifted to the right due to the existence of the uncorroded sites on the most anodic electrode that may support a higher cathodic current. At the coupling potential, E_{coup} (assuming only these two electrodes are coupled), the internal current, which is equal to I^{a}_{in}, is large and cannot be ignored. However, if the coupling potential can be altered to E'_{coup}, the corresponding $I^{a'}_{in}$ would be much smaller than the externally measured anodic current, I'_{ex}. In this case Equation [8.5] can be used to calculate the corrosion current. In the work by Yang *et al.*,[99] E'_{coup} was defined as a potential at which the current from the most cathodic electrode is about to become zero. In other words, E'_{coup} is the highest open-circuit potential measured on all the electrodes of a CMAS probe (when the electrodes are decoupled). Because E'_{coup} is the open-circuit potential of one of the electrodes which are made of identical metals, it is not an unreasonable potential for the metal in the solution of interest.

From a statistical point of view, the multiple electrodes in a CMAS probe simulate the different cathodic and anodic sites of a metal coupon; the

highest potential (usually the potential measured from the most cathodic electrode) can be considered to statistically represent the potential of the most cathodic site on the metal (after it is electrically isolated from the other sections of the metal). The potential measured from the most cathodic electrode may thus be considered as the highest bounding potential for all the cathodic sites on the most anodic electrode. Therefore, if the coupling potential of a CMAS probe is raised to a value that is slightly higher than the potential measured from the most cathodic electrode, there should be no cathodic reaction on the most anodic electrodes even though some areas are still uncorroded. Under these conditions, $\varepsilon \rightarrow 1$ and $I_{in}^{a} \rightarrow 0$, the uncertainty in the measured corrosion rate from the CMAS probe due to I_{in}^{a} can be ignored or eliminated.

A polarization unit, as shown in Fig. 8.26, was used for a CMAS instrument to dynamically adjust the potential of the coupling joint of the probe such that the current from the most cathodic electrode of the CMAS probe is zero or slightly anodic (lower than zero if an anodic current is recorded as a negative current by the instrument or higher than zero if a cathodic

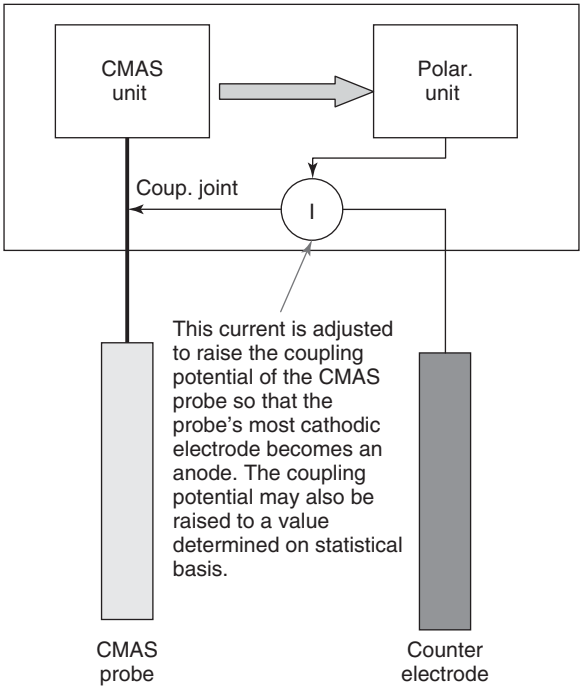

8.26 An improved CMAS instrument system that reduces or eliminates the effect of internal electrons on the most anodic electrode of a CMAS probe.[99] © NACE International 2005.

current is recorded as a negative current by the instrument). Under this condition, the coupling potential is higher than the open-circuit potential of the most cathodic electrode.

Because raising the coupling potential also increases the current from the active sites, the corrosion rate measured at the raised coupling potential may be higher than the actual corrosion rate. Thus, the corrosion rate measured at the raised coupling potential may be considered the upper bound of the corrosion rate. The corrosion rate measured at the natural coupling potential, E_{coup}, may be considered the lower bound of corrosion rate because of the possible non-zero internal flow of electrons on the most corroding electrode at E_{coup}.

Preliminary measurements were conducted in a 0.5 M NaCl solution using the improved CMAS method as shown in Fig. 8.26.[99] The upper bounds of the maximum localized corrosion rates were found to be 2.2 to 2.7 times higher than the lower bounds for the probes made of Alloy 276 (UNS N10276), Type 316 stainless steel (UNS S31600) and Type 1008 carbon steel (UNS G10080), respectively. Therefore, the maximum localized corrosion rate values measured at the natural coupling potential were close to the actual maximum localized corrosion rates for these three metals in 0.5 M NaCl solution.

8.8.2 Minimization of the effects by corrosion products formed in H_2S-containing environment on localized corrosion rate measurement using coupled multielectrode array sensors

As discussed in Chapters 3 and 11, both linear polarization resistance probes (LPR) and the electrical resistance (ER) probes are subject to the effect of electron-bridging caused by the corrosion products formed in H_2S-containing environments. The sulfide corrosion products, such as FeS, are semiconductors and have similar behaviors as metal conductors for conducting electrons. In an ER probe, the corrosion measurement is based on the increase in the resistance of the sensing element that is caused by corrosion. If the electron-conducting corrosion products are deposited onto the sensing element and cause the changes in the measured resistance, it is not difficult to understand that such changes would give false readings for the ER probe.

Figure 8.27a shows the effect of the electron-conducting deposits on the measurement of corrosion using an LPR probe. An external potential or current perturbation source (I source in Fig. 8.27a) is required to cause a slight polarization to the sensing electrode, and the change in current or voltage (measured by V in Fig. 8.27a) that is caused by the polarization is

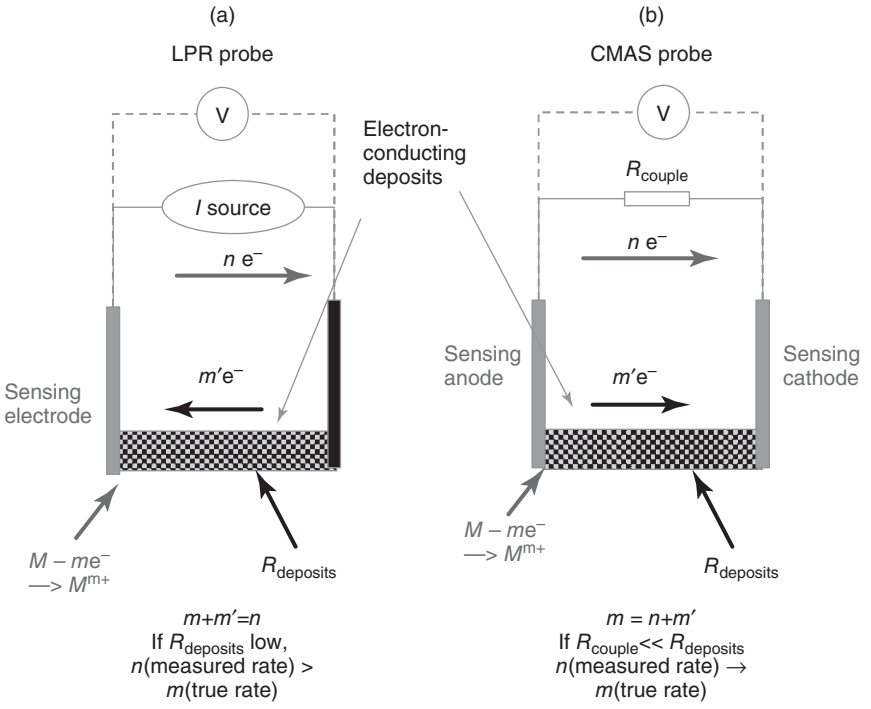

8.27 Schematic diagram for the effect of electron-conducting corrosion products on (a) linear polarization resistance (LPR) probe and (b) coupled multielectrode array sensor (CMAS) probe.

used to derive the corrosion rate (see Chapter 3). Normally, the conductivity between the two electrodes in the solution is provided purely by the ionic species in the solution, in which case, the number of electrons flowing through the solution, m', is zero, and the externally measured or supplied number of electrons, n, equal to the number of electrons that are as a result of the dissolution or corrosion reaction at the metal–solution interface, m. However, if an electron-conducting deposit is formed between the two electrodes in the solution, a portion of the electrons supplied or measured in the external circuit, m', would go through the electron-conducting deposits. Because this portion of electrons does not take part in the corrosion reaction at the metal–solution interface, the number of electrons that take part in the corrosion reaction, m, does not equal the externally supplied or measured number of electrons, n. Because there is no way of knowing the value of m', sulfide corrosion products severely affect the performance of an LPR probe. It also affects any other electrochemical methods that require an external perturbation source.

On the other hand, as shown in Fig. 8.27b, the corrosion current from a coupled multielectrode array sensor probe is obtained by measuring the currents generated by the coupling of an anode in the probe with the cathodes on the same probe. There is no external perturbation needed during the measurements. The coupling current is measured either by a coupling resistor (or a zero resistance ammeter which also has a defined internal resistance, especially when the current is low) that is in parallel with the resistance formed by the corrosion products. As long as the value of the coupling resistor (R_{couple}) is much smaller than the values of the electronic-conducting deposits ($R_{deposits}$), the number of electrons going through the electron-conducting deposit would be much smaller than that going through the coupling resistor ($m' \ll n$), and the current measured in the external circuit would be close to the current involved in the corrosion reaction ($n = m$).

Figure 8.28 shows the results obtained with a carbon steel CMAS probe in a solution saturated with 100% H_2S at ambient temperature and pressure using two CMAS analyzers.[106] The first analyzer used larger resistors as the coupling resistors, and the second analyzer used smaller resistors as the coupling resistors (see Fig. 8.10). The measured maximum localized corrosion rate was high initially, but decreased gradually with time when the

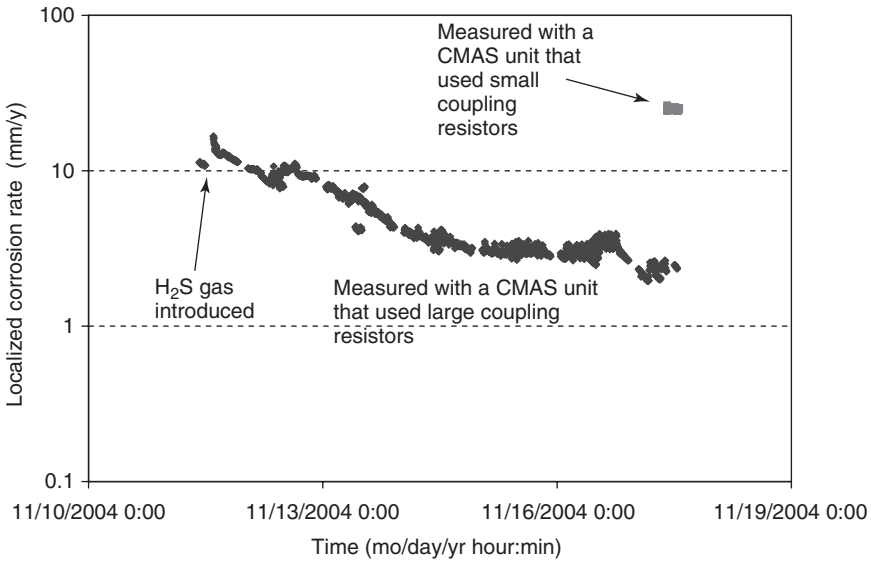

8.28 Maximum localized corrosion rate measured from a carbon steel CMAS probe in a solution saturated with pure H_2S at ambient temperature and pressure using two CMAS instrument units.[106] © NACE International 2006.

probe was connected to the instrument unit that had large resistors. Because the corrosivity of the solution should not decrease after introducing the H_2S, the decrease in the measured corrosion rate was apparently caused by the bridging effect. At the end of the experiment, the DC resistance measurement between each electrode and the coupling joint showed a significant decrease (from several megaohms to less than 100 ohms) which indicates the bridging effect. However, when the maximum localized corrosion rate for the same probe was measured with the second analyzer that had lower values of coupling resistors, the localized corrosion rate was close to the value measured initially when there were no corrosion products. Therefore, the CMAS probe works in H_2S environments as long as the coupling resistors are low.

An important criterion for the coupled multielectrode array sensor probes to perform properly in systems that contain H_2S is that the value of the coupling resistor must be substantially smaller than that of the corrosion products that bridge the anodes and the cathodes. A mechanism built in a coupled multielectrode array sensor instrument that measures the bridging resistance on a continuous basis would be ideal for this application. Based on the above analysis, galvanic probes using true zero-resistance ammeters (or low-input impedance ammeters) are also less affected by the bridging effects by the corrosion products in the H_2S system.

8.8.3 Minimization of the effect by crevice on corrosion rate measurement using coupled multielectrode array sensors

Similar to all electrochemical methods in corrosion rate measurements, the electrode surface area must be well known to apply Faraday's law to calculate the corrosion rate. For highly corrosion-resistant alloys or for corrosion in less corrosive environments, CMAS probes are sensitive to the presence of crevices that may be formed between each sensing electrode and the surrounding insulator. This is because the CAMS probes have a much smaller designated sensing surface area than the probes based on other electrochemical techniques (see Section 8.7.1). In addition, the crevice between the sensing electrode and the surrounding insulator, if formed, may also promote localized corrosion. If the objective is to measure localized corrosion, including crevice corrosion, such as in the case of steam generator tube corrosion under the tube sheet, measurement with a probe that has a crevice would not be a concern. But for cases where no crevice exists, the measurement with a probe that has a crevice would give false results. It should be mentioned that the concern only exists for highly corrosion-resistant alloys or for corrosion in less corrosive environments. If

the solution is highly corrosive or the metal is highly active, such as in the case of carbon steel in seawater,[102] most of the corrosion reactions would take place on the boldly exposed surfaces rather than deep in the crevice because of the limitation by mass transfer through the relatively thin crevice. If the solution is not corrosive or the metal is highly corrosion-resistant, however, mass transfer would not be a limiting factor and corrosion reactions may take place anywhere the metal is in direct contact with the solution, even if the location is deep inside the crevice. In this case, the effective corrosion area is the total area of the metal in contact with the solution.

At low temperatures (<80 °C), this requirement can be satisfied by using a proper sealing material such as an epoxy as the insulator,[51,53] or applying a proper coating[29,61] around the electrodes to achieve good bonding between the electrode and the insulating material or the coating. At elevated temperatures (e.g., 150 °C), however, it is difficult to find a proper coating or sealing material that would resist a harsh chemical environment. In the measurements of localized corrosion rate of Alloy 22 (UNS N06022) material in a NaCl-$NaNO_3$-KNO_3 brine at 150 °C, Chiang and Yang[119] successfully coated the sensing electrode with a diamond-like carbon coating using a chemical vapor deposition process. It was demonstrated that the electrical-insulating diamond-like carbon coating formed an excellent bonding with the Alloy 22 substrate. Figure 8.29 shows a comparison for the sensing electrode surface between a probe that was uncoated, and a probe that was coated with the diamond-like carbon (both were supported by an outer layer of epoxy) after the probes were exposed to a low pH NaCl-$NaNO_3$-KNO_3 brine at 150 °C for two weeks.

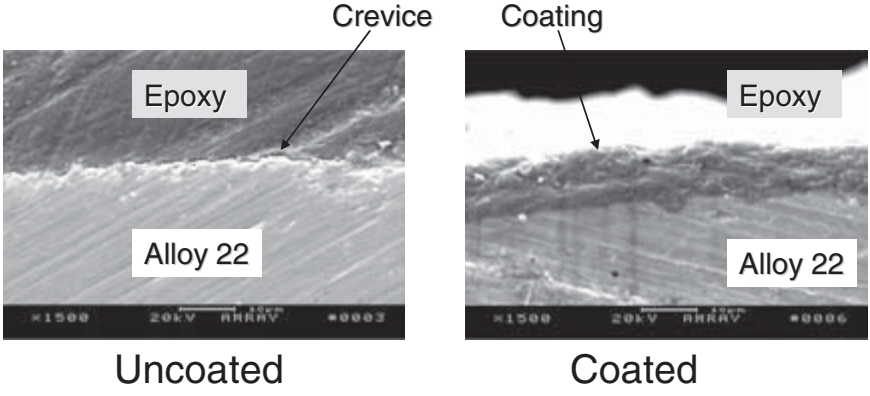

8.29 Post-test appearance of the electrode with and without the diamond-like carbon coating.[119] © NACE International 2007.

Clearly, a crevice was formed between the outer layer epoxy and the Alloy 22 electrode, but no degradation was observed at the interface between the diamond-like carbon coating and the Alloy 22 electrode. Measurements with electrochemical impedance spectroscopy (EIS) showed that the diamond-like carbon coating was highly protective before and after the exposure to the aggressive NaCl-$NaNO_3$-KNO_3 brine at 150 °C.[119]

8.9 Validation of corrosion rate measurement using coupled multielectrode array sensors

An important assumption in the derivation of the maximum localized corrosion rate using a CMAS probe is that if the number of electrodes is large enough, there is at least one electrode (the most corroding electrode) that would not have significant internal current flow (see Section 8.8.1). In addition, the insulator that separates the electrodes from electrically contacting each other and the spacing among the electrodes in typical CMAS probes would not have a significant effect on the measurements of the CMAS probe. Therefore, validations are required to compare the measured corrosion rates against those measured with coupons or other types of probes that measures the wall loss as a direct signal.

8.9.1 Comparison with coupon data for carbon steel in industrial cooling water systems

The coupled multielectrode array sensors were used to measure the localized corrosion rates of low carbon steel material in a chemical plant.[96] Carbon steel specimens were also installed in the system for comparison of the test results. Figure 8.30b shows the monitoring station for cooling water corrosivity and chemistry where CMAS probes and the carbon steel specimens were installed. Figure 8.30a shows the real-time maximum localized corrosion rates from two carbon steel CMAS probes during a five-month test. The five-month average of the maximum localized corrosion rate was 145 mil/y (3.68 mm/y). Figure 8.31 shows the appearance of the sensing electrodes of a CMAS probe and two carbon steel specimens after the test. The sensing electrodes of the probes were covered by a thick layer of deposits when they were removed from the monitoring station. This is also true on the surface of the carbon steel specimens. Bacteria were found in the water samples and in the corrosion products, and microbially influenced corrosion was attributed to the high corrosion rate of carbon steel in the system. The maximum pitting rate (149 mil/y) (3.8 mm/y) indicated in Fig. 8.31 was calculated based on the depth measurement for the most corroded

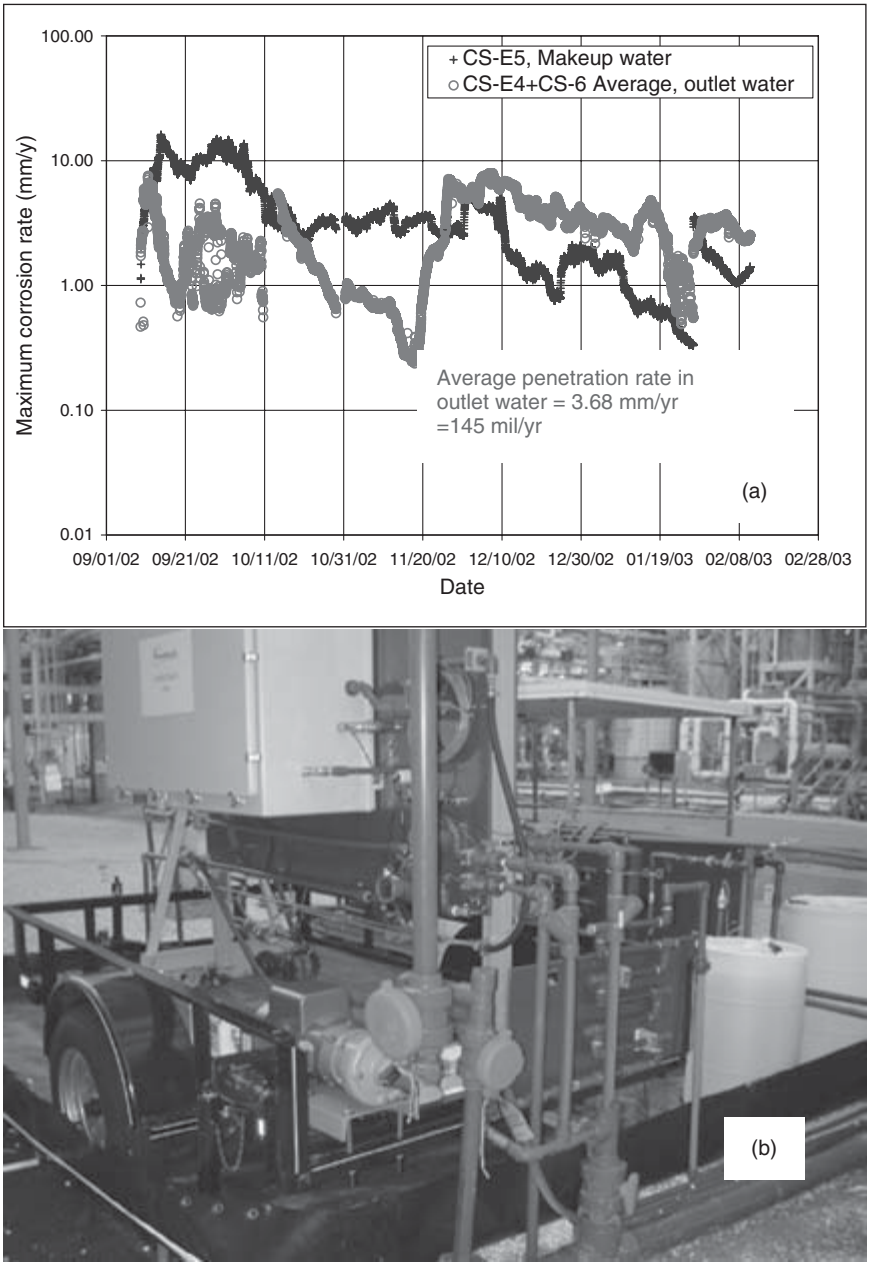

8.30 (a) Typical maximum localized corrosion rates of CMAS carbon steel probes measured in (b) a cooling water monitoring station of a chemical plant.[96] © NACE International 2004.

Coupon tests showed 100 to 200 mil/y (2.5 to 5 mm/y) pitting rate

(a)

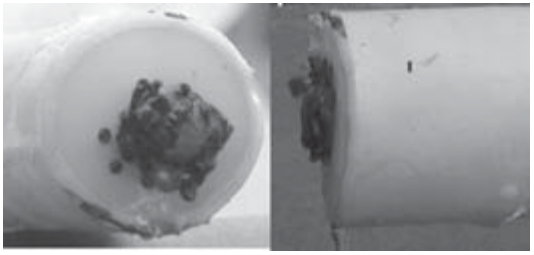

Before cleaning

(b)

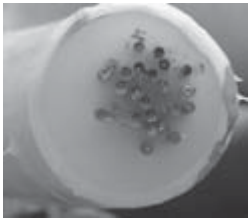

Maximum penetration rate: ~149 mil/y (3.73 mm/y)

After cleaning

(c)

8.31 Comparison of the post-test appearances of the CMAS carbon steel probes and the coupon test specimens in the cooling water system of a chemical plant.[96] © NACE International 2004.

electrode (the electrode that has the deepest pit) after the probe was cleaned. This maximum pitting rate is consistent with the real-time average maximum localized corrosion rate from the probe (145 mil/y (3.7 mm/y), see Fig. 8.30). The maximum localized corrosion rate from the probe (145 mil/y or 3.7 mm/y) is also consistent with the pitting rate measured from the specimens that were tested in the same water (100 to 200 mil/y (2.5 to 5 mm/y), see Fig. 8.31).

8.9.2 Comparison with coupon data for carbon steel, aluminum and stainless steels in seawater systems

Sun and Yang measured the corrosion rates of the following alloys in simulated seawater using coupled multielectrode array sensors:[103]

Type 1008 carbon steel (UNS G10080)
Type 304L stainless steel (UNS S30403)
Type 316L stainless steel (UNS S31603)
Type 904L stainless steel (UNS N08904)

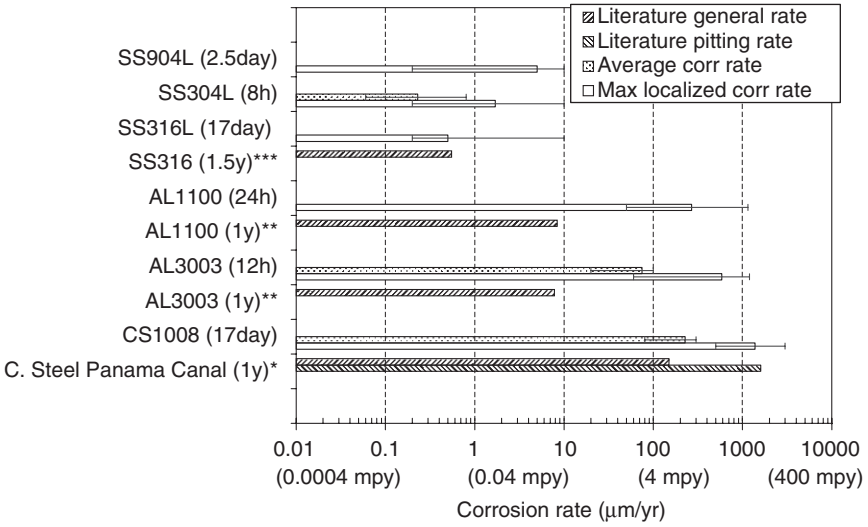

*From Southwell and Alexander, 1970; **From Hollingsworth and Hunsicker, 1987; ***From Pelensky et al. 1976.

8.32 Comparison between the corrosion rates measured with coupled multielectrode array sensors and literature data.[103] © NACE International 2006.

Type 1100 aluminum (UNS A91100)
Type 3003 aluminum (UNS A93003)

Figure 8.32 shows the comparison between the maximum localized corrosion rates averaged over the testing periods for the different types of alloys and the average corrosion rates averaged over the testing periods from the CMAS probes, and the pitting and general corrosion rates of relevant alloys from the literature.

The measured maximum localized corrosion rate (1380 μm/yr) and average corrosion rate (228 μm/yr) for carbon steel 1008 are in good agreement with the reported maximum pitting rate (1600 μm/yr) and general corrosion rate (228 μm/yr), respectively.[103] These reported corrosion rates for carbon steel were obtained from one-year immersion test in Panama Canal seawater. The average corrosion rates for the stainless steels (~0.25 μm/yr) are close to the reported general corrosion rates for stainless steel 316 (0.55 μm/yr). The reported stainless steel general corrosion rate was obtained in an 18-month test in seawater. The average corrosion rate for Al3003 (20 to 100 μm/yr) is slightly higher than the reported value (7.8 μm/yr). The reported general corrosion rate for Al3003 was obtained in a one-year immersion test in seawater.

8.9.3 Comparison with multielectrode penetration probe data for aluminum alloys

Recently, a multielectrode penetration probe was used to validate the corrosion rates measured with CMAS probes.[117] Figure 8.33 shows a schematic diagram of the multielectrode penetration probe with multilayer foils for measuring the penetration rate for a metal in a corrosive environment. The multiple electrodes were embedded inside one or more layers of metal foils in tube shape that were formed by spirally winding a piece of large foil onto a cylindrical bar. Two layers of acid free paper were placed between two layers of the foils and each of the electrodes was placed between the two layers of paper inside a given layer of the foil so that no electrode was electrically contacting the metal foil. The bottom end of the foil tubes was

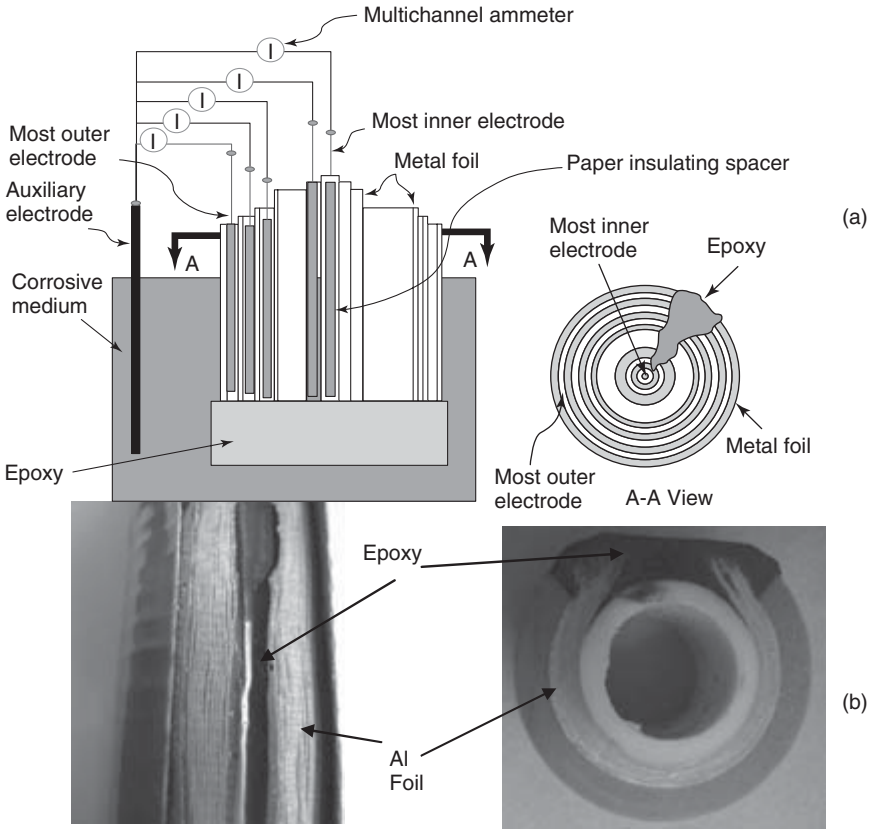

8.33 (a) Schematic diagram and (b) pictures of a multielectrode penetration probe made of aluminum foil.[117] © NACE International 2007.

sealed with epoxy. One side of the foil tube was cut and filled with epoxy so that the space within each layer of the foil was sealed (separated) from the neighboring layers, to avoid having the electrolyte migrate from the space inside one layer of the foil tube to the space inside another layer of the foil tube. The assembled system containing multiple electrodes and multiple foil tubes was then placed in a polyvinylchloride (PVC) protection tube to form an integrated multielectrode penetration probe. The protection tube had an opening (window) for the exposure of the foil to a corrosion environment. Figure 8.33b shows the horizontally-cut and vertically-cut sectional views of the multielectrode penetration probe made of a aluminum foil. During the measurements, the probe was exposed to a corrosive liquid and each electrode was connected to an auxiliary electrode placed in the same electrolyte through an ammeter. When a layer of foil and its outside layers of foil were penetrated by corrosion (both general corrosion and localized corrosion), the corrosive medium would wet the electrode inside that layer of foil and form an electrical path between the electrode and the auxiliary electrode and a galvanic current would flow through the electrode.

Figure 8.34 shows the anodic currents from the different electrodes in an eight-electrode multilayer penetration probe made of aluminum foil to a

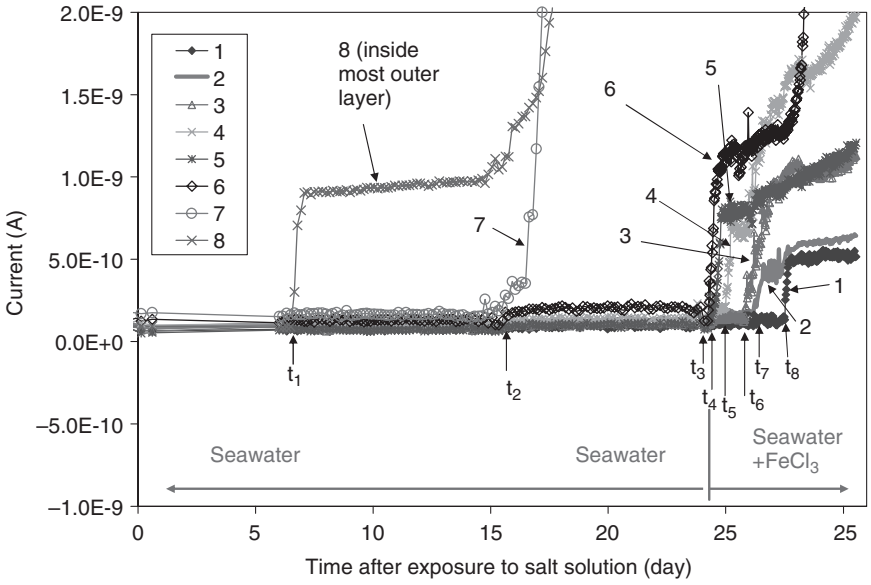

8.34 Typical responses of currents and breakthrough times measured from a multielectrode penetration probe.[117] © NACE International 2007.

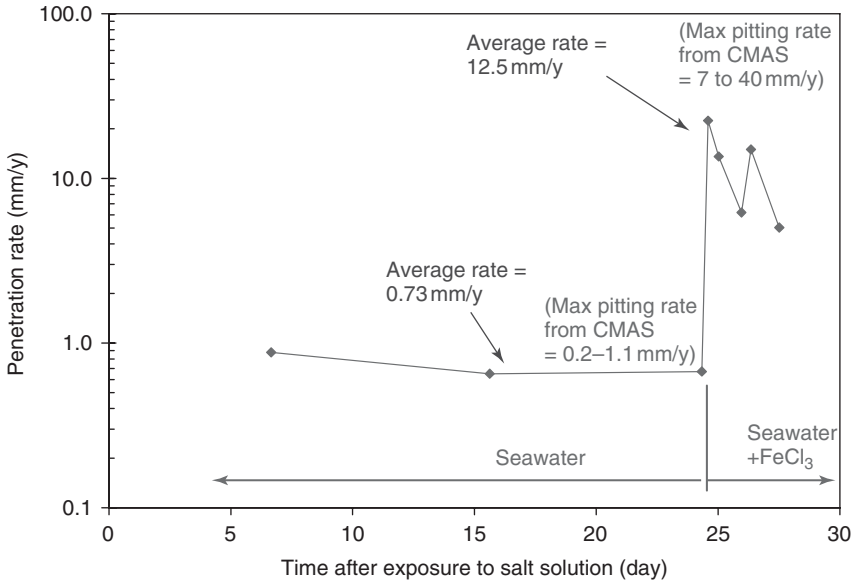

8.35 Comparison between the penetration rates calculated using the breakthrough times shown in Fig. 8.34 and penetration rates measured with coupled multielectrode array sensors.[117] © NACE International 2007.

Type 316L stainless steel auxiliary electrode in simulated seawater and a simulated seawater plus 10 mM ferric chloride solution. The breakthrough times ($t_1, t_2, \ldots$) are the times the current from the corresponding electrodes started to increase due to the perforation of the foils. Figure 8.35 shows the penetration rates calculated using the breakthrough times shown in Fig. 8.34 and the thickness of the foil (16 μm in thickness). The average penetration rates for the aluminum foil were approximately 0.73 mm/y (29 mil/y) in simulated seawater, and 12.5 mm/y (490 mil/y) in the simulated seawater plus ferric chloride solution, respectively. The aluminum foil was Type 8111 aluminum with a chemical composition of 98.5wt% aluminum and balance of iron and silicon. The maximum localized corrosion rates measured with the CMAS probes were 0.2 to 1.1 mm/y for Types 3003 aluminum (98.6% Al, 0.12% Cu and 1.2% Mn) and 0.2 to 0.5 mm/y for Type 1100 aluminum (99% minimum Al and 0.12% Cu) in simulated seawater, and 7 to 40 mm/y for Type 1100 aluminium in simulated seawater plus 10 mM $FeCl_3$ solution. These results from the CMAS probes are in good agreement with the results from the penetration probes.

8.10 Applications of coupled multielectrode array sensor for real-time corrosion monitoring

CMAS probes have been extensively used for monitoring localized corrosion of a variety of metals in the following environments:

- Cooling water[81,85,96,101,120]
- Simulated seawater[103,120]
- Salt-saturated aqueous solutions[86]
- Concentrated chloride solutions[82]
- Concrete[109]
- Soil[110]
- Low-conductivity drinking water[104]
- Process streams of chemical plants at elevated temperatures[89,93,98]
- Coatings[107,111]
- Deposits of sulfate-reducing bacteria[88,95]
- Deposits of salt in air[87,91]
- High pressure simulated natural gas systems[106]
- H_2S systems[106]
- Oil/water mixtures[100,116]
- High temperature acidic solution[119]
- Engine coolant.[115]

The CMAS probes were also used in the evaluation of corrosion inhibitors[81,121] and monitoring the effectiveness of cathodic protections.[108] In addition, CMAS probes have been used to measure the propagation rate of metals in crevices.[102]

Chapter 26 describes in detail the application of the CMAS probes in real time corrosion monitoring for cathodically protected systems in simulated seawater, drinking water, soil and concrete. For other applications, the users are encouraged to read the appropriate references.

8.11 Limitations of multielectrode systems

All electrochemical techniques have limitations. Coupled electrode systems, depending on their operating principles, have their own limitations. Corrosion engineers need to understand these limitations in order to use them effectively for research or monitoring. As previously discussed, an obvious limitation of the CMAS probe is a possible underestimation of actual dissolution rates because of concurrent cathodic reactions occurring on the most anodic electrode of the array. The corrosion rate from an unpolarized CMAS probe may be lower than the actual corrosion rate and is the lower bound of the corrosion rate. The proposed method to overcome this limitation is to slightly polarize the probe to or near the potential of the most

cathodic electrode. This polarization method gives the upper bound of the corrosion rate. Although the tests with selected systems showed that the lower bound values were close to the upper bound values (factors of 2.2 to 2.7), the lower and upper bound values may be significantly different for other systems. An alternative approach is to use small electrodes, because the smaller the electrode, the greater the probability for anodic reactions to completely cover the most anodic electrode surface. This, however, may not be practical for all situations. In addition, if the electrode is too small, it may no longer represent the corrosion behavior of a large metal. The electrode size effect should be determined before any attempt is made to use extremely small electrodes.

A second limitation, especially for purposes of research in localized corrosion phenomena, is the crevice between each electrode and the surrounding insulator. Although different methods and different types of epoxy or coatings have been used to reduce or eliminate the formation of crevices, the fabrication of a crevice-free multielectrode probe for certain environments, especially under elevated temperature conditions, has been a challenge. For a less corrosion-resistant metal in a corrosive environment, such as carbon steel in seawater, this may not be an issue because corrosion takes place mostly on the boldly exposed metal surfaces. If a crevice forms, the area of corrosion is less defined, and the calculation of corrosion rates may be difficult.

Finally, because the electrode areas are small and low levels of current are measured, precautions must be taken to minimize noise from thermal junctions, dissimilar electrode contacts, and other noise sources. Care must also be taken in the electrode preparation to ensure that the metallurgical state of the actual material of interest is adequately represented by the electrodes. Often, wires of an alloy do not have the same microstructure as other wrought forms. Special machining techniques have been used to fabricate the electrode from exactly the same kind of wrought forms for the probes, but the cost for such fabrication is high.

8.12 Summary

Coupled multielectrode systems have been used for qualitative corrosion detection in concrete for nearly two decades and for crevice corrosion detection for more than 15 years. Coupled multielectrode arrays with spatially patterned electrodes have been used for electrochemical studies for at least 12 years. The coupled multielectrode arrays that can be arranged in any given patterns have been used by many researchers for studying the spatial patterns and the electrochemical behaviors of the corrosion processes, especially the localized corrosion processes of metals.

With the advancement of the coupled multielectrode arrays and multichannel instrumentation, real-time CMAS probes have been developed. These probes give simple parameters, such as maximum localized corrosion rate, maximum localized corrosion penetration depth, and estimation for average corrosion rate. The CMAS probes have been extensively used for online and real-time corrosion monitoring in laboratories and industrial fields. Because CMAS probes do not require the presence of bulk electrolytes, they have been used not only in aqueous solutions, but also in wet gases, oil/water mixtures, salt deposits, biodeposits, soil, concrete and undercoatings. CMAS probes also have been used for real-time monitoring of the effectiveness of cathodic protection in cathodically protected systems. In addition to the real-time measurement of the quantitative rate of localized corrosion, such as pitting and crevice corrosion, CMAS probes have also been used to estimate the general corrosion rate based on the average corrosion rate. With proper design in seals and access fittings, CMAS probes also have been used for corrosion monitoring at high-pressure and elevated temperatures. Another important feature of CMAS probes is that the life of these probes is extremely long because there is no limit on the length of the sensing electrodes embedded in the insulators. The probes can be reused after the sensing surface is re-polished or after the severely corroded sensing tip is cut off.

At the present time, the costs of the multichannel high-resolution multielectrode instruments are rather high. As the demand for the multielectrode systems increases and the instruments as well as the probes can be mass produced, the costs of the multielectrode systems will decrease and the multielectrode systems will play an important role in corrosion monitoring.

8.13 References

1 T. Shibata and T. Takeyama, 'Stochastic Theory of Pitting Corrosion', *Corrosion*, 33, 12 (1977): p. 243–251.
2 Y-J. Tan and X. Xu, 'Evaluation of Corrosion Protective Oil Using Poly Working Electrode System', *Materials Protection* (Chinese), 20, 2 (1987): p. 38–40.
3 H.S. White, G.P. Kittlesen and M.S. Wrighton, 'Chemical Derivatization of an Arrray of Three Gold Microelectrodes with Polyrrote: Fabrication of a Molecule-Based Transistor', *J. Am. Chem. Soc.*, 106 (1984): p. 5375–5377.
4 G.P. Kittlesen, H.S. White and M.S. Wrighton, 'Chemical Derivatization of a Microelectrode Arrays by Oxidation of Polyrrote and N-Methylpyrrole: Fabrication of Molecule-Based Electronic Device', *J. Am. Chem. Soc.*, 106 (1984): p. 7389–7396.
5 E.W. Paul, A.J. Rico and M.S. Wrighton, 'Resistance of Polyaniline Film as a Function of Electrochemical Potential and the Fabrication of Polyaniline-Based Microelectronic Devices', *J. Phys. Chem.*, 89 (1985): p. 1441–1447.

6 S. S. Wang, 'Microelectrode Arrays for Lubrication Studies', *J. Electrochem. Soc.*, 136, 3 (1989): p. 713–715.
7 Y.J. Tan, 'The Effect of Inhomogeneity in Organic Coatings on Electrochemical Measurements Using a Wire Beam Electrode, Part 1', *Progress in Organic Coatings*, 19, (1991): p. 89–94.
8 Y.J. Tan and S.T. Yu, 'The Effect of Inhomogeneity in Organic Coatings on Electrochemical Measurements Using a Wire Beam Electrode, Part 2', *Progress in Organic Coatings*, 19, (1991): p. 257–263.
9 Y.J. Tan, 'A New Crevice Corrosion Testing Method and Its Use in the Investigation of Oil Stain', *Corrosion*, 50, 4, (1994): p. 266–269.
10 Q. Zhong, 'Electrochemical Technique for Investigating Temporarily Protective Oil Coatings', *Progress in Organic Coatings*, 30, 4, (1997): p. 213–218.
11 Q. Zhong, 'Wire Beam Electrode: A New Tool for Investigating Electrochemical Inheterogeneity of Oil Coating', *Progress in Organic Coatings*, 30, 4, (1997): p. 279–285.
12 Z. Qingdong, 'A Novel Electrochemical Testing Method and Its Use in the Investigation of Underfilm Corrosion of Temporary Protective Oil Coating', *Corrosion*, 56, 7, (2000): p. 722–726.
13 Q. Zhong, 'Potential Variation of a Temporarily Protective Oil Coating before Its Degradation', *Corrosion Science*, 43, 2, (2001): p. 317–324.
14 Q. Zhong, 'Study of Corrosion Behaviour of Mild Steel and Copper in Thin Film Salt Solution Using the Wire Beam Electrode', *Corrosion Science*, 44, 5, (2002): p. 909–916.
15 Q. Zhong, 'A Novel Electrochemical Testing Method and Its Use in the Investigation of the Self-Repairing Ability of Temporarily Protective Oil Coating', *Corrosion Science*, 44, 6, (2002): p. 1247–1256.
16 Q. Zhong and Z. Zhao, 'Study of Anti-Contamination Performance of Temporarily Protective Oil Coatings Using Wire Beam Electrode', *Corrosion Science*, 44, 12, (2002): p. 2777–2787.
17 P. Schiessl, United States Patent 5,015,355, 'Corrosion Measuring Cell', 14 May, 1991.
18 P. Schiessl, Federal Republic of Germany Patent Application 3,834,628, 'Corrosion Measuring Cell', 11 October 1988.
19 P. Schiessl and M. Raupach, 'Monitoring System for the Corrosion Risk for Steel in Concrete', *Concrete International*, 7 (1992): p. 52–55.
20 P. Schiessl and M. Raupach, 'New Approach for Monitoring of the Concrete Risk for the Reinforcement-Installation of Sensors', Proceedings, International Concrete: Across Borders, Odense, Denmark, June, 1994, p. 65–78.
21 R. Bassler, J. Mietz, M. Raupach and O. Klinghoffer, 'Corrosion Risk and Humidity Sensors for Durability Assessment of Reinforced Concrete Structures', Proc. EUROCORR 2000, London, article 100805 (2000).
22 R. Bassler, J. Mietz, M. Raupach and O. Klinghoffer, 'Corrosion Monitoring Sensors for Durability Assessment of Concrete Structures', Proc. SPIEs 7th International Symposium on Smart Structures and Materials, Newport Beach, article 3988 06 (2000).
23 R. Bassler, J. Mietz, M. Raupach and O. Klinghoffer, 'Corrosion Monitoring Sensors for Durability Assessment of Concrete Structures', Proc. SPIEs 7th International Symposium on Smart Structures and Materials, Newport Beach, article 3988 06 (2000).

24 O. Klinghoffer, P. Goltermann and R. Bassler, 'Embeddable Sensors for Use in the Integrated Monitoring Systems of Concrete Structures', First International Conference on Bridge Maintenance, Safety and Management IABMAS 2002, Barcelona, 14–17 July, (2002).
25 U. Steinsmo, 'The Effect of Temperature on Propagation of Crevice Corrosion of High Alloyed Stainless Steel in Natural Seawater', Progress in the Understanding and Prevention of Corrosion, 10th Eur. Corros. Congr. Paper, Volume 2, J.M. Costa and A.D. Mercer, Eds, Institute of Materials, London, UK, 1993, p. 974–982.
26 U. Steinsmo, T. Rone and J.M. Drugli, 'Aspects of Testing and Selecting Stainless Steels for Sea Water Applications', *CORROSION/94*, paper no. 492 (Houston, TX: NACE International, 1994).
27 U. Steinsmo, T. Rogne and J. Drugli, 'Aspect of Testing and Selecting Stainless Steels for Seawater Applications', *Corrosion*, 53, 12, (1997): p. 955–964.
28 U. Steinsmo, 'Test Method for Localized Corrosion of Stainless Steel in Sea Water', *Pitture Vernici Europe*, 74, 14, (1998): p. 15–18.
29 Z. Fei, R.G. Kelly and J.L. Hudson, 'Spatiotemporal Patterns on Electrode Arrays', *J. Phys. Chem.*, 100, (1996): p. 18986–18991.
30 Z. Fei, 'Spatiotemporal Behavior of Iron and Sulfuric Acid Electrochemical Reaction System', PhD Thesis, University of Virginia, Charlottesville, Virginia, *Diss. Abstr. Int.*, B 1997, 58, 3, 1402, May, 1997.
31 Z. Fei and J.L. Hudson, 'Pacemaker-Driven Spatiotemporal Patterns on an Electrode Array', *Journal of Physical Chemistry B*, 101, 49, (1997): p. 10356–10364.
32 Z. Fei and J.L. Hudson, 'Chaotic Oscillations on Arrays of Iron Electrodes', *Industrial & Engineering Chemistry Research*, 37, 6, (1998): p. 2172–2179.
33 J.L. Hudson, 'Spatiotemporal Patterns in Electrochemical Systems', in *Pattern Formation in Continuous and Coupled Systems, IMA Volume in Mathematics and its Applications 115*, p. 137–146, Martin Golubitsky, Dan Luss, and Steven H. Strogatz, eds., Springer, New York (1999).
34 Z. Fei, B.J. Green and J.L. Hudson, 'Spatiotemporal Patterns on a Ring Array of Electrodes', *Journal of Physical Chemistry B*, 103, 12, (1999): p. 2178–2187.
35 I.Z. Kiss, W. Wang and J.L. Hudson, 'Experiments on Arrays of Globally Coupled Periodic Electrochemical Oscillators', *J. Phys. Chem. B*, 103, (1999): p. 11433–11444.
36 W. Wang, I.Z. Kiss and J.L. Hudson, 'Experiments on Arrays of Globally Coupled Chaotic Electrochemical Oscillators: Synchronization and Clustering', *Chaos*, 10, 1, (2000): p. 248–256.
37 I.Z. Kiss, G. Vilmos and J.L. Hudson, 'Experiments on Synchronization and Control of Chaos on Coupled Electrochemical Oscillators', *J. Phys. Chem. B* 104, (2000): p. 7554–7560.
38 I.Z. Kiss, W. Wang and J.L. Hudson, 'Complexity of Globally Coupled Chaotic Electrochemical Oscillators', *Physical Chemistry Chemical Physics 2*, (2000): p. 3847–3854.
39 W. Wang, I.Z. Kiss and J.L. Hudson, 'Clustering of Arrays of Chaotic Chemical Oscillators by Feedback and Forcing', *Phys. Rev. Lett.* 86, 21, (2001): p. 4954–4957.

40 W. Wang, B.J. Green and J.L. Hudson, 'Periodic Forcing of Arrays of Chaotic Electrochemical Oscillators', *J. Phys. Chem. B*. 105, 30, (2001): p. 7366–7373.
41 W. Wang, I.Z. Kiss and J.L. Hudson, 'Synchronization and Clustering of Arrays of Electrochemical Oscillators with Global Feedback', *Ind. Eng. Chem. Res.* 41, (2002): p. 330–339.
42 I.Z. Kiss, W. Wang and J.L. Hudson, 'Populations of Coupled Electrochemical Oscillators', *Chaos* 12, 1, (2002): p. 252–263.
43 I.Z. Kiss, Y. Zhai and J.L. Hudson, 'Collective Dynamics of a Weakly Coupled Electrochemical Reaction on an Array', *Ind. Eng. Chem. Res.* 41, (2002): p. 6363–6374.
44 Y. Zhai, I.Z. Kiss, and J.L. Hudson, 'Amplitude Death through a Hopf Bifurcation in Coupled Electrochemical Oscillators: Experiments and Simulations', *Phys. Rev. E.* 69, 206–208 (2004).
45 T.T. Lunt, V. Brusamarello, J.R. Scully and J.L. Hudson, 'Interactions among Localized Corrosion Sites Investigated with Electrode Arrays', *Proceedings – Electrochemical Society* (1999), 99–27; (*Passivity and Localized Corrosion*), p. 414–424.
46 T.T. Lunt, V. Brusamarello, J.R. Scully and J.L. Hudson, 'Interactions Among Localized Corrosion Sites Investigated with Electrode Arrays', *Electrochemical and Solid State Letters* 3, 6, (2000): p. 271–274.
47 T.T. Lunt, J.R. Scully, V. Brusamarello, A.S. Mikhailov and J.L. Hudson, 'Spatial Interactions among Localized Corrosion Sites: Experiments and Modeling', *Proceedings – Electrochemical Society* (2001), 2000–25; (*Pits and Pores II: Formation, Properties, and Significance for Advanced Materials*), p. 115–125.
48 T.T. Lunt, J.R. Scully, V. Brusamarello, A.S. Mikhailov and J.L. Hudson, 'Spatial Interactions among Localized Corrosion Sites: Experiments and Modeling', *J. Electrochemical Soc.* 149, 5, B163–B173 (2002).
49 N.D. Budiansky and J.R. Scully, 'Origins of Persistent Interaction among Localized Corrosion Sites', *Proceedings – Electrochemical Society* (2003), 2002–24; (*Critical Factors in Localized Corrosion IV*), p. 133–146.
50 N.D. Budiansky, J.L. Hudson and J.R. Scully, 'Origins of Persistent Interaction among Localized Corrosion Sites on Stainless Steel', *Journal of the Electrochemical Society* (2004), 151(4), B233–B243.
51 N.D. Budiansky, F. Bocher, H. Cong, M.F. Hurley and J.R. Scully, 'Use of Coupled Multi-Electrode Arrays to Advance the Understanding of Selected Corrosion Phenomena', *CORROSION/2006*, paper no. 06677 (Houston, TX: NACE, 2006).
52 M.F. Hurley and J.R. Scully, 'Candidate Corrosion Resistant Reinforcement Materials for Concrete Structures: Corrosion Propagation Behavior', *CORROSION/2006*, paper no. 066340 (Houston, TX: NACE, 2006).
53 H. Cong, N.D. Budiansky, J.R. Scully and H.T. Michels, 'Use of Coupled Electrode Arrays to Elucidate Copper Pitting as a Function of Potable Water Chemistry', *CORROSION/07*, paper no. 07392 (Houston, TX: NACE, 2007).
54 D. Battocchi, J. He, G.P. Bierwagen and D.E. Tallman, 'Emulation and Study of the Corrosion Behavior of Al Alloy 2024-T3 Using a Wire Beam Electrode

(WBE) in Conjunction with Scanning Vibrating Electrode Technique (SVET)', *Corrosion Science* 47 (2005) 1165–1176.
55 N. Missert, R.G. Copeland, F.D. Wall, C.M. Johnson, J.C. Barbour and P. Kotula, 'Aluminum Corrosion at Systems of Engineered Copper Particles', *Proceedings – Electrochemical Society* (2002), 2002–13; (*Corrosion Science*), p. 307–313.
56 F.D. Wall, M.A. Martinez, C.M. Johnson, J.C. Barbour, N. Missert and R.G. Copeland, 'Does Anything Pin the Pitting Behavior of Aluminum?', *Proceedings – Electrochemical Society* (2004), 2003–23, 1–11.
57 F.D. Wall and M.A. Martinez, 'Using Microelectrodes to Determine the Availability and Behavior of Pit Initiation Sites in Aluminum', *Proceedings – Electrochemical Society* (2001), 2000–23 (Corrosion and Corrosion Prevention of Low Density Metals and Alloys), 229–238.
58 F.D. Wall and M.A. Martinez, 'A Statistics-Based Approach to Studying Aluminum Pit Initiation – Intrinsic and Defect-Driven Pit Initiation Phenomena', *Journal of the Electrochemical Society*, 2003, 150(4): p. B146–B157.
59 F.D. Wall, C.M. Johnson, J.C. Barbour, and M.A. Martinez, 'The Effects of Chloride Implantation on Pit Initiation in Aluminum', *Journal of The Electrochemical Society*, 151(2), B77–B81, 2004.
60 F.D. Wall, M.A. Martinez and J.J. Van den Avyle, 'Relationship between Induction Time for Pitting and Pitting Potential for High-Purity Aluminum', *Journal of the Electrochemical Society*, 2004, 151(6): p. B354–B358.
61 F.D. Wall, 'Applications of Multi-electrode Techniques to Aqueous and Atmospheric Corrosion Testing', *CORROSION/06*, paper no. 06672 (Houston, TX: NACE, 2006).
62 K.R. Cooper, M. Smith, J.R. Scully and N.D. Budiansky, 'Development of a Multielectrode Array Impedance Analyzer for Corrosion Science and Sensors', *CORROSION/06*, paper no. 06674 (Houston, TX: NACE, 2006).
63 W. Zhang, B. Hurley, R.G. Buchheit, 'Characterization of Chromate Conversion Coating Formation and Breakdown Using Electrode Arrays', *Journal of the Electrochemical Society* (2002), 149(8), B357–B365.
64 F.D. Wall and M.A. Martinez, 'The Effect of Electrode Thickness and Interelectrode Spacing on Electrochemical Signals at Low Humidity', Abs. 480, 204th Meeting, The Electrochemical Society, Inc. (2004).
65 Y.J. Tan, 'Studying Non-uniform Electrodeposition Using the Wire Beam Electrode Method', *International Journal of Modern Physics B (World Scientific)*, no.1&2 – special issue for proceedings of International Conference on Materials for Advanced Technologies, Singapore (1–6 July 2001), vol.16, p. 144–150 (2002).
66 Y.J. Tan and K.Y. Lim, 'Characterising Nonuniform Electrodeposition and Electrodissolution Using the Novel Wire Beam Electrode Method', *Journal of Applied Electrochemistry*, 34, 1093–1101 (2004).
67 Y.J. Tan, 'Wire Beam Electrode: A New Tool for Localized Corrosion Studies', *Proceedings of Australasian Corrosion Association, Corrosion & Prevention 97*, paper no. 52, Australasian Corrosion Association, Australia, 9–12, November 1997.
68 Y.J. Tan, 'Monitoring Localized Corrosion Processes and Estimating Localized Corrosion Rates Using a Wire-beam Electrode', *Corrosion*, 54(5), 1998, p. 403–413.

69 H. Eren, A. Lowe, Y.J. Tan, S. Bailey and B. Kinsella, 'An Auto-switch for Multi-sampling of a Wire Beam Electrode Corrosion Monitoring System', *IEEE Transaction on Instrumentation and Measurement*, 47, 1096–2001 (1998).
70 Y.J. Tan, 'Wire Beam Electrode: A New Tool for Studying Localized Corrosion and Other Inheterogeneity Electrochemical Processes', *Corrosion Science*, 41(2), 1999, 229–247.
71 Y.J. Tan, S. Bailey, B. Kinsella and A. Lowe, 'Mapping Corrosion Kinetics Using the Wire Beam Electrode in Conjunction with Electrochemical Noise Resistance Measurements', *Journal of the Electrochemical Society*, 147(2), 530–540 (2000).
72 Y.J. Tan, 'Method and Apparatus for Measuring Localized Corrosion and Other Heterogeneous Electrochemical Processes', United States of America Patent No. 6132593, 24pp (2000).
73 Y.J. Tan, S. Bailey and B. Kinsella, 'Mapping Non-uniform Corrosion in Practical Corrosive Environments Using the Wire Beam Electrode Method (I) – Multi-phase Corrosion', *Corrosion Science*, 43, 1905–1918 (2001).
74 Y.J. Tan, S. Bailey and B. Kinsella, 'Mapping Non-uniform Corrosion in Practical Corrosive Environments Using the Wire Beam Electrode Method (II) – Crevice Corrosion', *Corrosion Science*, 43, 1919–1929 (2001).
75 Y.J. Tan, S. Bailey and B. Kinsella, 'Mapping Non-uniform Corrosion in Practical Corrosive Environments Using the Wire Beam Electrode Method (III) – Water-line Corrosion', *Corrosion Science*, 43, 1930–1937 (2001).
76 Y.J. Tan, 'Measuring Localized Corrosion Using the Wire Beam Electrode Method', in special Electrochemical Society publication: *Corrosion Science: A Retrospective and Current Status*, the Electrochemical Society 201st Meeting, Philadelphia, USA, pp. 377–384 (2002).
77 N.N. Aung and Y.J. Tan, 'A New Method of Studying Buried Steel Corrosion and Its Inhibition Using the Wire Beam Electrode', *Corrosion Science*, 46, 3057–3067 (2004).
78 Y.J. Tan, 'An Experimental Comparison of Three Wire Beam Electrode Based Methods for Determining Corrosion Rates and Patterns', *Corrosion Science*, 47, 1653–1665 (2005).
79 L. Yang, N. Sridhar and O. Pensado, 'Development of a Multielectrode Array Sensor for Monitoring Localized Corrosion', Presented at the 199th Meeting of the Electrochemical Society, Abstract #182, Extended Abstract Volume I, 2001.
80 L. Yang, N. Sridhar, O. Pensado and D. Dunn 'An In-situ Galvanically Coupled Multi-Electrode Array Sensor for Localized Corrosion', *Corrosion*, 58, 1004, 2002.
81 L. Yang and D. Dunn, 'Evaluation of Corrosion Inhibitors in Cooling Water Systems Using a Coupled Multielectrode Array Sensor', *Corrosion/2002*, paper no. 004 (Houston, TX: NACE International, 2002).
82 L. Yang, N. Sridhar and G. Cragnolino, 'Comparison of Localized Corrosion of Fe-Ni-Cr-Mo Alloys in Concentrated Brine Solutions Using a Coupled Multielectrode Array Sensor', *NACE CORROSION/2002*, paper no. 545 (Houston, TX: NACE International, 2002).

83 C.S. Brossia, L. Yang, D.S. Dunn and N. Sridhar, 'Corrosion Sensing and Monitoring', Proceedings of the Tri-Service Corrosion Conference, Jan. 14–18, 2002, San Antonio, TX, USA.
84 L. Yang and N. Sridhar, 'Monitoring of Localized Corrosion', in *ASM Handbook, Volume 13A – Corrosion: Fundamentals, Testing, and Protection*, Stephen. D. Crammer and Bernard S. Covino, Jr., eds, ASM International, Materials Park, OH, p. 519–524, 2003.
85 L. Yang and N. Sridhar 'Coupled Multielectrode Online Corrosion Sensor', *Materials Performance*, 42(9), 48–52, 2003.
86 L. Yang, R.T. Pabalan, L. Browning and G.A. Cragnolino, 'Measurement of Corrosion in Saturated Solutions under Salt Deposits Using Coupled Multielectrode Array Sensors', *CORROSION/2003*, paper no. 03426 (Houston, TX: NACE International, 2003).
87 L. Yang, R.T. Pabalan, L. Browning and D.S. Dunn, 'Corrosion Behavior of Carbon Steel and Stainless Steel Materials under Salt Deposits in Simulated Dry Repository Environments', in *Scientific Basis for Nuclear Waste Management XXVI*, R.J. Finch and D.B. Bullen, eds, Materials Research Society, Warrendale, PA, M.R.S. Symposium Proceedings, Vol. 757, p. 791–797, 2003.
88 C.S. Brossia and L. Yang, 'Studies of Microbiologically Influenced Corrosion Using a Coupled Multielectrode Array Sensor', *CORROSION/2003*, paper no. 03575 (Houston, TX: NACE International, 2003).
89 A. Anderko, N. Sridhar, C.S. Brossia, D.S. Dunn, L. Yang, B.J. Saldanha, S.L. Grise and M.H. Dorsey, 'An Electrochemical Approach to Predicting and Monitoring Localized Corrosion in Chemical Process Streams', *CORROSION/2003*, paper no. 03375 (Houston, TX: NACE International, 2003).
90 V. Jain, S. Brossia, D. Dunn, and L. Yang, 'Development of Sensors for Waste Package Testing and Monitoring in the Long Term Repository Environments', *Ceramic Transactions*, 143, 283–290, 2003, American Ceramic Society, Westerville, OH.
91 L. Yang, R.T. Pabalan and D.S. Dunn, 'The Study of Atmospheric Corrosion of Carbon Steel and Aluminum under Salt Deposit Using Coupled Multielectrode Array Sensors', Presented at the 204th Meeting of the Electrochemical Society, Abstract #465, Extended Abstract Volume 2003-II.
92 L.Yang and N. Sridhar, 'Sensor Array for Electrochemical Corrosion Monitoring', US patent 6,683,463 (2004).
93 L. Yang, N. Sridhar, S.L. Grise, B.J. Saldanha, M.H. Dorsey, H.J. Shore and A. Smith, 'Real-Time Corrosion Monitoring in a Process Stream of a Chemical Plant Using Coupled Multielectrode Array Sensors', *CORROSION/2004*, paper no. 04440 (Houston, TX: NACE International, 2004).
94 L. Yang, N. Sridhar, D.S. Dunn and C.S. Brossia, 'Laboratory Comparison of Coupled Multielectrode Array Sensors with Electrochemical Noise Sensors for Real-time Corrosion Monitoring', *CORROSION/2004*, paper no. 04429 (Houston, TX: NACE International, 2004).
95 L. Yang and G.A. Cragnolino, 'Studies on The Corrosion Behavior of Stainless Steels in Chloride Solutions in the Presence of Sulfate Reducing Bacteria', *CORROSION/2004*, paper no. 04598 (Houston, TX: NACE International, 2004).

96 M.H. Dorsey, L. Yang and N. Sridhar, 'Cooling Water Monitoring Using Coupled Multielectrode Array Sensors and Other On-line Tools', *CORROSION/2004*, paper no. 04077 (Houston, TX: NACE International, 2004).
97 L. Yang, N. Sridhar, C.S. Brossia and D.S. Dunn, 'Evaluation of the Coupled Multielectrode Array Sensor as a Real Time Corrosion Monitor', *Corrosion Science*, 47, 1794–1809 (2005).
98 A. Anderko, N. Sridhar, L. Yang, S.L. Grise, B.J. Saldanha and M.H. Dorsey, 'Validation of a Localized Corrosion Model Using Real-Time Corrosion Monitoring in a Chemical Plant', *Corrosion Engineering, Science and Technology* (formerly *British Corrosion J.*), 40, 33–42, August, 2005.
99 L. Yang, D.S. Dunn and G. Cragnolino, 'An Improved Method for Real-time and Online Corrosion Monitoring Using Coupled Multielectrode Array Sensors', *CORROSION/2005*, paper no. 05379 (Houston, TX: NACE International, 2005).
100 L. Yang, D.S. Dunn, Y.-M. Pan and N. Sridhar, 'Real-time Monitoring of Carbon Steel Corrosion in Crude Oil and Brine Mixtures Using Coupled Multielectrode Sensors', *CORROSION/2005*, paper no. 05293 (Houston, TX: NACE International, 2005).
101 M.H. Dorsey, D.R. Demarco, B.J. Saldanha, G.A. Fisher, L. Yang and N. Sridhar, 'Laboratory Evaluation of a Multi-Array Sensor for Detection of Underdeposit Corrosion and/or Microbially Influenced Corrosion', *CORROSION/2005*, paper no. 05371 (Houston, TX: NACE International, 2005).
102 X. Sun and L. Yang, 'Real-time Measurement of Crevice Corrosion with Coupled Multielectrode Array Sensors', *CORROSION/2006*, paper no. 06679 (Houston, TX: NACE International, 2006).
103 X. Sun and L. Yang, 'Real-Time Monitoring of Localized and General Corrosion Rates in Simulated Marine Environments Using Coupled Multielectrode Array Sensors', *CORROSION/2006*, paper no. 06284 (Houston, TX: NACE International, 2006).
104 X. Sun and L. Yang, 'Real-Time Monitoring of Localized and General Corrosion Rates in Drinking Water Utilizing Coupled Multielectrode Array Sensors', *CORROSION/2006*, paper no. 06094 (Houston, TX: NACE International, 2006).
105 K.T. Chiang and L. Yang, 'Monitoring Corrosion Behavior of a Cu-Cr-Nb Alloy by Multielectrode Sensors', *CORROSION/2006*, paper no. 06676 (Houston, TX: NACE International, 2006).
106 N. Sridhar, L. Yang and F. Song, 'Application of Multielectrode Array to Study Dewpoint Corrosion in High Pressure Natural Gas Pipeline Environments', *CORROSION/2006*, paper no. 06673 (Houston, TX: NACE International, 2006).
107 X. Sun, 'Online Monitoring of Undercoating Corrosions Utilizing Coupled Multielectrode Sensors', *CORROSION/2004*, paper no. 04033 (Houston, TX: NACE International, 2004).
108 X. Sun, 'Online Monitoring of Corrosion under Cathodic Protection Conditions Utilizing Coupled Multielectrode Sensors', *CORROSION/2004*, paper no. 04094 (Houston, TX: NACE International, 2004).

109 X. Sun, 'Online and Real-Time Monitoring of Carbon Steel Corrosion in Concrete, Using Coupled Multielectrode Sensors', *CORROSION/2005*, paper no. 05267 (Houston, TX: NACE International, 2005).
110 X. Sun, 'Real-Time Corrosion Monitoring in Soil with Coupled Multielectrode Sensors', *CORROSION/2005*, paper no. 05381 (Houston, TX: NACE International, 2005).
111 X. Sun, 'Online Monitoring of Undercoating Corrosion Using Coupled Multielectrode Sensors', *Materials Performance*, 44(2), 28–32 (2005).
112 P. Angell, 'Use of the Multiple-Array-Sensor to Determine the Effect of Environmental Parameters on Microbial Activity and Corrosion Rates', *CORROSION/2006*, paper no. 06671 (Houston, TX: NACE International, 2006).
113 L. Yang and N. Sridhar, 'Sensor Array for Electrochemical Corrosion Monitoring', US Patent, #6,987,396 (United States Patent and Trademark Office, 2006).
114 X. Sun, Yang, 'Electronic System for Multielectrode Sensors and Electrochemical Devices', US Patent, #7,180,309 (United States Patent and Trademark Office, 2007).
115 B. Yang, F.J., Marinho, A.V. Gershun, A.V., 'New Electrochemical Methods for the Evaluation of Localized Corrosion in Engine Coolants', *Journal of ASTM International*, 4(1) (2007).
116 T. Pickthall, V. Morris and H. Gonzalez, 'Corrosion Monitoring of a Crude Oil Pipeline A Comparison of Multiple Methods', *CORROSION/07*, paper no. 07340 (Houston, TX: NACE International, 2007).
117 X. Sun and L. Yang, 'Multielectrode Penetration Sensor for Monitoring Localized and General Corrosion', *CORROSION/2007*, paper no. 07391 (Houston, TX: NACE International, 2006).
118 L. Yang and X. Sun, 'Measurement of Cumulative Localized Corrosion Rate Using Coupled Multielectrode Array Sensors', *CORROSION/2007*, paper no. 07378 (Houston, TX: NACE International, 2007).
119 K.T. Chiang and L. Yang, 'Development of Crevice-Free Multielectrode Sensors for Elevated Temperature Applications', *CORROSION/2007*, paper no. 07376 (Houston, TX: NACE International, 2007).
120 D. Duke and L. Yang, 'Laboratory and Field Studies of Localized and General Corrosion Inhibiting Behaviors of Silica in Zero Liquid Discharge (High TDS Cooling Water) using Real Time Corrosion Monitoring Techniques', *CORROSION/2007*, paper no. 07626 (Houston, TX: NACE International, 2007).
121 G. Tormoen, J. Dante and N. Sridhar, 'Correlation of In-Situ VCI Adsorption Monitoring with Real-Time Corrosion Rate Measurements', *CORROSION/2007*, paper no. 07356 (Houston, TX: NACE International, 2007).

Part II

Other physical or chemical methods for corrosion monitoring

9

Gravimetric techniques

K. CHIANG and T. MINTZ, Southwest Research Institute, San Antonio, Texas, USA

9.1 Introduction

Measuring weight is one of the fundamental techniques of corrosion sciences. Measurements of mass changes (weight loss or weight gain) of test specimens using analytical balances with various capacities and sensitivities have been widely used to evaluate materials degradation as a function of exposure times or temperatures in corrosive environments. In this chapter, two gravimetric techniques for corrosion monitoring will be described: thermogravimetric analysis (TGA) and quartz crystal microbalance (QCM). This chapter will examine the operating principles of TGA and QCM, and will review types of corrosion that can be evaluated with the two techniques. Additionally, the various types of TGA and QCM measuring and monitoring systems that are currently available on the market and future trends for applying these techniques will be discussed throughout the text.

9.2 Thermogravimetric analysis (TGA) technique

The thermogravimetric analysis (TGA) technique requires continuous weighing of a sample in a specific environment, either as a function of temperature or at a constant temperature. This technique is widely used to study oxidation and high-temperature corrosion. Gulbransen and Andrew (1961) developed vacuum microbalance to study and analyze the reaction rates of metals and alloys in controlled atmospheres of O_2, N_2, H_2 and H_2O. Such analysis relies on a high degree of precision in four measurements: specimen weight, temperature, rate of temperature change and exposure time. An automatic recording microbalance (Cahn and Schultz, 1962) with precision of 0.1 micrograms ($\mu g = 10^{-6}$ grams) permits long duration runs at high temperatures and has been commercially available since the 1960s. A schematic diagram of an automatic recording microbalance is shown in Fig. 9.1. The specimen is freely suspended from a precision microbalance

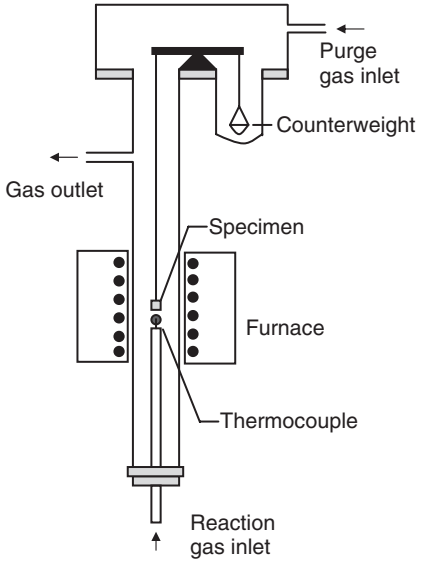

9.1 Schematic diagram of a thermogravimetric apparatus with automatic recording microbalance.

located outside the furnace chamber. The microbalance mechanism records weight change due to chemical reactions in a controlled environment, along with specimen temperature and elapsed time. The technique has been used to study the kinetics and mechanisms of engineering alloys in high temperature oxidation (Lai, 1990; Birks *et al.*, 2006). The technique was also used for laboratory study of high-temperature corrosion kinetics of nickel- and cobalt-based turbine alloys (Goebel and Pettit, 1970; Huang *et al.*, 1979; Chiang *et al.*, 1983, 1984; Cheruvu and Chiang, 2006). The effects of alloy composition, salt composition, gas composition, and temperature on the corrosion rates and mechanisms were reported.

9.2.1 Examples of microbalance applications

Multiple processes can lead to mass changes that would correspond to chemical reactions as a function of temperature. The types of processes that can be studied using microbalance systems include but are not limited to:

- Thermal stability and decomposition
- Surface adsorption/desorption
- Evaporation
- Oxidation rates of metals, alloys, polymers, ceramics, composites and coatings

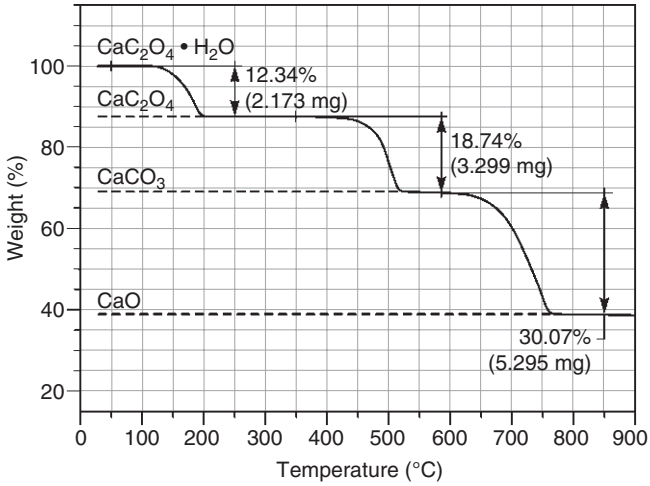

9.2 Thermogravimetric weight change curve as a function of temperature for calcium oxalate hydrate.

- Reaction rates in CO, CO_2, H_2O, N_2, H_2 and mixed gases
- Halogen corrosion
- Salt deposit corrosion.

Examples of microbalance applications are given next.

Thermal decomposition of calcium oxalate hydrate

Figure 9.2 shows the TGA weight change curve for calcium oxalate hydrate ($CaC_2O_4 \cdot H_2O$) compound when the sample is heated from 20 °C to 900 °C in a furnace with a heating rate of 10 °C/min. Each downward step in the weight change curve corresponds to a decomposition process for calcium oxalate hydrate compound. The three steps correspond to losing water (H_2O), carbon monoxide (CO) and carbon dioxide (CO_2). The specimen weight data were converted to percentage weight with respect to the original weight of calcium oxalate hydrate (Wendlandt, 1964).

Oxidation kinetics of nanostructured coatings

TGA technique was used to study the oxidation kinetics of a nanostructured Cu-Cr coating deposited on copper alloy substrate (Chiang *et al.*, 2007). The nanostructured coating was deposited using an ion-beam assisted deposition (IBAD) method (Chiang *et al.*, 2005). The oxidation rate of uncoated and IBAD single-layer Cu-Cr coated NARloy-Z (Cu-3

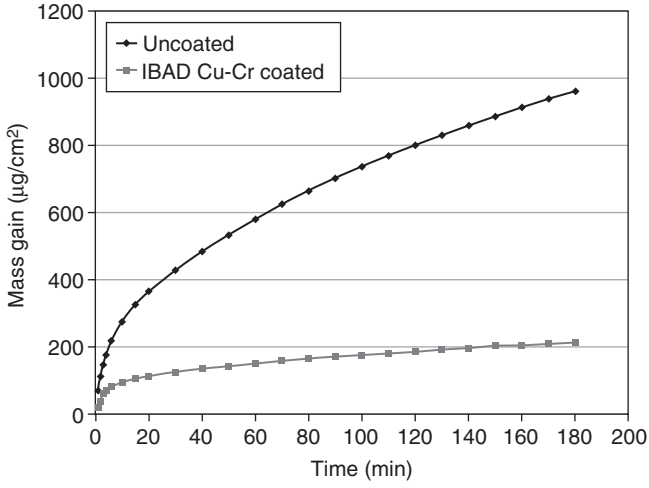

(a)

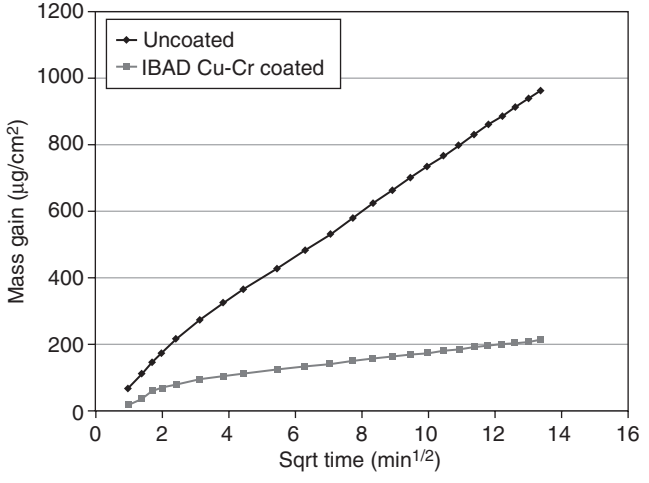

(b)

9.3 Oxidation kinetics of uncoated and IBAD Cu-Cr coated NARloy-Z (Cu-3 wt%Ag–0.5 wt%Zr) in air at 650 °C. (a) Mass gain versus time plot and (b) mass gain versus square root of time plot (Chiang *et al.*, 2007). (IBAD: ion-beam assisted deposition). © Southwest Research Institute 2007.

wt%Ag–0.5 wt%Zr) at 650 °C is shown in Figure 9.3(a) as mass gain as a function of exposure time. Both specimens exhibited high oxidation rates during an initial transient period of approximately 6 minutes, which was reduced to lower rates at longer times. Oxidation rate decreases markedly with the coating. The data are also plotted in Figure 9.3(b) as mass gain

versus square root of time. The data fall along a straight line, indicating that the oxidation kinetics after the initial transient period obeys parabolic rate law:

$$\Delta m/A = (K_p t)^{1/2} + C \quad [9.1]$$

where:

$\Delta m/A$ = mass change per unit area
K_p = parabolic rate constant
t = exposure time
C = a constant

The parabolic rate constant (square of the slope in Fig. 9.3b) for the uncoated NARloy-Z is $4.5 \times 10^3 \mu g^2 cm^{-4} min^{-1}$. In comparison, the IBAD Cu-Cr coated specimen has a parabolic rate constant of $1.3 \times 10^2 \mu g^2 cm^{-4} min^{-1}$, which is about 35 times smaller than the parabolic rate constant obtained for the uncoated specimen. The oxidation rate of NARloy-Z is controlled by outward diffusion of Cu ions to form external Cu oxide. In contrast, oxidation of the Cu-Cr coating surface is controlled by outward diffusion of chromium ions to form protective Cr_2O_3 scales.

Most commercial TGA systems are supplied with data acquisition and analysis software to display the test in progress on a monitor, store the data, and perform analyses of the data.

9.3 Quartz crystal microbalance (QCM) technique

The quartz crystal microbalance was initially used to measure mass changes during thin film deposition in a vacuum system and to study adsorption processes (Stockbridge, 1966; Eschbach and Kruidhof, 1966; Warner and Stockbridge, 1963). This technique can measure mass changes on the order of nanograms (10^{-9} grams) (Buttry and Ward, 1992) and with some new equipment may be able to measure picogram (10^{-12} grams) changes. Within the last 45 years, the QCM has become a highly useful instrument when *in situ* detection and monitoring of phenomena occurring on the surface of materials at the microscopic level is required (Lu and Czanderna, 1984).

9.3.1 Principle of QCM

The fundamental properties of quartz have been studied for over a century. QCM is based on the inverse piezoelectric effect, in which a shift in the resonance frequency of the quartz crystal is used for measuring shifts in mass of the crystal and any surface film. QCM consists of a thin plate of single-crystal quartz with electrodes affixed to each side of the plate. Synthetic quartz is composed of silicon and oxygen in the form of silicon

dioxide (SiO_2) and is normally made in autoclaves under high temperature and pressure. These quartz crystals exhibit piezoelectric properties, which means that they can generate an electric potential when pressure is applied to the crystal surfaces. If a current-measuring circuit is attached to the quartz crystal and compressive stresses are applied, current will begin to flow through the circuit in one direction. If tensile stresses are applied to the same quartz crystal, the current will flow in the reverse direction. Conversely, when an electric potential is applied to the surface of the crystal, mechanical deformation or vibrations are generated (Heising, 1946).

The main technology behind QCM is the piezoelectric properties of the quartz crystal sandwiched between two electrodes. In 1880, the Curie brothers discovered the piezoelectric effect on a quartz crystal (Heising, 1946). Their first test included placing a weight on the surface of a quartz crystal while measuring the electrical charge that appeared on the surface. It was discovered later that if an alternating current (AC) is applied to the electrodes, the quartz crystal will start to oscillate at its resonance frequency due to the piezoelectric properties. The resonance frequency of the crystal will be a function of its physical properties and environment. The theoretical resonance frequency for a bar can be determined by Equation [9.2] (Heising, 1946).

$$f_R = \frac{1}{2l}\sqrt{\frac{Y_o}{\rho}} \qquad [9.2]$$

where:

f_R = resonance frequency
l = length of the bar
Y_o = Young's modulus along the bar
ρ = density

Some factors affecting the frequency can be controlled, such as the density and viscosity of the phases adjacent to either side of the quartz crystal, the pressure differences across the crystal and the temperature. Other factors that affect the frequency that are not necessarily controllable are the mass of the attached electrode, an absorbed film or a thin deposited film (Deakin and Buttry, 1989).

The preparation of the quartz crystal will affect the crystal device's properties. The crystal's oscillation direction will depend upon the orientation of the crystal lattice. Quartz is typically a six-sided prism that ends in a six-sided pyramid, as seen in Fig. 9.4. Because of the quartz crystal structure, various types of crystal cuts can be made that will affect the piezoelectric properties of the crystal. One of the more important properties is the frequency stability: the amount that the frequency deviates from the ambient

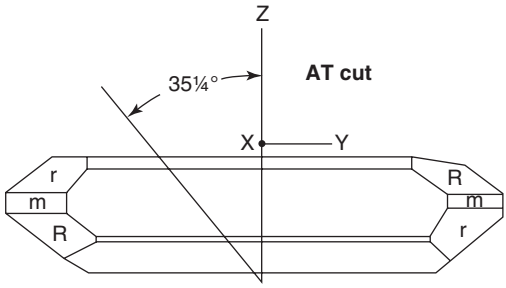

9.4 Quartz crystal AT cut. (Adapted from Heising, 1946.)

temperature frequency over the operating temperature range. As shown in Fig. 9.4, a quartz crystal that is cut so that the plate contains the X-axis and makes an angle of about 35 degrees with the optic or Z-axis is called an AT cut (Cady, 1964). Because of the frequency stability, this is one of the most common quartz crystal cuts, with fundamental resonance frequencies predominately in the range of 5–30 MHz (Lin *et al.*, 1993). An AT cut will lead to mechanical shear oscillations and displacements that are parallel to the wafer surface. Other types of cuts are available, but the AT cut is most often used for QCM. The frequency stability and the operating temperatures required by the type of testing will determine the necessary angle of the cut. Generally, the oscillations of quartz crystals are very stable due to the high quality of the oscillation (Q-factor). The ability to measure the resonant frequency for particular quartz crystals can be so accurate that it is possible to measure the adsorption of a monolayer of hydrogen in a vacuum system.

The QCM system utilizes the inverse piezoelectric effect to measure the changes in mass with time. The quartz crystal is coated by the material of interest, which is considered the working electrode. The material used for the working electrode will depend upon the type of test being performed. Any change in the mass that is rigidly attached to the working electrode will result in a change of the quartz crystal's resonance frequency. The mass change can be measured by comparing the frequency of the quartz/working electrode to the frequency of a standard reference quartz crystal and computing a differential frequency (Sauerbrey, 1959). The mass change is related to the differential frequency by the Sauerbrey equation, shown in Equation [9.3].

$$\Delta f = \frac{-2\Delta m f_o^2}{A\rho_q v_q} \qquad [9.3]$$

where:

Δf = change in oscillation frequency of a piezoelectric quartz crystal
Δm = change in mass of quartz crystal/working electrode system
f_o = resonant frequency of the crystal
A = active area of the crystal
ρ_q = density of quartz
v_q = shear wave velocity in the quartz

Sometimes the Sauerbrey equation is written as Equation [9.4].

$$\Delta f = -C_f \cdot \Delta m \qquad [9.4]$$

where:

$$C_f = \frac{2f_o^2}{A\rho_q v_q} = \text{sensitivity factor for the quartz crystal}$$

In this equation, the constant C_f (sensitivity factor) depends only upon the thickness of the quartz slab and on the intrinsic properties of the quartz. C_f will increase proportionally with the overtone number and depends upon the square of the fundamental frequency. For an AT-cut 10 MHz quartz crystal, C_f equals 0.444 $cm^2\,Hz\,ng^{-1}$ if changes of mass on each face of the quartz crystal are equal (Rodahl *et al.*, 1995).

Limitations to the Sauerbrey equation include high dissipation (i.e., damping) that affects the accuracy of the calculation when the mass that is added to the electrode surface (a) is not rigidly deposited, (b) slips on the surface, or (c) is not deposited evenly on the surface in the QCM system being evaluated. The damping effect can be measured and accounted for with more elaborate QCM testing equipment, which will be described in Section 9.3.3.

The Sauerbrey equation is also only useful for thin solid films, where the frequency shift is less than 1 percent of the initial quartz resonator frequency (Mecea *et al.*, 1996). To deal with this limitation, Miller and Bolef (1968) developed the composite acoustic resonator model to account for thicker films. Miller and Bolef developed an equation that maintains Sauerbrey-like results while treating the quartz resonator and deposited film as a composite resonator. Lu and Lewis (1972) further developed this technique for a more accurate equation.

An additional limitation to the Sauerbrey equation is that it assumes that a rigid mass is attached to the crystal in air and not in a liquid environment. When using the QCM system in a liquid, the viscosity of the liquid will decrease the amplitude of the oscillation and affect the resonance frequency (Martin and Hager, 1989). In the 1980s, both Kanazawa and Gordon (1985) and Nomura and Okuhara (1982) studied the use of QCM in a liquid environment to evaluate the effect of liquids on the QCM. Kanazawa and Gordon showed that an exponentially damped shear wave develops at

the surface of a QCM when it is submerged in a solution. The change in resonant frequency as a function of the liquid environment's viscosity can be calculated by Equation [9.5].

$$\Delta f = -f_o^{3/2}\left(\frac{\eta_l \rho_l}{\pi \rho_q \mu_q}\right)^{1/2} \qquad [9.5]$$

where:

η_l = viscosity of the liquid
ρ_l = density of the liquid
ρ_q = density of quartz
μ_q = shear modulus of quartz

Once it was found that the excess viscosity loading of a liquid did not affect the sensitivity of QCM to measurements in mass changes, QCM was utilized in direct contact with liquids and/or viscoelastic films. With this development, QCM could be used as a tool to measure corrosion processes in a range of aqueous environments.

9.3.2 Quartz crystal microbalance experiments and equipment

QCM was first used in 1959, when Sauerbrey published a paper showing that the change in frequency of a quartz crystal can be directly proportional to the change in mass. Since then, many different uses for this technology have been developed, some of which are described next.

Quartz crystal microbalance equipment

Many QCM systems are currently available on the market, with various features. A typical QCM system consists of a few components, as shown in Fig. 9.5. These include a controller, oscillator electronics, frequency counter, high precision digital voltmeter, crystal holder and quartz crystals with electrodes attached to each side. The controller is attached to the oscillator and the frequency counter. The controller sets the inputs for the experiment and outputs the measured frequency to the frequency counter. The oscillator is the electronic circuit that specifies the output signal and as such, controls the resonance frequency of the crystal. It receives input from the controller and then transmits the electric signal to the quartz crystal holder. The frequency counter measures the frequency from the output of the controller. The selection criteria for a frequency counter will include resolution speed, time-base stability, computer interfaces and software drivers. Careful selection is required; otherwise, the quality of the mass measurement may be degraded.

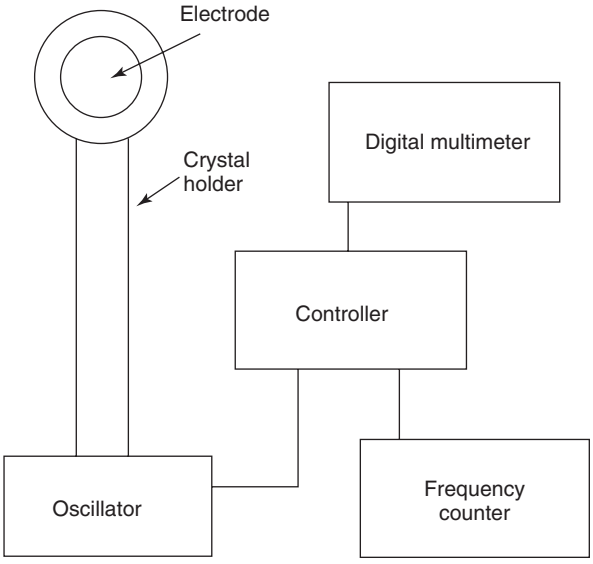

9.5 Schematic diagram of quartz crystal microbalance equipment.

Depending upon the experiments planned, a variety of quartz crystal coatings can be used to cover a wide range of physical and chemical properties, bonding properties and various interaction mechanisms. The most commonly used electrode for QCM is pure gold, which is chemically inert and can be chemically modified to allow users to optimize the test setup. For example, gold can be chemically modified to be hydrophobic rather than the customary hydrophilic surface. In addition to the gold sensor, there are silica-, stainless steel-, polystyrene- and titanium-coated surfaces that can be easily purchased. Silica surfaces are very hydrophilic and are mainly used to form lipid bilayers. Stainless steel surfaces have been used to examine biofilm formation. Polystyrene can be used to evaluate the interaction between polymers and various different biomolecules. Titanium-coated samples have been used for implant research. While these types of sensors can be purchased off-the-shelf, surface deposition techniques can also be used to develop specific sensors if there are none in stock that fit specific requirements.

In today's computer-based world, the newer systems have integrated some of the components shown in Figure 9.5 into a peripheral component interconnect (PCI) board/computer. The system is interfaced to a personal computer (PC) by means of a digital counter PCI board, which replaces the controller and frequency counter in the conventional setup. This type of system allows for simultaneous control of multiple quartz crystals. In

addition, very low noise electrogravimetric QCM systems have been developed that can measure picogram level changes in mass.

Quartz crystal microbalance applications

QCM experiments can be used to measure various types of phenomena. The working electrode is typically gold deposited onto the quartz crystal, unless specified as something other than gold. The working electrode is a thin film that is placed onto one side of the quartz crystal. The quartz crystal oscillates nominally in the shear mode due to the AT-cut crystal. Any change in the mass rigidly attached to the working electrode results in a change in the quartz crystal oscillation frequency, given by the Sauerbrey equation. Differential frequency measurements are recorded, which means the frequency of a reference quartz crystal is subtracted from the frequency of the working crystal.

There are multiple processes that can lead to mass changes which would correspond to an effective frequency change. The types of process that can be studied using QCM systems include, but are not limited to

- Corrosion and corrosion protection
- Surface oxidation
- Surfactant research
- Adsorption/desorption
- Metal/alloy plating
- Oxidation
- Etching
- Moisture accumulation.

9.3.3 Dissipation technique

As mentioned previously, the Sauerbrey equation is based upon having a rigid film form on the surface of the working electrode. However, not all processes such as adsorption or corrosion may lead to a rigid film being attached to the electrode surface. When certain layers on the surface of the working electrode have some degree of structural flexibility or viscoelasticity, another technique will be needed. An alternative method that has been developed for studying these types of surface properties using QCM is called the dissipation technique.

The viscoelasticity of a surface film can be measured by analyzing the energy loss, or dissipation, of the shear movement of the quartz crystal. One means to measure the dissipation is to drive the quartz crystal at its resonant frequency by an oscillator that is intermittently disconnected, causing the crystal oscillation amplitude to decay exponentially. The decay of the frequency is recorded which provides a method for measuring not

only the frequency but also the dissipative properties of the film. This data provides a wealth of knowledge on the film's viscoelastic properties. The dissipative properties can be measured by the dissipation factor (Rodahl *et al.*, 1995, 1997), which can be calculated using Equation [9.6].

$$D = \frac{E_{dissipated}}{2\pi E_{stored}} \qquad [9.6]$$

where:

D = dissipation factor
$E_{dissipated}$ = energy dissipated during one period of oscillation
E_{stored} = energy stored in the oscillating system

The total dissipation factor is the sum of all the losses due to damping in the system. Measurement of the dissipation factor can provide some quantitative analysis of the viscous nature of the film. For example, if an absorbed film is somewhat viscous, it will add to the total dissipation factor.

Dissipation monitoring equipment

There are no significant differences between the traditional QCM and equipment that allows for a dissipation study. The main difference is the addition of a relay which can pulse the quartz crystal A/C driver on and off.

9.3.4 Electrochemical quartz crystal microbalance

Because QCM was shown to be reliably operated in liquid environments, it was possible to develop a new technique called electrochemical quartz crystal microbalance (EQCM) (Deakin and Buttry, 1989). EQCM has been used for electrochemical studies including potentiostatic- and galvanostatic-controlled experiments. The typical configuration for these electrochemical studies is to place the quartz crystal between two O-rings. One side of the quartz crystal, including the deposited electrode, contacts the solution in the electrochemical cell. The electrode contacting the solution serves as both part of the QCM oscillator circuit and as the electrochemical working electrode. By combining the concepts from Sauerbrey's work with the frequency change due to a solution damping, the EQCM system can measure mass changes in solutions.

Electrochemical quartz crystal microbalance equipment

The EQCM is utilized to study electrochemical processes. The typical equipment is not much different from the standard QCM equipment. The main difference is that an electrochemical cell and some accessories are

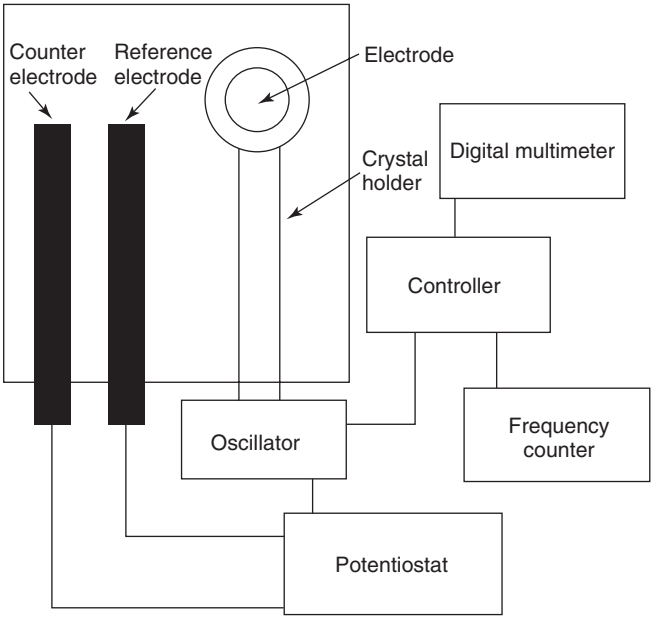

9.6 Schematic diagram of electrochemical quartz crystal microbalance equipment.

needed. A QCM crystal is mounted into a holder, which is connected to the chemical cell so that only one of the electrodes is exposed to the conductive solution. The holder is connected to a crystal oscillator, and the QCM crystal electrode exposed to the conductive solution is connected to the working electrode lead of a potentiostat. A standard reference electrode can be used in conjunction with a counter electrode (e.g., platinum mesh). A QCM controller provides independent frequency and conductance outputs. This data is collected and displayed by a frequency counter and digital multimeter, respectively. An example of the EQCM setup is shown in Fig. 9.6.

Applications

There are many potential applications for EQCM (Deakin and Buttry, 1989). One is to measure the mass changes in thin films on the electrode. Because of this measurement capability, it may be possible to use EQCM as a monitor in plating or stripping baths. In addition to its use as a monitor, EQCM may be used to measure mass changes associated with the reduction or oxidation reactions. The EQCM technique can also be used with dissipative techniques to quantitatively treat the influence of viscoelasticity. EQCM

has also been used to measure the formation of a monolayer on the electrode surface. One study by Quan *et al.* (2001) utilized QCM to examine the self-assembled monolayer of Schiff bases on copper surfaces in ethanol. AT-cut quartz crystal disks were precoated with a silver underlayer. Copper was then electroplated onto one side of the silver underlayer, and this side was used as the working electrode in the experiments. Once the copper was electroplated, it was initially rinsed with double distilled water, quickly rinsed with absolute ethanol, and immediately transferred to the QCM cell containing absolute ethanol. The adsorbate solutions were injected into the ethanol to start the process of forming the self-assembled monolayer. Two Schiff bases were used in this QCM study: N,N′-o-phenylen-bis-(3-methoxy-salicylindenimine) (V-o-Ph-V) and N-2-hydroxyphenyl-(3-mthoxy-salicylidenimine) (V-bso). Figure 9.7 shows the QCM results for the different self-assembled monolayers. As the Figure shows, after injection of either base, the frequency decreased very rapidly and reached a constant value within 15 and 30 minutes for V-o-Ph-V and V-bso, respectively. It was assumed that a monolayer of material had formed onto the surface once the frequency reached a steady state. A mass associated with the change in frequency can be calculated from the frequency results. QCM tests determined that the V-o-Ph-V formed a more densely packed film on the surface of copper than did the V-bso. This information along with additional corrosion data can be used to make conjectures about the inhibiting effect of the individual monolayer. This and other types of experiments are possible with the use of an EQCM system.

In addition, the EQCM system has been combined with other surface analysis techniques, such as x-ray photoelectron spectroscopy, infrared spectroscopy and electrochemical impedance spectroscopy to study the mechanisms of various corrosion reactions, including growth and dissolution of passive oxide films of alloys in corrosion environments (Olsson and Landolt, 2006).

9.4 Gravimetric techniques summary

Two gravimetric techniques are examined in this chapter: thermogravimetric analysis (TGA) and quartz crystal microbalance (QCM). The fundamental theories behind the techniques for corrosion monitoring are covered next, including some of the typical experiments that would be conducted and the equipment that would be used. Gulbransen and Andrew (1961) developed vacuum microbalance to study gas–metal reactions in a controlled environment at high temperatures. Automatic recording microbalance (Cahn and Schultz, 1962) with precision of 0.1 μg permits long duration runs at high temperatures and has been commercially available since the 1960s. The gravimetric method is widely used to study the kinetics of

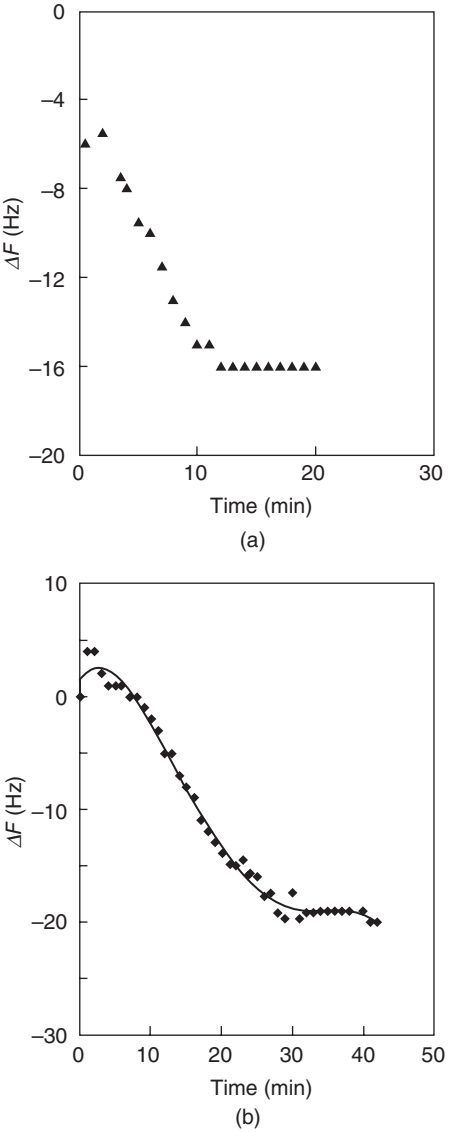

9.7 A plot of frequency change (ΔF) against time during the self-assembly of (a) V-o-Ph-V and (b) V-bso. The final concentration of the solution in both tests was 10^{-3} M with a total volume of 20 mL. Frequency change of 1 Hz corresponds to mass change of 18 ng/cm^2 (Quan *et al.*, 2001). © NACE International 2001.

oxidation and other forms of high-temperature corrosion, surface reaction, and protective coatings.

QCM is based on the inverse piezoelectric effect, where a shift in resonance frequency can be used to measure changes in mass. QCMs consist of a thin plate of single crystal quartz with electrodes affixed to each side of the plate. The crystal can be made to oscillate at its resonant frequency when an external potential is applied. The frequency of the quartz crystal will depend upon several factors, including physical properties of the quartz, properties of the environment, and changes in the mass attached to the electrode. The quartz crystal can be prepared in different ways, but the most common type of quartz used for QCM is an AT-cut quartz, which will produce a mechanical shear oscillation with displacements parallel to the wafer surface.

In 1959, Sauerbrey derived an equation (Equation [9.3]) that relates the change in resonance frequency to a change in mass. This equation was used to conduct early QCM experiments in vacuum and air. However, this equation assumed that the films on the QCM electrodes were thin, were rigidly deposited, did not slip on the surface, and were deposited evenly. The Sauerbrey equation does not account for any of these circumstances. Therefore, QCM was not initially used in a liquid environment due to the viscoelastic nature of the solution.

Kanazawa and Gordon (1985) evaluated the use of QCM in liquids, and in the mid-1980s, an equation was developed (Equation [9.5]) to account for the frequency change due to contact with a solution. These authors have conducted experiments that compared the variation in the QCM frequency to changes in solution density or viscoelasticity. Further experiments have been expanded to look at the electrochemical properties for different systems.

QCM experiments can examine many different types of phenomena. These include, but are not limited to, adsorption/desorption, oxidation, metal/alloy plating, corrosion, etching, corrosion protection, surfactant research and moisture accumulation. EQCM can be used to study the electrochemical properties of a system. One of the electrodes contacts the solution and is attached to a potentiostat as the electrochemical working electrode. EQCM can measure the formation of monolayers or mass changes in thin films. It can also measure mass changes in plating or stripping baths, or mass transport associated with redox reactions.

Finally, there is a dissipation technique that can be used to measure films that are not fully rigid and bonded to the electrode surface. A dissipative factor can be measured by intermittently disconnecting the driving potential to the QCM crystal holder. The crystal oscillation amplitude decay curve provides information about the dissipative properties of the film on the surface of the electrodes. QCM techniques offer a wide range of poten-

tial applications for conducting *in situ* experiments in various environments. Depending upon the properties that are being evaluated, different QCM techniques that have been developed over the last half-century may be applicable.

9.5 References

Birks, N., G.H. Meier and F.S. Pettit. *Introduction to the High-Temperature Oxidation of Metals* 2nd Edition. Cambridge University Press. New York. 2006.

Buttry, D.A. and M.D. Ward. 'Measurement of Interfacial Processes at Electrode Surfaces with the Electrochemical Quartz Crystal Microbalance.' *Chemical Reviews*. Vol. 92. pp. 1355–1379. 1992.

Cady, W.G. *Piezoelectricity*, Dover Publications. New York. 1964.

Cahn, L. and H.R. Schultz. 'The Cahn Gram Electrobalance', in *Vacuum Microbalance Techniques*. R.F. Walker. ed., Vol. 2. pp. 7–18. Plenum Press. New York. 1962.

Cheruvu, N.S. and K.T. Chiang, 'Isothermal and Cyclic Oxidation Behavior of Turbine Blade Alloys', Proceedings of Turbo Expo 2006: Power for Land, Sea and Air. Paper No. GT2006-90756. ASME. New York. 2006.

Chiang, K.T., F.S. Pettit and G.H. Meier. 'Low Temperature Hot Corrosion', *High Temperature Corrosion: NACE-6*. R.A. Rapp, ed. National Association of Corrosion Engineers. Houston, Texas. pp. 519–530. 1983.

Chiang, K.T., G.H. Meier and R.A. Perkins. 'The Effect of Deposits of CaO, $CaSO_4$, and MgO on the Oxidation of Several Cr_2O_3-Forming and Al_2O_3-Forming Alloys', *Journal of Materials for Energy Systems*, ASM. Vol. 6, No. 2. pp. 70–86. 1984.

Chiang, K.T., J.H. Arps and R. Wei. 'Oxidation Resistance of Multilayered Cu-Cr Coatings Produced by Ion-Beam Assisted Deposition', Proceedings of Coatings 2005 Symposium. N. Padture, L. Francis, J. Jampikian, and N. Dahotre, eds. pp. 7–10. Materials Science & Technology Conference. Pittsburgh, Pennsylvania. 2005.

Chiang, K.T., R. Wei and J.H. Arps. 'Development of Nanostructured Cu-Cr Coatings for Liquid Rocket Engine Applications', Proceedings of the 43rd AIAA/ASME/SAE/ASEE Joint Propulsion Conference, Paper No. 2007-5583. AIAA. Reston, Virginia. 2007.

Deakin, M.R. and D.A. Buttry. 'Electrochemical Applications of the Quartz Crystal Microbalance', *Analytical Chemistry*. Vol. 61. pp. 1147A–1154A. 1989.

Eschbach, H.L. and E.W. Kruidhof. 'A Direct Calibration Method for a Crystal Oscillator Film-Thickness Monitor', *Vacuum Microbalance Techniques*. K.H. Behrndt. ed. Vol. 5. pp. 207–216. Plenum Press. New York. 1966.

Goebel, J.A. and F.S. Pettit. 'Na_2SO_4-Induced Accelerated Oxidation (Hot Corrosion) of Nickel', *Metallurgical Transactions*. Vol. 1. pp. 1943–1954. 1970.

Gulbransen, E.A. and K.F. Andrew. 'An Enclosed Physical Chemistry Laboratory – The Vacuum Microbalance', *Vacuum Microbalance Techniques*. M.J. Katz, ed. Vol. 1. pp. 1–21. Plenum Press. New York. 1961.

Heising, R.A. *Quartz Crystals for Electrical Circuits*. D. Van Nostrand Company. New York. 1946.

Huang, T., E.A. Gulbransen and G.H. Meier. 'Hot Corrosion of Ni-Base Turbine Alloys in Atmospheres in Coal-Conversion Systems', *Journal of Metals*. Vol. 31(3). pp. 28–35. 1979.

Kanazawa, K.K. and J.G. Gordon. 'The Oscillation Frequency of a Quartz Resonator in Contact with Liquid', *Analytica Chimica Acta*. Vol. 175. pp. 99–105. 1985.

Lai, G.Y. *High Temperature Corrosion of Engineering Alloys*. ASM International. Materials Park, Ohio. 1990.

Lin, Z., C.M. Yip, I.S. Joseph and M.D. Ward. 'Operation of an Ultrasensitive 30-MHz Quartz Crystal Microbalance in Liquids', *Analytical Chemistry*. Vol. 65. pp. 1546–1551. 1993.

Lu, C. and A.W. Czanderna. *Applications of Piezoelectric Quartz Crystal Microbalances*. Elsevier. Amsterdam. 1984.

Lu, C.S. and O. Lewis. 'Investigation of Film-thickness Determination by Oscillating Quartz Resonators with Large Mass Load', *Journal of Applied Physics*. Vol. 43. pp. 4385–4390. 1972.

Martin, B.A. and H.E. Hager. 'Velocity Profile on Quartz Crystals Oscillating in Liquids', *Journal of Applied Physics*. Vol. 65. pp. 2630–2635. 1989.

Mecea, V.M., J.O. Carlsson and R.V. Bucur. 'Extensions of the Quartz-Crystal-Microbalance Technique', *Sensors and Actuators A*. Vol. 53. pp. 371–378. 1996.

Miller, J.G. and D.I. Bolef. 'Acoustic Wave Analysis of the Operation of Quartz-Crystal Film-Thickness Monitors', *Journal of Applied Physics*. Vol. 39. pp. 5815–5816. 1968.

Nomura, T. and M. Okuhara. 'Frequency Shifts of Piezoelectric Quartz Crystals Immersed in Organic Liquids', *Analytical Chimica Acta*. Vol. 142. pp. 281–284. 1982.

Olsson, C.-O.A. and D. Landolt. 'Electrochemical Quartz Crystal Microbalance', in P. Marcus and F. Mansfeld, eds. *Analytical Methods in Corrosion Science and Engineering*. CRC Press, Taylor and Francis Group. Boca Raton, Florida. pp. 733–751. 2006.

Quan, Z., X. Wu, S. Chen, S. Zhao and H. Ma. 'Self-Assembled Monolayers of Schiff Bases on Copper Surfaces', *Corrosion*. Vol. 57. pp. 195–201. 2001.

Rodahl, M., F. Höök, A. Krozer, P. Brzezinski and B. Kasemo. 'Quartz Crystal Microbalance Setup for Frequency and Q-factor Measurements in Gaseous and Liquid Environments', *Review of Scientific Instruments*. Vol. 66. pp. 3924–3930. 1995.

Rodahl, M., F. Höök, C. Fredriksson, C.A. Keller, A. Krozer, P. Brzezinski, M. Voinova and B. Kasemo. 'Simultaneous Frequency and Dissipation Factor QCM Measurements of Biomolecular Adsorption and Cell Adhesion', *Faraday Discussions*. Vol. 107. pp. 229–246. 1997.

Stockbridge, C.D. 'Effect of Gas Pressure on Quartz-Crystal Microbalances', *Vacuum Microbalance Techniques*. K.H. Behrndt, ed. Vol. 5. pp. 147–178. Plenum Press. New York. 1966.

Sauerbrey, G. 'Verwendung von Schwingquarzen zur Wägung dünner Schichten und zur Mikrowägung', *Zeitschrift für Physik*. Vol. 155. pp. 206–222. 1959.

Warner, A.W. and C.D. Stockbridge. 'Mass Measurement with Resonating Crystalline Quartz', *Vacuum Microbalance Techniques*. K.H. Behrndt, ed., Vol. 3. Plenum Press, New York. pp. 55–73. 1963.

Wendlandt, W.W. *Thermal Methods of Analysis*. John Wiley & Sons, Inc. New York. 1964.

10
Radioactive tracer methods

DOUGLAS C. EBERLE, Southwest Research Institute, San Antonio, Texas, USA

10.1 Principle and history

The radioactive tracer method was first conceived by George de Hevesy in the early 1900s. According to Van Houten (2002), De Hevesy was employed at Ernest Rutherford's lab in Manchester, England between 1910 and 1913. Rutherford was interested in studying the properties of a substance named radium-D. The problem was that the radium-D he had obtained was mixed with lead. Rutherford had been unable to separate it, so he challenged de Hevesy to the task. De Hevesy attempted the separation unsuccessfully for more than a year before he had the idea that if this substance was inseparable from lead, it might be used as a tracer to follow lead through chemical reactions by making radioactive measurements. This was the birth of the radioactive tracer method and it eventually led to de Hevesy winning the Nobel Prize for his work on the use of isotopes as tracers in the study of chemical processes in 1943. As a side note, it was eventually discovered that radium-D was actually an isotope of lead, namely ^{210}Pb.

Since de Hevesy's initial conception, radioactive tracer methods (sometimes known as radiotracers) have been used by industry to measure a wide variety of corrosion, erosion and wear mechanisms. The technique offers several advantages over conventional techniques. First of all, it is highly sensitive. Radioactive material can often be detected at quantities much lower than can be detected through other means such as chemical analysis or gravimetric or dimensional means. Material loss rates in the order of micrograms per minute (μg/min) or nanometers per minute (nm/min) can be measured with time resolutions in the order of several minutes. Under certain circumstances, the technique can make measurements in near real time without having to periodically take apart an assembly. This is a significant advantage when the component is difficult to get to and disassembly means having process downtime. It also means that measurements can be made under changing conditions. This allows for cause and effect analysis, such as the effect of temperature on corrosion rate. Lastly, the technique

can quantify material losses from discrete areas or surfaces of interest. This allows for tracing of corrosion, erosion or wear rates from a discrete component within an assembly, such as wear from piston rings in an engine, without the confounding effect of other sources of wear material from the engine.

The basic principle of operation is that a surface or volume of material to be tested is first labeled with a radioactive isotope or isotopes. Ehmann (1991, p. 8) defines isotopes as 'forms of an element with the same number of protons, but different masses due to different numbers of neutrons in their nuclei'. Isotopes are often an unstable form of the element and these unstable forms decay by various means at a known rate. As isotopes decay, they often emit emanations such as gamma rays, alpha particles or beta particles. These emanations are known as radioactivity and can be measured with different types of detectors.

Once a material has been radio-labeled, it is exposed to an environment (either a wearing or corroding condition, usually in a fluid) for a period of time. As the part wears or corrodes, labeled radioactive material is removed at the same rate as the unactivated parent material. Quantification can be made of this surface loss through either measuring the increase in radioactivity of the fluid, or by measuring the decrease in radioactivity from the activated surface, after accounting for natural radioactive decay.

To give an illustration of this technique, Treuhaft and Eberle (2007) describe a method often employed to measure real-time wear from components within internal combustion engines. In this case, the components of interest (piston rings, rod bearings, etc.) are made radioactive by exposing the parts to a thermal neutron flux (bulk or neutron activation) near the core of a nuclear reactor. The high energy neutrons penetrate the nucleus of a small number of atoms within the test component. For each interaction, there exists a probability that the free neutron will be captured. This results in an increase in the mass of the nucleus, transmuting the atom into a heavier isotope, which is often radioactive. The now radioactive component of interest is then installed in the engine. The engine is configured with a special sump oil loop for interrogation with a gamma spectroscopy system, see Fig. 10.1. As the engine is operated and the component wears, wear particles are abraded from the parent part and are transported into the lubricating oil. Since the wear debris consists of very small particles, the debris is readily suspended and distributed throughout the oil system. Oil is drawn from the sump and circulated past a gamma ray detector, which measures the buildup of radiation from the wear particles. The activity of the wear particles is mathematically proportional to the concentration of radioactive wear particles present, after making corrections for natural radioactive decay.

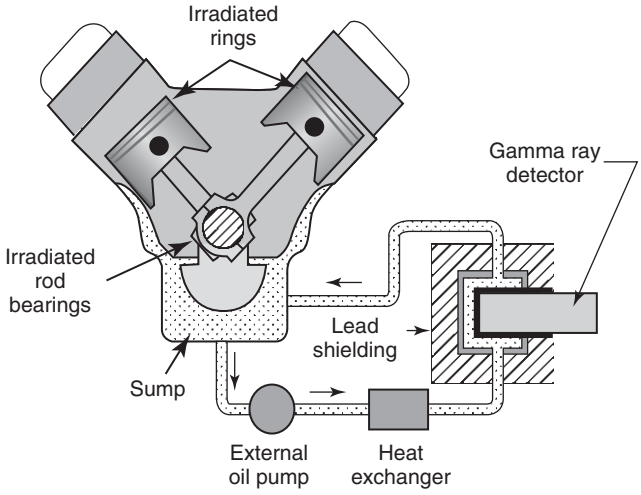

10.1 Wear measurement flow loop schematic, courtesy Southwest Research Institute.

10.2 Assumptions

The most important assumption that must be made is that the process of labeling a material with a radiotracer does not alter its mechanical or chemical properties. This is almost always valid for radiotracer studies. The amount of radioactively transmuted material is typically in the order of 1 ppm to 1 ppb and thus the gross material properties are not affected. The amount of radiation produced is also typically at a low enough level that the radioactivity itself does not significantly affect the system. In most cases, the process of activation produces isotopes that are chemically the same as the parent isotopes. These isotopes contain the same number of protons as the parent, with only an additional neutron. The electron structure is not affected. There is a slight difference in the mass of the nucleus caused by the additional neutron, which may have a minor effect on diffusion type studies of lighter elements. According to Ehmann and Vance (1991 p. 314), for heavy isotopes (such as ^{51}Cr or ^{59}Fe), the mass differences are minor and the isotopes behave so similarly in chemical and physical processes that they are very difficult to separate by chemical means. Some types of activations produce isotopes that contain an additional proton. While these isotopes are chemically different from the parent, they reside within the same grain structure as the parent isotope in the metallurgy. In wear and corrosion studies, the assumption is made that as the grain corrodes, the labeled atom becomes carried away with neighboring atoms.

Although not explicitly necessary for qualitative evaluations, quantitative evaluations require a few additional assumptions. When monitoring the

buildup of radioactivity in a fluid, it must be assumed that the entrained radioactive material is evenly distributed and is not removed from the fluid by means of other processes. In many cases this is a good assumption; however this must be considered as a source of potential error when designing an experiment, as it can have a significant effect on measurements. Examples of processes which can remove radioactive material from fluids include filtration, particle settling and plating of the radioactive materials onto other contacting surfaces.

When monitoring an activated surface for loss of activity through direct measurement, it must be assumed that all of the material that has been removed from the surface has been carried away from the immediate area such that it does not significantly affect the measurement. If material has re-plated on the surface, or has settled through another means near the detector, it can significantly skew the results.

10.3 Labeling methods

10.3.1 Bulk or thermal neutron activation

Thermal neutron activation is sometimes referred to as bulk activation. This technique (as well as thin layer activation, described below) creates radioactive isotopes from naturally abundant isotopes within the parent material. The component to be activated is placed in a neutron flux near the core of a nuclear reactor, where it is bombarded with thermal neutrons. There is a small probability (referred to as a cross-section) that a free neutron will directly interact with and be absorbed by a nucleus within the component. This causes a nuclear reaction to take place, sometimes resulting in the formation of a radioisotope. Since neutrons are uncharged particles, they can penetrate relatively large distances through matter without interaction. Thus, this method allows the creation of radioisotopes that are homogeneously distributed throughout the part.

There are several limitations to this technique. The physical size of components is limited by the space available near the core of the nuclear reactor. Typically research reactors are used that are available at certain governmental and university campuses around the world. Depending upon the design of the vessels used for activation, the size of components that can be activated is often limited to 15 to 20 cm in diameter. Some reactor setups have much smaller limitations.

Since the entire mass of the component is activated, the total induced radioactivity in the part is higher than in other methods. This higher activity often requires special licensing for increased radiation levels and additional safety precautions and facilities. In addition, to be able to obtain high sensitivity, measurement of corrosion or wear rates is accomplished by moni-

toring the buildup of radioactive material in the transport fluid. Monitoring for the loss of activity from the surface directly is typically not possible as the change in activity is generally too small to detect. In most cases, this requires a recirculating flow system in order to allow the cumulative radioactive corrosion product to build up to detectable levels. Certain processes do not lend themselves to recirculating systems. Sensitivity is also dependent upon the total volume of the recirculating fluid. If the system volume is too large, the radioactive material will be too dilute to detect.

Despite these limitations, there are a lot of good reasons to take advantage of the technique. For small components, the cost of irradiation is often much lower than other methods for the same specific activity. Multiple components can be activated at the same time for a lower cost and activating to a higher specific activity level increases the sensitivity of the experiment. Bulk activation can produce different isotopes from parent materials than other methods. This increases the choices of available radio-tracers. In some cases, bulk activation is the only way to produce useful isotopes from certain metallurgies. Since the available choice of isotopes is increased, bulk activation is sometimes combined with other techniques to produce multiple isotopes within an assembly from the same parent metallurgy. This is useful to be able to trace processes from multiple discrete components simultaneously. In the case of internal combustion engines, it has been used to measure piston ring wear and wear from localized areas of the engine bores in the same measurement.

10.3.2 Thin or surface layer activation

Thin layer activation (TLA) is sometimes referred to as surface layer activation (SLA) or as charged particle activation. Laguzzi *et al.* (2004) give a good description of this technique. To summarize, in TLA, a thin layer of material at the surface of a component is activated using a beam of charged particles (ions) from either a linear accelerator or a cyclotron. Typical ions used for activation include protons and deuterons although sometimes heavier ions such as ^{3}He are used. As in neutron activation, there is a small probability (cross-section) that a charged particle will directly interact with a parent nucleus, causing a nuclear reaction that can result in a radioactive isotope. Charged particles do not penetrate through matter without interaction as easily as neutrons. This characteristic limits the depth of activation to a very shallow layer on the surface of the component. Typically activation depths range from 50 to 150 microns and can be tailored by adjusting the energy of the particle beam or the angle of incidence.

One of the drawbacks of the technique is that activation is much more complicated. The charged particle beam is typically narrower than the area to be activated. This requires that either the beam be rastered or

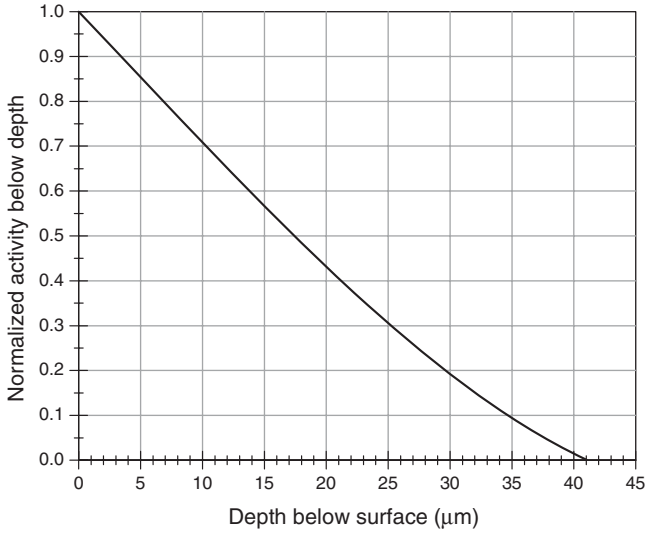

10.2 TLA activity to depth profile, courtesy Southwest Research Institute.

the part itself be accurately moved through either mechanical or electromechanical means. In order to readily quantify the loss of material, the material near the surface must be homogeneously and uniformly activated, without a surface dead-band. If a surface dead-band exists, the part will lose material initially without showing any loss of activity. This characteristic can be taken advantage of in certain applications as an indication that, for instance, a surface coating has been compromised. If the surface is not homogeneously or uniformly activated, the specific activity of the material changes with depth or position. Quantifying the loss of material requires that the specific activity be constant or significant errors can result.

In an activity to depth profile, a linear curve represents a homogeneous activation as shown in Fig. 10.2. While no profile is perfectly linear, an experienced activation facility should know how to generate a nearly linear profile with errors of less than a few percent over most of the useful depth. This curve can be generated by either empirical modeling or physical measurement as described in section 10.5.

10.4 Potential isotopes

Table 10.1 contains a sampling of available isotopes, related production methods, half-lives and gamma ray energies. For SLA production methods, the beam type is listed as p for proton or d for deuteron.

Table 10.1 A sampling of available isotopes, related production methods, half-lives and gamma ray energies. For SLA production methods, the beam type is listed as p for proton or d for deuteron

Parent element	Nuclide made	Production method	$t_{1/2}$ (days)	Gammas (keV)
Fe	^{59}Fe	Bulk	44.5	1099, 1291
Fe	^{56}Co	SLA, p	77.2	846
Fe	^{57}Co	SLA, d	272	122
Cr	^{51}Cr	Bulk	27.7	320
Cr	^{52}Mn	SLA, p	5.6	744, 935, 1434
Cr	^{54}Mn	SLA, p	312	835
Sn	^{113}Sn	Bulk	115	255
Sn	^{124}Sb	SLA, p	60.2	603, 1691
Ni	^{58}Co	Bulk	70.8	811
Zn	^{65}Zn	Bulk	244	1115
In	^{114m}In	Bulk	49.5	190
Cu	^{65}Zn	SLA, p	244	1115
Co	^{60}Co	Bulk	1925	1173, 1332
Sb	^{124}Sb	Bulk	60.2	602.7, 1691

10.5 Calibration and conversion to corrosion units

In order to quantify radiotracer measurements into physical units of either mass or thickness, a calibration must be accomplished. The method used for determining the calibration factor is dependent upon the method used to activate the sample. For bulk activated materials, since the activity is homogeneously distributed through the material, calibration to correlate measured activity to mass is relatively straightforward. Samples of the test material are activated simultaneously with the test article to ensure that the calibration samples have the same specific activity as the labeled part of interest. These calibration samples are accurately weighed, then dissolved into an acidic solution to form a base calibration solution. This base solution is then diluted through several orders of magnitude into a series of known concentrations. The detector is then sequentially exposed to this series of calibration solutions in the same or identical vessel as to be used during the experiment. Counts are accumulated for each sample and corrected for time decay to a fixed but arbitrary reference time, usually chosen as the time of activation. This series of counts is plotted as a function of concentration. If performed properly, a linear curve is developed relating measured counts for each isotope to solution concentration. A non-linear curve is an indication that the radioactive isotope has partially come out of solution as either a precipitate or as plating on the solution container walls. A sample calibration curve is shown in Fig. 10.3.

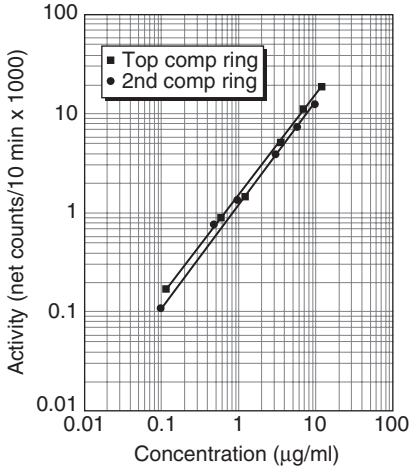

10.3 Bulk activation calibration curve, courtesy Southwest Research Institute.

Surface layer activation calibrations require a less direct approach, since the surface layer cannot easily be separated from the unactivated material below and the homogeneity of the activation must be checked. Several options are possible. If thin foils of known thickness made from the same or very similar parent material are available, the foils can be stacked and activated with the same accelerator setup as used for the primary activation. Care must be used to ensure that the accelerator parameters are held constant to produce the same activation profile in the foil stack as in the primary target. Following activation, the foil stack is exposed to the detector. Successive measurements are made in which one layer of foil at a time is stripped away. By performing time decay correction and plotting this series of measurements, a curve representing activity to depth is developed.

If adequate foils are not available, an ablation technique can be used. In the ablation technique, a calibration coupon made from a similar alloy material is activated using the same parameters as during the primary component activation. A calibration profile is developed by measuring the activity of the coupon between sequential abrasive ablation steps which remove a measured amount of material. The method is more prone to error than the foil technique as it is difficult to evenly remove material by abrasion and to accurately quantitate the material removed.

Finally if similar material activations have been previously accomplished and are well known, an empirically calculated activity profile can be used. While most commonly employed, this method is the least preferred as there is no confirmation of the actual depth profile.

10.6 Applications and limitations

10.6.1 Example application

Real-time crude oil corrosivity measurement

The corrosivity of crude oils has been a long term area of interest for refineries and crude oil buyers and sellers. Crude oils with higher total acid numbers (TAN) are becoming more prevalent on the market. Due to the perceived higher corrosivity of these high TAN crude oils, the crude oils are often sold at a discount. Though TAN has historically been used as an indicator of higher corrosivity, the correlation between TAN and corrosivity is poor. Crude oil corrosivity is a difficult parameter to measure under high temperature conditions, since the corrosive agents (typically a combination of naphthenic acids and sulfur compounds) can undergo thermal degradation. Traditionally, crude oil corrosion is measured by coupon weight loss techniques that range from 48 to 96 hours, or longer, exposure under various conditions. Weight loss has several confounding issues in that the oil properties can change in this time period and passivating or other types of films can build up on the surface of the coupon, potentially leading to coupon weight gain if not properly removed.

In order to obtain better sensitivity than loss-in-weight techniques, and to make the measurement prior to thermal degradation and without confounding film buildup, two techniques have recently been developed by Eberle *et al.* (2005) using radiotracers to measure crude oil corrosivity at elevated temperatures. One technique uses a heated, stirred autoclave, while the second uses a high shear stress flow loop arrangement. The flow loop technique allows for real-time measurement of corrosion with ten-minute resolution. In both techniques, 1018 carbon steel coupons were radio-labeled for demonstration studies with ^{59}Fe by bulk activation.

The first technique involves exposure of the activated coupon to heated oil in a stirred autoclave. A radio-labeled disk-shaped coupon is mounted between low conductivity ceramic spacers onto the autoclave's stirring rod to prevent galvanic corrosion. Test oil is added and the autoclave is sealed and pressurized with nitrogen gas to minimize oil phase change. The coupon is rotated while the oil is heated to the test temperature. The autoclave is held at this temperature for a period of 30 minutes and then is allowed to cool. Following disassembly, the coupon is removed from the test oil. The test oil is measured with a gamma spectrometer for the accumulation of radioactive soluble corrosion products. The test coupon is next tumbled in abrasive media to remove any adhered products on the coupon surface. The abrasive media is measured with a gamma spectrometer to measure the products which were removed during the tumbling process. In both cases,

measurements are first converted to mass units by applying appropriate time decay and calibration factors. Mass units can be converted to average thickness loss over the exposed coupon surface area. A chart showing soluble, adhered and total corrosion product loss resulting from testing is shown in Fig. 10.4.

In the flow loop technique, a rod-shaped coupon is installed in a special test fixture designed to create a constant shear stress along the coupon surface when oil flows through. As in the autoclave technique, the coupon is mounted between low conductivity ceramic isolators to prevent galvanic corrosion. The fixture is installed in a heated recirculating flow loop containing the test oil. An image of the flow loop is shown in Fig. 10.5. The flow loop is pressurized with nitrogen gas to minimize oil phase change. Shear stress is measured as pressure drop over the length of the coupon. Typically oil flow rate is adjusted during testing to maintain a constant shear stress as the oil is heated. As the coupon corrodes, corrosion products are entrained in the oil stream and carried past a calibrated gamma spectrometer. The spectrometer accumulates detected counts over a fixed time period. At the end of each period the accumulated counts are saved, the spectrometer is zeroed and the counts restarted. The counts for each period are time-decay-corrected and converted using calibration factors to accumulated corrosion product in the oil. Figure 10.6 shows a sample corrosion curve for a mineral oil spiked to a TAN of 3.0 mg KOH. In this curve, corrosion rate increases

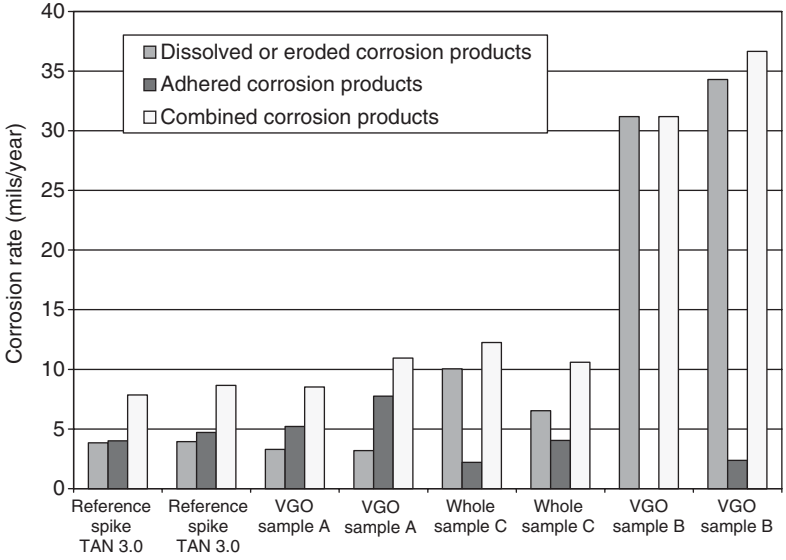

10.4 Grouped repeats of autoclave corrosivity tests, courtesy Southwest Research Institute.

10.5 Real-time corrosivity measurement flow loop, courtesy Southwest Research Institute.

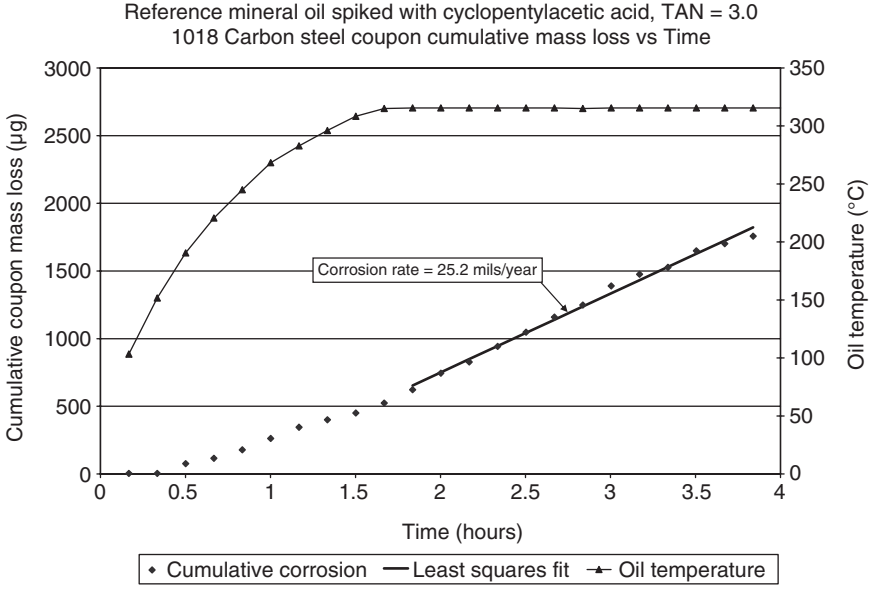

10.6 Sample flow loop test cumulative corrosion as a function of time and temperature, courtesy Southwest Research Institute.

as temperature increases and stabilizes once the system reaches a steady-state temperature.

10.6.2 Discussion of limitations

Although radiotracer corrosion measurement techniques have many significant advantages over other techniques, there are limitations as well. First of all the technique involves the use of radioactive materials. Although the relative activities are low and can be handled safely with appropriate precautions, radioactive materials are regulated materials. Laws vary in almost every country. In most cases, specific licenses to handle radioactive materials are required. Licenses can be costly both to obtain and to maintain.

Another significant limitation to the technique is that in order to make the measurement, the corrosion products must be physically separated from the originating surface. In many cases this is accomplished by transporting the corrosion products from the surface in the corroding fluid. In other cases the surface can be cleaned either mechanically or chemically to remove the products.

Measurement equipment costs are relatively high for this technique. Depending upon the instrumentation used, detector costs can range from several thousand to tens of thousands of US dollars.

10.7 Sources of further information

For information on radiation measurement equipment, refer to Knoll, G 2000, *Radiation Detection and Measurement, Third Edition*, Wiley, New York.

10.8 References

Eberle, DC, Wall, CM, Treuhaft, MB 2005, 'Applications of radioactive tracer technology in the real-time measurement of wear and corrosion', *Wear*, vol. 259, pp. 1462–1471.

Ehmann, WD, Vance, DE 1991, *Radiochemistry and nuclear methods of analysis*, Wiley, New York.

Laguzzi, G, Luvidi, L, De Cristofaro, N, Stroosnijder, MF 2004, 'Corrosion monitoring of different steels by thin layer activation', *Journal of Radioanalytical and Nuclear Chemistry*, vol. 262, no. 2, pp. 325–330.

Treuhaft, MB, Eberle, DC 2007 'The use of radioactive tracer technology to measure real-time wear in engines and other mechanical systems', SAE paper no. 2007-01-1437.

Van Houten, J 2002, 'A century of chemical dynamics traced through the Nobel Prizes, 1943: George de Hevesy', *Journal of Chemical Education*, vol. 79, no. 3, pp. 301–303.

11

Electrical resistance techniques

C. S. BROSSIA, CC Technologies,
Dublin, Ohio, USA

11.1 Introduction and background

Corrosion monitoring probes based on detecting and measuring changes in electrical resistance have been in use since the 1950s (Dravnieks and Cataldi, 1954; Freedman *et al.*, 1957). These electrical resistance (ER) probes, sometimes referred to as electronic coupons (Brown, 1996), monitor the electrical resistance of a sensing element that is exposed to the environment of interest. As the sensing element experiences corrosion, its cross-sectional area will decrease and the measured resistance will increase. ER probes are utilized in a wide range of application and industries including oil and gas production, pipeline, chemical process, pulp and paper, power generation and archeological preservation to name a few.

ER probes are often selected because of their relatively simple operations, relatively low maintenance, ease of data interpretation, real-time data collection and reliability. Because the probes essentially are exposed to the environment, they are relatively passive in nature and are no more difficult to install or utilize than traditional weight loss coupons. Thus, the main issues in utilizing ER probes include ensuring that the probe element is exposed to the environmental conditions of interest (e.g., the same chemistry, temperature, flow regime, etc. as the structure being monitored), safety considerations associated with ensuring that penetrations into a high pressure system are done correctly, and provisions are made for eventual retrieval for maintenance and replacement. Thus, ER probes are commercially available for service operations up to and exceeding pressures of 100 bar and temperatures of 500 °C. Higher pressure and temperature probes are often also available for specialized cases and can be custom produced without significant difficulties.

Maintenance of the probes usually arises due to deposit build up and precipitation. In cases where scaling formation is of interest, the probe can still be used with caution since some scale deposits can be electronic-conducting *(note, ionic conducting generally does not affect the measurements)*

and others are not. Thus, with conducting scales the overall resistance will tend to decrease with the time of exposure. Should corrosion occur simultaneously with scale formation, interpretation of the results may be difficult.

Data interpretation and decision-making are generally fairly easy. As the resistance increases, the loss of metal can be directly determined which will be discussed below. Because the effect of actual metal loss is measured, this can then be translated to a corrosion rate and provides a reliable indication of possible metal loss experienced by system components. It has been reported that the nominal minimum thickness loss that can be detected by ER probes is on the order of 1 μm (Clarke, 1991); however this is strongly dependent on the probe design. Though an indication of metal loss is obtained from ER probes, they do not measure the direct metal loss experienced by system components.

Unlike corrosion coupons, ER probes can be used to provide real-time corrosion rate information (see Fig. 11.1). For corrosion coupons, the corrosion rate is generally determined after a prescribed exposure period has been reached and the weight change of the specimens is then determined. The assumption in using these coupons is that the corrosion rate throughout the exposure period is relatively uniform. As a result, any process system upsets that dramatically increase the corrosion rate will be difficult to detect and tend to be minimized using coupons. In the case of ER probes, the corrosion rate can be determined either through periodic or continuous resistance change measurements. In the case of periodic measurements, the periodicity can be much more frequent than that employed with corrosion coupons. For example, typical coupon exposures might call for weight loss measurements after a period of several weeks or months whereas the ER probe can be interrogated as often as desired. Thus, the corrosion rate can be determined daily or more frequently. When monitored continuously, both the instantaneous effects of corrosion and the integrated time effects of corrosion can be determined. For example, a linear polarization resis-

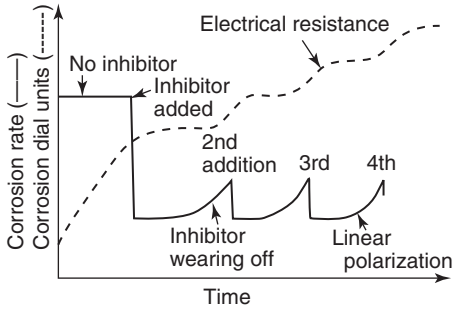

11.1 Illustration and comparison of ER probe data and linear polarization data as a function of time.

tance probe can provide a measure of the instantaneous corrosion rate but cannot provide the cumulative effects of corrosion. In the case of the ER probe, the cumulative effect of corrosion is always known and the instantaneous effects of corrosion, like the effects of a process upset, can be determined by comparing subsequent or a sequence of measurements over a short period of time. That is, if the resistance is noted to increase dramatically over a short period of time and then continues to increase at a slower rate consistent with the pre-event rate, then an upset or some other event can be concluded to have occurred.

Because of their relative simplicity, ER probes are generally quite reliable and cost effective. Issues and concerns that need to be considered include probe replacement due to corrosion and the resultant effect on useful life, the effects of non-uniform corrosion on rate measurements, and installation and manufacturing defects. Because the probe element corrodes away during exposure, eventually the probe will corrode to the point that unreliable measurements are obtained. These errors typically arise due to non-uniformity in corrosion of the sensing element after approximately half of the original thickness (one quarter of the diameter for wire elements) has been consumed (Davies, 1986). Non-uniform corrosion, such as pitting, crevice corrosion, and stress corrosion cracking can lead to errors in measurement. These errors can be both in the form of underestimation and overestimation of the true corrosion rate, thus visual inspection of the probe element on replacement is required. Installation and manufacturing defects can also be a source of errors and thus spurious readings should not always be associated with process system changes.

11.2 Sensing probe designs

In its basic form, an electrical resistance (ER) probes consists of a metal sensing element whose resistance is measured while the element is exposed to the environment of interest. As corrosion takes place and metal loss occurs, the cross-sectional area of the sensing element, shown generically in Fig. 11.2, will decrease and the electrical resistance will increase via Equation [11.1]:

$$R = \frac{\rho l}{A} \qquad [11.1]$$

Where ρ is the resistivity of the metal (element), l is the length of the element, and A is the cross-sectional area. Utilizing Ohm's law, the resistance can thus be measured by determining the potential (voltage) drop across the sensing element when a small current is applied. The resistance of the sensing element is then compared to the resistance of a separate element that is not exposed to the environment. Changes in the ratio of the two resistances as a function of time (the slope of the resistance ratios with

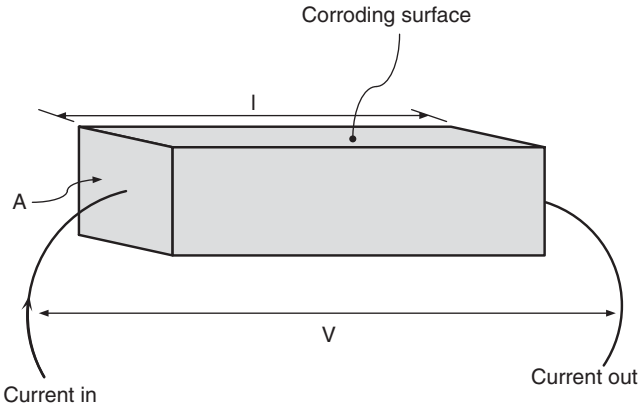

11.2 Schematic diagram of ER probe sensing element.

time) then yield the corrosion rate. Because resistivity is also a function of temperature, compensation for temperature effects separate from the effect of temperature on corrosion rate needs to be considered. To accomplish this, the reference element is allowed to reach the same temperature as the sensing element, thus any changes in the inherent resistivity due to temperature will be subtracted out.

Sensing probes come in a wide range of forms including wires and loops, tubulars and thin film/sheets and strips. Examples of some of these probe designs are shown in Fig. 11.3. The choice of probe element design is often driven by the application and conditions being monitored. For example, thinner elements such as thin films/sheets and small diameter wires can provide very high sensitivity and improved response times for detecting corrosion. However, these elements also will be perforated and will experience significant metal loss as a fraction of the total original much sooner than other forms. Thus, their life expectancy in service will be shorter than thicker forms. The relationship between ER probe response time, probe life and the expected corrosion rate is illustrated in Fig. 11.4. Because the temperature of the environment will change the resistance of the element and thus introduce an error in the corrosion rate measurement, a thicker probe, especially the tubular form, tends to counteract this and improves temperature compensation. By improving temperature compensation, the response time to corrosion rate changes also improves.

It is important also to note that probes can be designed to be inserted into the process stream as well as to be flush mounted. The use of flush mounted probes is important when the fluid dynamic properties play a significant role in performance. This could arise in multiphase systems such as mixed product pipelines where liquid petroleum, liquid water and various gases are present. Under stratified flow conditions, the water phase will settle to the bottom of the pipeline and thus corrosion monitoring for

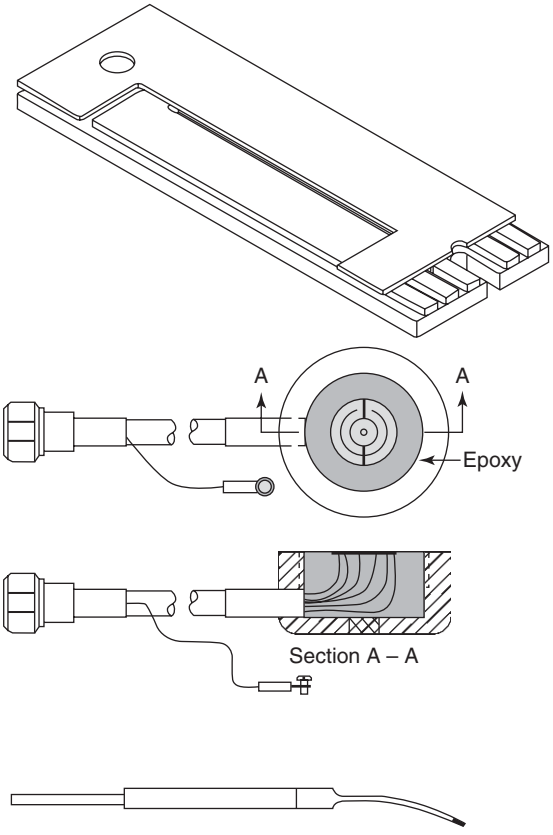

11.3 Examples of different commercially available ER probes.

inhibitor effectiveness at these locations is critically important. If the ER probe is located in the middle of the stream, it will predominantly see the oil phase which may be of lesser interest. Similarly, if entrained solids lead to erosion-corrosion, placement of the ER probe at locations within the system where erosion is most likely (e.g., bends, elbows) would be in order. Thus, not only the design of the probe element itself but how it is inserted and located within the system is important.

11.3 Examples of application and use

For the most part, all of these probe designs discussed previously are suitable for immersion service in any form of electrolyte including aqueous, non-aqueous (e.g., organic solvents, alcohols), concrete and soils. For some cases, such as atmospheric corrosion, the use of the thin film probe is preferred due to increased sensitivity. Examples of the use and application of ER probes for corrosion monitoring are described below.

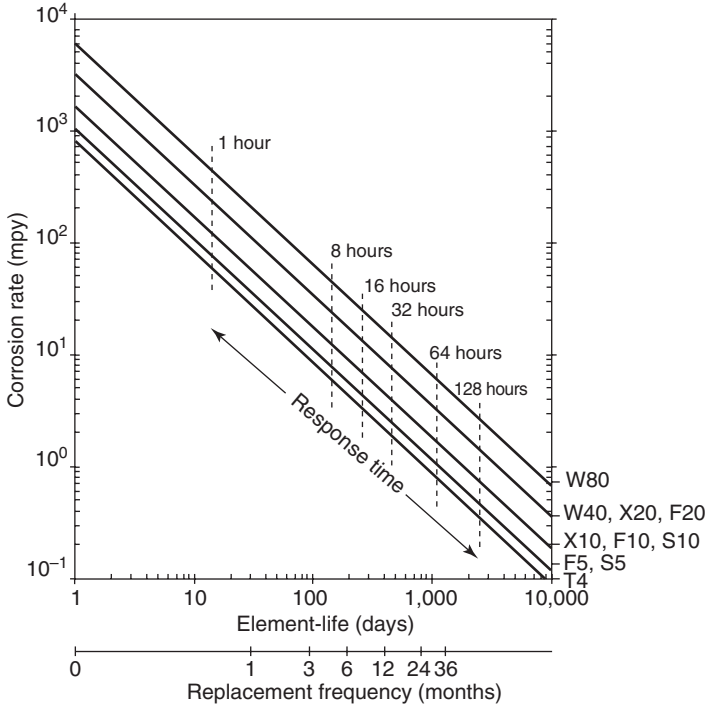

11.4 Expected life and response times for ER probes as a function of corrosion rate.

11.3.1 Chemical process and oil and gas industries

Bergstrom (1981) described results using an ER probe to monitor the corrosion rate in an acidified organic solvent process stream where attempts were made to neutralize the acid by caustic soda additions. The system had been experiencing a series of unexplained leaks that were diagnosed as caused by a faulty pH probe that was part of the caustic addition control system such that the pH remained very low and the corrosion rate high. In a separate example, Bergstrom (1981) showed where an ER probe was able to detect the failure of fluid velocity controlling baffles in a concentrated brine solution (Fig. 11.5). The resultant increase in corrosion rate experienced by the ER probe element was a direct result of the baffles failure leading to increased flow rates.

11.3.2 Concrete structures

Legat *et al.* (2003) demonstrated that ER probes could detect the addition of corrosion inhibitors to concrete and to measure the cumulative effects

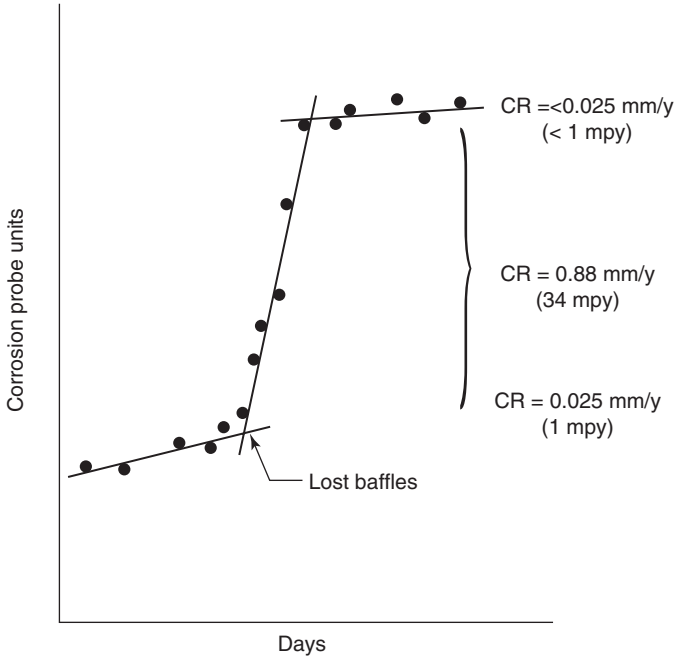

11.5 Response of an ER probe upon flow control baffle failure.

of corrosion damage. In their study, they also examined the effects of probe depth and the presence of salt on the corrosion rate. As shown in Fig. 11.6, the probes where deionized water (DI) water was used to wet the concrete showed consistently lower corrosion rates than the concrete wetted with a 3.5% NaCl solution (as would be expected). The thickness loss at locations closer to the surface was also noted to be more dramatic than deeper into the concrete. On the addition of inhibitor to the chloride solution wetted concrete, the thickness loss of the ER probe was noted to stop until the inhibitor was consumed.

11.3.3 Atmospheric

The thin film/strip probe can also be used for atmospheric corrosion monitoring. For example, McKenzie and Vassie (1985) used a thin film ER probe and compared the resultant corrosion to that measured using weight loss coupons over a period of 12 months. They demonstrated very good correlation (Fig. 11.7) in total metal loss experienced by the weight loss coupons and the corrosion loss measured using the ER probe at intervals of 3, 6, 9 and 12 months. They concluded that the ER probe results were comparable to the traditionally used standard weight loss coupon and thus could be used to provide better short term atmospheric corrosion rate estimates and

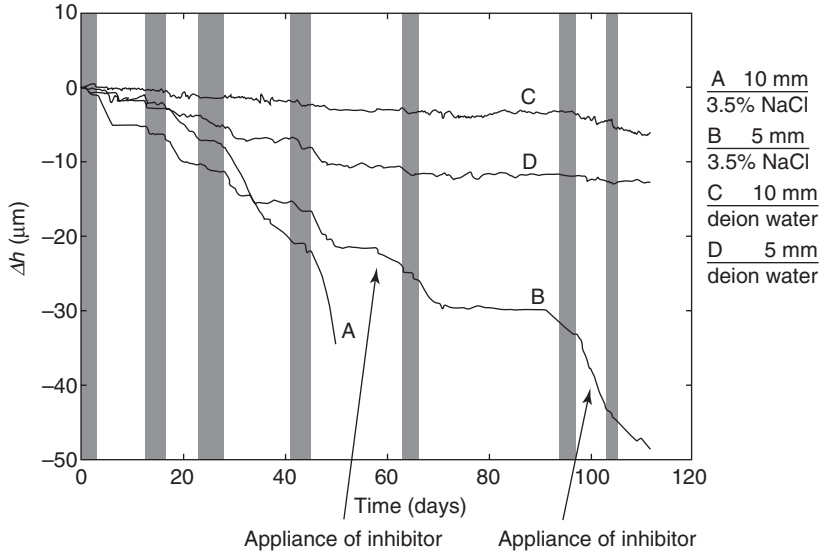

11.6 ER probe results embedded in concrete at different depths and exposed to different wetting environments.

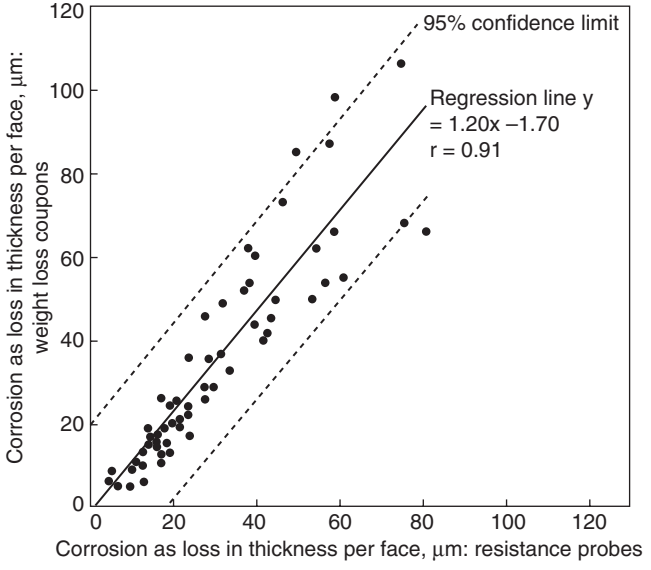

11.7 Comparison of ER probe results to weight loss coupons during atmospheric exposure.

importantly can provide an early indication of the onset of corrosion due to higher sensitivity. In addition, they found that the ER probe was able to more effectively determine and quantify the effects from directional wind/rain exposure than weight loss coupons.

Jung *et al.* (2003) constructed a thin film ER probe to monitor for atmospheric corrosion and compared its performance to a traditional time of wetness sensor. They were able to demonstrate that the ER probe was much more sensitive to alternating wet/dry conditions and could clearly show the elevated corrosion rates that result from salt concentration effects and increased oxygen transport during the dry out periods. In contrast, the time-of-wetness sensors were unable to clearly distinguish these episodic events.

11.3.4 Corrosion in soils

Thin film ER probes have also been used to monitor for the onset of microbially influenced corrosion in soils (Li *et al.*, 2001). Figure 11.8 shows the response of three individual probes that were exposed to soils containing sulfate reducing bacteria. Some differences in performance were noted and based on post-exposure examination showed that all the probe elements had formed FeS films but had experienced ruptures on two of the probes.

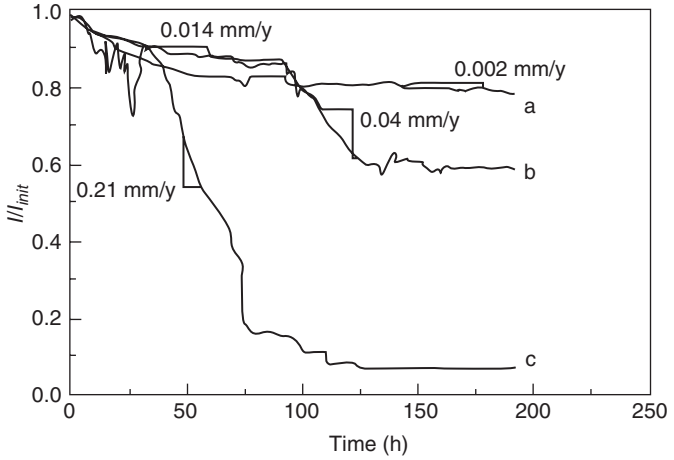

11.8 ER probe response in soils containing sulfate reducing bacteria.

Thus, where the ruptures were present, the corrosion rate was substantially higher and the remaining thickness considerably decreased.

Horton *et al.* (2006) described a program to monitor for possible corrosion of ductile iron pipe in the Florida Everglades, United States. The Florida Everglades environment is highly corrosive because of its high

concentration of decaying organic matter, brackish water chemistry and high microbial concentrations. Because these pipes traditionally were encased in polyethylene, a determination of the effectiveness of this encasement for this environment was needed. To aid in that determination, both bare and polyethylene encased ER probes were installed in several locations. The authors were able to distinguish corrosion rate differences between the encased and non-encased ER probes but also where the probes were located with respect to the pipe. For example, they noted that the corrosion rate measured on top of the pipe (12 o'clock position) showed virtually no corrosion whereas underneath the pipe (6 o'clock position) corrosion rates on the order of a few mils per year (mpy) (or 0.025 to 0.1 mm/y) were observed. This work helps to demonstrate not only that corrosion and where it occurs on a structure is highly spatially dependent but also the utility in using ER probes to help make these determinations.

Martin (1993) described efforts to better understand and mitigate potential telluric current (current induced in buried metallic structures due to the earth's magnetic field) corrosion effects on buried pipelines in Australia. To accomplish this, he attached a series of ER probes to the cathodic protection (CP) system of the pipeline and then compared the pipe potential and CP system current draw with the ER probe data. He was able to show that in some cases telluric currents did in fact result in appreciable changes in the corrosion rate. This work illustrates an important advantage that ER probes have over many other monitoring methods. If a system is protected using cathodic protection, the ER probe can likewise be polarized and the resultant corrosion rate while under CP can be determined. In contrast, other methods such as linear polarization resistance (see Chapter 3) cannot easily be modified to enable this capability.

11.4 Sensing probe electronics and instrumentation

The electronics used for ER probe measurements are shown schematically in Fig. 11.9 and essentially consist of a Wheatstone bridge configuration. A Wheatstone bridge is particularly well suited to determine the value of an unknown resistance (in this case the resistance of the sensing element, R_X). Because the values for the other resistances are known (R_1 and R_2 are in the meter and R_3 is the unexposed reference probe that has the initial resistance of the sensing element without experiencing any corrosion), if the ratio of R_X/R_3 equates R_2/R_1 then the current flow and voltage between points B and D will be zero. Using a sensitive galvanometer, the current between these two mid-points can be measured very accurately and can be nulled out by adjusting the resistance of R_2. With no current flow between the mid-points, the total resistance of the entire circuit is given by Equation [11.2]:

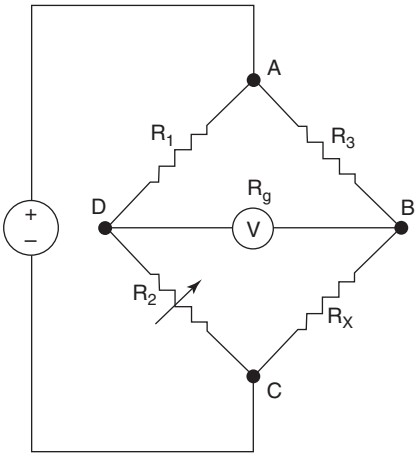

11.9 Wheatstone bridge.

$$R_T = \frac{(R_1 + R_2)\cdot(R_3 + R_X)}{R_1 + R_2 + R_3 + R_X} \qquad [11.2]$$

Since R_T can be measured and R_1, R_2, and R_3 are known, R_X can be solved for. Essentially all commercial instruments automatically determine the sensing element resistance and either provide that resistance value on the meter or take the additional steps to compare previous readings to determine a corrosion rate.

Several different instrumentation designs are available. Some of the more simple systems are battery powered and consist of a dial to adjust (null) out the sensing probe resistance thus providing its value. Other systems are more complex, but still in the form of battery powered portable units, that automatically convert the probe measurement response into a corrosion rate by comparing previous measurements and are displayed as a digital readout. Other systems are available that are intrinsically safe for applications in fire-hazardous locations and are permanently mounted in place. These permanently mounted systems are then read using a portable reader or are read automatically by a data logger.

11.5 Variations on the ER theme

Modifications and variations on the ER theme have also been developed that encompass changes to how the measurements are made to increase sensitivity and stability and to allow the application of ER measurement principles to the actual structure. Each of these advancements provides an improvement upon the overall ER probe concept but the underlying principles and applications still generally apply.

11.5.1 Inductance method

The use of inductive resistance to detect metal loss in the sensing element instead of directly measuring the resistance is an example of one of these changes. Patented under the trade name Microcor™, changes in the inductive resistance of a coil in proximity to the sensing element are monitored (Denzine and Reading, 1997a). Because changes in the magnetic permeability of the sensing element will be more pronounced than changes in its resistance, these magnetic changes result in potentially significant changes in the inductive resistance of the coil. As a result, it has been reported that this configuration results in decreases in response times by factors of between 100 and 2500. In addition to improvements in response times, improved temperature sensitivity (less sensitive to temperature changes) was also reported. (Microcor™ was originally developed and patented by Cortest Instrument Systems (Ohio, USA). Microcor is now available from Rohrback Cosasco Systems (California, USA).)

When compared to linear polarization resistance method (see Chapter 3) and traditional ER methods, the inductive resistance method was shown to provide comparable results (Figs 11.10 and 11.11). In Figs 11.10 and 11.11, the linear polarization resistance probe measurements are the same and the difference in response between the inductive resistance probe and the traditional ER probe can be seen. When the environment corrosivity changed from less than 5 mpy (0.125 mm/y) for steel to variable corrosion rates between 15 and 30 mpy (0.375 to 0.75 mm/y) the inductive resistance probe was able to detect the change in the corrosivity as evidenced by the change in slope. In contrast, the changes in corrosivity were not detected by the standard ER probe over the same time period. In addition, careful examination of the inductive resistance probe results also shows that some of the corrosion rate changes measured by linear polarization resistance method could also be detected as small changes and deviations in the slope of the inductive resistance probe data.

The inductive resistance probe, however, has some limitations. For example, because it relies on changes in the magnetic permeability of the sensing element as corrosion occurs, only highly magnetic materials can be used. Thus, carbon steel (and other ferritic steels) can be used, however non-magnetic materials cannot and weakly magnetic materials may not work as well. As a result, monitoring systems constructed from aluminum, copper and nickel alloys as well as austenitic stainless steels will not be possible with this probe system. For comparison purposes, the magnetic permeability of aluminum and copper are relatively similar and are only 0.1% of the value of steel. Other reported limitations with the inductive resistance probe include a short probe life, and the influence of mechanical stresses on magnetic properties resulting in erroneous readings.

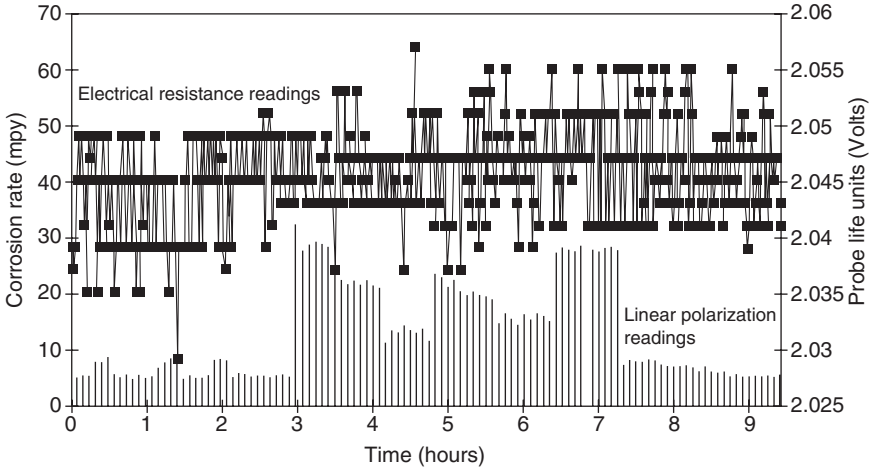

11.10 Comparison of standard ER probe to linear polarization resistance under the same conditions as shown in Fig. 11.9.

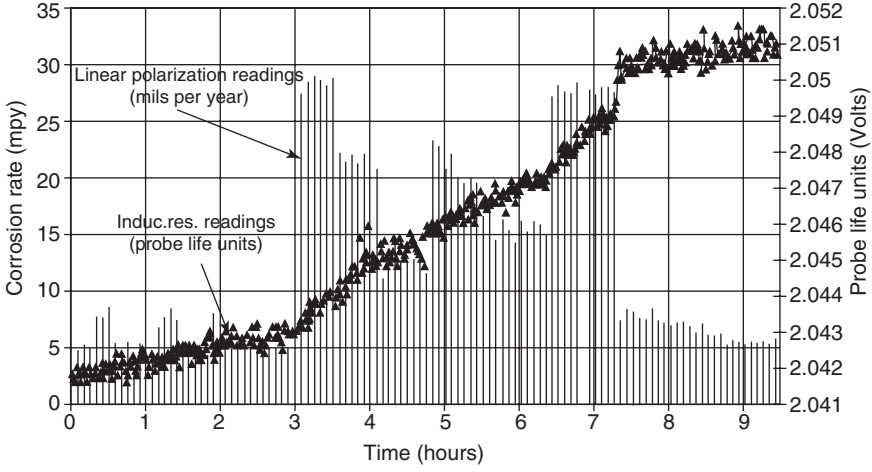

11.11 Comparison of linear polarization resistance to inductive resistance ER probe.

CEION®, produced and marketed by Cormon Ltd (UK) is also supposed to be based on an ER probe type concept. The probe, which appears to be in the form of a spiral ring embedded in epoxy, has been used in a wide range of oil field applications and has been shown to provide reasonable agreement with corrosion rate measurements found using other methods

(Fig. 11.12). Though this technology appears promising and seems to be based in some fashion on ER principles, the precise functionality and background of the method are unclear. Based on what is available in company provided information, the resistance of the element is apparently determined using alternating current methods rather than direct current. It has also been claimed that the resolution of the probe and its associated electronics is on the order of 1 nm (Hemblade *et al.*, 1999; Brown *et al.*, 2000). Others who report using ER probes that appear to be similar report resolutions that are sub-μm (Ridd *et al.*, 1998). Because of the limited amount of independent information available and the lack of details concerning the operating principles, it is difficult to determine the accuracy of these claims.

11.5.2 Field signature method

A slightly different variation on the ER probe concept is the use and application of the same operating principles but applied to the entire structure of interest. The Field Signature Method (FSM), developed by the University of Oslo in Norway in the mid-1980s and presently marketed by CorrOcean, is capable of detecting metal loss and other defects by observing the changes induced in the way that current flows through the structure. To accomplish this, a series of pins are attached to the structure in an array spaced at approximately two to three times the wall thickness. When a current is applied to the structure, the current flow and resultant potential drop due to the metal's resistance are measured. When corrosion occurs, this resistance between a given set of sensing pins will increase (similar to an ER

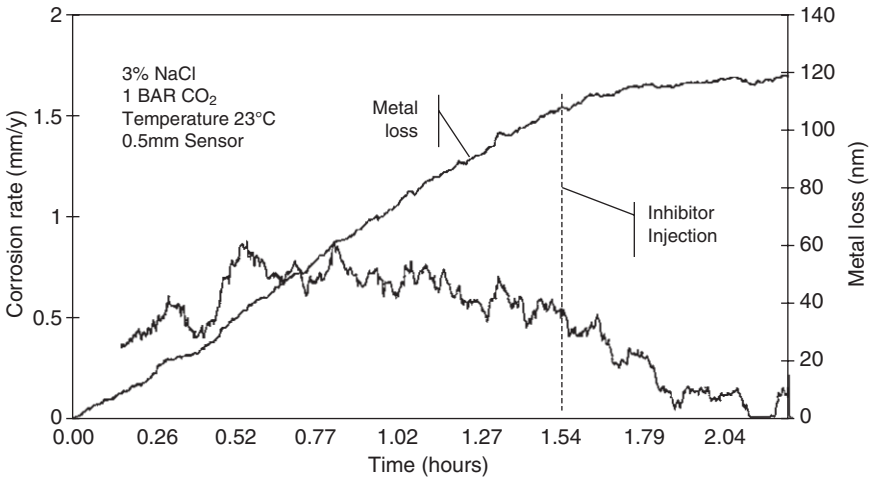

11.12 Corrosion response of CEION probe.

probe) and the potential drop across that region will also increase. When the original potential distribution 'signature' is compared to subsequent readings, the effects of corrosion can be determined. This method has a nominal sensitivity reported to be in the order of 0.1% of the wall thickness and has the significant advantage of monitoring the actual component. That is, instead of monitoring a sensing element, the structure in question is itself the sensing element. The other advantage of FSM is that it is non-intrusive, which is an important aspect for application in internal corrosion monitoring, especially if the system is pressurized.

FSM has been widely used for monitoring corrosion in subsea pipelines, onshore pipelines, in gas plants, and in the refinery industry. Strommen (2002) described the results of a seven year internal corrosion monitoring program using FSM on subsea pipelines. A comparison of the FSM response as compared to independent corrosion rate measurements in the well fluids showed excellent agreement (0.11 mm/y by FSM compared to 0.12 mm/y). Scanlan *et al.* (2003) used the FSM technique to monitor for possible corrosion at a series of locations within a refinery and noted that the method could provide a three-dimensional image of metal loss at bends and elbows and could distinguish between pitting and general corrosion.

11.6 Advantages and limitations

ER probes are often chosen due to their relatively simple operation, low cost, and ease of operation and interpretation. Because the ER probe method does not rely on electrochemistry, it can be used in nearly any condition including atmospheric and high resistivity environments where electrochemistry-based monitoring tools often experience difficulties or cannot be used. In addition, ER probes can be connected to a cathodic protection system which then enables the monitoring of structures that utilize CP for corrosion mitigation.

ER probes, however, do have some limitations. First, the sensitivity of the ER technique is generally too low to show rapid changes in corrosion conditions. As shown in Fig. 11.4 if a corrosion rate on the order of 1 mpy (25 μm/yr) is expected the response time for detecting that rate is between one and ten days. On the other hand, if the expected corrosion rate is 100 mpy (2.5 μm/yr) the response time is significantly diminished to a matter of less than a few hours. Increased sensitivity can be achieved using thinner/smaller elements but this comes at the sacrifice of probe life.

Limitations also arise when corrosion mechanisms other than uniform, general corrosion are expected or encountered. The reduction in the cross-sectional area that results in an increase in probe resistance is assumed to be uniform. Depending on the probe size and geometry, the presence of a

pit or stress corrosion cracking (SCC) may or may not be detected since the reduction in the cross-sectional area associated with a pit or a crack can be quite small.

Additional limitations arise when the possibility of conductive corrosion products or scales are precipitated on the probe. For example, sulfide environments are particularly difficult to interpret using ER probes because the iron sulfide corrosion product that forms is conductive which will tend to underestimate the amount of metal loss experienced. Iron sulfide precipitation has been heavy enough in some cases to indicate that metal gain had taken place. This type of response, then, somewhat limits the applicability of ER probes in sour oil and gas systems.

11.7 Summary and conclusions

ER probes have been in use since the mid-1950s and provide a valuable tool for the corrosion engineer. They are easy to use, interpret, and can provide highly valuable information regarding the propensity for a system to experience corrosion. Improvements and modifications have also been developed that help enhance the sensitivity and responsiveness of the overall ER probe concept.

11.8 References

D.R. Bergstrom, *Materials Performance*, p. 17, September (1981).
G.K. Brown, *Pipeline and Gas Industry*, p. 53, April (1996).
G.K. Brown, J.R. Davies, B.J. Hemblade, *Corrosion2000*, paper no. 00278 (2000).
M.A. Clarke, *Industrial Corrosion*, v. 9, p. 11 (1991).
R.D. Davies, *Appita*, vol. 39, p. 472 (1986).
A.F. Denzine and M.S. Reading, *Corrosion97*, paper no. 287 (1997a).
A.F. Denzine and M.S. Reading, *Corrosion97*, paper no. 288 (1997b).
A. Dravnieks, H.A. Cataldi, *Corrosion*, v. 10, p. 224 (1954).
A.J. Freedman, E.S. Troscinski, A. Dravnieks, *Corrosion*, v. 14, p. 175 (1958).
B.J. Hemblade, J.R. Davies, J. Sutton, *Corrosion99*, paper no. 225 (1999).
A.M. Horton, D. Lindemuth, G. Ash, *Materials Performance*, p. 50, May (2006).
S. Jung, Y.-G. Kim, H.-S. Song, S.Y. Li, S.-M. Le, Y.-T. Kao, *Corrosion2003*, paper no. 03392 (2003).
A. Legat, V. Kuhar, M. Leban, A. Vernekar, *Corrosion2003*, paper no. 03390 (2003).
S.Y. Li, Y.G. Kim, K.S. Jeon, Y.T. Kho, T. Kang, *Corrosion*, v. 57, p. 815 (2001).
B.A. Martin, *Corrosion*, v. 49, p. 343 (1993).
M. McKenzie, P.R. Vassie, *British Corrosion Journal*, v. 20, p. 117 (1985).
B. Ridd, T.J. Blakset, D. Queen, *Corrosion98*, paper no. 78 (1998).
R.J. Scanlan, R.M. Boothman, D.R. Clarida, *Corrosion2003*, paper 03655 (2003).
R.D. Strommen, *Corrosion2002*, paper no. 02251 (2002).

12

Nondestructive evaluation technologies for monitoring corrosion

G. LIGHT, Southwest Research Institute, San Antonio, Texas, USA

12.1 Introduction

Corrosion begins and increases over time and, in most cases, is hidden from view either inside a component such as a pipe or under a surface covering such as thermal insulation or concrete. Unfortunately, corrosion does not grow predictably. The present practice is to estimate a period of time over which corrosion will not cause a catastrophic failure and conduct an inspection to measure remaining wall thickness at specific intervals. This is usually done by marking certain areas on the component and attempting to collect data at the same location each time so that any changes in the component wall can be detected. This approach sounds like a logical one, but many times data are collected at specific spatial locations – for example, on 50-mm centers. There is no guarantee that the corrosion effect is occurring at one of the sites where data are collected. In fact, there can be a situation where a throughwall corrosion pit can grow next to a region that is being periodically inspected and the defect never detected. So this type of process has uncertainties and can lead to unexpected failure.

In addition, corrosion can occur on the inside or outside. The product flow or product process may lead to corrosion on the inside of the pipe or component. Other times, the corrosion is caused by the environment. For example, corrosion on the outside surface of a pipe under the insulation is caused by the moisture condensed between the outside surface of the pipe and the insulation.

A better way to determine the amount and severity of damage being caused by corrosion is to use sensor systems that can remain in place to monitor a component while the process that causes corrosion is ongoing. This process is called 'condition monitoring'. This monitoring can be either active or passive.

12.2 NDE methods for corrosion monitoring

There are a number of nondestructive evaluation (NDE) methods that can be used to monitor the condition of a component for defects such as corrosion. These include ultrasonics, eddy current, acoustic emission, guided waves, and infrared thermography. In the following sections, typical applications of these techniques and limitations are discussed, including probes, electronics and software.

For condition monitoring programs, it is necessary to establish the baseline condition of any component or installation. This may be done at any time, but should preferably be implemented directly after construction. In an early stage, one should consider using a type of inspection that may be applied in an equal fashion in a later stage during service. Periodic condition assessment allows trending and prediction of the remaining mean-time-to-failure (MTTF). Operational lifetime extension may be agreed upon with authorities, and increased plant availability is the result.[1] Lifetime calculation models may predict the remaining service time of any asset. These calculations require input data provided by the asset's history and available nondestructive testing (NDT) data. The outcome can be only as reliable as the input. High probability of detection (POD) is required to ensure reliable operation until the next shutdown, and a low false call rate (FCR) is desirable to avoid unnecessary maintenance work. Accurate and highly reliable data result in a reliable prediction of the remaining service time.

The number and methods of inspection are always a trade-off between the minimum requirements for safe operation and the amount of information needed for optimum maintenance management. In a baseline inspection, it is important to establish, as accurately as possible, the zero condition of the component. It is often good to use several complementary techniques, but one should definitely be the technique that will be used to monitor the equipment. For example, if ultrasonics is the method to be used for monitoring a region, the baseline condition might be obtained using radiography as well as ultrasonics. Care should be taken to precisely establish coordinate systems used for the component and to precisely mark and notate any anomalies that are found.

12.2.1 Ultrasonic monitoring technologies

Ultrasonic monitoring for corrosion/erosion and general wall thinning processes can be conducted by collecting periodic 0-degree L-wave wall thickness measurements using individual probes, a single probe that is scanned, or an array of probes. Ultrasonic corrosion mapping can provide quantitative information on corrosion of vessel plate and welds, and even the condition of certain internal coatings, and is an invaluable and widely used tool. Ultrasonic thickness is based on the time required for the ultrasonic pulse to travel from the front surface of the component to the back and return,

based on the known ultrasonic velocity in the component. The limitations of the method are the maximum temperature at which inspection may be carried out, usually lower than approximately 94 °C unless methods for keeping the ultrasonic sensor cool and maintaining fresh and effective couplant are part of the process.[2] One approach is to have a constant supply of couplant applied to the probes, but this could also lead to variations in coupling efficiency. However, the thickness measurement is primarily a time measurement, not an amplitude measurement. In addition, coatings on the probe surface can attenuate the ultrasonic energy going into the part. This is especially true if the coating is thick and possibly delaminated. Also, if the corrosion occurs on the front surface, the ultrasonic beam is scattered by the front surface corrosion, making this approach ineffective. Thus, ultrasonics should primarily be used when the corrosion process is on the inside surface of the component being monitored. Ultrasonic weld monitoring can be done as well, using fixed probes or arrays for shear wave and/or time-of-flight diffraction (TOFD) data to detect weld cracking. Again, the primary limitations of these techniques include providing sufficient long-term couplant as well as access and temperature.[1]

One example of a corrosion monitoring system that uses a 0-degree longitudinal mode thickness measurement transducer to measure wall thickness over a period of time under a transducer that is clamped in place is the MIST UT Monitor developed by CC Technologies, located in Dublin, Ohio, USA. The device is fairly simple but requires that the exact location be known where monitoring is required. This is best used when an inspection reveals a corrosion pit or defect that is at an acceptable level but is expected to grow. The MIST UT Monitor can be clamped onto the pipe or component at that location and ultrasonic thickness measurements collected periodically.

More complex units have also been developed because recent developments in the fields of electronics, computer systems, and communication technology have enabled the use of new concepts for inspection and monitoring. One such development is the ULTRAMONIT system developed by Cole and Gautrey,[2] where an array of 0-degree ultrasonic sensors is placed permanently onto the pipe. The location of the sensor array is usually at a field joint directly at or close to a weld so that the array can monitor for wall thinning corrosion and cracks. Permanently installed sensors are advantageous because exact position, orientation, and acoustic coupling are maintained between surveys. Compared to conventional ultrasonic inspection, this concept provides significantly improved possibilities for high-resolution data trend analysis. This technology has been applied for both subsea and land facility use.

In the subsea embodiment, the array of 0-degree transducers is implemented as an instrumented pipeline clamp, where the required electronics and sensors are placed and protected in a rugged steel structure as

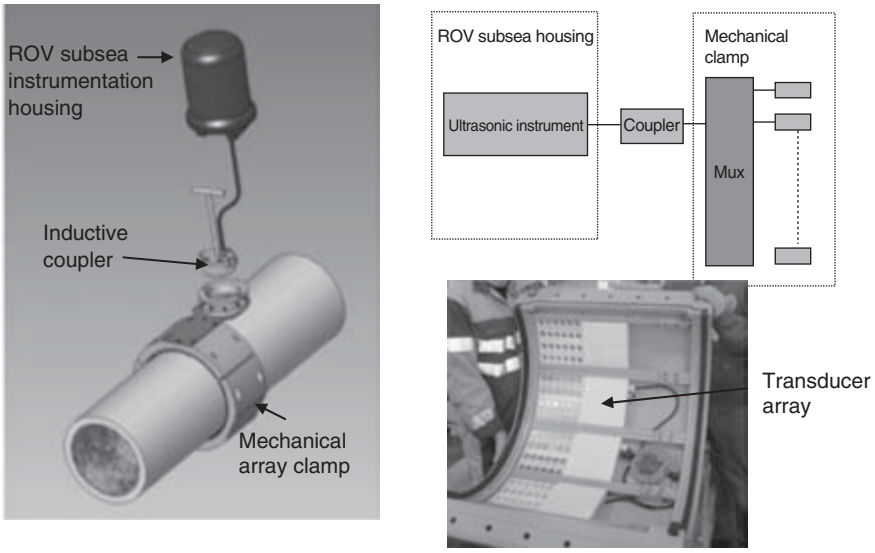

12.1 Illustration of the ULTRAMONIT array system used on subsea pipe applications with subsea sensor clamp, inductive coupler, and main instrumentation subsea housing that contains the ultrasonic instrument and multiplexer (MUX).

illustrated in Fig. 12.1.[3] Reliability was a key objective for this system and has been addressed by keeping the permanently installed electronics as simple as possible, while making the more complicated parts of the instrumentation accessible in a remotely operated vehicle (ROV)-carried unit. This ROV is used for interrogation with the sensors by the use of a specially developed inductive coupler, which provides power, analog signal for the ultrasonic transducers, and digital communication for the signal multiplexer. This unit is controlled digitally, and the number of channels is limited only by signal degradation due to total spanned length of analog cable, as the channel count gets very high. For the land facility version, the same system has been installed on a 30-cm pipe at the Kårstø gas processing plant located near Stavanger, Norway. This unit has run since December 2003.

It is important to understand that application of this technology is very localized and requires that the location of corrosion attack be known so the sensors can be placed in that area to effectively monitor for potential corrosion failure. If the corrosion begins to affect other parts of the component where the sensor is not located, corrosion could go undetected.

12.2.2 Eddy current

Eddy current inspection can also be a very useful method for monitoring external corrosion in components by measuring the liftoff between the

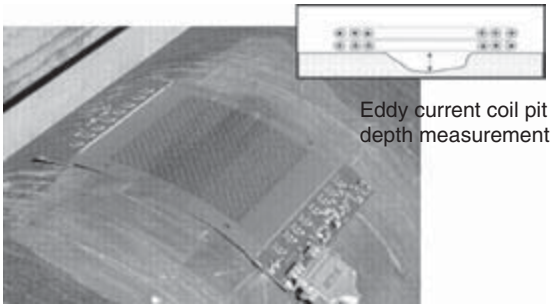

12.2 Photograph of the conformable array on top of a pipe monitoring the pit depth.

component nominal surface and the surface of the pit on the metal. This requires either a localized scanning method or an array of probes. An example of an eddy current array is the conformal array shown in Fig 12.2. The array is flexible; however, to effectively use this to monitor, a means to locate the array precisely each time is needed.[4] Temperature and access to the surface are the main limitations of eddy current.

Pulsed eddy current can operate without having close proximity to the surface. A pulsed eddy-current technique that uses a stepped or pulsed input signal for the detection of corrosion under insulation (CUI) has been evaluated. This allows the detection of wall-thinning areas in various types of pipe, including riser pipe, without removing the outside coatings. In addition, it is found that filmless, realtime, and digital radiography can be used to find internal and external corrosion defects in an insulated splash zone while the riser remains in service. A survey of NDE manufacturing companies, NDE inspection companies, and operating companies was completed to collect information about current instrumentation and inspection/operators' experience for riser inspection. Examples of advanced riser inspection instrumentation and field results were included. The ability of the candidate technologies to be adapted to riser variations, the stage of standardization, and costs were also discussed.

Pulsed eddy current equipment has been successfully applied in corrosion detection for several years. Whereas field experience on insulated objects has grown significantly, the technique's characteristics also make it highly suitable for other field situations where the object surface is rough or inaccessible. Because (surface) preparations can be avoided, the tool provides a fast, cost-effective solution for corrosion detection.

Röntgen Technische Dienst (RTD) developed a pulsed eddy current tool (called the RTD-INCOTEST) that has been used by the refinery industry for the detection of corrosion under insulation (CUI). It allows the detection of wall thinning areas without insulation removal. However, this is a

point measurement. Currently, a network of 12 companies worldwide operate a total of 32 systems. RTD-INCOTEST applies pulsed eddy currents for the detection of corrosion areas. A pulsed eddy current technique uses a stepped or pulsed input signal, whereas conventional eddy currents use a continuous signal. The advantages of the pulsed eddy current technique are its larger penetration depth, relative insensitivity to liftoff, and the possibility to obtain a quantitative measurement result for wall thickness. This leads to the characteristic that makes it suitable for the detection of CUI: no direct surface contact between the probe and the object is necessary. Also, this tool can be employed in other field situations where the object surface is rough or inaccessible.

The applied operating principle of pulsed eddy current systems can vary from system to system. In order to obtain a quantitative reading for wall thickness, the RTD-INCOTEST uses a patented algorithm[5] that relates the diffusive behavior in time to the material properties and the wall thickness. It operates on low alloy carbon steel, as illustrated in Fig. 12.3.

A pulsed magnetic field is sent by the probe coil. This penetrates through any nonmagnetic material between the probe and the object under inspection (e.g. insulation material). The varying magnetic field will induce eddy currents on the surface of the object. The diffusive behavior of these eddy currents is related to the material properties and wall thickness of the object.

The detected eddy current signal is processed and compared to a reference signal. The material properties are eliminated, and a reading for the average wall thickness within the magnetic field area results. One reading takes a couple of seconds. The signal is logged and can be retrieved for later comparison in a monitoring approach. An example of the RTD-INCOTEST data output is shown in Fig. 12.4.

The area over which a measurement is taken is referred to as the footprint. Probe design is such that the magnetic field focuses on an area on the surface of the object. The result of the measurement is a reading of the average wall thickness (AWT) over this footprint area. The size of this area is dependent on the insulation and object thickness, as well as the probe

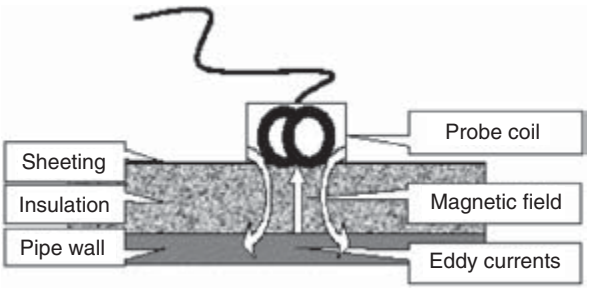

12.3 Principle of operation RTD-INCOTEST.

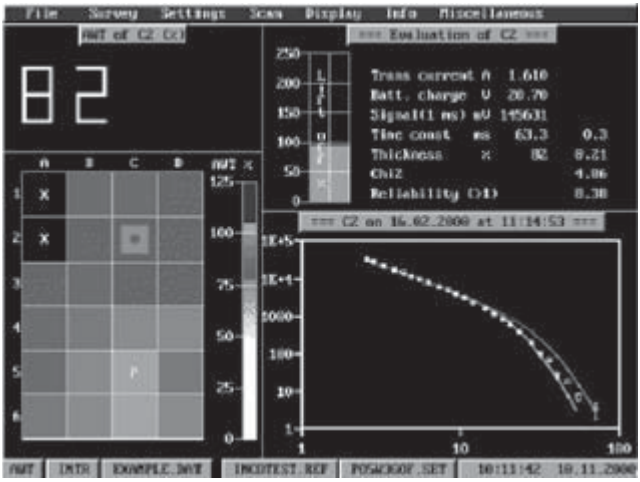

12.4 Display of RTD-INCOTEST showing AWT (Average Wall Thickness) reading (top left), logged inspection grid (bottom left) and the decay of the eddy currents (bottom right).

design. Roughly, the footprint can be considered to be in the order of the insulation thickness. Due to the averaging effect, detection of highly localized defect types like pitting is not reliable with this tool. Although the AWT reading is not a direct replacement of the commonly used ultrasonic testing (UT)-obtained minimum wall thickness, a quantitative result is obtained that can be interpreted unambiguously.

The outer application ranges of the RTD-INCOTEST tool can be described by:

- Low alloy carbon steel
- Pipe diameter >50 mm or 2 inches
- Nominal wall thickness between 6 and 65 mm
- Insulation thickness ≤150 mm
- Sheeting thickness ≤1 mm stainless steel, aluminum, galvanized steel
- Object temperature >–100 °C to <+500 °C

These ranges are determined on condition that a reliable signal can be obtained under regular field conditions.

12.2.3 Acoustic emission and equipment

Acoustic emission (AE) is a passive NDE technique that makes use of the high-frequency acoustic energy emitted by an object that is undergoing stress, such as when corrosion products formed on a corroding rebar push out on the concrete surrounding it. The primary advantage AE offers over

more conventional NDE techniques is that it results directly from the process of flaw growth. Slow crack growth in ductile materials produces few AE events, whereas rapid crack growth in brittle materials produces large numbers of AE events.[6–17]

Acoustic emission can also be created as a result of corrosion-induced phenomena. In concrete, for example, corrosion can produce cracking that generates acoustic emissions. In stainless steel, primary AE was produced by the falling-off of grains due to the mutual actions of anodic dissolution and mechanical fracture along a chromium-depleted zone in the grain boundary, and secondary AE was produced by hydrogen gas evolution and by the cracking of corrosion products.[6] AE is able to test/monitor 100% of a structure using relatively few stationary sensors mounted to the structure. AE techniques are primarily sensitive to active defects caused by stress. AE may also be generated by cracking of corrosion products. Unlike most methods, there is no probe temperature limitation with AE, as sensors may be coupled through metal acoustic waveguides welded to the plant, the sensor being outside the insulation.

This technology has been used for detection of corrosion in steel rebar encapsulated in concrete on bridges. AE monitoring of concrete was used to detect rebar corrosion, film cracking, gas evolution and microcracking. Although attenuation of the AE signal in the concrete was a concern in the past, unique placement of the AE transducers on the reinforcing steel and using the steel as the sound propagation medium allowed the onset of steel corrosion to be detected. In addition, it was possible to use the AE signal to calculate the location where the steel corrosion was occurring, allowing bridge inspectors to determine the extent of corrosion damage. Thus, AE monitoring appears to be a promising technique that can be used for bridge inspection to quantify the condition of steel-reinforced concrete, where corrosion is occurring, and where repair is needed.

A typical AE monitoring system uses piezoelectric sensors acoustically coupled to the test object with a suitable acoustic coupling medium (grease or adhesive). The output of the sensors is amplified and filtered by preamplifiers and then fed to the monitor via shielded coaxial cables. The monitor further filters and amplifies the AE signals, processes the data, and displays the results. Both results and raw data are typically recorded for archival purposes or for post-test analysis; for instance, to determine location of the AE signal.

The disadvantage of AE is that commercial AE systems can only estimate qualitatively how much damage is in the material and approximately how long the components will last, so other NDE methods are still needed to do more thorough examinations and provide quantitative results. Service environments are generally very noisy, and the AE signals are usually very weak. Thus, signal discrimination and noise reduction are very difficult, yet extremely important for successful AE applications.

12.2.4 Guided waves and equipment

One of the fastest growing techniques for monitoring corrosion is the use of long-range ultrasonics, primarily using guided waves. Guided waves refer to mechanical (or elastic) waves in ultrasonic and sonic frequencies that propagate in a bounded medium (pipe, plate, rod, etc.) parallel to the plane of its boundary. The wave is termed 'guided' because it travels along the medium guided by the geometric boundaries of the medium.

Since the wave is guided by the geometric boundaries of the medium, the geometry has a strong influence on the behavior of the wave.[18–20] In contrast to ultrasonic waves used in conventional ultrasonic inspections that propagate with a constant velocity, the velocity of the guided waves varies significantly with wave frequency and geometry of the medium. In addition, at a given wave frequency, the guided waves can propagate in different wave modes and orders.

The properties of guided waves and examples of their dispersion curves (which refer to the relationship between the velocity and the wave frequencies) are given in Figs. 12.5 and 12.6 for pipe and plate geometries, respectively. In pipe, the guided waves exist in three different wave modes: longitudinal (L), torsional (T), and flexural (F). In plate, they exist in two different wave modes: longitudinal that is generally called 'Lamb' waves and exists in symmetric (S) and antisymmetric (A) modes; and shear horizontal (SH).

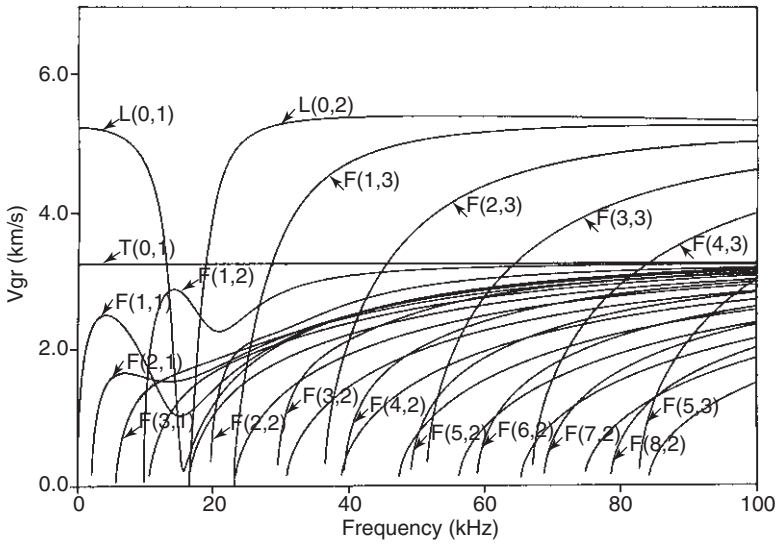

12.5 Examples of dispersion waves of various guided wave modes in pipe (for 114-mm-OD, 8.6-mm-thick pipe). The numbers in parentheses indicate the order of the wave mode.

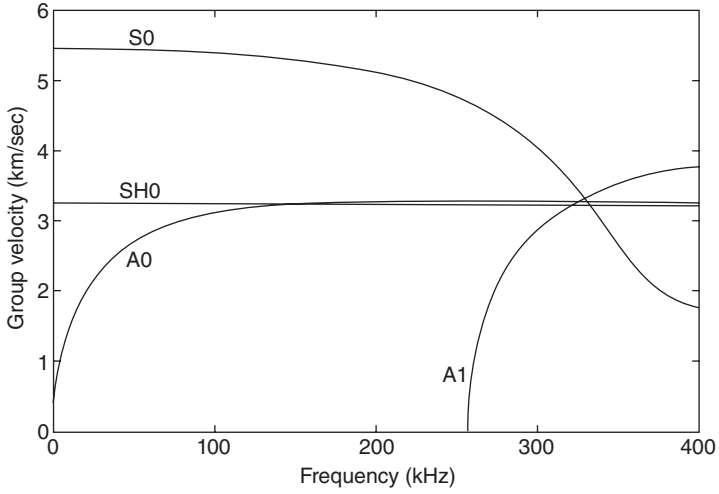

12.6 Example of dispersion curves of various guided wave modes in plate (for 6.35-mm-thick plate). The numbers after the letter (0 and 1) indicate the order of the wave mode.

Although the properties of guided waves are complex, with judicious selection and proper control of wave mode and frequency, the guided waves can be used to achieve 100% volumetric inspection of a large area of a structure from a single sensor location.

Guided waves can be developed at a single location on a component and then travel long distances from the source point to monitor the condition of that component. The guided wave fills the entire volume of the component, and any change in cross-section of the component, such as a weld or corrosion/erosion, usually reflects or scatters the guided wave so that the change in cross-section is detected. Depending on frequency and material conditions, guided waves can travel as far as 150 m or more from one source, and defects such as corrosion scatter back the guided waves, thus giving an indication of corrosion locations.

There are two types of guided wave systems based on the physics of generating the guided waves. One type uses a large number of piezoelectric transducers that are pressure coupled to the pipe. This technology was developed and distributed by Guided Wave Ultrasonics Limited[21] and requires a mechanical fixture to squeeze the transducers onto a pipe. This fixture can be expensive and can only be used on cylindrical-type geometries such as pipe. The defect detection sensitivity is estimated to be 5 to 10% of the pipe cross-section.

The other type uses a thin ferromagnetic strip (approximately 0.15 mm) that has a high magnetostrictive property and is bonded to the pipe[21–28]

and is referred to as magnetostrictive sensor (MsS) technology. The ferromagnetic strip and excitation coil are relatively inexpensive and can be used on piping, plate, bar and a wide range of geometries. However, time for bonding the ferromagnetic strip onto the geometry is required.

Generally speaking, the MsS approach can be used as an inspection mode to detect defects on the order of 3 to 5% of the component cross-section, but if the sensor can be left in place for long periods of time (most feasible with the ferromagnetic strip concept) and data are collected at various times during its life, defects as small as 0.5% can be detected. However, guided waves tend to be poor at quantifying the corrosion and should really be used as more of a screening and locating tool.

The piezoelectric sensor system is limited in temperature applications of 70 °C to 120 °C. The MsS technology has been used on components ranging from approximately –150 °C to 300 °C.

Guided waves have been used to inspect various types of pipeline, on land as well as offshore. An example of an offshore application is the inspection of risers. Offshore pipeline failure statistics have been collected for more than 30 years and illustrate that the riser predominantly fails as a result of corrosion. The consistent wetting and drying in the splash zone, combined with defects in the coatings, are the usual contributors to the problem. A guided wave approach using torsional waves can be deployed to detect significant reduction in wall thickness. This allows the detection of wall-thinning areas in the riser without removing the outside coatings. For detecting and monitoring corrosion under insulation, the MsS can be placed on a pipe with many welded sections as shown in Fig. 12.7, with the data shown in Fig. 12.8. The directionality of the guided wave from the MsS is controlled so the wave can be transmitted to the right of the sensor or to the left.

Presently, the MsS technology uses the T-wave mode primarily for piping inspection that is generated and detected with the thin ferromagnetic

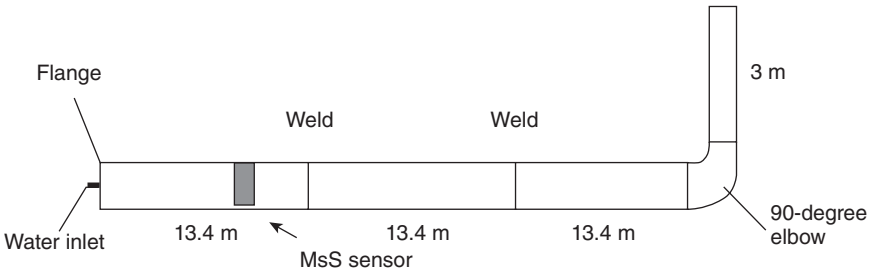

12.7 Illustration of MsS guided wave sensor attached to pipe.

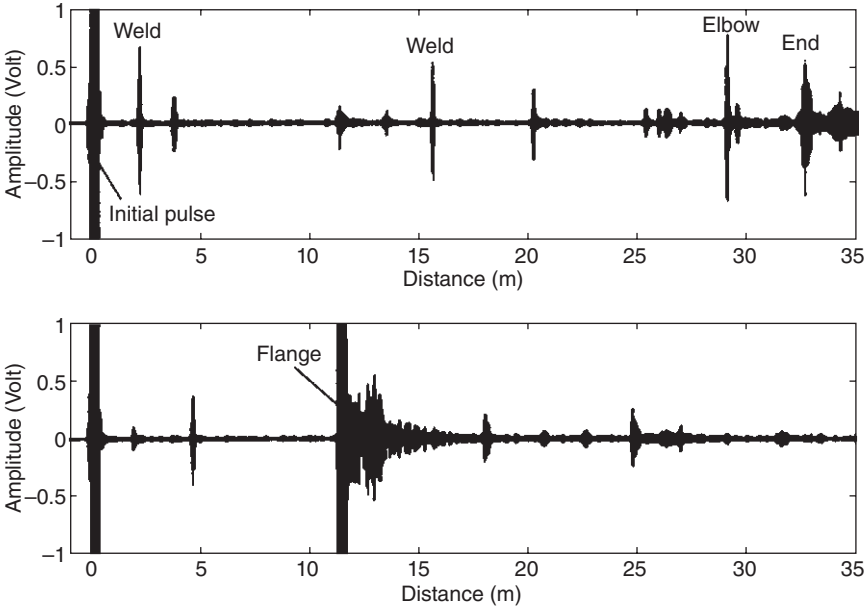

12.8 Illustration of guided wave data collected by MsS system. The top waveform directed to right of the MsS sensor shown in 12.7 and the lower waveform is directed to the left of the MsS sensor shown in 12.7.

(typically nickel) layer approach. Reasons for this practice include: (1) the fundamental T-wave mode is not dispersive and, therefore, no consideration is necessary for possible dispersion effects that exist in the L-wave mode; (2) the T-wave MsS has fewer effects than other extraneous wave modes and, therefore, it gives better signal-to-noise ratio and its data are easier to analyze; (3) the T-wave does not interact with liquid inside the pipe and, therefore, is far superior to the L-wave[24] for inspection of liquid-filled pipes; and (4) the T-wave MsS does not require heavy bias magnets and, therefore, is much easier and safer to handle than the L-wave counterpart. The disadvantage of the T-wave MsS is the requirement for direct physical access to the pipe surface for bonding of the thin ferromagnetic layer. Therefore, to apply the T-mode MsS for bitumen-coated piping, for example, the coating must be removed beforehand, whereas the L-mode MsS can be applied without removing the coating. However, the advantage of the T-mode MsS greatly outweighs the disadvantage and, consequently, the T-mode MsS is used primarily for long-range piping inspection.

Table 12.1 summarizes the capabilities and limitations of the present guided wave technology for long-range piping inspection in bare pipes. The effects of pipeline geometric features and other conditions such as coating and liquid inside pipe on the inspection capabilities are also summarized in Table 12.2.

Table 12.1 Capabilities and limitations of guided wave systems for pipe inspection

Item	Capabilities/limitations
Spatial resolution	3 to 7 inches (7.5 to 17.8 cm), depending on frequency and mode
Pipe material	Any material
Pipe size	Up to 60 in. (152 cm) diameter for MsS technology, approximately 32 in. (81.3 cm) for piezoelectric system and less than 0.75 in. (19 mm) wall thickness
Inspection range	100 ft (30 m) or greater, depending on coating and for aboveground piping
Detectable defect type	Isolated corrosion pits and circumferential cracks
Minimum detectable defect size	2 to 5% of pipewall cross section
Defect location	Axial location within ±2 in. (5 cm), depending on operational frequency and mode
Defect characterization	Limited to rough estimation of circumferential cross-section
Long term monitoring	Only with MsS system because cost of MsS sensors are much less than piezoelectric sensor belt

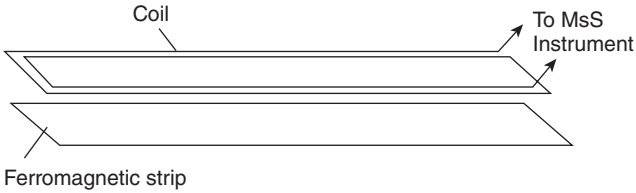

12.9 Illustration of the flat MsS guided-wave probe for structural health monitoring. The coil is placed directly on the nickel layer.

Corrosion monitoring on other components, such as plate, has been demonstrated in the laboratory using MsS technology. For this application, the ferromagnetic sensor (Fig. 12.9) is permanently bonded to the surface of the structure with appropriate adhesive, such as epoxy, and then magnetically conditioned. The coil is used to generate a guided wave in the ferromagnetic strip and also to receive any guided waves scattered from defects. Because the sensor is fixed to the surface, the data collected periodically can be carefully compared to the baseline data established at the time of sensor installation. This allows trending of the structural condition changes as a function of time. An effective determination of damage and its location can be obtained through the monitoring mode and used in a suitable structural management decision code.

An example application is on aircraft structures such as fuselage and wing skins that are assembled with fasteners. Corrosion and cracking that occur around and under fasteners are major concerns for assuring structural

Table 12.2 Effects of pipeline geometric features and other conditions on inspection capabilities

Features/conditions	Effects
Flange/valve	Prevents wave propagation; forms end point of inspection range
Tee	Causes a large disruption in wave propagation and limits inspection range up to that point
Elbow	Causes a large disruption in wave propagation and limits inspection range no farther than the elbow region
Bend	Has negligible effect if the bend radius is greater than three times the pipe OD; if the bend radius is less than the above, behaves like an elbow
Side branch	Causes a wave reflection and thus produces a signal; no significant effects on inspection capabilities
Clamp	Causes a wave reflection and thus produces a signal; no significant effects on inspection capabilities
Weld attachment	Causes a wave reflection and thus produces a signal; if the attachment is large (such as pipe shoes), can reduce inspection range
Paint	Has negligible effects
Insulation	Has no effects unless the insulation is bonded to the pipe surface, in which case the inspection range will be shortened due to higher wave attenuation
Coating	Has negligible effects if the coating is thin (e.g. fusion-bonded epoxy coating); thicker coating (e.g. bituminous coating, polyethylene coating) increases wave attenuation and shortens inspection range
Liquid in pipe	No effect on torsional-wave; significant degradation on longitudinal-wave
General surface corrosion	Increases wave attenuation and shortens inspection range
Soil	If pipe is buried, the surrounding soil greatly increases wave attenuation, and the inspection range is significantly shortened

safety of the aircraft. Because of the complicated geometry of the fastened structure and the large number of fasteners, inspection of such structures is time consuming and difficult. Cost-effective and economical maintenance of fastened aircraft structures could be achieved by applying a suitable structural integrity monitoring (SIM) method.

An example of this application is shown in Fig. 12.10 for an aluminum test panel that was a 1/4 in. thick (6.3 mm), 3×4 ft (0.9 m $\times$ 1.2 m) aluminum

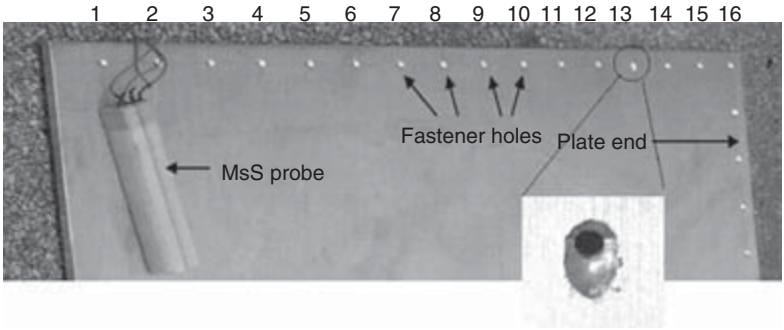

12.10 Configuration of test panel and laboratory MsS probe and photograph of fastener hole showing simulated corrosion.

plate and had a large number of 1/4 in. (6.3 mm) diameter tapered fastener holes along two edges of the plate. The center of each hole was located at approximately 1 inch (25.4 mm) from the edge of the plate, and the distance between the centers of the adjacent holes was approximately 3 in. (76.2 mm). As the simulated corrosion was increased from approximately 0.05 in. (1.3 mm) on the side to 0.2 in. (5 mm) on the side, the monitoring showed that the changes in the corrosion could be detected and monitored, as illustrated in the data shown in Fig. 12.11.

12.2.5 Infrared thermography

Infrared thermography is an NDE tool that images a range of the infrared spectrum given off by a component that is heated. The imaging technology is most useful to detect thermal radiation differences in a component. For example, in the case where a component might have wall thickness changes caused by corrosion or erosion, discontinuities in solid materials can change the heat flow condition, which can result in the fluctuation of the temperature on the surface of the materials. Both infrared testing and thermal image testing use this principle to measure the change of the surface temperature and then to deduce the discontinuity condition in the materials. Care must be taken to properly register images that are periodically collected. This technology has been applied to high-temperature and high-pressure pipelines used in petrochemical plants and power stations. Infrared thermography techniques have advantages over some other NDE technologies because a full-field image is obtained very quickly and there is no harmful radiation required and no contact with the part under inspection.

In the aspect of NDT for industrial equipment, infrared thermography testing is applied to operation condition monitoring of electrical equipment, power plant machinery, and high-temperature equipment.[29–38] Though

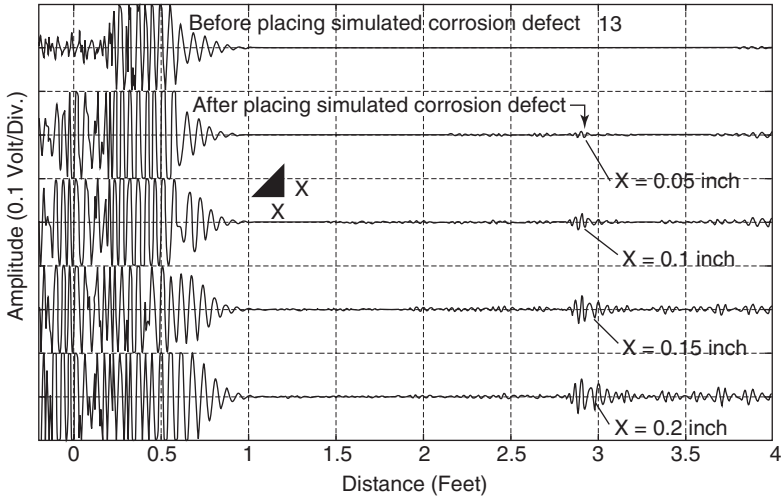

12.11 Monitoring data showing the defect signal increasing as the simulated corrosion increases from no corrosion to 0.2 in. by 0.2 in. (5.1 mm × 5.1 mm) by approximately 0.05 in. (1.3 mm) deep.

metals have very high thermal conductivity and detection of wall loss defects for steel pipes by use of infrared thermography has been difficult, this work has shown that wall thinning can be detected. An example of this was the work by Shen[29] in which a series of infrared thermography experiments were performed for four kinds of stainless steel and carbon steel pipes during heating and cooling. The pipes had different size holes drilled on inner surfaces. The experiments were performed using the TVS-2100 Thermal Video System. The infrared camera head of this system is an optically mechanical scanning type. The detector is InSb with 10 × 10 cell arrays. The detecting wavelength is about 3 to 5.4 μm. The operating range of temperature is about –40 °C to 950 °C. The minimum detecting temperature difference is 0.1 °C at 30 °C, and the sensitivity is 0.01 °C. The field of view is 10° (V) = × 15° (H). The field resolution is 2.2 mrad. The images were taken at 30 frames per second. For the test, steam at a temperature of 150 °C was passed through the pipe to heat from normal temperature. The thermal images of the defects obtained are shown in Fig. 12.12.

This work showed that thermography can be used to detect and monitor corrosion if a thermal gradient can be observed. In many cases, the components being monitored are at a thermal equilibrium, and for these cases, thermography may not be the best approach. However, under the conditions of thermal gradient, the technique is sensitive to small defects. Furthermore, a number of factors affect the potential capability of thermography such as:

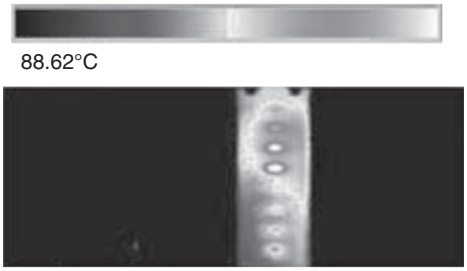

(b) (Φ15, Φ10) X (20%, 40%, 60%, 80%)

12.12 Infrared image of pipe with simulated corrosion defects.

1. The thermal conductivity of materials is a key factor affecting the sensitivity of infrared thermography. The lower the thermal conductivity, the higher the sensitivity and the longer the duration of defects emerging.
2. The shape and size of defects is another key factor affecting the sensitivity of infrared thermography. The larger the area of defect, the higher the sensitivity of wall loss.
3. The thickness is also a key factor affecting the sensitivity of infrared thermography. The thicker the material, the lower the testing sensitivity, but the longer the duration of defects emerging.

12.3 Future trends

The industry will tend to use monitoring technologies that leave the inspection sensors in place and to retrieve data as required. To achieve this goal, monitoring technologies will have to incorporate wireless communication technologies so that sensors can be left on a component and be queried at an appropriate time by a base control station. This will require that the sensors and associated instrumentation be inexpensive yet effective. This also will require computerized data acquisition and analysis systems that autonomously detect and analyze acquired data and alert the plant operators when a defect is determined to be growing and possibly heading toward ultimate failure. This is, in effect, diagnosis.

Further, the monitoring technology will be required to handle the operational environment. In most cases, the components that encounter significant corrosion issues are operated at temperatures around 150 °C to 650 °C. Only a few sensor technologies can continually operate at temperatures above 250 °F.

The ultimate trend is to head toward prognosis. This means that the monitoring data have been fed into the diagnosis system to determine the condition of the component and then the results of the diagnosis put into the prognosis system to determine the remaining life of the component being inspected. Prognosis will incorporate the present condition of the part

determined by the monitoring system with the expected operational conditions that the component will be subjected to and, with the understanding of how the material behaves under that operational condition, predict remaining life of the component. Work has been reported[39–42] primarily in high-value components like aircraft rotors and blades. Work[41] has been completed demonstrating that MsS technology, when used in a thin-film, multilayer format, has potential for use in the harsh thermal environments encountered in jet engines.

Although more work and more collaboration between sensor and material technologies is needed, it appears that the ability to continually monitor high-value components during operation will be available in perhaps five years. This means that periodic inspection requiring shutdown of a plant operation may be a thing of the past.

More information can be obtained primarily from the internet as well as the American Society of Nondestructive Testing. The following websites can provide additional information: www.swri.org; www.rtd.nl; www.asnt.org; www.pacndt.com; www.ewi.org; www.statoil.com; www.ndt.net.

See also Roderic K. Stanley, Patrick O. Moore, and Paul McIntire (eds), *Nondestructive Testing Handbook, Volume 9*, 'Special Nondestructive Testing Methods,' American Society for Nondestructive Testing, 1995.

12.4 References

1 M. B. Hoppenbrouwers, 'Advanced Ultrasonic Methods for In Service Condition Assessment of Industrial Process Installations,' Röntgen Technische Dienst BV, Rotterdam, http://www.rtd.nl.
2 P. T. Cole and S. N. Gautrey, 'In-Service Testing and Monitoring of Process Plant,' *2nd MENDT Proceedings*, *NDT.net*, 9 (6), June 2004.
3 Ø. Baltzersen, A. Solstad, A. Daaland and J. K. Holberg, 'Multichannel Ultrasonic Monitoring of Corrosion on Subsea Pipelines', NDT.net, 10 (6), June 2005, http://www.ultrasonic.de/article/v10n06/baltzers/baltzers.htm.
4 T. Goyen, 'Conformable Array for Characterization of Surface Corrosion,' *Proceedings of ASNT 14th Annual Research Symposium*, Albuquerque, NM, 14–18 March, 2005.
5 M. A. Robers and R. Scottini, 'Pulsed Eddy Current in Corrosion Detection,' *Proceedings of 8th ECNDT*, Barcelona, June 2002.
6 A. Yonezu, H. Cho and M. Takemoto 'Monitoring of Stress Corrosion Cracking in Stainless Steel Weldments by Acoustic and Electrochemical Measurements,' *Meas. Sci. Technol.* 17, 2447–2454, doi:10.1088/0957-0233/17/9/011, 2006.
7 A. D. Zdunek, D. Prine, Z. Li, E. Landis and S. Shah, 'Early Detection of Steel Rebar Corrosion by Acoustic Emission Monitoring,' Paper No. 547, *CORROSION95*, the NACE International Annual Conference and Corrosion Show© 1995 by NACE International.
8 M. Huang, L. Jiang, P. K. Liaw, C. R. Brooks, R. Seeley and D. L. Klarstrom, 'Using Acoustic Emission in Fatigue and Fracture Materials Research,' *JOM*, 50 (11) (November 1998).

9 A. Almeida and E.V. K. Hill, 'Neural Network Detection of Fatigue Crack Growth in Reveted Joints Using Acoustic Emission,' *Mat. Eval.*, 53 (1), 76–82, 1995.
10 J. Baram, 'Fatigue-Life Prediction by an Order Statistics Treatment of Acoustic-Emission Signals,' *Exper. Mech.*, 33, 189–194, 1993.
11 B. A. Barna, J. A. Johnson, and R. T. Allemeier, 'Determination of Acoustic-Emission Sites Using a Digital Nondestructive-Evaluation Workstation,' *Exper. Mech.*, 28, 210–213, 1988.
12 S. Barre and M. L. Benzeggagh, 'On the Use of Acoustic Emission to Investigate Damage Mechanisms in Glass-Fibre-Reinforced Polypropylene,' *Comp. Sci. and Tech.*, 52, 369–376, 1994.
13 R. B. Clough, J. C. Chang and J. P. Travis, 'Acoustic Emission Signatures and Source Microstructure Using Indentation Fatigue and Stress Corrosion Cracking in Aluminum Alloys,' *Scripta Met.*, 15, 417–422, 1981.
14 J. E. Coulter, S. Gehl, J. R. Scheibel and D. M. Stevens 'Acoustic Emission Monitoring of Fossil-Fuel Power Plants,' *Mat. Eval.*, 46, (2) 230–237, 1988.
15 D. Fang and A. Berkovits, 'Fatigue Design Model Based on Damage Mechanisms Revealed by Acoustic Emission Measurements,' *Trans. of ASME*, 117, 200–208, 1995.
16 K. F. Graff, *Wave Motion in Elastic Solids* (Columbus, OH: Ohio State University Press, 1975).
17 S. Yuyama, 'Fundamental Aspects of Acoustic Emission Applications to the Problems Caused by Corrosion,' in *Corrosion Monitoring in Industrial Plants Using Nondestructive Testing and Electrochemical Methods,* eds. G. C. Moran and P. Labine ASTM STP 908, (Philadelphia, PA: *ASTM*, 1986), pp. 43–74.
18 M. Redwood, *Mechanical Wave-Guides, The Propagation of Acoustic and Ultrasonic Waves in Fluids and Solids with Boundaries* (New York: Pergamon, 1960).
19 J. L. Rose, *Ultrasonic Waves in Solid Media*, (Cambridge: Cambridge University Press, 1999).
20 M. G. Lozev, R. W. Smith and B. B. Grimmett, 'Evaluation of Methods for Detecting and Monitoring of Corrosion Damage in Risers,' *Journal of Pressure Vessel Technology*, 127, 3, 244–254, August 2005.
21 D. N. Alleyne, B. Pavlakovic, M. J. S. Lowe and P. Cawley, 'Rapid Long-Range Inspection of Chemical Plant Pipework Using Guided Waves,' *15th World Conference on NDT*, Rome 2000.
22 H. Kwun, S. Y. Kim and G. M. Light, 'Development of a Torsional Guided Wave Probe for Heat Exchanger Tube Inspection,' Paper Summaries for the ASNT Fall Conference, Las Vegas, NV, 15–19 November 2004, pp 71–73.
23 G. M. Light, H. Kwun, S. Y. Kim and R. L. Spinks, 'Health Monitoring for Aircraft Structures,' *Mat. Eval.* 61 (7), pp. 844–847, 2003.
24 G. M. Light, H. Kwun, S. Y. Kim and R. L. Spinks, 'Deeply Probing,' *World Pipelines*, May 2003.
25 H. Kwun, S. Y. Kim and G. M. Light, 'The Magnetostrictive Sensor Technology for Long-Range Guided Wave Testing and Monitoring of Structures,' *Mat. Eval.* 61 (1), 80–84.
26 G. M. Light, H. Kwun, S. Y. Kim and R. L. Spinks, 'Magnetostrictive Sensor Technology for Monitoring Bondline Quality of and Defect Growth Under Adhesively Bonded Patches on Simulated Wing Structure,' *Proceedings of the Aging Aircraft Conference*, San Francisco, CA, 16–19 September, 2002.
27 H. Kwun, G. M. Light, S. Y. Kim, R. H. Peterson and R. L. Spinks, 'Permanently

Installable, Active Guided-Wave Sensor for Structural Health Monitoring,' *Proceedings of Structural Health Monitoring Conference*, Paris, France, 10–12 July, 2003.
28 H. Kwun, G. M. Light, S. Y. Kim, C. J. Schwartz, C. P. Dynes and R. L. Spinks, 'Cost Effectiveness of Magnetostrictive Sensor Technology for Inspection of Corrosion Under Insulation,' *Proceedings of the 1st Middle East Nondestructive Testing Conference & Exhibition*, 24–26 September, 2001, Bahrain, pp. 79–92.
29 G. Shen and G. Chen, 'Infrared Thermography Test for High Temperature Pressure Pipe,' 10th APCNDT, Brisbane, Australia.
30 X. Maldague (ed.), *Nondestructive Testing Monographs and Tracts, Volume 7*, *Infrared Methodology and Technology*, (New York: Gordon and Breach Science Publishers, 1994).
31 R. K. Stanley, P. O. Moore and P. McIntire (eds), *Nondestructive Testing Handbook, Volume 9*, *Special Nondestructive Testing Methods*, (Columbus, OH: American Society for Nondestructive Testing, 1995).
32 T.-M. Liou, C.-C. Chen and T.-W. Tsai, 'Heat Transfer and Fluid Flow in a Square Duct with 12 Different Shaped Vortex Generators,' *Transactions of the ASME. Journal of Heat Transfer*, 122 (2), 327–335, May 2000.
33 R. N. Wurzbach and D. A. Seith, 'Infrared Monitoring of Power Plant Effluents and Heat Sinks to Optimize Plant Efficiency,' *Proceedings of SPIE – The International Society for Optical Engineering Thermosense XXII*, 24–27 April, 2000, Orlando, FL, USA.
34 R. Rozenblit, M. Simkhis, G. Hetsroni, D. Barnea and Y. Taitel, 'Heat Transfer in Horizontal Solid-liquid Pipe Flow,' *International Journal of Multiphase Flow*, 26 (8), 1235–1246, 2000.
35 S. Yamawaki, T. Yoshida, M. Taki and F. Mimura, 'Fundamental Heat Transfer Experiments of Heat Pipes for Turbine Cooling,' American Society of Mechanical Engineers (Paper), *Proceedings of the International Gas Turbine & Aeroengine Congress & Exposition*, 2–5 June, 1997, Orlando, FL, USA.
36 Y. Qin and N. Bao, 'Thermographic Nondestructive Testing Technique for Delaminated Defects in Composite Structure,' *Proceedings of SPIE – The International Society for Optical Engineering Thermosense XVII*, 1995, Orlando, FL, USA.
37 K. R. Maser and M. S. Zarghamee, 'Leakage Evaluation of a Buried Aqueduct,' *Proceedings of the Specialty Conference on Infrastructure Condition Assessment*, 25–27 August, 1997, Boston, MA, USA.
38 X. Maldague, 'Pipe Inspection by Infrared Thermography,' *Mat. Eval.*, 57 (9), 899–902, 1999.
39 J. M. Larsen and L. Christodoulou, 'Integrated Damage State Awareness and Mechanism-Based Prediction,' *Journal of Metals*, TMS, March 2004, p. 14.
40 L. Christodoulou and J. M. Larsen, 'Using Materials Prognosis to Maximize the Utilization Potential of Complex Mechanical Systems,' *Journal of Metals*, TMS, March 2004, pp. 15–19.
41 S. J. Hudak, Jr., M. P. Enright, R. C. McClung, H. R. Millwater, A. Sarlashkar and M. J. Roemer, 'Potential Benefits of Adding Probabilistic Damage Accumulation to Prognosis of Turbine Engines Reliability,' SwRI Final Report to AFRL/DARPA , Contract No. F33615-97-D-5271, 30 June 2002.
42 S. J. Hudak, Jr., B. R. Lanning, G. M. Light, J. M. Major, J. A. Moryl, M. P. Enright, R. C. McClung and H. R. Millwater, 'The Influence of Uncertainty in Usage and Fatigue Damage Sensing on Turbine Engine Prognosis,' *TMS (The Minerals, Metals & Materials Society)*, 157–166, 2005.

13

Hydrogen flux measurements in petrochemical applications

FRANK DEAN, Ion Science Ltd., UK

13.1 Introduction

The movement of mobile atomic hydrogen through steel, known as hydrogen permeation, is a pre-requirement for most types of hydrogen damage, including hydrogen induced cracking (HIC), stress oriented hydrogen induced cracking (SOHIC), sulfide stress cracking (SSC) and disbonding. Hydrogen emanating from the external or *exit* face of a pipe or vessel is known as *hydrogen flux*. Flux measurements provide information relating to cracking risk, and also to the causes of hydrogen permeation. Specifically, hydrogen permeation may be caused by the formation of hydrogen on a steel surface due to some corrosive process, or dissolution of hydrogen into steel at the high temperatures encountered in steel manufacture, milling or welding, or due to release of trapped hydrogen in traps in the steel upon high temperature excursions, as in hydrogen bakeouts. The objective in this chapter is to define the particular circumstances conducive to hydrogen permeation through steel, and provide the means to relate hydrogen flux to hydrogen damage risk, and rate of corrosion, where appropriate.

13.2 Scenarios leading to hydrogen permeation and detection

The progress of hydrogen to a flux detector on the external surface of a steel pipe or vessel face involves essential, sequential steps:

1. Active corrosion causing hydrogen to enter steel
2. Sufficient permeability of hydrogen in steel for flux to pass through it
3. Permeability of hydrogen through external surface oxides and coatings
4. Adequate measurement tool, operating and being used correctly

Certain flux measurement tools require surface coatings to be removed in order to operate correctly. Then, step 4 is critical, and step 3 is not rele-

Table 13.1 Required conditions for the existence of a hydrogen flux in typical industrial scenarios. *CP = cathodic protection

Temperature, °C	**(A)** Hydrogen source	**(B)** Permeable alloys	**(C)** Permeable coatings
0 to 120	H_2S, amine, NH_4HS / HCN and HF[1,2] corrosion. CP.*[3] Electroplating.	<5% alloy ('carbon' or 'mild' steel)	Most,[7] not zinc.
80 to 200	Severe acid corrosion e.g. acetic.	<10% alloy	Uncoated. Depending on temperature, alloy oxides present a partial barrier to permeation.
200 to 300	Protonic corrosion, e.g. naphthenic acid[4–5] . . .	<13% alloy	
300 to 400	. . . also H from traps in pre-weld H bakeouts[6]	All non-austenitic	
400+	H from steam, grease etc. in high T steel forming	All steels	
From 1540	H in molten steel (e.g. welds, any H source)		

vant. For the purposes of this discussion we assume an adequate and correctly deployed tool (4), which does rely upon spontaneous flux exit from the steel surface. Hydrogen more freely permeates steel as the temperature increases, so conditions for flux measurements are nicely defined in terms of temperature, as shown in Table 13.1.

Table 13.1 shows distinct trends with temperature. At low temperatures (less than 100 °C), hydrogen flux sources are restricted to a few 'hydrogen promoters', almost exclusively encountered in petrochemical operations upon corrosion of mild steel. At higher temperatures, hydrogen flux may occur as a consequence of corrosion involving naphthenic acid[4–5] or acidic salts[8] – it does not depend so crucially upon the presence of hydrogen promoters. Molten steel will uptake hydrogen from any hydrogen source. The reason for this trend is that the movement of hydrogen through steel is more facile as the temperature increases:

(a) Internal barriers (e.g. corrosive scale) are less prone to prevent hydrogen access to the steel surface
(b) the kinetic barrier to hydrogen dissolution is more easily overcome
(c) the solubility of hydrogen, S, and diffusivity of hydrogen, D, through steel increase markedly with temperature of all steels, hence more alloys permeate a significant flux as temperature increases, step 2, Table 13.1
(d) less hydrogen is retarded or permanently trapped in traps, voids or pre-existing blisters as the temperature increases.

For steel walls of greater than a few millimetres in thickness,[9–10] a well defined corrosion activity at an entry face will generate a steady state flux through steel inversely proportional to its thickness. Further, the time required for hydrogen to establish a steady state steel increases as the square of thickness: At 300 °C (750 °F) ½ in. (1.3 cm) thick steel requires less than an hour for flux to reach 90% of its steady state value following a step increase in hydrogen entry at the inside face; 2 in. (5 cm) steel will require half a day. At 20 °C (68 °F) the corresponding times are about 16 h and a week respectively. This time delay precludes the use of flux measurements on thick (>1 in.) cold (<30 °C) steel, particularly if the interest is in using flux to discern hydrogen damage episodes lasting less than a day.

13.3 A measurement of hydrogen activity based on flux measurement

As indicated above, the hydrogen efflux emanating from steel is influenced by both temperature and thickness. Thus it is preferable to 'normalise' flux measurements for steel temperature and thickness, to obtain a more universally comparable parameter indicating HIC risk and corrosive action. It is also desirable for this normalised parameter to have some physical meaning. The activity of hydrogen in steel, $\boldsymbol{a}$, is defined by $\boldsymbol{a} = c/c^0$, where c^0 is the solubility of hydrogen in steel in equilibrium with H_2 gas at 7 bar. Solubility varies with H_2 pressure p according to $c = c^0.\, p^{1/2}$. Thus the hydrogen activity $\boldsymbol{a}$ corresponds to an equivalent equilibrium H_2 gas pressure of $\boldsymbol{a}^2$ bar: because it is dissolved in a solid – it is an equivalent pressure of gaseous hydrogen that would dissolve at equilibrium. At the hydrogen entry (internal, reaction) face, $\boldsymbol{a}_0$, which drives through wall permeation, is the parameter of choice. Physically, $\boldsymbol{a}_0$ is an equivalent hydrogen gas pressure which would be in equilibrium with hydrogen concentration at the entry face necessary to deliver the measurable flux at the exit face. Severe corrosion from a hydrogen promoter is studied, for example by Mishael *et al.*[11] A solution saturated with 1 bar H_2S at 20 °C, can generate $\boldsymbol{a}_0$ values exceeding millions of bar hydrogen equivalent (100s GPa). Flux-thickness-temperature conversion to $\boldsymbol{a}_0$ is obtained from the equation $J_{ss} = P\boldsymbol{a}_0/\boldsymbol{w}$, where J_{ss} is the steady state flux, P the steel permeablity and $\boldsymbol{w}$ the steel thickness. P values are obtained from Grabke and Reicke[12] using the McNabb model[13] developed therein. This can be compared with a typical Young's modulus for 200 Gpa steel. Not surprisingly, it is feasible for atomic hydrogen in steel, associating within steel defects, to form blisters and cracks. Thus activity $\boldsymbol{a}_0$ is a direct measure of the crack susceptibility of a corrosion scenario causing a hydrogen flux.

Table 13.2 Typical calculated hydrogen activities for a number of scenarios, compared with the Young's modulus or mild steel

Scenario	Typical flux (at typical temp.)	Activity / bar hydrogen	Comments
15 atm. H_2S	7335 (30 °C)	9 100 000	50 cm dia 8.7 mm wall line pipe. Mn 1.0. Ni flash Dev. Cell[14*]
NACE TM0284 (H_2S 1 bar, pH 2.7 buff.)	2100 (20 °C)	2 500 000	16 mm A516 steel[11]
0.1 mm/yr sour corrosion, <50 °C, typical	120 (20 °C)	6 500	Probably dependent on scale type. Caution co-corrodants
MRO175 'sour' threshold (>0.03 bar)	80 (20 °C)	2 200	Based on NACE MR0175 definition of sour service,[15] without low-pressure cut-offs
1 ppm H in ferritic steel, deemed to require PWHT	–	40 000	Assumes S = 5 ppb at ambient temperature
0.1 mm/yr nap. acid corrosion, typical	200 (250 °C)	0.5	Limited data
Ferritic steel Young's modulus, typical	–	2 000 000	=200 GPa

*Devanathan cell, PWHT – postweld heat treatment.

Hydrogen activities are shown in Table 13.2 for typical scenarios in which hydrogen in mild steel is of critical interest. At present there is little reliable hydrogen permeation data available in the literature. However, the data from Grabke and Riecke from which the values in Table 13.2 are derived is authoritative, and show a few 10s per cent of variation of P between low alloy steels. Interestingly, corresponding D values vary much more, typically ten-fold. Increased trapping in steels causes the solubility S of hydrogen in steel to vary in inverse proportion. Permeability $P = D.S$, so P is fairly invariant. Figure 13.1 provides a graphical means by which flux and steel thickness may be used to determine activity $\boldsymbol{a}_0$.

There are several flux sensing technologies that have been used in recent decades, based on the sensing of the hydrogen located at, or exiting from, the steel surface. Figure 13.2 shows kit employing the 'hydrogen collection method', in which hydrogen is swept up in an air stream from the surface of steel, and through a capillary into a remote hydrogen analyser.

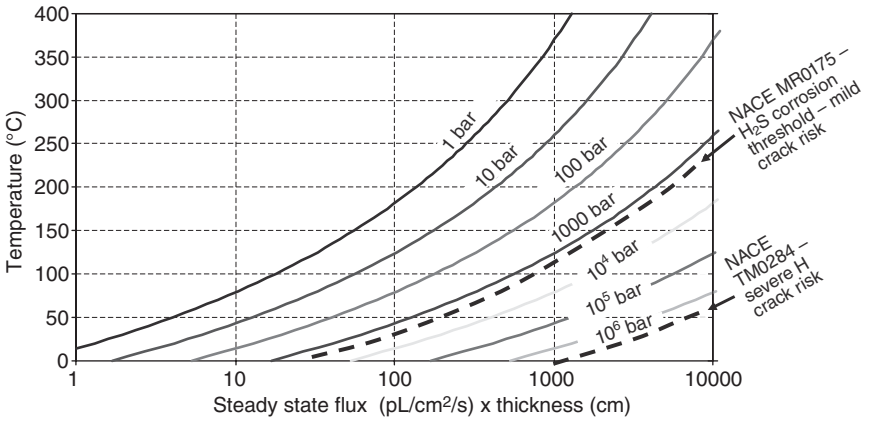

13.1 Plot flux-thickness versus mild steel temperature which can be used to estimate hydrogen activity.

13.2 A commercial hydrogen flux probe (Hydrosteel® 6000, AT-S, Ion Science Ltd, UK). An analyser is attached to the central capillary and air drawn through it as described in the text. The probe, about 6 in. (15 cm) diameter, is flexible and can tolerate steel temperatures to at least 500 °C. Photograph courtesy Ion Science Ltd, UK.

13.4 Comments pertaining to particular flux measurement applications

13.4.1 Using flux to assess hydrogen damage risk

Hydrogen damage is never acceptable and rarely anticipated. The strategy is generally to prevent hydrogen damage, as its occurrence is sometimes catastrophic. It is usually associated with severe sour corrosion. Field applications of flux monitors in the assessment of crack risk are therefore chiefly confined to monitoring equipment with a chronic history of unremediable hydrogen damage, and to determining the effectiveness of process or corrosion control measures intended to mitigate that damage. Laboratory measurements of flux are extremely valuable in assessing hydrogen damage risk and its remediation.

There is a substantial literature on critical concentrations, c_{crit}, at which hydrogen causes steel cracking. The variance of solubility of hydrogen in steel, S, discussed above, as well as the common method of using thin membranes in Devanathan cells to derive the data (from steady state flux and inferred values of D from flux transients) prevent confident comparisons between c_{crit} values. A critical hydrogen activity at which steel cracks, $\boldsymbol{a}_{crit}$, is much to be preferred as a 'stand alone' measure of crack susceptibility. Using Fig. 13.1 to obtain activity from flux, thickness and temperature, 10^6 bar is considered sufficient activity to initiate damage in crack susceptible steels; 10^4 bar is a risk to poor steels.

However, it should be remembered that the activity conversion assumes steady state hydrogen diffusion through the steel; damage can occur before an appreciable flux exits a steel. Very poor, and previously damaged, steels will not even deliver a substantial hydrogen flux when exposed to hydrogen charging a corrodant, because most hydrogen is taken up by the steel. *Any* activity – any hydrogen flux – is probably symptomatic of damage to steel which is already micro-delaminated due to historical hydrogen damage. Further, flux measurements on large blisters tell us more about the pressure (activity) of hydrogen in the blister than at the entry face behind it.

Activity $\boldsymbol{a}_0$ is derived from the permeability P of hydrogen in steel, which is equal to the product of diffusivity D and solubility S. Since both D and S increase rapidly with temperature, so does P. Thus steel is thousands of times more permeable to hydrogen at say 300 versus 30 °C. Not surprisingly, hydrogen damage at temperatures exceeding 100 °C is rare. Correspondingly, diffusible hydrogen in steel in service at high temperatures needs to be allowed to diffuse away before the steel is cooled, lest it increase too much in activity. The use of flux monitoring in this area is likely to increase with increasing acceptance of fieldworthy flux measurement tools.

13.4.2 Hydrogen bakeouts

Prior to welding steel which may have been subject to hydrogen charging by one of the sources cited in Table 13.1, it is often deemed necessary to raise the steel temperature (typically to 350 °C) for a number of hours (typically 2–48 h, depending on the steel type and thickness) to 'bake out' hydrogen which may have become entrapped in the steel. Otherwise, during welding, the hydrogen content of the parent steel is liable to concentrate at the weld's heat affected zone, causing hydrogen cracking. About 1 ppm hydrogen is often considered an upper acceptible threshold for diffusible hydrogen content of the steel at the elevated temperature. Fick's First Law of Diffusion states that flux

$$J = D.\mathrm{d}c/\mathrm{d}x \qquad [13.1]$$

During hydrogen bakeouts, the hydrogen concentration gradient, $\mathrm{d}c/\mathrm{d}x$, at the steel face is expected to be greater than anywhere in the steel interior at all times while the flux is decreasing from its maximum value. It is possible to conservatively cite a critical, decreasing flux during bakeout as indicating that the steel contains negligible hydrogen. For mild steel at 350 °C and <5 cm thickness, the flux is estimated at 500 pL/cm^2/s. This flux provides a real time criterion for extending the time of hydrogen bakeout if necessary, whereby prospective weld damage can be avoided. Correspondingly, if a flux fails to reach, or decreases to below, the threshold flux, the bakeout may be curtailed, and the repair schedule re-adjusted, whereby the product downtime is shortened.

Steel which has been in high temperature service is occasionally retained at temperature after service, to allow hydrogen in the steel to escape before cooling, sometimes forcibly, under nitrogen. It is possible to forecast a 'safe' flux threshold below which the steel may be safely cooled. However, this application of flux monitoring is not reported to date in the literature.

13.4.3 Using flux to indicate corrosion by sour gas and related species

The most well known conventional cause of hydrogen flux through steel is corrosion by sour gas (H_2S) condensate in pipes and vessels, in both upstream and downstream petrochemical equipment. Different sulfide scales form on steel as a result of sour gas corrosion of steel, depending on sour gas concentration, co-corrodants, pH, ambient temperature and steel composition. In most cases, it is likely that both the corrosion, and corrosion induced flux, are completely suppressed by scales. However, since some of the scales formed are semiconducting (in particular, pyrrhotite),[16] thereby providing a means of electrochemical hydrogen formation, not on the steel, but on a

scale through which atomic hydrogen migration is unlikely, it is probably best not to assume that the correlation of hydrogen flux with corrosion obtained in one sour corrosion scenario is applicable in another.

To be sure, sour corrosion is more episodic than is commonly supposed, and generally, successful deployment of a flux tool depends on the experience of the operator in knowing where and when to use it, particularly as a near real time indicator of sour corrosion, and its control. Flux measurements on sour systems are most valid:

- where there is a history of hydrogen damage
- where inhibitors of corrosion of steel are deemed to be effective
- where corrosion is known to be episodic due to modification, removal or dissolution of scale, as a consequence of pH change, oxygen, cyanide or erosion (the latter particularly in relation to ammonium bisulfide corrosion).

Because the permeability of steel is very temperature sensitive, any attempt to correlate flux with corrosion rate will benefit from conversion of flux to activity, as described above. A more approximate method is simply to compensate for thickness, by multiplying a flux reading (in pL/cm^2/s) by thickness (in cm), to obtain readings in pL/cm/s. Field flux due to sour corrosion rarely exceeds 1000 pL/cm/s and values of 10s of pL/cm/s are much more common in the field (cf. values in Table 13.1), typically indicative of corrosion rates of about 0.1 mm/y (a few mil/y).

13.4.4 Using flux to indicate corrosion by HF acid

Flux from steel in HF acid alkylation units is more substantial than from sour systems, and more long-lived. This is probably because iron fluoride scales are more soluble and less passivating than sulfide scales. Also, HF corrosion is much less variant than sour corrosion, occuring as it does in a much more well defined product stream. It is generally not mitigated by inhibitors.

As above, conversion to hydrogen activities is advisable if readings from different sites are to be compared. Flux-thickness of a few 100 pL/cm/s are quite typical, probably indicative of a few tenths of mm/y (about 10 mil/y).

13.4.5 'Naphthenic acid' and sulfidic corrosion

Naphthenic acid is the generic name given to cyclic carboxylic acids produced from 'acid crude', obtained from deeper, more ancient oil deposits. Sulfidic corrosion is attributed to sulfur compounds, also particularly prevalent in more newly producing wells. The acids concentrate in distillation column sidecuts at temperatures between approximately 250 and 400 °C

(480 and 750 °F). They are corrosive, generating carboxylic iron salts and hydrogen, which, due to the high temperature of the steel, is prone to diffuse through the wall sufficiently to deliver hydrogen flux[4,5] of up to a few thousand pL/cm^2/s. Thiols and hydrogen sulfide – present as a thermal breakdown product – react similarly to form hydrogen and sulfide salts.

Naphthenic acid corrosion is complicated by the plethora of different prospective compounds involved,[17] their respective temperature stability and solubility, and interaction with, for example, hydrogen sulfide.[18] Corrosion depends on the process stream sheer velocity, and therefore is prevalent at pipe elbows, where flux tools at the time of writing were not easy to deploy. As the service steel may not have been designed to sustain this corrosion, any monitoring technique is liable to be of interest. Flux measurement, as a near real time corrosion indicator, is very attractive. At the time of writing there is a strong commercial interest in this application for flux monitors. For all these reasons, data pertaining to flux measurements at high temperatures is limited in the public domain.

13.5 References

1 F.W.H. Dean, P.A. Nutty, M. Carroll, *Corrosion 2001*, paper 01636, NACE.
2 F.W.H. Dean, S.W. Powell, *Corrosion 2004*, paper 04472, NACE.
3 J. Woodward, R.P.M. Procter, R.A. Cottis, 'The Effect of Hydrostatic Pressure on Hydrogen Permeation', in '*Hydrogen Effects in Materials*' p 657 ed. A.W. Thomson, N.R. Moody, Minerals, Metals and Materials Soc., 1996.
4 F.W.H. Dean, *Corrosion 2002*, paper 0234, NACE.
5 F.W.H. Dean, S.W. Powell, *Corrosion 2006*, paper 06436, NACE.
6 C.N. Brown, M.J. Carroll, F.W.H. Dean, J.H. Harrison, A. Kettle, *Corrosion 2004*, Paper 04478, NACE.
7 R.D. Tems, A.L. Lewis, A.L. Abdulhadi, *Corrosion 2002*, paper 02345, NACE.
8 F.W.H. Dean, D.J. Fray, T.M. Smeeton, *J.Materials Sci. and Technol.*, 18 (2002), 851–855.
9 M.R. Bonis, J-L. Crolet, *Corrosion 2002*, paper 2036, NACE.
10 F.W.H.Dean, *Materials Sci. and Technol.*, 21(3) (2005), 347–351.
11 S.J. Mishael, F.W.H. Dean, C.M. Fowler, *Corrosion 2004*, paper 04476, NACE.
12 H.J. Grabke, E. Riecke, *Materiali in Tehnol.*, 34(6) (2000), 331–342.
13 A. McNabb, P.K. Foster, *Trans. Metallurg. Soc.*, AIME, 227 (1963), 618–627.
14 M. Shimitsu, M. Iino, M. Kimura, N. Nakate, K. Ume, 'Corrosion Control and Monitoring in Gas Pipelines and Well Systems', *Proc. of Corrosion/87 Symposium*, NACE, Houston, TX., 1989.
15 NACE MR0175/ISO 15156-1 International Standard, 'Petroleun and Natural Gas Industries – Materials for use in H2S-containing environments in Oil and Gas Production', NACE, 1st edition (2001).
16 J. C. Ward, *Rev. Pure and Appl. Chem.*, 20 (1975), 175–206.
17 E. Slavcheva, B. Shone, A. Turnball, *Corrosion 1998*, Paper 579, NACE.
18 R.D. Kane, M.S. Cayard, *Corrosion 2002*, San Diego, CA, Paper 02555, NACE.

14

Rotating cage and jet impingement techniques

SANKARA PAPAVINASAM, CANMET Materials Technology Laboratory, Natural Resources Canada, Ottawa, Ontario, Canada

14.1 Introduction

This chapter presents an overview of two laboratory methodologies that are generally used to simulate flow conditions of the field in the laboratory. The methodologies described are rotating cage and jet impingement. They are compact, inexpensive, hydrodynamically characterized, and scalable, i.e., can be used under various flow conditions. Using these methodologies several variables that influence the corrosion rate in the field can be simulated in the laboratory, e.g., compositions of material, composition of environment (gas and liquid), temperature, pressure and flow.

Equations are developed to characterize the flow in these methodologies. These equations are, however, developed based on some assumptions and approximations. In view of these approximations these equations should be used with caution. The geometry of the apparatus including vessel length and diameter, sample holder length (and, as a consequence, the sample length), diameter, rotation speed, volume of liquid, controls the flow pattern as well as the corrosion rates. Therefore all pertinent parameters should be carefully designed and recorded. This chapter also provides an approach to predict field performance based on the results obtained by these methodologies.

14.2 Rotating cage

14.2.1 History

In 1990, the rotating cage (RC) was introduced as a promising laboratory methodology, to simulate pipe flow in the laboratory by rotating the specimens at speeds up to 1500 rpm.[1–5] In the literature, rotating cage experiments are also reported as high-speed autoclave tests (HSAT)[6,7] or rotating probe[4,5] experiments. In 1999, the atmospheric pressure rotating cage was described, together with a systematic analysis of flow patterns.[8,9]

In the results of a study published in 2001, the rotating cage was identified as the preferred methodology for evaluating corrosion inhibitors.[10–14] This

assessment was based on a quantitative comparison of field and laboratory data on general corrosion rates, pitting corrosion rates and percentage inhibition (calculated from general and pitting corrosion rates) under three different field conditions using three continuous and three batch inhibitors. The rotating cage methodology was also identified as an inexpensive and relatively simple methodology to carry out.

In 2001, ASTM published a standard guide, ASTM G170, 'Evaluating and Qualifying Oilfield and Refinery Corrosion Inhibitors in the Laboratory'.[15] This Standard presents rotating cage as a compact, inexpensive, hydrodynamically characterized, and scalable (i.e., they can be carried out under various flow conditions) methodology. Using this methodology, several variables that influence inhibitor performance in the field can be simulated, including composition (of the steel, brine, oil and gas); temperature; pressure; and flow. In 2002, the application of the atmospheric pressure rotating cage for simultaneous determination of inhibitor efficiency and drag reduction properties of corrosion inhibitors was demonstrated.[16] In 2003, the influence of rotating cage geometry on the flow pattern and on the corrosion rate was published.[17] In 2006, ASTM published a Standard Practice ASTM G184, 'Evaluating and Qualifying Oil Field and Refinery Corrosion Inhibitors using Rotating Cage', which describes a procedure to conduct experiments using a rotating cage.[18]

14.2.2 Rotating cage apparatus

Figure 14.1 shows a schematic diagram of the rotating cage system. The vessel can be manufactured from acrylic or polytetrafluoroethylene (PTFE). At the bottom of the container, a PTFE base is snugly fitted. At the center of the PTFE base, a hole is drilled, into which the lower end of the stirring rod is placed. This arrangement stabilizes the stirrer and the coupons. Multiple coupons, typically eight (each of surface area 35.8 cm^2) are supported between two PTFE disks mounted 76 mm apart on the stirring rod of the autoclave. Holes are drilled in the top and bottom PTFE plates of the cage to increase the turbulence on the inside surface of the coupon. This experimental set-up can be used at temperatures up to 70 °C and rotation speeds up to 1000 rpm. For elevated pressure experiments an autoclave is used instead of acrylic or PTFE vessel.[8,9]

14.2.3 Flow characteristics of rotating cage

Before rotating cage experiments can be performed the hydrodynamic conditions of the cage should be understood. The flow characteristics of a rotating cage vary with cage dimensions, liquid levels, rotation speeds and liquid types. The flow pattern in the absence of rotating cage is similar to

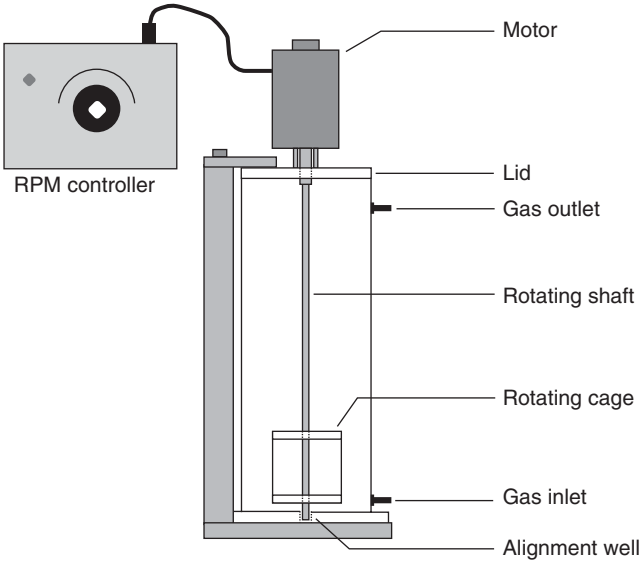

14.1 Schematic diagram of a rotating cage.

the flow pattern of the rotating cylinder electrode (RCE) because the experimental set-ups are similar. Under this condition the rotation of the shaft causes the fluid movement.

In the presence of a block, a vortex is formed whose dimensions (both length and width) increase with rotation speed until the width reaches the side walls of the container.

Blocks with larger diameter generally produce a larger vortex at the same rotation speed and volume (Fig. 14.2). Similarly blocks with longer length generally produce a larger vortex at the same rotation speed and volume (Fig. 14.3). In addition the position of the block also affects the flow pattern. As shown in Fig. 14.4, the higher the position of the block, the greater is its influence on the vortex at the same rotation speed and volume.[17]

Figure 14.5 presents the variation of vortex length with volume of liquid for a block and rotating cages containing coupons in two configurations, with aligned and non-aligned holes at 800 rpm. The dimensions, i.e., diameter (3.1 in. (8 cm)) and length (3.3 in. (8.5 cm)) of all three configurations are the same. In the aligned position, the holes drilled in the top and bottom PTFE plates were vertically aligned. In the unaligned case, the holes were separated by 180 degrees around the circumference of the cylinder. It can be seen from Fig. 14.5 that for the same length and diameter, at the same volume of liquid and at the same rotation speed, the vortex length decreases in the order: the cage with holes aligned > cage with holes un-aligned > solid block.

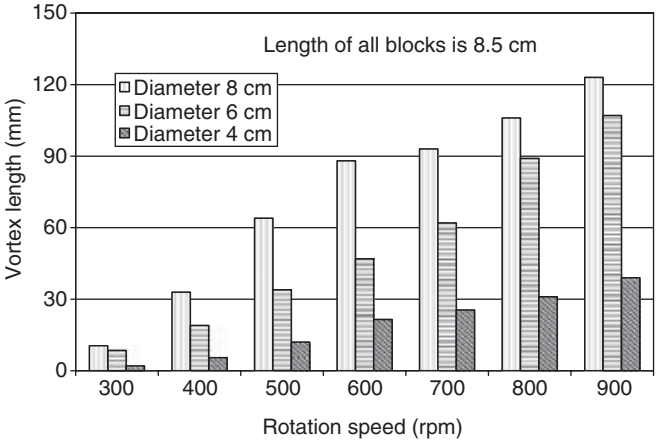

14.2 Variation of rotation speed with vortex length for various block diameters (solution volume 4 L).

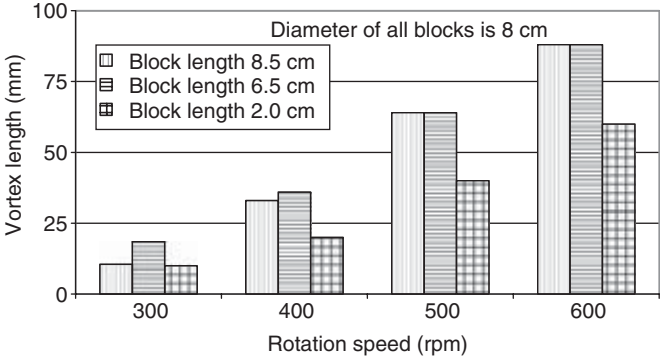

14.3 Variation of rotation speed with vortex length for various block lengths (solution volume 4 L).

The flow patterns of a rotating cage can be qualitatively divided into four zones:

Homogeneous zone:	Vortex dimensions length and width increase with rotation speed
Side-wall affected zone:	Vortex length increases but the width has reached the side and collides with the wall
Turbulent zone:	Vortex length penetrates into the rotating cage unit and creates turbulent flow
Top-cover affected zone:	The liquid level oscillates and rises to the top, pushing the flow pattern due to the backward movement of the fluids, and changing the flow pattern (the rate of vortex length increases at a lower rate)

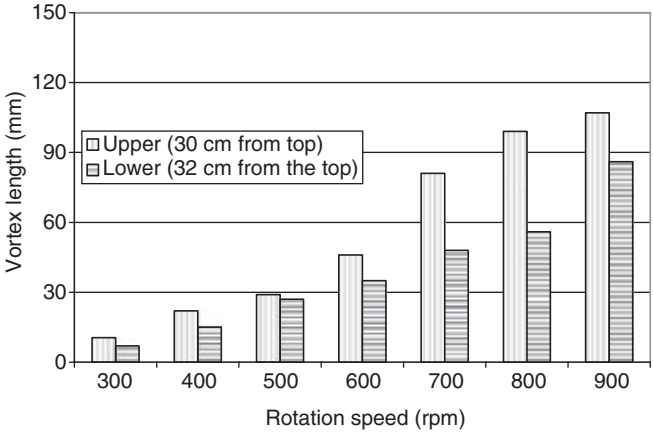

14.4 Effect of position of block 8 cm diameter and 6.5 cm long on the vortex length (solution volume 5 L).

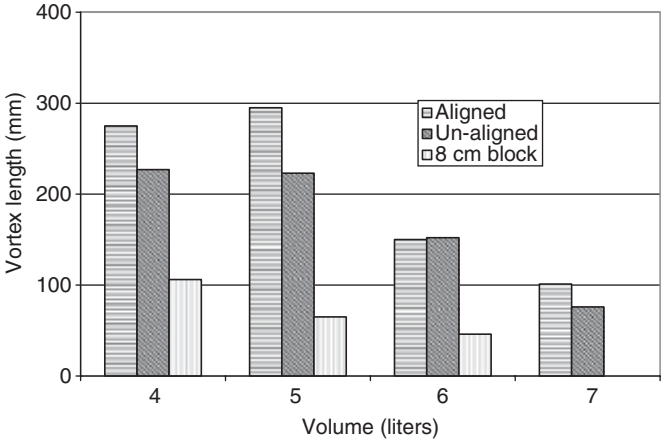

14.5 Effect of alignment of holes on flow pattern (800 rpm).

In the absence of a rotating cage, vortex formation does not occur. In the presence of a block of the same dimension as the RC, a vortex forms, and its dimensions increase with the speed of rotation. When the block is replaced with the rotating cage containing coupons, the flow pattern does not change significantly, but the vortex growth rate is high; i.e., under the same conditions, the vortex dimensions (length and width) increase at a higher rate with the rotating cage (containing multiple, e.g., eight coupons with gaps between them) than with the block (no gaps). The vortex dimensions depend on the fluid type and quantity. The fluid patterns in the homo-

geneous, side-affected and turbulent zones are similar, but the top-cover affected zone decelerates the vortex growth rate due to the motion of fluids in the opposite direction.

In all zones, except in the top-cover affected zone, the solution is dragged toward the coupons, due to the vortex formation, increasing the wall shear stress at least on the outer surface of the coupons. Based on the above observations, it can be assumed that the rotating cage wall shear stress (τ_{RC}) consists of two components of wall shear stress of the RCE, τ_{RCE} and wall shear stress caused by the movement of the solution resulting from vortex formation, τ_{vortex}.

Under most conditions, the slope of vortex length with rotation speed is about 3 mm/100 rpm. In order to account for the drag coefficient induced by the vortex the slope of the plots of vortex dimensions with rotation speed should be considered. As a first approximation, rotating cage wall shear stress can be calculated using Equation [14.1], which includes both τ_{RCE} and τ_{vortex}.[19]

$$\tau_{RCE} = 0.079\ Re_{RC}^{-0.3}\ \rho r_{RC}^{2}\ \omega^{2.3} \qquad [14.1]$$

where r_{RC} is the radius of the rotating cage, $Re_{RC}(=\omega r_{RC}^2/\nu)$ is the Reynolds number of rotating cage, ω is the angular velocity, and ν is the kinematic viscosity.

Equation [14.1] can be used to calculate the wall shear stresses in the homogeneous zone only. In the turbulent zone, the wall shear stress may be higher than predicted by Equation [14.1]; on the other hand, in the side-affected and top-cover affected zones, the wall shear stress may be less than predicted by Equation [14.1], because of the movement of a portion of the fluids in the opposite direction by the vortex driven flow. Local wall shear stresses at coupons in the rotated cage arrangement has been carried out using microelectrode arrays incorporated flush to the surface of plastic dummy probes.[20] A suitable redox couple, e.g., hexacyanoferrate, is used as a tracer system for the evaluation of local wall shear stresses from diffusion controlled electrochemical reaction.

The local wall shear stresses are strongly influenced by liquid viscosity. Highest wall shear stresses are encountered in the middle of the coupon close to the inner corner of the leading edge. The wall shear stresses at the outer corner of the leading coupon edge are roughly one-third lower than at the inner corner of the leading edge. In the middle of the outer coupon surface the maximum average wall shear stresses are roughly two-thirds less than at the inner corner of the leading edge. The highest wall shear stress at the outer coupon surface is close to the leading edge. The gradient of wall shear stresses between leading and trailing edge on the outer coupon surface is significant only at higher hydrodynamic viscosities. Vertically, the local wall shear stresses at the inner or outer corner of the leading coupon

edges exhibit a much smaller gradient. They are in the order of 10 to 20% of the local maximum value with little dependency on liquid viscosity.

Computational fluid dynamics (CFD) analysis indicates that the wall shear stress varies somewhat with time. The shear stress is generally higher on the leading edge compared to the trailing edge, and higher on the outer face compared to the inner face. On the leading edge, the shear stress is higher toward the inner face. On the trailing edge, the shear stress is higher toward the inner face. On the outer face, the shear stress is higher toward the trailing edge and on the inner face, the shear stress is higher toward the leading edge.[21]

The fluid dynamics lead to the shear stress distribution on the coupons. The highest speeds occur near the coupons, since they drive the flow. Relative variation in velocity leads to variation of shear stress. The flow speed past the coupon is low due to the fact that the coupons and the water are moving in the same direction. Another interesting feature of rotating cage flow is the complicated flow in the wake region following the trailing edge of the coupon; each coupon has a significant effect on the one that follows. The third feature to note is that the blunt leading edge presents a formidable obstacle to flow around the coupon. Finally, because the coupons are flat and rotating about a center, the ends of the coupon are traveling on a larger radius than the middle and are, therefore, moving faster. Relative to the flow of water moving in a circular path, the ends of the inner face are effectively moving away from the flow while the ends of the outer face are effectively moving toward the flow.

At the leading edge, the flow accelerates toward the inner face causing a higher shear stress toward the inner face. On the inner face, the flow impacts near the center of the coupon causing a higher shear stress. However, the end of this face is effectively moving away from the flow and, therefore, the flow is very slow toward the trailing edge causing a low shear stress. The opposite occurs on the outside face. The flow has to travel around the leading edge and, as a result, the flow is relatively slow along most of the outer face. As the flow approaches the trailing edge, which is moving fast and toward the flow, it accelerates and causes a higher shear stress. The flow is not able to penetrate the wake region behind the coupon so the shear stress is low on the trailing edge. Flow that does circulate back into the wake region comes from the outside face and flows back toward the inside face, causing the shear stress on the trailing edge to be higher near the inner face.

14.2.4 Simulation of general and localized corrosion

Rotating cage is an efficient tool to investigate the effect of flow on general corrosion rates. Figure 14.6 for example compares the general corrosion

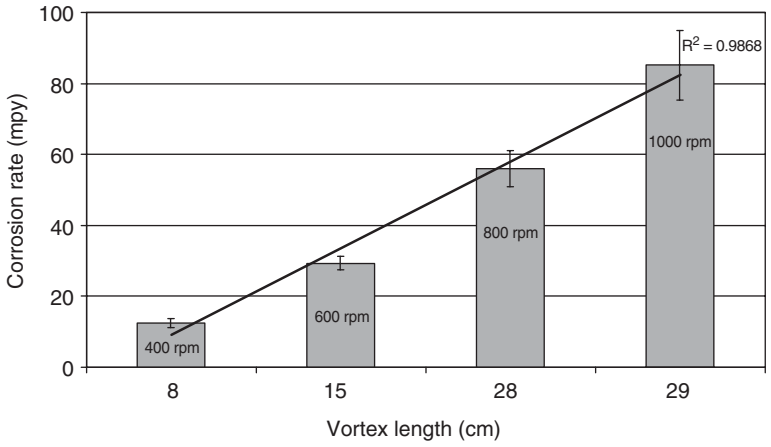

14.6 Relationship between the corrosion rate (mpy) and the vortex length (cm): 4 liters of solution with holes aligned. Note: 1 mpy = 0.025 mm/yr.

rate to the vortex length. As vortex length increases, i.e., rotation speed increases, the corrosion rate increases.

A study that compared the pitting corrosion rates of laboratory methodologies with those of field conditions found rotating cage to be an ideal methodology to simulate pitting corrosion. In this study, by comparing the results of the field and laboratory experiments at the same inhibitor concentrations, a preliminary ranking of test methodologies at each inhibitor concentration was developed. From these rankings, the cumulative ranking was deduced by summing the preliminary rankings. That study found that the RC test was the top-ranked laboratory methodology based on the comparison of laboratory and field general and pitting corrosion rates. This methodology produced higher pitting corrosion rates, and is a tougher test for the inhibitor to pass. Several inhibitors exhibited lower efficiencies when tested in this methodology.[19] The simulation of pitting corrosion in a rotating cage is due to the variation in the flow pattern on various sides of the coupons, as described in section 14.2.3.

14.2.5 Typical applications of rotating cage

Corrosion inhibitors

Selection of corrosion inhibitor for oil field and refinery applications involves qualification of corrosion inhibitors in the laboratory. Field conditions should be simulated in the laboratory in a fast and cost-effective manner. Oil field corrosion inhibitors should provide protection over flow

conditions ranging from stagnant to that found during typical production conditions. Not all inhibitors are equally effective over this range of conditions so it is important for a proper evaluation of inhibitors to test the inhibitors using a range of flow conditions. Because the rotating cage is relatively inexpensive and uses simple flat specimens that allow replicates to be run with each set-up it is widely used to evaluate corrosion inhibitors for oil-field and refinery applications. ASTM Standard Practice G184 and ASTM Standard Guide G170 present a general procedure to obtain reproducible results using RC to simulate the effects of different types of coupon materials, inhibitor concentrations, oil, gas and brine compositions, temperature, pressure and flow.

Materials selection

Because the rotating cage uses multiple specimens (typically eight) which are separated by an insulator, it is valuable to simultaneously evaluate corrosion behavior of materials in a particular environment. When using a rotating cage for materials selection caution should be exercised in that the holes on the top and bottom covers are plugged. Only when the holes are plugged are all the coupons exposed to the same flow pattern. Leaving one or both holes open makes the flow pattern of the two coupons around the holes different from that of the rest.

Drag reduction property evaluation

Drag reduction is a physical phenomenon that causes friction to be reduced and fluid flow to be increased. Chemicals that reduce drag are known as drag-reducing agents (DRA). Several polymeric compounds can reduce the wall shear stress of flowing liquids at low concentrations. Several studies have pointed out that part of the corrosion inhibitory effect may be due to the drag reduction properties (i.e., reducing the wall shear stress) of the chemicals. It is assumed that the drag reduction exerted by corrosion inhibitors is due to the interaction of shear-deformed surface active compound (SAC) aggregates in the near-wall liquid boundary layer with adsorbed self-assembled structures on the solid surface.

The rotating cage can be used to determine drag reduction properties. Several rotating cage parameters can be used to determine the drag reduction properties of corrosion inhibitors, including vortex length, vortex width and increase of the liquid level. But vortex length is the parameter that can be easily measured under all conditions. Liquid level, rotation speed and equations to correlate rotation speed and wall shear stress are based on the vortex length.

In order to evaluate the drag reduction property of a chemical, the vortex length measured during the experiments should be compared to the corro-

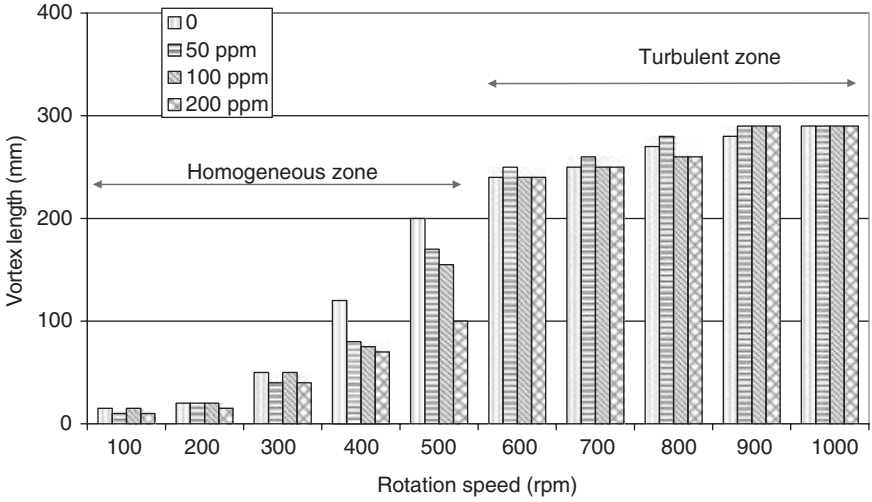

14.7 Variation of vortex length with rotation speed (with and without corrosion inhibitor): volume of liquid = 4 liters.

sion rates of coupons in the presence of the chemical. Figure 14.7 presents a typical result, in which the chemical exhibits drag-reduction properties ~500 rpm (homogeneous zone). Beyond 500 rpm, the flow pattern becomes turbulent, and the chemical loses its drag-reduction properties.

14.3 Jet impingement

14.3.1 History

Failure of a condenser tube by erosion-corrosion caused by high-velocity salt water provided an opportunity to develop a laboratory methodology to simulate high velocity in the laboratory. In the 1920s it was found that jet impingement could be used to reproduce the type of attack encountered in service, by subjecting specimens to jets of sea water containing air bubbles of a particular size.[22]

In the 1950s a comparison was made between two jet impingement apparatuses installed in London and in Harbor Island, USA. The 24-unit jet impingement apparatus installed in London was the recirculating type, whereas that installed in the USA was once-through. Tests with recirculating water showed a less severe attack than those with once-through water. It was also found that air bubbles in the water are necessary for an attack to occur.[23]

During the early 1970s, the ability of jet impingement to simulate high heat and mass transfer rates at surfaces even when the bulk of the surround-

ing fluid is stagnant, and to simulate different flow regimes simultaneously were recognized. With the reorganization, jet impingement found applications in non-corrosion fields including simulation of glass toughening, paper drying, solids leaching and welding processes as well as in aero- and space research to simulate vehicle vertical take-off and landing conditions.[24–27]

By the 1980s jet impingement apparatus was commonly used in electrochemical machining and erosion-corrosion (including nuclear reactor conditions).[28,29] By the 1990s application of jet impingement for corrosion studies was established. Several studies which compared the corrosion rates of various methodologies found that jet impingement was most suitable for simulating flow conditions of pipes and for the evaluation of oil-field corrosion inhibitors.[30–32] In the 2000s high-temperature, high-pressure jet impingement apparatus and jet impingement apparatus with vibrating specimens were designed.[33–35]

In 2001, ASTM published a Standard Guide, ASTM G170, *Evaluating and Qualifying Oilfield and Refinery Corrosion Inhibitors in the Laboratory*.[15] This standard describes the usefulness of jet impingement apparatus as a laboratory apparatus to simulate fluid conditions.

14.3.2 Jet impingement apparatus

Jet impingement apparatus can be operated in three different configurations. Depending on the configuration, the flow region in jet impingement can be stagnation, transition and wall-jet. The boundaries between these regions are not sharp and different values are provided in the literature (see Table 14.1). The experimental configuration for each flow region is discussed below. The flow characteristics are discussed in section 14.3.3 of this chapter.

Set up of jet impingement apparatus in stagnation region (disk electrode)

The advantage of conducting experiments in the stagnation region include:

- Fluid flow is well characterized
- The hydrodynamic shear is a linear function of radial position
- Mass transfer and convective diffusion to the surface are uniform
- Prevents the establishment of differential oxygenation cells
- The electrode is stationary and allows use of *in situ* determination of film thickness, e.g. by ellipsometry. Rotating disk electrode and rotating cylinder electrodes also provide well-characterized fluid flow with uniform mass transfer; however, they cannot be used for *in situ* techniques.[36,37]

Table 14.1 Flow characteristics of jet impingement

Flow zone	Characteristics
Stagnant	Well characterized for mass transfer, but not based on wall shear stress (because the flow vector changes rapidly as radial distance increases). Extends from the central axis to the point of maximum velocity and minimum jet thickness at $r_{jet,radial}/r_{jet} = 2$
	Extends up to $d_{jet,radial}/d_{jet} = 2.35$ for $H/d_{jet} = 8$. Sherwood numbers beyond $d_{jet,radial}/d_{jet} \simeq$ are independent of nozzle height in the range $0.2 \leq H/d_{jet} \leq 19.23$, and for Reynolds numbers from 25 000 to 125 000
	Up to $r_{jet,radial}/r_{jet} \leq 1.2$ (for Re 375) and ≤1.5 (for Re 1740 and above). For nozzle closer than $<0.5r_{jet}$ no significant change in the transfer rate ($r_{jet,radial}/r_{jet} < 0.2$). $r_{jet} = 2$, 1.25 and 0.72 inches $x/d_{jet} = 0.1$ to 1.0 (for turbulent nozzle) and $x/d_{jet} = 0.1$ to 0.5 (for laminar nozzle). Mass transfer rate is independent of the electrode size for $0.1 \leq H/d_{jet} \leq 6$. (Radii of disk electrodes used 0.0127, 0.0495, 0.0787, 0.157, 0.265, 0.634, 1.27 and 1.91 cm. Nozzle i.d. 0.635 and 0.292 cm and length 20.3 and 63.5 cm)
	Wall shear stress increases linearly with H/d_{jet} up to $H/d_{jet} = 8.0$, beyond which the effect levels off (because for nozzle height beyond eight diameters, the oncoming jet profiles are similar). This effect is seen between ($r_{jet,radial}$/free jet half radius at distance above the plate where the impingement region begins = up to 1.2). Shear stress data determined at $H/d_{jet} = 8.24$ and Re 10 600 to 36 200 agree with the theory, but for larger distances the data level off at about 15% below predictions. Data obtained at $H/d_{jet} = 18$ and Re ~ 160 000 also agree with the model, but experimental shear value was higher than the predicted value by a factor of 2
	Variation of dimensionless mass transfer coefficient ($Sh/Re^{0.5}$) with $r_{jet,radial}/r_{jet}$ is a function of H/d_{jet}. In general, the $Sh/Re^{0.5}$ is constant in the range of $r_{jet,radial}/r_{jet}$ up to 1.0 (for $H/d_{jet} = 1.2$ to 5.0); the $Sh/Re^{0.5}$ decreases with $r_{jet,radial}/r_{jet}$ in the range of $r_{jet,radial}/r_{jet}$ 0 to 5. The rate of decrease is a function of H/d_{jet}. At $H/d_{jet} = 6.0$–14, it decreases up to 2.5 and then becomes constant; at $H/d_{jet} = 17$–20, it continues to decrease
Transition	Not rigorously characterized mathematically
	Wall shear stress is proportional to the velocity squared ($r_{jet,radial}/r_{jet} = 2$ and 4)
	No transition zone (for Re 375). Between[24] $r_{jet,radial}/r_{jet} \geq 1.5$ and ≤ 3.0
	Mass transfer rate decreases with the radial position
Wall jet zone	Beyond $r_{jet,radial}/r_{jet} \geq 4$ ($r_{jet} = 2$ mm, $x = 4$ mm)
	Begins at $x/d_{jet} = 3.0$ ($d_{jet} = 0.254$ or 0.508 cm)
	$r_{jet,radial}/r_{jet} \geq 1.2$ (for Re 375) and ≥3 (for 1740). For nozzle-to-surface distances in the range 0.5 and $12r_{jet}$ mass transfer from the impingement surface is independent of nozzle distance. For nozzle closer than $<0.5r_{jet}$, transfer rate increase with decreasing nozzle height (due to constriction of flow between nozzle and impingement surface)
	Begins at $d_{jet,radial}/d_{jet} = 4$

Proper design of the impinging jet electrode system requires that the electrode be situated within this region. Stagnation regions of different lengths are reported in the literature. Stagnation regions extending up to a radius of jet (r)/radial distance (d) ratio of 0.5, 1, and 1.4 are reported. Therefore a jet impingement disk electrode of size less than 0.5 to 1.4 should be used. Typically a disk (rather than a ring) of r/d less than 0.5 is used. Under this condition the distance (h) between the nozzle and the electrode has no effect on the stagnation region, but typically an h/r ratio of 2 is used. A disk electrode that is large enough to extend into the region where stagnation flow theory does not apply still has a significant portion of the disk in the stagnation flow region. In contrast, a ring electrode can be constructed to lie wholly inside or outside the stagnation region. The ring-electrode measurements are therefore more sensitive to changes in the flow pattern. For this reason the disk electrode rather than the ring electrode is used to carry out jet impingement apparatus in the stagnation region.

Set up of jet impingement apparatus in turbulence and in wall-jet regions (ring electrodes)

Ring electrodes are used to conduct jet impingement experiments in the wall-jet region. Fluid jet can be produced using a non-metallic layer with a machined center hole with a tapered inlet to smooth the flow. The length of the cylinder is designed to ensure flow stabilization before the fluid exits. This provides a stable, reproducible jet impinging on the sample surface.

The jet impinged on the center of the flat surface of the test sample consists of one or more concentric ring working electrodes separated by a non-metallic spacer ring. The probe can be constructed to allow electrochemical corrosion measurements. The threaded back section of the probe allows precise adjustment of the distance between the test surface and the jet. The concentric ring working electrode centered at $d/r = 3$ is used to simulate a turbulence zone and $d/r = 5$ is used to simulate a wall jet zone.

Set up of jet impingement apparatus in stagnation to wall-jet region (disk electrode)

The jet impingement apparatus consists of a central cell with four arms containing nozzles (Fig. 14.8).[21] The impeller, housed in the cell body, is driven by an electric motor magnetically coupled to the impeller drive shaft. Fluid from the cell is forced by the impeller through the nozzles and aimed directly and symmetrically onto the disk specimens mounted at the end of

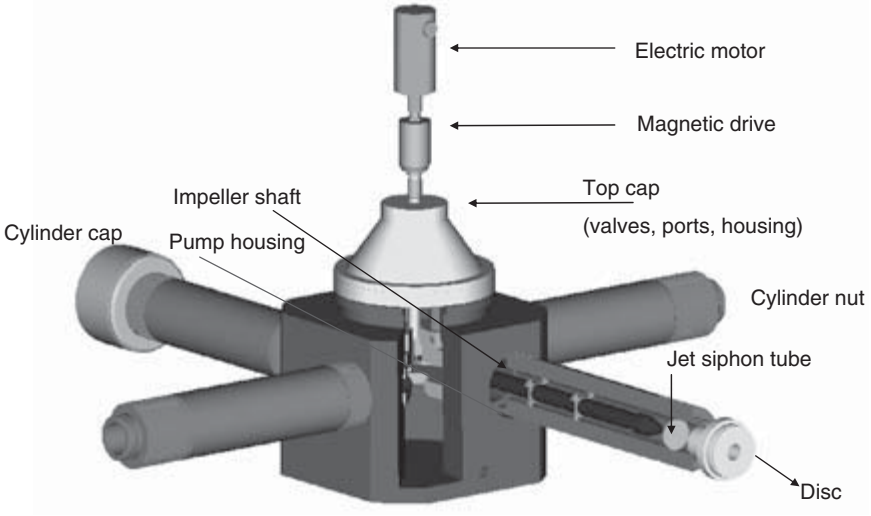

14.8 Schematic diagram of high-temperature, high-pressure jet impingement apparatus.

the jet arm, within the jet arm caps. The fluid returns to the cell body through the jet arms. This impinging jet design has submerged nozzle where the flow confining wall is the jet arms. Multiple (typically four) samples can be used. Corrosion rates can be measured using both weight-loss and electrochemical techniques. The radius of the disk should be larger, typically more than $d/r = 5$ so that all three jet regions exist on the surface.

14.3.3 Flow characteristics of jet impingement

The flow field established for a circular jet impinging on a flat plane with the jet's central axis normal to the plane is illustrated in Fig. 14.9. Under these conditions, a stagnation point will exist at the intersection of the axis with the plane, and the flow will be symmetrical about the axis. Because the flow is axisymmetric, only the flow and fluid properties in the radial plane normal to the disk are considered.

Region *A* in Fig. 14.9 is the stagnation zone. The flow is essentially linear near the plate, and the principal velocity component changes from axial to radial, with a stagnation point at the center. The wall shear stress within the stagnation region is given by:

$$\tau_{stag} = -1.312r(\mu\rho)^{1/2}a^{3/2} \qquad [14.2]$$

where τ_{stag} is wall shear stress in the stagnation region, r is the radius of the disk electrode, μ is the kinematic viscosity, ρ is the density of the fluid, and

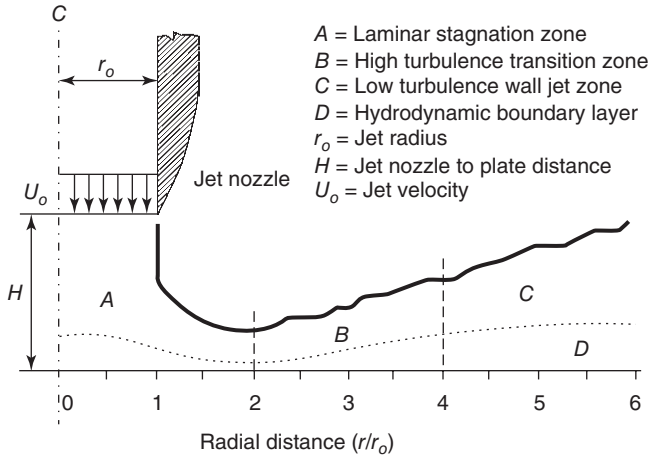

14.9 Hydrodynamic characteristics of jet impingement on a flat plate.

a is hydrodynamic constant, proportional to the average jet velocity, and is a function of cell geometry.

Region *B* in Fig. 14.9 is the turbulent region in which the flow is increasingly turbulent and develops into an all jet (i.e., the primary flow vector is parallel to the solid surface). The flow pattern is characterized by high turbulence, a large velocity gradient at the wall, and high wall shear stress. Thus, Region *B* is of primary interest for studying fluid flow effects on corrosion in high-turbulence areas. The region has not been rigorously characterized mathematically, but published work indicates wall shear stress is proportional to the velocity squared. The wall shear stress in this region is given by:

$$\tau_{turb} = 0.179\rho U^2 Re^{-0.182}\left(\frac{r}{r_o}\right)^{-2.0} \quad [14.3]$$

Where τ_{turb} is the jet wall shear stress in the turbulent region, U is the jet velocity, Re is the Reynolds number, and r_o is the jet radius.

Region *C* in Fig. 14.9 is the wall jet region. In this region the bulk flow rate and turbulence decay rapidly as the thickness of the wall jet increases, momentum is transferred away from the plate, and the surrounding fluid is entrained in the jet. This region is amenable to mathematical characterization, but the flow cannot be related to field conditions because momentum transfer and fluid entrainment are in the opposite direction to the pipe flow.

14.3.4 Simulation of general and localized corrosion

Jet impingement is a widely used technique to study flow-accelerated corrosion. Experimental results at very high wall shear stress, up to 1000 Pa,

have been reported in the literature.[38] In one study it was found that the jet impingement apparatus simulated the extreme flow conditions of the pipe, but in this methodology the inhibitors also exhibited higher inhibitor efficiencies. This study also found that the jet impingement did not effectively simulate pitting corrosion. Whenever pits were initiated in the JI, inhibitors controlled their propagation.[19] The critical radii for transition from uniform to localized corrosion typically occur around $2.46 < r/r_o < 2.88$. This region is also the region that displays the transition from the turbulent to the wall-jet region.[35]

14.3.5 Typical applications of jet impingement apparatus

Jet impingement apparatus can be used in all applications where rotating cages can be used, but typically jet impingement is useful to create high-shear stress flow conditions, typically above 200 Pa.[39]

14.4 Prediction from laboratory test result to field application

In order for a laboratory methodology to be useful, it must simulate the combined effects of parameters that influence corrosion inside an actual pipeline. Despite the difficulties in correlating corrosion data from samples in the laboratory and from pipe in the field, laboratory methods are invaluable as a first step to evaluate corrosion inhibitors and to select inhibitors for further testing in the field.

There are two types of variables, direct and indirect. Composition of material, composition of gas and liquid (oil and water), temperature and pressure are direct variables. Simulation of these variables in the laboratory is direct. Flow, on the other hand, is an indirect variable, and simulation of flow in the laboratory is not direct.[40] The influence of both types of variable should be understood and simulated.

Flow is the main indirect variable. To simulate the effect of flow, the hydrodynamic parameters are determined, and then the laboratory corrosion tests are conducted under the calculated hydrodynamic parameters. The fundamental assumption in this approach is that, when the hydrodynamic parameters in two different geometries are the same, then the corrosion rates are similar. The parameter used to describe the flow conditions in a pipe is wall shear stress.

14.4.1 Pipe wall shear stress

Pipe wall shear stress, τ_p, can be measured experimentally in terms of the pressure drop (ΔP) over a specific length of pipe (ΔL) with a specific diameter (d):

$$\tau_p = \left(\frac{\Delta P}{\Delta L}\right)\left(\frac{d}{4}\right) \quad [14.4]$$

By measuring the pressure drop (ΔP) over a specific length of pipe (ΔL) with a specific diameter (d), τ_p can be experimentally determined.

Alternatively, the wall shear stress can be calculated as follows. The ratio of τ_p to the kinetic energy pressure loss per unit volume of fluid defines a dimensionless friction factor (f) that is a measure of the energy loss as a result of wall turbulence, accounting for both viscous shear in the fluid and the surface roughness. This relationship is expressed as:

$$\tau_p = \frac{fU^2\rho}{2} \quad [14.5]$$

where f is the friction factor (dimensionless), U is flow velocity and ρ is density.

Moody has derived an approximate equation (Equation [14.6]) which agrees within +5% of f values calculated using other more complicated but more accurate equations. This formula covers the usual range of engineering problems.

$$f = 0.0055\left[1 + \left(20000\frac{\varepsilon}{d} + \frac{10^6}{Re}\right)^{1/3}\right] \quad [14.6]$$

where Re is the Reynolds number (dimensionless), ε is surface roughness (4.57×10^{-5} m for commercial welded pipe), and d is pipe diameter.

For pipes in the rough zone of complete turbulence, where f is independent of the Reynolds number, the final term can be dropped and Equation [14.6] becomes:

$$f = 0.0055 + 0.15(\varepsilon/d)^{1/3} \quad [14.7]$$

To complete the equation set, the Reynolds number for pipe flow can be calculated as:

$$Re = (U^*d)/\nu \quad [14.8]$$

where ν is kinematic viscosity.

The density and flow velocity terms used in Equation [14.8] are fairly simple in cases where the substance flowing through the pipe is homogeneous. The use of these terms becomes more complex when a multiphase fluid is being transmitted. A simple average of the density and flow rates is insufficient if the quantity of each phase flowing through the pipe is not equal. In order to calculate the wall shear stress, the weighted averages of the density and flow rate of each phase flowing through the pipe must be known. The percentage of each phase must be calculated

and used to produce a weighted average. The rates of water, oil and gas need to be compared in order to determine the percentage of each phase and from which the weighted averages of density and flow rate are determined.

The flow rates through a pipe (of diameter, d) are calculated as: Flow rate (m/s) = volume transmitted/pipe area. Calculation of flow rate of gas presents a unique mathematical problem. The gas volume is normally presented at standard temperature and pressure (STP). The gas in the pipe, however, is not at standard temperature and pressure and, in fact, occupies a different volume than that reported. From Van der Waals' gas equation, it is known that a given quantity of gas takes up a different volume at different pressures:

$$\left(P+\frac{an^2}{V^2}\right)^2(V-nb)=nRT \qquad [14.9]$$

where P is pressure, a and b are Van der Waals constants, n is the number of moles of gas, R is a constant equal to 8.31441 J/K.mol , V is the volume of the substance and T is the temperature. In order to solve the equation, it is assumed that the gas flowing in the pipe is pure methane; thus, $a = 2.300$ bar L^2/mol and $b = 0.04301$ L/mol.

In order to convert the volume of gas from STP values to the pipeline operational pressure and temperature, Equation [14.9] is solved for the number of moles at STP and then this value is substituted into Equation [14.6] for the volume under pipeline operational conditions. In order to solve for n, the number of moles, a cubic equation of the form must be solved:

$$An^3 + Bn^2 + Cn + D = 0 \qquad [14.10]$$

where $A = ab/V^2$, $B = -a/V$, $C = (RT + Pb)$ and $D = -PV$. The general form of the solution is as follows:

$$n = y - B/3A \text{ where } y = Ya + Yb \qquad [14.11]$$

$$Ya=\left(-\frac{Q}{2}+[(Q/2)^2+(S/3)^2]^{1/2}\right)^{1/3} \qquad [14.12]$$

$$Yb=\left(-\frac{Q}{2}-[(Q/2)^2+(S/3)^2]^{1/2}\right)^{1/3} \qquad [14.13]$$

$$S=\frac{C}{A}-\frac{B^2}{3A^2} \qquad [14.14]$$

$$Q = \frac{D}{A} + \frac{2B^3}{27A^3} - \frac{CB}{3A^2} \quad [14.15]$$

Solving Equation [14.7] results in a value for n, the number of moles. Substituting this value back into Equation [14.6] and using the pipeline operating pressure and temperature, another cubic equation is obtained of the form:

$$AV^3 + BV^2 + CV + D = 0 \quad [14.16]$$

where $A = P$, $B = -(\{bnP\} + \{nRT\})$, $C = (an^2)$ and $D = -(abn^3)$. The volume under pipeline operational conditions can be calculated by solving Equation [14.13] using the same technique as presented in Equation [14.16].

14.4.2 Correlation between pipe and rotating cage

As a first approximation, the rotating cage wall shear stress can be calculated using Equation [14.1]. Re_{rc}, Reynolds number of the rotating cage required in Equation [14.1] is calculated as:

$$Re_{rc} \ (= \omega r_{rc}^2/\nu) \quad [14.17]$$

Solving Equations [14.1] and [14.17] for angular velocity yields:

$$\omega = \left(\frac{3.55\tau_{RC}^{0.5}}{\nu^{0.15}\rho^{0.5}r^{0.7}} \right) \quad [14.18]$$

Equation [14.8] is valid only if the flow in the rotating cage is in the homogeneous zone. Flow in the side-wall is affected by top-wall and turbulent zones experiences a different wall shear stress, and thus, the equation for angular velocity is not valid under these conditions.

14.4.3 Correlation between pipe and jet impingement

The corrosion rates in the jet impingement experiments and in the pipe are correlated when the wall shears for both geometries are the same. This correlation is valid only when r/r_o is between 2 and 4. Solving Equation [14.3] for jet velocity using $\mathrm{Re} = 2r_oU_j/\nu$, Equation [14.19] is obtained:

$$U_j = 2.7613(\tau_j/\rho)^{0.5501}\,\nu^{-0.1001}\,(r^{1.1001}/r_o) \quad [14.19]$$

14.5 Future trends

At the time of writing this chapter, standard procedure is available for evaluating corrosion inhibitors using the rotating cage[17] but not for jet impingement. In addition the reproducibility of the rotating cage and jet

impingement is not known. A standard for conducting jet impingement experiments is being developed. In the future, the reproducibility of results achieved by different operators of the rotating cage and jet impingement using procedures described in this chapter will be established.

Once the standard test procedures are developed and their reproduci bility established, a laboratory could carry out one test using the conditions described in the standard to qualify the test equipment, before conducting experiments under field conditions for selecting corrosion inhibitors. By following such a procedure, the reliability of inhibitor selection will be increased.

14.6 Further information

The purpose of this chapter is to provide an overview of the rotating cage and jet impingement apparatus that are widely used to simulate corrosion in the laboratory. The discussions provided are not exhaustive. Several advances have been made to use them efficiently and new standards are developed every day. Most advances are published in corrosion journals (including those published by NACE: *Corrosion Journal, NACE Material Performance*; *The Journal of the Electrochemical Society*, *British Corrosion Journal*, and *Corrosion Science*), symposia (including those organized by ASTM, NACE, the European Federation of Corrosion (EFC), books (including those published by ASTM, ASM, NACE and EFC), and standards (including those developed by ASTM G01 committee and NACE STG 62 committees).

14.7 References

1 H. Gytzeit, C. Samans and F.B. Bulls, *Mater. Prot*., 12 (7) (1973) p. 12.
2 K. Faessler and G. Blummel, *Werkstoffe und Korrosion* 42 (1991) p. 55.
3 G. Schmitt and W. Bruckhoff, *NACE CORROSION/88*, Paper #357 (1988).
4 G. Schmitt, W. Bruckhoff, K. Faessler and G. Blummel, *NACE CORROSION/90*, Paper #23 (1990).
5 G. Schmitt, W. Bruckhoff, K. Faessler and G. Blummel, *Material Performance* 30 (2) (1991) p. 85.
6 D.W. Stegmann, R.H. Hausler, C.I. Cruz and H. Sutanto, *NACE CORROSION/90*, Paper #5 (1990).
7 V. Jovancicevic, S. Ramachandran, Y.S. Ahn and B.A.M. Oude Alink, *NACE CORROSION/2001*, Paper #1052, NACE International, Houston, TX (2001).
8 S. Papavinasam, R.W. Revie, M. Attard, A. Demoz, H. Sun, J.C. Donini and K. Michaelian, *CORROSION/99* Paper # **1,** NACE International, Houston, TX (1999).
9 S. Papavinasam, R.W. Revie, M. Attard, A. Demoz, H. Sun, J.C. Donini and K. Michaelian, 'Laboratory Methodologies for Corrosion Inhibitor Selection', *Materials Performance*, 39 (2000) p. 58.

10 S. Papavinasam, R.W. Revie, M. Attard, A. Demoz, H. Sun, J.C. Donini and K. Michaelian, *CORROSION/2000,* Paper # 55, NACE International, Houston, TX (2000).
11 S. Papavinasam, R.W. Revie, M. Attard, A. Demoz, H. Sun, J.C. Donini and K. Michaelian; 9th European Symposium on Corrosion Inhibitors, University of Ferrara, Ferrara, Italy, 4–8 September 2000.
12 S. Papavinasam, R.W. Revie, M. Attard, A. Demoz, H. Sun, J.C. Donini and K. Michaelian, *EUROCORR 2000*, 10–14 September 2000, University of London, London, UK.
13 S. Papavinasam, R.W. Revie, M. Attard, A. Demoz, D.C. Donini and K. Michael ian, 'Standardized Methodology for Inhibitor Evaluation and Qualification for Pipeline Applications', IPC2000, ASME, Calgary, AB, Canada, 1, p. 901, 1–5 October (2000).
14 S. Papavinasam, R.W. Revie, M. Attard, A. Demoz, H. Sun, J.C. Donini and K. Michaelian, *CORROSION/2000,* Paper # 1061, NACE International, Houston, TX (2001).
15 ASTM G170, 'Standard Guide for Evaluating and Qualifying Oilfield and Refinery Corrosion Inhibitors in the Laboratory', ASTM, Barr Harbor Driver, West Conshohocken, PA 19428-2959, US.
16 S. Papavinasam, M. Attard, R.W. Revie and J. Bojes, 'Rotating Cage – A Compact Laboratory Methodology for Simultaneously Evaluating Corrosion Inhibition and Drag Reducing Properties of Chemicals', *CORROSION/2002,* Paper # 2271, NACE International, Houston, TX (2001).
17 S. Papavinasam, A. Doiron and R. Winston Revie, 'Effect of Rotating Cage Geomery on Flow Pattern and Corrosion Rate', *CORROSION/2003*, Paper #3333, NACE International, Houston, TX (2003).
18 ASTM G184, 'Standard Practice for Evaluating and Qualifying Oil Field and Refinery Corrosion Inhibitors using Rotating Cage', ASTM, Barr Harbor Driver, West Conshohocken, PA 19428-2959, US.
19 S. Papavinasam, R.W. Revie, M. Attard, A. Demoz and K. Michaelian, 'Comparison of Laboratory Methodologies to Evaluate Corrosion Inhibitors for Oil and Gas Pipelines', *Corrosion* 59 (10), 2003, p. 897.
20 C. Deslouis, A. Belghazi, Y. T. Al-Janabi, P. Plagemann and G. Schmitt, 'Quantifying Local Wall Shear Stress in the Rotating Cage', CORROSION/2004, #4727, NACE, Houston, TX (2004).
21 Allan report
22 G.D. Bengough and R. May, *J. Inst. Metals*, 32, 1924, pp. 81 and 40, 1928, p. 141.
23 P.T. Gilbert and F.L. Laque, 'Jet Impingement Tests', *Journal of the Electrochemical Society*, 101 (9), 1954, p. 448.
24 F. Giralt, C.J. Chia, and O. Trass, 'Characterization of the Impingement Region in an Axisymmetric Turbulent Jet', *Ind. Eng. Chem. Fundam*., 16 (1), 1977, p. 21.
25 F. Giralt and O. Trass, 'Mass Transfer From Crystalline Surfaces in a Turbulent Impinging Jet: Part 1. Transfer by Erosion', *The Canadian Journal of Chemical Engineering,* 53, 1975, p. 505.
26 F. Giralt and O. Trass, 'Mass Transfer from Crystalline Surfaces in a Turbulent Impinging Jet: Part 2. Erosion and Diffusional Transfer', *The Canadian Journal of Chemical Engineering,* 54, 1976, p. 148.

27 M.T. Scholtz and O. Trass, 'Mass Transfer in a Nonuniform Impinging Jet', *AIChE Journal*, 16 (1), 1970, p. 82.
28 D.T. Chin and C.H. Tsang, 'Mass Transfer to an Impinging Jet Electrode', *J. Electrochemical Society*, 125 (9), 1978, p. 1461.
29 D.A. Jones, 'Effect of Water Chemistry on the Erosion-Corrosion of Aluminum in High Temperature High Velocity Water', *Corrosion* 37 (10) 1981, p. 563.
30 J.L. Dawson, C.C. Shih, R.G. Miller and J.W. Palmer, 'Inhibitor Evaluations Under Controlled Hydrodynamic Shear', *Materials Performance* 30 (1), 1991, p. 43.
31 K.D. Efird, E.J. Wright, J.A. Boros and T.G. Hailey, *Corrosion* 49 (12), 1993, p. 992.
32 J.M. Esteban, G.S. Hickey and M.E. Orazem, 'The Impinging Jet Electrode: Measurement of the Hydrodynamic Constant and Its Use for Evaluating Film Persistency', *Corrosion*, 46 (11), 1990, p. 896.
33 A. Demoz, T. Dabros, K. Michaelian, S. Papavinasam and R.W. Revie, 'A New Impinging Jet Device for Corrosion Studies', *CORROSION 2003*/Paper #3322, NACE International, Houston, TX 2003.
34 G. Schmitt, C. Bosch, U. Pankoke, W. Bruckhoff and G. Siegmund, 'Evaluation of Critical Flow Intensities for FILC in Sour Gas Production', *CORROSION 1998*/Paper #46, NACE International, Houston, TX, 1998.
35 A. Demoz, T. Dabros, K.H. Michaelian, S. Papavinasam and R.W. Revie, 'A New Impinging Jet for Corrosion Studies', *Corrosion* 60(5), p. 455 (2004).
36 J.C.C. Filho and M.E. Orazem, 'Application of a Submerged Impinging Jet to Investigate the Influence of Temperature, Dissolved CO_2, and Fluid Velocity on Corrosion of Pipeline-Grade Steel in Brine', *CORROSION/2001*, Paper #1058, NACE International, Houston, TX, 2001.
37 J.M. Esteban, G.S. Hickey and M.E. Orazem, 'The Impinging Jet Electrode: Measurement of the Hydrodynamic Constant and Its Use for Evaluating Film Persistency', 46 (11) 1990, p. 896.
38 M. Bartos and J. Watson, 'Oilfield corrosion inhibition under extremely high shear conditions', *CORROSION/2000*, Paper # 68, Houston, TX, 2000.
39 S. Papavinasam, R.W. Revie, T. Panneerselvam and M. Bartos, 'Standards for Evaluation of Corrosion Inhibitors for Oil-field Applications', *Materials Performance* 46 (5), 2007, p. 46
40 S. Papavinasam, A. Doiron, G. Shen and R.W. Revie, 'Prediction of Inhibitor Behaviour in the Field from Data in the Laboratory', *CORROSION/2004,* Paper #4622, NACE International, Houston, Texas, 2004.

Part III

Corrosion monitoring in particular environments and other issues

15

Corrosion monitoring in microbial environments

PIERANGELA CRISTIANI, Cesiricerca SPA, Milan, Italy

15.1 Introduction

In many cases, corrosion damage to industrial equipment cannot be directly attributed to 'chemical' effect. They are often referred to as microbial corrosion, which ascribes the decrease of material performance to the activity of living micro-organisms. These kinds of phenomena are often observed in process waters as well as in cooling circuits, including the facilities exposed to simple air condensates. Nevertheless, it is indeed very difficult to demonstrate exhaustively that these kinds of corrosion are due to a single cause because they usually involve complex systems both temporally and spatially. Taking into account this concern, the 'verdict' should be almost always more properly 'Microbial Influenced Corrosion' usually abbreviated as MIC. A necessary condition for the development of MIC phenomena in industrial plants is the presence of a 'biofilm' covering or underlaying the surface of the materials equipment.

15.1.1 Biofilm

Biofilm is the first layer of biofouling growing on the surface of wetted structures in contact with natural waters, whose thickness can range from a few microns to a few millimetres. It is constituted by microbial cells (bacteria, fungi and algae) imbued in extra-cellular polymeric substances (EPS): a complex mixture of macromolecules such as polysaccharides, proteins, nucleic acids and lipids produced by the cells themselves (Wingender and Flemming, 1999). EPS facilitate cell adhesion to the substratum and give structural integrity to the biofilm matrix (Sutherland, 2001). Depending on the environment (aerobic or anaerobic for instance), several inorganic precipitates enrich biofilm.

Many metallic materials commonly utilised in plant can be affected by MIC. Stainless steel and copper alloys are no exception because the biofilm

protects micro-organisms from the toxic effect of copper. The biofilm enhances bacterial resistance against several external factors, including biological competitors and chemical biocides action, forcing the use of intensive antifouling and disinfecting water treatments.

It is now acknowledged that bacteria form synergistic communities that are able to catalyse electrochemical processes within biofilms and, typically, both the aggressive and inhibitory effects from the metabolism of bacterial population on corrosion reactions are due to complex interactions, involving corrosion products on the material surface, seldom linked to a single bacterial species (Geesey *et al.*, 2000).

It must be stated that all the bacteria secreting organic acids and EPS or slime are able to play relevant roles in aerobic as well as in anaerobic environments (Chandrasekaram and Dexter, 1993; Beech and Sunner, 2004; Wardell and Chamberlain, 1995).

Some representative specific types of bacteria that were demonstrated to influence corrosion of metals are sulphate-reducing bacteria (SRB) in anaerobic conditions, sulphur-oxidising bacteria (SOB), iron-oxidising/reducing bacteria (IOB/IRB), and manganese-oxidising bacteria (MOB).

The cost of MIC is very high: in the particular case of heat exchangers 20% of all the corrosion damages were attributed to this type of corrosion (Flemming, 1991) and a similar percentage was reported in other cases.

A study related to Italian power plants reports, at a first approximation, that 50% of the corrosion cases of the condenser tubes might be prevented by better cleaning during the plant operation (Cristiani and Bianchi, 1997).

15.1.2 MIC monitoring

A survey recently conducted by European specialists coming from universities, research laboratories and industries, on the basis of their personal experience (Cristiani, 2000) concluded that many techniques can be employed in the laboratory, and some of them can be used in the field, for MIC monitoring. Even though some of the methods are very effective for monitoring biofilm and others for monitoring corrosion, none of them can be used alone to effectively follow the development of microbial attack in all the possible combinations of metals, environments and biofilms.

The corrosion rate, especially after the biofilm overcomes the first phase of its development, was found to be independent of parameters such as the biofilm thickness, its roughness, or the number of settled micro-organisms. It is widely accepted that many of the metabolic products of micro-organisms inside the biofilm (enzymes within the EPS matrix, organic and

inorganic acids, as well as volatile compounds such as ammonia or hydrogen sulphide) can alter electrochemical processes at the metal/biofilm interface (Geesey *et al.*, 2000; Characklis and Marshall, 1990; Beech, 2002; Lee and Newman, 2003; Hamilton, 2003) and lead to MIC. Furthermore, the occasional direct correlation between microbial metabolism and the corrosion rate has been well documented (Neal *et al.*, 2003, Dinh *et al.*, 2004).

Most of the MIC cases are reported as localized attacks and the localization is connected to non-homogeneous morphology and 'composition' of the biofilm. In fact, in a biofilm the type of settled micro-organisms and the nature/concentration of their extra-cellular products can change over a distance of a few micrometres. Because of these facts, a wide range of monitoring approaches should be considered and tested before a suitable approach could be determined. The final solution should be selected on a case-by-case basis, taking into account the type of material, the environment at the metal–biofilm interface and, last but not least, the suitability for industrial applications.

In the case of stainless steels in aerated waters, the electrochemical monitoring devices proposed for direct evaluation of MIC risk must be considered as an exception to mature industrial application (see section 15.3).

15.1.3 Off-line biofilm monitoring

The traditional way to document biofilm presence involves the use of 'hand-made' probes and coupons inserted directly into the plant facility, or in a by-pass of a process stream, and periodically collected for off-line analyses (Pope, 1987). Some systems for the exposure of samples are commercially available (for instance Bioprobe™ by Petrolite (Texas, USA) and Robbin's Device such as that used by Tyler Research Corporation (Alberta, Canada) (Nickel *et al.*, 1985). Some of these systems can also be used in high pressure.

It is important to make test lines being representative of the real process. Indeed, as the positioning of the probes and the water flow influence the results strongly, they must be chosen to reproduce, at least, the same (or most critical) conditions.

Samples, in addition, must be made of the representative materials. It has been shown, in fact, that bacteria populations are colonised to varied extents on different materials, including metals, even though the planktonic bacterial growth conditions are identical (Beech and Coutinho, 2003). Many analyses can be performed off-line (see Table 15.1), to gain better knowledge of the structure and distribution of the collected biofilm (Videla *et al.*, 1992).

There are already several tools and kits available on the market to analyse the biofilm and to count the cultivable bacteria in it (see Table 15.2).

Table 15.1 Off-line techniques used to document MIC

Analyses	Technique	Comment
Sampling	Coupons	Always necessary
Deposit analysis	Determination of dry weight, Visual observation of corrosion products, slime, sludge	To document and quantify the corrosion case
Microscopy observations in plant	Stereo zoom microscopy, Optical microscopy, Epi-fluorescence microscopy	Biofilm observation in field, Bacteria counts, ATP and bacteria count
Microscopy observation in laboratory	Scanning Electron Microscopy (SEM)	Fixed biofilm observation and bacteria count
	Environmental SEM (ESEM) for non-fixed and wet samples	Living biofilm morphology
	X-Ray XPS (X photoemission Spectroscopy), EDS (Electron Diffraction Spectroscopy) microprobe	Chemical analyses of corrosion products and biofilm components
	Atomic Force Microscopy (AFM)	Three-dimensional vision of living biofilm morphology
	Confocal Laser Scanning Microscopy (CLSM)	Section analyses of living biofilm layer allowing the three-dimensional vision of it
Chemical analyses	Colorimetric kits	Analyses of corrosion products in plants
	Laboratory techniques Inductively Coupled Plasma (ICP)	Analyses of corrosion products in laboratory
	Gas Chromatography (GC) Gas Chromatography/Mass Spectroscopy (GC/MS) FT-IR (Fourier Transform Infra-Red spectrometer)	Analyses of chemical components of biofilm (fatty acids, chlorophylls, organic compounds) in laboratory
Microbiological analyses	Coupons, dipstick, culture medium and laboratory equipment	Plate counts of micro-organisms
Immunological analyses	Colorimetric assays, ELISA-kits, luminometric assays, laboratory equipment	Detection of enzymes
Genetic analyses	PCR (Polymerase Chain Reaction) FISH (Fluorescence In Situ Hybridization), laboratory equipment	Amplification and detection of DNA or RNA genetic matter in micro-organisms

Some systems are able to give a rough quantification of cell proliferation biomass measuring the cellular ATP (adenosine triphosphate) activity (Petty *et al.*, 1995). The ATP assays are often based on the detection of the light produced by the reaction of ATP with added luciferase and D-luciferin

Table 15.2 Off-line analyses of biofilm components sustainable in plant

Analyses	Technique	Comments
Microbiological analyses	Plate count of total viable bacteria. Plate count of specific bacteria (as anaerobics, iron-bacteria, pathogens etc.) Kit for luminescent bacteria	Dipstick, kits and assays for in-field application
Immunological analyses	Analyses of ATP Analysis of APS (adenosine-5′ phosphosulphate reductase, the enzyme reducing sulphate to H_2S in SRB) Analyses of hydrogenase (the enzyme removing hydrogen in SRB)	Kits for in-field use
Staining	DAPI (4′,6-Diamidino-2-phenylindole) epifluorescent reactive to reveal DNA Acridine orange to reveal adenosine Other stains to reveal specific cell components	Simple microscopy observation in laboratory (epifluorescent, optical microscopy)
Chemical analyses	H_2S; other specific chemical substance by bacteria metabolism	Kits for in-field use

(Britelite™ Perkin Elmer, MA, USA, TRACIDE™, Improchem, South Africa). ATP is present in all metabolically active cells and it declines very rapidly when the bacteria die and the cells decay.

Commercial kits can facilitate the analysis if the number of cultivable bacteria or the presence of some specific bacteria has to be assessed in plant procedures mandatorily (Pope, 1987). The simplest device contains dipsticks or glass beads (or coupons made of different materials) that can be removed for testing. They can be sonicated and the bacteria of detached biofilm counted (plate count) or placed in a specific lysing solution for cellular ATP analysis. Otherwise, the beads may be treated with specific staining and directly observed under optical microscopy. Some commercial kits analyse specific enzymes (Enzyme-Linked ImmunoSorbent Assay, or ELISA test), for instance: the sulphate reductase, common to sulphate reducing bacteria (SRB) (Rapidcheck™ Strategic Diagnostic Inc., Newark, DE, USA) as well as the hydrogenase responsible for the acceleration of corrosion through the rapid removal of hydrogen formed on the metal surface (Bryant *et al.*, 1991) (Hydrogenase, Caproco International Inc. TX, USA).

Other kits specific to SRB analyse the development of hydrogen sulphide (Sanicheck^{TR}, Biosan Laboratories Inc., MI, USA; BTI-SRB^{TR}, Bioindustrial Technologies Inc., TX, USA).

In addition to the methods listed in Tables 15.1 and 15.2, other analyses are possible and sometimes utilised, especially in laboratories for mechanistic studies (Videla *et al.*, 1992). These methods are usually time consuming, expensive, complex and require expert people. However, simple visual observations of coupons and their viscid tactile sensation can provide a 'rough' proof of biofilm presence.

15.1.4 On-line fouling monitoring

A traditional approach for the on-line evaluation of fouling growth is the measurement of physical effects, such as the decrease of the heat exchange efficiency and/or the increase of the friction factor, induced by biofilm as well as other kinds of fouling (Hillman, 1985).

In power plants, because biofilm is one of the major concerns for heat exchange efficiency, the whole condenser can be used as a biofilm sensor; the measurement of plant parameters such as the value of the condensate back pressure can provide information on the fouling developed on the condenser tubes. The same effects (heat transfer and pressure drop) can also be measured, on a piece of pipe mounted inside the condensers or in a by-pass.

Some of these monitoring devices are available on the market (for instance that by Bridge Scientific, US, Micheletti and Miller, 1993) some others are proprietary equipment (Stuart *et al.*, 1990). Main disadvantages of physical devices are:

1. They are not specific for biofilm. Indeed they signal not only biofilm but the growth on the condenser walls of the whole fouling, scale and eventual corrosion products.
2. They are able to signal the presence of a biofilm only if its thickness is ≥30–40 μm (Characklis and Marshall, 1990; Chu and Mochizuki, 1985). As a consequence they do not provide information on the first phase of the biofilm growth, which is crucial for MIC. Furthermore, they do not reveal residual living micro-organisms that have survived the antifouling procedures, leading to a fast re-growth after treatment (Lewis, 1982).

Several on-line fouling sensors based on optical effects have also been developed. Optical fibres detect all kinds of deposit, living or dead biofilm, scale, etc. A simple fibre optic device is based on light reflectance measurement (Bott, 1995). A differential turbidity measurement device is another optical method based on detection of the deposition of reflecting material.

The optical sensors could be employed particularly to detect fouling in high turbidity solutions (as in pulp and paper mills) and for non-conducting materials. Their sensitivity to the biofilm layer could be bigger than that of pressure drop sensors (Flemming *et al.*, 1998). The more sophisticated Fourier Transform Infrared Spectrometry (FTIR) flow cell operating in the attenuated total reflectance mode allows the detection of bacterial biofilms as they form on a crystal of zinc selenide or germanium, and also gives information about the chemical nature of the deposit. In this case it could be possible to separate the signal coming from the different fouling components. However it is currently only limited to laboratory applications.

Optical systems are often exclusively licensed by manufacturers to a single service company (as in the case of Nalco Optical Fouling Monitors OFM (Wetegrove *et al.*, 1996). Another recent system proposed by Nalco Ondeo company (IL, USA) for monitoring and on-line optimisation of biocide treatments in cooling towers, is a fluorometer. It detects a fluorescent molecule (bio-sensor) that interacts with both planktonic and sessile micro-organisms and changes its fluorescence spectrum when added to re-circulating water (Hatch *et al.*, 2003; Chattoraj *et al.*, 2003).

There are a number of other methods employed for the measurement of biofouling. The Laser Light Scattering Device of Wyatt Industries (Santa Barbara, CA, USA) is a commercial system for bulk phase monitoring based on the detection of colloidal particles of bacteria by laser light scattering (Wyatt, 1972; Wyatt and Jackson, 1989). In a method based on a 'Mass Transport Device', the estimation of the biofilm thickness is obtained measuring the tracer transport rate through the fouling layer on a gold electrode. Other techniques require a quartz crystal microbalance or various sophisticated ultrasonic devices (Herbert-Guillou *et al.*, 1999). Most of these methods have been developed only on a laboratory scale or they were used only in special applications, although they might have the potential for wider use.

15.2 Corrosion monitoring applied to MIC

15.2.1 Off-line method

The traditional and widely used system to detect and measure corrosion phenomena consists of metallic coupons inserted directly in the plant facility and then extracted for evaluation of the corrosion attacks. The advantages and the disadvantages of this method are essentially the same as those already discussed regarding the off-line biofilm monitoring method. There are essentially no limits to the number and complexity of the possible off-line analyses (from simple weight loss to microscopic observation, corrosion products analyses, etc.) so that a detailed information on corrosion can be

obtained; in addition biofilm can concurrently be studied and possibly correlated with the morphology and the propagation rate of the corrosion attacks.

15.2.2 On-line techniques

A number of traditional electrochemical techniques for on-line corrosion monitoring were employed to detect MIC in the laboratory and some in the field (Borenstein, 1994). The criteria in the selection of the measurements are mainly related to:

- nature of the metals to monitor (carbon steel, passivable alloys, etc.)
- environmental conditions (aerobic, anaerobic)
- physico-chemical characteristics of the water (temperature, flow, conductivity, chemical treatments, pH)
- applications (field, plant, laboratory).

Linear polarisation resistance (LPR)

Several commercially available and relatively cheap devices are available for the measurement of the uniform corrosion rate on metallic coupons based on the LPR technique (see Chapter 3). In its basic form, a potentiostat is used to move the potential of the coupon a few mV (normally at maximum of 10 mV) near its free corrosion potential and to concurrently measure the current (ASTM Standard G96-90 (96)). Assuming that in the aforementioned small potential range, the current is proportional to the potential shift, and the so called 'linear polarisation resistance', Rp is evaluated using Ohm's law. Stern and Geary showed that, in case of uniform corrosion in conductive acid solutions, corrosion rate is inversely proportional to Rp.

Taking into account that this technique is relatively easy to perform not only in the laboratory but also in the field and that it is able to provide information in real-time on corrosion rate, the LPR method was applied also in environments different from the ones in which it was originally defined. Indeed this technique was also applied to study MIC on iron in a neutral anaerobic environment, on copper alloys in condensers treated with biocides and so on. It should be noted that the data provided by the LPR technique cannot always be accepted without additional information. One of the reasons is that the method refers to uniform corrosion, but localised corrosion often happens in MIC. The other reason is that the presence of corrosion products on samples exposed to a neutral environment can make the interpretation of the data very complicated (see Borenstein, 1994, for instance); LPR measurements on carbon steel under anaerobic conditions and in the presence of sulphide (5 mg/L or more) creates a risk of very large

errors due to the formation of porous corrosion products (Hilbert, 2000). Also the potential scanning rate during LPR measurement can play an important role: due to a high capacitive current, LPR technique was found to overestimate corrosion rate of carbon steel in an anaerobic SRB environment and, attempting to reduce this effect, very long measurement times, in the range of hours, were found necessary (Hilbert, 2000; Little *et al.*, 2000). Really the value of the resistance measured with the LPR technique is the sum of the true polarisation resistance Rp and of the solution resistance Rs between the coupon and the reference electrode: a large Rs caused by low conductivity of the electrolyte (such as in some potable waters) can result in a large error in the evaluation of the corrosion current. Data provided by the instrument must be corrected when the conductivity of the electrolyte is lower than about 0.5 mS cm^{-1} depending on the probe geometry (Perboni and Radaelli, 1998). These low values are often found, for example, in fresh waters, tap waters, boiler waters and so on.

The geometry of the electrodes and the finishing of its surface can play a determinant role in MIC monitoring more than any other kind of corrosion for high conductive waters, such as seawater, because the biofilm growth is strongly influenced by the value of water flow rate and surface roughness.

Finally, the following suggestions should be taken into account in the installation of the electrochemical cells:

- Use the same kind of alloys that are used in the plant for the electrodes
- Use electrodes with the same surface finishing and corrosion stage development as actually occurs on the surface of the materials operating in the plant
- Use electrodes with the same geometry as the monitoring equipment (tubes of a similar diameter for heat exchangers, tubes or pipelines, or plates for wall or plate exchangers and so on)
- Make sure that the water flow on the electrodes is representative of the plant condition to be monitored
- Make sure there are no thick or abundant deposits on the electrode surfaces.

Figure 15.1 shows an example of an LPR probe set-up used in industrial MIC environments.

Redox potential and open circuit potential measurement (OCP)

These measurements are very easy to perform both in the laboratory and in the field: they require an electrometer, a reference electrode, a platinum wire for Redox and a metallic coupon whose corrosion is evaluated. (see Chapter 7). The Redox potential is used in plant mainly to establish whether

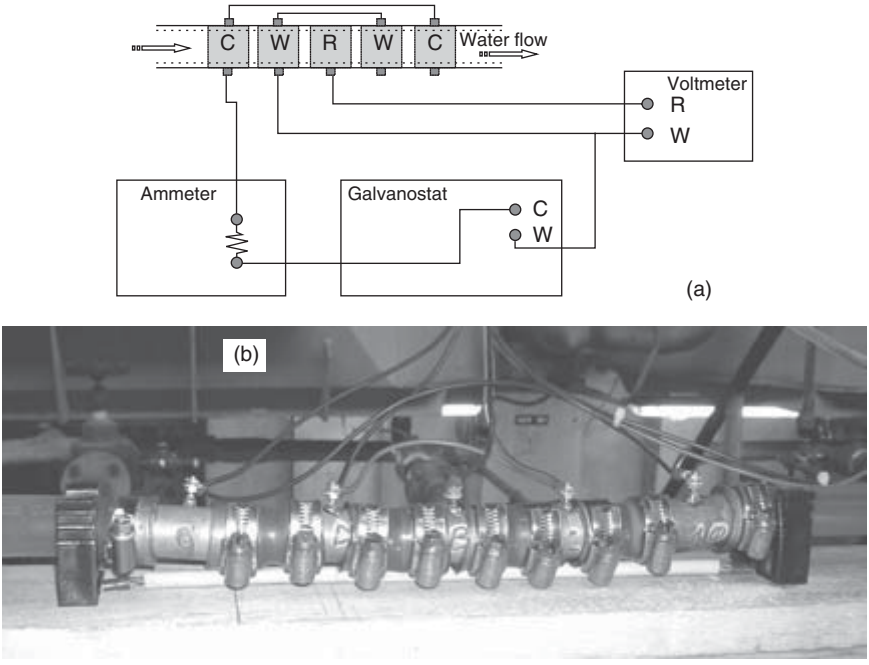

15.1 (a) Schematic of LPR technique. (b) Image of the electrochemical cell inserted in a test line of plant by-pass.

aerobic or anaerobic conditions are developing in water, or oxidant biocides are decaying in the solution.

Open circuit potential may give information about the passivation layer of metals and the thermodynamic risk for the integrity of the protective layer. Problems during in-field applications can occur if the reference electrode is not stable in the chosen environment. Zinc and commercial silver/silver chloride reference electrodes were found suitable for seawater; copper/copper sulphate reference electrodes have been found to be stable in soils. This technique does not give information on the actual corrosion rate and, if not integrated with other techniques, it could provide ambiguous indications about MIC (Borenstein, 1994).

The following are two examples concerning the use of OCP and Redox potential measurements:

- a high Redox potential suggests that planktonic bacteria are mainly aerobic but the corrosion of a metal exposed in the same environment can occur under a thick biofilm, at the bottom of which a prevailing anaerobic bacteria population may be present because the oxygen diffused from water is totally consumed in the upper biofilm layers

- a low free corrosion potential measured on an active-passive alloy can indicate corrosion in a passive state, i.e. a low general corrosion rate, in an anaerobic environment or, on the contrary, severe localised corrosion in an aerated one.

Electrochemical Impedance Spectroscopy (EIS)

The instrument used for the Electrochemical Impedance Spectroscopy (EIS) measures the impedance, in a wide frequency range, between a metallic coupon and a reference electrode.

In practice a small sinusoidal potential perturbation (<10 mV in amplitude) at a given frequency is added to the free corrosion potential and, joined with the resulting alternating current, sent to a frequency response analyser; the result of the analysis is the value of the electrode impedance at the tested frequency; the procedure can be repeated at other frequencies chosen over a wide possible range (e.g. from mHz to MHz, see ASTM G106-89, 1994) so that the impedance spectrum is obtained.

From the impedance values respectively measured at high and low frequencies the values of the solution resistance (Rs) and polarisation resistance (Rp) can be obtained, so that the main disadvantage of the LPR method when applied in a low conductivity solution is eliminated.

By looking at the trend of the impedance values in the intermediate frequency region, one can obtain additional information (double-layer capacitance, diffusion phenomena, etc.) about the corrosion mechanism. The analyses of the data are usually complex and must be done by experts. As a result, this technique for mechanistic studies is more applicable in the laboratory than in the field. Nevertheless if a 'model' for data interpretation in the considered system is already known the analysis of the data is greatly simplified.

Specific tentative studies were made in laboratory experiments with EIS to verify whether the formation of a biofilm affects the value of Rs, measured as a real part of the impedance at high frequencies. Unfortunately, the EIS technique was unable to reveal clearly the first crucial phase of biofilm less than about 200 µm in thickness (Feron, 2002). Nevertheless, other authors (Nagiub and Mansfeld, 2002) are using this technique extensively at laboratory level to study MICI (microbial influenced corrosion inhibition); they monitored, for instance, specific strains of *Shewanella sp.* able to provide excellent corrosion protection of Al 2024.

Electrochemical Noise (EN)

The EN technique consists of the measurement of spontaneous fluctuations (no external signal is applied) of the potential or of current between two

identical metal samples as a function of time (see Chapter 4). This technique was able to detect the initiation of localised corrosion, which is the most important feature of MIC (Little *et al.*, 2000), but it does not provide information on the corrosion propagation rate.

Researchers at Argonne laboratories (Tennessee, USA) have developed an online, real-time method to detect sustained localized pitting (Lin *et al.*, 2003). This approach includes new software and improved probes to interpret real-time electrochemical noise signals.

Because this technique is relatively easy to apply, EN appears suitable for increasing applications in the field. The technique is limited by the need for particular instrumentation and expert people for data analysis/interpretation. Laboratory applications of EN coupled with corrosion rate measurements permit the study of the influence of SRB and other organisms in promoting the pitting corrosion of iron in reinforced concrete. In particular, different steps of growth/rupture of the iron sulphide film on the metal surface were documented (Moosavi *et al.*, 1986). Results demonstrate that bacteria are preferentially attracted to iron corrosion products, these last determining their spatial distribution (Little *et al.*, 2000).

Electrical Resistance (ER)

The measure of the Electrical Resistance (ER) of a metallic sample can be used to evaluate the thickness decrease of the sample due to corrosion (see Chapter 11). The measurements give cumulative corrosion but, if measured as a function of time, they can provide an almost real time average corrosion rate. Sensitivity depends on the design of the probes and on the instrumentation; probes can be designed with different sensitivities and expected lifetimes. A new, improved highly sensitive ER-technique probe (by Metri-Corr, Denmark) has increased sensitivity and reduced the response time to the levels of other electrochemical techniques such as LPR. The advantage of ER is that this technique can be applied in any media, without limitation regarding the conductivity of the solution (Nielsen and Nielsen, 2003), and the data analysis is very simple. ER is therefore a widely used monitoring technique and has the potential to be useful also for MIC.

Precipitation of semi-conducting ferrous sulfides on ER probes does not seem to affect accuracy in the ER measurements when comparing weight loss, or in the low activity SRB media. The risk of underestimation is often the major reason for not recommending ER for sulfide media (the opposite is the case with LPR), but it seems that with proper sensor design and by avoiding probes that may short circuit, the error will be small due to the lower conductivity of ferrous sulfide to that of steel (Hilbert *et al.*, 2005). The main disadvantage of this technique is that the basic hypothesis of uniform corrosion is seldom respected in MIC.

Other techniques

Other various sophisticated electrochemical methods have been experimented: large signal polarisation techniques, random potential pulse method, electrochemical relaxation methods (programmed pulse relaxation, sinusoidal AC relaxation), scanning vibrating electrode techniques (a review in Schmitt, 1997). Various micro-sensors have also been used (Lewandowski *et al.*, 1988), but these tools at this moment remain useful mainly for laboratory studies in full controlled 'microcosmos'.

In the field, macroscopic MIC cases concern the oil industry pipeline. In a large waxy crude oil pipeline under low flow conditions, MIC corrosion is more of an issue, expecially for older fields where reservoir pressure is being supported by water injection. Mitigation methods usually involve periodic biocide treatments of the pipeline.

The monitoring of corrosion in the pipelines requires the use of in-line inspection (ILI) tools often consisting of 'intelligent pig runs' equipped with devices and sensors. ILI tools are forced to pass through the pipeline driven by the fluid flow or towed by a vehicle or cable. The most common technologies used for pipeline inspections are Magnetic Flux Leakage (MFL) and Ultrasonics (UT) associated with geometry measurement tools. The information which can be provided by these intelligent pigs covers a much wider range of inspection and troubleshooting needs, they are not specific for corrosion, but often the MIC monitoring programmes refer to the data collected with that facility (Farquhar *et al.*, 2005).

The field signature method (FSM, CorrOcean ASA, Norway), is one of the techniques applied to monitor corrosion inside buried pipes and subsea flowlines. It is a variant of the ER technique (see Chapters 11 and 28): an array of metallic pins (electrodes) are fixed on the external surface of a specially prepared section of pipe in which an aggressive solution flows. A known direct current is applied and it flows through the pipe wall. Voltage drops between the pins are recorded as a function of time and converted into losses of the wall thickness in different areas of the pipe. The sensitivity is claimed to be 1/1000 of wall thickness, or better, in case of general corrosion.

The non-uniformity of the attack can be revealed if the spatial resolution of the pins is high. For example, a resolution of less than 12 mm for the distance between the pins may reveal a pit of 2 mm × 2 mm × 2 mm in a plate 24 mm thick. For corrosion control the pipe section for FSM is designed to last over the total operational lifetime of the structure and can be engineered for a variety of situations and geometries, e.g. a pipeline on the seabed. This technique is obviously quite expensive and the number of electrodes fixed on the pipe wall can be very high if a good resolution for localised attacks is required. In practice the

sensitivity is not high enough for monitoring initiation of pitting and small attacks.

In addition the formation of sulphide layers generated by SRB might complicate the signals, as in the cases of ER probe and also the LPR probe.

15.3 Electrochemical sensors for the evaluation of MIC risk

In industrial practice, it is obviously more important (and more effective) to prevent MIC and minimise corrosion risk than monitor the evolution of corrosion phenomena. In this light, during recent years some innovative electrochemical probes for MIC prevention were proposed and implemented for application in plants. The working principle of these sensors is based on an effect of the biofilm initially observed on stainless steel exposed to aerated seawater: the increase of oxygen reduction when biofilm covers the metal surface.

This phenomenon, often known as 'cathodic depolarisation' (Mollica and Trevis, 1976; Mollica *et al*., 1990; Mollica, 1992) was repeatedly observed later by several researchers (Ishihara *et al*., 1995; Eashwar and Maruthamuthu, 1993; Videla *et al*., 1989; Lee *et al*., 1984) so that it is now widely recognised as a 'property' of marine biofilm. The same effect was later observed in other natural waters such as estuarine, river (Dexter and Zhang, 1990; Maruthamuthu *et al*., 1995), in wastewaters and in mineral waters (Cristiani, 2005b). It is also widely accepted that the 'cathodic depolarisation' is a common cause of MIC on stainless steel (and similar active-passive alloys) in seawater: indeed it was shown that, as a result of a gradually faster oxygen reduction induced by biofilm growth, the probability of localised corrosion onset increases, the propagation rate of localised corrosion is faster and the galvanic current between passive alloys and less noble alloys present in the plant becomes higher (Licina, 1989; Scotto *et al*., 1985). It follows that a device able to signalise the first appearance of biofilm activity can be used to signalise the presence on the metal surface of MIC risk.

Although there are variations in the different techniques, all the electrochemical devices to monitor biofilm currently on the market reveal biofilm activity as they influence cathodic depolarisation and other anodic effects. Examples of electrochemical devices includes the BIoGEORGE™ probe (by Structure Integrity Associates, USA) suitable for detecting biofilm effects induced by aerobic or anaerobic bacteria, and the BIOX probe (by CESI, Italy), set up to detect also cathodic processes due to oxidant biocides added to water. The BIoGEORGE and BIOX probes will be described in detail in Sections 15.3.1 and 15.3.2. Despite the simplicity of the probes, these devices are extremely sensitive to the effects generated by biofilm during the first phases of growth.

It must be noted, in addition, that these electrochemical sensors are able to signalise the biofilm also in the presence of complex fouling on the metal surface (scale, deposits, mud, etc.)

The main limits of the electrochemical biofilm sensors are:

- they cannot be used if temperature is higher than about 40 °C (at higher temperatures 'cathodic depolarisation' induced by biofilm growth decreases)
- they signalise the biofilm growing on the surface of a stainless steel (or titanium) sample but the biofilm growing on the surface of different alloys exposed in the same environment can be different.

15.3.1 BIoGEORGE system

BIoGEORGE™ (Structural Integrity Associates, USA) was the first system commercialised. It utilises a potentiostatic technique: an electrode made of a series of stainless steel discs (or titanium discs for saline waters) is polarised at a fixed cathodic potential, with respect to an identical stainless steel electrode, for one hour a day. The resulting current reaches a fixed potential drop between the two electrodes and the residual current measured when the external polarisation is switched-off (measured every 10 minutes during the rest of the day), is used as an index of the biofilm development on the probe surface. A gradual increase of the measured current (the first 'applied' during the polarisation and the second 'generated' after polarisation) is a result of biofilm development.

Possible explanations of the generated current circulating in the biofouled probe may be as follows. Different polarization is applied on each disc of the electrodes inducing the development of different biofilms (which may be 'patchy' or continuous) on each electrode. These biofilms include non-homogeneous microbial populations as number and kind of micro-organism (Licina *et al.*, 1990; Licina and Nekoksa, 1993). Difference in anaerobic species was documented on cathodically protected structures (Guezennec, 1991; Nekoksa and Gutherman, 1991).

A specific electrochemical condition occurs on the anodic sites of the probe during polarization, such as local pH decreases. Inhibition of biofilm development by decreasing the seawater pH to 6.3 has been documented on stainless steel and other active-passive alloys (Cristiani *et al.*, 1995). When polarization has stopped, the shift of the free corrosion potential induced by biofilm only on the cathodic sites sustains the current flowing between the electrodes. In Figs. 15.2 and 15.3 the BIoGEORGE™ probe and typical graphics are reported.

(a,b)

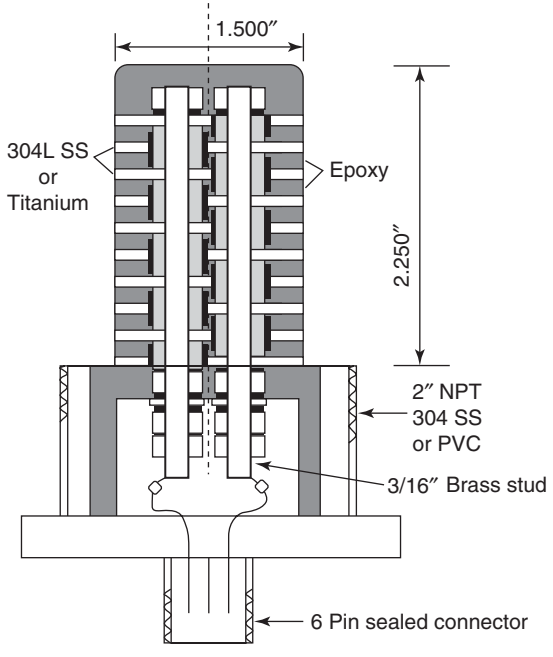

(c)

15.2 BIoGEORGE™ system: electronic probe (a,b) and schematic of the probe (c) showing the two electrodes made of the same materials but alternated on the probe surface.

The commercial system consists of a cylindrical probe, its integrated electronics, interconnecting cable, display software, user's manual, and product support.

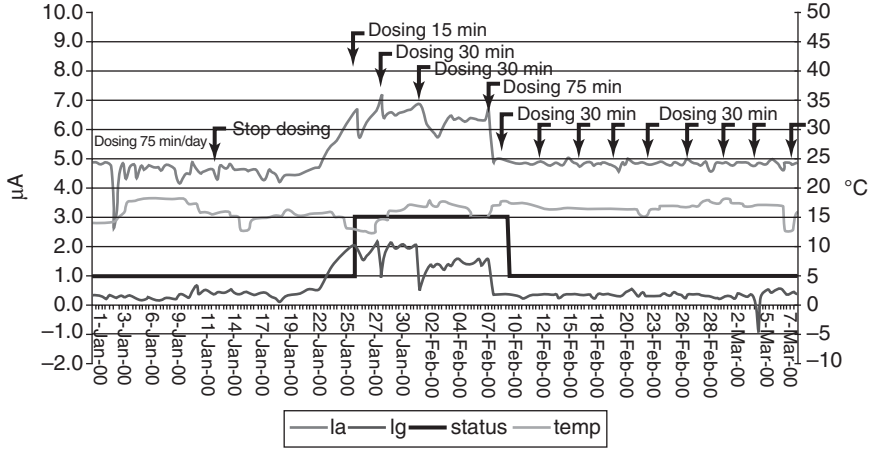

(a)

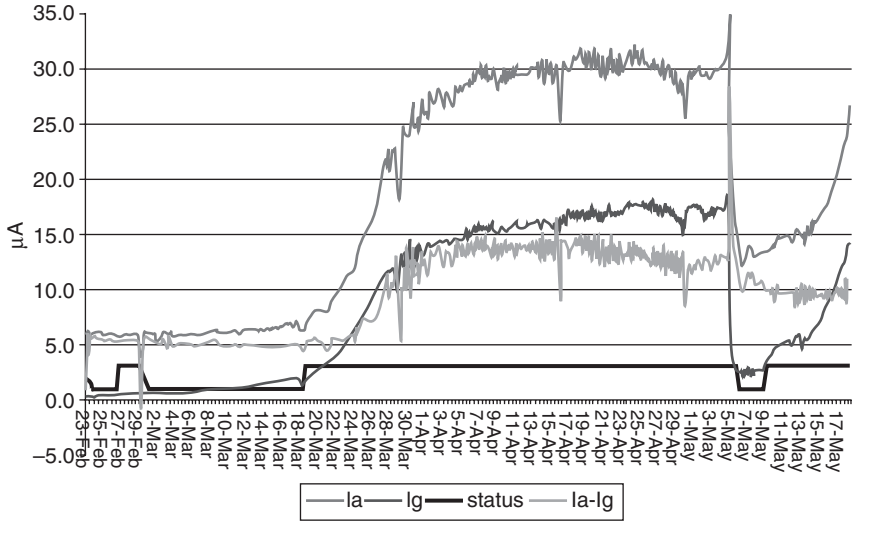

(b)

15.3 BIoGEORGE™ typical graphics of signal trend. The graphic (a) shows the signal trend in a cooling water circuit during the optimisation of sodium hypochlorite treatment (TRO = 0.6 mg Cl_2/L). Status Code: 1,0 = Clean, 2,0 = Waiting to establish baseline, 3,0 = Fouled/Alarm. Graphic (b) shows the start of biofilm growth on 1 March (the alarm parameter for 'Ia' was significantly increased) and the effect of chlorination injection on 5 March.

Probe status is indicated on the integrated electronics enclosure by an LED indicator (red light/green light) on the controller. The controller compares the applied and generated currents to baseline levels for each

current type. When the applied or generated current deviates from the steady baseline (that is indicative of a clean probe surface, green light), an alarm (red light) is indicated. A yellow light appears as the system is establishing a steady baseline condition.

The probe can be installed into a piping system or side stream via a 1-inch or 2-inch threaded connection. Special probes can also be built for 'hot tap' type fittings or flow-through probes. The unit operates on 110 or 220 VAC and has built-in battery backup. System data can be downloaded to the user's PC. Software is included with the system for analysing the data and creating detailed trend plots.

The sensor can work in different kinds of industrial water, including seawater as well as water with the lowest conductivity and in anaerobic conditions (Licina and Nekoksa, 1993). There are many industrial applications of BIoGEORGE™, for instance in nuclear and thermal power plants, cooling towers and in gas field produced waters, since the 1990s (Licina, 2001; 2004; Fallon and Licina, 2004; Andrade, 2006).

15.3.2 BIOX system

The BIOX system was developed specifically to improve the antifouling treatments of cooling systems of industrial plants (Cristiani and Giancola, 2000; Mollica and Cristiani, 2002). The system utilises an electrochemical probe in a specific configuration allowing the continuous detection of two phenomena: the aerobic biofilm growth on the working electrode and the cathodic effect of oxidant biocides added to the water (such as chlorine, bromine, chlorine dioxide, hydrogen peroxide, peracetic acid, ozone and others) (Cristiani *et al*., 2001; 2004, Cristiani, 2005a).

The probe consists of a bi-metallic couple: a stainless steel sample is coupled to a zinc electrode through a high resistor which strongly limits the galvanic current (Fig. 15.4). This assembly simulates a quasi-intentiostatic technique and the evolution of 'cathodic depolarisation' on stainless steel induced by biofilm development is signalised by an increase in the ohmic drop across the resistor. The design of the BIOX probe permits its application also in low conductivity water.

The electrical voltage across the resistor is the BIOX signal and falls in the range of 300–1400 mV. A typical trend of the BIOX signal in the presence of chlorine and during biofilm growth is reported in Fig. 15.4.

In the case of the addition of oxidant (chlorine for instance) to the solution, the probe response is immediate. In the case of biofilm growth on to electrodes the time response is considerably longer, because several days may be required to completely cover a clean probe with biofilm. By analysing the probe signal trend under regular operation conditions, it is possible

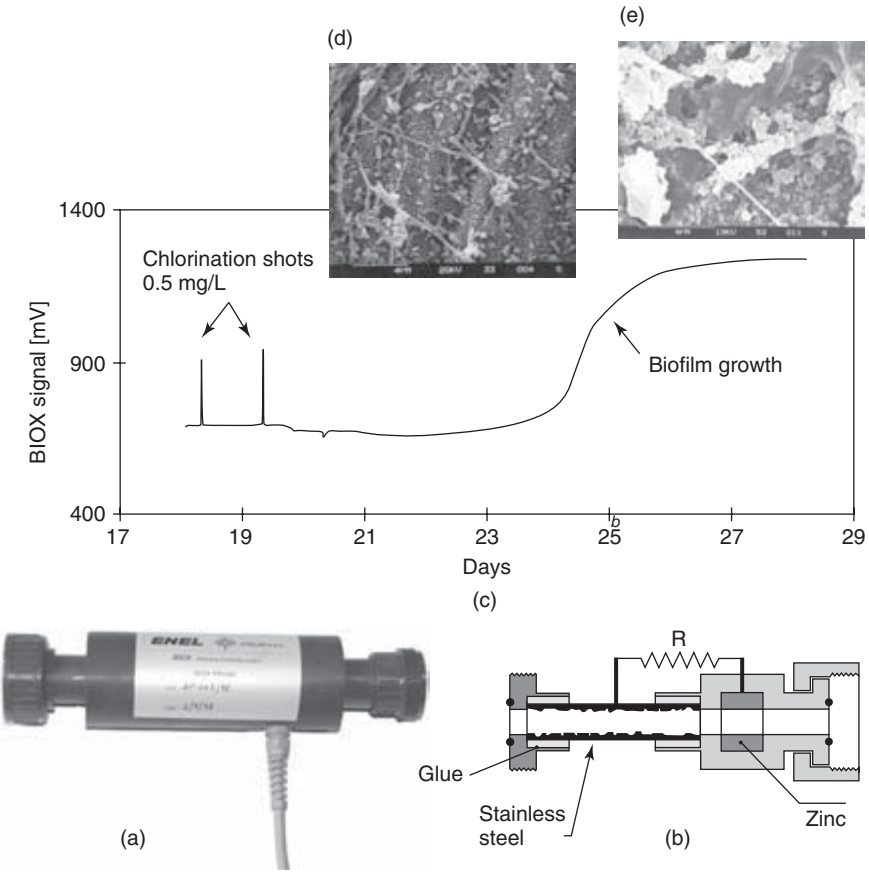

15.4 BIOX probe (a) and schematic (b). Typical graphic of the signal (c) showing the trend in the case of chlorine addition in the water or biofilm growth on the probe. Two micrographs of marine biofilm, corresponding to two different levels of the signal: low (d) and close to saturation (e).

clearly to distinguish the contributions of the two phenomena. The Industrial BIOX system (Fig. 15.5) consists of a dedicated industrial computer with a monitor showing a signals trend, one or more probe set, integrated electronics, interconnecting cable, software, user's manual, and product support. Each probe set generally consists of a BIOX tubular electrochemical sensor of internal diameter of 16–20 mm and, optionally, with a titanium cathode, a temperature meter and a flow-meter. The data video graphic output on the monitor permits a complete on-line visual check of biocide oxidant treatments. All stored data can be shown on site or exported to

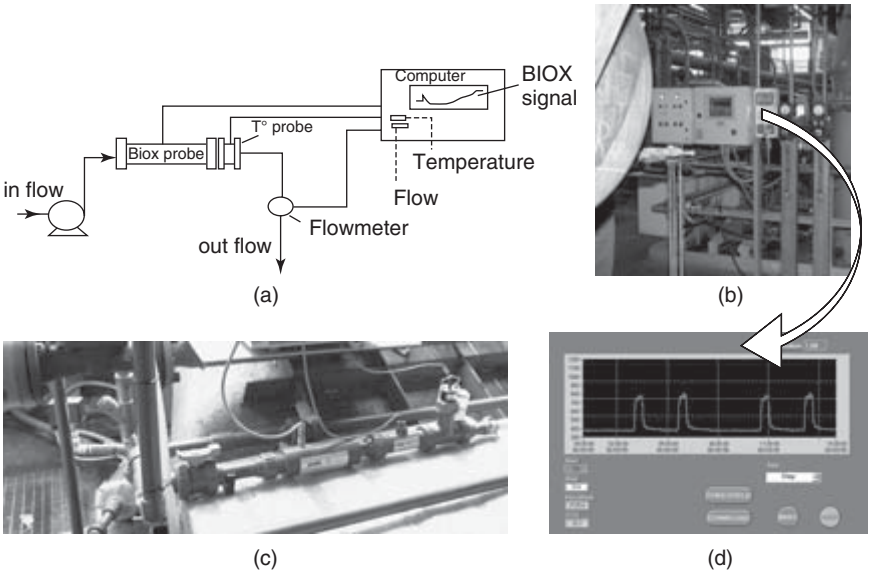

15.5 Industrial BIOX system: schematic of the system (a), computer box installed in a power plant (b), probe set (c), layout of the computer display (d).

other programs by a floppy disc drive, a USB port or by remote control. Default measuring is every 10 seconds and data storage is every 30 seconds. It is also possible to vary the frequency. This last aspect permits the acquisition of details of signal trends during treatment based on a short biocide dosage.

In seawater, it was found that BIOX was able to clearly signalise the corrosive effects generated by a biofilm covering close to 1% of the surface area of the stainless steel cathode (i.e. a number of settled bacteria in the order of 10^6 bacteria/cm^2). Further biofilm development generates a signal almost proportional to the surface coverage; the signal provided by the sensor goes to saturation when biofilm coverage reaches a value close to 100% (i.e. a number of settled bacteria in the order of 10^8 bacteria/cm^2). An additional increase in the amount of biofilm is no longer signalised.

The sensitivity of the probe to the oxidants depends on the nature of the oxidant but, generally, falls in the range of concentration normally useful for antifouling treatments. The linearity of the slope with respect to the concentration of biocide oxidants results less in fresh water than in seawater, but concentration in the range 0.2 to 1 mg/L of chlorine can be effectively detected in every kind of water. In seawater, concentrations of

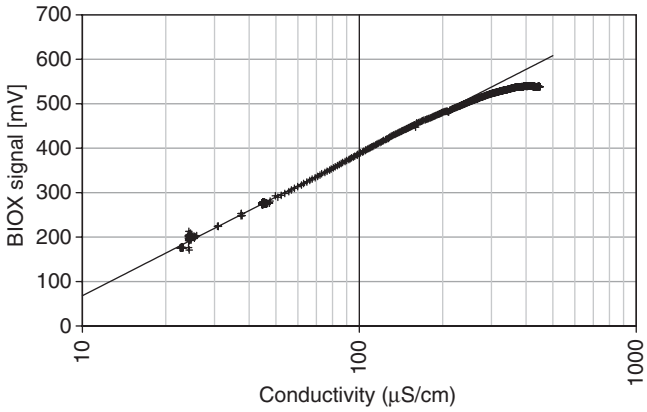

15.6 Contribution of water conductivity on the baseline value of BIOX probe. (Cristiani 2005, Eurotherm77, with permission.)

0.02 mg/L of chlorine dioxide have been effectively detected as well as concentrations of 1–10 mg/L of peracetic acid.

Tests confirmed that the BIOX sensor can work in the same configuration in seawater as well as in river water and mineral water with low conductivity (>50 µS/cm, Fig. 15.6), signalising a growth of between about 10^6 to 10^7 bacteria/cm^2 (Cristiani, 2005b). Confirmation came from several field applications performed with the BIOX system in environments such as river water, drinking water, re-circulated waters, wastewaters. The baseline value of the BIOX signal is not significantly influenced by temperature in the range of 5–40 °C, or by sunlight as shown in Fig. 15.7. Decrease in pH is clearly detected with an increase of the signal as shown in Fig. 15.8. The pH effect is of particular relevance in the case of monitoring in cooling tower circuits. The BIOX signal fails in the case of significant developments of anaerobic bacteria in the biofilm and in anaerobic water environments.

This probe is not affected by carbonate formation on the cathode, because of the very low circulating current. The presence of metal ions (ferrous ion for instance) or the high temperature of the water (more than 32 °C) can promote the growing of inorganic scale on all the surfaces exposed. When metal deposit or thick scale covers the electrodes, the signal baseline falls below its normal value, indicating the necessity to clean the probe. The cleaning operation of the probe can be done by mechanical scrubbing or chemical treatments taking a few minutes, filling the probe with (or circulating) hydrochloric acid 5% for few minutes.

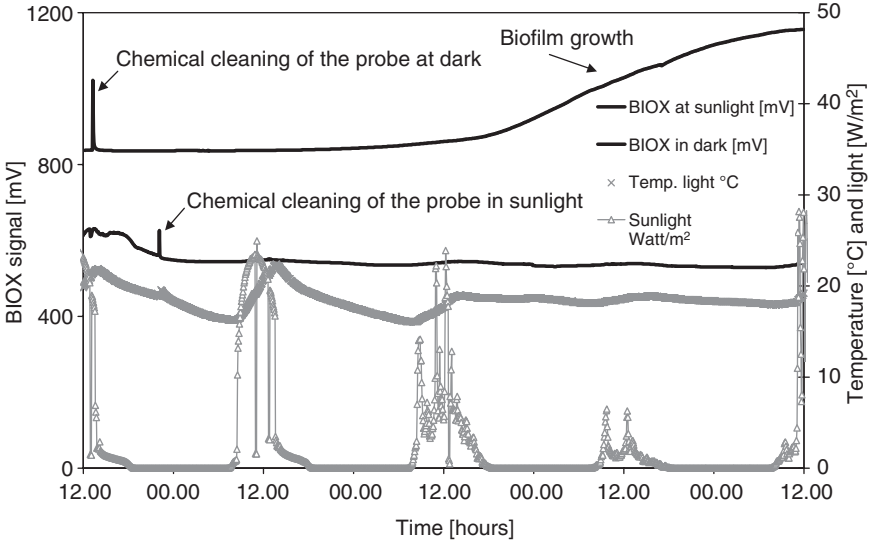

15.7 Signals of two BIOX probes exposed to sea water respectively in sunlight and darkness: it shows the fast signal increase due to biofilm growth on the probe kept in the dark. Temperature and light variations during the day do not influence the baseline of the BIOX probes.

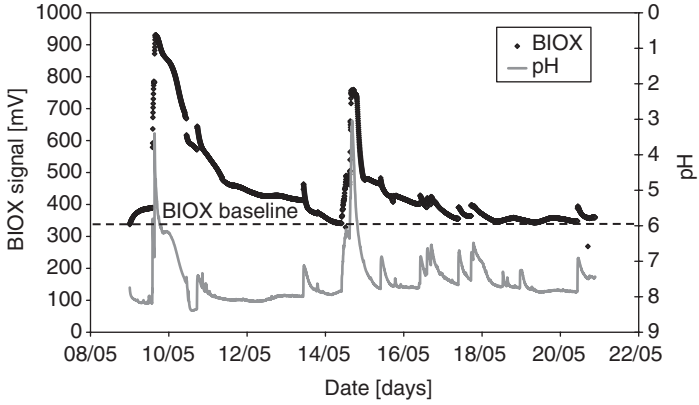

15.8 Decrease in pH lowers the baseline value of BIOX probe. Test performed adding hydrochloric acid to demineralised water.

Because of the promising results obtained for the first applications, the BIOX system is now used alone or integrated with other corrosion monitoring techniques in order to optimise different kinds of industrial antifouling, anticorrosive and disinfecting water treatments. Some tests are still in progress for the application of a new version of the system in soil.

15.4 Integrated on-line monitoring systems

Usually, the same chemical treatment performed against biofilm growth in industrial facilities is targeted to prevent deleterious effects other than MIC, such as the reduction of heat exchange efficiency, increased friction factor or the development of pathogen micro-organisms in the water. Nevertheless, it must also take into account the fact that biofilm enhances bacterial resistance against several external factors, including biological competitors and the action of chemical biocide, which forces operators to use more intensive disinfection programmes than those effective in breaking down the sole bioburden of bulk water. On the other hand, biocides could play an active role in corrosion development processes in particular the oxidant agents which are utilized most. They could also be involved in environmental concerns, because of the discharge of residuals and by-products (Rook, 1974; Symons *et al*., 1996; Jenner *et al*., 1997).

In these cases a higher level of attention is required to reach treatment optimisation. It means, in practice, that an effective monitoring system must be able, at least, to signalise on line and in real time if treatments and procedures applied are to play the role of a corrosion inhibitor and provide information to rationalise, and then minimise, the application of these procedures. Furthermore, the biocide dosage, in many cases, is mixed or alternated with other chemicals. The phenomena commonly affecting the industrial process/cooling waters that should be controlled by the chemical treatment include macrofouling growth, scale deposition and chemical pollution (see Table 15.3). In the light of all these aspects, reliable monitoring of the water treatment (anticorrosive, antifouling or disinfecting) results in the best way to prevent MIC and the other negative, correlated risks.

At this level of knowledge a reasonable amount of 'cross-validated' information can, normally, be provided by a set of a few sensors concurrently working in the plant associated with the MIC risk. The number and type of these sensors depends on the specific environment, the metal(s) utilised in the plant and the nature and sensitivity level of the requested information (see Tables 15.3 and 15.4). One important conclusion to the experience collected from the case histories was to verify, by comparing the data from the different devices employed in the practical applications, that complete or sufficient information is often achievable from a single electrochemical MIC risk monitoring device, operating on-line and in real time.

The base system, from the author's experience, includes a single electrochemical probe, a flow meter and a temperature meter in the standard configuration of the BIOX system, but the BIoGEORGE system associated with other commercial sensors and hand-made coupons should also work well in several similar applications. A data acquisition system and a computer (used for the storage/elaboration/presentation of the data) has to

Table 15.3 Stages/kinds of fouling sensible to the chemical treatments of industrial waters

Stage of fouling	Typical application
First stage of living biofilm growth	Wide range of application for MIC risk assessment
Stage of biofilm influencing process parameters	Food industry, pharmaceutical industry, desalination plants, demineralisation process (membranes), heat exchangers
Biofilm with micro-organisms producing toxics, pollutants	
Clusters of micro-organisms in the bulk waters (total viable bacteria, specific bacteria as pathogens, fungae, moulds, micro-algae)	Process waters of food industry, pharmaceutical industry, wastewaters, drinking water, pulp and paper industry, cooling towers
Algae, macrofouling growth, larval settlement	Open cooling circuits, cooling towers
Solids, organic matters, oils	Wastewaters, drinking water plants
Scale deposition	Fresh waters, cooling towers, re-circulating waters, hot waters

complete the monitoring system in any case. An additional electrochemical cell, made with material from monitoring equipment using the LPR technique is necessary when the corrosion rate monitoring is requested.

Other on-line sensors such as a turbidimeter (in open circuits), a pH meter or Redox measurement (in cooling towers) may be useful. In the latter case, when scale deposition represents the main topic, a scale sensor could be equally useful, but reliable sensors for industrial application need to be assessed. In the case of chlorination treatments, it must be taken into account that most of the commercially available systems to monitor the TRO (Total Residual Oxidant) on-line work quite well in fresh and drinking waters (the amperometric ones in particular, commonly used in swimming pools, drinking water plants and so on), but very few of them, based on colorimetric or potentiometric measure (Mod. ORION 1770, Thermo Scientific, USA for instance) are able to give correct and effective measurements in seawater, least of all in cases of concentration less than 0.2 mg/l. A set of sample coupons for weight loss determination and visual observations of biofouling and corrosion (Fig. 15.1) may be inserted in the test line to collect additional confirmation of the phenomena monitored.

In the case of macrofouling risk (algae, hydroids, mussels and other sessile organisms), specific panels (concrete, ropes and plastic supports) can also

Table 15.4 On-line sensors used for integrated monitoring of corrosion, biofilm and industrial water treatments

Parameter	Sensors	Application
Biofilm growth	BIOX probe BIoGEORGE probe	Almost always
Corrosion rate	Corrosion-meter LPR cells	When corrosion phenomena or the metal passivation processes have to be monitored
Oxidant biocide concentration (above 0.2 mg/L of chlorine)	BIOX probe Redox probe Amperometric systems Colorimetric systems Sens-ion probe	For oxidant biocide treatments (chlorination and the others based on bromine, chloramines, chlorine dioxide, peracetic acid, hydrogen peroxide, ozone, etc.)
Oxidant residual concentration (below 0.2 mg/L of chlorine)	Total Residual Oxidant sens-ion probe Colorimetric systems Amperometric systems	To control very low residual concentration at the discharge Amperometric systems work best in fresh, clean waters
Non oxidant chemicals	Colorimetric systems Specific systems	Water treatments alternative to chlorination, such as quaternary ammonium salts or filming amines
pH	pH-meter	Fresh waters, cooling towers
Redox potential	Redox potential-meter	Wastewaters When the aerobic condition has to be monitored
Temperature	Thermometer	For optimisation of biocide dosage according to season In case of macrofouling risk monitoring For optimisation of scale control Supporting the precision of other measurements
Water flow	Industrial flow-meter	Always in the cases of test line in by-pass: to be sure to have the same flow in the measure line as in the plant facility

be immersed at a critical (but reachable) point of the plant. This is typically the case of open marine cooling circuits.

Microbiological kits for bacterial counts could be useful only in the specific cases where the bioburden of bulk water has to be necessarily controlled (as in wastewater or re-circulating systems).

15.4.1 Costs of monitoring equipment

The cost of each sensor mentioned above is not very high. The most expensive is the on-line Total Residual Oxidant Meter for seawater applications (more than 10000 US$). This sensor needs analytical chemical supply and frequent maintenance (at least monthly). Consequently, the use of that sensor is suggested only when a very low concentration of oxidant (chlorine less than 0.2 mg/L for instance) needs to be rigorously controlled, typically at the discharge of open cooling circuits. In these cases, the device must be installed for the other monitoring probes requiring an extra cost to collect the output signal. The computer and the data acquisition system is the most critical and expensive component of the integrated monitoring system, especially when an industrial computer is preferred to solutions with remote control, because the industrial environment (coal dust, atmospheric agents, humidity, high temperature, etc.) is deleterious for the standard electronic components. Commercial software developed for specific applications is already available (e.g. in BIOX, BIoGEORGE and LPR commercial systems). The most complex ones are able to drive both the LPR electrochemical measures and the acquisitions of all the other probe signals (e.g. the software for the Integrated BIOX system). The cost depends mainly on the number of probes and to the application.

The basic BIOX and BIoGEORGE systems cost about the same they are a bit more expensive than the LPR commercial systems. The electrodes for LPR probes, the coupons of metal samples and the supports for macrofouling may be prepared in situ using the material coming from the equipment/circuit of the plant. On-line sensors and the cases in which they had been frequently integrated into the loop are summarised in Table 15.4. In Section 15.5, some examples of integrated monitoring systems for MIC risk prevention applied in industrial plants to optimise water treatments are described.

15.5 Case histories

15.5.1 Inhibition of crevice corrosion on stainless steel

Several field tests were conducted to determine whether electrochemical sensors can really be utilised to minimise corrosion problems in plants and if these sensors are reliable for long term application without maintenance. The results of a test lasting one year in 1996 (Mollica and Scotto, 1996) are briefly described as follows.

In the tests, seawater was pumped, once, through a series of tubes of external diameter 25 mm, wall thickness 1.5 mm, made of stainless steel (UNS31600). In order to promote the onset of localised corrosion the stainless steel tubes were connected using rubber hose which was pressed on the external surface of the stainless steel tubes: in this way artificial crevices are pre-formed on the metal under the rubber. An electrochemical probe, in the configuration of a BIOX sensor, was inserted at the end of the test line. It was utilised to evaluate an antifouling procedure to apply to the stainless steel tubes and to the sensor itself.

When the BIOX signal was increased above a prefixed value (as a result of the biofilm growth), a single standard chlorination (at 0.5 mg/L for 30 minutes) was started automatically and chlorine was added in the middle of the test line, leaving half of the samples upstream unchlorinated. At the end of chlorination, the biofilm on the probe was partially destroyed and, as a consequence, the BIOX signal decreased. When new biofilm was growing, the above described procedure was automatically repeated. The test started in August 1994 with the seawater temperature close to 28 °C. During the year the temperature first decreased to about 14 °C in winter and then rose again to 28 °C in the following summer. No maintenance was applied to the probe during the test. The trends of the signal provided by the sensor indicate that during the two summers, it was judged sufficient to apply a single chlorination approximately every 1.5 days. In winter the sensor indicated that only one chlorination was sufficient about every six days as a consequence of decreased biological activity.

The tubes exposed to untreated seawater were heavily fouled whereas the tubes exposed to the automatically treated seawater looked totally clean. In the latter case, observation of the surfaces by the Scanning Electron Microscopy (SEM) revealed only the presence of a few settled bacteria, randomly distributed. Heavy crevice corrosion, leading to perforation of a 1.5 mm thick pipe wall, was observed on the stainless steel tube exposed for three months to untreated seawater. Only a shallow attack was observed on the stainless steel pipe exposed, for the same time length, to automatically chlorinated seawater (Fig. 15.9). Additional tests showed that the application of a weak and inexpensive cathodic protection is also sufficient to avoid the onset of crevice corrosion on stainless steel exposed to automatically chlorinated seawater.

In conclusion electrochemical sensors were found reliable also for long time application without maintenance, and able to provide a set of information which can be used to minimise the application of antifouling procedures in seawater, increasing plant efficiency and, concurrently, decreasing corrosion problems on the active-passive alloys.

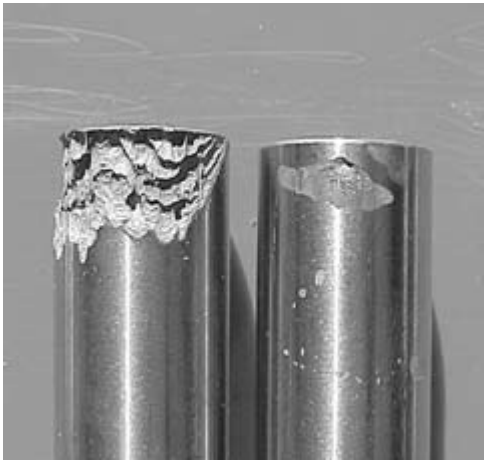

15.9 Crevice corrosion propagation on AISI 316 pipes after 3 months of exposure to untreated (left side) and automatically chlorinated seawater (right side) Mollica and Scotto (1996).

15.5.2 Optimisation of cooling water treatment in power plants

The industrial version of the BIOX system was successfully applied in seawater cooling systems of Italian power plants from 1996 to optimise chlorination treatments (Cristiani and Agostini, 1999). Figure 15.10 shows examples of signal trends provided by the sensor during approximately one month of exposure (Mollica and Cristiani, 2002). The trend of the BIOX signal can be described as composed of several sharp peaks superimposed over a stable base line at about 500 mV. Peaks were observed when intermittent chlorination (20 minutes at 0.5 mg/L of residual oxidant) were used in the plant following the program routinely applied during summer (four chlorinations per day); the height of the peaks was found proportional to the residual chlorine concentration in the range 0.2 to 1 mg/L. The sensor suggests that this chlorination program was sufficient to avoid biofilm growth. Indeed the base line continuously has the same value that was measured at the beginning of the test on the clean probe.

When the chlorination program was not run for three days (from 17 September 1996 to 20 September 1996) the slope of the sensor base signal was positive. The increase of the base signal towards 700 mV means that biofilm was growing but it was still in the first phase of its development (in this period no valuable decrease of the condenser efficiency was observed). Once the normal chlorination programme was restored the base value of

the signal returned rapidly to the value observed on the clean probe. This suggests that the chlorination programme usually applied in the plant was not only able to prevent biofilm formation but also to rapidly destroy the biofilm once formed.

The antifouling programme was changed after ten days and the chlorination frequency was strongly decreased. The graph in Fig. 15.10 indicates that a reasonable control of biofilm growth was obtained with only one chlorination per day, i.e. with 25% of the chlorine previously utilized.

Following this first study, many antifouling treatments for condensers of power plant based on chlorination and other chemicals (chlorine dioxide and peracetic acid included) have been monitored by BIOX system (Cristiani, 2005a). The results obtained underlined that:

- at the beginning of the BIOX signal increase, the sterilisation does not require a huge quantity of biocide, and a continuous, low level of chlorine dioxide results are very effective against biofilm at this stage;

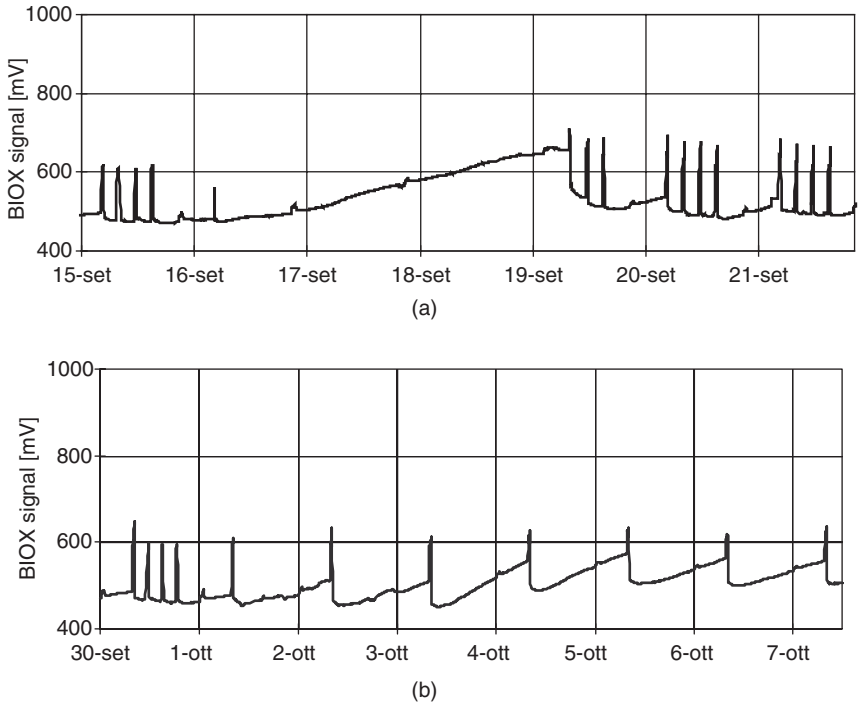

15.10 Optimisation of chlorination in an Italian power plant by using a BIOX system. Treatment based on 0.5 mg/L dosage of sodium hypochlorite for 20 minutes (peaks of the BIOX signal), 4 shots/day in September (a) and 1 shot/day in October (b).

- the exponential signal increase, coinciding with the exponential growth of the bacteria community has very short duration, but it is still easy to chemically control the biofilm at this stage
- after reaching the platform, the steady state could require a stronger dosage of chemicals; the complete disinfection could not be guaranteed.

Very low levels of chlorine and peracetic acid were not so effective in controlling biofilm growth as a lower level of chlorine dioxide. However, shot dosage of few mg/L of each chemical was effective enough to destroy mature, untreated biofilms.

Another positive performance of the BIOX system concerned the monitoring of in-service mechanical cleaning by sponge balls. In particular, the monitoring permitted the documentation of different chemical and mechanical force against the biofilm (Cristiani, 2005a). With a water flow of about 1 m/s in the 20 mm diameter tubular probe, the mechanical treatment was found very effective: a BIOX signal of about 900 mV, corresponding fell down to a 'moderate' biofilm growth, after the passage of a single ball. However, with a flow above 2 m/s, 1 mg/L of chlorine dioxide dosed for 1 h was necessary to destroy microbiological activity.

15.5.3 Detection of biofilm in mineral water plant

During a two month test conducted with a BIOX system inserted in a bypass in-line with an industrial tank of mineral water (Fig. 15.11) (Cristiani, 2005b), under a flow of 1100 l/h, corresponding to 1.5 m/s in the tubular

15.11 On-line monitoring of biofilm absence in mineral water plant by the BIOX system (Eurotherm77, 2005 with permission).

probe of 16 mm diameter, the probe signal held down around 400 mV during all the period of the test, indicating the complete absence of biofilm. The tests confirmed the laboratory results showing that the BIOX system works correctly with water having a low conductivity of 350 µS/cm. In a subsequent test performed with the same water at low flow of about 0.4 m/s, but outlet to a bacteria contaminated tank, the BIOX probe was able to detect the first stages of biofilm growth reaching the value of 800 mV. The test line was then cleaned and disinfected with a dosage of about 15 mg/L of chlorine for 15 minutes.

The BIOX signal reached values not more than 900 mV during chlorination (in spite of the high concentration used) and it came back to baseline values after the dosage was complete, keeping the baseline value for a long duration. SEM micrographs of stainless steel coupons sampled from the test line before and after chlorination documented the presence of a thin uniform biofilm on all the surfaces detaching in consequence of chlorination.

15.5.4 Testing of a disinfecting treatment in wastewater

A treatment based on peracetic acid (PAA) to control microbiological growth in a pilot serpentine reactor (10 m^3/h) fed by secondary settled effluent coming from the wastewater treatment plant in Southern Italy was investigated using a BIOX probe with external electrodes submerged into the water flow exposed at sunlight. A number of treatments were carried out during a six month period at different PAA continuing dosages ranging from 2 to 13 mg/L. PAA decay was determined by monitoring the residual concentration during each treatment using both electrochemical on-line BIOX signals and standard chemical off-line methods. Data coming from biofilm electrochemical monitoring were integrated and compared with microbiological analytical results. A residual of 3–4 mg/L of PAA was required in order to destroy the biofilm already grown on the electrochemical probes submerged in the final part of the serpentine pilot reactor. PAA dosages lower than 2 mg/L were found sufficient to prevent the early stages of biofilm development on the clean probes. The total microbial charge and amount of *Escherichia coli* in the bulk water of the pilot plant remained under control even at the same lowest tested PAA dosages (Cristiani *et al.*, 2004; Dell'Erba *et al.*, 2007).

15.5.5 Monitoring of copper alloy condenser tube passivation in a power plant

Microbial activity negatively influences the passivation process of copper alloys, in seawater in particular. In the light of some recorded case histories, an integrated monitoring of corrosion, biofilm and chlorine dosages has

been performed on Copper-Nickel 70/30 coupons (UNS C71500, external diameter of 22 mm, wall thickness 1.6 mm) made of the same condenser tubes used in the marine cooling circuit of an Italian power plant.

The study documented how the 'little economy' in biocide treatments during the start-up period of exchanger equipment can return severe additional costs because of early failures of the bundle (Cristiani *et al.*, 2007). The following sensors have been chosen for monitoring, inserted in a by-pass close to the condenser:

- one BIOX tubular sensor to monitor the biofilm growth and the chlorination treatment;
- one tubular electrochemical cell made of coupons from the condenser tubes to monitor the corrosion rate of CuNi 70/30 by LPR technique;
- one flow-meter, one temperature sensor and one turbidity meter to monitor the physical-chemical parameters of the water flow.

Weight loss determination, chemical and metallographic analyses have also been done off-line during the monitor programme on tubular coupons of the condenser tubes.

The data collected documented the occurrence of localised corrosion on the surface of the CuNi 70/30 specimens in the case of events causing the enrichment of biologically active mud in sea water (big ships moving or strong rain close to the inlet of cooling circuit) or after the stagnant condition occurring in the tubes. The integrated monitoring permitted an effective chlorination treatment of the condenser cooling water, able to promote the development of a firm 'passive layer' on the CuNi 70/30 tubes.

Figure 15.12 shows two periods of integrated monitoring. In Fig. 15.12a, the CuNi 70/30 passivation layer was well established and the detected corrosion rate was very low. In Fig 15.12b, the peak of corrosion appeared after an intensive mechanical cleaning of the probe surfaces that removed part of the passive layer. The corrosion rate trend shows a significant reduction as a consequence of the chlorination treatments. The same positive reduction did not occur on untreated samples.

15.5.6 Monitoring of cooling water treatment in a steel factory

Another integrated monitoring of corrosion, biofilm and water treatment was performed with the metal alloys used (principally carbon steel) in a very large seawater cooling circuit of a steel factory treated with a daily intermittent dosage of chlorine dioxide. The following sensors driven by a computer-data acquisition system were inserted in a by-pass close to the condenser:

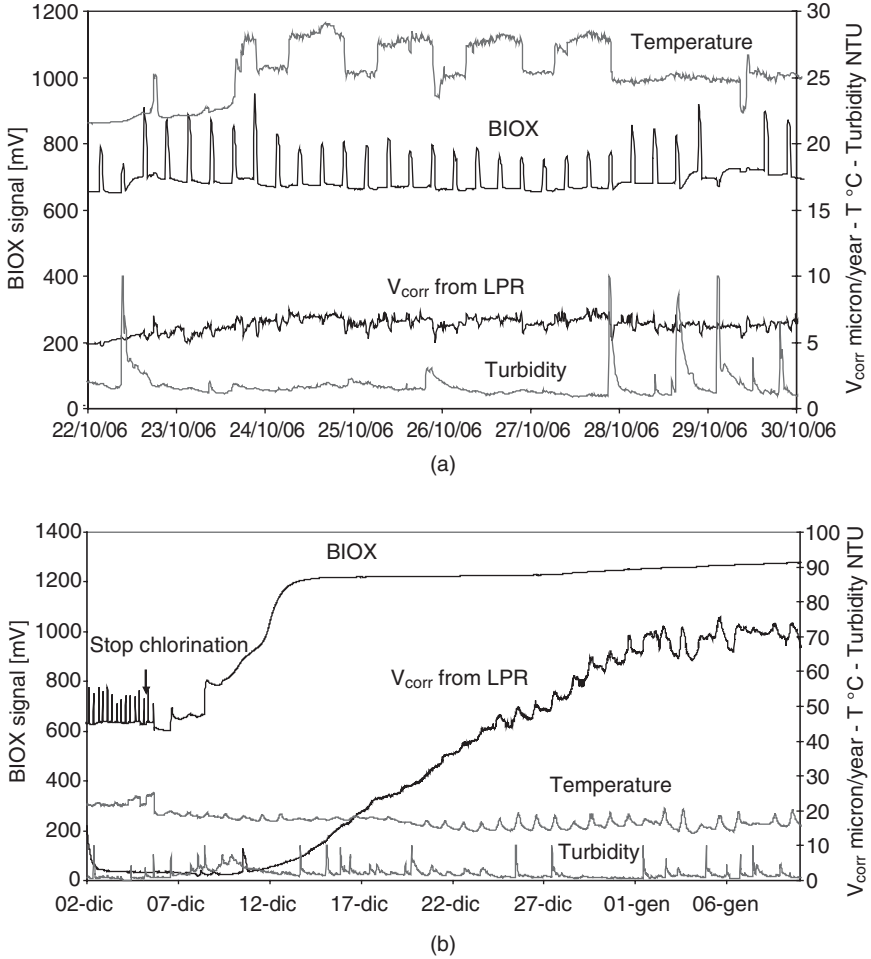

15.12 Details of an integrated monitoring of corrosion, biofilm, chlorination and water turbidity in seawater circuit rich in mud (corresponding to the turbidity signal increase) and treated with 0.5 mg/L TRO (chlorine-bromine) one hour four times/day, corresponding to steps of the BIOX signal. The LPR technique has been applied on electrodes in CuNi 70/30. In the graphic (a), CuNi passivation layer is well established and corrosion rate (by the LPR technique) is very low. On 5 December, the test line was moved before the chlorination point and specimens in the LPR cell were substituted with new ones: graphic (b).

- one BIOX tubular sensor to monitor the biofilm growth and the chlorine dioxide treatment;
- three tubular electrochemical cells to monitor the corrosion rate by LPR technique; coupons of carbon steel, stainless steel (UNS 31600) and copper-nickel 70/30 UNS C71500 respectively, with diameter of about 20 mm in each case;

- zinc anodes to monitor the free corrosion potential of the three alloys;
- one flow-meter and one temperature sensor to monitor the physical-chemical parameters of the water flow.

Several tubular coupons made of the same three materials were inserted for the off-line visual observations and weight loss determinations.

The treatment in the first period was not effective and a thick layer of iron corrosion products covered the whole surface in the test line. Biofilm growth on corrosion products increased the BIOX base line. Crevices were found on stainless steel; the general corrosion rate of the carbon steel was very high; the copper alloy showed localised corrosion. On the basis of the monitoring results, the surfaces were brushed mechanically and following that, the treatment became more effective to prevent a new corrosion product and biofilm deposition (see Fig. 15.13). The responses coming from the electrochemical instrumentation were found to be in a good agreement with the data from the analyses performed on the coupons (visual observations and weight loss) off-line. Subsequently good control of crevice phenomena on stainless steel as well as the corrosion of carbon steel and copper alloy were kept with a few small adjustments of the treatment.

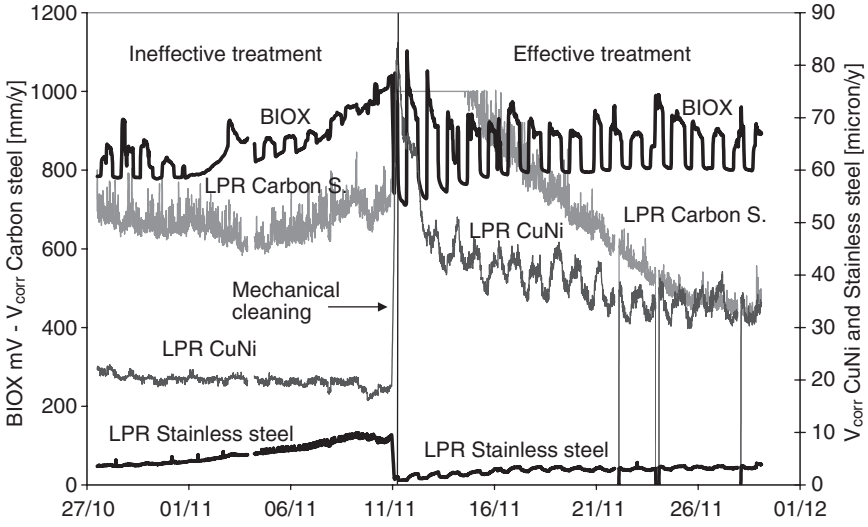

15.13 Integrated monitoring of corrosion, biofilm and treatment in cooling circuit of steel factory. Seawater treated with a very low and intermittent dosage of chlorine dioxide. LPR techniques have been applied on electrodes in CuNi 70/30, AISI 316 stainless steel and carbon steel.

15.5.7 Evaluation of a water treatment in a cooling tower

A final example of integrated monitoring of corrosion, biofilm and water treatment refers to a cooling tower fed by river water and treated with short, daily dosages of peracetic acid at different concentration (Fig. 15.14). The following sensors driven by a computer-data acquisition system were used in the test line:

- one BIOX tubular sensor to monitor the biofilm growth and the peracetic acid treatment
- one electrochemical cell to monitor the corrosion rate by the LPR technique with coupons of carbon steel with diameter of about 20 mm
- one pH meter, one flowmeter and one temperature sensor to monitor the physical-chemical parameters of the water.

Several coupons made of carbon steel for visual observation and weight loss determination completed the test line.

The increase of the BIOX base line detected during the first period indicated too light treatment. Increasing the PAA dosages in the range of 8–10 mg/L, the treatment became effective to control biofilm. Furthermore, the measures of corrosion rate remained at the lowest level. Too strong dosages, with concentration of PAA more than 100 mg/L, tested during the

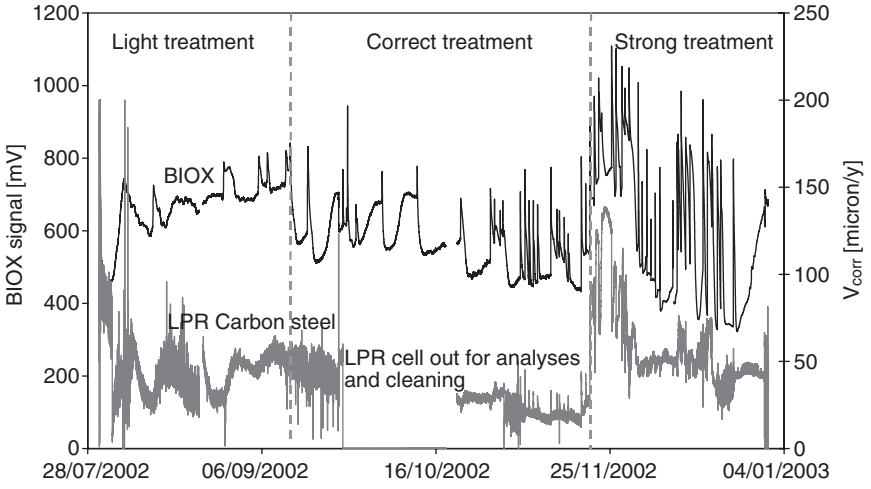

15.14 Integrated monitoring applied to a treatment based on peracetic acid (PAA) dosages for cooling tower. The LPR technique has been applied on electrodes in carbon steel. A significant decrease of pH around 25/11/2002 caused the corrosion rate increase. The peaks of too strong treatment correspond to PAA concentration of 100 mg/L.

final period, associated with a significant decrease of pH, caused an increase in the rate of corrosion.

15.6 Summary

The micro-organisms' attachment to wetted supports leads to the development of a biofilm that results in the negative deterioration and corrosion of materials, decaying the performance of equipment and process waters. MIC risk mitigation usually coincides with biofilm risk mitigation.

Biofilm also causes other deleterious effects, reducing heat transfer and promoting the biological risk in industrial facilities; consequently, the biofilm control permits several issues to be avoided, not only MIC. The existing procedures of MIC risk prevention often require the use of biocide treatments, such as chlorination, but standard treatment procedures, field experiences and macro-analysis of the phenomena are insufficient to build an effective and exhaustive risk assessment. Valid help, often decisive, comes from simple, rugged and innovative electrochemical sensors, able to monitor on-line and in real time the first stage of biofilm growth. This electrochemical probe, applied alone or integrated with a few other traditional sensors and devices, could allow the direct evaluation of MIC risk in several field applications. Industrial and commercial versions of electrochemical MIC risk monitoring have been already successfully used in several plants to optimise the chemical treatments of cooling water circuits.

15.7 References

Andrade C (2006), 'Real Time Monitoring Of Biofilms In Seawater Injection Environments', *CORROSION06*, Paper 06660, Houston, TX, NACE International.

Beech IB (2002), 'Biocorrosion: role of sulphate-reducing bacteria', in: Bitton G, ed. *Encyclopaedia of Environmental Microbiology*. London: John Wiley; 465–75.

Beech IB and Coutinho CLM (2003), 'Biofilms on corroding materials', in Lens P, Moran A P, Mahony T, Stoodly P, and O'Flaherty V, eds, *Biofilms in Medicine, Industry and Environmental Biotechnology – Characteristics, Analysis and Control*. London: IWA Publishing of Alliance House, 115–31.

Beech IB and Sunner JA (2004), 'Microbially-influenced corrosion: towards understanding of interactions between bacterial biofilms and metallic materials', *Current Opinions in Biotechnology*, 15: 181–6.

Borenstein SW (1994), *Microbiologically Influenced Corrosion Handbook*, Industrial Press inc., New York.

Bott TR (1995), *Fouling of Heat Exchangers*, Chemical Engineering monograph no. 26, Amsterdam: Elsevier.

Bryant RD, Janssen W, Bolvin J, Laishley EJ and Corterson JW (1991), 'Effect of hydrogenase and mixed sulfate-reducing bacterial population on the corrosion of steel', *Appl. Environ. Microbiol.*, 57: 2804–2809.

Chandrasekaram P and Dexter SC (1993), 'Factor Contributing to Ennoblement of Passive Metals Due to Biofilm in Seawater', *Proc. of 12th Int. Corr. Cong.*, NACE, article n. 493, 3696–707.

Characklis WG and Marshall KC (1990) *Biofilms*, New York: John Wiley and Sons.

Chattoraj M, Stonecipher DL and Borchardt SA (2003), 'Demand-based, real-control of microbial growth in air-conditioning cooling water system', *ASHRAE Transactions*, v.109, 1.

Chu K and Mochizuki F (1985), 'The effect of biofouling on fouling resistance', *Proceedings of Condenser Biofouling Control: The State of The Art*, Menlo Park, CA: CS-4339 April 1985, Electric Power Research Institute, 3-140–3-150.

Cristiani P (2000) 'Biofilm and MIC monitoring: State-of-the-art', Venice,13/04/2000, Second Workshop of Brite-Euram Thematic Network *BIOCORROSION – MIC of industrial materials*' (BRRT–CT98–5084), UE report 'biocorrosion 00–01' http://www.corr-institute.se/english/Web_DT/files/Biofouling1.pdf

Cristiani P (2005a) 'Solutions to fouling in power station condensers', *Applied Thermal Engineering Journal*, 25(16), November 2005, Elsevier, 2630–40.

Cristiani P (2005b) 'Biofilm growth and destruction: electrochemical monitoring for food processing plants', Proceedings of *Eurotherm Seminar 77 Heat and MassTransfer in Food Processing*, 20–22 June 2005 Parma: ETS Pisa.

Cristiani P and Bianchi G (1997) 'Microbial corrosion prevention in ENEL power plants', European Federation of Corrosion Publications, NUMBER 22: *Aspects of Microbial Induced Corrosion*, London: The Institute of Materials, 137–55.

Cristiani P and Giancola U (2000) 'Prevention of fouling and microbial corrosion in power stations using seawater as a coolant', in *Heat Exchanger Fouling Mitigation and Cleaning Technologies* H. Muller-Steinhagen ed., Essen: Publio, 334, 349.

Cristiani P, Belluato M, Balacco V, Bartole L and Bressan G (2001) 'Chlorine dioxide treatment optimisation by monitoring systems', New York Engineering Foundation Conferences: *Heat Exchanger Fouling – Fundamental Approaches and Technical Solutions*, 8–13 July 2001, Davos, Switzerland.

Cristiani P, Dell'Erba A, Falsanisi D, Notarnicola M and Liberti L (2004) *Tecnologie antifouling ad impatto ambientale minimizzato: Valutazione sperimentale dell'effetto della crescita di biofilm e degli inibitori, con particolare riferimento all'acido per acetico*, Ricerca di Sistema, Report A4524785, http://www.ricercadisistema.it

Cristiani P, Rocchini G and Mazza F (1995) 'Influence of Metal-Biofilm interface pH on aluminium brass corrosion in seawater', *Microbial Corrosion Proceedings of the 3th Int. EFC Workshop Portugal*, *1994*, London, The Institute of Materials, 243–60.

Cristiani P, Perboni G and Debenedetti A (2007) 'Effect of chlorination on the corrosion behavior of CuNi 70/30 condenser tubing', *Biocorys 2007* International Conference on Biocorrosion and Materials, Paris, F, 11–14 June 2007.

Dell'Erba A, Cristiani P, Falsanisi D, Notarnicola M and Liberti L (2007) 'Peracetic Acid Treatment for Biofilm Control' Engineering Conferences International *Water Treatment and Reuse*, 11–16 February, Tomar, Portugal.

Dexter SC and Zhang HJ (1990), 'Effect of Biofilm on Corrosion Potential of Stainless Alloys in Estuarine Waters', *Proc. of 11th Int. Corros. Congr.*, 4 April 1990, Firenze: AIM, 333–40.

Dinh HT, Kuever J, Mussmann M, Hassel AW, Stratmann W and Widdel F (2004), 'Iron corrosion by novel anaerobic micro-organisms', *Nature*; 427: 829–32.

Eashwar M and Maruthamuthu S (1993) 'Ennoblement of stainless alloys by marine biofilm: an alternative mechanism', *Proc. of 12th Int. Corros. Congr.*, Houston, TX, NACE International, 3708–16.

Fallon H and Licina GJ (2004) 'Plant experience with dosing optimisation of an environmentally friendly biocide, *Int. Cong. CORROSION 2004*, Paper 04086, Houston, TX, NACE International.

Farquhar GB, Thomas W, Pickthall TW and DeCuir JA (2005) 'Solving Gulf Coast oil pipeline bacteria-related corrosion problem, *Pipeline and Gas Journal*, 232(3), 28–30, www.pipelineandgasjournal.com

Feron D (2002) in Task 5 Final Report 'Guidelines', *Brite-Euram Thematic Network MIC of Industrial Materials* (BRRT – CT98-5084), 14

Flemming HC and Geesey GG, eds (1991) *Biofouling and Biocorrosion in Industrial Water Systems*, Springer-Verlag, Berlin, 47–80.

Flemming HC, Tamachkiarowa C, Klahre JA and Schmitt J (1998) 'Monitoring of fouling and biofouling in technical systems', *Wat. Sci. Tech*, 38(8–9), pp 291–8.

Geesey GG, Beech IB, Bremmer PJ, Webster BJ and Wells D (2000) 'Biocorrosion', in Bryers J, ed. *Biofilms II*: *Process Analysis and Applications*. London: Wiley-Liss, Inc, 281–326.

Guezennec J (1991) 'Influence of cathodic protection of mild steel on the growth of sulphate-reducing bacteria at 35 °C in marine sediments', *Biofouling*, 3(4), 339–48.

Hamilton WA (2003) Microbially influenced corrosion as a model system for the study of metal microbe interactions: a unifying electron transfer hypothesis, *Biofouling*; 19: 65–76.

Hatch SR, Stonecipher DL, Willer M, Yu P and Borchard SA (2003) 'Real word experience with a new cooling water automation system', *Int. Congr. CORROSION/2003* Paper No. 3075, Houston, TX, NACE International.

Herbert-Guillou D, Tribollet B, Festy D and Kiéné L (1999) 'In situ detection and characterization of biofilm in waters by electrochemical methods' *Electrochimica Acta,* 45, 1067–75.

Hilbert LR (2000) 'Monitoring techniques for microbially influenced corrosion of carbon steel', *Biocorrosion – Monitoring Techniques*, Annual meeting of Danish Metallurgical Society, January, Vintermodet, 5–7.

Hilbert LR, Hemmingsen T, Nielsen LV and Richter S (2005) 'When can electrochemical techniques give reliable corrosion rates on carbon steel in sulfide media?', *CORROSION/2005* paper No. 05346, Houston, TX, NACE International.

Hillman RE (1985), *Biofouling Detection Monitoring Devices: Status Assessment*. Battelle New England Marine Research Laboratory, EPRI Report CS-3914.

Ishihara Y, Motoda SI, Suzuki Y and Tsujikawa S (1995) 'Effect of environmental factors on ennobled electrode potential attained in natural sea water for stainless steels', *Corros. Eng.* 44, 421–33.

Jenner HA, Taylor CJL, van Donk M and Khalanski M (1997) 'Chlorination by-products in chlorinated cooling water of some European coastal power stations', *Marine Environmental Research*, 43(4), June, 279–93(15).

Lee AK and Newman DK (2003) 'Microbial iron respiration: impacts on corrosion processes', *Appl Microbiol Biotechnol*., 62: 134–9.

Lee TS, Kain RM and Oldfield JW (1984) 'The effect of environmental variables on crevice corrosion of stainless steels in seawater', *Mat. Perform.*, 23, 9–15.
Lewandowski Z, Lee WC, Characklis WG and Little BJ (1988) 'Dissolved oxygen and pH microelectrode measurements at water-immersed metal surfaces', Paper No. 93, *CORROSION 88*, Houston, TX, NACE International.
Lewis RO (1982) 'The influence of biofouling counter measures on corrosion of seat exchanger materials in seawater', *Material Performance*, September, 31–8.
Licina GJ (1989) 'Microbial corrosion: 1988 Workshop Proceedings', EPRI report ER-6345, April 1989, 1-1/1–14.
Licina GJ (2001) 'Monitoring biofilms on metallic surfaces in real time', *CORROSION/01 annual int. congr.*, Paper No. 1442, Houston, TX, NACE International.
Licina GJ (2004) 'Optimizing Biocide Additions via Real Time Monitoring of Biofilms', *CORROSION/04* Int. Conference, Paper No. 04582, Houston, TX, NACE International.
Licina GJ and Nekoksa G (1993) 'An electrochemical method for on-line monitoring of biofilm activity', *CORROSION/93 annual int. congr*. March 1993, New Orleans LA, paper No. 403, Houston, TX, NACE International.
Licina GJ, Nekoksa G and Ward G (1990) 'An electrochemical method for monitoring the development of biofilm in cooling water' in Dowling NJ, Mittelman MW, Danko JC, *Microbial and Biodeterioration*, Knoxville, TN, paper 541.
Lin J YuPo, St. Martin EJ and Frank JR (2003) *Monitoring and Mitigation of Sustained Localized Pitting Corrosion*, Argonne National Laboratory Argonne IL, January 2003 Final Report DOE FEW 49297.
Little B, Ray RI, Wagner PA, Jones-Meehan JC, Lee C and Mansfield F (2000), 'Diagnosing microbiologically influenced corrosion', COST 520 *Biofouling and Materials*, Budapest, 31 May–3 June.
Maruthamuthu S, Rajagopal G, Sathianarayannan S, Eashwar M and Balakrishnan K (1995) 'A photoelectrochemical approach to the ennoblement process: proposal of an adsorbed inhibitor theory', *Biofouling*, 8, 223–32.
Micheletti W and Miller M (1993) 'Condensor microbiofouling control handbook', EPRITR-102507, 4(1)–4(33).
Mollica A (1992) 'Biofilm and corrosion on active-passive alloys in seawater', *International Biodeterioration and Biodegradation*, 29, 213–29.
Mollica A and Cristiani P (2002) 'On-line biofilm monitoring by electrochemical probe "BIOX"', IWA journal *Water Science and Technology* 47(5), 45–9.
Mollica A and Scotto V (1996) 'Mechanisms and prevention of biofilm effects on stainless steel corrosion: Inhibition of crevice corrosion on stainless steel test, European Federation of Corrosion Application no. 19, *Sea Water Corrosion of Stainless Steels – Mechanisms and Experiences*, London, The Institute of Materials, 23–43.
Mollica A and Trevis A (1976) *Proc.of 4th Int. Cong. Marine Corros. and Fouling*, Antibes, France, June 1976, 351–65.
Mollica A, Traverso E and Ventura G (1990) 'Electrochemical monitoring of the biofilm growth on active-passive alloy tubes of heat exchange using sea water as cooling medium', XI *Proceedings of International Corrosion Congress*, Firenze 2–6 April 1990, Italy, AIM Ed., vol. 4, 333–40.
Moosavi AN, Dawson JL and King RA (1986) 'The effect of sulphate reducing bacteria on the corrosion of reiforced concrete' in *Biologically Influenced Corrosion*, Dexter SC, ed. reference Book N. 8, Houston, TX, NACE International.

Nagiub A and Mansfeld F (2002) 'Evaluation of microbiologically influenced corrosion inhibition (HICI) with EIS and ENA', *Electrochemical Acta*, 47, 2319.

Neal AL, Rosso KM, Geesey GG, Gorby YA and Little BJ (2003) 'Surface structure effects on direct reduction of iron oxides by *Shewanella oneidensis*', *Geochim Cosmochim Acta*, 23, 4489-503.65 G.

Nekoksa G and Gutherman B (1991), 'Cathodic protection criteria for controlling microbially influenced corrosion in power plants', EPRI report NP-7312, New York.

Nickel JC, Ruseska I, Wright JB and Costerton JW (1985) 'Tobramycin resistance of Pseudomonas aeruginosa cells growing as a biofilm on urinary catheter material', *Antimicrob. Agents Chemother*. 27, 619–24, http://www.tylerresearch.com/instr/biofilm/lpmr.shtml

Nielsen LV and Nielsen KV (2003) 'Differential ER-technology for measuring degree of accumulated Corrosion as well as Instant Corrosion Rate', *CORROSION2003*, Paper No. 03443, Houston, TX, NACE International.

Perboni G and Radaelli M (1998) *Monitoraggio elettrochimico ad alta temperatura del trattamento ossidante nel generatore di vapore con corpo cilindrico di Turbigo 4*, Report ENEL-SRI-PDM-CPC-98-003, Luglio 1998.

Petty RD, Sutherland LA, Hunter EM and Cree IA (1995) 'Comparison of MTT and ATP-based assays for the measurement of viable cell number', *J. Biolumin. Chemilumin.*10, 29–34.

Pope DH (1987) *Microbial Corrosion in Fossil-Fired Power Plants* EPRI CS-5495 Project 2300–12 Final Report November 1987, Research, 43(4): 1–15.

Rook JJ (1974) 'Formation of haloforms during chlorination of natural waters', *Wat. Treat. Examin.*, 23, 234–41.

Scotto V, Di Cinto R and Marcenaro G (1985) 'The influence of marine aerobic microbial film on stainless steel corrosion behaviour', *Corrosion Science*, 25(3), 185–94.

Schmitt G (1997) 'Sophisticated electrochemical methods for MIC investigation and monitoring', *Materials and Corrosion* 48, 586–601.

Stuart CM, Kaufmann MK and Brundage ER (1990) 'Practical experience with advanced on-line monitoring techniques', *CORROSION/90* Las Vegas, Nevada, April 23–27, Paper n. 360, Houston, TX: NACE International.

Sutherland IW (2001) 'The biofilm matrix – an immobilized but dynamic microbial environment', *Trends Microbiol*; 9, 222–7.

Symons JM, Krasner SW, Sclimenti MJ, Simms LA, Sorensen HWJ, Speitel GEJ and Diehl AC (1996) 'Influence of bromide ion on trihalomethane and haloacetic acid formation', in *Disinfection By-Products in Water Treatment: The Chemistry of Their Formation and Control*, Eds. Minear RA, and Amy GL, CRC Press Inc, 91–130.

Videla HA, De Mele MFL and Brankevich G (1989) 'Biofouling and corrosion of stainless steel and 70/30 copper-nickel samples after several weeks of immersion in seawater', *Corrosion/89*, Houston, TX: NACE Paper N°291.

Videla HA, Silva RA, Canales CG and Wilkes JF (1992) 'Monitoring biocorrosion and biofilms in industrial waters: a pratical approach', in *Proceeding of The International Symposium on Microbiologically Influenced Corrosion (MIC) Testing*, by ASTM Committee G-1 on Corrosion of metal, Miami, Florida, November 1992.

Wardell JN and Chamberlain AHL (1995) 'Bacteria associated with MIC of copper: characterisation and extracellular polymer production', in Tiller AK and Sequeira CAC, *Microbial corrosion*, European Federation of Corrosion publication N. 15, London, The Institute of Materials, 49–63.

Wetegrove RL, Banks RH and Hermiller MR (1996) 'Optical monitor for improved fouling control in cooling systems', Cooling Technology Institute, Technical paper TP 96–09. http://www.cti.org/tech_papers/fouling.shtml

Wingender J, Neu TR and Flemming HC (1999) 'What are bacterial extracellular polymeric substances?' in Wingender J, Neu TR, Flemming HC, *Microbial Extracellular Polymeric Substances: Characterization, Structure and Function*, New York, Springer-Verlag, 1–15.

Wyatt PJ (1972) 'Light scattering in the microbial world', *Journal of Colloid and Interface Science* 39, 479–91.

Wyatt PJ and Jackson C (1989) 'Discrimination of phytoplankton via light scattering properties', *Limnology and Oceanography* 34(1), 96–112.

16

Corrosion monitoring in concrete

PETER SCHIEßL and CHRISTOPH DAUBERSCHMIDT,
Technical University of Munich, Germany and
Ingenieurbuero Schiessl Gehlen Sodeikat, Germany

16.1 Introduction

The major part of the European infrastructure has reached an age where capital costs have decreased. But inspection and maintenance costs have grown so extensively that they constitute the major part of current costs. Repair of damage caused by rebar corrosion causes a major part of repair costs, consuming annual costs for maintenance and repair up to 2.5% of building costs (Bergmeister, 2004). According to international research 66% of all assessed damage to bridges arises from the ingress of chlorides in concrete and the subsequent onset of corrosion of the reinforcement (Gaal, 2004). Thus in recent years the need has arisen to monitor time dependent chloride penetration and corrosion behaviour of the reinforcement in order to be able to take early protective measures.

The reinforcement of concrete, reinforced steel as well as pre-stressed steel, ensures the load carrying capacity of most structures such as bridges, parking decks, tunnels, etc. Steel reinforced concrete is normally protected against corrosion due to a thin and impermeable dense passive layer formed in the alkaline medium of the pore solution of concrete (pH ≈ 13.3). This passive layer can break down in the presence of chlorides at the steel surface or due to the decrease of the pH-value caused by carbonation of the concrete. After the breakdown of the passive layer, corrosion at the reinforcement can be initiated which can cause severe deterioration of the steel and the concrete and thus can significantly reduce the load carrying capacity.

During the initial phase of ingress of chlorides or the carbonation front as well as in the early corrosion phase no visible damage can be assessed at the concrete surface. Only later, when cracks are formed or spalling of the concrete covers occurs, can deterioration be assessed by visual inspection; but then repair measures are likely to be more cost- and time-intensive compared to earlier stages of damage as repair costs increase exponentially as the damage increases.

Corrosion monitoring is a cost-effective and non-destructive method of assessing the ingress of the depassivation front and corrosion of the reinforcement during the early stages. As a result repair measures are much more cost-efficient. Thus it enables measures to be taken at an early stage and in this way minimises the overall costs of maintenance of the structure.

16.2 Deterioration mechanisms for corrosion in concrete

16.2.1 General deterioration model

The development over time of most types of deterioration mechanisms in concrete structures may be modelled by a two-phase-curve illustrated in Fig. 16.1, which is the basis for defining the service life of a structure. The two phases of deterioration are the following (fib 1999):

- **Initiation phase**: During this phase no noticeable weakening of the material or the function of the structure occurs, but some of the protec-

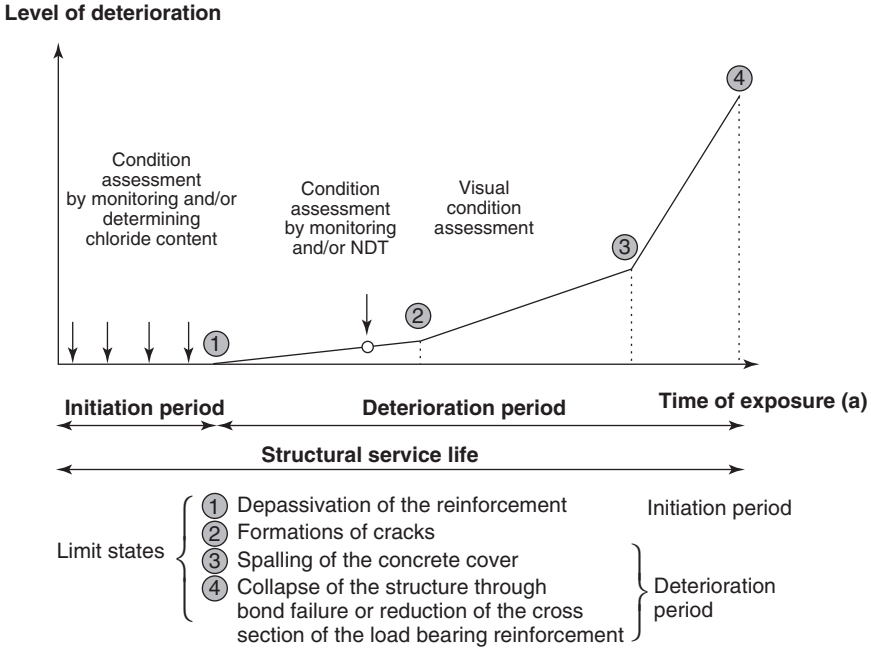

16.1 Service life of concrete structures. A two-phase modelling of deterioration (adapted from Tuutti, 1982) with possibilities of assessment.

tive barrier is broken or overcome by aggressive media. Carbonation, chloride penetration and sulphate accumulation are examples of such mechanisms. In the case of corrosion the duration of the initiation period is determined by the thickness and permeability of the concrete cover and the exposure conditions (e.g. chloride ingress can be accelerated by cyclic wetting and drying).

- **Deterioration phase**: During this phase active deterioration develops and loss of function is observed. Figure 16.1 shows a deterioration mechanism that develops an increasing deterioration rate over time. Reinforcement corrosion is one such important propagating deterioration.

The most common mechanisms leading to corrosion of steel in concrete under moderate climatic conditions are carbonation and chloride penetration in the initiation phase. Both mechanisms are described in Section 16.2.2.

16.2.2 Initiation phase

Carbonation

As already noted in Section 16.1, it is well known that steel in concrete is protected against corrosion by the fact that, owing to the alkalinity of the pore solution (pH = 12.5–13.5) a microscopic oxide layer is formed at the steel surface preventing the dissolution of the steel. The formation and maintenance of the passive film electrochemically is also a corrosion process, however the 'corrosion rate' of passive steel in concrete is 1–2 μm/year at most, and is therefore negligible from a practical point of view.

If the pH value drops below 9 the passive layer and, consequently, corrosion protection will be lost over greater surface areas. Such a drop in pH value can be evoked under normal exposure conditions by carbonation of the concrete. Carbonation of concrete normally involves a chemical reaction between atmospheric carbon dioxide (CO_2) and the products of cement hydration. The normal CO_2 content of the air is 0.03% by volume, but in particular conditions, as in road tunnels and parking garages, it may easily reach much higher values.

In very simplified terms, the main chemical reaction may be described as follows:

$$Ca(OH)_2 + CO_2 \Rightarrow CaCO_3 + H_2O \qquad [16.1]$$

accompanied with a drop of pH value from 12.4 ($Ca(OH)_2$) to 8 to 9. Similarly, the other alkalis, contained in small amounts in the pore solution (KOH, NaOH) combine with carbon dioxide to form potassium and sodium carbonate. After nearly all the potassium, sodium and calcium hydroxides

in the pore cavities have been re-dissolved and carbonated, the pH will decrease to values of about 8–9.

For calculating the time-dependent depth of the carbonation front it is essential to set up a model for the carbonation process considering the physical and chemical interaction of CO_2 with the concrete. The model is based on diffusion as the prevailing transport mechanism of CO_2 by using Fick's first law of diffusion. An easy model to evaluate the time-dependent carbonation depth is the so-called square root time equation:

$$x_c(t) = \sqrt{\frac{2 \cdot D \cdot C_s}{a}} \cdot \sqrt{t} = k \cdot \sqrt{t} \qquad [16.2]$$

with

D = carbon dioxide diffusion coefficient [mm^2/a]
C_s = carbon dioxide concentration at the surface [kgCO_2/m^3]
a = binding capacity [kgCO_2/m^3]
t = concrete age [a]
x_c = depth of carbonation front at time t [mm]

In order to consider the influence of a natural exposure condition and the influences on the concrete, Equation [16.2] has been modified by Gehlen (2000) as follows:

$$x_c(t) = \sqrt{2 \cdot k_e \cdot k_c \cdot (k_t \cdot R_{ACC,0}^{-1} + \varepsilon_t) \cdot C_S} \cdot \sqrt{t} \cdot W(t) \qquad [16.3]$$

with

$$k_e = \left(\frac{1 - \left(\frac{RH_{real}}{100} \right)^{f_e}}{1 - \left(\frac{RH_{ref}}{100} \right)^{f_e}} \right)^{g_e}$$

$$k_c = a_c \cdot t_c^{b_c}$$

$$C_S = C_{S,atm.} + C_{S,emi.}$$

$$W = \left(\frac{t_0}{t} \right)^{\frac{(\rho_{SR} \cdot ToW)^{b_w}}{2}} = \left(\frac{t_0}{t} \right)^{w}$$

$$ToW = \frac{\text{days with rainfall } h_{Nd} \geq 2.5\text{mm per year}}{365}$$

k_e = sub-function considering the influence of environment (e.g. realistic moisture at the concrete surface during use; RH_{real}) on the effective inverse carbonation resistance [–]
RH_{real} = relative humidity of the carbonated layer [%]
RH_{ref} = reference humidity [%]
f_e = exponent [–]
g_e = exponent [–]

k_c = sub-function taking into account the influence of curing on the effective carbonation resistance [–]
$a_c = 7(^{-b_c})$
b_c = exponent of regression [–]
t_c = period of curing [*d*]
k_t = variable, which considers the influence of test method on the ACC-test (**Ac**celerated **C**arbonation-Test) [–]
$R_{ACC,0}^{-1}$ = inverse effective carbonation resistance of dry concrete, determined at a certain point of time t_0 on specimens with the accelerated carbonation test ACC [$(mm^2/a)/(kgCO_2/m^3)$]
ε_t = error term considering inaccuracies which occur conditional on the ACC test method [$(mm^2/a)/(kgCO_2/m^3)$]
C_S = CO_2 concentration to which the structure is exposed [$kgCO_2/m^3$]
$C_{S,atm.}$ = CO_2 concentration of the atmosphere [$kgCO_2/m^3$]
$C_{S,emi.}$ = CO_2 concentration of additional emission sources [$kgCO_2/m^3$]
T = time in service [*a*]
W = weather function considering the influence of meso-climatic conditions (rewetting) [–]
t_o = time of reference [*a*]
w = weather exponent [–]
ToW = time of wetness [–]
p_{SR} = probability of driving rain [–]
b_w = exponent of regression [–]

The duration of the initiation phase for carbonation will be prolonged by:

- increasing the concrete cover of the reinforcement
- decreasing the permeability of concrete (low w/c ratio i.e. water/cement ratio, sufficient curing) with high $Ca(OH)_2$ content of the cement
- increasing water content of the pores (water saturated concrete cannot carbonate)
- decreasing CO_2 content of the surrounding atmosphere.

Chloride ingress

Chlorides may be present in the fresh mix or may penetrate into the hardened concrete. During use of the structures, chlorides may penetrate from the surface into the concrete from various sources. The most important of these are sea water, de-icing salts and PVC (polyvinyl chloride) fires. Chlo-

rides penetrate into the concrete as ions within partly or completely water-filled pores. They are partially bound chemically or physically within the cement matrix.

Unlike carbonation penetration, chloride penetration is not associated with a distinct reaction front. On the contrary, a chloride profile with a chloride content decreasing from the concrete surface to the interior is usually found for chloride exposure conditions (Brite/EuRam, 2002).

When chlorides penetrate into hardened concrete, the following main transport mechanisms are involved (Lay, 2006):

- pure chloride ion diffusion
- convection (due to 'pickaback' transportation of chlorides in ingressing water e.g. capillary suction)
- dispersion (due to inhomogeneous velocity-distribution of water transportation).

Further mechanisms are retardation (filter effect), backwards transportation (in drying phases), chloride binding, interaction of ions and self-sealing of concrete.

When assessing the penetration of chlorides into concrete and the associated risk of reinforcement corrosion, it is necessary to differentiate between two basic influencing parameters:

- the diffusion resistance of the concrete against ingress of chlorides which is described by the diffusion coefficient of the concrete; this diffusion resistance depends primarily on the pore size distribution of the concrete
- the binding capacity of the concrete with respect to chloride ions (physical and chemical binding). This binding capacity influences both the penetration rate and the ratio of bound to free chloride ions in the pore water.

The binding capacity of concrete is particularly influential, since the risk of corrosion at the reinforcement is determined solely by the free chlorides in the pore water. Consequently, free chlorides in the pore water or the ratio of bound to free chlorides at the steel surface are the decisive factors in judging the reinforcement corrosion risk.

Pure chloride diffusion can be described according to Fick's second diffusion law. To take into account the changes of permeability of concrete over time and real exposure conditions Fick's diffusion law has been modified extensively. A widely used modified model, taking into account practice observations related to chloride ingress, is according to Gehlen (2000):

$$C(x,t) = C_0 + (C_{S,\Delta x} - C_0) \cdot \left[1 - \operatorname{erf} \frac{x - \Delta x}{2 \cdot \sqrt{D_{app,C}(t) \cdot t}} \right] \qquad [16.4]$$

with $D_{app,C}(t) = k_e \cdot D_{RCM,0} \cdot k_t \cdot A(t)$

and $k_e = \exp\left(b_e\left(\frac{1}{T_{ref}} - \frac{1}{T_{real}}\right)\right)$

$$A(t) = \left(\frac{t_0}{t}\right)^a$$

$C(x,t)$ = content of chlorides in the concrete at depth x and at time t, [wt.-%/c] as the output of Equation [16.4]
C_0 = initial concentration of chlorides in the concrete due to chloride containing components (e.g. aggregate) [wt.-%/c]
$C_{S,\Delta x}$ = concentration of chlorides at depth Δx, depending on the chloride impact [wt.-%/c]
x = depth with a corresponding content of chlorides $C(x,t)$ [mm]
Δx = depth of concrete layer, in which the process of chloride penetration differs from Fick's second law of diffusion [mm]
$D_{app,C}$ = apparent coefficient of chloride diffusion of concrete at time t [m²/s]
k_e = sub-function considering the dependency of $D_{app,C}$ on the temperature [–]
b_e = regression variable [K]
T_{ref} = reference temperature [K]
T_{real} = temperature of the ambient air, respectively of the structure part [K]
$D_{RCM,0}$ = chloride migration coefficient of water saturated concrete, measured at the reference period t_0 on specimens which have been produced and stored under exactly defined conditions [m²/s]
k_t = variable, which converts the under accelerated conditions measured chloride migration coefficient (Rapid Chloride Migration, $D_{RCM,0}$) into a chloride diffusion coefficient, whereby the specimens have been exposed to natural conditions (Chloride Profiling Method, $D_{CPM,0}$) [–]
$A(t)$ = sub-function considering the ageing [–]
a = ageing exponent taking the time dependent behaviour of $D_{app,C}$ into consideration [–]
t_0 = time of reference [a]
t = time of exposure [a]

Corrosion at the reinforcement can occur, when the so-called 'critical chloride content' of the concrete at the reinforcement is exceeded. In principle two definitions of 'critical chloride content' are conceivable:

1. A critical chloride content at which depassivation of the steel surface commences, whether or not this leads to visible corrosion damage at the concrete surface
2. A critical chloride content which over time leads to a corrosion phenomenon classified as damage.

Critical chloride content may be considerably higher according to definition 1 than definition 2, because corrosion damage occurs only if, in addition to depassivation of the steel surface, other conditions conducive to a correspondingly accelerated rate of corrosion (e.g. oxygen supply, humidity) are fulfilled (see Section 16.2.3).

It is evident from current knowledge that the critical chloride content is not a fixed value but is dependent both on the quality of the concrete cover (type of cement, w/c ratio, curing, thickness) and on environmental conditions. Thus concrete in permanently dry environmental conditions as well as constantly water saturated conditions the critical chloride content according to definition 2 is much higher than in frequently changing exposure conditions (e.g. splash water zone). The much-criticized chloride content of 0.4% in relation to the cement content was arrived at through research into the chloride binding capacity of concrete (Richartz, 1969), and generally is on the safe side. Under certain conditions, much higher chloride contents may be uncritical.

The duration of the initiation phase for chloride penetration will thus be prolonged by:

- increasing concrete cover of the reinforcement
- using concrete mix with low permeability (with low w/c-ratio and, which is much more decisive, the appropriate type of cement, like blast-furnace slag or fly ash cements, adequate curing)
- increasing binding capacity of the concrete (increasing the C_3A content (C_3A = tricalciumaluminate) of the cement)
- reducing water content of the concrete and the depth of the changing water content caused by the exposure condition (splash zone or spray fog zone)
- reducing temperature of surrounding atmosphere
- increasing age of concrete at the first chloride attack, as older concrete has higher resistance against chloride ingress than younger concrete (e.g. by protecting the young concrete against chloride attack).

16.2.3 Deterioration phase

Corrosion mechanisms

After the depassivation front has reached the reinforcement (either by carbonation of the concrete or by exceeding the critical chloride content)

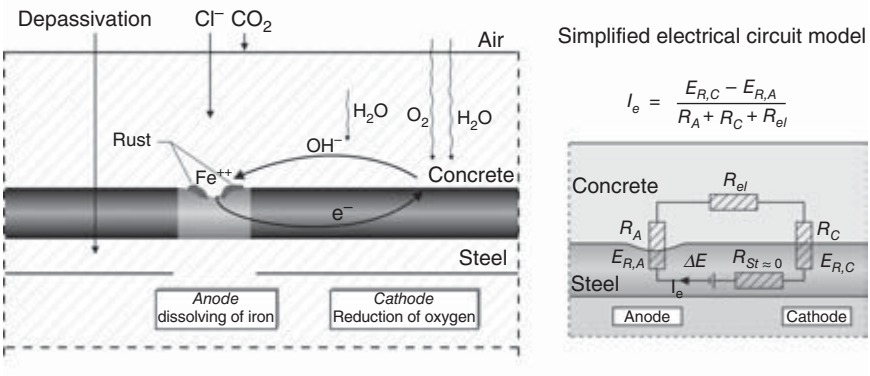

16.2 Corrosion of steel in concrete (left: corrosion mechanism, right: simplified electrical circuit model with $E_{R,C}$ and $E_{R,A}$: potentials at the anode and cathode; R_A, R_C and R_{el}: polarisation resistances at the anode and the cathode, electrolytic resistance; I_e: macro-cell current (approximately equal to corrosion rate) (Raupach, 1996).

corrosion can be initiated. The corrosion process takes place in two sub-processes, as outlined in Fig. 16.2:

- At the **anode**, iron ions pass into solution, separating from the electrons. They are converted into rust products in further reactions.
- At the **cathode**, electrons, water and oxygen are converted into hydroxyl ions. The cathodic process does not cause any deterioration of the steel.

These hydroxyl ions transport the negative charge in the electrolyte through the electrical field created between the anode and the cathode, towards the direction of the anode. Near the anode, they react with the iron ions in solution. Depending on moisture and aeration conditions, this intermediate product may continue to react, producing the final corrosion products. The individual processes are in fact much more complicated, and are described by Raupach (1992) and Schießl (1988).

In order for the corrosion process to take place, a number of preconditions for the anodic and cathodic process and for the electrolytic process must be satisfied simultaneously:

- There must be differences in potential between anodes and cathodes. The preconditions for sufficiently large differences in potential are, however, usually met, and in the case of chloride-induced corrosion these may be several 100 mV.
- Anodic and cathodic surface zones of the steel must be connected electrically and electrolytically, i.e. a flow of electrons and ions between them must be possible. The metallic connection necessary for an elec-

tron flow from the anode to the cathode is provided by the reinforcement system in the reinforced concrete. The electrolytic connection is represented by the concrete. This must, however, be sufficiently wet, since otherwise there can be virtually no migration of ions. In dry interior situations, for example, the electrolytic conductivity of the concrete is too low to permit corrosion of the reinforcement, even if the carbonation front reaches the reinforcement, leading to loss of alkalinic protection.

- Anodic dissolution of iron must be possible due to depassivation of the steel surface. The cathodic process can, however, take place even in zones with a passive steel surface.
- Sufficient oxygen must be available at the cathode. There must be continuous diffusion of oxygen from the surface of the concrete to the steel surface acting as the cathode. There is therefore practically no risk of corrosion to reinforced concrete components which are permanently and completely immersed in (deep) water.

If all conditions for corrosion are fulfilled simultaneously, the reinforcement will corrode. If only one of the conditions can be eliminated, corrosion can be prevented or halted. Fundamental repair principles may be deduced from this knowledge.

As described in Chapter 2, corrosion phenomena may be sub-divided into uniform corrosion and local pitting. Pitting may be understood as a form of corrosion in which crater shaped hollows undermining the surface or appearing in the form of needles occur without any attack outside the pitting location point.

Uniform corrosion is generally caused by carbonation of the concrete over a wide area or uniformly very high chloride contents in the vicinity of the steel. This leads to the formation of so-called micro-cells, consisting of pairs of immediately adjacent anodes and cathodes. These are microscopic in size, so that externally they appear to produce uniform removal of the steel.

Pitting generally results from chloride-induced corrosion. In this case, so-called macro-cells are formed, with the pits acting as the anodes and the neighbouring sections of the reinforcement as cathodes. Anodes and cathodes are not necessarily adjacent; they may well be situated at a considerable distance from each another.

Rate-determining parameters

The corrosion rates at anodic sites in macro-cells are generally much greater than in micro-cell corrosion, as the anodes of macro-cells are usually very small in relation to the cathodes, leading to high current densities and hence

high corrosion rates. The potential size of a macro-corrosion cell is determined largely by the electrolytic resistivity of the concrete, i.e. by its water content, and by the permeability of the concrete and chemical composition of the pore solution. In dry concrete with extremely low permeability, the rate of corrosion remains low. Macro-cells may, however, also occur where there is carbonation of the concrete over a wide area, with uneven moisture distribution or aeration, or in zones with localised depassivation, e.g. in the regions of cracks or honeycombs. Here again, corrosion rates higher than those encountered with uniform corrosion of the reinforcement may be expected.

As expected, the chloride content in the concrete at the steel surface has a decisive influence on the corrosion rate. If the chloride content rises above a critical, corrosion-initiating value, there will be a roughly linear increase in the corrosion rate with increasing chloride content.

According to Fig. 16.2 the corrosion rate of the steel is, besides other resistances, dependent on the polarisation resistance at the cathode, which is linked to the oxygen diffusivity of the concrete, being mainly influenced by capillary porosity and the water content of the concrete. Permanently water saturated concrete structures are unlikely to show significant corrosion rates, as the resistance against oxygen diffusion is very high. Also the concrete cover has a significant influence on the oxygen diffusion in concrete mixes with low permeability.

Furthermore the corrosion rate is dependent on the electrolytic resistance of the concrete. If the water content of the concrete decreases, the electrolytic resistance increases significantly (up to several decades). Thus corrosion causing damage can only occur when the electrolytic resistance of the concrete is below a range of 100 to 150 Ωm (Nürnberger, 1995), which is normally reached in concrete exposed to 85 to 90% relative humidity and under. So technically relevant corrosion can only occur in weathered or water-exposed structures, but not in dry indoor conditions. The electrolytic resistance is also dependent on the ion-concentration of the pore solution, the temperature and the permeability of the concrete.

Whereas in uncracked concrete a good quality concrete cover will generally prevent depassivation of the reinforcement for a long period (initiation phase), prevention is practically impossible in the area of cracks crossing the reinforcement, since both the carbonation front and the chlorides penetrate much more rapidly into the crack zone than elsewhere (Schießl, 1976). The capillary suction capacity of the cracks plays an important role in the penetration of chlorides.

The corrosion mechanism in the crack zone is of decisive significance for the corrosion rate of the reinforcement. In laboratory investigations cell current and voltage measurements on cracked reinforced steel beams

exposed to chloride attack clearly demonstrate that large macro-cells are formed under certain conditions. The reinforcement in the crack zone acts as an anode, the reinforcement between the cracks set up at a distance of several decimetres as a cathode, often leading to extremely high corrosion rates in the crack zone. The corrosion rates within the cracks are more dependent on concrete cover and composition than on crack width (Schießl, 1997).

16.2.4 Structural service life management

The design service life is the assumed period for which a structure or part of it is to be used for its intended purpose with anticipated maintenance but without major repair being necessary. The design service life is defined by:

- the definition of the relevant limit state
- the number of years of the service life
- the level of reliability for not passing the limit state during this period.

Durability of the structure in its environment shall be such that it remains fit for use during its design service life. This requirement can be considered in one of the following ways:

- by using materials that, if well maintained, will not degenerate during the design service life
- by giving such dimensions that deterioration during the design service life is compensated
- by designing protective and mitigating systems
- by choosing a shorter lifetime for structural elements, which may be replaced one or more times during the design life.

All the above approaches are possible in combination with appropriate inspection at fixed or condition dependent intervals and appropriate maintenance activities.

Designing for long service life needs some form of verification during the use of the structure. This becomes a natural part of the operation and maintenance activities, the so-called structural service life management. The service life design is based on some assumptions regarding deterioration mechanisms related to the aggressiveness of the environment. Due to the uncertainties between the prior assumptions made at the design stage and the reality of the service conditions of the finished structures, a need arises with time to verify – or adjust – the initial assumption and revise the service life forecast accordingly, see Fig. 16.3. This need for adjustment, and the benefits of obtaining a more reliable forecast of the service life to be expected, leads naturally to a need to monitor the durability performance

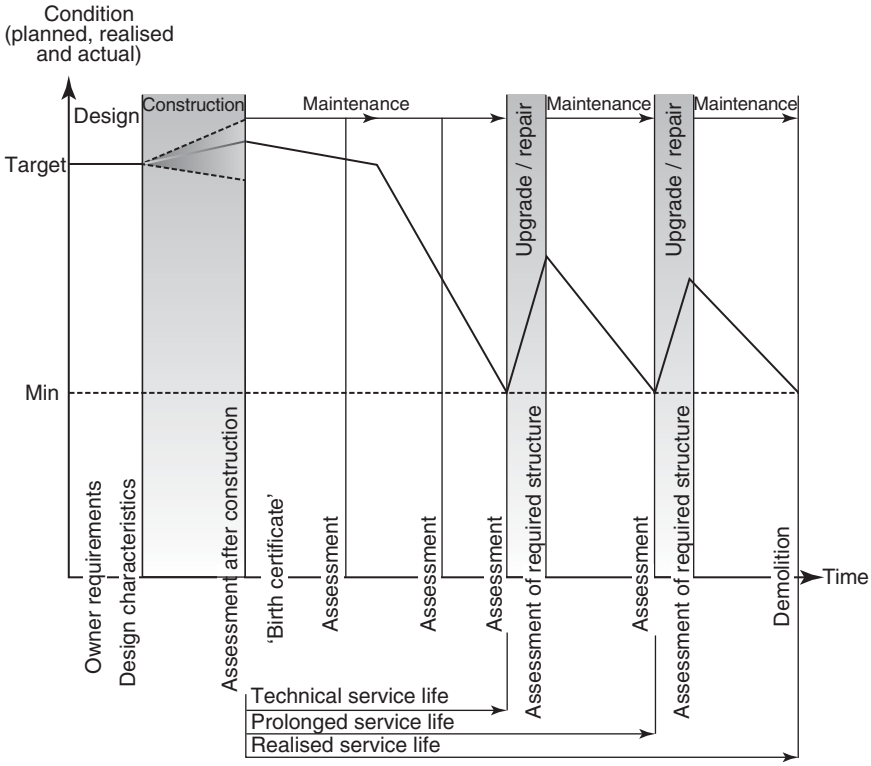

16.3 Structural service life management as structural flow from birth to exitus, adapted from fib (2002).

of the structure in service (fib, 1999). This monitoring can be done destructively but preferably non-destructively.

The term 'maintenance' is used on activities that are planned to take place during the service life of the structure in order to ensure the fulfilment of the assumptions in the service life design. A maintenance plan shall state type and frequency of the foreseen activities. The maintenance plan might comprise activities such as general cleaning, drainage, addition of sealants, replacement of components, etc. Condition control is mainly made to verify the design assumption. From the regularly updated condition control (information from monitoring and inspection) the risk of having depassivation of the reinforcement can be determined more precisely. From this information, if necessary, an optimal point in time can be determined when to introduce preventive measures, for example a preventive coating or a cathodic protection.

16.3 Assessment of corrosion and corrosion risk in concrete

16.3.1 Carbonation

In this Section, describing the carbonation of concrete, it is very well in evidence that only one key parameter has to be controlled in order to evaluate the risk of corrosion of reinforcement in the case of carbonation: the pH value is at the heart of the reinforcement.

Indicator

A minimal destructive method to measure the pH value or, better, the pH range, is the use of a pH indicator applied at freshly fractured concrete surfaces. For the situation encountered Phenolphthalein solutions have been proven to work excellently. Phenolphthalein is a pH indicator, which gradually changes from colourless to purple as the pH rises from 8.3 to 10. The purple colour rapidly becomes visible on a broken concrete surface at a pH greater than about 9 to 9.5, while the carbonated surface zone remains uncoloured. The depth of carbonation can be measured directly at the fracture surface.

Percussive drilling

Minimally invasive are the methods that use percussive drilling. Drilling dust is collected on paper, wetted by phenolphthalein; or alternatively the drilled hole can be sprayed. When the dust becomes magenta, the drilling is stopped and the depth of the hole is considered to equal the carbonation depth. This test is less precise and more tests will be needed. Larger granulates can easily lead to wrong conclusions (CEB, 1998).

Alternative methods

A number of alternative methods are available for monitoring carbonation although none are as convenient as the phenolphthalein indicator method. These alternative methods are X-ray diffraction (to measure the reduction of calcium hydroxide and the increase of various forms of calcium carbonate), thermal analysis and infra-red absorption (formation of silica gel when calcium silicate hydrate carbonates).

The above survey shows that only the phenolphthalein indicator method can be practically used to monitor the pH changes in concrete structures, and therefore to obtain indications concerning the risk of corrosion of the reinforcement by knowledge of the carbonation depth. Besides, this method is destructive, requiring the drilling of cores or other similar samples. Therefore it cannot be considered as an adequate continuous monitoring system.

PH sensors

Recently, pH sensors that are to be embedded in concrete have been designed and tested (Burkert *et al.*, 2006) but the development has not exceeded the status of prototypes. As the carbonation front is generally well defined, requirements on the accuracy of pH sensors are not necessarily high, but stability should be sufficient for long-term performance.

Commercial pH-electrodes for long-term use in concrete are currently unavailable. As the usual glass-electrodes for laboratory purposes are not suitable, other systems have to be discussed, e.g. metal/metal oxide electrodes, with a typically pH-dependent equilibrium potential and a sufficiently steep current/potential characteristic at the free corrosion potential (Brite/EuRam, 2002).

16.3.2 Chloride content

The concentration of chlorides in concrete can be determined by chemical analysis of drilled samples (dust or cores) in a laboratory. The chloride content may be related to the weight of the concrete or to the weight of cement if the content of cement of the concrete is known or obtained by analysis. Several field tests for determining chloride contents from drilled samples are commercially available. The tests are generally easy and quick to perform, but a regular confirmation by laboratory-based determinations is advisable.

When external chloride penetration has occurred, the chloride ion concentration versus depth as chloride profile is required. This profile can be obtained by taking drilling dust samples in different depth ranges and determining the chloride content by chemical analysis. The chloride ion concentration at the depth of the rebar will determine whether there is a risk of corrosion. The satisfactory future performance of both repair works and areas not yet actively corroding will also depend on future movement of chlorides and hence on the critical chloride content in front of and behind the reinforcement, and whether chlorides can still penetrate from an external source (CEB, 1998). Taking into account the critical chloride content (defined in Section 16.2.2) the determined chloride content at the reinforcement can be estimated according to Table 16.1 (CEB, 1989).

16.3.3 Water content and concrete resistivity

As described in Section 16.2 the water content of concrete has a significant influence on chloride penetration as well as on carbonation and, even more important, on the corrosion rate after depassivation. The direct determination of water content by the gravimetric method (drying the concrete at 105 °C until weight stability) is the most precise but is also a destructive test

Table 16.1 Critical chloride levels and the resulting corrosion risk (CEB, 1989)

wt.-% Cl (cement)		
Added in mix	Penetrated	Corrosion risk
<0.6	<0.4	Low
0.6–1.0	0.4–1.0	Medium
>1.0	>1.0	High

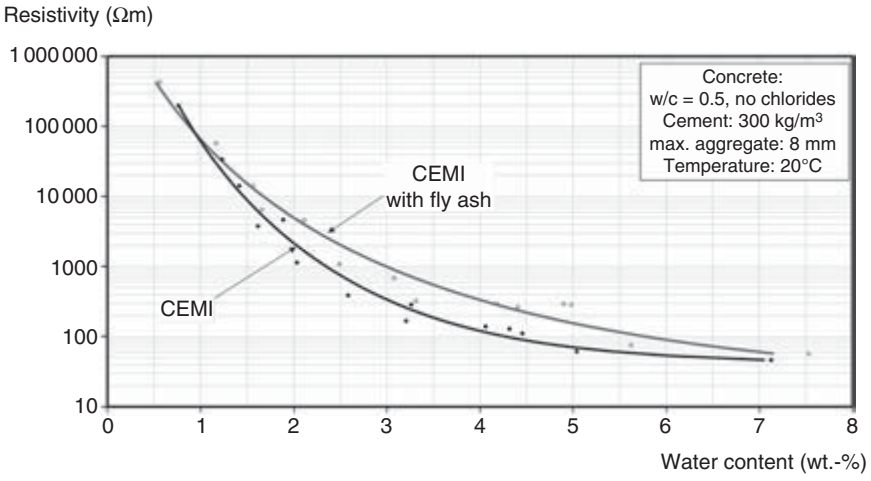

16.4 Correlation between water content and resistivity of two concrete mixtures, adapted from Raupach (2005).

method and thus not suitable for permanent monitoring. Therefore a number of non-destructive test methods have been developed, like resistivity measurement, di-electric methods, capacity methods, methods using microwaves, nuclear magnetic resonance, neutron probe, etc.

Influences on resistivity

The most common method for monitoring water content is the resistivity measurement of the concrete. The resistivity of the concrete depends mainly on the water content, the temperature, the type of cement, the chemical composition of the pore water and the pore structure. Figure 16.4 shows the correlation of water content to resistivity of the concrete for two different concrete mixtures.

The influence of temperature on the electrolytic resistance can be taken into account with the following equation:

$$R_{el} = R_{el,0} \cdot e^{b \cdot \left(\frac{1}{T} - \frac{1}{T_0}\right)} \quad [16.5]$$

with:

R_{el} = Electrolytic resistance at temperature T (e.g. 20 °C)
T, T_0 = Absolute temperatures [K] (e.g. 293 K)
$R_{el,0}$ = Electrolytic resistance at temperature T_0
b = Constant in K (activation energy)

Values between 3000 and 5000 K are quoted in the pertinent literature for the temperature constant b. Under normal conditions a decrease in temperature of 1 °C causes an increase in resistance of approximately 3%.

A non-destructive determination of the electrical resistivity of the concrete can be carried out by commercially available Wenner four-point arrays. No electrical connection to the reinforcement is required, but a temporary connection of the measuring electrodes to the concrete surface is needed, for which conductive liquids and gels have been developed. Using special embedded measuring electrodes the resistivity of the concrete can also be measured as two-point arrays in different depth steps (see Section 16.4.3). Electrical resistance measurements are usually carried out using AC (alternating current) impedance measurements with frequency ranges from 100 to 1000 Hz to avoid polarisation effects at the electrodes. Another method uses DC (direct current) measurements of the voltage drop of the concrete induced by an applied direct current (IR drop).

As the concrete resistivity strongly influences the corrosion rate of the reinforcement (see Fig. 16.2), the electrolytic resistivity acts as an important parameter for the estimation of the corrosion state of rebars. Assessment criteria for resistivity measurements in regard to the risk of corrosion are given in Table 16.2 (Brite/EuRam, 2002).

Table 16.2 Correlation between resistivity and corrosion risk (Brite/EuRam, 2002)

Resistivity [Ωm]	Corrosion risk
>1000	Negligible
500–1000	Low
100–500	Moderate
<100	High

Table 16.3 Probability for corrosion according to ASTM-C 876

Potentials related to CSE-electrode [mV]	Probability of corrosion
<–350	90%
–350 to –200	Uncertain range
>–200	10%

In the case of carbonation, unfortunately, the value of the resistivity is influenced by the formation of calcium carbonates which often contributes to close the pores and causes an increase in resistivity; this fact is in contrast with the above classification, which assesses that a decrease in resistivity corresponds to an increase in corrosion. Therefore, when assessing resistivity measurements, effects of carbonation need to be taken into account.

16.3.4 Potential values

Potential measurement or potential mapping is the most widely used non-destructive assessment technique for assessing the actual corrosion behaviour of the reinforcement. It is a very efficient method for detecting localised areas of corrosion such as that due to chloride ingress. Compared with the other existing techniques it is the only commonly recognized and standardized method (see e.g. ASTM-C 876, SIA Merkblatt 2006). It gives an indication of the probability of corrosion by relatively simple voltage measurements between a reference cell either held on to the concrete surface or an embedded reference electrode and the reinforcement.

The evaluation criteria for the potentials related to the saturated copper/copper-sulphate electrode (CSE) as given in the Standard ASTM-C 876 can be found in Table 16.3. These criteria have to be used very cautiously. Their interpretation should always be compared with the interpretation of the results of other inspections (e.g. resistivity measurement) or evaluations (e.g. potential gradient) (Lay, 2003).

Experience over the years has shown that an evaluation of the absolute potential as shown in Table 16.3 often leads to wrong interpretations, because the basis for this standard was an evaluation of data from bridge decks which cannot be transferred to other types of structure having different environmental conditions. Therefore more reliable evaluation methods have been developed. An overview of newly developed methods can be found in the report by Lay (2003).

The most common types of electrode are the saturated copper/copper-sulphate-electrode (CSE) for potential mapping on the concrete surface and the manganese oxide electrode (MnO_2), which can be embedded into

concrete for monitoring. In the case of uniform corrosion induced by carbonation the potential values often lead to inconclusive results.

16.3.5 Corrosion rates

Potential measurements just give information whether active corrosion is actually probable or not. To get more detailed information on corrosion behaviour than from simple potential mapping, on-site corrosion rate measurement methods have been developed, like anodic pulse measurements, linear polarisation resistance measurements, AC impedance and electrochemical noise measurement. Most of these methods have this in common: the potential of the steel (reinforcement) changes electrochemically by using an external current; and it monitors the electrochemical response of the reinforcement.

The anodic pulse measurements use a galvanic direct current pulse over a period of a few seconds to the reinforcement and the influence on the potentials of the reinforcement is monitored. This potential change consists of the IR-drop occurring immediately after applying the pulse (which enables the resistivity to be determined) and later on of a further increase of the potential describing the polarisation behaviour of the steel. Altogether three parameters are determined by anodic pulse measurements: the potential, the resistivity and the polarisation behaviour of the reinforcement. However, the determination of the exact corrosion rate under practical conditions is normally not possible, because the calculation models (suitable equivalent electrical circuits) are only rough approximations. Furthermore the measurement is influenced by the ratio between the reinforcement surface and the concrete surface, which can vary widely. Additionally galvanic effects in the case of macro-cell corrosion (localised corrosion) cannot be determined, i.e. only an average corrosion rate is measured (CEB, 1998).

Similar to the anodic pulse measurements linear polarisation measurements can be carried out to determine the potential and polarisation behaviour of the reinforcement and the resistivity of the concrete. Instead of an anodic pulse a small voltage variation (±10 to ±20 mV) is applied sinusoidally to polarise the reinforcement slightly. The induced electrical current is measured and evaluated allowing the determination of the IR-drop and polarisation behaviour. Assuming a linear relationship between potential and current near the free corrosion potential, a so-called linear polarisation resistance (LPR) (see Chapter 3 for more details) can be calculated from the measured data. This LPR is often used to calculate a corrosion current for the reinforcement.

A further improvement is a commercially available special device for LPR measurements: the so-called guard-ring. This confines the area of

Table 16.4 Limit values for LPR-measurements often used as evaluation criteria (RILEM, 2004)

Current densities [μA/cm²]	Corrosion rates
0.1 to 0.2	Passive condition
0.2 to 0.5	Low to moderate
0.5 to 1.0	Moderate to high
>1.0	High

measurement on the reinforcement if placed around the counter electrode used for applying external voltage. When interpreting data from the LPR measurement it should also be noted that the corrosion rate of the reinforcement can only be estimated because some parameters cannot be quantified as a ratio between reinforcement and concrete surface and macro-cell corrosion effects. The limit values according to RILEM (2004) are given in Table 16.4.

Similarly to the case of potential measurements, the corrosion rate may be measured by means of either external devices (cathode, reference electrode) for existing structures, or internal probes to be positioned inside the structure at the casting stage.

16.4 Sensors for corrosion monitoring

16.4.1 Measurement categories for durability assessment

The measurement categories for durability assessment can be subdivided into assessed parameters, location of the measured parameter and whether the measuring system is either portable or permanently installed in the structure. The parameters determined for durability assessment are either indirect or direct parameters:

- **Indirect parameters** are resistivity of the concrete, water content, chloride content or chloride profiles and depth of the carbonation front. These parameters give no direct information on the state of corrosion of the reinforcement, but the risk of corrosion and/or the rate of corrosion can be estimated.
- **Direct parameters** like the potential or corrosion rate of the reinforcement provide direct information on the corrosion state of the reinforcement.

Another category to distinguish between the monitoring systems is the depth of the assessed condition related to the concrete surface.

- **Mono-depth systems** provide information on the condition only at one fixed depth (which is normally the location of the reinforcement). These systems can only be used to assess the actual state of the reinforcement. However durability prediction as part of the structural service life management (see Figure 16.3) is not possible in the initiation period (see Figure 16.1). In many cases intervention, like repair measures, is much more expensive, when the deterioration period has started compared with intervention during the initiation period.
- **Multi-depth systems** allow the assessment of parameters (e.g. resistivity or corrosion rate) in several depth steps, especially between the concrete surface and the reinforcement. In this way information of the condition is time- and depth-dependent. For example, these data enable the prediction of the time to onset of corrosion at the reinforcement and thus can be part of a structural service life management system.

The monitoring systems are either portable or permanently installed. The main advantages of **permanently installed monitoring** systems are:

- Continuous monitoring of the process of corrosion that is affected by many factors and shows daily variations and seasonal changes.
- Monitoring of inaccessible areas of structures (e.g. exterior of tunnels) or areas hard to reach (structures under water) is possible.
- By the use of multi-depth sensors, for example, it is possible to monitor the ingress of the depassivation front versus time and thus use the data from monitoring for a durability assessment.
- No interference with traffic in case of bridges, tunnels etc.
- Time saving as measurements with portable equipment take more time to be carried out (including personnel costs).

The use of **portable monitoring equipment** for corrosion monitoring can be recommended as follows (Brite/EuRam, 2000):

- Portable equipment for monitoring corrosion activity is a convenient tool for supplementing the current practice of surveillance, based mainly on visual inspections. It gives some semi-qualitative (potentials) and quantitative information (corrosion rate) on the level and progress of damage thus giving an input for the prediction of deterioration, definition of alarm thresholds and time to repair.
- Portable systems are in most cases rather handy and easy to use. They allow measures to be taken extensively along the structure, provided access is guaranteed.
- Measures can be repeated at regular intervals over the years, however access to the structures may be costly and cause interference to traffic.

- It may be used in conjunction with permanent monitoring on existing structures or it may suggest the best location for probes and sensors, as it gives information on the location and extension of the most corroded or risky parts.
- It may be used to check the performances of permanent monitoring (working conditions of sensors and probes).

As monitoring structures using multi-depth and permanently installed sensors provides the most important information to assess the durability of these structures sections 16.4.2–16.4.5 focus mainly on these types of sensor. Most sensors can also be used for mono-depth monitoring. If portable systems that provide useful additional information are available, they are briefly described.

16.4.2 Sensors for determining the chloride content

The chloride-sensitive sensors are normally based on a solid silver/silver chloride electrode and a reference electrode for use in concrete. The central, active, chloride-sensitive element is a silver wire coated with electrochemically deposited silver chloride. The potential at the silver/silver chloride electrode is strongly dependent on the chloride content of free chlorides in the pore solution, but also on the temperature, the water content and the concentration of other ions in the pore water of the concrete. As reference electrode a manganese oxide electrode is recommended (Schiegg, 2002).

By installing several silver/silver chloride electrodes at different depths in a structure, together with the manganese oxide electrode, a non-destructive determination of a chloride profile and the time-dependent change of the chloride content is possible. The sensors can also be embedded in existing structures by using a special connecting mortar, which is adjusted to the water and chloride transportation properties of the surrounding concrete. Long-term exposure revealed a strong humidity influence, e.g. by drying out, on the measured values. The interpretation of the monitored data must therefore take humidity into account. Additionally a long-term potential shift has been determined even in chloride-free specimens as well as an influence of corrosion processes on the measured values. Thus the long-term stability of chloride-sensitive sensors is doubtful (Brite/EuRam, 2002; Bergmeister, 2004).

16.4.3 Sensors for concrete resistivity measurement

The resistivity of concrete can be determined either by using two-point arrays or four-point arrays (see Section 16.3.3). A portable monitoring system is the so-called Wenner-probe as a four-point-electrode which is connected to the concrete surface. The Wenner-probe is not suitable for

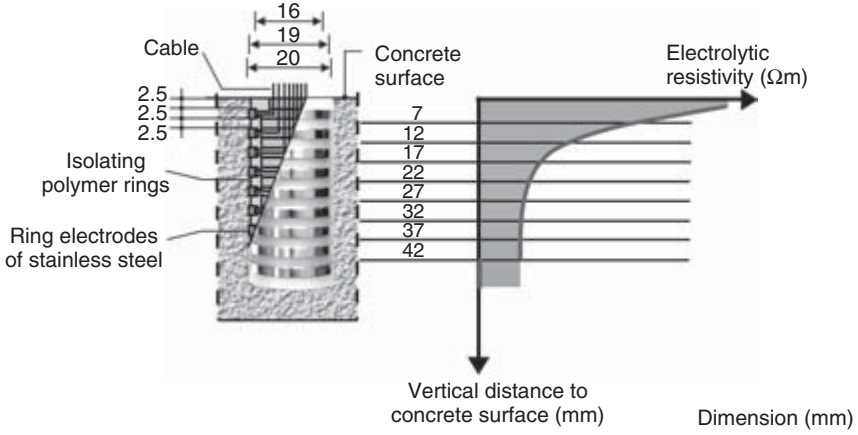

16.5 Schematic set-up of the Multiring-Electrode for measurements of depth-dependent resistivity of concrete (Sensortec, 2006).

concrete structures with a distinct profile of resistivity in the concrete cover, which is often the case in naturally weathered structures.

A depth-dependent resistivity-profile can be determined with the so-called Multiring-Electrode (MRE S + R Sensortec GmbH), see Figure 16.5. It consists of alternating stainless steel and polymer rings. Typically the sensor consists of nine stainless steel rings enabling the measurement at eight depths with a distance of 5 mm, and single measurements being done between two neighbouring steel rings. The cell constant k of the MRE sketched in Fig. 16.5 was determined to a value of 0.1 m by experiments and by numeric simulation.

The Multiring-Electrodes are cast into the concrete with a concrete cover of the uppermost stainless steel ring of 2.5 mm. The resistivity of the surrounding concrete between the adjacent pairs of stainless steel rings (1–2, 2–3, . . . , 8–9) can be measured resulting in a local electrolytical resistivity profile of the concrete cover zone (approx. 40 mm). For installation in existing concrete structures a special connecting mortar is used, which provides a humidity balance to the surrounding old concrete.

16.4.4 Sensors for potential measurement

As described in Section 16.3.4 potential measurement can be conducted either using a portable system (potential mapping) by means of an external reference electrode (like a saturated copper/copper-sulphate electrode) or using an internally installed system e.g. by means of manganese oxide electrodes. Internal reference electrodes are normally embedded close to the reinforcement to minimise the influences arising from concrete resistivity

16.6 MnO_2-reference electrode for measuring the potential of the steel attached to the reinforcement (ERE 20, Force Technology).

(IR-drop). The most common type of reference electrodes are the manganese oxide (MnO_2) electrodes (see Fig. 16.6) having proven long term stability in concrete. Cast into the cover concrete of new or existing structures the corrosion state of reinforcing steel or effectiveness of cathodic protection can be monitored. The potential of MnO_2 is virtually independent of changes in the chemical properties of the concrete. It can, therefore, be used in wet or dry concrete, whether exposed to chlorides or to carbonation. But a total drying of the electrode should be prevented, because inside the steel housing an alkaline, chloride-free gel is required as an electrolyte (Burkert *et al*., 2006).

The use of a solid reference electrode for corrosion measurements of steel in concrete has been investigated by Sagüés (1994), testing activated titanium rods. For installed electrodes in the same pH-range an excellent short-term stability and a reasonable long-term stability with little sensitivity to variations in the partial pressure of oxygen was determined. Reference electrodes made of activated titanium are used for additional potential measurements in some corrosion sensors (e.g. Anode Ladder).

16.4.5 Sensors for depassivation and corrosion rate measurement

The most common portable corrosion monitoring system is the so-called GalvaPulse (Force Technology) (Force, 2006), which is described in Section 16.3.5. The GalvaPulse allows a rough estimation of the corrosion rate of the reinforcement, see Fig. 16.7.

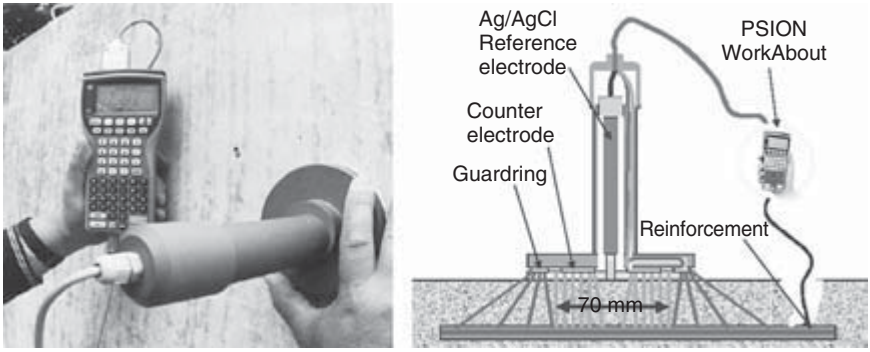

16.7 The GalvaPulse computer and the electrode for measurements of the corrosion rate (left, Force, 2006) and schematic conditions at the electrode (right, Brite/EuRam, 2002).

Sensors for permanently installed corrosion monitoring can be subdivided for new constructions (or installed during repair measures with renewal of the concrete cover) and for existing structures. Most of these sensors, such as the so-called Anode Ladder (S + R Sensortec GmbH) or the Expansion-Ring-System consist of different single sensors at defined distances from the concrete cover, e.g. of six steps, each of about 10 mm width, depending on the thickness of the concrete cover. The basic measuring principle of the sensors for the determination of time-to-corrosion is to place electrodes at different depths related to the concrete surface and to measure the onset of corrosion of these electrodes one after the other (see Fig. 16.9). The measuring principle of the Anode Ladder is the successive connection of each anode with a cathode consisting of noble metal (activated titanium) and the measurement of the corrosion current via cables which connect the sensor to a external terminal box.

For new structures the Anode Ladder has been used world-wide in concrete structures exposed to aggressive environments since 1990 (Schießl, 1992) (see Fig. 16.8). The measuring electrodes are made of steel with a similar composition to reinforcing steel to ensure that they will start to corrode at the same time that a rebar at the same depth would start to corrode. Comparative tests have been carried out at the Institute for Building Materials Research of the RWTH Aachen, ibac (Germany) showing that there was no significant difference in the corrosion behaviour of the steel used for the measuring electrodes (anodes) and reinforcing steel with different degrees of pre-rusting before installation into the concrete specimens.

Measurement of the Anode Ladder is carried out automatically in three steps: first the voltage difference between each electrode and the activated titanium rod acting as a solid reference electrode as well as a

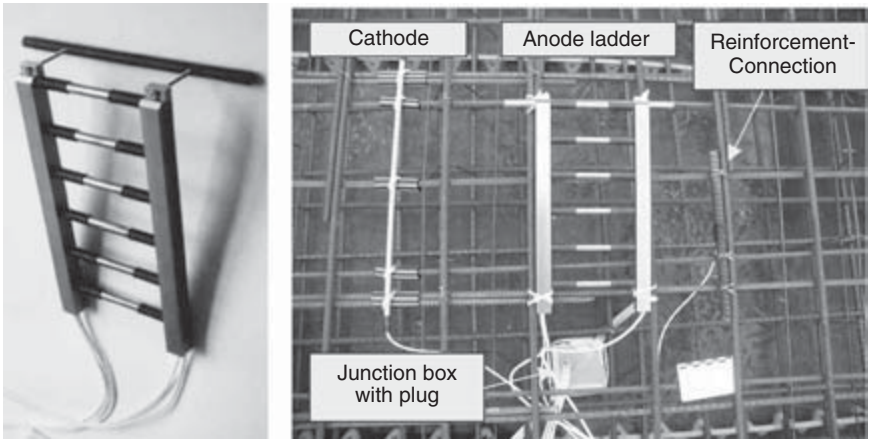

16.8 Anode Ladder to determine the depth of the critical chloride front (left: design of the Anode Ladder, right: installed Anode Ladder before concreting) (Sensortec, 2006).

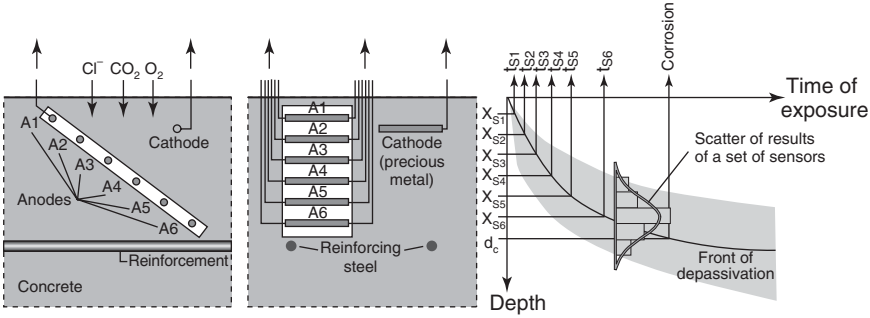

16.9 Basic principle of the Anode Ladder and the determination of the time to corrosion of the reinforcement.

cathode. Then the electrical current is determined for each electrode five seconds after coupling of the anodes against the cathode and finally the AC-resistance is measured (at 10 Hz) between neighbouring anodes and also the temperature of the integrated platinum PT 1000 sensor. Experience has shown that for activity limit values of single anodes under normal conditions an electrical current of about 10 to 15 µA after a short circuit time of five seconds is used. For special conditions regarding concrete composition or environment, e.g. for nearly water saturated concrete, other limit values might be relevant, which have to be determined by calibration tests using the same concrete under the same conditions. Thus the critical depth of the depassivation front can be determined at any time (see Fig. 16.9).

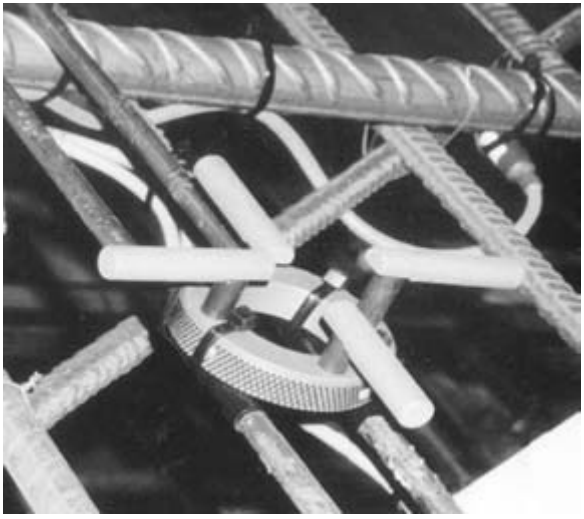

16.10 Design of the CorroWatch to determine the depth of the critical chloride front (Force, 2006).

By installing sufficient sensors, the scatter in the depths of the depassivation front can be considered and implemented in a probabilistic update of the service life design (see Fig. 16.9: scatter of results). A comparable sensor from another producer is the so-called CorroWatch (Force Technology), with circularly placed electrodes, a MnO_2-reference electrode and a cathode, which enables the determination of the corrosion current and the potential of the anodes depth-dependently (see Fig. 16.10).

To enable such monitoring for existing structures another system, the so-called Expansion-Ring-System (ERA) (S + R Sensortec GmbH) has been developed (see Fig. 16.11). Tests on drilled-in sensors were first carried out in 1996 (Raupach, 1998). After several improvements, sufficient experience is now available for the system to be used in existing buildings in non-submerged exposure conditions. The principle of the Expansion-Ring-System is similar to the Anode Ladder. It consists of the Expansion-Ring-Anode and a Cathode. Both are inserted into holes, which have to be drilled into the concrete. The measuring part is the Expansion-Ring-Anode. The sensor consists of six measuring rings at different distances from the concrete surface, 10 mm increments from 10 mm to 60 mm. The electrolytic connection of the sensor is carried out by expanding the rings during installation and pressing them strongly into the concrete surface of the drilled hole. In this way the ingress of chloride and/or carbonation from the concrete surface into the concrete

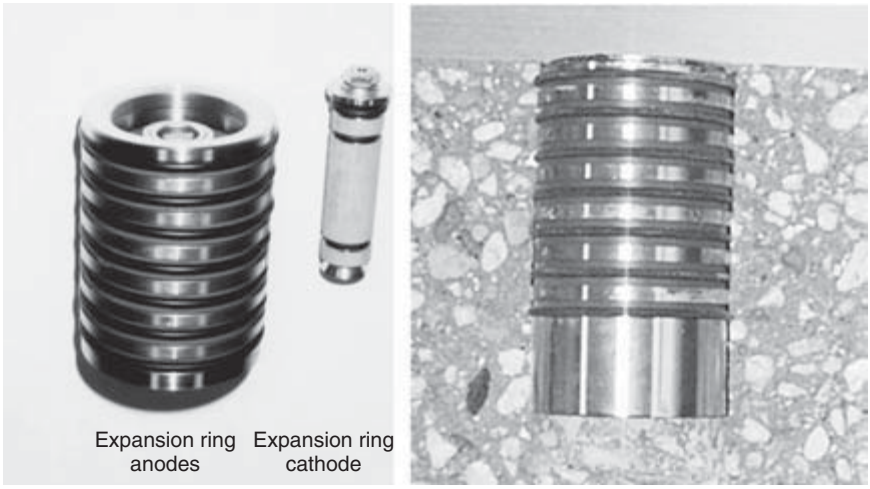

16.11 Design of the Expansion-Ring-System to determine the depth of the critical chloride front for existing structures (left) and the Expansion-Ring-Anode after installation in concrete (Sensortec, 2006).

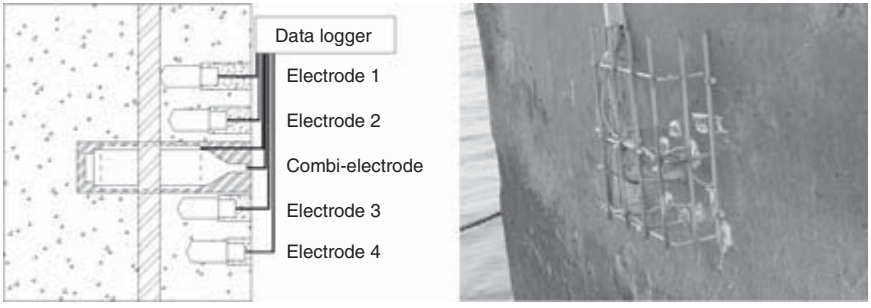

16.12 Design of the CorroRisk to determine the depth of the critical chloride front for existing structures (left: sectional view on the mounted CorroRisk probe, right: CorroRisk mounted on bridge pillar and covered with latticework) (Force, 2006).

and the subsequent corrosion risk of the reinforcement can be measured by the same method as the Anode Ladder. The performance of the Expansion-Ring-System has been tested both in the laboratory and on-site (Brite/EuRam, 2002).

Another sensor for existing structures, the so-called CorroRisk probe (Force Technology) (see Fig. 16.12), is based on metallic nails with a cathode and a MnO_2-electrode. These nails are installed in existing structures by hammering through pre-drilled holes. The nails are made from a material

similar to that of the reinforcement. They are therefore expected to corrode when the chloride is penetrating the concrete and reaches critical concentration at the level of the single nails. The cathode is an activated titanium mesh. For existing structures under submerged conditions a new type of sensor is currently under development by S + R Sensortec, Germany.

16.5 Data evaluation

16.5.1 Discussion of the data gathering rate

When a structure is monitored with regard to the durability or to corrosion of the reinforcement the data gathering rate has be specified carefully. For all permanent installed sensor-systems automatic measuring systems with data-loggers are available. This enables measurements to be carried out in very small cycles resulting in a huge amount of data. However for life management of structures a measuring period of approximately 30 to 50 years is required for most sensors. Even taking into account the rapid development of soft- and hardware, it is unlikely that a monitoring system with a PC-remote-control installed today will run for 10 or 15 years. Furthermore experience shows that receiving a huge amount of data to be analysed normally distracts the person in charge from really important questions. For these reasons a portable measuring system for permanently installed sensors and a data gathering rate of every 6 to 12 months (t_{insp}) will prove to be sensible in most cases. Furthermore readings of the sensors can then be carried out in combination with a visual, routine or in-depth inspection of the structure.

16.5.2 Implementation of monitoring data in durability evaluation

The best case for information provided by monitoring is: How deep the depassivation front develops with time. This information can be used to update durability calculations (e.g. fully probabilistic) at regular intervals. If the measured depth of the depassivation front at time t_{insp} is lower than expected *a priori* or if the expected depth at time t_{insp} will be confirmed by corrosion sensor readings, the reliability of the service life predictions is improved. On the other hand, if the environmental load is underestimated (*a priori*) the remaining maintenance free service life will be reduced compared with the original *a priori* calculation. Updated and consequently regularly improved information about the present state of the structure can be used to decide upon the optimal point in time, if necessary, for protective measures. A mathematical approach for implementation of monitoring data in durability evaluation is introduced by Sodeikat *et al.* (2006).

16.6 Applications

16.6.1 Fields of application

Reasonable fields of application of corrosion sensors are primarily structures, which are generally inaccessible following construction, but are exposed to an aggressive environment. These include structures such as the exterior of tunnels in soil containing chlorides, foundations or piles in sea water, console areas in exposure conditions containing de-icing-salt and other structures in severe conditions. An overview of fields of application for corrosion monitoring is shown in Fig. 16.13.

16.6.2 Basic requirements and limitations

The basic requirements for sensors for corrosion monitoring in concrete are as follows:

- Sensors need to be robust, all components must be designed to be durable and long-term-stable in the alkaline environment of concrete containing chlorides.
- The installation should be easy to handle.
- Any negative effects on the structural behaviour (e.g. changes of the exposed surface, deformation due to temperature) should be excluded.
- Redundant systems help to check the sensors and to locate malfunction.

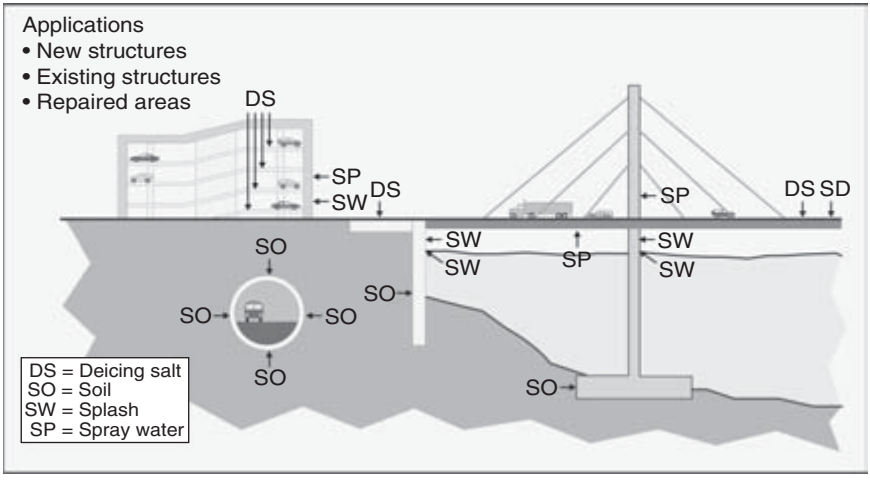

16.13 Fields of applications for corrosion monitoring (examples).

- Furthermore it is advisable to use specially protected cables (e.g. Teflon coated cables) if a replacement is virtually impossible (e.g. connections within the concrete).
- Finally an external measuring unit can easily be replaced in case of malfunction.

Corrosion monitoring has some limitations, too:

- Limitations in regard to **durability of the monitoring system**
  Because the durability of a structure is aimed to be monitored, the service life of the monitoring system consisting of the sensor itself, cables and measuring unit should exceed the service life of the structure. As already mentioned above the durability of some sensors is limited (like chloride sensitive sensors), therefore these sensors should not be used for durability monitoring.
- Limitations in regard to **kind of corrosion**
  Available corrosion sensors are designed to monitor either uniform or pitting corrosion. Other kinds of corrosion like stress corrosion or corrosion fatigue crack cannot be determined with these sensors.
- Limitations in regard to **cracks or other weak points** in the construction
  Permanently installed sensors are able to monitor the condition in the surrounding area only, they give no information on cracks or other weak points outside the location of the sensor. In cracked structures sensors in an uncracked area can easily interpret the structure as in a better condition than it actually is. If the location of probably arising cracks or other weak points (e.g. joints, honeycombs) is known in advance, sensors can be placed there to monitor those weak points. Nevertheless monitoring cannot substitute further inspections (visual, routine or in-depth), to determine any anomaly of the structure which cannot be monitored by the used sensors.

16.6.3 Examples of applications

Storebaelt

The 18 km long crossing over/under the Great Belt in Denmark, consisting of two bridges and a railway tunnel, is one of the most famous major building structures for which a durability design covering a period of 100 years has been carried out (e.g. Rostam, 1993). This assessment also included various scenarios regarding possible future problems, like the consideration of possible repair measures over several decades. With regard to the risk of reinforcement corrosion, the following concept was pursued:

- The concrete cover and the quality of the concrete were designed so as to ensure corrosion protection for 100 years according to knowledge currently available and on the basis of comprehensive laboratory experiments carried out specifically to examine the properties of the concrete mixtures, in particular the chloride penetration characteristics.
- As no adequate long-term experience was available with regard to the durability of the employed high-performance concrete under practical conditions, corrosion monitoring sensors (Anode Ladders) were installed in order to reduce the risk of unidentified corrosion problems (e.g. Schießl, 1995) and preparations were undertaken for protection measures which might subsequently become necessary. In order to ensure that the subsequent installation of a cathodic corrosion protection system would be possible, the reinforcement was welded such that all rods are interconnected in an electrically conductive configuration.
- The low permeability of the concrete has been proven by laboratory testing permanently within the construction phase. The design assumptions are reviewed by regular examination of the structures, including readings of the corrosion sensors which have been installed, particularly at inaccessible points (Raupach, 2002).

Bibliotheca Alexandrina

The Bibliotheca Alexandrina (Egypt) which was opened in 2002 represents a building with a special historical background. In view of the fact that it had been destroyed twice, the scheduled service life was set at 400 years, in order to outlast the two previous periods of use.

As the library building is located in the direct vicinity of the Mediterranean Sea on the coast of Alexandria, the foundation elements, consisting of a diaphragm wall of around 35 m in depth and several hundred piles, are exposed to severe chloride attack. As numerous piles were systematically subject to tension as a result of water pressure on the foundation slab, there was an additional danger of cracks crossing the main reinforcement. In order to ensure long service life, the following corrosion protection concept was selected:

- The tension piles were provided with a second reinforcing cage that is capable of bearing the tensile forces, should the outer reinforcement corrode away completely.
- A blast-furnace cement containing a high slag content and a concrete with a low water/cement ratio were used for all foundation elements, in order to achieve a high level of resistance to both sulphate and chloride penetration. A minimum thickness of 15 cm was specified for the concrete cover.

- Similar to the Great Belt project, the reinforcement was totally interconnected in electrically conductive configuration by means of welding, in order to enable the subsequent installation of a cathodic corrosion protection system. A sensor-based corrosion monitoring system using Anode Ladders has been deployed to determine whether and when such a protection system becomes necessary (Raupach, 2002).

Hangzhou Bay Bridge

In east China a 36 km long bridge began construction in 2003 and will be opened in 2009 as the longest sea bridge in the world, crossing the bay of Hangzhou. The target service life was set at 100 years, although the bridge will be exposed to extreme severe environmental conditions, like tremendous tidal range, changing water currents, earthquakes, typhoons and chloride attack. To monitor the penetration of chlorides and, if necessary, to start further protection actions (like cathodic protection) a long-term-monitoring system is actually being installed including corrosion monitoring sensors (Raupach, 2006).

Parking deck at the football stadium Allianz-Arena in Munich

In Munich, Germany, a new football arena was built. In 2006 the world championship was opened there. In order to provide an adequate infrastructure for visitors, the arena is connected to the underground railway as well as to two highways. To provide adequate parking space, a huge multi-storey car park with 11 000 parking spaces, the biggest in Europe, was constructed. The car park consists of four parking decks, with three made from reinforced and pre-stressed concrete. As de-icing salts, often in combination with frost attack are expected on the horizontal parking deck surfaces, the design of the three parking decks should provide adequate durability against chloride induced corrosion and freeze-thaw attack. As the dimension of the multi-storey car park is about 425 m in length and 152 m in width a preventive coating of all three decks is very costly (extra investment costs of about €7 500 000).

Considering that only during football matches is the car park frequented (event dependent utilisation), it was decided that a preventive coating of the whole area of all decks was not justifiable from an economical point of view at this early time (the service life of coatings is expected to be no longer than about 15 years). At the design stage, it was assumed that an excellent quality concrete in combination with an adequate concrete cover in an uncracked situation can provide acceptable resistance against chloride ingress and frost attack even if the concrete surface is uncoated. Only in the surface areas, where cracking has to be expected is extra protection definitively needed. With this approach the high investment costs for a

complete coating of all surfaces could be reduced substantially. The target service life was set at 50 years (owner requirement).

To operate the structure safely and to ensure the functionality a condition control plan was established. The plan consists of:

- types of inspection/monitoring
- definitions of components of the structure to be inspected/monitored
- frequency of condition control
- performance criteria to be met
- possible documentation/interpretation of the results
- action in the case of non-conformity with the performance criteria.

Initial inspection was made to verify that areas supposed to be uncracked are in fact uncracked (verification of design assumption). If not, a crack-bridging coating (intervention) was applied immediately.

In the uncracked surface area a monitoring system was installed locally, providing information about depth-dependent corrosion risk at specific locations. Sensors (Anode Ladders) were installed at different locations, mainly at low points, expected hot spots with regard to reinforcement corrosion and frost deterioration. The information that will be provided by the sensors at low points is the depth of the depassivation front over time. This information will be and has been used to continuously update the durability calculation.

From the continuously updated information (monitoring, inspection) about the probability of occurrence that the reinforcement is starting to corrode, an optimal point in time can be determined to apply a preventive coating if necessary. The application of the coating has to be accurately timed, so that a possible redistribution of chlorides (equalisation of concentrations) after application of the coating does not lead to corrosion of the reinforcement/pre-stressing bars.

Due to the expected low frequency of the parking deck during operation (event-dependent utilisation) it is expected that the durability of an uncoated but corrosion-resistant-optimised structure is much higher than experience shows for parking decks located in congested urban areas. Depending on the regularly controlled ingress of chlorides one or two coating measures and their associated costs may be saved without any restriction to safe operation if compared with the situation of preventive coating at the beginning and renewal every 15 years.

16.7 Conclusions

Like in many other industrial sectors the request for on-line monitoring of corrosion relevant parameters arises in civil engineering. As corrosion of reinforcement is the main cause of deterioration and thus of repair

measures, corrosion monitoring is a useful and powerful tool which enables the condition of a structure to be assessed permanently and therefore the date of intervention optimised. A pre-condition for successful corrosion monitoring is a detailed design of the monitoring system with a clear description of the monitoring target and a subsequent choice of suitable sensors. Furthermore part of the design of a monitoring system is to plan installation carefully while the structure is being constructed, to define threshold values of the sensors in advance, to describe possibilities of checking the system and the data gathering rate. Finally an 'information plan' has to be developed in case the condition of the structure should fall below a defined threshold, including the description of repair measures.

A significant difference from other industrial sectors (like the chemical industry) is that in civil engineering the changes of corrosion relevant parameters in structures take place rather slowly, thus a low data gathering rate is recommended (maybe in combination with a higher data gathering rate when the structure is young). Meanwhile many types of corrosion sensor measuring either direct parameters (e.g. corrosion rate, depassivation depth) or indirect parameters (e.g. resistivity) are commercially available. Some of them have been tested in practice for longer periods of time. As the durability of the whole corrosion monitoring system (sensor, cables and measuring unit) is a pre-condition for successful monitoring, particular attention should therefore be paid to the choice of sensors and system. At best the corrosion monitoring system is part of a service life management system, which includes service life design calculations. Thereby data from corrosion monitoring can be implemented into the update of service life design calculations permanently.

16.8 References

Bergmeister K (2004), 'Brückeninspektion und – überwachung', in Wörner J. D., *BetonKalender 2004*; Berlin, Ernst & Sohn, 409–481.

Brite/EuRam (2002), *Smart Structures (Integrated Monitoring System for Durability Assessment of Concrete Structures), Final Technical Report and Report of Task 2.1: Determination of Key Parameters,* Bruxelles.

Burkert A, Eich G, Bäßler R, Isecke B (2006), 'Corrosion Monitoring im Bauwesen', in *Sicherheitsgewinn durch Monitoring?*, Darmstadt, Freunde des Institutes für Massivbau der Technischen Universität Darmstadt e.V., 115–135.

CEB Bulletin 192 (1989), *Diagnosis and Assessment of Concrete Structures – State-of-Art Report,* Lausanne, CEB.

CEB Bulletin 243 (1998), *Strategies for Testing and Assessment of Concrete Structures – Guidance report*, Lausanne, CEB.

fib (1999), *Structural Concrete, the Textbook on Behaviour, Design and Performance, Volume 3*. Lausanne, International Federation for Structural Concrete (fib).

fib (2002), *Working Party 5.3–1, Assessment and Residual Service Life Evaluation: Technical Report on 'Assessment and Residual Service Life Evaluation on Concrete Structures'*, Draft per 15 March 2002 (unpublished).
Force (2006), Brochures 'CorroWatch Multiprobe & ERE 20 Reference Electrode', 'GalvaPulse' obtainable from Force Technology, Denmark.
Gaal GCM (2004), *Prediction of Deterioration of Concrete Bridges: Corrosion of Reinforcement Due to Chloride Ingress and Carbonation*, Delft, Technische Universiteit, Civil Engineering and Geosciences Concrete Structures.
Gehlen C (2000), *Probabilistische Lebensdauerbemessung von Stahlbetonbauwerken – Zuverlässigkeitsbetrachtungen zur wirksamen Vermeidung von Bewehrungskorrosion*. Berlin, Heft 510 der Schriftenreihe des DAfStb.
Lay S (2003), *Prototype of Condition Assessment Protocol – Life Cycle Management of Concrete Infrastructures for Improved Sustainability*, Project LIFECON, cbm – Technische Universität München.
Lay S (2006), *Abschätzung der Wahrscheinlichkeit tausalzinduzierter Bewehrungskorrosion – Baustein eines Systems zum Lebenszyklusmanagement von Stahlbetonbauwerken*, Berlin, Heft 568 der Schriftenreihe des DafStb.
Nürnberger U (1995), *Korrosion und Korrosionsschutz im Bauwesen*, Wiesbaden. Bauverlag.
Raupach M (1992), *Zur chloridinduzierten Makroelementkorrosion von Stahl in Beton*. Berlin, Heft 433 der Schriftenreihe des DAfStb.
Raupach M (1996), 'Chloride-Induced Macrocell Corrosion of Steel in Concrete – Theoretical Background and Practical Consequences', *Construction and Building Materials* 10 (5), 329–338.
Raupach M (1998), 'A New Sensor System for Monitoring the Corrosion Risk in Existing Structures', Second International Conference *Concrete Under Severe Conditions – Environment and Loading (CONSEC 98)*, Tromsö, Norway, 565–573.
Raupach M, Dauberschmidt C (2002), 'Stahlbeton mit planmäßiger Nutzungsdauer von 100 Jahren', *Beton* 52 (5), 236–240.
Raupach M (2006), 'Korrosions-Monitoring an der 36 km langen Hangzhou Bay Bridge in China', *Sicherheitsgewinn durch Monitoring?*, Darmstadt, Freunde des Institutes für Massivbau der Technischen Universität Darmstadt e.V.
Raupach M, Dauberschmidt C, Wolff L (2005), 'Monitoring the Moisture Distribution in Concrete Structures', *International Conference on Concrete Repair, Rehabilitation and Retrofitting (ICCRRR)*, Cape Town, South Africa, 2005, 6–8.
Richartz W (1969), 'Die Bindung von Chlorid bei der Zementerhärtung', *Zement-Kalk-Gips* 58 (10), 447–456.
RILEM (2000), TC 154-EMC (Polder R, Raupach M, Weydert R, *et al.*) 'Electrochemical Techniques for Measuring Metallic Corrosion: Test Methods for On Site Measurement of Resistivity of Concrete', *Materials and Structures (RILEM)* 33 (234), 603–611.
RILEM (2003), TC 154-EMC (Elsener B, Andrade C, Gulikers J, Raupach M), 'Half-Cell Potential Measurements – Potential Mapping on Reinforced Concrete Structures', *Materials and Structures (RILEM)* 36 (261), 461–471.
RILEM (2004), TC 154-EMC (Andrade C, Alonso C, Gulikers J, Polder R, Cigna R, *et al.*), 'Electrochemical techniques for measuring metallic corrosion, Test methods for on-site corrosion rate measurement of steel reinforcement in con-

crete by means of the polarization resistance method', *Materials and Structures (RILEM)* 37 (273), 623–643.
Rostam S (1993), 'Service Life Design – The European Approach', *Concrete International* 15 (7), 24–32.
Tuutti K (1982), *Corrosion of Steel in Concrete*, Stockholm, Cement och Betong Institutet.
Sagüés AA, Castro P, Moreno EI, Maldonado L, Genesca J (1994), 'Characterization of Activated Titanium Solid Reference Electrodes for Corrosion Testing of Steel in Concrete', *Corrosion, 52*, 609, 1996.
Schiegg Y (2002), *Online-Monitoring zur Erfassung der Korrosion der Bewehrung von Stahlbetonbauwerken,* Zürich, ETH Zürich.
Schießl P (1976), *Zur Frage der zulässigen Rißbreite und der erforderlichen Betondeckung im Stahlbetonbau unter besonderer Berücksichtigung der Karbonatisierung des Betons*, Berlin, Heft 255 der Schriftenreihe des DAfStb.
Schießl P (1988), (RILEM; Technical Committee 60-CSC) *Corrosion of Steel in Concrete*, New York: Chapman and Hall.
Schießl P, Raupach M (1992), 'Monitoring System for the Corrosion Risk of Steel in Concrete Structures', *Concrete International* July, 52–55.
Schießl P, Raupach M (1997), 'Laboratory Studies and Calculations on the Influence of Crack Width on Chloride-Induced Corrosion of Steel in Concrete', *ACI Materials Journal,* 94 (1), 56–62.
Schießl P, Rostam S, Raupach M (1995), 'Corrosion Monitoring Systems Installed in the Structures of the Great Belt Link Projects – Monitoring as Part of a Multi-Barrier-Protection Strategy', International Symposium *Non-Destructive Testing in Civil Engineering (NDT-CE),* Berlin, 1995.
Sensortec (2006), Brochures 'Multiring-Electrode', 'Anode Ladder', 'Expansion Ring Anode', S + R Sensortec GmbH, Germany.
Sodeikat C, Dauberschmidt C, Schießl P, Gehlen C, Kapteina G (2006), 'Korrosionsmonitoring von Stahlbetonbauwerken für Public Private Partnership Projekte: Dauerhaftigkeit sichtbar gemacht', *Beton- und Stahlbeton*, 101 (December), 932–942.

17

Corrosion monitoring in soil

NAEEM KHAN, Saudi Aramco, Saudi Arabia

17.1 Introduction

In the early days of the corrosion control industry, buried corrosion coupons were used for metal weight loss measurements in soil side applications. More recently, instrumented probes have been adapted for use in soils. When used in soil side applications, these probes are referred to as 'soil corrosion probes' (SCP).

SCP are typically used where cathodic protection (CP) potentials cannot be reliably measured and corrosion rate measurements are used as an alternative to conventional CP criteria for buried pipelines. SCP are connected to the structure so that they receive the same level of CP as the structure. Thus even if the measured potential reading on the structure is not at the minimum required level, the corrosion rate measurement (millimeters per year, or mils per year) can be used as an alternative criterion to assess CP effectiveness. Situations where SCP can be useful include low levels of cathodic polarization in high resistivity soils, or erroneous potential readings due to poor soil contact.

17.2 Types of soil corrosion probes

The pipeline corrosion control industry has moved from using buried corrosion coupons for weight loss measurements to modified electrical resistance (ER) probes[1–2] and linear polarization resistance (LPR) probes, typically used for internal corrosion monitoring, for use in soil side applications. As discussed in Chapters 11, and 3, respectively, the ER probes indicate the cumulative metal loss of the sample, while the LPR probes give the instantaneous corrosion rate of the exposed metallic sample. Newer types of probes have also been developed[3] which have a faster response time than that of 'standard' ER probes. Another new type of device being developed is the multielectrode array sensor (Chapter 26), for use in corrosion monitoring under cathodic protection conditions.

17.3 Electrical resistance probes

Chapter 11 has described the general aspects of electrical resistance probes. This chapter will focus on the application of ER probes in soil environments. As discussed in Chapter 11, ER probes are based on the principle of increase in resistance of a metal strip or wire as a function of metal loss, and the resultant reduction in the cross-sectional area of the metal. They indicate the cumulative metal loss of the sample. The measurements taken using an ER probe are evaluated over time to calculate a corrosion rate in millimeters or mils per year.

In applying this technique to soil environments, the probe element of known cross-section is exposed to the soil. The electrical resistance of the probe is measured after initial installation and at subsequent time intervals. As metal is lost from the exposed surface of the probe element, the measured electrical resistance will increase, allowing the amount of loss to be quantified with an ER instrument.

ER soil corrosion probes are available in various sizes, shapes and sensitivities. The size of the probe element must be representative of the possible coating defect sizes of the pipelines or structures under investigation. As the probe is located in the same soil environment as the protected structure, it is assumed that it replicates the effectiveness of the CP applied to the structure. The sensitivity of an ER probe is a compromise between the response time and the lifetime of the probe. For a probe with 0.635 mm (25 mils) useful life and assuming a sensitivity and repeatability of 1% of the full scale, the soil corrosion probe system can detect metal thickness losses of approximately 0.005 mm (0.2 mils). The life of a probe connected to the CP system is usually long because it is protected by the CP. However, a probe installed unconnected to the CP to measure the unprotected corrosion rate will have a shorter life. The probe must be replaced when half of its thickness has been consumed. The probe element material should normally match that of the pipeline or structure as closely as practicable, e.g. carbon steel or ductile iron.[4]

17.3.1 Types of ER probes

ER probes fall into two types:

(a) individual probe
(b) probe installed as part of a test station.

Three designs of individual ER probes are shown below. The flat surface probes in Figs 17.1 and 17.2 are typically used in pipeline applications. The probe in Fig. 17.1 is more adaptable to direct burial while the probe in Fig. 17.2 is better for placement under coatings or poly wrap because it has a

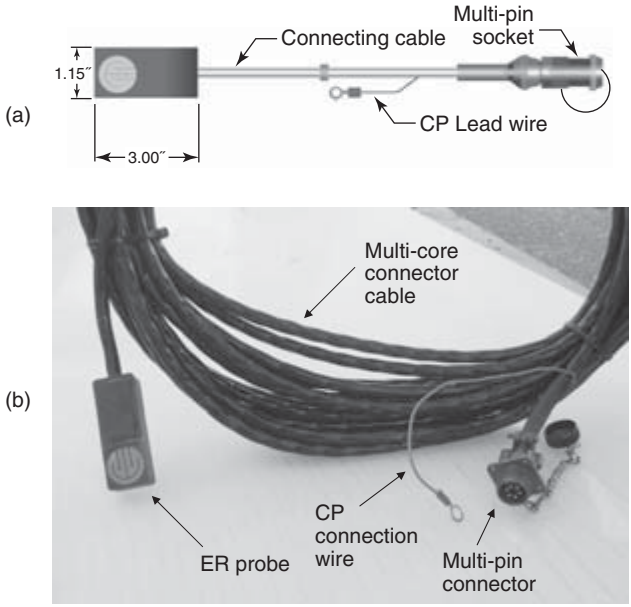

17.1 Flat surface type ER probe.

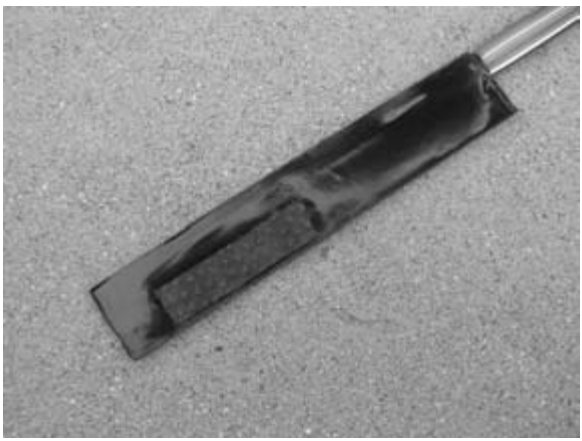

17.2 Low-profile sensor for soil or under wrap.

low profile. The multi-core connecting cable is terminated on a multi-pin connector that is used to connect to the ER instrument. A separate CP connection wire is provided to connect the probe element to the CP circuit by connecting it to the protected structure, thus providing CP to the probe and allowing the effectiveness of the CP system to be monitored. The CP

17.3 Cylindrical-type ER probe for concrete.

connection wire can be at the probe end or the connector end. The advantage of having the CP connection at the connector end is that, if required, it is possible to disconnect the CP connection in order to obtain the probe 'off' potential measurement. The third design shown in Fig. 17.3 uses a cylindrical element and is typically used for concrete applications where it simulates a reinforcing bar.

The ER probes shown in Figs 17.1, 17.2 and 17.3 are installed directly in the soil or concrete with the connecting cable brought up to a test/monitoring station. ER probes installed as part of a test station are typically ring-type probes, usually installed at the bottom of a combined probe/test station mounting tube, as shown in Figure 17.4. In this configuration, the probe element has been combined with a coupon ring that can be used as a 'native' potential reference. Both the probe element and the coupon are wired up through the mounting tube to the test station head (Fig. 17.5), which includes an on/off switch in the circuit connecting the probe element to the CP circuit, and a multi-pin socket for connection of the instrument used to take a probe measurement. The switch allows 'off' potentials to be measured on the probe element.

The potentials of the probe element can be recorded using a reference cell installed inside the test station mounting tube or in a soil-access tube installed next to the test station (Fig. 17.6). This latter arrangement is used in high soil resistivity areas, where water-wetting of the reference electrode contact point is typically used to counter the high-soil contact resistance.

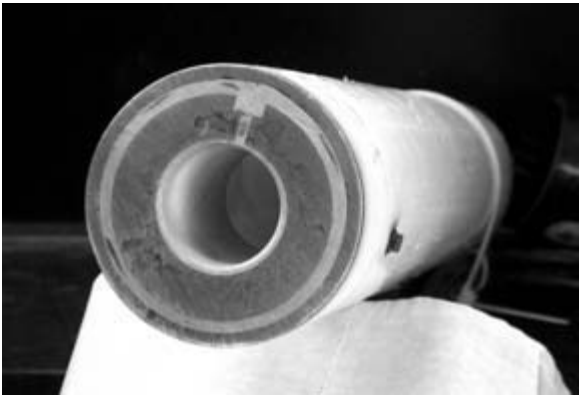

17.4 Ring-type ER probe.

17.5 ER probe test station head.

Pouring water inside the test station mounting tube is not advisable, as water seeping down to the probe element will change the soil environment in the vicinity of the probe, leading to a change in the CP levels, and therefore erroneous corrosion rate results. In the installation arrangement shown in Fig. 17.6, the ER probe is connected to the CP source by connecting to the CP test station lead wire, rather than directly to the pipeline. This simplifies the installation, as a wire connection to the pipe is not typically made.

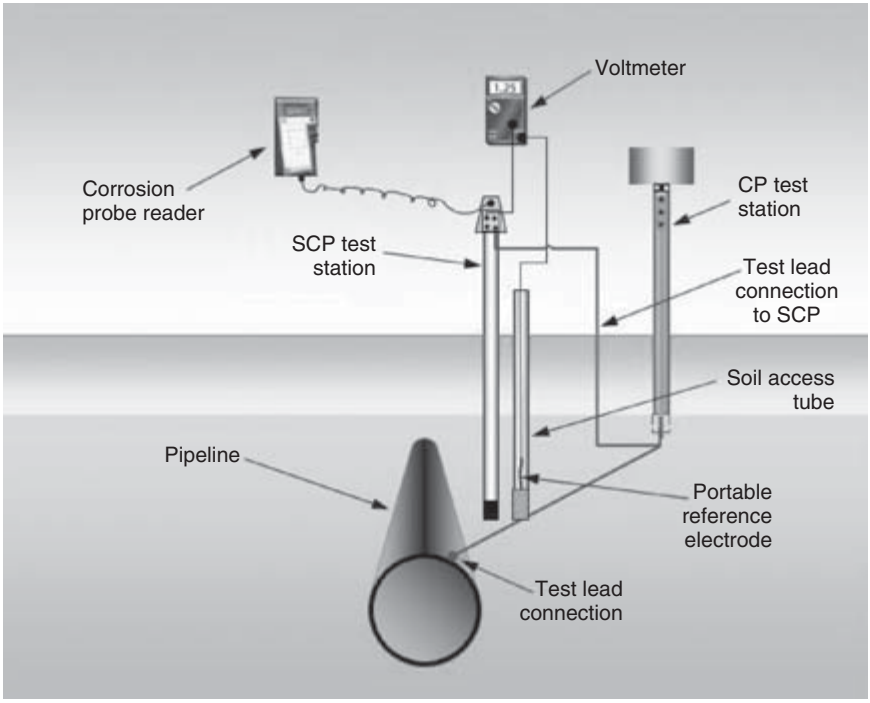

17.6 Typical ER probe test station installation on pipeline.

An even more simplified installation routes the cable from a low-profile ER probe (as shown in Fig. 17.2) mounted adjacent to the pipe or under a wrap, directly to a connector in the CP test station.

17.3.2 Typical applications

ER soil corrosion probes have been used to determine general corrosion rates to determine the effectiveness of CP. ER probes can represent the corrosiveness of a bare (uncoated) pipeline in a particular environment. ER probes are also employed to model the corrosiveness of a coated pipeline at a typically sized defect. This information is typically used for design of CP systems or determination of appropriate CP criteria, for example, in aggressive environments such as high temperatures or areas susceptible to microbiologically influenced corrosion (MIC), in mixed-metal systems, or in areas susceptible to stray current, telluric currents, alternating current (AC) induction and AC induced corrosion.

Data can also be used to establish criteria for protection of ductile or cast iron pipe, in mixed-metal systems, systems with cyclical variations in level

of protection, areas with surface conditions limiting access to the electrolyte (such as cased crossings, backfill with significant rock content or rock ledges, gravel or dry vegetation). Additionally, data can also be used to establish criteria for pipelines buried very deep, areas of high contact resistance such as pipe located under concrete or asphalt pavement, frozen ground or very dry conditions.

ER probes are used in areas where potential criteria are difficult or impractical to apply. These include: pipelines with adjacent buried or submerged metallic structures; locations at which coatings cause electrical shielding; and pipelines with lack of electrical continuity, such as with some forms of mechanically coupled pipe that have not been made electrically continuous through the use of bonding cables or straps welded across each coupling. ER probes are installed at locations that are difficult to monitor using structure-to-electrolyte potentials, such as the bottom of large-diameter pipelines. In addition, data are often used to determine whether existing CP levels are adequate for pipelines that have proven impractical to meet existing CP criteria.

Other typical applications of ER probes include installations adjacent to underground storage tanks, installations under aboveground storage tanks, internal surfaces of water tanks and reinforced concrete structures.

17.3.3 Selection of ER probe installation locations

The ER probe is typically installed near the pipe or structure in the same soil/electrolyte or environment as the pipe or structure, and the entire surface of the probe element typically maintains contact with the soil or environment. Loss of contact due to shrinkage, freezing or drying out of the soil results in loss of the CP protection, as it would also on the pipe or structure.

The ER probe needs to be installed close to the pipe or structure, in the same soil/electrolyte as the pipe and structure, and distance from the anode, so that the probe sees the same potential field as the structure. This is typically not a problem on a pipeline where the anode is some distance from the pipeline. It is much more critical in situations in which the anode is relatively close to the structure, such as in double-bottomed tanks with an anode grid.

Generally, corrosion probes are installed on well-coated pipelines, with no history of corrosion in the area, but which have low or erratic potentials. They are not recommended for use on pipelines with coatings such as PE tapes or three-layer PE coatings, which do not allow CP current to flow to the pipe surface ('shielding') when disbonded from the pipeline. The installation of probes adjacent to pipelines with poor or disbonded coatings may result in erroneous corrosion rate interpretation, if the size of the probe is

much smaller than the exposed surface area of the pipe due to coating defects, or if corrosion occurs under disbonded coating due to CP current shielding. Low profile type probes (Fig. 17.2) can be used under pipeline coatings, to detect and quantify under-coating corrosion at known disbonded coating locations, or under poly wrap on ductile iron pipes.[4]

17.4 Monitoring and data interpretation

Probes are permanently installed and measurements should be made on a periodic basis. As a guide, the probe is typically monitored at least once a month for the first 12 months. Thereafter, the monitoring frequency is re-evaluated to determine whether more or less frequent readings are warranted. An ER instrument is used to measure the cumulative metal loss on the corrosion probe (see Figs. 17.7 and 17.8). For probe potential measure-

17.7 Portable ER instrument.

17.8 Portable ER instrument connected to SCP test station.

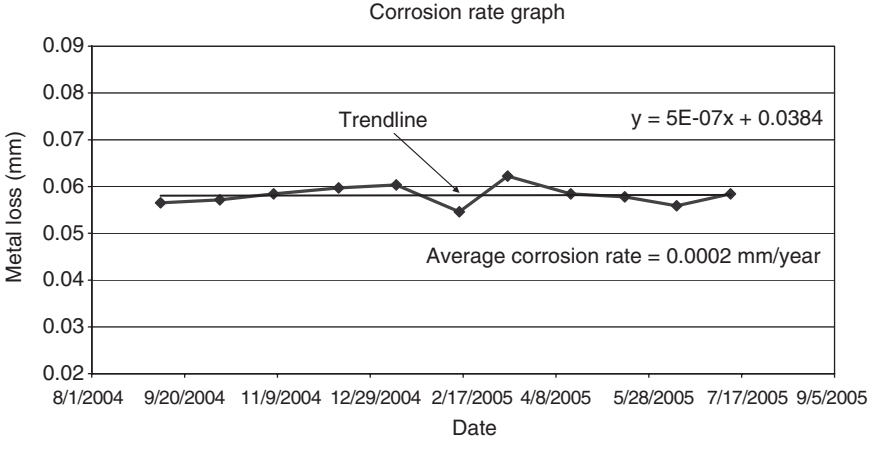

17.9 Typical corrosion rate graph.

ments, the probe 'off' potential is measured by interrupting the current flow to the probe.

The graph in Fig. 17.9 is an example of the data derived from ER probe measurements. The corrosion rate between any two measurement times is

the difference in metal-loss measurements divided by the time difference and annualized, i.e., the slope of the metal-loss curve between the selected times. For a series of measurements, the average corrosion rate is calculated using regression analysis from the slope of the trendline as calculated by the least squares method. Most graphing programs, such as an electronic spreadsheet, have built-in capability to calculate slopes.

The average corrosion rate (C) can also be calculated using Equation [17.1]:

$$C = \frac{P \times 365(S_2 - S_1)}{\Delta T \times 1000} \qquad [17.1]$$

Where:

S_1 = the first reading
S_2 = the second (later) reading in divisions (1/1000 of probe span) from typical ER instrument readings
ΔT = the time in days between readings
P = the 'probe element span' ('probe constant') specified by the probe manufacturer.

If the probe element span is entered in millimeters the corrosion rate will be in millimeters per year. If the probe span is entered in mils the corrosion rate will be in mils per year.

17.5 Effectiveness criteria

An average corrosion rate of less than 0.025 mm/year (1.0 mil/year) over a 12-month monitoring period is generally accepted as an indication that CP is effective at the location of the probe. This criterion is often modified based on visual examination of the probe element after a burial time exceeding 12 months, and also depending on the condition/integrity of the structure during this time period.

SAA AS 2832.1[5] includes a protection criterion incorporating a corrosion rate not exceeding approx. 0.005 mm/year (0.2 mils/year) in combination with an instantaneous 'off' potential of –850 mV or 100 mV more negative than the depolarized potential.

17.6 References

1 Fitzgerald, J. H., P. R. Nichols and R. Niebling. 'Measuring the Effectiveness of Cathodic Protection on the Exterior Bottoms of New Aboveground Asphalt Storage Tanks Using Corrosion Monitoring Probes', NACE International, *CORROSION/99*, paper no. 519, (Houston, TX, NACE International, 1999).
2 Khan, Naeem A. and Mathieu, J. B. 'Assessing the Effectiveness of Cathodic Protection in High Resistivity Soils', Proceedings of the 9th Middle East Corrosion

Conference, p. 141 (Bahrain, Bahrain Society of Engineers/NACE International, February, 2001).
3 Kempe, Phillipe, A. Denzine and E. Tiefnig. 'Rapid Underground Corrosion Measurements for Buried Pipelines', NACE International, *CORROSION/2000*, paper no. 92, (Houston, TX, NACE International, 2000).
4 G. E. C. Bell, C. G. Moore and S. Williams. 'Development and Application of Ductile Iron Pipe Electrical Resistance Probes for Monitoring Underground External Pipeline Corrosion,' *CORROSION/2007*, paper no. 07335 (Houston, TX: NACE International, 2007).
5 SAA AS 2832.1 (latest revision), 'Cathodic Protection of Metals: Pipes and Cables' (Sydney, New South Wales, Australia: Standards Australia Limited).

17.7 Bibliography

Baeckmann, W. V., A. Baltes and W. Prinze, *New Developments in Measuring the Effectiveness of CP*, Victoria, Australia: Australasian Corrosion Association (ACA) 8(1) (1983), 4–9.

Fitzgerald, J. H., 'Use of Corrosion Measurement Probes to Evaluate the Effectiveness of Cathodic Protection on the Exterior Tank Bottoms of Aboveground Asphalt Storage Tanks', NACE International, *CORROSION/98*, paper no. 668. Houston, TX: NACE International, 1998.

Khan, N. A. 'Use of ER Soil Corrosion Probes to Determine the Effectiveness of Cathodic Protection', NACE International, *CORROSION/2002*, paper no. 104. Houston, TX: NACE International, 2002.

Khan, N. A., 'Using Electrical Resistance Soil Corrosion Probes to Determine Cathodic Protection Effectiveness in High Resistivity Soils', *Material Performance* 43(6) (2004), 20–25.

Khan, N. A., 'Use of CP Coupons and ER Soil Corrosion Probes in Application of Pipeline Cathodic Protection Criteria', *Materials Performance* 46(4) (2007), 26–30.

18

Corrosion monitoring under coatings

FENG GUI and C. SEAN BROSSIA, CC Technologies, Dublin, OH, USA

18.1 Introduction

Coatings, including organic and metallic coatings, have been used in many industries as a means to provide protection from a corrosive environment and thus extend the lifetime of the protected structure. Although organic and metallic coatings are both used for protection, most metallic coatings usually serve as the sacrificial anode in the coating–substrate couple, such as a zinc coating on steel and the aluminum clad layer on aluminum alloys, whereas organic coatings provide protection mainly through the barrier properties of the film. In some industries (e.g., aircraft industry), other coating-like products – corrosion prevention compounds (CPC) – have also been widely used to provide protection for the interior surface of joints due to the wicking and water displacement ability that CPCs possess.

An organic coating system often consists of a conversion coating, primer and a top coating. Sometimes, inhibitors such as chromate are incorporated into the organic coating to further inhibit corrosion. Some researchers are also working on developing a smart coating system through which inhibitors can be delivered to a corroded site as needed.[1]

The protection offered by organic coatings is mainly determined through isolation from the aggressive environment, by adhesion opposing corrosion initiation at the metal/coating interface, and through structural changes taking place during curing of the coatings.[2] Therefore, many times, coatings that have good barrier properties would be better choices for isolating the corrosive environment from the protected structure, although sometimes it is necessary to have a porous coating so that the penetrated electrolyte can trigger the inhibitive action of the pigment in the coating.[3] Frequently, however, corrosion could initiate if aggressive species and water are transported through the defects (pores) in the coating and reach the substrate/coating interface.

The initiation of corrosion and failure of coatings usually can be identified via visual inspection because the failure of protection from organic coatings generally results in the formation of blisters and delaminated regions. However, these features usually cannot be observed until the later stages of corrosion. Most times, it is desirable to identify corrosion at an earlier stage to reduce the impact of corrosion and to reduce the overall maintenance that is needed. Thus, monitoring of coating degradation is of great importance to the corrosion engineer.

18.2 Corrosion monitoring methods under coatings

It is usually desired that any technique capable of monitoring under coating corrosion not be destructive so that corrosion could be detected while maintaining the integrity of the protected structure. Both Electrochemical Impedance Spectroscopy (EIS) and Electrochemical Noise (EN) are non-destructive techniques. In particular, EIS has been successfully used in many cases to detect coating delamination, corroded area under coatings. During the last decade, many efforts have been made in order to use it for under coating corrosion monitoring. One typical benefit of EN technique over EIS is that it does not require any perturbation of the system of interest.

The theories of EIS and EN techniques were introduced in Chapter 4. Although the use of these two techniques is not limited to coatings, this section will only review the applications where EIS and EN were used to detect and monitor corrosion under organic coatings. The applications of several other techniques will also be reviewed.

18.2.1 Electrochemical Impedance Spectroscopy (EIS)

The use of EIS to study the corrosion has been broadened significantly since it was introduced by I. Epelboin and coworkers.[4] The behavior of a coated metal can be represented with an equivalent circuit model, which has been well developed.[5] The typical models for a coated metal are shown in Fig. 18.1. An equivalent circuit model usually consists of *Rs*, *Rp* and *Cc* that characterize the solution resistance, coating resistance (or pore resistance), and coating capacitance, respectively. The *Z1* component in the general model in many systems consists of a capacitance that characterizes the double layer behavior and a resistance that reflects the charge transfer resistance (or polarization resistance). In the case that diffusion through the coating is of concern, the *Z1* component can be characterized with the charge transfer resistance and a Warburg impedance.

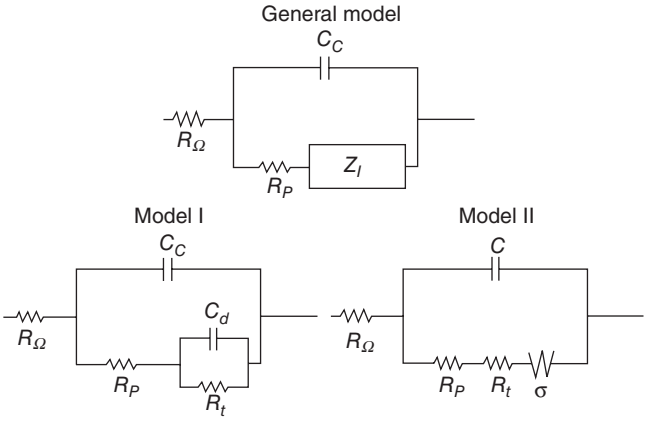

18.1 Typical equivalent circuit models for a coating.[5]

Much information can be obtained by carefully fitting the EIS data to a meaningful equivalent circuit model, such as coating capacitance, pore resistance (coating resistance), double layer capacitance and charge transfer resistance (polarization resistance). These parameters can be related to the coating performance, such as delamination area and corroded area under coating, for many coating systems.

Coating capacitance depends on the thickness of the coating (d) and the total sample area (A) that was tested:

$$C_c = \frac{\varepsilon \varepsilon_0 A}{d} \qquad [18.1]$$

where ε and ε_0 are the coating dielectric constant and the free space dielectric constant, respectively. Thus, by monitoring the change in the coating capacitance, it is possible to monitor possible water uptake in a coating system. This is an essential step to evaluate the coating performance because water uptake would subsequently cause the loss of adhesion at the coating–metal interface.[6–8] The coating dielectric constant is very sensitive to the uptake of water. The volume fraction (v) of electrolyte absorbed by the coating can be determined based on the coating capacitance:[9]

$$v = \log[C(t)/C(0)]/\log 80 \qquad [18.2]$$

where $C(t)$ and $C(0)$ are the coating capacitance after exposure of time period t and that at time zero, respectively. Water uptake determined from coating capacitance has been found to correlate well with that determined gravimetrically, as shown in Fig. 18.2.[10] In many cases, a coating that absorbed less water is likely to indicate better performance as the water/electrolyte

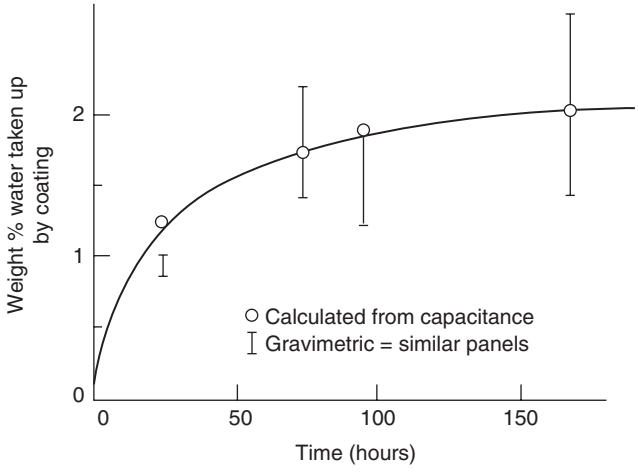

18.2 Weight percent water uptake by a polybutadiene coating as determined from the capacitance and as determined gravimetrically.[10]

that diffuses through the coating and reaches the metal/coating interface could often serve as the precursor of localized corrosion. Thus, the ranking of coating performance determined by water uptake during the earlier time period of exposure could correlate well with that obtained by other variables such as coating resistance.[11] Touhsaent and Leidheiser also found that coatings that absorbed less water at earlier times calculated according to coating capacitance performed better than others that showed more water uptake during two years of atmospheric exposure.[12] In some cases, studying water uptake is essential for understanding the protective mechanism through which a coating provides protection. Deflorian and Felhosi found that the low barrier properties of a coating, meaning more water uptake, actually induced the activation of the pigment inhibitive action.[3] Therefore, in this case, the coating provided protection not simply through the barrier properties.

Coating resistance is usually influenced by the presence of defects and conductivity through the pores.[3] Frequently, coating resistance was observed to decrease as the exposure time increased.[13,14] Haruyama *et al.* suggested that the coating resistance was related to the delamination area:[15]

$$R_p = R_P^0/A_d \qquad [18.3]$$

where $R_P^0 = \rho d(\text{ohm-cm}^2)$ and A_d is the delamination area. The coating resistivity (ρ) and the coating thickness (d) were assumed to be constant during the exposure. Thus caution should be taken when water uptake in the coating resulted in the change in the coating thickness. Mansfeld and Tsai found that there was an excellent agreement between the estimated

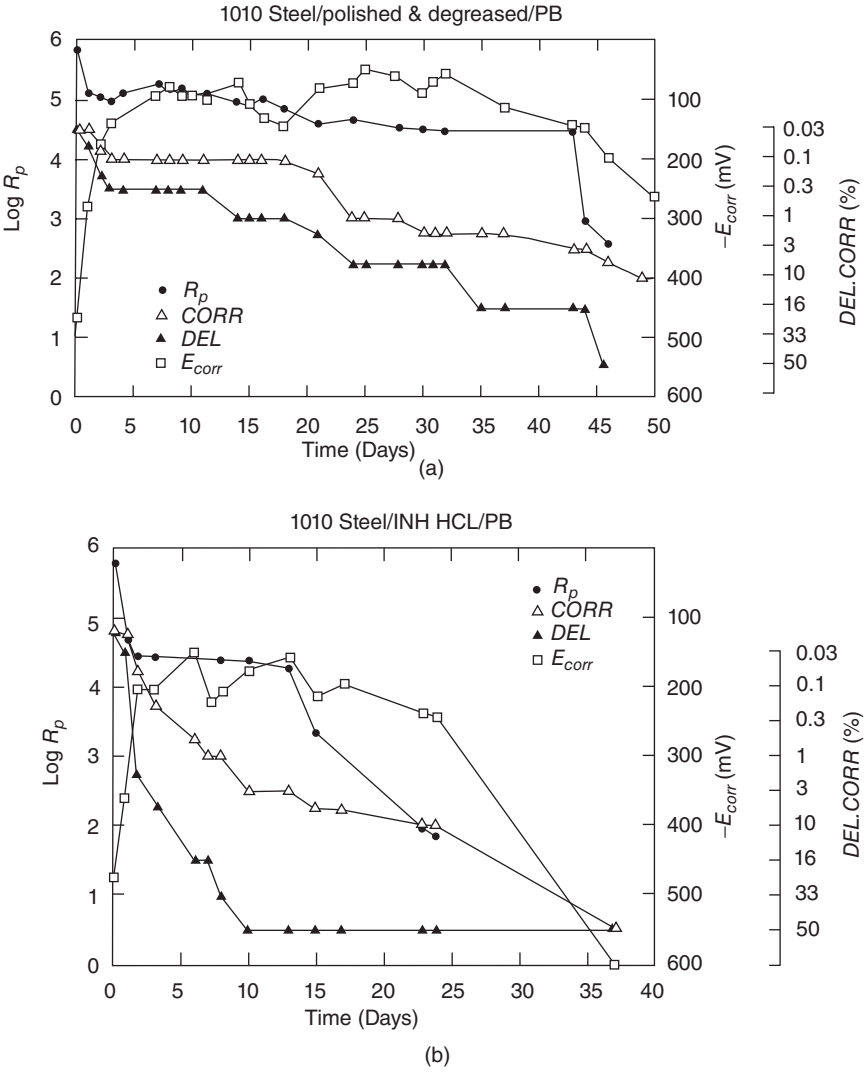

18.3 The comparison of coating resistance and the visual observation of the coating performance.[5] E_{corr}, corrosion potential; *DEL*, delamination; *CORR*, corrosion extent.

delamination degree based on the coating resistance and visual observation. And thus, it is possible to determine the delaminated area under the coating from EIS data.[14] Kendig *et al.* have demonstrated the correlation of coating resistance and the under-corrosion extent as determined based on ASTM D610.[5] As shown in Fig. 18.3, the corrosion extent (CORR) increased with the decrease in the coating resistance (*Rp*).

After the electrolyte is absorbed by the coating and the metal/coating interface penetrated, a double layer forms and corrosion is initiated. As a result, the double layer capacitance is increased from zero and can be related to the disbonded area (A_d):[6]

$$C_d = C_d^0 A_d \qquad [18.4]$$

where C_d^0 is the area specific capacitance that can be determined from bare metal with known area in a simulated underfilm solution.[6] Using Equation [18.4], the disbonded area could be determined from double layer capacitance. The double layer capacitance has been used by people to calculate the corroded area or delaminated area under coatings.[8,16–19]

Charge transfer resistance R_t (polarization resistance) describes the electrochemical processes taking place at the metal/coating interface. Similar to the polarization resistance determined via DC electrochemical techniques, such as the linear polarization resistance (LPR) method, a corrosion rate could be obtained but this rate corresponds with the undercoating corrosion.[20] Frequently, however, the low frequency impedance (sometimes corrected by the solution resistance), which is the summation of coating resistance and sometimes the charge transfer resistance, has been used to evaluate the coating performance. Scully found that the low frequency impedance correlates well with the open circuit potential (OCP) measurement.[21] Specifically, the OCP for an epoxy polyamide-coated steel sample is either unstable or positive when low frequency impedances are high. When impedances decreased below 10^7 ohms/cm^2, the OCP was measured as –650 mV vs. Ag/AgCl, as shown in Fig. 18.4. Others also found that low frequency impedances could be correlated to the coating performance in various application cases and thus a critical value of low frequency impedance could be used to identify the failure of a coating.[16,22]

Another approach that has been used frequently to detect corrosion under coatings is the breakpoint frequency method. Breakpoint frequency is defined as the frequency where the phase angle drops to 45°.[15] The breakpoint frequency at high frequency is related to the disbonded area (A_t):

$$f_h = (1/2\pi\varepsilon\varepsilon_0\rho) = K_f(A_t/A_0) \qquad [18.5]$$

where A_0 is the surface area of the coated sample and K_f is a material constant. Hack and Scully demonstrated the correlation of high frequency breakpoint frequency and the ASTM D-610 rating of an epoxy coated steel sample (Fig. 18.5).[23]

Clearly, the breakpoint frequency was higher as coating damage increased. Since the breakpoint frequency can be determined at high frequency and without running a full frequency sweep, the measurement can be performed rapidly.[6] A few others have also demonstrated the use of breakpoint

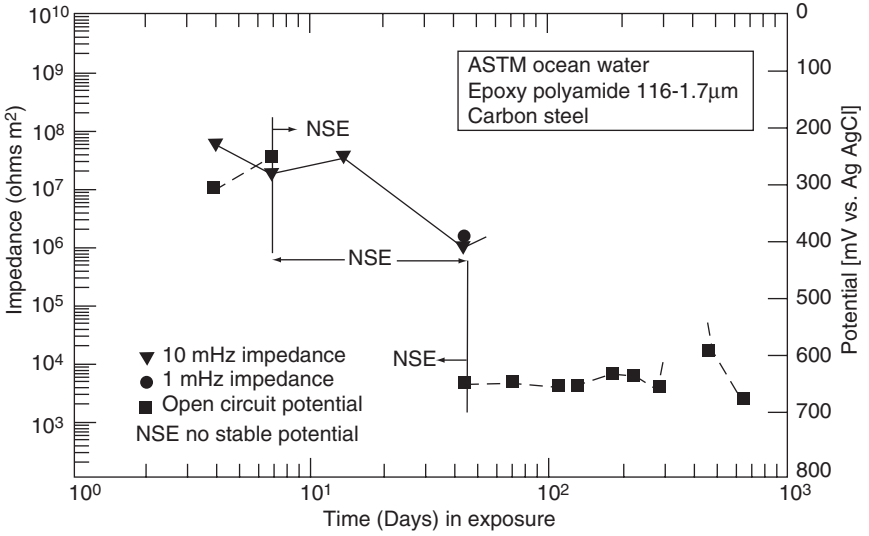

18.4 Low frequency impedance behavior as a function of exposure time for 11μm thick epoxy polyamide-coated steel.[21]

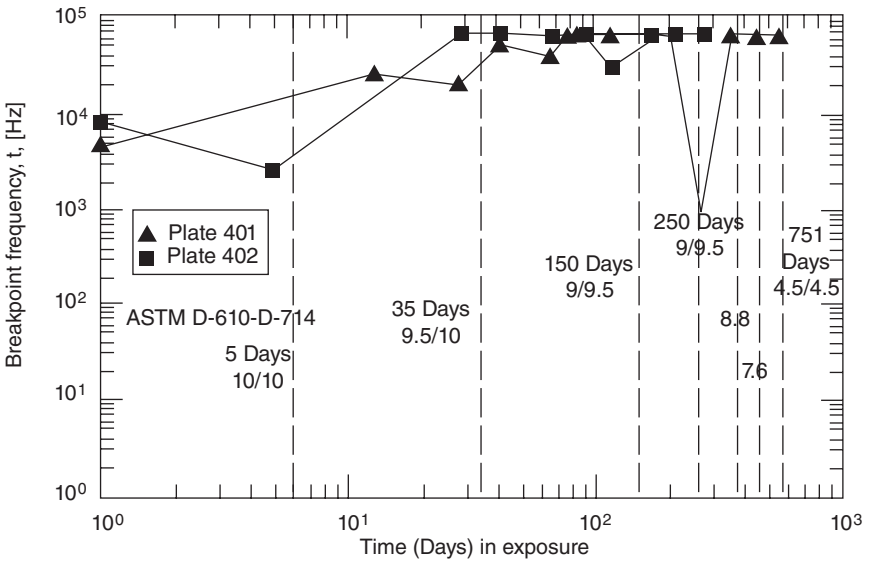

18.5 Increase in the higher breakpoint frequency with exposure time for 55μm thick epoxy coated steel in ASTM seawater.[23]

frequency to evaluate coating performance and detect coating delamination.[13,14,24]

Note Equation [18.5] is valid based on the assumption that the electric constant and the coating resistivity did not change significantly during exposure. This situation is usually not true considering that the coating electric constant will change as water uptake occurs. To overcome this problem, Mansfeld proposed to use the ratio of breakpoint frequency and the minimum of frequency (f_{min}):[13]

$$f_b/f_{\min} = (C_{dl}/C_c)^{1/2} = (C_{dl}^0/C_c^0)D^{1/2} \quad [18.6]$$

This ratio is independent of coating resistivity. The results by this method agree with the time dependence of R_{po}.[13]

Like many other corrosion mitigation methods, the challenge of corrosion prevention is to be able to predict when the coating will fail based on short term test data. To achieve this, many authors have successfully correlated several different parameters determined from impedance to the long-term performance of coatings. Kendig *et al.* found that the time dependence of polarization resistance for a coated steel observed with five days of exposure in 0.5 M NaCl predicts the failure that occurred at three weeks.[5] With the impedance at 10 mHz and breakpoint frequency determined at ten days' exposure, Scully was able to predict the coating performance after 550 days in service.[21,25] Scully also found that the prediction was successful only at times sufficient to permit permeation of specifically H_2, O_2, Na^+ and to a lesser extent Cl^- through the coating to the reacting metallic interface.[21] When using impedance to study the performance of CPC, Gui and Kelly also found that the low frequency impedance at short time period of exposure was able to predict the coating performance after six months of exposure.[16]

The nondestructive nature of EIS has made it one of the most frequently used electrochemical techniques for corrosion performance evaluation of coating systems. As discussed, the parameters determined from impedance data can generally be related to the coating performance, characterized by water uptake, delaminated or disbonded area, and corroded area under coating. However, caution needs to be taken when using EIS simply because much information could be obtained from a single measurement. Specifically, the determination of the parameters described in this chapter is not a simple task. Many models could be obtained by fitting the impedance data but only the one that has physical meanings should be considered as the representative model for the coating behavior. Additionally, some of the parameters, such as low frequency impedance, could be time consuming especially at extremely low frequency range.

Although the bulk of the efforts in EIS so far have been limited to laboratory investigations, some efforts have been undertaken to apply this technol-

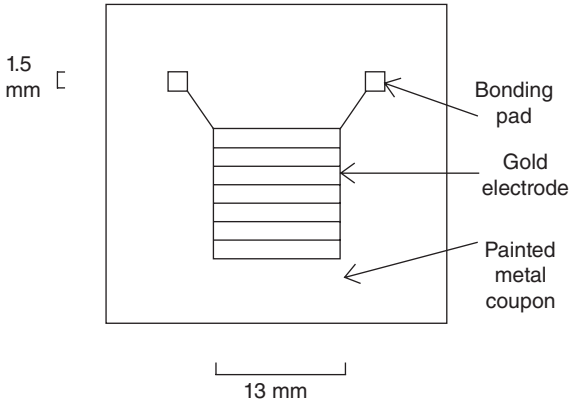

18.6 Schematic of the atmospheric electrochemical monitor used by Simpson *et al.*[26]

ogy to field measurements of coating performance. Several authors have demonstrated the use of impedance-based sensors for monitoring undercoating corrosion. Although the design of these sensors is different, essentially they function by measuring the impedance of a two-electrode system under the coating. Simpson *et al.* demonstrated the use of an atmospheric electrochemical sensor to monitor coating degradation in atmosphere (Fig. 18.6).[26] The sensor consists of a painted steel coupon on which a sputter coated electrode has been deposited to serve as a reference/counter electrode combination. Van Westing *et al.* was able to monitor the curing extent of coatings with a dielectric sensor that consists of a glass plate with a golden grid applied to the surface.[27] With a sensor buried in the structure in question, Brossia and Dunn successfully monitored the coating degradation.[28] In the work by Brossia and Dunn, a parameter was obtained from three different frequencies and the authors were able to identify the quality of the coating during approximately one month of exposure. Similarly, Dacres and Davis also developed an electrochemical *in situ* sensor for detecting corrosion under coatings on aging aircraft. Essentially, the low frequency impedance (defined as Near-DC impedance) was monitored with the sensor embedded in the coating system. The results obtained from this sensor were consistent with that obtained by conventional three electrodes measurement.[29] Tsai and Mansfeld demonstrated the use of the impedance at 100 Hz and 10 000 Hz to detect delamination ratio D (the ratio of the delaminated area to the initial sample area).[11] All these methods did not require the use of the conventional electrochemical cell or a sweep over a relatively wide frequency range. Therefore, the detection and monitoring of corrosion under coatings can be achieved in the field with proper design and consideration of probe/element/electrode placement.

18.2.2 Electrochemical Noise (EN)

The impedance technique, although powerful and capable of detection under coating delamination via several parameters, can be complicated. Compared to the impedance technique, electrochemical noise does not introduce any perturbing signal to the system of interest. Instead, the current and voltage fluctuations are obtained at the open circuit potential.[30] Many efforts have been made to use electrochemical noise for coating evaluations.[30–37]

Although many different parameters could be determined from the analysis of impedance data, in general the analysis of electrochemical noise only generates the electrochemical noise resistance (R_n), defined as:

$$R_n = \sigma_V/\sigma_I \qquad [18.7]$$

where σ_V and σ_I are the standard deviation of the potential noise and the current noise, respectively. Many authors have demonstrated that the electrochemical noise usually decreases with increases in exposure time, which is very similar to that observed from EIS.[30,34–37] Skerry and Eden also found that good paints exhibited relatively large voltage noise and relatively small current noise compared to poor paint coatings.[37] However, many also agreed that although the general trend of noise resistance change with time is similar to the parameters (e.g. R_t) determined from impedance, the numerical values were considerably different. As a result, most of the published work has been using EN techniques in conjunction with electrochemical impedance techniques. Further research and theoretical work still needs to be conducted to build more confidence in using electrochemical noise to monitor corrosion under coating.

18.2.3 Other techniques

Besides the conventional electrochemical techniques, some other techniques have also been developed as an effort to provide alternative means to monitor under-coating corrosion.

For field application, online monitoring of corrosion under coatings is always a challenge. Using coupled multielectrode sensors, Sun monitored the degradation process of a few different coatings on carbon steel.[38] The current signal changed with the increase in exposure time and the signal from the sensors was sensitive enough for detecting the corrosion that had initiated under coating. The sensitivity makes this technique appropriate for field applications but the author did not address how to implement the sensors with a protected structure.

Recently, the development of imaging techniques has made it possible for them to be used to study corrosion under coating. Schneider *et al.* suc-

cessfully used confocal laser scanning microscopy (CLSM) as a tool to monitor the corrosion underneath organic coatings.[39] The ability of CLSM to monitor the topography change of the substrate surface and the coating due to the initiation of corrosion under coating was demonstrated. Souto *et al.* demonstrated the use of scanning electrochemical microscopy to monitor electroactive species so that the activity under coating could be identified.[40] Many authors have also used a Scanning Kelvin Probe (SKP) to detect the initiation of corrosion under coating and to understand the initiation mechanism.[41–44] However, these techniques usually require expensive instruments. Furthermore, some instruments such as CLSM and SKP are extremely sensitive to the environment. The requirement on the samples is also often more strict than that for EIS and EN. Therefore, these microscope techniques are more suitable for using in the laboratory for mechanistic study.

18.3 Summary and conclusions

Several methods have been employed to study coating performance and degradation with the bulk of previous efforts focused on laboratory studies. Some of these approaches have begun to be adopted and applied for field monitoring of coating performance to varying degrees. Of these methods, EIS appears to have shown the greatest promise but more efforts need to be undertaken to broaden its application in fields. Other techniques, such as EN and impedance based sensors, have been employed in the field of monitoring although some more studies have to be performed to correlate EN results with the coating performance. Furthermore, the implementation of the techniques with real structures still needs to be further addressed.

18.4 References

1 M. Kendig, M. Hon and L. Warren, *Progress in Organic Coatings, Keystone 2002*, **47**, 183 (2003).
2 M. I. Karyakina and A. E. Kuzmak, *Progress in Organic Coatings*, **18**, 325 (1990).
3 F. Deflorian and I. Felhosi, *Corrosion*, **59**, 112 (2003).
4 I. Epelboin, C. Gabrielli, M. Keddam and H. Takenouti, in *ASTM STP*, p. 150 (1981).
5 M. Kendig, F. Mansfeld and S. Tsai, *Corros. Sci.*, **23**, 317 (1983).
6 M. Kendig and J. Scully, *Corrosion*, **46**, 22 (1990).
7 F. Mansfeld, *J. Appl. Electrochem.*, **25**, 1145 (1995).
8 P. L. Bonora, F. Deflorian and L. Fedrizzi, *Electrochim. Acta*, **41**, 1073 (1996).
9 D. M. Brasher and A. H. Kingsbury, *J. Appl. Chem.*, **4**, 62 (1954).
10 H. Leidheiser and M. Kendig, *J. Electrochem. Soc.*, **123**, 982 (1976).
11 C. H. Tsai and F. Mansfeld, *Corrosion*, **49**, 726 (1993).

12 R. Touhsaent and H. Leidheiser Jr., *Corrosion*, **28**, 435 (1972).
13 F. Mansfeld, *J. Appl. Electrochem.*, **25**, 187 (1995).
14 F. Mansfeld and C. H. Tsai, *Corrosion*, **47**, 958 (1991).
15 S. Haruyama, M. Asari and T. Tsuru, in *Corrosion Protection by Organic Coatings*, M. M. Kendig and H. Leidheiser, Editors, PV 87-2, p.197, The Electrochemical Society Proceedings Series, Pennington, NJ (1987).
16 F. Gui and R. G. Kelly, *Corrosion*, **61**, 119 (2005).
17 F. Deflorian, L. Fedrizzi and P. L. Bonora, *Prog. Org. Coatings*, **23**, 73 (1993).
18 F. Deflorian, V. B. Miskovic-Stankovic and P. L. Bonora, *Corrosion*, **50**, 336 (1994).
19 R. D. Armstrong and J. D. Wright, *Corros. Sci.*, **33**, 1529 (1992).
20 A. Amirudin and D. Thierry, *Prog. Org. Coatings*, **26**, 1 (1995).
21 J. R. Scully, *J. Electrochem. Soc.*, **136**, 979 (1989).
22 J. A. Grandle and S. R. Taylor, *Corrosion*, **50**, 792 (1994).
23 H. P. Hack and J. R. Scully, *J. Electrochem. Soc.*, **138**, 33 (1991).
24 F. Deflorian, L. Fedrizzi and P. L. Bonora, *Corrosion*, **50**, 113 (1994).
25 J. R. Scully and S. T. Hensley, *Corrosion*, **50**, 705 (1994).
26 T. C. Simpson, P. J. Moran, W. C. Moshier, G. D. Davis, B. A. Shaw, C. O. Arah and K. L. Zankel, *J. Electrochem. Soc.*, **136**, 2761 (1989).
27 E. P. M. van Westing, G. M. Ferrari and J. H. W. de Wit, *Corros. Sci.*, **34**, 1511 (1993).
28 C. S. Brossia and D. S. Dunn, Paper 02161, *Corrosion 2002*, NACE, Houston, TX (2002).
29 G. D. Davis, C. M. Dacres, M. Shook and B. S. Wenner, in *Intelligent NDE Sciences for Aging and Futurisitc Aircraft*, C. Ferregut, R. Osegueda and A. Nunez, Editors, University of Texas, El Paso, TX (1998).
30 Q. Le Thu, G. P. Bierwagen and S. Touzain, *Progress in Organic Coatings*, **42**, 179 (2001).
31 B. S. Skerry and D. A. Eden, *Progress in Organic Coatings*, **15**, 269 (1987).
32 C. P. Woodcock, D. J. Mills and H. T. Singh, *Progress in Organic Coatings AETOC 2003*, **52**, 257 (2005).
33 G. P. Bierwagen, X. Wang and D. E. Tallman, *Progress in Organic Coatings Jurata 2001*, **46**, 163 (2003).
34 R. L. De Rosa, D. A. Earl and G. P. Bierwagen, *Corros. Sci.*, **44**, 1607 (2002).
35 D. J. Mills and S. Mabbutt, *Progress in Organic Coatings*, **39**, 41 (2000).
36 F. Mansfeld, L. T. Han, C. C. Lee and G. Zhang, *Electrochim. Acta*, **43**, 2933 (1998).
37 B. S. Skerry and D. A. Eden, *Progress in Organic Coatings*, **19**, 379 (1991).
38 X. D. Sun, *Mater. Perform.*, **44**, 28 (2005).
39 O. Schneider, G. O. Ilevbare, J. R. Scully and R. G. Kelly, *J. Electrochem. Soc.*, **151**, B465 (2004).
40 R. M. Souto, Y. Gonzalez-Garcia and S. Gonzalez, *Corros. Sci.*, **47**, 3312 (2005).
41 B. Reddy and J. M. Sykes, *Progress in Organic Coatings AETOC 2003*, **52**, 280 (2005).
42 A. P. Nazarov and D. Thierry, *Electrochim. Acta*, **49**, 2955 (2004).
43 B. Reddy, M. J. Doherty and J. M. Sykes, *Electrochim. Acta*, **49**, 2965 (2004).
44 M. Stratmann, A. Leng, W. Furbeth, H. Streckel, H. Gehmecker and K.-H. Gro-Brinkhaus, *Progress in Organic Coatings – Proceedings of the 20th International Conference in Organic Coatings Science and Technology*, **27**, 261 (1996).

19

Cathodic protection monitoring

ALLEN CARLILE, Kinder Morgan, USA

19.1 Introduction

Cathodic protection is the application of a DC current onto a metal structure that is in contact with an electrolyte. Cathodic protection is provided from a DC current flowing from an anode into an electrolyte. The current flows from the anode into and through the electrolyte and onto the protected structure (cathode) and back to the anode by a metallic path. Sacrificial and Impressed systems are used to provide cathodic protection for buried or submerged structures.

For cathodic protection to be effective the DC current needs to be applied to the structure in amounts that will cause the positive and negative charges in metal that are contacting the electrolyte to polarize (Fig. 19.1 intergranular pattern not polarized and Fig. 19.2 intergranular pattern polarized). Cathodic protection can be provided from sacrificial or impressed systems (Fig. 19.3 typical impressed). The design of cathodic protection systems is key to insuring that cathodic protection currents are applied to the structures in adequate amounts to insure polarization is established and to insure current distribution is optimal. Monitoring cathodic protection is important in insuring that the structure being protected is receiving adequate current to insure cathodic protection is effective. Monitoring can be comprised of different techniques, equipment and methods. Information gained from monitoring cathodic protection can be used to determine effectiveness of cathodic protection, tracking how environmental changes affect structures, graphing, trending and interacted with risk modeling.

19.2 Cathodic protection monitoring

19.2.1 Cathodic protection monitoring to insure value of assets

Cathodic protection and monitoring of cathodic protection systems are crucial in insuring the functionality and long term financial gain of assets.

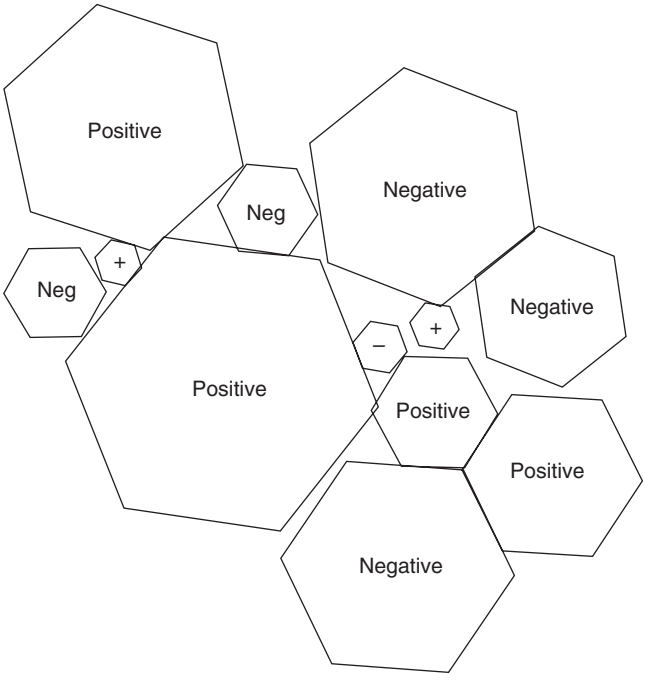

19.1 Intergranular pattern, no polarization.

It was reported that one particular system was having three or four leaks per month. The cathodic protection systems had not been kept in a functional state. Ground beds had depleted and were in need of replacement allowing the corrosion process to be active in areas where the structure was in contact with soil. After an upgrade and addition of cathodic protection systems and close monitoring to insure effectiveness, the leak rate dropped by 85%. There was obvious immediate financial gain and the assets are still functional today. The value of the assets is substantially more today, than in the 1970s. Cathodic protection monitoring can consist of many different items. Some of the components to be monitored after a system is energized, functional and adjusted are structure to soil potentials, rectifier output, impressed anode current output, galvanic anode output and bonds mitigating interference corrosion. NACE Standard RP0169-2002 – Standard Recommended Practice – Control of External Corrosion On Underground or Submerged Metallic Piping Systems – Section 10 – Operation and Maintenance of Cathodic Protection Systems states:

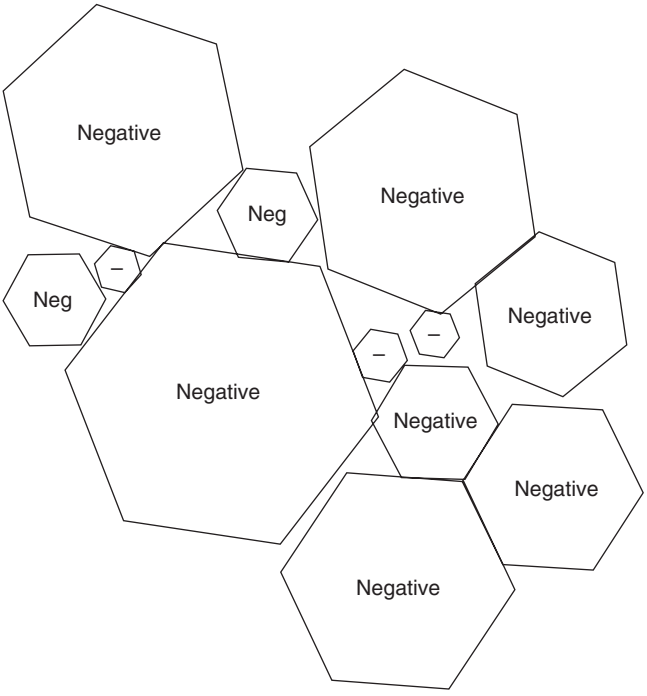

19.2 Intergranular pattern, polarized.

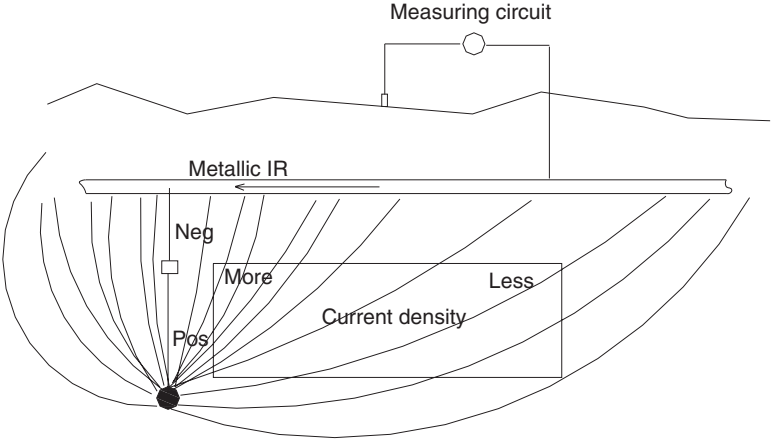

19.3 Typical impressed cathodic protection system.

10.1 Introduction

10.1.1 This section recommends procedures and practices for energizing and maintaining continuous, effective, and efficient operation of cathodic protection systems.

10.1.1.1 Electrical measurements and inspection are necessary to determine that protection has been established according to applicable criteria and that each part of the cathodic protection system is operating properly. Conditions that affect protection are subject to change. Correspondingly, changes may be required in the cathodic protection system to maintain protection. Periodic measurements and inspections are necessary to detect changes in the cathodic protection system. Conditions in which operating experience indicates that testing and inspections need to be made more frequently than recommended herein may exist.

10.1.1.2 Care should be exercised in selecting the location, number, and type of electrical measurements used to determine the adequacy of cathodic protection.

10.1.1.3 When practicable and determined necessary by sound engineering practice, a detailed (close-interval) potential survey should be conducted to (a) assess the effectiveness of the cathodic protection system; (b) provide base line operating data; (c) locate areas of inadequate protection levels; (d) identify locations likely to be adversely affected by construction, stray currents, or other unusual environmental conditions; or (e) select areas to be monitored periodically.

10.1.1.4 Adjustments to a cathodic protection system should be accompanied by sufficient testing to assure the criteria remain satisfied and to reassess interference to other structures or isolation points.

10.2 A survey should be conducted after each cathodic protection system is energized and/or adjusted to determine whether the applicable criterion or criteria from Section 6 have been satisfied.

10.3 The effectiveness of the cathodic protection system should be monitored annually. Longer or shorter intervals for monitoring may be appropriate, depending on the variability of cathodic protection factors, safety considerations, and economics of monitoring.

10.4 Inspection and tests of cathodic protection facilities should be made to ensure their proper operation and maintenance as follows:

10.4.1 All sources of impressed current should be checked at intervals of two months. Longer or shorter intervals for monitoring may be appropriate. Evidence of proper functioning may be current output, normal power consumption, a signal indicating normal operation, or satisfactory cathodic protection levels on the pipe.

10.4.2 All impressed current protective facilities should be inspected annually as part of a preventive maintenance program to minimize in-service failure. Longer or shorter intervals for monitoring may be appropriate. Inspections may include a check for electrical malfunctions, safety ground connections, meter accuracy, efficiency, and circuit resistance.

10.4.3 Reverse-current switches, diodes, interference bonds, and other protective devices, whose failures would jeopardize structure protection, should

be inspected for proper functioning at intervals of two months. Longer or shorter intervals for monitoring may be appropriate.

10.4.4 The effectiveness of isolating fittings, continuity bonds, and casing isolation should be evaluated during the periodic surveys. This may be accomplished by electrical measurements.

10.5 When pipe has been uncovered, it should be examined for evidence of external corrosion and, if externally coated, for condition of the external coating.

10.6 The test equipment used for obtaining each electrical value should be of an appropriate type. Instruments and related equipment should be maintained in good operating condition and checked for accuracy.

10.7 Remedial measures should be taken when periodic tests and inspections indicate that cathodic protection is no longer adequate. These measures may include the following:

10.7.1 Repair, replace, or adjust components of cathodic protection systems;

10.7.2 Provide supplementary facilities where additional cathodic protection is necessary;

10.7.3 Thoroughly clean and properly coat bare structures if required to attain cathodic protection;

10.7.4 Repair, replace, or adjust continuity and interference bonds;

10.7.5 Remove accidental metallic contacts; and

10.7.6 Repair defective isolating devices.

10.8 An electrical short circuit between a casing and carrier pipe can result in inadequate cathodic protection of the pipeline outside the casing due to reduction of protective current to the pipeline.

10.8.1 When a short results in inadequate cathodic protection of the pipeline outside the casing, steps must be taken to restore cathodic protection to a level required to meet the cathodic protection criterion. These steps may include eliminating the short between the casing and carrier pipe, supplementing cathodic protection, or improving the quality of the external coating on the pipeline outside the casing. None of these steps will ensure that external corrosion will not occur on the carrier pipe inside the casing; however, a shorted casing does not necessarily result in external corrosion of the carrier pipe inside the casing.

10.9 When the effects of electrical shielding of cathodic protection current are detected, the situation should be evaluated and appropriate action taken.

In addition to consistent monitoring of these items NACE Standard RP0169-2002 – Standard Recommended Practice – Control of External Corrosion On Underground or Submerged Metallic Piping Systems – Section 11 recommends that records be kept on the following:

Section 11: External Corrosion Control Records

11.1 Introduction

11.1.1 This section describes external corrosion control records that will document in a clear, concise, workable manner, data that are pertinent to the

design, installation, operation, maintenance, and effectiveness of external corrosion control measures.

11.2 Relative to the determination of the need for external corrosion control, the following should be recorded:

11.2.1 Corrosion leaks, breaks, and pipe replacements; and

11.2.2 Pipe and external coating condition observed when a buried structure is exposed.

11.3 Relative to structure design, the following should be recorded:

11.3.1 External coating material and application specifications; and

11.3.2 Design and location of isolating devices, test leads and other test facilities, and details of other special external corrosion control measures taken.

11.4 Relative to the design of external corrosion control facilities, the following should be recorded:

11.4.1 Results of current requirement tests;

11.4.2 Results of soil resistivity surveys;

11.4.3 Location of foreign structures; and

11.4.4 Interference tests and design of interference bonds and reverse-current switch installations.

11.4.4.1 Scheduling of interference tests, correspondence with corrosion control coordinating committees, and direct communication with the concerned companies.

11.4.4.2 Record of interference tests conducted, including location of tests, name of company involved, and results.

11.5 Relative to the installation of external corrosion control facilities, the following should be recorded:

11.5.1 Installation of cathodic protection facilities:

11.5.1.1 Impressed current systems:

11.5.1.1.1 Location and date placed in service;

11.5.1.1.2 Number, type, size, depth, backfill, and spacing of anodes;

11.5.1.1.3 Specifications of rectifier or other energy source; and

11.5.1.1.4 Cable size and type of insulation.

11.5.1.2 Galvanic anode systems:

11.5.1.2.1 Location and date placed in service;

11.5.1.2.2 Number, type, size, backfill, and spacing of anodes; and

11.5.1.2.3 Wire size and type of insulation.

11.5.2 Installation of interference mitigation facilities:

11.5.2.1 Details of interference bond installation:

11.5.2.1.1 Location and name of company involved;

11.5.2.1.2 Resistance value or other pertinent information; and

11.5.2.1.3 Magnitude and polarity of drainage current.

11.5.2.2 Details of reverse-current switch:

11.5.2.2.1 Location and name of companies;

11.5.2.2.2 Type of switch or equivalent device; and

11.5.2.2.3 Data showing effective operating adjustment.

11.5.2.3 Details of other remedial measures.

11.6 Records of surveys, inspections, and tests should be maintained to demonstrate that applicable criteria for interference control and cathodic protection have been satisfied.
11.7 Relative to the maintenance of external corrosion control facilities, the following information should be recorded:
11.7.1 Maintenance of cathodic protection facilities:
11.7.1.1 Repair of rectifiers and other DC power sources; and
11.7.1.2 Repair or replacement of anodes, connections, wires, and cables.
11.7.2 Maintenance of interference bonds and reverse current switches:
11.7.2.1 Repair of interference bonds; and
11.7.2.2 Repair of reverse-current switches or equivalent devices.
11.7.3 Maintenance, repair, and replacement of external coating, isolating devices, test leads, and other test facilities.
11.8 Records sufficient to demonstrate the evaluation of the need for and the effectiveness of external corrosion control measures should be maintained as long as the facility involved remains in service. Other related external corrosion control records should be retained for such a period that satisfies individual company needs.

19.3 Cathodic protection monitoring techniques

Monitoring of cathodic protection can be accomplished using several different methods. One tool for monitoring cathodic protection effectiveness on a structure is using portable copper/copper sulfate reference cells for measuring structure to soil potentials. The reference cells are placed in close proximity to the structure on which the cathodic protection levels are being measured. It is important to insure good technique is used when obtaining structure to soil information and be sure to observe the polarity of the reading insuring the polarity is correct and the structure is polarized negative. In addition to portable copper/copper sulfate reference cells permanent reference cells can be used. Common locations for permanent reference cells are under the floors of above ground tanks, structure crossings where interference corrosion is a concern or areas on a structure where environmental changes can influence the structure in an undesirable way. Permanent reference cells can be used with remote monitors. Cathodic protection coupons can also be used to monitor effectiveness and levels of cathodic protection. Electrical measurement of coupons can be used to determine the effectiveness of cathodic protection systems. Coupons that are installed for electrical measurement need to be buried in the same electrolyte as the structure to be evaluated. Coupons that are used for electrical measurement need a wire connecting them to the cathodic protection circuit being evaluated. Structure to soil measurements can be made on the coupon allowing evaluation of structure to soil measurements with current applied and structure to soil measurements that are IR free. The

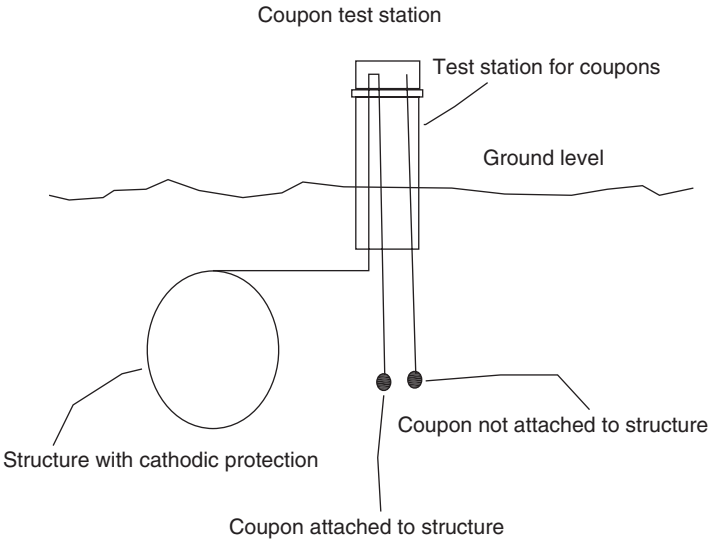

19.4 Coupon test station.

use of another (second) coupon in electrical measurements where the second coupon is not attached to the structure will allow the evaluation of static potentials on the coupon (Figure 19.4 coupon test stations). ANSI/NACE RP0104-2004 Standard Recommended Practice – The Use of Coupons for Cathodic Protection Monitoring Applications – Section 3 – Applications states:

> 3.1 Coupons may be used for potential measurements on pipelines and many other structures. When properly installed and maintained, coupons may be used, either by themselves or in conjunction with other measurement techniques, for evaluating compliance with CP criteria. It has long been realized that an IR drop that produces an error in the structure-to-electrolyte on potential exists in the electrolyte and across the coating. This IR-drop error varies from pipeline to pipeline and along the length of a given pipe because of variations in soil resistivity, depth of burial, coating condition, stray current, local and long-line corrosion cells, and the magnitude of CP current. This IR drop may be determined by measuring the difference between the on potential and the instant-off potential of a structure immediately after interrupting the CP current. The instant off potential measured without perceptible delay after interruption is an accepted method of determining the polarized potential of the pipe.
>
> 3.2 The CP coupon methodology may be used as an alternative to the conventional instant-off potential measurement for evaluating the effectiveness of a CP system. By disconnecting the coupon from the pipe (and therefore, from the CP system as well) and measuring the potential of the coupon

surface with a reference electrode located very close to the coupon or in a soil-access tube, the instant-off potential errors for the coupon are either eliminated or minimized.

3.3 The CP coupon polarized (off) potential is not identical to the conventional structure-to-electrolyte off potential measured from the surface of the ground. The structure-to-electrolyte off potential is affected by many factors, including:

- the number and distribution of holidays along and around the structure surface both near to and far from the coupon,
- variations in the specific conductance of the coating along and around the structure surface both near to and far from the coupon,
- possibly large surface areas exposed to the electrolyte (especially for bare pipe),
- different electrolyte conditions (soil type, moisture content, chemistry, resistivity, temperature, and amount of oxygen) along the length and depth of the pipe,
- different current densities along and around the surface of the pipe, resulting in different levels of polarization,
- long-line currents and local currents established between areas with different levels of polarization,
- interference effects from foreign CP systems, telluric currents, and other alternating current (AC) and direct current (DC) stray current sources, and
- bimetallic structure connections that may be inadvertently or deliberately in contact with the cathodically protected structure.

3.4 Because of these differences, when a structure-to-electrolyte potential is measured, each measurement is actually a weighted average of all the areas exposed to the electrolyte. It has been demonstrated that the polarized potential of exposed steel at small holidays on large diameter pipelines can vary significantly over small distances because of the factors listed in Paragraph 3.3. The significance of these differences on an individual structure-to-electrolyte measurement is usually difficult to determine. In contrast, the polarized potential of the coupon represents the polarized potential of a single, small area of either an uncoated structure or a coating defect (holiday) on a coated structure.

3.5 When a coupon is installed close to the structure and the electrolyte around each is the same, the coupon essentially receives the same level of CP current and attains the same level of polarization as an adjacent equal area of the structure that has the same resistance-to-earth. This allows CP measurements to be made on the coupon from which the CP status of the structure in that area may be determined. The coupon method evaluates the effectiveness of a CP system based on an accurate polarized potential measurement of a coupon (representing an equivalent surface on the structure) rather than a structure-to-electrolyte off-potential measurement that may contain errors. This is especially true when error sources are known to be near the measurement area. Coupons may be

used to obtain significant information on the level of protection supplied by a CP system to a structure. The instant-disconnect potential, depolarization behavior, and the current picked up by the CP coupon can be easily measured.

3.6 Coupons may be used in a wide variety of applications. The most common usage is for buried or submerged pipelines. They are also used for USTs, on-grade storage tank bottoms, reinforcing steel in concrete, internal surfaces of elevated or on-grade water storage tanks, and various other structures in aqueous environments. Information on these applications can be found in Appendices A, B, and C. Pipelines that can use coupons include transmission, distribution, gathering, utility, and in-plant piping. Coupons may also be used for cable-carrying piping or conduit that is buried or submerged and protected from external corrosion with CP.

3.7 Coupons may be used when any of the following conditions occur:

(a) current from multiple rectifiers must be interrupted synchronously (or a nonsynchronous interruption method, like the wave-form analyzer or stepwise reduction method, must be used);
(b) foreign CP systems are present in the area, for which either the locations are unknown or the rectifiers cannot be interrupted, resulting in IR-drop errors in the off-potential measurement;
(c) the presence of directly connected sacrificial anodes that cannot be interrupted, resulting in IR-drop errors in the off-potential measurement;
(d) long-line or telluric currents that result in IR-drop errors that interruption cannot eliminate;
(e) stray current that causes significant IR-drop errors in the off-potential measurement;
(f) structures utilizing polarization or depolarization criterion;
(g) locally corrosive areas in an otherwise noncorrosive environment;
(h) rapid IR transients (spikes) immediately following interruption that cause errors in the off-potential measurement;
(i) simple averaging over a length of pipe based on structure-to-electrolyte measurements made at grade that cause local potential fluctuations to be underestimated;
(j) multiple pipelines in the same right-of-way that produce interference with one another, thus preventing an accurate measure of any individual line;
(k) the structure may be under the influence of alternating current; and
(l) no known CP problem exists, but additional information is desired.

3.8 In areas where multiple impressed-current sources influence the structure-to-electrolyte potential, interruption of all current sources is not always practical. A coupon may be disconnected from the structure and its instant-disconnect potential measured to evaluate the protection level with respect to the relevant polarized potential criterion. Additionally, a coupon may be allowed to depolarize, permitting evaluation with respect to the relevant polarization criterion without the need to turn off CP systems for extended periods.

3.9 Coupons may be used to assess the level of protection on structures affected by stray currents. Stray current sources include DC traction systems, foreign rectifiers, telluric earth currents, and high-voltage direct-current (HVDC) electrodes.
3.10 In some cases, galvanic anodes are directly connected to the structure and cannot be interrupted to reduce the measurement error caused by the IR drop. In such cases, coupons may be used because their potential may be measured after they are disconnected from the structure.
3.11 In complex piping environments, such as industrial plants in which mixed metals can be electrically continuous with the affected structure, application of polarized potential or polarization criteria has not always been technically correct or practical. The measured potential is a result of a combination of the potentials of the metals involved. In a similar way, during current interruption, secondary IR drops from circulating galvanic current can cause errors in potential or polarization measurements on structures with widely varying potentials. When coupons are used, potential and polarization measurements should be made by locally disconnecting the CP coupon from the affected structure, thus avoiding the problem.
3.12 When several structures are bonded together, the structure-to-electrolyte potential measured at grade above one structure is actually a mixed potential of all the structures. The use of coupons is a means for determining a more local potential because each pipeline or structure can have its own coupon.
3.13 A CP coupon or a free-corrosion coupon as described in this standard, installed adjacent to a location with a disbonded, high-dielectric coating that shields CP current from reaching the structure surface, may not represent the CP protection status of the structure under the disbonded coating.

Data loggers are another method that can be used in monitoring cathodic protection. Data loggers can be used to evaluate structure to soil potentials, current amounts and current direction. Data loggers allow real time data collection and can be key in helping identify problem areas and trouble shooting. Data loggers will also allow data to be moved electronically into data management programs. Close interval surveys are another method used to monitor structures such as pipelines. Close interval surveys are structure to soil surveys that are taken at approximate 3 ft (91 cm) intervals using data loggers. Close interval surveys can be used to determine areas of a structure that do not meet NACE criteria, possible coating degradation areas and interference corrosion concerns. Power sources for cathodic protection (rectifiers, solar panels, gas generators, etc.) should be monitored to insure DC voltage and DC amperage are consistent and stable. Typically readings showing the date and time of the reading, DC voltage output, DC amperage output, power meter usage, and power source setting are obtained. The information obtained is maintained allowing presentation for necessary audits, tracking and trending. One thought is, if the power source

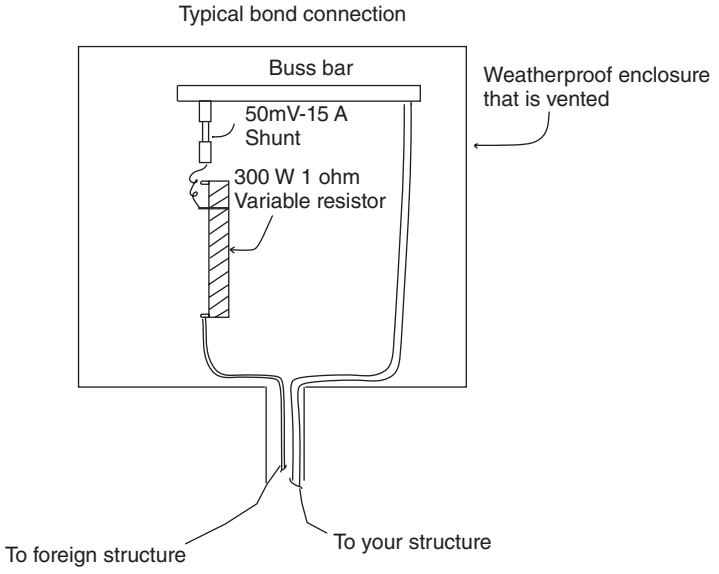

19.5 Typical bond connection.

is adjusted correctly with a stable output then the structure to soil potentials on the structure are also stable insuring effective corrosion control. Obtaining a structure to soil potential at the power source at the time the output information is obtained is a monitoring method that allows you to see if structure to soil potentials have changed drastically.

Bonds that are used in cathodic protection are typically a wire that has been sized appropriately that is connected between two structures, each having their own cathodic protection system. The electrical bond between the two wires allows a path (Fig. 19.5 shows a typical bond connection) for cathodic protection current to return to its original source without creating interference corrosion. Amounts of current and current direction should be monitored on bonds insuring the cathodic protection current is traveling in the correct direction and with the correct amount of current. Bonds can be critical to the integrity of a structure and should be monitored frequently to insure correct operation is maintained. Calibrated shunts are typically installed in bonds to allow proper measurement.

In the process of monitoring cathodic protection it is good to remember that the focus of cathodic protection is to polarize the metal contacting the electrolyte so that all components of the metal are negative in relation to a copper/copper sulfate reference cell. The definition of polarization is 'The deviation from the corrosion potential of an electrode resulting from the flow of current between the electrode and the electrolyte'. One description of polarization is:

A battery, a corrosion cell, or a cathodic protection system consists of many series and parallel circuits. The characteristic of a series circuit is that the same current flows through each element in series. The total potential difference in a series circuit is the algebraic sums of the potential differences and IR drops added to zero. The total resistance of a series resistance network is the sum of the individual resistance values. In a series circuit, the circuit resistance is dominated by the high-test resistance. Consider a network of four resistors: 1 000 000, 10, and 0.1 ohms. The total resistance is 1 000 110.1 or almost the resistance of the largest resistor.

Four calculations are important in series circuits for cathodic protection measurement:

(a) computation of total resistance
(b) computation of potential difference
(c) computation of current
(d) computation of IR drop through each resistor.

The total resistance is the sum of the individual resistances (Fig. 19.6). R1 is 100 000 ohm, R2 is 0.01 ohm, R3 is 0.2 ohm, R4 is 0.4 ohm, R5 is 2750 ohm, R6 is 4250 ohm, R7 is 0.4 ohm and R8 is 0.09 ohm. The total resistance is 108 001.1 ohm. The total potential difference is

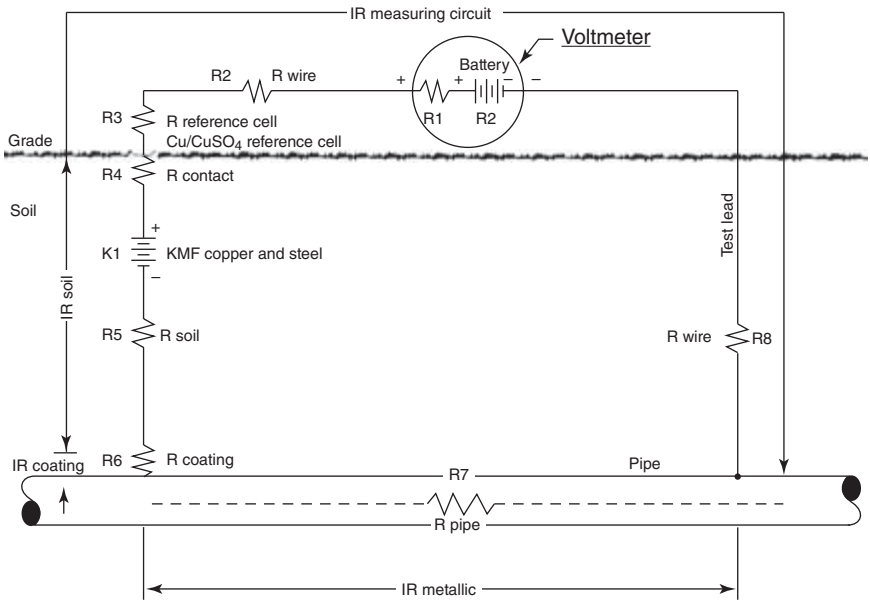

19.6 IR drop in pipe to soil measurements.

the sum of the individual potential deferences. If E1 is 9V and E2 is 8.15V the total E is 0.850V. The potential differences are actually subtracted since the batteries are connected with opposite polarity. The total current is the total potential difference divided by the total resistance. The total current is 0.0000079A. The IR drop through each resistor is the total current multiplied by the resistance of each resistor. The sum of the IR drops must equal the total potential difference. Most of the voltage is dropped in the largest resistor.

Polarization is important as when cathodic protection is applied to a structure the potential across the corrosion cells should be polarized.

Polarization

Polarization is caused by some slow step in the electrode reaction.

Further insight into polarization can be gained by considering the reduction of hydrogen ions (electroplating). This is an important cathodic reaction in corrosion, electroplating, and battery operation. The overall reaction is:

$2e^-$ +	$2H^+$ →	2H →	H_2 →
Electrons	H ions	Hydrogen atoms	Hydrogen molecule
In electrolyte		At cathode	

H_2O +	$2e^-$ +	$\frac{1}{2}O_2$ →	2 (OH)-
Water molecule	Electrons	Oxygen molecule	Hydroxyl ions

Reaction at cathode with available oxygen

The following steps are required:

1. H^+ must travel from the bulk of the electrolyte to the metal surface
2. H^+ must lose its water on solvation
3. An electron must be added to H^+ forming an atom on the surface
4. The atom on the surface must react with another forming a molecule
5. Many molecules must collect to form a bubble
6. The gas bubble must escape to the surface

Any slow step among these can cause polarization. In general, polarization is related to the depletion of reactants and buildup of a reaction product. Anything that favors the buildup of reaction products or the depletion of reactants increases polarization. Conversely, anything that causes the removal of reaction products or the replenishing of reactants will reduce polarization.

There are several ways to determine the IR drop at the test location. Bear in mind once the IR drop is determined then you know what your

polarized potential is and whether or not you are within the parameters of criteria. Some of the ways for determining what or how much IR drop is affecting your voltage reading is as follows:

1. Measuring or calculating voltage drops
2. Reviewing the historical performance of the cathodic protection system
3. Evaluating the physical and electrical characteristics of the pipe and its environment
4. Determining whether or not there is physical evidence of corrosion
5. Side drain extrapolation
6. Wave form analysis
7. Wave form digitizing.

By having an understanding of IR drop and using the proper criteria it is possible to have an effective and economical corrosion control system.

The most common method for measuring polarization levels is interrupting the cathodic protection circuit while measuring structure to soil potentials. Interruption of the cathodic protection circuit eliminates the current flow and driving voltage from the cathodic protection power source allowing an IR free measurement and being able to electrically evaluate the polarization level (polarized potential). The definition of polarized potential is 'The potential across the structure/electrolyte interface that is the sum of the corrosion potential and the cathodic polarization'. While observing high impedance digital voltmeters approximately two seconds should be given while the cathodic protection circuit is interrupted to allow the digital voltmeter to process the measuring circuit and display an OFF, IR free or polarized potential reading.

Calibrated test stations are a useful tool in monitoring cathodic protection current flow on pipelines. A calibrated test station is two test leads connected to the pipe line. The test leads are connected with a definitive space between the connections (50 or 100 feet (15 or 30 m)). The test leads are typically color coded allowing identification of the location/orientation of the test leads and terminate in a test station with each test lead clearly identified as to its location on the pipe. This process allows the pipe to be used as a shunt measuring DC current flow and direction. The resistance value of the pipe can be calculated or a small amount of DC current voltage and amperage can be passed through the calibrated test station. If DC voltage and amperage are passed through the calibrated test station Ohm's law can be used to determine the actual resistance of the circuit. Once the test station resistance is determined electrical measurements can be taken as needed to measure cathodic protection current amounts and direction. As the information from the calibrated test station is obtained, recorded and filed the ability to track and trend the data will allow identification of

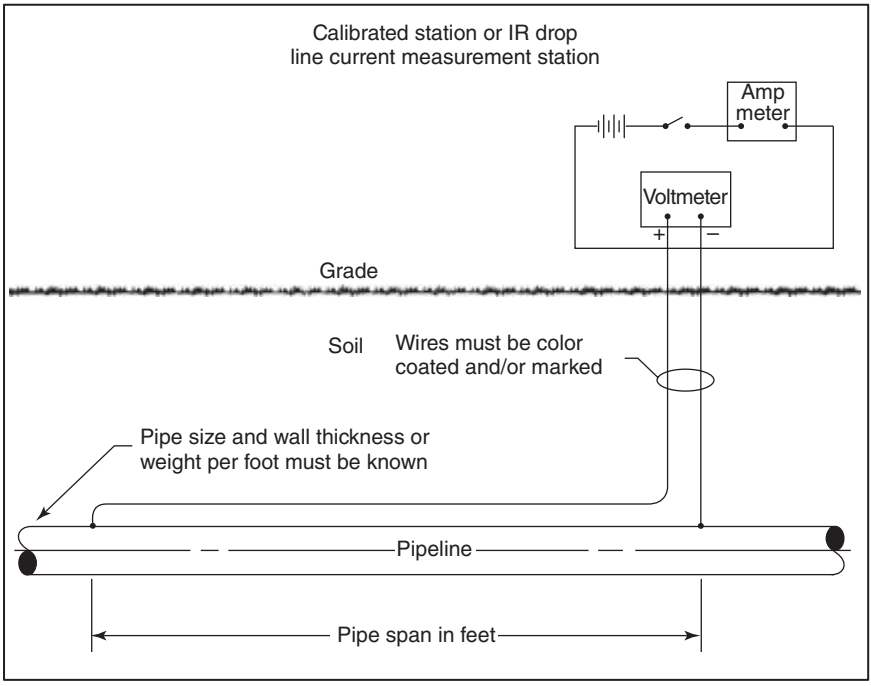

19.7 Calibrated station or IR drop line current measurement station.

changes in cathodic protection current flow and allow possible coating degradation areas to be identified. This type of monitoring will help identify areas where foreign structures may be in contact with your structure (Fig. 19.7).

19.4 Cathodic protection monitoring technology

19.4.1 Pickup trucks and voltmeters

The most common way of obtaining structure to soil, rectifier, bond and other CP monitoring information is by having a technician go to the locations to be monitored, with the needed equipment and obtain the needed data and information (Fig. 19.8). This process can take some time to be completed. It can also be labor intensive and difficult especially on cross-country pipelines that are in rugged terrain. If electronic data loggers are not being used the information is recorded on paper. The process is effective and is the typical method used to monitor cathodic protection systems (Fig. 19.9).

Cell phone technology allows cathodic protection systems to be remotely monitored. The technology is cost effective, dependable and integrates with

19.8 Oil immersed rectifer and deep well.

19.9 Air cooled rectifier.

data management systems. For areas that may require more frequent monitoring, remote monitoring using cell phone technology is a good tool. One thing to bear in mind with cell phone technology is there may be areas that are not covered by cell towers or where directional antennas may be needed. The ability to obtain data more frequently will allow trending and tracking of data. Typically after installation most owner operators are surprised at

the amount of 'down time' a unit will have. If monitoring bond currents or structure to soil potential, there typically are eyebrows raised at the amount of time a structure is not meeting protection criteria or influence from other cathodically protected structure being adjusted and having adverse affects on the one being remotely monitored.

Satellite technology used for remote monitoring has made major steps over recent years. The use of satellites has enhanced the ability to move data from the field to desktops. The technology using satellite technology first came into play on pipelines in 2000 and was used in monitoring rectifiers. The ability to determine power outages, rectifiers that needed repair or adjustment, or a structure that has been adversely affected by stray currents or environmental changes and have the information on your desktop within minutes of its occurrence is a major step in insuring that the value of assets does not decline and continues to increase.

19.5 Effectiveness of corrosion control after installation and monitoring

After energizing cathodic protection systems, the asset or structure should be monitored at many and various locations to insure NACE criteria (RP 0169-2002 Section 6, Criteria & Other Considerations for Cathodic Protection) are met. The Criteria and Other Considerations state:

Section 6: Criteria and Other Considerations for Cathodic Protection

6.1 Introduction

6.1.1 This section lists criteria and other considerations for cathodic protection that indicate, when used either separately or in combination, whether adequate cathodic protection of a metallic piping system has been achieved (see also Section 1, Paragraphs 1.2 and 1.4).

6.1.2 The effectiveness of cathodic protection or other external corrosion control measures can be confirmed by visual observation, by measurements of pipe wall thickness, or by use of internal inspection devices. Because such methods sometimes are not practical, meeting any criterion or combination of criteria in this section is evidence that adequate cathodic protection has been achieved. When excavations are made for any purpose, the pipe should be inspected for evidence of corrosion and/or coating condition.

6.1.3 The criteria in this section have been developed through laboratory experiments and/or verified by evaluating data obtained from successfully operated cathodic protection systems. Situations in which a single criterion for evaluating the effectiveness of cathodic protection may not be satisfactory for all conditions may exist. Often a combination of criteria is needed for a single structure.

6.1.4 Sound engineering practices shall be used to determine the methods and frequency of testing required to satisfy these criteria.

6.1.5 Corrosion leak history is valuable in assessing the effectiveness of cathodic protection. Corrosion leak history by itself, however, shall not be used to determine whether adequate levels of cathodic protection have been achieved unless it is impractical to make electrical surveys.

6.2 Criteria

6.2.1 It is not intended that persons responsible for external corrosion control be limited to the criteria listed below. Criteria that have been successfully applied on existing piping systems can continue to be used on those piping systems. Any other criteria used must achieve corrosion control comparable to that attained with the criteria herein.

6.2.2 Steel and Cast Iron Piping

6.2.2.1 External corrosion control can be achieved at various levels of cathodic polarization depending on the environmental conditions. However, in the absence of specific data that demonstrate that adequate cathodic protection has been achieved, one or more of the following shall apply:

6.2.2.1.1 A negative (cathodic) potential of at least 850 mV with the cathodic protection applied. This potential is measured with respect to a saturated copper/copper sulfate reference electrode contacting the electrolyte. Voltage drops other than those across the structure-to-electrolyte boundary must be considered for valid interpretation of this voltage measurement.

Note: Consideration is understood to mean the application of sound engineering practice in determining the significance of voltage drops by methods such as:

6.2.2.1.1.1 Measuring or calculating the voltage drop(s);

6.2.2.1.1.2 Reviewing the historical performance of the cathodic protection system;

6.2.2.1.1.3 Evaluating the physical and electrical characteristics of the pipe and its environment; and

6.2.2.1.1.4 Determining whether or not there is physical evidence of corrosion.

6.2.2.1.2 A negative polarized potential (see definition in Section 2) of at least 850 mV relative to a saturated copper/copper sulfate reference electrode.

6.2.2.1.3 A minimum of 100 mV of cathodic polarization between the structure surface and a stable reference electrode contacting the electrolyte. The formation or decay of polarization can be measured to satisfy this criterion.

6.2.2.2 Special Conditions

6.2.2.2.1 On bare or ineffectively coated pipelines when long-line corrosion activity is of primary concern, the measurement of a net protective current at predetermined current discharge points from the electrolyte to the pipe surface, as measured by an earth current technique, may be sufficient.

6.2.2.2.2 In some situations, such as the presence of sulfides, bacteria, elevated temperatures, acid environments, and dissimilar metals, the criteria in Paragraph 6.2.2.1 may not be sufficient.

6.2.2.2.3 When a pipeline is encased in concrete or buried in dry or aerated high resistivity soil, values less negative than the criteria listed in Paragraph 6.2.2.1 may be sufficient.

6.2.2.3 Precautionary notes

6.2.2.3.1 The earth current technique is often meaningless in multiple pipe rights-of-way, in high-resistivity surface soil, for deeply buried pipe, in stray-current areas, or where local corrosion cell action predominates.

6.2.2.3.2 Caution is advised against using polarized potentials less negative than –850 mV for cathodic protection of pipelines when operating pressures and conditions are conducive to stress corrosion cracking (see references on stress corrosion cracking at the end of this section).

6.2.2.3.3 The use of excessive polarized potentials on externally coated pipelines should be avoided to minimize cathodic disbondment of the coating.

6.2.2.3.4 Polarized potentials that result in excessive generation of hydrogen should be avoided on all metals, particularly higher strength steel, certain grades of stainless steel, titanium, aluminum alloys, and prestressed concrete pipe.

6.2.3 Aluminum Piping

6.2.3.1 The following criterion shall apply: a minimum of 100 mV of cathodic polarization between the structure surface and a stable reference electrode contacting the electrolyte. The formation or decay of this polarization can be used in this criterion.

6.2.3.2 Precautionary notes

6.2.3.2.1 Excessive Voltages: Notwithstanding the minimum criterion in Paragraph 6.2.3.1 if aluminum is cathodically protected at voltages more negative than –1200 mV measured between the pipe surface and a saturated copper/copper sulfate reference electrode contacting the electrolyte and compensation is made for the voltage drops other than those across the pipe–electrolyte boundary, it may suffer corrosion as the result of the buildup of alkali on the metal surface. A polarized potential more negative than –1200 mV should not be used unless previous test results indicate that no appreciable corrosion will occur in the particular environment.

6.2.3.2.2 Alkaline Conditions: Aluminum may suffer from corrosion under high-pH conditions and application of cathodic protection tends to increase the pH at the metal surface. Therefore, careful investigation or testing should be done before applying cathodic protection to stop pitting attack on aluminum in environments with a natural pH in excess of 8.0.

6.2.4 Copper Piping

6.2.4.1 The following criterion shall apply: a minimum of 100 mV of cathodic polarization between the structure surface and a stable reference electrode contacting the electrolyte. The formation or decay of this polarization can be used in this criterion.

6.2.5 Dissimilar Metal Piping

6.2.5.1 A negative voltage between all pipe surfaces and a stable reference electrode contacting the electrolyte equal to that required for the protection of the most anodic metal should be maintained.

6.2.5.2 Precautionary note

6.2.5.2.1 Amphoteric materials that could be damaged by high alkalinity created by cathodic protection should be electrically isolated and separately protected.

6.3 Other Considerations

6.3.1 Methods for determining voltage drop(s) shall be selected and applied using sound engineering practices. Once determined, the voltage drop(s) may be used for correcting future measurements at the same location, providing conditions such as pipe and cathodic protection system operating conditions, soil characteristics, and external coating quality remain similar. (Note: Placing the reference electrode next to the pipe surface may not be at the pipe–electrolyte interface. A reference electrode placed at an externally coated pipe surface may not significantly reduce soil voltage drop in the measurement if the nearest coating holiday is remote from the reference electrode location.)

6.3.2 When it is impractical or considered unnecessary to disconnect all current sources to correct for voltage drop(s) in the structure-to-electrolyte potential measurements, sound engineering practices should be used to ensure that adequate cathodic protection has been achieved.

6.3.3 When feasible and practicable, in-line inspection of pipelines may be helpful in determining the presence or absence of pitting corrosion damage. Absence of external corrosion damage or the halting of its growth may indicate adequate external corrosion control. The in-line inspection technique, however, may not be capable of detecting all types of external corrosion damage, has limitations in its accuracy, and may report as anomalies items that are not external corrosion. For example, longitudinal seam corrosion and general corrosion may not be readily detected by in-line inspection. Also, possible thickness variations, dents, gouges, and external ferrous objects may be detected as corrosion. The appropriate use of in-line inspection must be carefully considered.

6.3.4 Situations involving stray currents and stray electrical gradients that require special analysis may exist. For additional information, see Section 9, "Control of Interference Currents."

6.4 Alternative Reference Electrodes

6.4.1 Other standard reference electrodes may be substituted for the saturated copper/copper sulfate reference electrode. Two commonly used reference electrodes are listed below along with their voltage equivalent (at 25 °C [77 °F]) to –850 mV referred to a saturated copper/copper sulfate reference electrode:

6.4.1.1 Saturated KCl calomel reference electrode: –780 mV; and

6.4.1.2 Saturated silver/silver chloride reference electrode used in 25 ohm-cm seawater: –800 mV.

6.4.2 In addition to these standard reference electrodes, an alternative metallic material or structure may be used in place of the saturated copper/copper sulfate reference electrode if the stability of its electrode potential is ensured and if its voltage equivalent referred to a saturated copper/copper sulfate reference electrode is established.

It may take several trips to the field to obtain needed data to insure polarization is established and criteria are met.

Although structure to soil surveys are typically done on an annual basis additional monitoring of mid-points between rectifiers and critical locations on a structure will help insure effective levels of cathodic protection are being maintained year round. It will also help identify when cathodic protection levels are below criteria. If areas are found that are not meeting NACE criteria then an action plan can be put into place to overcome the problem to include upgrades of systems if needed.

The same perspective can be applied to critical bonds and rectifier operation. If a rectifier is read every 60 days and quits operating the day after it is read/monitored and not discovered until the next 60 day reading cycle then the structure being protected by the rectifier will have been without protection for 16% of the year. One of the tools in today's world that helps overcome such lapses in cathodic protection is remote monitoring. Remote monitoring allows readings to be obtained on a more frequent basis. Critical bonds can be an even bigger concern. Loss of a critical bond will typically allow an interference corrosion process to initiate as soon as the bond is broken. More frequent monitoring of critical bonds will help insure your asset stays intact.

19.6 Monitoring results and maintenance opportunities

Efforts and monies spent for maintaining cathodic protection can be identified, planned for and improved. Monitoring cathodic protection can result in identifying maintenance concerns. While obtaining cathodic protection information from structure/assets, repair information can be trended. An example would be numbers of test locations each year that require repair. This information can then be extrapolated and budgeted for, on an annual basis. The same thought can be applied to rectifier maintenance, bond repair, etc.

19.7 Value of structure increases

Effective cathodic protection insures the economic value of an asset does not decay. A cathodic protection system that is monitored, maintained and effective insures the economic value of assets increase. Monitoring cathodic protection plays a key role insuring the integrity of assets. Thorough monitoring and taking corrective actions when deficiencies are found insure the value of the assets will increase and not decline.

19.8 Less replacement and maintenance cost for the company

Cathodic protection systems that are monitored and are effective result in less money being spent for replacement due to external corrosion. Cost associated with down time, repair, over time and environmental clean up are reduced as used in the example on the system constructed in the 1930s. An 85% reduction can be expected in these costs.

19.9 Cathodic protection monitoring as required by US government as a minimum requirement and other considerations

Government regulations are a minimum requirement. With that in perspective, monitoring performed beyond the minimum requirement insures that the integrity of the asset will be maintained. The value added for the extra work far outweighs the cost of performing the task needed to perform the additional monitoring, as well as the ability to be proactive in identifying problems that can be corrected.

Government regulations (CFR 195, Subpart H) identify test lead locations (except offshore pipelines) to be placed at intervals frequent enough to obtain electrical measurements indicating the adequacy of cathodic protection. Peabody's Control of Pipeline Corrosion (Second Edition) indicates that test station location should be placed (on well coated pipelines) at a minimum of half-mile (0.8 km) intervals to a maximum of one-mile (1.6 km) intervals along the route of the pipeline. Additional test leads will be needed for foreign line crossings, buried insulated joints, and at cased crossings. High consequence areas or areas of high population may require more test station locations to insure cathodic protection monitoring is effective and representative.

Above-ground tanks can be monitored at eight locations typically North, North East, East, South East, South, South West, West and North West. A technique in monitoring large diameter tanks (100 ft (30 m) diameter or larger) that may be useful is to measure structure to soil potentials at 20 ft (6 m) intervals circumferentially around the tanks. Installation of permanent half cells with slotted tubes for profiling structure to soil potentials under the tank floor will help to insure effective levels of cathodic protection under the tank floor.

Underground tanks can have access tubes or permanent half cells placed at each end of the tank, underneath the tank and point representing the horizontal center of the tank. These locations will allow representative data to be obtained.

Structure to soil monitoring requirement for a regulated pipeline is once a year not to exceed 15 months. As mentioned earlier it would be prudent to check midpoints between rectifiers on a regular basis (once a quarter). The additional information will help to insure protective levels are maintained year round. Other structures (above-ground storage tanks, underground storage tanks, submerged structures) that are monitored on a frequent basis will also allow data to be trended insuring effective levels of cathodic protection are maintained.

Rectifier and bond monitoring requirements for regulated pipelines are six times a year not to exceed 2½ months. As mentioned earlier in the chapter as much as 16% of the year can have equipment not functioning properly. In order to insure that the value of assets is maintained, more frequent monitoring may prove to be a worthwhile effort.

19.10 Monitoring frequency helps determine effectiveness of corrosion program

The more often a cathodic protection system is monitored the better the data base is for trending. Downtime or areas that are influenced by cyclic environmental changes are easier to identify and correct. The information gathered from frequent monitoring of cathodic protection systems allows a data base to be enhanced. As the environment changes, required amounts of current to protect buried structures will also change. The ability to identify the changes (seasonal or cyclic) will allow rectifier output to be adjusted (based on historical monitoring data) to compensate for increased or decreased current demands. If sacrificial systems are being used the effectiveness of the system can be verified as needed.

19.11 NACE recommendations

The recommendations made in NACE RP0-169-2002, Control of External Corrosion On Underground or Submerged Metallic Piping Systems, Section 10 Operation and Maintenance of Cathodic Protection Systems, 10.1.1.1 states:

> Electrical measurements and inspections are necessary to determine that protection has been established according to applicable criteria and that each part of the cathodic protection system is operating properly. Conditions that affect protection are subject to change. Correspondingly, changes may be required in the cathodic protection system to maintain protection. Periodic measurements and inspections are necessary to detect changes in the cathodic protection system. Conditions in which operating experience indicates that testing and inspections need to be made more frequently than recommended herein may exist.

NACE Standard RP0193-2001, External Cathodic Protection of On-Grade Carbon Steel Storage Tank Bottoms, Section 11, 11.2.2 states:

> Annual surveys should be conducted to verify that the cathodic protection system is meeting the protection criteria. Making more frequent surveys of the system may be desirable in critically corrosive environments or where highly variable conditions are present. The accuracy of stationary reference electrodes should be evaluated during these surveys. The effectiveness of isolating fittings and continuity bonds should also be evaluated during the periodic surveys.

Corrosion Control of Under Ground Storage Tank Systems by Cathodic Protection, NACE Standard RP0285-2002 Section 8, 8.1.3 states:

> Periodic measurements and inspections are necessary to detect changes in the CP system. Conditions in which operating experience indicates testing should be conducted more frequently than recommended in this standard may exist.

When cathodic protection monitoring is performed at frequent intervals data and information obtained should indicate when cathodic protection is at the point of becoming non-effective. Using this information will allow cathodic protection to be used in an effective manner insuring the value of assets is maintained and continues to be profitable, requiring minimal maintenance and/or replacement.

19.12 Cathodic protection monitoring relative to unusual or at-risk environments

Unusual environments may require more monitoring. Environments that are aggressive and allow corrosion processes to function at high rates may require more frequent monitoring. Soil resistivities that are below 2000 ohm-cm would be an example of an area where additional monitoring would be a useful tool. A critical bond that is a high amp drain (1 amp or higher) would be an example of a point where monitoring other than minimum requirements would helpful in insuring the value of assets is maintained.

Installation of remote monitoring systems may be a great tool for tracking cathodic protection voltage and currents that tend to change drastically due to influence from 'Mother Nature' and other entities. Today's technology is very functional, dependable and interactive with data management programs. Units can be set with definitive high or low alarm parameters and predefined to read at specific times. The remote monitoring technology is not costly and allows an owner operator to easily obtain information and data insuring cathodic protection is effective and the value of assets continues to increase.

19.13 Field data to aid in cathodic protection monitoring

When evaluations are being done in the field on structures, tanks, or pipelines information can be obtained to help determine the effectiveness of cathodic protection. Some of the information that can be obtained to determine the effectiveness would be:

- Structure to soil potentials on the area being examined at various points.
- Soil or water resistivities can be obtained to clearly identify the aggressiveness of the environment.
- Soil or water samples can be obtained for defined analysis and chemical composition.
- Coating systems can be evaluated to insure the coating is bonded and signs of failure are not present.
- If a coating is disbonded measurements can be taken using appropriate instruments to determine the area of disbondment.
- If a coating is disbonded pH measurements should be taken under the disbonded level to determine if hydroxyl ions are going under the disbonded coating.

The data obtained from a field analysis can be used to determine whether cathodic protection is effective. The obtained data can also be integrated into risk management systems to help evaluate and determine whether other areas of concern exist (Fig. 19.10).

19.10 Coating evaluation.

19.14 Data management

Data management technology or the programs that manage data gained from monitoring cathodic protection systems allows the data to be used in many ways. In addition to being able to readily access data for audits the data can be overlaid with inline inspection information, integrated with Risk Management programs. The ability to move reports around electronically improves communication and awareness in organizations (Figs 19.11 and 19.12). Other attributes would be:

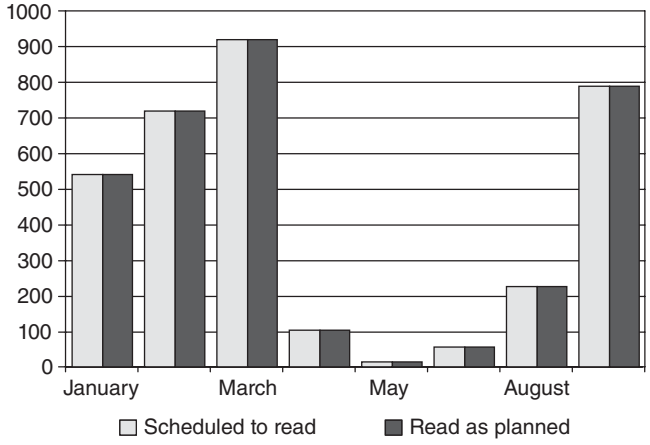

19.11 Annual test station readings.

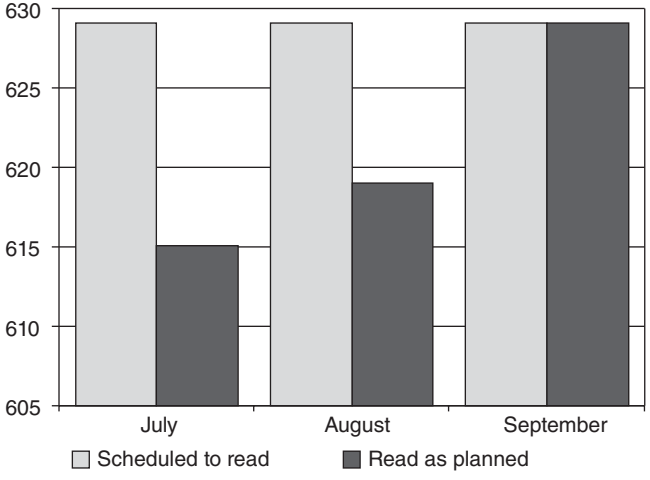

19.12 Monthly rectifier readings.

- tracking percentages of work complete
- graphing
- trending
- identification of missed readings
- areas not meeting NACE criteria
- ground bed ohm age changes
- equipment that malfunctions frequently
- specific points that were not included in survey
- easily available for presentation.

Data management programs that interphase with data loggers also allow the ability to electronically move information from the field to administrative levels within a matter of minutes. This process takes a lot of human error out of the cathodic protection monitoring equation not to mention time saved in hand data entry.

19.15 Overview

Monitoring cathodic protection systems is the key to insuring that they are functioning properly. Frequent monitoring insures that the value of assets increases with time and does not decline. Use of remote monitoring and data management programs allows the frequent monitoring of cathodic protection to be done with relative ease and minimal cost.

19.16 References

NACE RP0-169-2002 Standard Recommended Practice – Control of External Corrosion on Underground or Submerged Metallic Piping.

NACE RP0-193-2001 Standard Recommended Practice – External Cathodic Protection of On-Grade Carbon Steel Storage Tank Bottoms.

NACE RP0-285-2002 Standard Recommended Practice – Corrosion Control of Underground Storage Tank systems by Cathodic Protection.

ANSI/NACE Standard RP 104-2004 Standard Recommended Practice – The use of Coupons for Cathodic Protection Monitoring Applications.

Peabody's Control of Pipeline Corrosion, Second Edition, Edited by R. L. Bianchetti. Published 2001, pp 244 and 245.

University of Oklahoma College of Continuing Education Corrosion Control Course: 'An Explanation of Criteria and IR Drop', Allen Carlile, 2001.

20

Remote monitoring and computer applications

RICH SMALLING and LEE BLANKENSTEIN,
American Innovations, USA

20.1 Introduction

20.1.1 Why remote monitoring?

'Once a new technology rolls over you, if you're not part of the steamroller, you're part of the road.' – Stewart Brand. (As creator of the Whole Earth Catalog, his ideas were forerunners of the Internet. He is noted as an editor who published writings by many of the now-acknowledged innovative thinkers of today, early in their careers. He is one of the co-founders of the Global Business Network. Brand was also one of a group of 'futurists' consulted in the planning stage of the feature film *Minority Report*.)

From electronic mail and the Internet to satellite and cellular networks, there are more ways to communicate than ever before. People are constantly looking for more information in order to make good decisions and prevent problems. Those who embrace new technologies are likely to reap the benefits of reduced expenses, safer operations and more efficient use of scarce resources.

Remote monitoring is one such technology that has established itself in a number of applications including the monitoring of cathodic protection systems, gas measurement devices, storage tanks, pumps, compressors and site security. With a remote monitoring system, crucial information about the health of a piece of equipment is available at any time, not only at the time of a site visit. Monitoring devices may also employ a function to alert operators immediately when an alarm condition has occurred, thus improving response time and preventing minor problems from developing into more serious situations. While the idea of remote monitoring for corrosion control systems is not necessarily new, there has been a dramatic increase in the application of this technology driven by advances in communications technology, the prevalence of the Internet and a growing shortage of qualified technicians to assess those systems manually.

The production and transportation of oil and gas is a dangerous business. Pipeline companies are constantly striving to improve their safety records to protect their employees and the public. Data from remote monitoring systems is extremely important to operators of oil and gas-related equipment to help them improve the operation of their assets. Many of the large and most respected oil and gas companies in the world are using remote monitoring to improve their operations and safety performance.

The United States National Pipeline Mapping System reports that there are over 1.7 million miles (2.7 million km) of natural gas and hazardous liquid pipelines operated by more than 3000 companies in the United States alone.[1] According to the US Office of Pipeline Safety, 2006 statistics show:

- 102 accidents resulting in $33 352 005 of property damage and two injuries as reported by Hazardous Liquid Operators
- 133 accidents resulting in $47 739 029 of property damage, two fatalities and four injuries as reported by Natural Gas Distribution Operators
- 128 accidents resulting in $22 280 131 of property damage, 16 fatalities and 25 injuries by Natural Gas Transmission Operators.[2]

Careful monitoring of equipment operation allows rapid corrective action, which may help prevent the loss of life and reduce the expense associated with malfunctioning equipment. Closely monitoring corrosion systems also provides more valuable data for broader examination of pipeline safety aimed at predicting failures before they occur. While complying with regulations remains the strongest driver for the remote monitoring of corrosion systems, a growing shortage of qualified labor, safety and operating efficiency are driving increasing application of this technology.

20.1.2 Chapter contents

This chapter addresses remote monitoring of external corrosion control systems. External corrosion control is only one of many remote monitoring applications. It is important to provide a general overview of any remote monitoring system including the critical elements. The goal of this chapter is to help the reader understand the current state of remote monitoring technology, the trade-offs required when deciding upon a particular technology and the challenges of remote monitoring that are particular to corrosion control systems.

It is also important to point out what will not be covered in this chapter. This chapter considers relatively low cost systems that are suitable for the monitoring of corrosion systems. Thus this chapter will not consider Supervisory Control and Data Acquisition ('SCADA') or factory control systems

as those are typically designed for applications requiring a higher degree of reliability and response than corrosion monitoring (e.g., valve control on a petroleum pipeline).

The main application considered in this chapter is the monitoring of a corrosion control system along a piping system including those utilized in the transportation and distribution of oil, gas and hazardous liquids. Many other applications for corrosion control systems exist; however, one must consider the cost justification of using a remote monitoring system for these applications. For example, monitoring corrosion in a processing plant is certainly important, and can be accomplished remotely, but would most likely be done using the plant's existing process control system and/or manually. While a process control system can be considered 'remote' monitoring, such systems are beyond the scope of this chapter.

Except in a cursory sense, this chapter does not consider the corrosion sensor or data probe because they are the topics of the other chapters of this book. This discussion assumes that there is an existing sensor or data probe that requires monitoring and that this data source provides the remote monitoring system with a fairly standard industrial input (e.g., digital signal, 0–5 volts, 4–20 milliamps). In the more specific case of corrosion monitoring, this chapter focuses on the particular challenges of monitoring an impressed current cathodic protection system on a pipeline. Monitoring corrosion sensors in a tank farm is sometimes done remotely, but that application is more often considered as leak detection and, as such, is beyond the scope of this chapter except in a more general sense. Monitoring coupons, or other such indicators of degradation, might also be done remotely if the sensor could provide an appropriate output, but any changes typically happen too slowly for a remote monitoring system to be justified.

20.1.3 Remote monitoring basics

Remote monitoring systems continuously check the condition of field equipment and communicate this information to a central location where it can be routed to others or accessed by those with appropriate security clearance. The essential parts of a remote monitoring system are: the remote monitoring device, the communications network, and the central data warehouse. The central data warehouse is sometimes referred to by a term used in the telecommunications industry: the Network Operations Center (NOC). The remote monitoring device is often called the Remote Monitoring Unit (RMU); it may also be called the Remote Terminal Unit (RTU), but that term is most often reserved for SCADA systems or other more advanced field electronics with sophisticated sensors and programming capabilities.

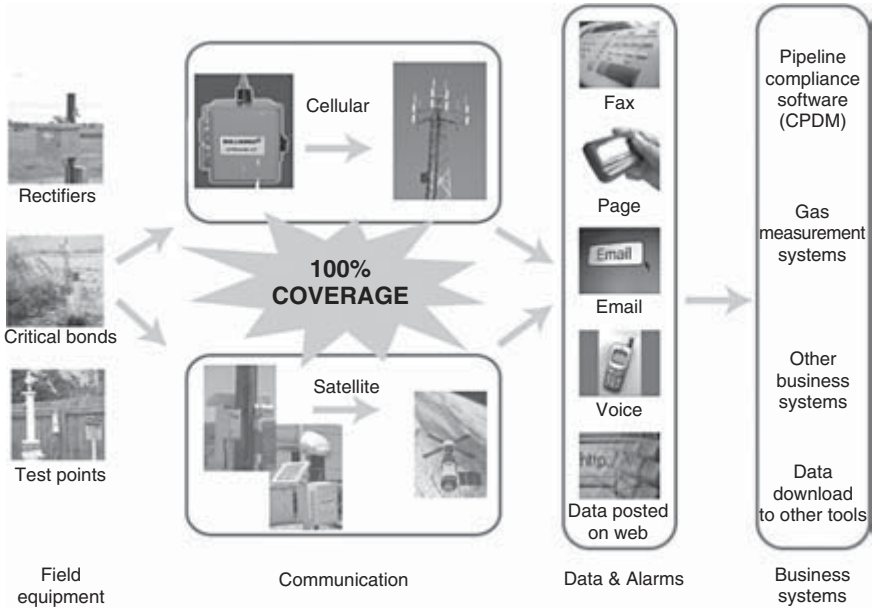

20.1 A remote monitoring system.

The most effective monitoring systems use existing wireless networks to transfer information from an RMU on any remote piece of equipment to the NOC where it is stored in a secure database that is accessible via the Internet. Using a commonly available, user-friendly Internet browser with proper authorization, information can be viewed from the main office, remote sites, or anywhere in the world 24 hours per day. Data may also be automatically transferred to clients by the NOC. In some instances, data is transferred from the field to the NOC, automatically retrieved by the client's information system and published directly to end-users without any human intervention. Most NOCs also provide users with the ability to set up automated notifications via electronic mail, pager, facsimile, voice mail or any combination thereof. Figure 20.1 provides an overview of the essential parts of a remote monitoring system.

The cathodic protection data manager (CPDM) is a data repository with superior capabilities of analysis and reporting used to better manage assets and meet regulations.

20.1.4 Critical decisions in a remote monitoring system

There are several important questions one must ask when considering a remote monitoring system. These can generally be grouped as follows:

1. Data questions. What is the nature of the data you wish to collect? How critical is it? How much needs to be transmitted? How often does it need to be transmitted? What are you willing to spend to gather it remotely?
2. Network questions. What communications network(s) are available? Are the sites you wish to monitor clustered within a small geographic area (e.g., one site, one city) or spread across a country, a continent or the world? Do the sites you wish to monitor move around or are they fixed in one location?
3. Application questions. Is power available at the remote site or required by the sensor(s)? Do you require two way communications with the site allowing for requesting current status 'on-demand' or remote control? Are there any other site or application specific requirements?

Each of these questions impacts one or more essential elements of the remote monitoring system. In the following sections, we consider how the answers to these questions guide one through the trade-offs required by the current limits of technology. The data questions help determine whether a remote monitoring system is suitable for the application or whether SCADA or manual data collection is warranted. These questions also help the user narrow the communications network options. The data requirements and characteristics of the site to be monitored determine the communications network(s) to be employed, which then drives the basic design of the RMU. Finally, the RMU may need to be tailored specifically to the application, which may then cause one to reconsider the communications network and/or the suitability of the application for remote monitoring. In the following sections, each of these questions is discussed in further detail. Once one determines what data are required and how communication will be accomplished with the remote sites, the often-overlooked NOC and the always-underestimated support systems will be discussed.

20.2 Data considerations

As discussed in Section 20.1.2, many applications fall outside of the scope of a remote monitoring system. The characteristics of the data required by the application determine whether a remote monitoring system is technologically or economically viable. The limits of current technology will simply not allow one to consider remote monitoring for every application. Careful consideration of the data requirements will provide a quick answer to the question of viability. Table 20.1 summarizes these considerations.

Table 20.1 Data considerations

Criticality	Informational	Operational	Life support
Cost of monitoring system failure	Low	Low–moderate	High
Rate of data capture from the sensor(s)	Broad range – likely instantaneous	Seconds	Micro-seconds
Frequency of data transmission	Quarterly–annually	Hourly–monthly	Real-time, <1 minute
Amount of data transmitted	Broad range – bits to megabytes	<1 megabyte, typically <100 bytes	Typically >1 megabyte
Maintenance and training required	Low	Low–moderate	Very high
Justifiable system costs	Cost of quarterly or annual site visits	<$5000 equipment <$50/month	>$5000 equipment >$100/month
Typical monitoring system choice	Manual	Remote monitoring	SCADA and/or manual
Example applications	Test points, coupons	Rectifiers, critical bonds	Emergency valves, large compressors

20.2.1 Nature and criticality of the data

Since most corrosion occurs at such a slow rate that instantaneous measurement and communication is not required, data requirements for a corrosion control system are not likely to warrant a SCADA system. Even though the characteristics of corrosion are consistent across industries and applications, in a processing plant environment if control system capacity is available and if the proximity of signal wires makes it viable to monitor with the existing control system, it is likely that the corrosion monitoring need will be filled by the existing system. Most other cases requiring instantaneous response to prevent catastrophic results driven by corrosion fit into the category of leak detection and are not, *per se*, corrosion system monitoring.

The nature and criticality of the data for a corrosion control system is not nearly as important a factor as it is in other applications. For example, the types of remote monitoring system contemplated herein would not be suitable for life support or when a failure of the system could lead to loss of human life or other catastrophic results. The data from a corrosion control system on a pipeline is certainly important, and it is important to know when the system is operating outside acceptable parameters, but it is not critical that such information be delivered with 100% certainty and/or nearly instantaneously because the rate of corrosion on a pipe is not likely

to result in catastrophe if one message is missed. Remote monitoring systems are almost always equipped with programming that ensures the message will be delivered at some point. United States Department of Transportation regulations require corrosion system measurements on a bi-monthly basis for pipeline corrosion system rectifiers, and a remote monitoring system that delivers data and alarms on a daily or weekly basis meets the demands for criticality by a wide margin. More often than not, it is the frequency of data transmission required and the geographic locations of the sites that determine the suitability of remote monitoring for corrosion systems.

20.2.2 Frequency and amount of data transmitted

The amount of data to be transmitted and the transmission frequency required are key factors in determining whether remote monitoring is viable or if another real time control system is demanded. Some applications do not warrant the cost of transmitting large amounts of data over commonly available wireless networks on a daily or hourly basis. Of course, this is changing faster than any other technological element involved in a remote monitoring system; in the time it took to write this sentence, the price of sending a digital photograph from your cellular telephone has probably dropped by 20%. However, even at reduced rates, the cost of sending a megabyte of data any more often than monthly would not be economically justifiable for many applications. In contrast, such data requirements would be warranted when monitoring a 3000 horsepower compressor moving millions of cubic feet (or cubic meters) of gas. Today's corrosion monitoring applications do not require that amount of data or justify the requisite cost of gathering it.

The frequency of data transmission required for external corrosion monitoring often determines whether remote monitoring is justified. In the United States, the Department of Transportation (DOT) regulation contained in the Code of Federal Regulations Title 49, Part 192, Subpart 1 (49 CFR 192.465) require that rectifiers must be inspected six times each calendar year, but with intervals not exceeding two and one-half months. Critical bonds (reverse current switch, each diode and each interference bond whose failure would jeopardize structure protection) must be inspected at the same frequency. Test points and non-critical bonds, however, must be tested at least once each calendar year, but with intervals not exceeding 15 months. Due to the quantity of test points, the remote nature of these devices, and the inherent lack of available power, most companies have not found a cost justifiable way to automatically monitor these points. As costs continue to come down, technology might advance in the future to change this situation. Thus, for cost justification reasons,

most companies to date have chosen to manually monitor test points while automating monitoring of rectifiers and critical bonds.

Of course, regulatory requirements are only one consideration. Monthly or daily monitoring of cathodic protection systems, including rectifiers, test points and critical bonds provides operational data that is useful for the safe and efficient operation of a pipeline. In a worse case scenario, a rectifier or critical bond may fail immediately after a manual visit and remain undetected for up to two and one-half months. Even though corrosion happens at a relatively slow rate, the failure of a corrosion system for a month or more may cause significant damage to the pipe depending upon the general quality of coating and the quantity of 'holidays' (flaws in the coating systems protecting the pipelines) in the specific area of the failure. If this situation occurs, at best, the risk of failure increases, and at worst, the pipe might require mitigation activities that exceed the cost of a remote monitoring system by an order of magnitude. While many monitoring systems are typically configured to report data on a daily or weekly schedule, they might also be configured to monitor the corrosion system continuously and report an alarm condition upon occurrence.

Technology often provides information that users are not prepared to use effectively. Regulations and corrosion professionals are geared toward looking at bi-monthly data to ensure that all readings are 'in compliance'. Daily measurements are of little use today because they would provide 60 times more data than people are prepared to handle. In time however, both the regulations and the technicians may come to see the value of looking for 'out of compliance' events within thousands of data points to more effectively predict the risk of failure on a pipeline.

Generally, in today's environment, remote monitoring is difficult to justify when the data is needed any less often than bi-monthly. However, the justification of a remote monitoring system becomes easier when the sites that must be monitored are more difficult to access manually; i.e. when the sites are very remote, geographically spread over a wide area or in instances where access to the right of way is behind several locked gates.

20.3 Communications networks

20.3.1 Private networks

Once you have determined that the data requirements are suitable for a remote monitoring system, the next step is to determine the best method for communicating with the site. Site locations have a significant impact on the selection of the communications network(s). Table 20.2 presents an overview of commonly available public communications networks. Of course, you may always elect to build and operate your own communica-

Table 20.2 Network options

	Analog Cellular (AMPS)	Digital Cellular (GSM/CDMA)	LEOS	GEOS
Coverage	North America	Metropolitan much better than rural	Worldwide	Worldwide
Data payload	16 bytes	SMS: 160 bytes GPRS: MB+	Typically few bytes to KB	Flexible: few bytes to MB
Message latency	Typically <30 s	Typically <30 s	Often <1 min.	Typically <1 min.
Reliability	Proven reliability over years	Proven reliability over years	Good	Very good
Transceiver cost	US$75–150	US$75–150	US$100–300	US$300–1000
Monthly fees	US$5–25	US$10–50	US$10–50	US$15–100
Risk of obsolescence	Very High (Feb. 2008)	Very Low	Low	Low
Transceiver size	10 cm × 5 cm	5 cm × 5 cm	>20 cm × 10 cm	>20 cm × 10 cm
Commercial providers	Aeris, Cellemetry, carriers	Kore, Aeris, Cellemetry, carriers	ORBCOMM, Iridium	Inmarsat, Globalstar
Installation, ease of use	Very easy; Must determine coverage first	Very easy; Must determine coverage first	Very easy	Requires clear line of site to satellite

Notes: AMPS: Advanced Mobile Phone Service, GSM: Global System for Mobile communications, CDMA: Code Division Multiple Access, LEOS: Low Earth Orbiting Satellites; GEOS: Geosynchronous Earth Orbiting Satellites, MB: megabyte, KB: kilobyte, s: second, cm: centimeter.

tions network. Companies sometimes install a private network to communicate along a pipeline or other transmission system. However, those networks are most often used for SCADA. The operators of those networks do not typically allow traffic from non-critical applications that could potentially affect the SCADA system. Often the SCADA system does not extend to all of the sites one wishes to monitor remotely and the cost of extending the system is prohibitive.

Some utility distribution companies, whether gas, electricity or water, are installing a network for the remote monitoring of utility meters. The network infrastructure is typically owned by the distribution company and may be operated by the distribution company or managed by the supplier of the network equipment. These networks may be ideal for remotely monitoring sites that are owned by the distribution company including corrosion systems. However, similar to SCADA systems, these networks are private, primarily used to collect data from the utility meters

and designed to exclusively serve the owner of the network, and thus, have limited application. While there are gas distribution companies monitoring corrosion systems with such networks, even those systems cannot be economically extended to reach every point requiring monitoring.

Power lines are increasingly used for data transmission. As many external impressed current corrosion systems are powered by alternating current, most rectifier sites are connected to power lines. However, the power lines are owned and operated by the electric utility which is most often not the owner of the corrosion system. Again, the 'power line network' is often privately held by the electric utility and not available to others seeking to use it for data transmission. This is an area of change however as some power companies begin to use their power line networks for broadband Internet access. In addition, standardized, low cost transmitters are not readily available for this type of network. The current highly sporadic availability of such technology makes the 'power line network' a largely private and impractical choice for broad implementation of remote monitoring today. This is an area, however, that warrants continued observation as a practical option.

As with data, several important questions need to be answered before an appropriate network can be selected. One such question has already been covered – if you have your own network available that serves all of your sites, skip the remainder of this section.

20.3.2 Landline and local area networks (LAN)

Please note that the networks presented in Table 20.2 are all wireless networks. Landline networks (also known as Plain Old Telephone Systems or POTS) are of limited value in remote monitoring systems mainly because installation and operating cost can be excessive and it can be quite an ordeal to get the phone company to install a new connection. By definition, most sites that are candidates for remote monitoring are, you guessed it, remote. In this context, remote often means remote from the nearest connection and difficult to reach with a wired system. The explosion in availability of reasonably priced, reliable, publicly available wireless networks over the last 20 years has made POTS obsolete as a mainstream choice for remote monitoring.

Also note that the networks in Table 20.2 are all wide-area networks (WAN). Some LAN technologies like Bluetooth® wireless, with a range of only a meter or two, have such a limited range as to be obviously unsuitable for 'remote' monitoring. But what of technologies like spread spectrum or WiFi with a range of several kilometers? Are those networks WAN or LAN? Are they suitable for remote monitoring? For most remote monitor-

ing applications, the answer is 'no'. Unless the remote sites you wish to monitor are clustered in a relatively small geographic area, e.g., solely within one town or city, such networks are unsuitable. In the case of a pipeline covering 100 km, a single network of the type shown in Table 20.2 is clearly the network of choice. In applications covering a territory, country, continent or the world, one or more of the networks listed in Table 20.2 will provide the best balance of coverage, reliability and cost.

LAN technologies may be very useful in gathering data from a number of sensors within a small area such as a tank farm or wellhead. In such cases, it is much more cost effective to use low cost wireless LAN transceivers to communicate from the individual sensors to a central location equipped with a WAN radio for communication to the NOC. The alternatives would be to 'hard-wire' each sensor to the central WAN device or to put a WAN radio at each sensor. Hard-wiring is expensive, time consuming and sometimes must be installed in protective conduit to meet electrical code and/or regulatory requirements. Given the cost difference between WAN and LAN transceivers (US$50–100 or more), using LAN transceivers is the most effective route when there are multiple sensors at a remote site that are located more than a meter or two away from each other. This type of configuration would likely be the most effective route to monitoring corrosion sensors at a tank farm. In this case, since a WAN transmitter is still required to get data from the farm to the NOC, the ensuing discussions are still relevant. Likewise, there may be corrosion systems deployed at a wellhead and often there are many other sensors within the wellhead that need to be monitored. Tying LAN transceivers to each point, including the corrosion system, into a single WAN transceiver RMU that communicates to the NOC is likely to be the most cost effective solution.

20.3.3 Fixed versus mobile sites

At this point, you have determined that your application involves monitoring a number of remote sites that are geographically dispersed (i.e. more than a few kilometers, more than one or two metropolitan areas). The data you require is not critically important, you do not require more than about one megabyte of data each month or several bytes each day, and you do not own a private network that reaches all of the sites you wish to monitor. Before moving on to choosing one or more WAN for your application, consider whether the application involves fixed points or mobile sites.

It is difficult to imagine a corrosion monitoring application that would be mobile. While one may wish to monitor corrosion on a vehicle, e.g., a piece of heavy equipment, it is unlikely that one would require that data while the vehicle is moving. Corrosion is not likely to occur quickly enough

to require that data on a daily or weekly basis in such a case. Example monitoring applications involving mobile remote assets include capturing and communicating the location and key operating parameters of heavy equipment, vehicles and storage containers. Mobile applications have different needs than fixed points. Most often, multiple WAN must be employed to ensure that contact is maintained with the mobile asset at all times. Another important difference is that mobile assets are more easily maintained; i.e. at some point, they are likely to return 'home' where they can more easily be upgraded, repaired or maintained.

The best (and potentially worst) aspect about fixed point monitoring is that the asset does not move. It is typically easier to select one WAN for each fixed site since that WAN, once installed, is likely to remain available at the site for ten years or more because of the enormous fixed cost involved with installing the WAN. The problem with fixed points is that any maintenance or repair requires a site visit. Remote monitoring is most valuable at the most remote sites. Therefore, any visit for repair or maintenance at such a site is likely to be very expensive. In extreme cases, the visit may require transportation by boat or aircraft. Reliability therefore becomes an important factor in the selection of a WAN and the design of the remote monitoring device for fixed sites. It should be noted however, that it is becoming increasingly easier to perform remote diagnostics, repair or firmware upgrades on fixed sites as more bandwidth becomes available at increasingly reasonable prices. As the corrosion monitoring application is likely to be a fixed site, e.g., a rectifier on a pipeline cathodic protection system, the remainder of this section will focus on selecting a WAN for fixed points and mobile asset monitoring will be ignored from this point forward.

20.3.4 WAN obsolescence

Note that the Advanced Mobile Phone Service (AMPS) listed in Table 20.2 has a very high risk of obsolescence. The detailed standards for AMPS, also known as 'analog' cellular service, were established in 1981 as the first standardized cellular service in the world. It uses an 800 MHz to 900 MHz frequency band and a 30 kHz bandwidth for each channel as a fully automated mobile telephone service. The AMPS control channels used for data transmission are different from the 'talk channels'. The control channels transmit data only, so they have voluminous message handling capacities and are extremely robust due to the fact that the cellular telephone network providers (also commonly known as 'carriers') use this technology to determine who and where you are so that they can charge accordingly. The key advantages to using AMPS control channels for remote monitoring are: seamless coverage within North America, low cost service and transceivers,

near real-time connectivity (very little latency), and robust and proven technology. This combination of attributes resulted in over 25 million AMPS-based remote monitoring devices being installed in North America. However, the technical advantages of digital service over analog led the wireless carriers to lobby for the removal of the requirement to provide AMPS. The US Federal Communications Commission has announced that carriers will no longer be required to provide AMPS after February 2008. For this reason, AMPS would no longer be a wise choice for remote monitoring. As it has been perhaps the most widely deployed WAN choice for many years, AMPS is shown in Table 20.2 for comparison.

Wireless telecommunication is marked by rapid technological change. As stated earlier, such change can make choosing a technology for fixed point remote monitoring a challenge. Hence, Table 20.2 attempts to focus on networks that appear to be relatively stable and without significant risk of technological obsolescence in the next decade or so. However, the reader is advised to remain aware of technological shifts in WAN technology. As an example, you may note that Cellular Digital Packet Data (CDPD) does not appear in Table 20.2. Just a few years ago, before the explosion in digital cellular services, CDPD would have been considered a viable option for remote monitoring. However, CDPD is no longer available and any remote monitoring devices employing that WAN must be removed from service and upgraded to a new WAN transceiver.

Also note that Low Earth Orbiting Satellite (LEOS) would not have been listed in Table 20.2 had it been published five years ago. The only commercial providers of such service were in bankruptcy, and thus, the technology was not a commercially viable option. However, the providers have emerged from bankruptcy, the technology has emerged as a leading option and both the providers and the technology appear to be stable for at least the next few years.

20.3.5 WAN choice for fixed sites

All of the networks listed in Table 20.2 are suitable for remote monitoring requiring the exchange of hundreds of bytes up to one megabyte over the course of a month from fixed points spread over a large geographic area. Other important factors to consider when selecting one or more WANs are coverage area, transceiver cost, monthly fees, network/carrier reliability, network latency and size of the transceiver.

Networks fall into one of three general categories: digital cellular, LEOS or Geosynchronous Earth Orbiting Satellites (GEOS). Digital cellular service is complicated by the existence of two competing standards for service: Global System for Mobile communications (GSM) and Code Division Multiple Access (CDMA). (Note: while there are still some systems

deploying Time Division Multiple Access transceivers (TDMA), those systems are obsolete.)

Each 'flavor' of cellular service requires a different transceiver so you must know what coverage is available for each in order to gage the viability for a given application. Because it is more common globally, GSM transceivers are typically 10–50% less expensive and smaller than CDMA. However, GSM service is further complicated by the presence of four different bandwidths: two for North America and two for the rest of the world. Transceivers that employ all four bandwidths are increasingly available, but it is advised that you become aware of the different 'flavors' of GSM and the availability of the various bandwidths when selecting a network for any given location. An exhaustive discussion of GSM versus CDMA service, including the relative merits of the technology and the current available coverage, is beyond the scope of this chapter. A couple of useful references are provided in the bibliography.

For most applications, it is unlikely that 100% of the sites you wish to monitor will be covered by any one WAN. Even if all of the sites were located within metropolitan areas covered by the same type of digital cellular service, it is likely that there will be one or two sites that cannot connect to the network for some site specific reason. It is desirable to use the minimum number of WAN possible to cover 100% of the sites for a number of reasons, including: volume discounts on equipment and service, training required on device installation and system configuration and the cost of maintaining multiple WAN technologies. Consider the specific needs of the application in question and select the network that fits the majority of those sites as the primary network, but be aware that it is likely that a secondary WAN will be required for complete coverage.

Cost is often a primary WAN consideration – both for the monitoring device and the service – but is also the factor that changes most rapidly. Just a few years ago, LEOS transceivers were prohibitively expensive for some applications at an approximate cost in excess of US$300. However, that cost has been cut in half or more resulting in LEOS becoming a much more competitive option to digital cellular systems. GEOS transceivers are more expensive than LEOS transceivers by an order of magnitude (typically 2–4 times) because of the power required to communicate with satellites that are much farther away.

The size of the transceiver, while typically of less importance in external corrosion applications, has a similar story as cost. The main benefit of a smaller transceiver is that it allows for a smaller RMU that is less obtrusive and more easily hidden to protect it from vandalism. GSM transceivers are the smallest in size and getting smaller every day. A small transceiver allows for a smaller package and often reduces the

total cost of the RMU. CDMA transceivers are not much larger than GSM transceivers and thus are unlikely to be at much of a disadvantage for most applications. LEOS transceivers are rapidly shrinking in size and cost as deployments increase. In most remote external corrosion applications, the half-wave whip antenna commonly utilized with the LEOS is a suitable solution because vandalism is less of a concern. However, in certain applications a lower profile LEOS antenna is preferred and available. GEOS transceivers are the most difficult to deal with from a size perspective; for some networks, the antenna alone may be one-half meter square. Vandalism is often more of a concern in metropolitan areas where a digital cellular service is likely to be readily available. Thus, transceiver and antenna size are other considerations in the selection of a WAN for a remote monitoring system, and it is possible that the deployment of multiple WAN types may be required.

20.4 Application specific requirements

20.4.1 Power requirements

The RMUs require power to operate. Thus, understanding the power requirements of the monitoring site is one of the most important aspects in designing and selecting a system. Many sensors will have their own power supply and will not require power from the RMU, but it is important to make sure that is the case, because an RMU is often designed to provide power solely for itself and some sensors can require a significant amount of additional power.

If the RMU only needs to power itself, the next choice is to determine what type of power is available. In many corrosion applications, alternating current (AC) power is used to power the external corrosion control system. AC power is rectified to direct current (DC) power, adjusted to the appropriate level and applied to an anodic ground bed that is used to flow direct current into the metal structure to prevent corrosion. Most remote monitoring applications today are in fact measuring the output current and voltage provided by the rectifier to the ground bed. If there is AC power at the rectifier, the RMU has a ready power source available and thus can avoid the use of a standalone power system consisting of batteries and/or solar panels. Batteries, even those that are recharged by solar power, need to be replaced periodically and thus add maintenance cost. However, few savings in RMU cost are achieved through the use of AC power over batteries as the electronics in the RMU require additional components to make effective use of the AC and protect the electronics from power fluctuations.

At those sites where AC power is available for remote monitoring, an important advantage emerges in that unlimited power allows for near-immediate two-way communications between the RMU and the NOC. Most battery powered designs provide limited power and thus the transceiver is turned off or put in standby mode until a data transmission is required by an alarm condition or scheduled report. Batteries can be sized such that the transceiver may be left on all the time, but such designs are often economically impractical. Transceivers are being introduced that require less power all the time, and thus, it is becoming easier to leave those devices on for at least some portion of each day, but even that type of design does not allow for immediate two-way access to the RMU on demand.

Two-way communications between the RMU and the NOC provide a number of important features. First, it allows the user to check the status at the remote site at any time instead of waiting for the RMU to make a scheduled report. Second, it allows the NOC to send firmware and/or configuration program updates remotely. For fixed point locations, this feature is particularly attractive, because it allows for trouble shooting, reconfiguration and new features without a site visit. Mobile sites will eventually return 'home' where such activities can be completed at low cost, but it can be expensive to accomplish those items in fixed point installations.

Finally, two-way communications also allow for remote control. A user may wish to take action at the site remotely through the RMU instead of passively monitoring the status of the site. Examples of such actions are activating ancillary equipment such as turning on pumps, adjusting the operating parameters of a compressor or opening a valve. The need for remote control in corrosion applications will be discussed later in this chapter.

Often, the user will want to know when AC power is off at the site since it means that the site equipment is no longer operational or is relying on limited back-up power supplies. If the RMU is also relying on AC power, it must be designed with a back-up power supply of its own in order to report the outage. This requirement further reduces the cost differential in the AC powered RMU compared to a battery powered unit.

Many remote monitoring applications, however, do not have AC power readily available. Most critical bonds and test points are simple test stations inside plastic risers sticking out of the ground in the middle of a field without any power supply in sight. In those applications, the RMU is typically powered by batteries. In most cases, the RMU will be located where there is enough sunshine to power a solar panel used to recharge the battery. The use of such rechargeable batteries is most economical as they require less frequent replacement and often last for the useful life of the RMU. In cases where the RMU is installed indoors, or where vandalism of the solar panel is a particular concern, disposable lithium batteries are often

used. Maintenance of the power supply is another factor that is more important for fixed sites than mobile applications.

20.4.2 Environmental requirements

Most remote monitoring applications are outdoors, and the RMU must be protected from the elements to insure reliable operation of the electronics and transceiver. The environmental requirements and methods used to protect the RMU are similar to those of many other outdoor industrial applications. The RMU must be designed to handle wide variations in temperature and relative humidity. Choosing an RMU with a suitable enclosure for the conditions is important. Many enclosures also provide latches that may be locked to prevent tampering.

An environmental concern that is more specific to external corrosion monitoring is protection from power surges. Essentially, the pipelines are huge conductors capable of carrying large surges of current that can damage sensitive electronics if not properly protected. Sources of these surges can include lightning hitting an exposed portion of the pipe creating large potential energy or other external sources such as high voltage AC induction. Various techniques exist to protect the electronics, but as always, there is a cost/benefit tradeoff. One technique that is commonly used is to keep the RMU inputs isolated from the pipeline at all times except when a measurement is in process. This technique reduces the probability of failure significantly. In lightning prone areas, it might be necessary to add external lightning protection devices to the remote monitoring inputs to protect them from likely close proximity lightning strikes.

20.4.3 Input requirements

An RMU is typically designed to monitor a limited number of inputs from sensors at the site. Most sensors at remote sites provide a standard type of input that can be grouped into three categories: digital, analog or serial. Digital inputs are often used to sense a simple state change: ON versus OFF, OPEN versus CLOSED, 1 versus 0. Analog inputs are often used to measure a value and most analog sensors provide a standard range of 0–5 volts or 4–20 milliamps. Most RMUs are designed to accommodate several digital inputs and are limited to monitoring state changes. Some RMUs have the added capability of being able to monitor analog inputs along with digital inputs and can therefore be used to monitor a wide variety of applications. Analog inputs are required for external corrosion system monitoring. A general monitoring example of how analog signals are utilized would involve a level sensor on a storage tank that may be calibrated to provide a 4 to 20 milliamp current signal relating to the actual level. The signal is

converted to a voltage signal acceptable to the RMU such that four milliamps equates to one volt or empty and 20 milliamps equates to five volts or full. The voltage measured by the RMU at any given point in time is assessed for alarm conditions. The voltage value is also potentially transmitted to the NOC on a scheduled basis and is converted to a volume measurement by knowing the size of the tank being monitored at the site.

Serial connections are often used to allow the RMU to communicate with an intelligent device at the site. Many intelligent industrial devices employ a standard language called Modbus. According to Wikipedia: 'Modbus is a serial communications protocol published by Modicon in 1979 for use with its programmable logic controllers (PLC).'[3] It has become a de facto standard communications protocol in industry and is now the most commonly available means of connecting industrial electronic devices. The main reasons for the extensive use of Modbus over other communications protocols are:

1. it is openly published and royalty-free
2. it can be implemented in days, not months
3. it moves raw bits or words without placing many restrictions on vendors.

So, an RMU with a serial connection and Modbus capability can be used in a wide variety of applications including gas volume correctors, electronic flow measurement systems, gas pressure monitors or more sophisticated level sensors. Thus an RMU equipped with a serial connection may be able to determine not only the level of the tank, but also its contents, temperature, pressure and the last time the valve was opened or closed.

Basic corrosion monitoring typically involves reading two analog inputs from a rectifier. Typical measurements at the rectifier include DC output voltage and DC output current from the rectifier. Current is determined by taking a voltage reading across a 'shunt' of known resistance. That voltage level is then scaled to represent the appropriate current level once the signal reaches the website. Required rectifier output voltage levels are determined by a number of environmental and pipeline construction factors. The DC output voltage of the rectifier may be sensed and converted to a range that the RMU accepts, and then, the voltage measured by the RMU at any given point in time after transmission to the NOC can be scaled to display on the website the actual DC voltage level leaving the rectifier. Like the current reading, this value is scaled for display at the website. Sometimes, additional measurements like test point and critical bond voltage levels might also be taken by the RMU at the rectifier. These measurement characteristics are described below.

As discussed earlier, test point and non-critical bonds (places where two or more pipelines cross) may not warrant the cost of remote moni-

toring systems because of the relatively infrequent need for the data. However, when these points are located in close proximity to the rectifier, the RMU must also have the capability to read them. Regardless of whether these test points and non-critical bond measurements are taken along the pipeline or at the rectifier, the characteristics are the same. These measurements require bi-polar analog inputs since these voltages are typically negative in polarity. They are also usually at a relatively low level; i.e. usually zero to two volts in magnitude. It is important to obtain a clean signal, and thus, AC filtering is a requirement.

20.4.4 Remote control; output requirements

In Section 20.4.1, the importance of two-way communications was briefly discussed. In corrosion monitoring, two-way communications are needed for remote control to support two specific needs: (a) turning the rectifier on and off at specific intervals and (b) remotely adjusting the rectifier to tune the corrosion control system.

While basic monitoring of rectifier voltage and current is employed in the majority of remote sites, there is increasing demand for remote synchronized current interruption (i.e. using relays to cycle rectifier output voltage at specific timing intervals). The RMU typically accomplishes this by enabling or disabling a program within an optional current interrupter that uses the Global Positioning System (GPS) to provide timing synchronization. Each current interrupter is pre-programmed with a variety of interruption schedules. The user can remotely trigger a specific interruption program through the RMU. Significant savings are available due to the elimination of a costly manual interruption set up. When a series of rectifiers are interrupted in a concurrent, synchronized manner, additional data can be gathered on the operation of the system via manual survey techniques using handheld computers with the same GPS time synchronization techniques. These devices are equipped with integral digital voltmeters to allow for collecting voltages along the expanse of the pipeline at close intervals for later analysis of the viability of the impressed current protection. Once collected, this data is moved electronically into a historical database for analysis, remediation and regulatory audit purposes.

In the United States, the DOT has established rules regarding External Corrosion Direct Assessment (ECDA) as part of the holistic pipeline integrity management requirement. Pipeline companies are expected to utilize at least two techniques to assess whether their pipelines are properly protected from corrosion. Generally, one chosen technique is focused on finding and sizing ‘holidays’. The other technique described directly above is intended to assess where the pipeline is being protected

by the cathodic protection system and where it is not in order that remediation may be achieved. This technique is commonly known as Close Interval Survey (CIS) or Close Interval Potential Survey (CIPS). Readings are taken every few feet while the power to the pipeline is cycled so that a pair of readings at each point (Instant On and Instant Off) might be obtained. The need to collect this information from at least two ECDA techniques and analyze the results concurrently is already a DOT requirement.

The other important use of two-way communications in corrosion monitoring is to allow for adjustment of auto-potential rectifiers. By using an analog output from the RMU, the user can command that the set point of the rectifier change to support changing environmental conditions. Most often, the need for this type of adjustment is driven by extreme variation in ground moisture that will result in a need for more or less power output from the rectifiers.

20.5 NOC and supporting systems

20.5.1 Network operating center basics

The NOC is an often overlooked piece of the remote monitoring system. The RMU and WAN most often get lots of attention, because that is where specific design questions must be answered prior to implementation and is most often where the system breaks down. However, the RMU is just an attractive doorstop without the NOC to gather, decode, store and disseminate the information gathered remotely. The point of remote monitoring is to improve the speed of collection, accuracy and value of the data measured at the remote site. The NOC is responsible for delivering information. An NOC typically includes a significant investment in computer hardware and software – machines that are connected to WAN and the Internet 24 hours a day and seven days a week, a database to store the data and software to distribute information.

20.5.2 Data security and redundancy

In some remote monitoring applications, security of the data during transport can be a very important feature. For example, if detailed gas measurement data could be intercepted, a competitor might gain an important advantage. However, in most practical cases, the data being collected by remote monitoring has limited value even if it could be understood by the intercepting party. Most of the data collected is encoded and compressed by the RMU in order to save money by using less bandwidth. Even if the data packet sent from the RMU was readily transparent, the

WAN employed likely has extensive data encryption to provide security during transport. While this question may come up in remote monitoring discussions, it is of little importance for monitoring corrosion systems.

In some non-corrosion remote monitoring applications, NOC uptime is critical. Designing an RMU and choosing a WAN for maximum reliability will be efforts made in vain if the NOC is not on-line because of power outages, software defects or lost connectivity. For critical data needs, it is important to have a back-up NOC that is automatically set in operation, with a current copy of all data collected, whenever the primary NOC is down for any reason. For corrosion monitoring however, this is of less concern for all of the reasons discussed in earlier sections about the nature of the data collected in remote monitoring.

Some applications rely on the NOC to be the primary storage site for operational data. In some remote monitoring applications, it may be critical that the NOC database maintain a long history of the data collected from RMU over time. However, most applications, including corrosion monitoring, allow the user to export the data from the NOC database to operational software for further analysis and warehousing. In the case of corrosion monitoring, the data is often exported to a package such as the Pipeline Compliance System™ software where it is archived for regulatory reporting and analyzed against other corrosion data, such as manually collected test point readings, to identify system defects. Storage capacity therefore is not typically an issue with the NOC database unless one is relying on it to be the primary data warehouse.

20.5.3 Data export, analysis and grouping

Once collected, decoded and effectively stored within the NOC database, users must be able to manipulate the data. As discussed above, data is most often exported from the NOC to other operational software for further processing and analysis. The NOC software must make data export possible in a variety of formats. The optimum system allows for the data to be automatically exported and electronically delivered to client business systems. It is important to understand how one wants to use the data collected by the remote monitoring system and ensure that the NOC can accommodate effective and correct delivery of the data.

Some companies may not have access to operational systems for analysis of the data collected from the remote monitoring system. In that event, it is important to ensure that the NOC software provides analytical tools. Those tools may be as simple as providing for export to a common commercial package like Microsoft® Excel® software or as complex as providing route scheduling features and Graphical Information System support to map locations.

Users often wish to group remote sites according to departments or regions formally responsible for manually collecting data. For example, a pipeline may be separated into different operating areas with different management, personnel and resources responsible for maintaining the corrosion system on that segment of pipe. The NOC software must be capable of grouping RMUs for appropriate visibility by the supporting personnel. The optimum system provides security features that allow for varying levels of access to the data according to functional need. Some users might be allowed to make changes while others are only allowed to view data. Finally, visibility might be controlled according to breadth of responsibility, so a regional manager might have access to a broader range of data than a local technician.

20.5.4 Alarm notifications

Some remote monitoring applications exist solely to screen for alarm conditions – to provide an indication that operating characteristics are outside normal conditions. Some remote monitoring systems allow for the periodic collection of data and the essential capability of immediately notifying users that an alarm condition exists at the site. Corrosion monitoring applications are not particularly time critical; however, it is still important to know that a problem exists at the remote site as soon as it occurs. Users should be able to program any number of notification methods including voice, facsimile, electronic pager, numeric pager and electronic mail. The message should provide the recipient with basic facts about the alarm condition so that effective action may be taken. This information should be delivered reliably. Clients should be offered the option of escalating the notifications – if the recipient does not acknowledge receipt of the alarm notification within a certain amount of time, the NOC sends additional notifications to ensure that the alarm condition is communicated and addressed.

False alarms can be a significant problem in remote monitoring systems and can result in excessive communication costs if not managed properly. The RMU must have the ability to distinguish a true alarm from a false alarm. This is often accomplished by requiring that the alarm condition persist for a given time period. Likewise, false alarms can also be controlled by using a technique called ‘deadband’ whereby an input is not allowed to alarm again until certain characteristics have been met.

20.5.5 Supporting systems

If the NOC is often ignored, supporting systems are almost always ignored. An effective remote monitoring system includes a software system that

supports production of RMU and ensures that the NOC knows what devices may be reporting to it. Each RMU must be married to its transceiver and stored in the NOC database before it can report from the remote site. Its transceiver must also be activated on the WAN so it can be tested 'end to end' prior to shipment. These processes must be accomplished correctly and efficiently prior to installation at the site. Such systems also must provide for pre-programming of parameters according to client specifications so that the user does not have to do so on-site.

Like it or not, products break and must be repaired. An effective monitoring system is tied to a return processing system that ensures returns are processed effectively and network fees are properly assigned while the RMU is in repair. A user should be able to tell which RMUs are in repair, how long they have been there, when to expect them back and be confident that it will not be charged for communications fees while the RMU is in repair.

Finally, a remote monitoring system needs an effective billing system for communications fees. Clients need to be billed accurately for tens or thousands of RMUs transmitting megabytes worth of information each month. Clients may wish to group RMUs for billing to different departments or companies and will need to see detail on billing charges.

20.6 Sources of further Information

1 'Office of Pipeline Safety: Pipeline Safety Initiatives' 2007. http://ops.dot.gov/init/init.htm#safety (19 January 2007).
2 'Office of Pipeline Safety: Pipeline Statistics' 2007. http://ops.dot.gov/stats/stats.htm (19 January 2007).
3 'Modbus' 2007. http://en.wikipedia.org/wiki/Modbus (19 January 2007).

20.7 References

Argent, Colin, Kevin Prosser, David Norman, Peter Morgan and Roger Weatherhead, *Macaw's Pipeline Defects*, Andover: Yellow Pencil Marketing. 2003.
Baboian, Robert, ed, *NACE Corrosion Engineer's Reference Book*, 3rd ed. Houston, TX: NACE Press. 2002.
Bedell, Paul, *Wireless Crash Course*, 2nd ed. New York: McGraw Hill. 2005.
Gralla, Preston and Eric Lindley, *How Wireless Works*, 2nd ed. Indianapolis, PA: Que. 2005.
Roberge, Pierre R, *Corrosion Inspection and Monitoring*, Hoboken, NJ: John Wiley & Sons. 2007.
Schwartz, Mischa, *Mobile Wireless Communications*, Cambridge: Cambridge University Press, 2005.

21

Models for predicting corrosion

N. SRIDHAR, Det Norske Veritas, USA

21.1 Introduction

Monitoring and modeling may be considered as components of an Integrated System Health Management (ISHM) approach (Fig. 21.1). In this intertwined approach, monitoring and modeling constitute the assessment aspect of ISHM, while feedback and decision-making ensure that the monitoring and modeling tools are revised in order to provide greater confidence to the prognosis and appropriate decisions to repair or mitigate the corrosion damage. Communication in terms comprehensible to other teams implementing these decisions is also important. If one considers the timeline of performance, monitoring provides information on the current extent and mode of corrosion. Inspection techniques (e.g., ultrasonic examination) provide information on total material loss or defect size due to corrosion that happened in the past. The inspection information has also been referred to as a 'lagging indicator' (Hedges *et al.*, 2006) because by the time the defect indications appear, significant corrosion may have already taken place (Fig. 21.2). Monitoring tools (e.g., electrochemical sensors), provide information on damage that is occurring at present, the time resolution of which depends on the specific technique used. If the sensor readings are integrated, material loss due to corrosion that occurred in the past can be determined. Thus, the inspection and monitoring tools provide the diagnostic elements of system health management. However, inspection and sensors by themselves cannot predict the future state of the system – a corrosion model is required for this purpose. Thus, models may be regarded as the 'leading indicators' or the prognosis elements of an ISHM program (Fig. 21.2).

In an approach developed by the Electric Power Research Institute (EPRI) in the United States for assessing the remaining life of power plant equipment, a three level process is identified (Dooley, 1990). In Level 1, essentially a review of equipment design, visual inspection, and simple empirical modeling using design parameters is considered

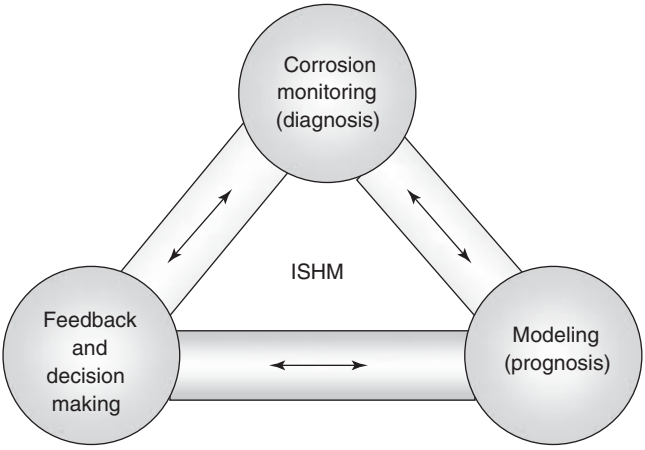

21.1 The three elements of an Integrated System Health Management (ISHM) relevant to corroding systems.

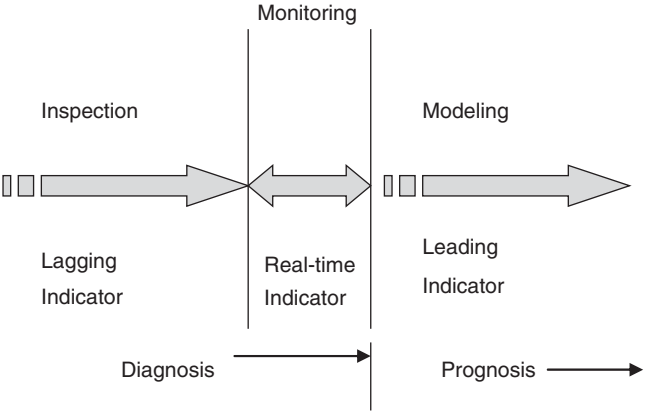

21.2 Elements of corrosion assessment.

sufficient for estimating remaining life. If key information on equipment history and operations is missing or if visual examination indicates that the expected life is less than the design life, then a Level 2 assessment is recommended. In Level 2 assessment, non-destructive examination and/or monitoring techniques are employed to characterize defect sizes and corrosion growth. In Level 2 as in Level 1, simple models are used to predict remaining life, but the models use operating parameters, rather than design parameters. If Level 2 assessment is not considered sufficient, then a Level 3 assessment is recommended. The Level 3 assessment involves root cause analysis, testing, and detailed modeling. Thus, in the EPRI

framework, as in ISHM, modeling forms an integral part of health management.

This chapter will outline how models can be used along with monitoring to predict the future state of a system. Models may derive functional relationships from empirical data on corrosion using a variety of statistical methods or use fundamental laws of processes involved in corrosion (also called variously mechanistic, physics-based, physicochemical, deterministic, etc.). Typically, the empirical models cannot be extended beyond the range of parameters used to develop the models. Section 21.2 provides some examples of empirical models. Fundamental models, in contrast, provide a framework through which predictions can be extended beyond the limits of the data. It must be emphasized however, that fundamental models also require experimental data. Indeed, elaborate models may contain many parameters that require 'calibration' from experimental data because independent measurements of these parameters are either difficult to obtain or do not yet exist. However, these data may be generated under conditions not directly related to the actual application, thus providing greater freedom from the constraints of the application. Furthermore, good modeling practice ensures that even where calibration of the model parameters is done, verification of the model predictions is performed against independent data sets.

Fundamental models may be developed for different size and time scales. The atomic and molecular level models focus on the interactions between the environment and the material at the atomic/molecular size scales. Examples of such models include the point defect model (PDM) for passive dissolution and localized corrosion initiation and molecular dynamics models for examining the interactions between inhibitors and metal surfaces. Because they consider detailed interactions at atomic/molecular levels, they are also typically constrained to short time scales. Fundamental models can also exist at macroscopic scales. Examples of such models include crevice chemistry models and mixed potential models. The time scales of these models can vary from minutes to years. Section 21.3 provides examples of fundamental models. Often, fundamental models have to be 'abstracted' into simplified numerical or analytical schemes in order to enable system-level assessments. Section 21.4 discusses integration of models with monitoring and future directions in ISHM of corroding systems.

21.2 Examples of empirical models

Because empirical models often mimic a particular application condition, the variety of empirical models is almost endless. Therefore, this section provides some examples from different corrosion applications. Also, models

to extract corrosion rate information from electrochemical impedance, noise, or other electrochemical measurements are discussed elsewhere in this book and therefore will not be covered in this chapter. The focus will be on time dependence of corrosion rate predicted by the models since this is of greatest importance in prognosis based on sensor measurements. Mention will also be made of empirical models that address extrapolation with respect to area and environmental parameters.

21.2.1 General corrosion models for natural environments

As discussed in Chapter 2, corrosion is seldom completely uniform and most of the corrosion that is considered to be uniform corrosion or general corrosion has some waviness to the morphology. Therefore, the term general corrosion is invoked here to indicate that the corrosion is governed by a relatively uniform spatial distribution of anodic and cathodic sites, in contrast to localized corrosion where the anodic and cathodic sites are separated spatially by a significant distance (see Chapter 2.2 and Sections 21.2.4 and 21.3.3 for more details). General corrosion rates follow a variety of rate laws depending on the rate determining steps for cathodic and anodic processes.

For atmospheric corrosion, a number of empirical rate laws have been proposed on the basis of long-term exposure data. The simple power law (Equation [21.1]) is most often used, but tends to under-predict the corrosion rate at short and long time periods.

$$CR = b_0 t^{b_1} \qquad [21.1]$$

Where CR is the corrosion rate, b_0 and b_1 are constants. A major international program called ISO CORRAG has developed methodologies to predict the corrosion behavior of iron and zinc in various atmospheric conditions (Konatkova *et al.*, 1995) using Equation [21.1] as the form of corrosion rate function. As a part of this program, Dean and Reiser (2002) examined eight-year atmospheric corrosion data on zinc panels from 51 sites around the country in the United States (marine, rural, urban and industrial sites) out of which they selected 23 sites to develop a regression equation for calculating corrosion rate. The corrosion rate of zinc was calculated as a logarithmic version of Equation [21.1]:

$$\text{Log}\,(M) = a + b\log(time) \qquad [21.2]$$

Where 'M' stands for metal loss per unit area (in micrometers) and the constants 'a' and 'b' are constants that depend on the specific location. Based on the 23 sites examined, they developed a regression equation for 'a' and 'b':

Table 21.1 Calculated corrosion rate of zinc using Equations [21.1] to [21.4]

Site	SO_2, mg/m^3	Cl, mg/m^2.d	TOW, h/Y	Parameters b	Parameters a	Corrosion loss, mils 1Y	Corrosion loss, mils 75Y
Kure Beach, NC, USA	0.61	184	4289	0.81	0.22	0.07	2.18
Los Angeles, USA	1.28	0	4003	0.75	0.15	0.06	1.39
Panama Coastal	3.3	619	7598	0.93	0.51	0.13	6.98

Note: 1 mil = 25 μm

$$b = 0.804 + 7.72 \times 10^{-4}\,(so_2) - 1.48 \times 10^{-5}\,(TOW) + 3.77 \times 10^{-4}\,(Cl^-) \quad [21.3]$$

$$a = 0.007 + 42.6 \times 10^{-4}\,(so_2) + 3.43 \times 10^{-5}\,(TOW) + 3.68 \times 10^{-4}\,(Cl^-) \quad [21.4]$$

Where *TOW* is the average Time of Wetness in hours per year when the temperature is greater than 0 °C and relative humidity (RH) is greater than 80%, the sulfur dioxide is the average concentration in mg/m^3, and the chloride is the average deposition rate in mg/m^2 day. Therefore, the corrosion loss can be calculated at any given location if the above parameters are known. An example calculation is shown in Table 21.1 for zinc at three different locations to illustrate the wide range in corrosion behavior. Galvanized iron corrodes at a slightly higher rate than zinc due to the porous nature of the zinc coating and the galvanic action between the iron and zinc that accelerates the zinc corrosion.

The representation accuracy of Equation [21.1] can be improved (McCuen and Albrecht, 1994) by the power-linear model with constant intercept (Equations [21.5] and [21.6]), where the power model represents the short-term data and the linear model represents the long-term data, the two models being equated at a transition time period.

$$CR = b_0 t^{b_1} \quad \text{for } t \le t_c \quad [21.5]$$

$$CR = b_0 t_c^{b_1}\left[1 + \frac{1}{t_c} b_1 (t - t_c)\right] \quad \text{for } t > t_c \quad [21.6]$$

The choice of transition time is critical to the accuracy of the model (McCuen and Albrecht, 1994). Therefore, a variable intercept model (Equations [21.7] and [21.8]), where the transition time is another parameter that has

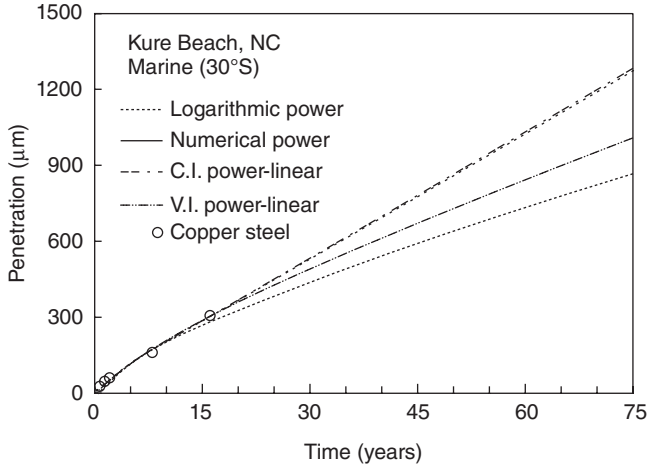

21.3 Atmospheric corrosion penetration depth predicted by three different empirical models at the end of a 75-year design life. The data points shown were used to generate the three models (McCuen and Albrecht, 1994).

to be numerically fitted, provides greater accuracy in representing the data.

$$CR = b_0 e^{-b_2 t} t^{b_1} \quad \text{for } t \le t_c \qquad [21.7]$$

$$CR = b_0 e^{-b_2 t} t_c^{b_1} \left[1 + \frac{1}{t_c} (b_1 - b_2 t_c (t - t_c) \right] \quad \text{for } t > t_c \qquad [21.8]$$

In these applications, the typical engineering design life is 75 years, whereas the experimental data set is for a much shorter-period of time. The impact of the choice of the empirical model on predicted corrosion penetration is shown in Figure 21.3. The models described in Equations [21.1]–[21.8] may be used in conjunction with atmospheric exposure tests. Coupon exposure tests are also conducted in other types of applications, notably in the process industry. While, most of the time, a single exposure test is conducted and therefore, the time dependence of corrosion rate cannot be determined, interval tests can be conducted to derive a time-dependent corrosion rate. The functionality may depend on the environmental condition being tested.

Corrosion of iron and steel under immersion conditions in marine exposure sites takes on a more complex form due to the interplay between film formation, dissolution, and microbiologically influenced corrosion. Melchers (2006) identified four different stages in corrosion growth as illustrated in Fig. 21.4. In the initial stages, identified as Stages 0 and 1, corrosion is

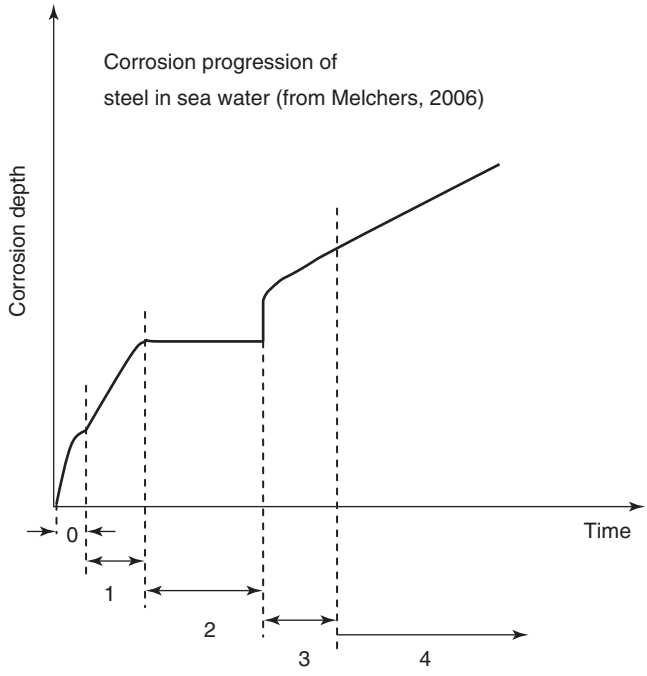

21.4 Different stages of corrosion penetration on carbon steel immersed in sea water (Melchers, 2006).

essentially in the active mode unrestricted by corrosion product. Therefore, a constant rate of corrosion prevails. Although Melchers argues that Stage 0 is not governed by oxygen transport to the surface, it is inconceivable that oxygen transport does not limit the cathodic reaction rate under immersion conditions, except for an extremely short period of time where the diffusion boundary layer is getting established. It is likely however, that a constant rate of corrosion prevails because of unrestricted access to the steel surface of the corrosive environment. Thus, Stages 0 and 1 cannot be easily distinguished in practice. The constant rate of corrosion can be calculated from the active anodic polarization of iron corrosion and transport-limited cathodic polarization of oxygen reduction reactions. Melchers (2006) showed that this initial corrosion rate primarily depends only on sea water temperature.

In Stage 2, a relatively thick corrosion product build-up occurs that may be a mixture of iron oxyhydroxides, primarily β-FeOOH. The build-up of corrosion product establishes a diffusion-controlled anodic dissolution rate that decreases with time. The build-up of corrosion product creates an anaerobic environment at the steel surface leading to the attachment of

sulfate reducing bacteria (SRB). The time for the start of SRB-induced corrosion depends on the seawater temperature, dissolved oxygen levels, nutrients, etc. Once SRB colonies attach themselves to the steel, an upsurge in corrosion (Stage 3) is noted. Stage 4 represents a steady-state corrosion behavior possibly determined by dissolution rate of the outer corrosion product layer, transport of nutrients to the SRB colonies, and the dissolution rate of the steel by SRB colonies.

21.2.2 General corrosion models for process environments

Another application of empirical model to predict uniform corrosion rates is in the area of CO_2 corrosion. The most widely used model in the industry, for CO_2 corrosion prediction, is the semi-empirical model originally developed by de Waard and Milliams (1975) and modified by de Waard *et al.* (1991, 1995) and de Waard and Lotz (1993). The basis of these models is the de Waard and Milliams equation:

$$\log(CR, \text{mm/y}) = 5.8 - \frac{1780}{T(^\circ\text{C})} + 0.67\log(p\text{CO}_2) \qquad [21.9]$$

Although this model and its variants introduced later by de Waard *et al.* incorporated CO_2 pressure, pH, temperature, flow rate, inhibitor, scale formation and steel microstructure, it is not directly applicable for use when the environment contains H_2S or O_2 or both. Other empirical models that are used by industry (Jepson *et al.*, 1997; Palacios and Corpoven, 1997; Halvorsen and Sontvedt, 1997; Gunaltun, 1996; Gunaltun and Larrey, 2000; Bonis and Crolet, 1989; Sangita and Srinivasan, 2000) are mainly applicable for production systems in the temperature range of 30 to 120 °C. Their validity at lower temperature is questionable. Furthermore, with the exception of the model by Sangita and Srinivasan (2000), the other empirical models are valid for CO_2 only systems. It is well-known that the presence of small concentrations (ppm levels) of H_2S can decrease the corrosion rate in CO_2 environments due to the formation of iron sulfide films. An empirical model available to account for the combined effect, on the steel corrosion rate, of CO_2, H_2S and O_2 was developed by Sridhar *et al.* (2001a). The multiple regression model, developed from short-term experimental data in static and gently flowing solutions, is given in Equation [21.10]:

$$\begin{aligned} CR = {} & 8.7 + 9.86 \times 10^{-3}\,(\text{O}_2) - 1.48 \times 10^{-7}\,(\text{O}_2)^2 - 1.31(\text{pH}) \\ & + 4.93 \times 10^{-2}\,(\text{CO}_2)(\text{H}_2\text{S}) - 4.82 \times 10^{-5}\,(\text{CO}_2)(\text{O}_2) \\ & - 2.37 \times 10^{-3}\,(\text{H}_2\text{S})(\text{O}_2) - 1.11 \times 10^{-3}\,(\text{O}_2)(\text{pH}) \end{aligned} \qquad [21.10]$$

where the corrosion rate, CR, is in mils/year (1 mil = 25.4 μm), O_2 concentration is in ppmv, CO_2 is in psi (1 atm =14.7 psi), and H_2S is in psi. Equation

[21.10] shows that O_2 is the most important accelerator to the steel corrosion and there is a synergistic effect between CO_2 and H_2S and between O_2 and H_2S, CO_2 or pH. Although Equation [21.10] is useful for corrosion rate estimation, it is based on only a limited number of data points and rather simple flow conditions. Another important drawback in using Equation [21.10] is that the pH is an important variable, but is not always known. If water condenses from the gas phase, the pH of the water in equilibrium with CO_2 and H_2S is about 4.5. Equation [21.10] cannot be used for systems involving flow other than stratified flow. Both Equations [21.9] and [21.10] assume that the corrosion rate is constant with time. Finally, in the presence of H_2S and O_2, localized corrosion is highly likely, which is not predicted either by Equations [21.9] or [21.10].

21.2.3 Empirical models for flow assisted corrosion

In cases where corrosion rate is controlled by the transport of species to or from the corroding electrode, the corrosion rate can be calculated from the product of the mass transfer coefficient and the concentration difference of the rate controlling species in the solution between the electrode surface and the bulk solution. Flow-induced corrosion is discussed in more detail in another chapter; therefore this chapter provides a brief description of the empirical models in the context of other empirical modeling.

Empirical models in these cases help translate the results from one geometry (e.g., a rotating cylinder electrode test in the laboratory) to a different geometry (e.g., a pipe flow condition in the field) (Silverman, 2004). For the rotating cylinder electrodes, Silverman (2004) showed that general relationship of the form

$$Sh = a[Re]^b[Sc]^c \qquad [21.11]$$

In Equation [21.11], the Sherwood number (Sh) is related to the mass transfer coefficient given by $Sh = (kd/D)$, where k = mass transfer coefficient in cm-s^{-1}, d = diameter of cylinder in cm, and D = diffusion coefficient of the rate controlling species in cm^2-s^{-1}; the Reynolds number (Re) is given by $\rho ud/\mu$, where ρ is the density of the fluid in g-cm^{-3}, u is the fluid velocity in cm-s^{-1}, and μ is the absolute viscosity of the fluid in g-cm^{-1}-s^{-1}; and the Schmidt number (Sc) is given by $Sc = \mu/\rho D$. In Equation [21.11], the values of 'a' ranged from 0.0489 to 0.219, 'b' ranged from 0.6 to 0.748, and 'c' ranged from 0.27 to 0.41 for a smooth, rotating cylinder electrode. Thus, once the mass transfer coefficient is determined from Equation [21.11], it can be used for other geometries, if self-similarity in mass transfer coefficient is assumed. For example, in order to maintain equal mass transfer coefficient between a rotating cylinder electrode and a pipe

under turbulent flow conditions, Equation [21.12] (Silverman, 2004) may be used:

$$u_{cyl} = 0.1185\left[\left(\frac{\mu}{\rho}\right)^{-0.25}\left(\frac{d_{cyl}^{3/7}}{d_{pipe}^{5/28}}\right)(Sc)^{-0.0857}\right]u_{pipe}^{5/4} \qquad [21.12]$$

21.2.4 Empirical models for localized corrosion

The empirical approaches to localized corrosion prediction utilize a number of factors that are known to affect localized corrosion initiation and propagation. Some of these approaches are shown below.

Critical pitting/crevice temperature

This is used mostly to provide a relative ranking of alloys in a standard environment, such as 6 wt% $FeCl_3$. It is known that either pitting or crevice corrosion initiate (at a macroscopic level) above a critical temperature that is a function of alloy content, surface preparation, environmental composition and test time. Relative ranking of alloys in a standardized environment can be used to make judgments on the selection of appropriate alloys in a given application, by comparing the performance of another alloy in the standard test to that alloy's performance in the application of interest. Because it is impossible to make quantitative determination of the relationship between the severity of the standard test environment and the service environment, this is not a predictive technique. The critical temperature for pitting is typically higher than for crevice corrosion.

Depassivation pH (pH_D)

Depassivation pH is the pH value at which passivity is lost and the alloy exhibits an active polarization curve. According to a mechanism of crevice corrosion, originally proposed by Galvele (1976), the electrolyte composition inside a pit or a crevice becomes acidic due to the hydrolysis of the metal ions according to reactions such as that shown in Equation [21.13]:

$$Fe^{2+} + 2H_2O = Fe(OH)_2 + 2H^+ \qquad [21.13]$$

At a critical pH known as the pH_D, crevice corrosion initiates due to depassivation of the oxide film in the crevice. The pH_D value has been shown to be dependent on the alloy content (Okayama *et al.*, 1987) and therefore could be used as a predictive method for localized corrosion. The main limitation of this method is that crevice corrosion initiation may not be preceded by a critical pH, but may be succeeded by it (Sridhar and Dunn, 1994).

Critical crevice geometry

The rate of acidification of the crevice and therefore the time to initiate crevice corrosion is a function of crevice gap and length. The crevice geometry essentially controls the rate of accumulation of dissolved cationic and anionic species. Galvele (1976) originally proposed the parameter, $x \cdot i$, where 'x' is the pit depth and 'i' is the current density, as a critical parameter that determines pitting or crevice corrosion initiation. Variations of this type of approach have been evaluated by Pride *et al.* (1994).

21.2.5 Statistical approaches to predicting localized corrosion

It has been long recognized that localized corrosion is a stochastic process and needs a statistical treatment to predict its initiation and growth. A historical background for the statistical treatment of localized corrosion has been provided by Shibata (1996). In the initiation stage, the initiation potential for pitting as well as for crevice corrosion (see Chapter 2 for more details) can vary by as much as several hundred millivolts depending on the number of specimens tested even under apparently identical conditions (Fig. 21.5). This distribution of pit initiation potential can be understood by considering pit initiation as a dynamic event consisting of both nucleation and repassivation of small pit nuclei. The change in the probability of pit initiation with time is given by Equation [21.14]

$$\frac{\mathrm{d}P(t)}{\mathrm{d}t} = -\lambda P(t) + \mu(1 - P(t)) \qquad [21.14]$$

where P is the probability of pit nucleation, λ is the pit generation rate, and μ is the pit repassivation rate. In this approach, the observed pit initiation potential depends on the potential dependence of λ and μ. The probability of pit nucleation in Equation [21.14] has also been called the survival probability, i.e. the probability of the specimen without any pits. The parameters λ and μ are obtained from experimental measurements of pit nucleation. For example, if N samples are tested at a constant potential, then the survival probability is given by

$$P(t) = 1 - \left(\frac{n}{1+N}\right) \qquad [21.15]$$

where n is the number of specimens that showed pitting at any given time and applied potential and N is the total number of specimens tested (Shibata and Takayama, 1977). The survival probability plotted as a function of applied potential is shown in Fig. 21.6. From the survival probability versus time curve, using Equation [21.14], the pit generation rate,

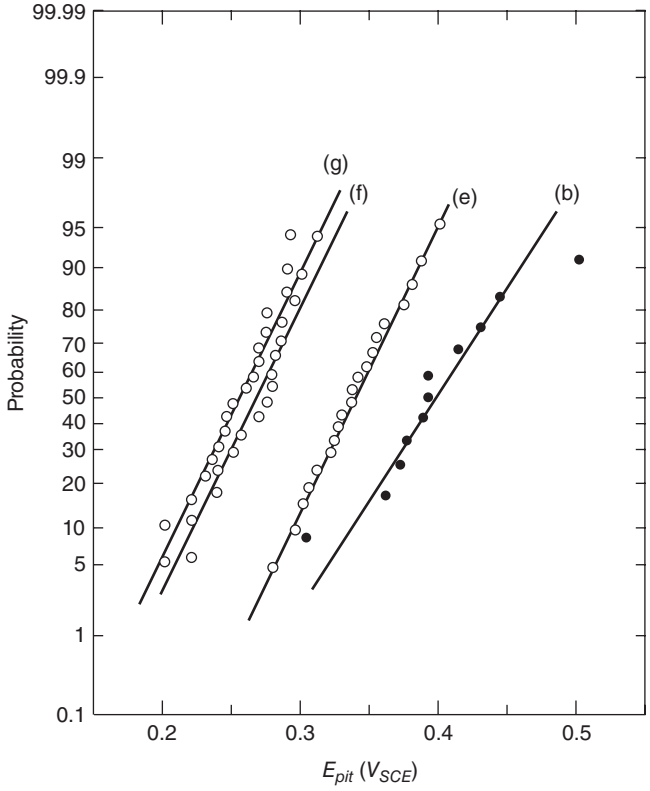

21.5 Distribution of pit initiation potentials of type 304 stainless steel in 3.5 weight percent NaCl at 303K (Shibata, 1996). The potential sweep rate was 0.33 mV/s. Lines (g) and (f) are results from a round-robin test conducted by the Japanese Society of Corrosion Engineers. Line (e) was obtained using a multichannel pit initiation measurement system described by Shibata and Takayama (1977). Line (b) was obtained by Shibata (1996).

repassivation rate, and induction time can be derived through curve fitting (Shibata, 1996). A similar approach was used by Kehler *et al.* (2001) for crevice corrosion. Although the statistical treatment of pit nucleation and stabilization has validity and support from experimental observations, the use of such an approach to prognostication is not clear. For example, the pit generation and repassivation rates, λ and μ, are derived from relatively short-term experiments and their dependence on time or potential over long time periods cannot be derived from these experiments. Mechanistic models to deal with this limitation have been proposed and will be discussed later (Macdonald and Urquidi-Macdonald, 1992; Williams *et al.*, 1985).

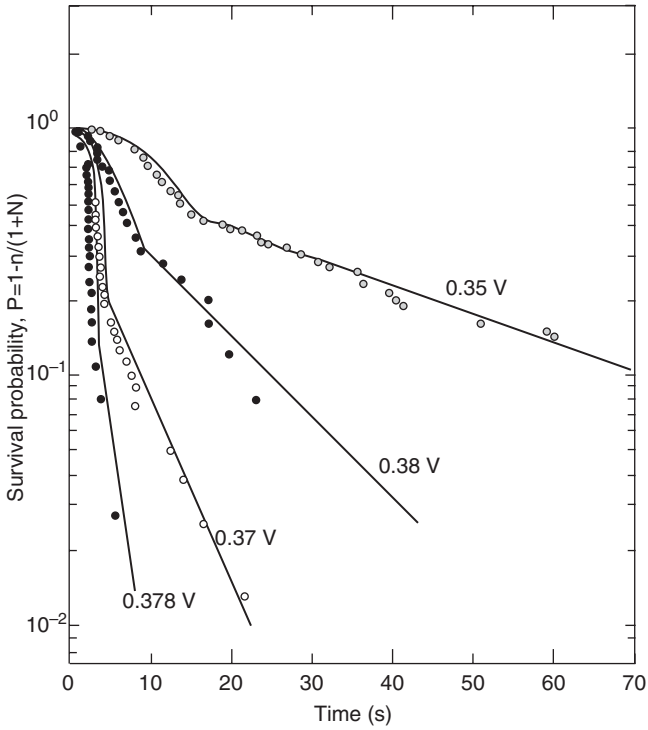

21.6 Survival probability of Type 304 stainless steel in 3.5% NaCl at 308K at constant applied potentials (Shibata and Takayama, 1977).

Statistical methods have also been used to predict pit growth rates in large structures by the use of Extreme Value methods (Shibata, 1996). The General Extreme Value (GEV) distribution has the form:

$$F(x) = \exp\left(-1 - k\frac{x-u}{\alpha}\right)^{\frac{1}{k}} \qquad [21.16]$$

where x is the reduced variable, and k, u, and α are the shape, location, and scale parameters, respectively. For $k = 0$, Equation [21.16] reduces to Type I distribution (also called Gumbel distribution):

$$F(x) = \exp\left(-\exp\left(\frac{x-u}{\alpha}\right)\right) \qquad [21.17]$$

For $k < 0$, Equation [21.16] becomes Type 2 extreme value distribution (Cauchy's distribution)

$$F(x) = \exp(-x^{-k}) \qquad [21.18]$$

And for $k > 0$, Equation [21.16] reduces to Type 3 extreme value (Weibull) distribution:

$$F(x) = \exp(-(\omega - x)^k) \quad [21.19]$$

Typically, experimental data are used to determine the type of extreme value statistical distribution to be used. The important property of the extreme value statistical distribution is the scaling of the maximum pit depth with surface area exposed, assuming otherwise identical exposure conditions (Shibata, 1996). For example in Type 1 (Gumbel) distribution, the pit depth for a surface area 'T' times larger than the test surface area, the distribution of pit depth is given by:

$$F_T(x) = (F(x))^T = \exp\left(-\exp-\left[\frac{x-(u-\alpha ln(T))}{\alpha}\right]\right) \quad [21.20]$$

In Equation [21.20], the location parameter 'u' is displaced by the logarithm of the area ratio. In determining the parameters, the sample area is divided into identical areas or a number of small samples are exposed simultaneously to the same conditions and for each area the deepest pit is determined. These deepest pits can then be rank ordered and the appropriate parameters determined using the procedures described by Shibata (1996). An important assumption in the GEV distribution discussed by Shibata is that the probability of pitting is not spatially correlated, i.e. the probability of observing pits of certain depths at one location is completely independent of their probability at another location. This essentially means that the environment, metallurgy and operating conditions are identical throughout the spatial extent of a system (e.g., a pipeline). This is seldom the case. For example, in pipelines, it is more probable to encounter pitting at points near the location where pits were originally observed (i.e. positive correlation of pitting). The methods to handle spatial correlations in estimating maximum pit depths and uncertainties in the estimation are discussed by Martinsek (2003).

While the extreme value statistical approaches provide a means to extrapolate the deepest pit in terms of area exposed (for example extrapolating from a lab sample to a pipeline), the time dependence is assumed or derived from short-term tests. Second, even area extrapolation assumes that the exposure conditions and mechanism are identical for all samples and that the neighboring pits on a sample are not correlated. Both these assumptions are suspect in many cases. It should be noted that the multielectrode array sensor (see Chapter 8 for more details) readings can be subjected to extreme value statistical analysis.

21.2.6 Artificial Neural Network type models

Artificial Neural Network models are best used when there is a significant body of experimental data, but no coherent theoretical framework exists to develop predictive relationships. An overall approach of this type of model is shown in Fig. 21.7 (Hernandez *et al.*, 2006; Kumar and Buchheit, 2004). The model consists of several input values connected to hidden nodes through weighing factors. The hidden nodes sum the input values using weighing factors that are determined during the training step. The weighing factors imitate the strength of the neural connections. Each hidden node can be biased by an activating signal such that it produces an output only if the sum of the input signals exceeds a pre-set threshold condition. A typical activating signal has the sigmoidal form shown in Equation [21.21]:

$$O_j = \frac{1}{1+\exp^{-(\sum input+\theta_j)}} \qquad [21.21]$$

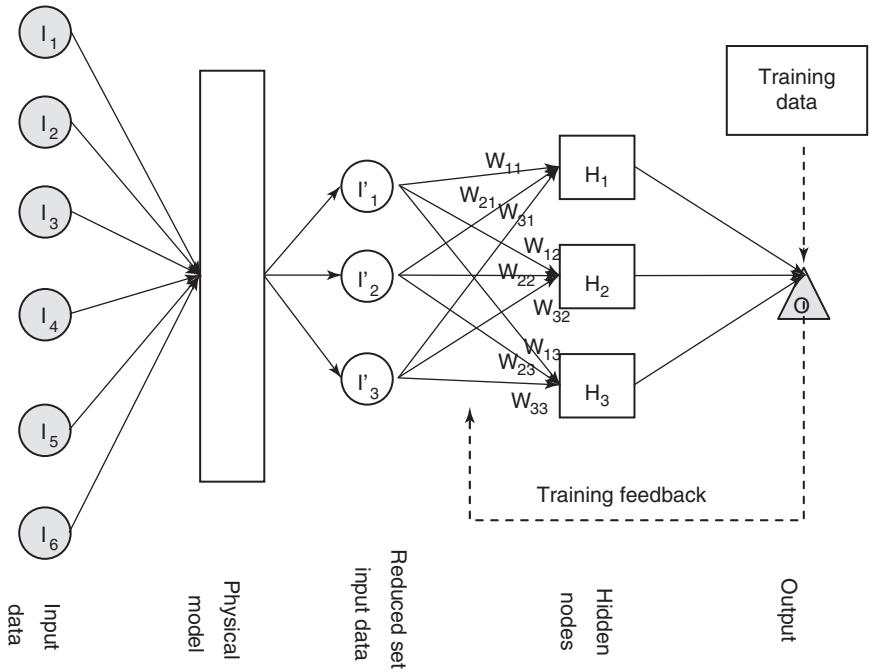

21.7 Artificial Neural Network modeling approach. A physical model block has been added to indicate that the typical ANN approach can be augmented through the use of physical models.

where O_j is the output of the jth node and θ_j is the threshold value of the jth node for output. The output of the hidden nodes may also be conditioned by a non-linear function to provide limits on output values. The hidden nodes (there may be several layers of the hidden nodes) form the black box of the model. The major use of neural network modeling has been in identifying trends and relationships in complex data sets that depend on a number of parameters. Although such relationships can also be established using well-designed statistical experimental approaches, neural network modeling can elicit trends in data even when experimental data sets are not part of a well-designed study or when data sets from a number of sources are used. For example, Kumar and Buchheit (2004) used such an approach to extract parameters from short-term electrochemical impedance data to predict longer-term behavior in salt spray tests. Nor and Cottis (2004) used a neural network model to reconstruct polarization curves of steel in chloride solutions. The limitation of neural network modeling is that it is correlative, not predictive, i.e. there is no element in the model that will enable one to extrapolate the data to future time periods. Short-term data can be correlated to long-term behaviors, as seen in Kumar and Buchheit (2004), but such correlation depends on the availability of longer-term data and is constrained by the available data, since that data is used to train the model.

21.2.7 Expert systems

Expert systems are conceptually similar to semi-empirical correlations and may include several individual correlations that cover various physical aspects of the process in addition to electrochemical corrosion (e.g., multiphase flow effects). They also may include facilities for recommending materials for service in the presence of target environments. For example, the Materials Technology Institute of the Chemical Process Industries (MTI) has developed a series of expert system advisors to select process equipment materials for service in the most common hazardous chemicals (the CHEM*COR modules). These models address selected single-component process environments. Several expert systems have been developed for CO_2 corrosion of carbon steels (Srinivasan and Kane, 1996; Garber *et al.*, 1994; Bonis and Crolet, 1989; and Zhang *et al.*, 1997). While the expert systems are valuable because they incorporate the plant experience in realistic systems, they are limited by the inability to reliably extrapolate beyond the experience base.

21.3 Mechanistic (physics-based) models

Some have referred to the mechanistic or physics-based models as 'deterministic models' (Macdonald and Urquidi-Macdonald, 1992). Despite

historical precedence, such a terminology can be confusing because deterministic models also often refer to models (whether empirical or mechanistic) that produce a single-valued output (e.g., failure time) for a set of input parameters, in contraposition with 'probabilistic models' which produce a distributed output (e.g., cumulative probability of failure) for a set of distributed inputs. Therefore, in this section, they are referred to as mechanistic or physics-based models, although they are mostly chemical and electrochemical models! These models embody basic physical laws to varying degrees, both explicitly and implicitly.

One such basic law is mass conservation, which is written in differential form as (Lichtner, 1996):

$$\frac{\partial}{\partial t}(p\Psi_j)+\nabla\cdot(\Omega_j^d+\Omega_j^e)=-\sum_i \nu_{ji}^e I_i^e-\sum_m \nu_{jm}^e I_m^e-\sum_m \nu_{jm} I_j \qquad [21.22]$$

Where p is the porosity, ν is the stoichiometric coefficient, I^e is the electrochemical reaction rate, and I_j is the non-electrochemical reaction rate. The generalized concentration, ψ_j, is given in terms of the primary species, C_j, and secondary species, C_i, by

$$\Psi_j = C_j + \sum_i \nu_{ji} C_i \qquad [21.23]$$

The primary and secondary species arise in Equation [21.23] because there is an essentially instantaneous equilibrium reaction between some species that needs to be considered. The secondary species in Equation [21.23] can be solved using matrix methods for a general system involving a number of species in equilibrium. The diffusive flux, Ω_j^δ, is given by

$$\Omega_j^d = -p\left(\nabla\cdot\left(D_j C_j + \sum_i \nu_{ji} D_i C_i\right)\right) \qquad [21.24]$$

The electromigration flux, Ω_j^e is given by

$$\Omega_j^e = -p\left(D_j C_j z_j + \sum_i \nu_{ji} D_i C_i z_i\right)\frac{F}{RT}\nabla\cdot\Phi \qquad [21.25]$$

Note that the Φ in Equation [21.25] is the potential in solution, not the potential difference between the metal and solution, although it may be related to the latter. Another fundamental law is charge conservation (in reality, the charge conservation law is a simplified form of Poisson's equation for charge at a point) given by:

$$\sum_j z_j \Psi_j = 0 \qquad [21.26]$$

Combining these equations and applying various simplifications can lead to other well-known electrochemical principles. For example, if we multiply

the two sides of Equation [21.22] by Z_j and combine it with Equation [21.26], we obtain,

$$\sum_j z_j \nabla \cdot (\Omega_j^d + \Omega_j^e) = -\sum_i z_i^e I_i^e - \sum_m z_m^e I_m^e \qquad [21.27]$$

Note that in Equation [21.27], the right hand side involves only electrochemical reaction rates multiplied by the net charge involved in each reaction. In the absence of concentration gradients in the solution, one obtains from Equation [21.27], the well-known relationship between the sum of anodic and cathodic currents that forms the basis for predicting mixed potentials:

$$\sum_i z_i^e I_i^e + \sum_m z_m^e I_m^e = 0 \qquad [21.28]$$

21.3.1 Thermodynamic models

A fundamental natural law governing corrosion reactions is the thermodynamic relationship of half-cell potential to the activity of species involved in the electrochemical reactions, as defined by the Nernst equation:

$$\Delta G = zFE^0 \qquad [21.29]$$

where ΔG is the free-energy change corresponding to the half-cell reaction, z is the charge involved, F is the Faraday's constant, and E^0 is the equilibrium half-cell potential. The free energy change is given by

$$\Delta G = \Delta G^0 + RT\, ln\left(\frac{\prod (m_i\gamma_i)_{ox}}{\prod (m_j\gamma_j)_{red}}\right) \qquad [21.30]$$

where ΔG^0 is the standard-state partial Gibbs free energy, m_i and m_j are the concentrations in molality (or other desirable units) of oxidized and reduced species, respectively, and γ_i and γ_j are their activity coefficients. In the classic Pourbaix diagrams, highly dilute solutions are considered and therefore, the activity coefficients are all considered to be equal to 1. In concentrated solutions, such simplifications cannot be made. However, recent advances in electrolyte speciation models have provided sophisticated tools to model the electrochemical potentials of metals and alloys in electrolytes over a wide concentration range (Rafal *et al.*, 1994; Anderko *et al.*, 2002). In addition to representing the thermodynamic regions of stability of various species in the form of potential–pH diagram, other types of stability diagrams (potential–chloride, species–species, etc.) can be constructed.

Pourbaix (1974) used the potential–pH diagram to identify regions of localized corrosion. Staehle (2000) and Parkins (1990) have used Pourbaix diagrams to delineate regions of SCC of iron, stainless steels, and Ni-base

alloys in various applications. An example of the use of Pourbaix diagram to delineate various regions of SCC of a Ni-base alloy, alloy 600, in the secondary side of a steam generator is shown in Fig. 21.8 (Staehle and Gorman, 2004). Secondary side stress corrosion cracking in steam generators predominantly occurs in crevices between tubes and tube-supports, tube sheets, or sludge formed on tube sheet. Many different types of SCC have been identified in the field and the authors assembled the extremely diverse range of observations into a Pourbaix diagram. They also used the Pourbaix diagram to explain the effectiveness of various mitigation treatments and to identify potentially new cracking modes. The major limitations of this approach are: (a) the thermodynamic diagrams used are for pure metals, not alloys; (b) in most crevice situations in steam generators high concentrations of salts are present due to evaporation that is not properly considered by Pourbaix diagrams; and (c) these diagrams provide a context for SCC to occur, not the rates of SCC.

In SCC or localized corrosion occurring in highly concentrated aqueous systems or in essentially non-aqueous systems, Pourbaix diagrams developed for dilute aqueous environments are not valid. Thermodynamic models of mixed solvent electrolytes (Anderko *et al.*, 2002) provide the means to visualize the domains of corrosion in such systems. An example of a potential–pH diagram for Fe in ethanol containing 100 ppm water is shown in Fig. 21.9 (Sridhar *et al.*, 2006). In this case, the SCC of steel in fuel-grade ethanol was studied using slow strain rate test method under different redox conditions induced by varying the aeration and ethanol source. SCC was found only when the potential was within a certain range (noted in Fig. 21.9). The ranges of potential and pH for SCC noted in Fig. 21.9 are approximate because the upper end of the potential for SCC has not been defined completely and the equilibrium pH conditions for such systems are not easy to measure. Nevertheless, this diagram shows that SCC in this system occurs in the stability region of iron oxides, suggesting that perhaps a localized dissolution of an oxide film may be responsible for SCC.

Although thermodynamic diagrams provide the constraints and context under which potential corrosion modes could occur in a given application, they suffer from the following major limitations:

1. They represent equilibrium, not kinetically determined conditions. Therefore, they provide no means to prognosticate corrosion.
2. They ignore the effects of microstructure, mechanical loading, and fluid flow.
3. The choice of a particular diagram (potential–pH or potential–chloride) to represent failure modes is arbitrary. In the case of iron, the passivity is marginal and is sensitive to pH, therefore, potential–pH is perhaps an

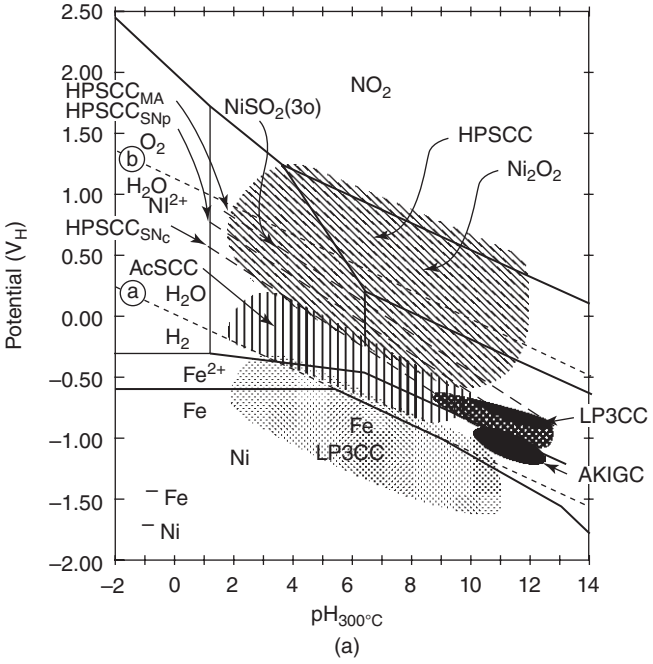

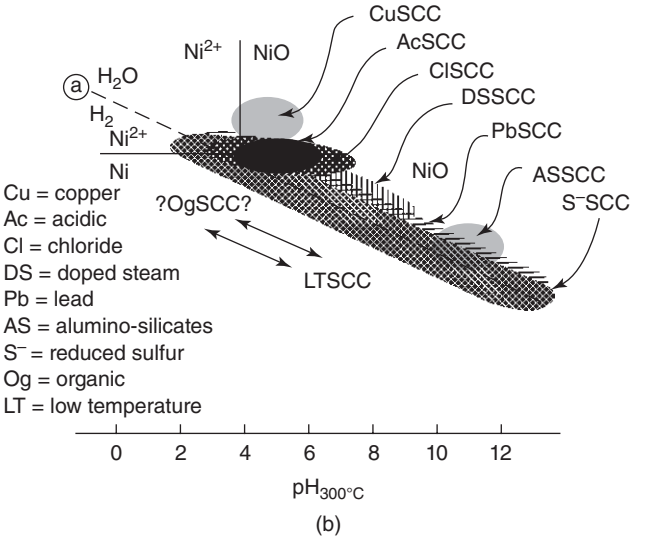

21.8 (a) Major submodes of SCC plotted with respect to coordinates of potential for significant reactions of Ni and Fe at 300 °C. Extent of the submodes based on experience from laboratories and reasonable interpolations and extrapolations. Submodes applicable to Alloy 600MA (Mill Annealed) in the range from 300 °C to 350 °C. Diagram calculated based on a 0.01 M Na_2SO_4 titrant. (b) Minor submodes of SCC for Alloy 600MA plotted with respect mainly to the NiO/Ni half-cell equilibrium at 300 °C (Staehle and Gorman, 2004).

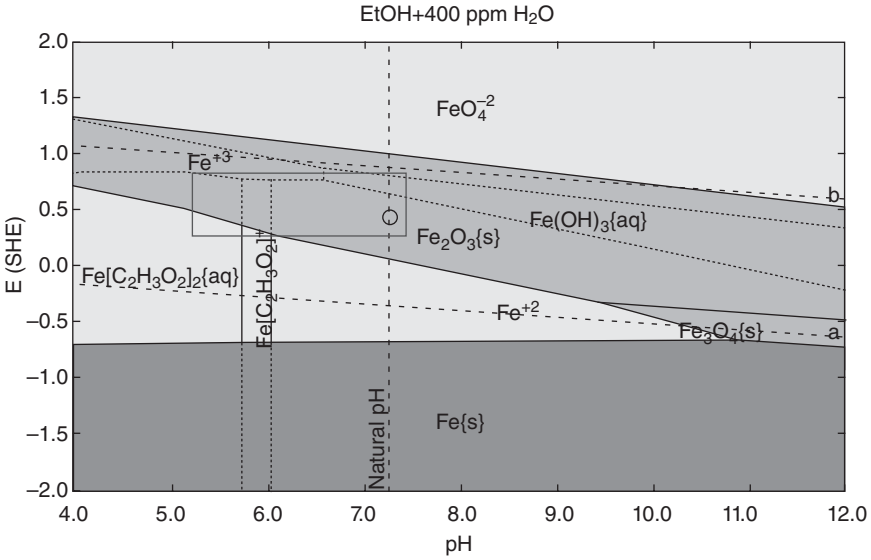

21.9 Potential–pH diagram of Fe in ethanol containing 400 ppm water at 25 °C. The rectangular box indicates the approximate potential and pH ranges in which SCC has been observed (Sridhar *et al.*, 2006).

adequate representation of various corrosion regimes. However, for stainless steels, potential–chloride or temperature–chloride, or cationic species–anionic species diagrams may all be appropriate depending on the corrosion phenomenon under consideration. The choice of which diagram to use is not always clear *a priori*.

21.3.2 General corrosion models

Most fundamental models of general corrosion rely on the relationship between potential and current density. In the case of an electrochemical reaction subject to transport limitation, a generalized Butler–Volmer kinetic relationship can be written as:

$$I_m^e = s_m \sum_l P_{ml} k_{ml} \left[\frac{e^{-\alpha_m \eta_m} - e^{\beta_m \eta_m}}{1 + \frac{s_m P_{ml} k_{ml}}{r_{lim}} \left(e^{-\alpha_m \eta_m} + e^{\beta_m \eta_m} \right)} \right] \qquad [21.31]$$

where P_{ml} is the prefactor consisting of concentrations of species considered to affect the kinetics (e.g. halides that increase anodic dissolution rate), r_{lim} is the limiting rate of reaction, α_m and β_m are transfer coefficients, and the dimensionless overpotential is defined as

$$\eta_m = \frac{n_m F}{RT}(E - E_m^{eq}) \qquad [21.32]$$

where n_m is the number of electrons involved in the reaction, F is the Faraday constant, R is the gas constant, T is the absolute temperature, E is the potential at any spatiotemporal point, and E_m^{eq} is the equilibrium potential that is dependent on the concentrations of species involved in the electrochemical reaction. Kinetic equations, such as Equation [21.31], can be written both for anodic dissolution and cathodic reduction reactions. Then, the corrosion potential is determined using Equation [21.28]. At potentials sufficiently anodic to the reversible equilibrium potential, and if transport limitation is not an important factor, Equation [21.31] reduces to the Tafel relationship:

$$i_a = i_a^0 \exp\left[\frac{\alpha_a n F (E - E_m^{eq})}{RT}\right] \qquad [21.33]$$

The active–passive transition is introduced into the electrochemical model by considering a current that leads to the formation of a passive layer in addition to the current that leads to active dissolution. At any instant, a certain fraction of the surface θ_P is assumed to be covered by a passive layer. The change of the passive layer coverage fraction with time is expressed as (Anderko *et al.*, 2001)

$$\left(\frac{\partial \theta_P}{\partial t}\right)_{E,a_i} = c i_{MeO}(1 - \theta_P) - K\theta_P \qquad [21.34]$$

where i_{MeO} is the current density that contributes to the formation of a passive layer. The second term on the right-hand side of Equation [21.33] represents the rate of dissolution of the passive layer, which is proportional to the coverage fraction. Solution of this equation in the steady-state limit yields an expression for the anodic dissolution current:

$$i_{Me,TOT} = \frac{i_{Me} + i_{MeO}}{1 + \frac{c i_{MeO}}{K}} = \frac{i_{Me} + i_{MeO}}{1 + \frac{i_{MeO}}{i_P}} \qquad [21.35]$$

where i_{Me} is the dissolution current density in the active state (Equation [21.33]), the parameters c and K are proportionality constants for the formation and dissolution of the passive film, respectively. The ratio $i_p = c/K$ constitutes the passive current density. For calculating the corrosion potential of passive alloys, the quantitative modeling of passive dissolution is of primary importance. In the absence of specific active ions, the passive current density depends primarily on the pH of the solution.

For acidic solutions, Anderko and Young (2000) considered a dissolution reaction between the passive oxide/hydroxide surface layers and protons from the solution, i.e.

$$\equiv MeO_a(OH)_b + (2a + b - x)H^+ = Me(OH)_x^{(2a+b-x)+} + (a + b - x)H_2O \quad [21.36]$$

where the symbol '≡' denotes surface species. The corresponding kinetic equation is

$$i_{p,H^+} = k_{H^+} a_{H^+}^{*s} \quad [21.37]$$

where $a_{H^+}^{*s}$ denotes the surface concentration of hydrogen ions and s is a reaction order, which is not necessarily related to the stoichiometric coefficient in the dissolution reaction. In neutral solutions, the predominant dissolution reaction is:

$$\equiv MeO_a(OH)_b + aH_2O = Me(OH)_{(2a+b),aq}^0 \quad [21.38]$$

where the predominant species on the right-hand side of Equation [21.38] is a neutral complex as indicated by the superscript 0. The corresponding kinetic equation is:

$$i_{p,H_2O} = k_{H_2O} a_{H_2O}^{*u} \quad [21.39]$$

where the reaction order with respect to water indicates that dissolution may be affected by water activity. Similarly, the predominant reaction in alkaline solutions is

$$\equiv MeO_a(OH)_b + (x - 2a - b)OH^- + aH_2O = Me(OH)_x^{(x-2a-b)-} \quad [21.40]$$

with a corresponding kinetic equation given by

$$i_{p,OH^-} = k_{OH^-} a_{OH^-}^{*v} \quad [21.41]$$

The total passive current density as a function of pH is given by

$$i_p = i_{p,H^+} + i_{p,H_2O} + i_{p,OH^-} \quad [21.42]$$

An example of the various component (partial) polarization curves in sulfate-nitrate environment and the composite polarization curve is shown in Fig. 21.10 (Anderko *et al.*, 2005a). The corresponding calculation of corrosion rate is shown in Fig. 21.11 (Anderko *et al.*, 2005a). Although the above model is phenomenological (i.e. it does not describe in detail the atomic processes occurring in the passive film), its main advantage lies in its ability to model a wide range of environments and alloy systems. Although the general corrosion model described in Equations [21.31]–[21.42] for active–passive metals provides a fundamentally sound method for predicting the general corrosion of alloys in complex chemical environments, it cannot predict the time evolution of the corrosion rate. The time

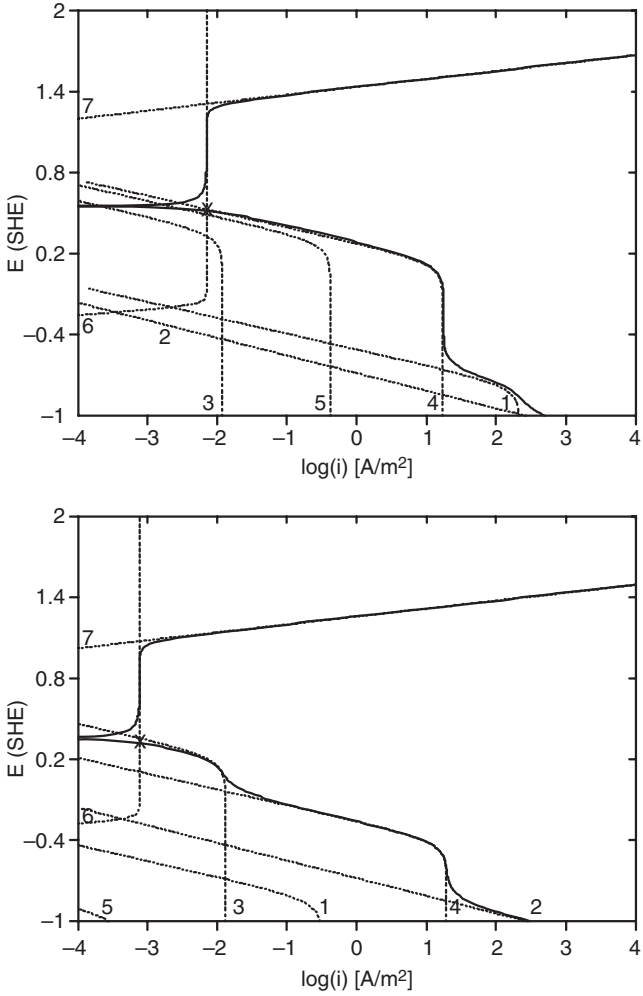

1: $H(+) = 0.5H_2 - e$
2: $H_2O = 0.5H_2 + OH(-) - e$
3: $O_2 + 4H(+) = 2H_2O - 4e$
4: $NO_3(-) + wH(+) = NOx + yH_2O - ze$
5: $HNO_3 + wH(+) = NOx + yH_2O - ze$
6: C-22 = {Ni,Cr,Mo,W}(x+)+xe
7: $Cr_2O_3 + 5H_2O = 2CrO_4(2-) + 10H(+) + 8e$

21.10 Calculated current density – potential relationship for alloy C-22 in a 0.5 M NO_3^- – 0.5 M SO_4^{2-} solution with pH = 0 (upper diagram) and pH = 3 (lower diagram). In both cases, the dissolved oxygen concentration is 1.2 ppm. Partial electrochemical processes are shown as dotted lines and labeled with numbers, which are explained in the legend (Anderko *et al.*, 2005).

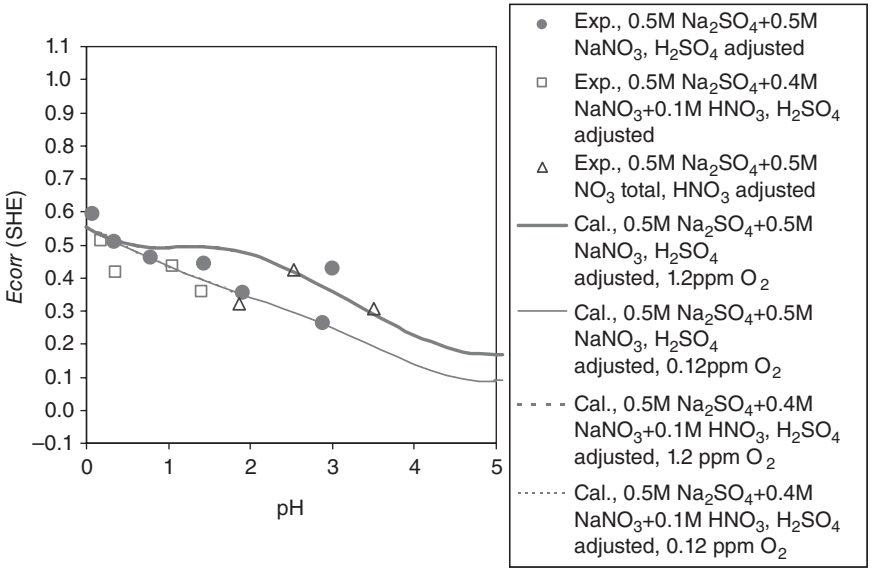

21.11 Calculated and experimental corrosion potentials of alloy 22 as a function of pH in nitrate solutions with a total nitrate concentration of 0.5 M. Two different concentrations of dissolved oxygen (1.2 ppm and 0.12 ppm) have been assumed in the calculations (Anderko *et al.*, 2005).

evolution of passive dissolution was modeled by Pensado *et al.* (2003), adapting the point defect model developed by Macdonald and his group (Macdonald, 1992). In this model, the assumption is made that passive dissolution occurs through the transport of cationic or anionic point defects in the oxide film under an applied potential. The various reaction steps leading to the dissolution of Ni, Cr and Mo in UNS N06022 (a Ni-22Wt%Cr-13Wt%Mo alloy) are illustrated in Fig. 21.12 (Pensado *et al.*, 2003). Based on these reactions, the overall passive current density was derived as:

$$i_p \approx F[\chi\, a_{Cr}(k_1^{Cr} + k_3^{Cr}) + \delta a_{Ni}(k_1^{Ni} + k_3^{Ni} + \xi a_{Mo}\, k_1^{Mo}] \qquad [21.43]$$

where a_{Cr}, a_{Ni} and a_{Mo} are the atomic fractions at the metal–film interface and the kinetic parameters, k_1 and k_3 are associated with interstitial and oxygen vacancy transport, respectively. Since injection of interstitials into the film from the metal would create vacancies in the metal to preserve charge transfer, the resulting decrease in the concentration of Cr, Ni, and Mo at the metal–film interface would cause a decrease in passive current density (Equation [21.43]). Thus, the model would predict that the time evolution of passive current density is related to the transport and annihilation of these vacancies in the metal. The results of the numerical calculation

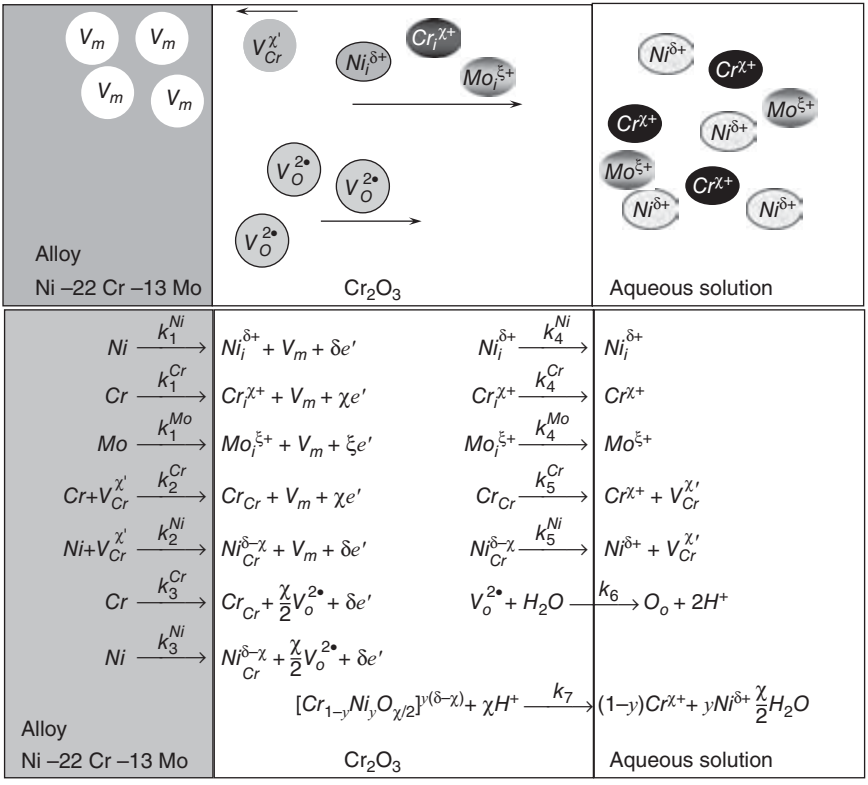

21.12 Various reactions involved in the passive dissolution of a Ni-Cr-Mo alloy. For simplicity, the passive film is shown as a single layer. In reality, multi-layer film may be present with an inner non-porous and outer porous layer, but the non-porous layer resembling chromium oxide is expected to govern the overall passive dissolution rate. y = [Ni]/[Ni] + [Cr], where [Ni] and [Cr] are nickel and chromium fractions in the passive film–solution interface (Pensado *et al.*, 2003). V_m is metal vacancy, V_{Cr} is cation vacancy for *Cr*, V_O is anion vacancy.

are compared to the measured range of passive current density for alloy UNS N06022 (Fig. 21.13).

21.3.3 Models of localized corrosion

In this section, pitting and crevice corrosion are treated together. The stochastic nature of pitting has already been discussed. However, the stochastic models treat pit nucleation phenomenologically, describing them in terms of pit generation and repassivation rate. The point defect model (PDM) mentioned above has been used to model pit initiation by

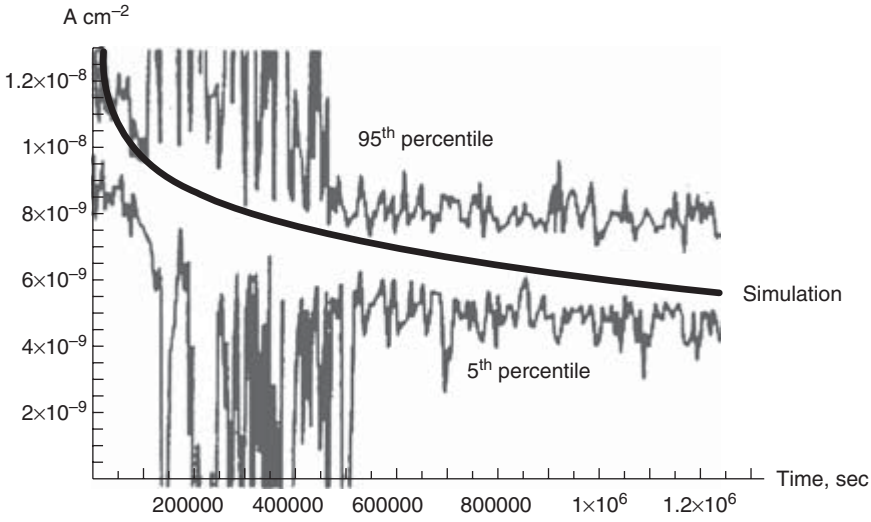

21.13 Anodic passive current density of alloy 22 versus time in a solution containing 1000 ppm chloride plus 1000 ppm sulfate – modeling versus experiments (Pensado *et al.*, 2003).

considering the transport of cation vacancies in the passive film toward the film–metal interface, where they condense to form voids or nascent pits. The PDM treats the transport of cation vacancies using Equations [21.31] and [21.32]. The effect of an aggressive species, such as chloride, is to alter the generation and transport of cation vacancies and thus the model successfully predicts the logarithmic dependency of pit initiation potential on chloride concentration and the effects of some alloying elements. The model does not differentiate between metastable pit nucleation events and pit stabilization. The latter phenomenon involves the evolution of local solution chemistry within the nucleated pit (Burstein *et al.*, 2004).

A different approach to modeling localized corrosion relies on predicting the evolution of chemistry inside pits and crevices. As mentioned in Section 21.2.4, the generation and hydrolysis of cations in the pit solution leads to acidification that can result in depassivation. Therefore, the pit/crevice chemistry models (e.g., Oldfield and Sutton, 1978; Gravano and Galvele, 1984; Sharland and Tasker, 1988; Watson and Postlethwaite, 1990; Walton *et al.*, 1996) attempt to compute the time evolution of pit chemistry using Equations [21.31] and [21.32] or variants of these equations constrained by suitable boundary conditions. The initiation time for pitting or crevice corrosion is the time required for the pH inside the pit to reach the depassivation pH. However, these models have not been successful in predicting

the long-term pit or crevice corrosion initiation. It is well established that when the potential is only slightly above the repassivation potential, the initiation time for stable crevice or pitting is extremely long (lasting months to years) (Dunn *et al.*, 2000). However, the chemistry models usually predict a very short time to reach depassivation pH. Because, prior to initiation, the passive dissolution rate is independent of potential, these models would not predict the dependence of initiation time on potential, another major observation.

Anderko *et al.* (2004a, 2004b, 2005a, 2006) developed a general model of localized corrosion by adapting Okada's irreversible thermodynamic model. This approach essentially divides the task of predicting localized corrosion into two parts: (a) calculating the corrosion potential; and (b) predicting the repassivation potential, also called the protection potential (see Chapter 2 for more details). The repassivation potential (E_{rp}) is a measure of the tendency of an alloy to undergo localized corrosion in a given environment. The underlying justification for the use of E_{rp} is the fact that, for engineering applications, only the fate of stable pits or crevice corrosion is important. Pits that nucleate, but do not grow beyond an embryonic stage (metastable pits) do not adversely affect the performance of engineering structures. It has been shown in a previous paper (Dunn *et al.*, 2000) that (a) E_{rp} is the potential below which stable pitting or crevice corrosion does not occur and (b) it is relatively insensitive to prior pit depth and surface finish. The predicted repassivation is then compared to the corrosion potential (E_{corr}) in the same environment to determine the alloy's susceptibility to localized corrosion. The separation of localized corrosion modeling into two steps is valid as long as the initiation of stable localized corrosion is being considered because the corrosion potential is not affected at this stage by the localized corrosion processes and the interaction between pits can be ignored. However, such a separation is not valid once significant pit or crevice corrosion growth occurs.

The concept is illustrated schematically in Fig. 21.14. For a given alloy, the E_{rp} decreases with an increase in chloride concentration (cf. Fig. 21.14a). In the general case, the main regions of the E_{rp} versus chloride concentration plot are a low-slope portion at high chloride concentrations and a high-slope portion at low concentrations. On the other hand, the corrosion potential is not a strong function of chloride concentration unless significant localized corrosion occurs. The critical chloride concentration for localized corrosion is observed when E_{corr} exceeds E_{rp} (Fig. 21.14a). Similarly, for a given chloride concentration, a critical temperature exists (Fig. 21.14b). The repassivation potential is also strongly affected by the presence of inhibitors. As shown in Fig. 21.14c, this gives rise to a critical inhibitor concentration. In many environments, the presence of oxidants may increase E_{corr}, so that localized corrosion may occur beyond a critical concentration of redox

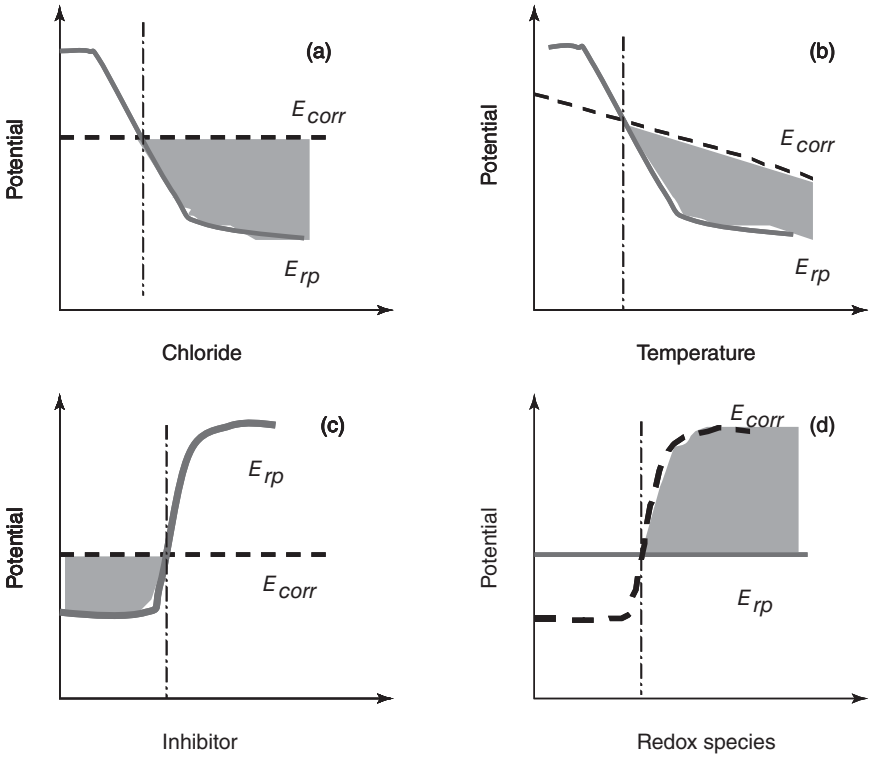

21.14 Schematic diagram of the effect of chloride ions (a), temperature (b), inhibitors (c), and oxidizing redox species (d) on the relative values of the repassivation potential (E_{rp}) and corrosion potential (E_{corr}). The shaded areas denote the ranges in which localized corrosion can be expected.

species (Fig. 21.14d). The actual conditions in a system may be a combination of the idealized cases shown in Fig. 21.14a–d.

The E_{corr} is calculated using the model for general corrosion described in Section 21.3.2. The E_{rp} is derived from fundamental equations that represent the electrochemistry of a metal in a localized corrosion environment. The metal (M) undergoes dissolution underneath a layer of concentrated metal halide solution MX. The concentrated solution may or may not be saturated with respect to a hydrous solid metal halide. The thickness of the hydrous halide layer is assumed to be much smaller than the size of the pit so that the system may be regarded as one-dimensional. In the process of repassivation, a thin layer of oxide forms at the interface between the metal and the hydrous metal halide. The model assumes that, at a given instant, the oxide layer covers a certain fraction of the metal surface. This fraction increases as repassivation is approached. Further, the

model includes the effects of multiple aggressive and non-aggressive or inhibitive species, which are taken into account through a competitive adsorption scheme. The aggressive species form metal complexes, which dissolve in the active state. On the other hand, the inhibitive species and water contribute to the formation of oxides, which induce passivity. In general, the equations that describe these processes are complex and can be solved only numerically. However, a closed-form equation has been found in the limit of repassivation, i.e., when the current density reaches a predetermined low value i_{rp} (typically $i_{rp} = 10^{-2}\,\mathrm{A/m^2}$) and the fluxes of metal ion become small and comparable to those for passive dissolution. This closed-form expression, which can be solved to calculate the repassivation potential, is given by:

$$1+\sum_k\left[\left(\frac{i_{rp}}{i_p}-1\right)\frac{l_k''}{i_{rp}}\right]\theta_k^{n_k}\exp\left(\frac{\xi_k FE_{rp}}{RT}\right)=\sum_j\frac{k_j''}{i_{rp}}\theta_j^{n_j}\exp\left(\frac{\alpha_j FE_{rp}}{RT}\right) \quad [21.44]$$

where E_{rp} is the repassivation potential, i_p is the passive current density, T is the temperature, R is the gas constant and F is the Faraday's constant. The summation on the right-hand side of Equation [21.44] is performed over all aggressive species (j) and the summation on the left-hand side pertains to water molecules and inhibitive species (k).

The partial coverage fraction of a species j is related to the activity of this species in the bulk solution by

$$\theta_j=\frac{r_j a_j}{1+\sum_k r_k a_k} \quad [21.45]$$

Equation [21.44] contains the following parameters:

1. Scaled rate constant for aggressive ions, which can be expressed using a scaled Gibbs energy of activation $\Delta g_{A,j}^{\neq}$:

$$k_j=\frac{k_j''}{i_{rp}}=\exp\left(-\frac{\Delta g_{A,j}^{\neq}}{RT}\right) \quad [21.46]$$

2. Scaled rate constant for inhibitive species, which is also expressed using a scaled Gibbs energy of activation $\Delta g_{I,k}^{\neq}$:

$$\left(\frac{i_{rp}}{i_p}-1\right)\frac{l_k''}{c}=\exp\left(-\frac{\Delta g_{I,k}^{\neq}}{RT}\right) \quad [21.47]$$

3. Reaction orders with respect to aggressive ions, n_j, and those with respect to inhibitive species, n_k. The latter quantities are assigned a default value of one for simplicity.
4. Electrochemical transfer coefficients for the inhibitive species, ξ_k.

5. Scaled Gibbs energy of adsorption $\Delta G_{ads,i}$, which defines the adsorption coefficient in Equation [21.45]:

$$r_j = \exp\left(-\frac{\Delta G_{ads,j}}{RT}\right) \quad [21.48]$$

The latter property can be assigned a common default value for the majority of species.

The scaled Gibbs energies of activation may be further related to temperature as

$$\frac{\Delta g^{\neq}_{A,j}}{T} = \frac{\Delta g^{\neq}_{A,j}(T_{ref})}{T_{ref}} + \Delta h^{\neq}_{A,j}\left(\frac{1}{T} - \frac{1}{T_{ref}}\right) \quad [21.49]$$

for aggressive ions and

$$\frac{\Delta g^{\neq}_{I,k}}{T} = \frac{\Delta g^{\neq}_{I,k}(T_{ref})}{T_{ref}} + \Delta h^{\neq}_{I,k}\left(\frac{1}{T} - \frac{1}{T_{ref}}\right) \quad [21.50]$$

for water and inhibitive species. For simplicity, the electrochemical transfer coefficients for aggressive species (α_j) are assumed to be equal to one. The parameters of the repassivation potential model are typically determined as follows:

1. Since E_{rp} data are most abundant for chloride solutions, the scaled rate constant for the chloride ions ($\Delta g^{\neq}_{A,Cl}$), reaction order with respect to chlorides (n_{Cl}), scaled rate constant for water ($\Delta g^{\neq}_{I,H_2O}$), and electrochemical transfer coefficient for water (ξ_{H_2O}) are determined based on data for chloride solutions. As discussed by Anderko *et al.* (2004b), this procedure can be simplified by the fact that the n_{Cl} and ξ_{H_2O} parameters have universal values for Fe-Ni-Cr-Mo-W alloys and do not need to be individually determined. If the temperature range of the data is sufficient to establish the temperature dependence, $\Delta h^{\neq}_{A,Cl}$ and $\Delta h^{\neq}_{I,H_2O}$ may also be determined.
2. The $\Delta g^{\neq}_{A,j}$ and, if necessary, n_j parameters are determined for other aggressive species j (e.g., bromide ions) using E_{rp} data for either pure or mixed solutions containing such ions.
3. The $\Delta g^{\neq}_{I,k}$ parameters for inhibitive ions k are determined on the basis of data for mixed solutions containing chlorides and inhibitors. Data for mixed systems are necessary because E_{rp} is undefined in solutions containing only inhibitors. If necessary, the activation enthalpy $\Delta h^{\neq}_{I,k}$ is also determined to reproduce the temperature dependence of the inhibition effect.

These parameters are listed for type 316L stainless steel (UNS S31603) in Table 21.2. Fig. 21.15 shows the calculated and experimental repassivation

Table 21.2 Parameters of the repassivation potential model for type 316L stainless steel in contact with the chloride, molybdate and vanadate ions (Anderko *et al.*, 2006).

Parameter	Physical meaning	Values for selected species				Units
		H_2O	Cl^-	MoO_4^{2-}	VO_3^-*	
$\Delta g^{\neq}_{A,j}(T_{ref})$	Gibbs energy of activation for dissolution reaction mediated by adsorption of aggressive species at reference T (298.15K)	Not applicable	–10.92	Not applicable	Not applicable	kJ/mol
$\Delta h^{\neq}_{A,j}$	Enthalpy of activation for dissolution reaction mediated by adsorption of aggressive species	Not applicable	0.040	Not applicable	Not applicable	kJ/mol
$n_{A,j}$	Reaction order with respect to aggressive ions	Not applicable	1.46	Not applicable	Not applicable	
$\Delta g^{\neq}_{I,k}(T_{ref})$	Gibbs energy of activation for the formation of oxide mediated by the adsorption of inhibitive species at reference temperature	19.31	Not applicable	–7.39	–5.02	kJ/mol
$\Delta h^{\neq}_{I,k}$	Enthalpy of activation for the formation of oxide mediated by the adsorption of inhibitive species	0**	Not applicable	0.023	0.017	kJ/mol
$\xi_{I,k}$	Electrochemical transfer coefficient for inhibitive species	0.743	Not applicable	0.99	0.99	
$\Delta G_{ads,j}$	Gibbs energy of adsorption	10***	10***	10***	10***	kJ/mol

Notes: *Includes hydrolyzed species such as $H_2VO_4^-$, HVO_4^{2-}, etc.
**The value of 0 indicates that the temperature dependence of the Gibbs energy of activation is insignificant
***Default value, not adjusted using experimental data

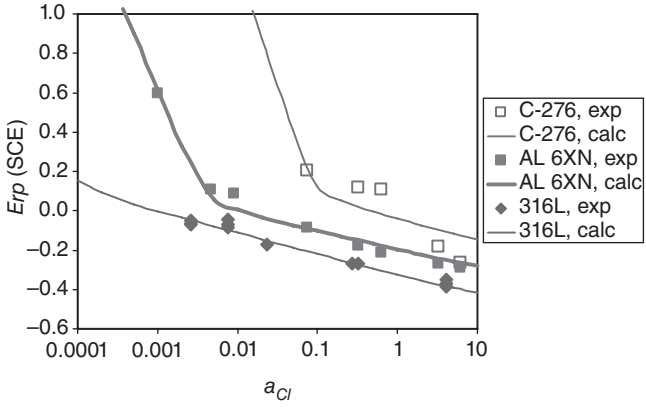

21.15 Calculated and experimental repassivation potentials for type 316L stainless steel and alloys AL6XN and C-276 at 368 K.

potentials for type 316L stainless steel, alloy AL-6XN (UNS N08367) and alloy C-276 (N10276) in chloride solutions (Anderko *et al.*, 2004a). As shown in this Figure, the slope of the repassivation potential changes as a function of chloride activity. This is a general phenomenon for alloys. However, the transition between the low-slope and high-slope segments of the curves strongly depends on the alloy and temperature. For alloys, such as type 304L stainless steel (UNS S30403), the transition may occur at very low chloride concentrations and only a single logarithmic slope is generally reported. The low-slope portion of the curve at higher chloride activities is determined by the parameters that represent the dissolution of the metal through the formation of metal–chloride complexes (i.e., $\Delta g^{\neq}_{A,Cl}$ and n_{Cl}). The steeper portion at lower chloride concentrations is additionally determined by the parameters that represent the formation of the oxide through a reaction with water molecules (i.e., $\Delta g^{\neq}_{I,H_2O}$ and ξ_{H_2O}). The slope of this segment increases with an increase in the parameter ξ_{H_2O}. Using these parameters, the model represents the data essentially within experimental uncertainty. The effect of an inhibitive species on E_{rp} is shown in Fig. 21.16 (Anderko *et al.*, 2006).

As described above, the repassivation potential model has a limiting character, i.e., it accurately represents the state of the system in the repassivation potential limit. In addition to the value of the repassivation potential, the model predicts the correct limiting slope of the current density versus potential relationship as the potential deviates from E_{rp} (Anderko *et al.*, 2004b). As discussed in a previous paper (Anderko *et al.*, 2004b), the predicted slope is accurate in the limit of repassivation (i.e., for $E \rightarrow E_{rp}$). As the potential increasingly deviates from E_{rp}, the predicted current density becomes progressively larger than the experimental values. In such cases,

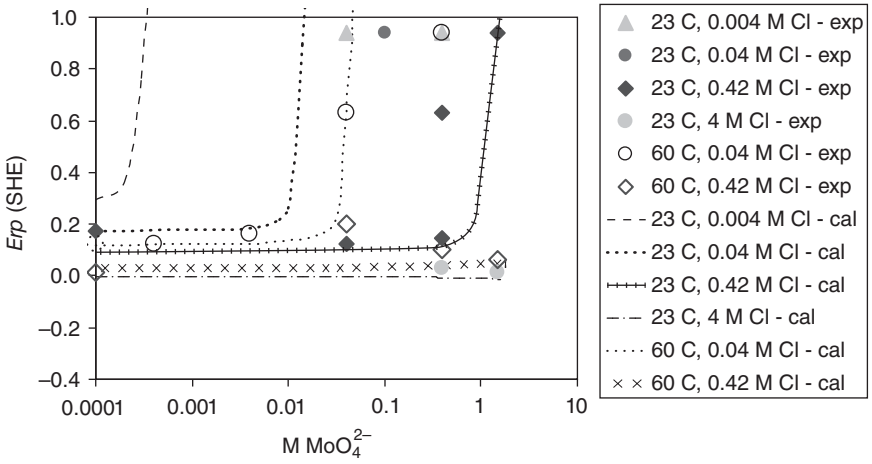

21.16 Calculated and experimental repassivation potentials of type 316L stainless steel in solutions containing sodium chloride and molybdate as a function of MoO_4^{2-} molarity at 23 °C and 60 °C.

the model provides an upper estimate for the current density for the propagation of individual pits. The current density predicted by the model as a function of potential is given by

$$i = \frac{\sum_j k_j'' \theta_j^{n_j} \exp\left(\frac{\alpha_j FE}{RT}\right) + \sum_i l_i'' \theta_i^{n_j} \exp\left(\frac{\xi_i FE}{RT}\right)}{1 + \frac{1}{i_p} \sum_i l_i'' \theta_i^{n_j} \exp\left(\frac{\xi_i FE}{RT}\right)} \qquad [21.51]$$

Equation [21.51] reduces to Equation [21.44] for $E = E_{rp}$ and $i = i_{rp}$. Since Equation [21.51] is a limiting law, its accuracy gradually deteriorates as the potential increasingly deviates from E_{rp}. Equation [21.51] cannot be regarded as a complete model for the propagation rate of an actively growing pit because it does not take into account factors such as the ohmic potential drop, diffusion limitations, etc. However, the current density predicted using Equation [21.51] for $E > E_{rp}$ is useful because it provides an estimate of the maximum propagation rate of an isolated pit as a function of potential. Such an upper estimate is particularly convenient because it relies only on parameters that have been calibrated using repassivation potential data. The measured and computed pitting rates are shown in Fig. 21.17 for three alloys in a chemical plant environment (Anderko *et al.*, 2005b).

The localized corrosion rate over the long-term depends on a number of factors including potential and chemical gradients, geometry of the pit or crevice, external potential, flow, and bulk chemistry. Solution of such a

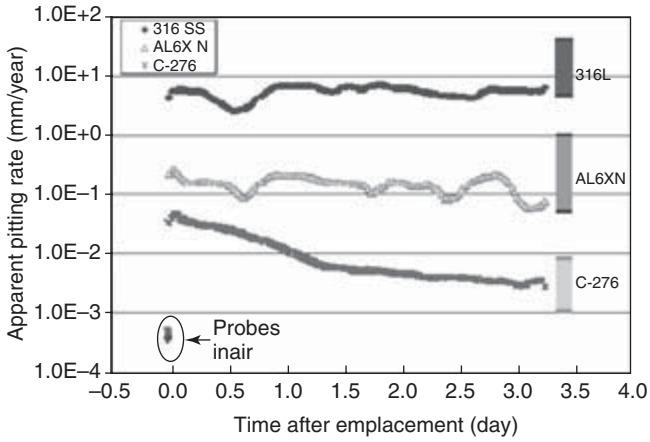

21.17 Comparison of experimental apparent pitting rates with calculated maximum rates of pit propagation for corrosion potentials obtained from short-term experiments (cf. Figure 21.5). The vertical bars show the range of predicted pitting rates when the corrosion potential varies from –0.20 V to –0.14 V (vs. SCE) and the temperature varies from 95 °C to 105 °C.

complex problem under moving boundary conditions is a challenging undertaking. However, simplified models have been developed for certain conditions (Engelhardt and Macdonald, 2004; Song and Sridhar, 2006a,b).

21.4 Future directions

This chapter described the different types of models available to the user interested in predicting or correlating the corrosion of metallic materials in various applications. It does not aim at comprehensiveness, since to do so would require a volume of its own. It is clear, however, that models of some sort will be needed to interpret monitoring results and to predict future health of the system. Models and monitoring can be used in one of three ways:

1. Monitoring can provide input parameters to a model that then is used to predict future state of the system. These monitored parameters may be environmental conditions (pH, temperature, chloride, TOW, etc.) or they can be corrosion parameters (impedance, corrosion depth, etc.).
2. Monitoring can provide verification of the models that are then used to extrapolate beyond the measurement period. In this case, the monitored parameters can be intermediate results of the modeling (e.g., corrosion potential) or predicted result (pit depth).

3. Monitoring can only be conducted at a few selected locations in a plant or field system. Modeling can help operators to select the worst case locations to monitor and predict the material performance in other locations.

Although empirical models are unsatisfactory because they are only valid under limited conditions, the current state of understanding of corrosion processes as well as computational limitations mean that empirical models will continue to be developed and used. This does not mean that continued development of fundamental models needs to be abandoned. After all, fundamental models are being used to predict very complex phenomena such as climate and weather patterns, albeit with mixed success. Therefore, corrosion science and engineering may one day also evolve out of the patchwork quilt of models that exist today. In the mean time, the hope is that the fundamental models may serve as tools to conduct sensitivity analyses (i.e. identify which parameters in a given process are most important so empirical modeling can focus on those parameters) and means to gain confidence in the simplified models that can be more amenable for practical implementation in the field.

The continual increase in computational processing speeds and memory means that ever more complex numerical simulations can be performed to capture more of the physics of the system. In this regard, multi-scale modeling involving integrated modeling at different size scales (from molecular to macroscopic level) is getting greater recognition. Improved computers and miniaturization also means that predictive models, at least the abstracted models, can be installed in monitoring systems such that the user obtains 'actionable intelligence' from the monitoring tools. Finally, models are only as good as the input data that go into determining model parameters. Unfortunately, in today's research climate, fundamental electrochemical data generation does not receive the necessary priority. It is hoped that as ISHM of corroding systems begin to be used widely, the need for augmenting the fundamental data base is recognized and fulfilled.

21.5 References

21.5.1 General reading and sources of further information

Parkins, R.N. (editor) 1994. *Life Prediction of Corrodible Structures*, Houston, TX: NACE International.

Cragnolino, G.A. and N. Sridhar (editors), 1993. *Application of Accelerated Corrosion Tests to Service Life Prediction of Materials*. ASTM STP 1194. ASTM.

Pourbaix, M. 1974. *Atlas of Electrochemical Equilibria in Aqueous Solutions* (Translated into English by J. A. Franklin), Houston, TX: NACE International.

Barber, Z. H. (editor), 2005. *Introduction to Materials Modeling*, Institute of Materials, Minerals, and Mining, Maney Publishing.

21.5.2 Specific references

Anderko, A., P. Mackenzie and R.D. Young, 2001. Computation of rates of general corrosion using electrochemical and thermodynamic models, *Corrosion*, 57 (3), 202–213.

Anderko, A., N. Sridhar and C.S. Brossia, 2005. Prediction of corrosion of nickel-base alloys and stainless steels in oxidizing environments using thermodynamic and electrochemical models, *Corrosion/2005*, Paper No. 05053, Houston, TX: NACE International.

Anderko, A., P. Wang and M. Rafal, 2002. Electrolyte solutions: from thermodynamic and transport property models to the simulation of industrial processes, *Fluid Phase Equilibria*, 194–197, 123–142.

Anderko, A., N. Sridhar and D.S. Dunn, 2004a. A general model for the repassivation potential as a function of multiple aqueous solution species, *Corrosion Science*, 46, 1583–1612.

Anderko, A., N. Sridhar, C.S. Brossia and D.S. Dunn, 2004b. A computational approach to predicting the occurrence of localized corrosion in multicomponent aqueous solutions, *Corrosion/2004*, Paper 04061, Houston, TX: NACE International.

Anderko, A., N. Sridhar and C.S. Brossia, 2005a. Prediction of corrosion of nickel-base alloys and stainless steels in oxidizing environments using thermodynamic and electrochemical models, *Corrosion/2005*, Paper No. 05053, Houston, TX: NACE International.

Anderko, A., N. Sridhar, L.T. Yang, S.L. Grise, B.J. Saldanha and M.H. Dorsey, 2005b. Validation of localized corrosion model using real time corrosion monitoring in a chemical plant, *Corrosion Engineering Science and Technology*, 40 (1), 33–42.

Anderko, A., N. Sridhar, C.S. Brossia and G. Tormoen, 2006. Modeling localized corrosion in complex process environments in the presence of inhibitors, *Corrosion/2006*, Paper No. 06215, Houston, TX: NACE International.

Bonis, M.R. and J.L. Crolet, 1989. Basics of the prediction of the risks of CO_2 corrosion in oil and gas wells, *Corrosion/89*, Paper 466, Houston, TX: NACE International.

Burstein, G.T., C. Liu, M. Souto and S.P. Vines, 2004. Origins of pitting corrosion, *Corrosion Engineering Science and Technology*, 39 (1), 25–30.

Dean, S.W. and D.B. Reiser, 2002. Analysis of long-term atmospheric corrosion results from ISO CORRAG program, in *Outdoor Atmospheric Corrosion, ASTM STP1421*, H. Townsend (editor), Conshohocken, PA: American Society for Testing and Materials, p. 3.

de Waard, C. and D.E. Milliams, 1975. Carbonic acid corrosion of steel, *Corrosion*, 31 (5), 177–181.

de Waard, C., U. Lotz and D.E. Milliams, 1991, Predictive model for CO_2 corrosion engineering in wet natural gas pipelines, *Corrosion*, 47 (12), 976–985.

de Waard, C. and U. Lotz, 1993. Prediction of CO_2 Corrosion of Carbon Steel, *Corrosion/93*, Paper 69. Houston, TX: NACE International.

de Waard, C., U. Lotz, and A. Dugstad, 1995. Influence of liquid flow velocity on CO_2 corrosion: a semi-empirical model, *Corrosion/95*, Paper 128. Houston, TX: NACE International.

Dooley, R.B., 1990. *Condition Assessment Guidelines for Fossil Fuel Power Plant Components*, Topical Report on Project 2596-10, EPRI GS-6724, Palo Alto, CA: Electric Power Research Institute, March.

Dunn, D.S., G.A. Cragnolino and N. Sridhar, 2000. An electrochemical approach to predicting long-term localized corrosion of corrosion resistant high-level waste container materials, *Corrosion*, 56(1): 90–104.

Engelhardt, G. and D.D. Macdonald, 2004. Estimation of corrosion cavity growth rate for predicting system service life, *Corrosion Science*, 46, 1159–1187.

Galvele, J.R., 1976. Transport processes and the mechanism of pitting of metals, *J. Electrochem. Soc.*, 123 (4), 464–474.

Garber, J.D., F.H. Walters, R.R. Alapati and C.D. Adams, 1994. Paper No. 25, *Corrosion/94*, Houston, TX: NACE International.

Gravano, S.M. and J.R. Galvele, 1984. Transport processes in passivity breakdown – III. Full hydrolysis plus ion migration plus buffers, *Corrosion Science*, 24(6), 517–534.

Gunaltun, Y.M., 1996. Combining research and field data for corrosion rate prediction, *Corrosion/96*, Paper 27. Houston, TX: NACE International.

Gunaltun, Y.M. and D. Larrey, 2000. Correlation of cases of top of line corrosion with calculated water condensation rates, *Corrosion/2000*, Paper 71. Houston, TX: NACE International.

Halvorsen, A.M.K. and T. Sontvedt, 1999. CO_2 corrosion model for carbon steel including a wall shear stress model for multiphase flow and limits for production rate to avoid mesa attack, *Corrosion/99*, Paper 42. Houston, TX: NACE International.

Hedges, B., K. Sprague, T. Bieri and H.J. Chen, 2006. A review of monitoring and inspection techniques for CO_2 and H_2S corrosion in oil and gas production facilities: location, location, location, Paper No. 06120, *Corrosion/2006*, 61st Annual conference, Houston, TX: NACE International.

Hernandez, S., S. Nesic, G. Weckman and V. Ghai, 2006. Use of artificial neural networks for predicting crude oil effect on carbon dioxide corrosion of carbon steels, *Corrosion*, 62(6), 467–482.

Jepson, W.P., C. Kang, M. Gopal and S. Stitzel, 1997. Model for sweet corrosion in horizontal multiphase slug flow, *Corrosion/97*, Paper 11, Houston, TX: NACE International.

Kehler, B.A., G.O. Ilevbare and J.R. Scully, 2001. Crevice corrosion stabilization and repassivation behavior of alloy 625 and alloy 22, *Corrosion*, 57(12), 1042–1065.

Konatkova, D., P. Boschek and K. Krieslova, 1995. Results of ISO CORRAG program: processing of one-year data in respect to corrosivity classification, in *ASTM STP 1239*, W.W. Kirk and H.H. Lawson (editors), Conshohocken, PA: American Society for Testing and Materials, p. 38.

Kumar, G. and R.G. Buchheit, 2004. Use of artificial neural network models for predicting coated component life from short term EIS measurements, Paper No. 04062, *Corrosion/2004*, Houston, TX: NACE International.

Lichtner, P.C., 1996. *Modeling reactive flow and transport in natural systems*, Proceedings of the Rome Seminar on Environmental Geochemistry,

L. Martini and G. Ottonello (editors) (Rome, Italy: University of Genoa), pp. 5–72.
Macdonald, D.D., 1992. The point defect model for the passive state, *J. Electrochem. Soc.*, 139, 3434–3449.
Macdonald, D.D. and M. Urquidi-Macdonald, 1992, Corrosion Damage Function – Interface between corrosion science and engineering, *Corrosion*, 48(5) 354–367.
Martinsek, A.T., 2003, Reliable inference for the maximum pit depth within pitting colonies on long pipelines, *Corrosion*, 59(12), 1058–1063.
McCuen, R.H. and P. Albrecht, 1994. Composite modeling of atmospheric corrosion penetration data, in Application of Accelerated Corrosion Tests to Service Life Prediction of Materials, in *ASTM STP 1194*, G. Cragnolino and N. Sridhar (editors), American Society for Testing and Materials, pp. 65–102.
Melchers, R.E., 2006. Examples of mathematical modeling of long term general corrosion of structural steels in sea water, *Corrosion Engineering Science and Technology*, 41 (1), 38–44.
Nor, A.M. and R.A. Cottis, 2004. Neural network modeling of the electrochemical behavior of steel in chloride solutions of varying pH, Paper No. 04063, *Corrosion/2004*, Houston, TX: NACE International.
Okayama, S., S. Tsujikawa and K. Kikuchi, 1987. Effects of alloying elements on stainless steel depassivation pH, *Corrosion Engineering*, 36, 631–638.
Oldfield, J.W. and W.H. Sutton, 1978. Crevice corrosion of stainless steels I. A mathematical model, *British Corr. J.*, 13(1), 13–22.
Palacios, C.A., T. and S.A. Corpoven, 1997. Application of simulation techniques for internal corrosion prediction, *Corrosion/97*, Paper 2. Houston, TX: NACE International.
Parkins, R.N., 1990. Stress corrosion cracking, in *Environment-Induced Cracking of Metals*, pp. 1–20, R.P. Gangloff and M.B. Ives, (Editors), Proceedings of the First International Conference on Environmental-Induced Cracking of Metals, NACE-10, Houston, TX: NACE International.
Pensado, O., D.S. Dunn, G.A. Cragnolino and V. Jain, 2003. *Passive Dissolution of Container Materials – Modeling and Experiments*, San Antonio, TX: Center for Nuclear Waste Regulatory Analyses, CNWRA-2003-01.
Pourbaix, M., 1974. *Atlas of Electrochemical Equilibria in Aqueous Solutions*, (Translated into English by J. A. Franklin), Houston, TX: NACE International.
Pride, S.T., J.R. Scully and J.L. Hudson, 1994. Metastable pitting of aluminum and criteria for transition to stable growth, *J. Electrochem. Soc.*, 141 (11), 3028–3040.
Rafal, M., J.W. Berthold, N.C. Scrivner, S.L. Grise, 1994. Models for electrolyte solutions in: *Models for Thermodynamic and Phase Equilibria Calculations*, S.I. Sandler (editor), New York: Marcel Dekker, p. 601.
Sangita, K.A. and S. Srinivasan, 2000. An analytical model to experimentally emulate flow effects in multiphase CO_2/H_2S Systems, *Corrosion/2000*, Paper 58. Houston, TX: NACE International.
Sharland, S.M. and P.W. Tasker, 1988. A mathematical model of crevice and pitting corrosion – I. The physical model, *Corrosion Science*, 28(6), 603–620.
Sharland, S.M., 1992. A mathematical model of the initiation of crevice corrosion in metals, *Corrosion Science*, 33(2), 183–201.

Shibata, T., 1996. W.R. Whitney Award Lecture: Statistical and stochastic approaches to localized corrosion, *Corrosion*, 52 (11), 813–830.

Shibata, T. and Y. Takayama, 1977. Stochastic theory of pitting corrosion, *Corrosion*, 33, 243–251.

Silverman, D.C., 2004. The rotating cylinder electrode for examining velocity-sensitive corrosion – a review, *Corrosion*, 60(11), 1003–1023.

Song, F.M. and N. Sridhar, 2006a. A two-dimensional model for steel corrosion under a disbonded coating due to oxygen with or without cathodic protection – Part 1: Full numerical solution, *Corrosion*, 62 (8), 676–686, August.

Song, F.M. and N. Sridhar, 2006b. A two-dimensional model for steel corrosion under a disbonded coating due to oxygen with or without cathodic protection – Part II: Model simplification for practical application, *Corrosion*, 62 (10), 873–882, October.

Sridhar, N. and D. S. Dunn, 1994. Effect of applied potential on changes in solution chemistry inside crevices on type 304L stainless steel and alloy 825, *Corrosion*, 50 (11), 857–872.

Sridhar, N., D.S. Dunn, A.M. Anderko, M.M. Lencka and H.U. Schutt, 2001a. Effects of water and gas compositions on the internal corrosion of gas pipelines – modeling and experimental studies, *Corrosion*, 57 (3), 221–235.

Sridhar, N., D.S. Dunn and M. Seth, 2001b. Application of a general reactive transport model to predict environment under disbonded coatings, *Corrosion*, 57 (7), 598–613.

Sridhar, N., C.S. Brossia, D.S. Dunn and A. Anderko, 2004. Predicting localized corrosion in seawater, *Corrosion*, 60 (10), 915–936.

Sridhar, N., K. Price, J. Buckingham and J. Dante, 2006. Stress corrosion cracking of carbon steel in ethanol, *Corrosion*, 62 (8), 687–702.

Staehle, R.W., 2000. Framework for Predicting Stress Corrosion Cracking, in *Environmentally Assisted Cracking: Predictive Methods for Risk Assessment and Evaluation of Materials, Equipment, and Structures, ASTM STP 1401*, R.D. Kane (ed.), West Conshohocken, PA: ASTM International, 131–165.

Staehle, R.W. and J.A. Gorman, 2004. Quantitative assessment of submodes of stress corrosion cracking on the secondary side of steam generator tubing in pressurized water reactors: Part 2, *Corrosion*, 60 (1), 5–63.

Walton, J.C., G. Cragnolino, S.K. Kalandros, 1996. A numerical model of crevice corrosion for passive and active metals, *Corrosion Science*, 38(1), 1–18.

Watson, M. and J. Postlethwaite, 1990. Numerical simulation of crevice corrosion of stainless steels and nickel alloys in chloride solutions, *Corrosion*, 46(7), 522–530 (see also discussion of this paper in *Corrosion*, 47(8), 590–591, 1991).

Williams, D.E, C. Westcott and M. Fleischmann, 1985. Stochastic models of pitting corrosion of stainless steels, *J. Electrochem. Soc.*, 132(8), 1796–1811.

Zhang, R., M. Gopal and W.P. Jepson, 1997. Development of a mechanistic model, Paper No. 601, *Corrosion/97*, Houston, TX: NACE International.

Part IV

Applications and case studies

22

Corrosion monitoring in engine exhaust systems

MICHAEL D. KASS, Oak Ridge National Laboratory, USA

22.1 Introduction

Corrosion of engine exhaust components has been a concern since the reciprocating engine was developed. Exhaust system corrosion can occur via internal corrosion (a result of the exhaust gas chemistry and temperatures inside the exhaust piping) or via exterior corrosion, whereby corrosion of the underbody materials such as the outer surfaces is caused by rock salt and chlorine. While both are important, we will only consider the topic of internal corrosion. During the early years of engine development, the corrosion rate of exhaust components was likely no greater than for other engine components, such as the block, cylinders, etc., since the overall life expectancy for engines was relatively short. However, as engines became more improved and reliable in robustness, special consideration was given to the engine and in particular the moving components. Since the exhaust components are not necessary to maintain engine (and hence, vehicle) operation, they did not receive equal attention to material improvements. However, as engine technology advanced and the powertrain components became more durable, corrosion of the exhaust system became more noticeable. With the advent of mufflers, and later three-way catalysts, the durability of exhaust systems became a serious concern.

Over the course of automotive development there have been primarily two noteworthy aspects of corrosion associated with engine exhaust systems and both were related to the fuel chemistry. For gasoline engines prior to 1986 corrosion was a serious concern. In fact, replacement of tailpipe and muffler components was fairly common and whole industries were established catering to periodic replacement of corroded exhaust (esp. muffler and tailpipe) components. The reason for the high corrosion rates of exhaust systems was related to the lead additive used to improve the octane number of gasoline. In order to prevent lead buildup on cylinder walls and valve seats, lead was introduced into the fuel primarily as lead halides containing chlorine or bromine. The chlorine and bromine anions served to scavenge the lead atoms to prevent excessive surface accumulation. However, during

combustion, hydrochloric and hydrobromic acids were formed, and subsequently corroded the sparkplugs, cylinder liners and exhaust components.[1] Following the introduction of unleaded fuel into the automotive fuel market in 1986, the corrosion rate of mild steel exhaust components was dramatically reduced.

Because corroded engine exhaust components are relatively inexpensive to replace, engine manufacturers historically paid little or no attention to exhaust corrosion. In contrast, the exhaust stacks of coal and oil burners are extremely costly and accordingly, a high level of research has been performed to understand the corrosion behavior of those systems.[2–4]

Recently, however, corrosion of diesel engine exhaust systems has become a serious concern.[5–7] This concern is driven by the incorporation of exhaust gas recirculation (EGR) as a means of lowering NOx (or oxides of nitrogen, NO and NO_2) emissions in order to meet US Environmental Protection Agency (USEPA) mandated limits. However, EGR has been shown to accelerate corrosion and wear in the intake manifold along with fouling in the EGR cooler. During EGR, a portion of the exhaust is recirculated back to the cylinder where the exhaust gas acts as a diluent to lower combustion temperature, thereby reducing the formation of NOx.[8–10] Within the intake manifold, ambient conditions (such as temperature and humidity) and coolant conditions are believed to play a critical role in the formation of highly corrosive acidic compounds, especially sulfuric acid and perhaps to a lesser extent nitric and acetic acids. EGR has been widely used in passenger car engines (diesel and gasoline) since the 1980s. However, these systems require only modest amounts of recirculated exhaust (and no cooling) to meet emission targets. In heavy-duty diesel engines, EGR was widely introduced in 2002 in North America to meet the 2.0 g/bhp-hr (2.7 g/kWh) on-highway Tier 3 NOx emission standard.[11]

In order to meet the more stringent 2008 and 2010 NOx emission standards, very high levels of EGR are being considered. Very high levels of EGR (in excess of 40%) have been shown to push combustion to low temperature combustion regimes where both NOx and particulate matter (PM) emission levels are low. Since NOx production is directly related to combustion temperature, an EGR cooler is normally used to lower the exhaust gas temperature, thereby reducing NOx emissions by an additional 10%. Cooled EGR is currently an area of intense study and high EGR strategies are expected to be used in diesel engines to assist in meeting even more stringent NOx and PM emission targets beginning in 2010.[11] However, the incorporation of EGR is not without its drawbacks. The unburned hydrocarbons and PM from recirculated exhaust have been shown to build up on chilled surfaces (especially within the intake and cooler) causing airflow problems. This fouling also has the potential for causing premature engine wear and durability problems. Another area of concern is enhanced

corrosion resulting from the formation and condensation of sulfuric acid, which is the primary motivation for assessing corrosivity within EGR exhaust components. Recent efforts have shown that relative corrosivity (i.e. sulfuric acid concentration) formed in diesel exhaust condensate is a direct consequence of fuel sulfur concentration and subsequent condensation during low temperature operating conditions.[6–7] This effect was mitigated by the utilization of diesel fuel having ultra-low sulfur content (<15 ppm). What is not known is the influence of catalysts to increase the concentrations of nitric and carboxylic acids. Another potential concern with the high EGR combustion is that the aldehyde emissions are four to five times higher than for conventional combustion. This translates into high carboxylic acid concentrations (formic, acetic and benzoic) in the exhaust. Their concentrations in exhaust condensate have not yet been measured or modeled. Although these acid types are considered weak, they may contribute to significant corrosion problems over time.

Another area gaining interest is galvanic corrosion of new turbocharger housings. Once again this problem is related to the presence of condensate where two metals having dissimilar electrical potential undergo galvanic corrosion when condensation forms and is in contact with the two metals.

22.2 Reciprocating engine combustion and exhaust chemistry

22.2.1 The combustion process and factors affecting combustion

Reciprocating engines operate by converting the heat and pressure released during combustion of fuel mixed with air into mechanical energy. A schematic depicting the process combined with EGR is shown in Fig. 22.1. Fuel is injected into the cylinder where it reacts with air entering from the intake manifold. The resulting exothermic reaction creates gases under high temperature and pressure, which expand by driving the piston downward to produce rotational energy. During the upward exhaust stroke the gases exit the cylinder and enter the exhaust system. A schematic showing the intake and exhaust sections of a typical diesel engine is shown in Fig. 22.2. After leaving the exhaust manifold, a portion of the exhaust is directed through a heat exchanger (EGR cooler) to lower the recirculated exhaust temperature. The cooled exhaust is sent to the intake where it mixes with the compressed air entering the manifold. The mixing region is darkened in the diagram.

The chemical composition of the exhaust products is primarily influenced by the fuel chemistry, fuel to air (F/A) ratio, and combustion temperature, with the F/A ratio being the most important.[12] Typical transportation fuels,

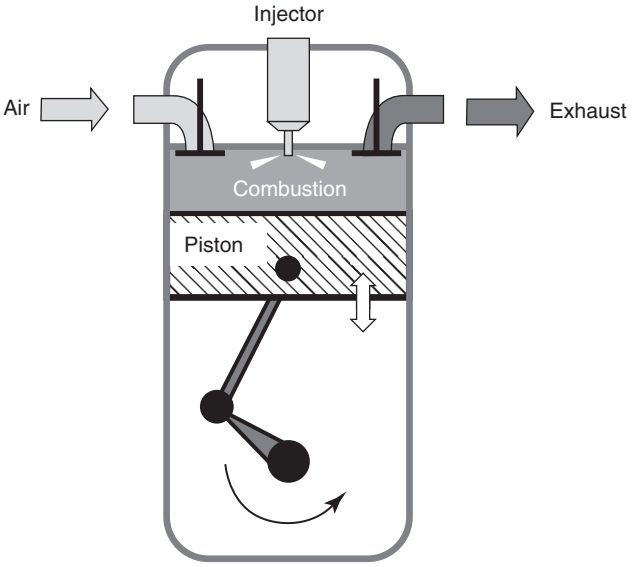

22.1 Schematic showing the operation of a reciprocating internal combustion engine.

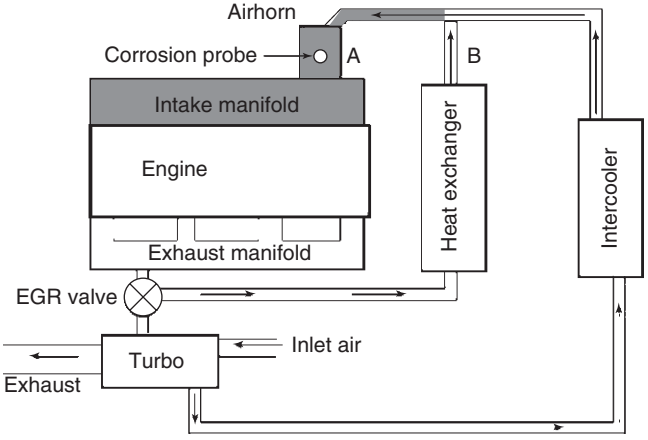

22.2 Schematic showing optimal placement of coupon specimens within the recirculated exhaust of a diesel engine.

whether gasoline or diesel, consist of a combination of paraffin compounds and aromatic rings of varying chain lengths. Paraffin and aromatic composition and concentration vary for fuel type but in general gasoline consists primarily of light hydrocarbon chains while diesel fuel is composed of heavier (longer) hydrocarbon chains and a significant level of aromatic

Table 22.1 Concentration variability of combustion products in diesel and gasoline engines

Product of combustion	Diesel	Gasoline
N_2	~75%	~75%
O_2	5–11%	0%
CO_2	6–10%	8–15%
H_2O	5–8%	5–12%
NO_x	100–1000 ppm	100–1000 ppm
CO	0–100 ppm	0–100 ppm
HC	0–300 ppm	0–100 ppm

compounds. The bulk of typical gasoline consists of hydrocarbons having between 5 and 12 carbon atoms per molecule. Diesel fuel on the other hand has between 10 and 15 carbon atoms per molecule. This molecule size is important since the fuel volatility greatly influences the combustion kinetics and, therefore, the products to a small degree. The fuel is injected into the combustion chamber and may or may not be premixed with air. The combustion of the fuel in air mixture forms CO, CO_2, NO, NO_2, H_2O, and unburned hydrocarbons (HC). If the mixture contains excess air, as in the case for diesel combustion, then O_2 will also be present in the exhaust stream. Of these components, the most important are NO, CO_2, and H_2O. However, if there is sulfur present in the fuel (which is usually the case for diesel), then the sulfur will be oxidized during combustion to form SO_2 and SO_3.[4,13–15] The concentration of the primary components is important since they are affected by the engine bulk combustion temperature and the equivalence ratio, which is a function of the fuel air mixture ratio. In general the exhaust gas composition for diesel and gasoline-based reciprocating engines is shown in Table 22.1.

As shown in Table 22.1 the primary exhaust gas species are CO_2, H_2O, N_2, and in diesels O_2 as well. Important minor constituents include unburned HC and CO. These species generally constitute about 99% of the exhaust from an engine. Since diesel fuels are mixtures of hydrocarbons of variable composition, a certain variability of the above carbon and hydrogen designations will be seen in real life samples.

22.2.2 Influence of operating variables on the combustion product formation

A number of factors affect the formation of combustion products, but the two most important are the fuel/air equivalence ratio and the combustion temperature (or bulk combustion temperature). It is important to note that

the combustion flame temperature directly influences the bulk combustion temperature but, for brevity, is not included in this discussion. The fuel/air equivalence ratio (Φ) is the ratio of the actual F/A ratio to the stoichiometric F/A ratio. The stoichiometric F/A ratio relates the theoretical proportions of fuel and air to completely oxidize all the fuel with no excess oxygen remaining. Therefore, when $\Phi < 1$, then the mixture is fuel-lean and there will be oxygen in the exhaust (as is the case for diesel combustion). When $\Phi > 1$, then the mixture is fuel-rich and there will be no residual oxygen present in the exhaust, but there will be carbon monoxide and unburned hydrocarbons present.[12]

Since EGR, engine speed and load all directly influence Φ, it is normally used as the parameter most often associated with combustion processes and exhaust chemistry. The other predominant factor is the combustion temperature since it directly affects the rates of reactions between fuel and air. Low combustion temperatures mean lower oxidation reaction rates, thereby inhibiting complete oxidization of the fuel and resulting in excess oxygen and unburned hydrocarbons along with increased CO, even at stoichiometric proportions. Likewise, high combustion temperatures increase oxidation of the fuel hydrocarbons and, for fuel-lean mixtures, increase the formation of oxides of nitrogen (especially NO). Because NOx compounds contribute to smog formation, engine NOx emission levels must meet stringent limits set by the US EPA and other regulatory agencies.

22.2.3 Catalyst effects

Catalysts are introduced into engine exhausts to reduce the emissions of NOx, HC, CO, and also particulate matter. They are used on all automotive gasoline engines to convert NOx to elemental nitrogen, and are being evaluated for potential NOx and PM control on diesel engines. In general, NOx-reducing catalysts are most effective under reducing conditions where there is no oxygen present in the exhaust, otherwise they promote oxidation reactions. In gasoline-fueled engines the fuel/air mixture is maintained near stoichiometry to eliminate oxygen and promote NOx reduction while simultaneously oxidizing CO and HC. In diesel engines this approach is less feasible since diesels operate most efficiently under lean conditions. The effects of catalysts to promote acid formation have not been well studied but it is theorized that catalysts (especially those used in PM control) will enhance the formation of oxides that will readily convert into acid compounds.

22.3 Formation of corrosive species

With the advent of cooled EGR in diesel engines, engine-induced exhaust corrosion has become a serious concern. Particularly worrisome for engine

manufacturers is the potential for severe engine damage caused by recirculating a portion of the exhaust back to the cylinders because diesel combustion can form corrosive gases containing sulfur and nitrogen. With EGR these corrosive gases are returned to the intake manifold where ambient conditions (such as temperature and humidity) and coolant conditions are believed to play a critical role in the formation of highly corrosive acidic compounds, especially sulfuric acid. Corrosion studies on coal and oil burners have shown that the main cause of corrosion and fouling of low-temperature oil-fired power plant preheater elements is the condensation of sulfuric acid (H_2SO_4) and sulfurous acid (H_2SO_3) at concentrations of only a few ppm (by volume) combined with water in the flue gas.[14–15]

Theoretical analysis of EGR conditions and sulfuric acid formation has shown that nominal levels of fuel sulfur (such as contained within No. 2 diesel fuel) could provide a highly corrosive situation for an engine equipped with cooled EGR.[5–6] As a result, several studies were initiated to monitor corrosion behavior in the EGR section of a diesel engine. The initial focus for these efforts has been the formation and corrosivity associated with sulfuric acid. However, concerns have also been raised regarding the potential corrosivity associated with the formation of nitric and carboxylic acids.

22.3.1 Sulfuric acid formation

During the combustion of sulfur-bearing fuel with excess air, most of the sulfur is converted into gaseous SO_2 or absorbed into the PM emissions. A small fraction is also converted into gaseous SO_3 (5–6). Sulfuric acid is primarily formed in diesel exhaust by a three-step process. In the first step sulfur (present in the fuel) reacts with oxygen to form gaseous SO_2. This reaction occurs during the combustion process. As the combustion products travel through the exhaust, SO_2 reacts with oxygen form SO_3 according to the following reaction:

$$2SO_2 + O_2 \rightarrow 2SO_3$$

This reaction proceeds slowly and the concentration of SO_3 formed in the exhaust is theorized to be low (<10 ppm). However, the SO_3 subsequently reacts with moisture in the exhaust to form highly corrosive sulfuric acid according to the following reaction:

$$2SO_3 + H_2O \rightarrow H_2SO_4$$

Under typical exhaust conditions sulfuric acid will condense around 150 °C while water condensation will occur at temperatures close to 25–30 °C.[5–6,16–17] SO_2 and SO_3 have boiling points of –10 °C and 45 °C, respectively and both are stable if kept anhydrous and deoxygenated. In the presence of water

and oxygen, both will rapidly convert to sulfuric acid. Theoretically-based analysis by McKinley *et al*. indicated that a mixture of sulfuric acid and water will condense in the temperature range between 63 and 156 °C and that the concentration of acid in the condensate will be 60–80% by weight.[6] The McKinley study (6) was the first to consider that condensation below the water dewpoint might be a larger concern since there will be significant conversion of SO_2 to H_2SO_4 with the onset of water condensation.

Although most of the sulfur emitted from diesel exhaust currently originates from the fuel, this may not be true in the near future. Beginning in 2006, the sulfur concentration for on-highway diesel fuel used in the United States began phasing-in to levels at or below 15 ppm. When these regulations are fully implemented, sulfur originating in the lubricant and atmospheric sources will likely be the primary contributors. At this point corrosion may be driven primarily by nitric and carboxylic acid formation.

22.3.2 Nitric acid formation

An undetermined level of nitric acid is also formed in the engine exhaust. Here the relevant species is NO_2 not NO, which normally makes up over 90% of the generated NOx emissions. However, under lean conditions most catalysts will convert NO to NO_2, especially urea-selective catalytic reduction (urea-SCR) and continuously regenerating traps-diesel particulate filter (CRT™-DPF) systems which employ an oxidation catalyst to convert NO to NO_2 to assist in PM and NOx reduction. Nitric acid is a strong acid, and in aqueous solution, it completely dissociates into the nitrate ion NO_3^- and a hydrated proton, known as a hydronium ion, H_3O^+. Nitric acid will also form when the dewpoint temperature is reached inside the engine exhaust according the reaction:

$$2NO_2 + H_2O \rightarrow 2HNO_3$$

22.3.3 Carboxylic acids

Carboxylic acids are organic acids characterized by a carboxyl group (COOH). They are widespread in nature and are typically weak acids, meaning they can only dissociate into H^+ cations and $RCOO^-$ anions in aqueous solutions. The presence of electronegative groups (such as OH^- or Cl^-) next to the carboxylic acid increases the acidity through inductive effects. In engine exhaust they are created through the complete oxidation of primary alcohols (methanol and ethanol may be present in exhaust under certain conditions) and aldehydes (which are frequently present in diesel and natural gas engine exhaust). The reaction with aldehyde is the one of most concern:

$$RCOH + \tfrac{1}{2}O_2 = RCOOH$$

Since catalysts may promote the oxidation of aldehydes, the presence of carboxylic acid may be a concern for exhaust components downstream of a catalyst.

22.4 Monitoring techniques

Corrosion monitoring of engine exhaust is relatively recent and as mentioned previously is driven by the incorporation of cooled EGR to reduce NOx emissions from reciprocating engines. In contrast, corrosion monitoring in the exhaust stacks of coal and oil combustion burners is commonplace and widespread.[13–15] This industry incorporates a number of methods to monitor and assess corrosion potential in the flue gas within the stack. They include measurement of the SO_3 content in the flue gas via chemical analysis, measurement of the acid buildup using electrical conductivity methods, and direct measurement of mass-loss using electrical resistance (ER) based probes. In contrast, corrosion measurement within the engine exhaust has been limited primarily to gravimetric methods based on coupon exposures. More recent efforts have included ER probes and wet chemistry methodologies. Each of these methods has its advantages and disadvantages and each is described below in detail.

22.4.1 Classical gravimetric method

The oldest and most traditional method of monitoring corrosion is to employ pre-weighed specimens composed of a metal alloy, frequently mild steel. For engine exhaust consideration, these will typically be composed of steel and aluminum alloys. The geometry of the coupons varies according to the test conditions but needs to be small enough to fit inside the exhaust stream and inside the component of interest. In one study, mild steel coupon specimens (weighed to 0.1 mg accuracy) were placed at the airhorn position (A) and at exit of the heat exchanger (B) as shown in Fig. 22.2 of a heavy-duty diesel engine.[17] These sampling locations were chosen because the potential for corrosion at these points was considered relatively high. The engine was fueled with a 2004 No. 2 certification fuel with a nominal sulfur content of ~350 ppm. The temperature of the gas exiting the chiller was maintained near 60 °C, which is above the water dewpoint but below the temperature required for the condensation of sulfuric acid.

The corrosion rate is determined by measurement of the mass lost due to corrosion and/or erosion from the exposed coupon's surface. This technique may necessitate very long exposure times to accurately assess a rate of corrosion. For engine experiments this means long exposure durations

in an engine test cell, which can be very expensive and time consuming. This method also requires careful specimen preparation and measurement of the mass, usually to within 0.01 g accuracy. A key advantage with this approach is that details of the microstructure can be ascertained and the precise nature of the corrosive effect can be determined. Structural features, such as pitting, occlusions, spalling, and intergranular degradation can be directly observed. Another advantage is that the formation of corrosive products can often be detected via electron microscopy techniques and spectrographic techniques such as diffuse infrared Fourier transform (DRIFT) spectroscopy.[17]

In the above-mentioned study, the coupons were removed after four hours of exposure.[17] The surfaces of the specimens were relatively free of particulate matter but did appear to be slightly corroded. The corrosion rates were found to be very low (<10 mm/y) at both the EGR cooler exit and intake. This result indicates that the coupon measurements may not be the most efficient method for determining corrosivity within engine exhaust during short periods of engine operation. In order to get a reliable measurement, engine operating times approaching 100 hours are normally required. Note that corrosion may be a complex process incorporating PM and HC accumulation along with condensation and corrosion. In addition the corrosion is likely not to be steady state but more transient in nature which would also require long exposure times.

The surfaces of the exposed coupons were scanned using DRIFT spectroscopy to determine the presence of possible corrosion products. The results shown in Fig. 22.3 revealed that the corrosion product, iron sulfate, was formed on the surface indicating that sulfuric acid was reacting with the mild steel coupon. Further DRIFT spectrographic analysis also observed that the surface chemistry of the specimen exposed in the intake differed from the specimen placed in the chiller exit.[17]

Preliminary studies have shown that the corrosion rates of exposed mild steel specimens are too low for this technique to be utilized to assess corrosivity in a reasonable timeframe; however, this method provided important information regarding possible corrosion mechanisms.

22.4.2 *In-situ* measurement of corrosivity using an electrical resistance-based probe

The utilization of an electrical resistance (ER) probe to elucidate corrosion behavior via corrosion rate measurement is a relatively recent application of this technology. The driving force for utilizing ER probes is the ability to obtain accurate corrosion rates within a reasonable time via *in-situ* measurement. The speed of this approach allows engine designers to quickly evaluate a large number of engine operating parameters to assess

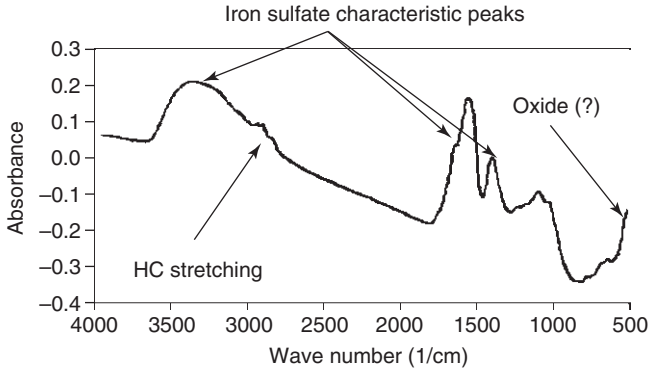

22.3 Diffuse infrared Fourier transform (DRIFT) spectroscopy results from a mild steel coupon exposed to recirculated exhaust of a diesel engine fueled with No. 2 diesel fuel. The peaks correspond to the signature stretching modes associated with specific molecular structures. The HC stretching indicates that unburned hydrocarbons were also present on the exposed coupon surface.

the corrosion potential associated with EGR. The goal is to enable engine manufacturers to establish boundary conditions on engine operation in order to avoid enhanced corrosion. Kass *et al.* (16) performed a study to determine the effectiveness of an advanced ER probe system to evaluate corrosion behavior in heavy-duty diesel exhaust as a function of intake conditions and engine operation. The instrument used in this study was a commercially-available probe manufactured by Cormon Ltd (Sussex, United Kingdom). The probe utilizes their proprietary CEION™ technology to enable high resolution measurement (<1 micron) at relatively high sample rates (up to 0.25 Hz).[18] A photograph of the probe tip is shown in Fig. 22.4. The probe measures 2.54 cm in diameter and consists of two, essentially identical, spiral elements. One of the elements measures the fluid temperature and also provides for temperature compensation (since temperature has a pronounced influence on electrical resistance) (see Chapter 11). A key feature of this probe is the ability to compensate for temperature fluctuations which is necessary for assessing corrosivity within engine exhaust. The system was originally developed to monitor oil pipeline wear and this effort was the first to apply this technology to engine exhaust. In effect, the corrosion probe offers an *in-situ* method of assessing the potential of corrosion in near real time. Prior evaluations using the Cormon probe have shown that an accurate measurement could be made within 30 minutes for each operating setpoint and the measured corrosion rates were determined to be highly repeatable (typically within 5%). However, because of sample rate limitations this method cannot be used

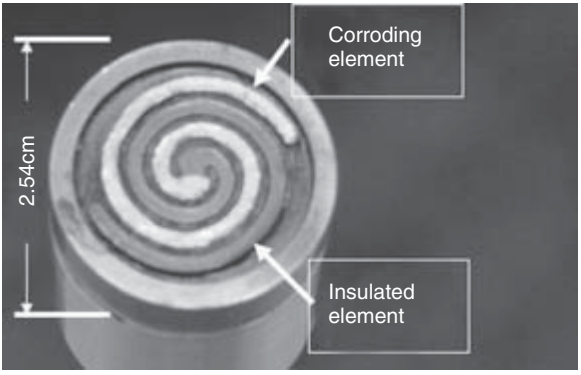

22.4 Photograph of corrosion probe tip showing element configuration.

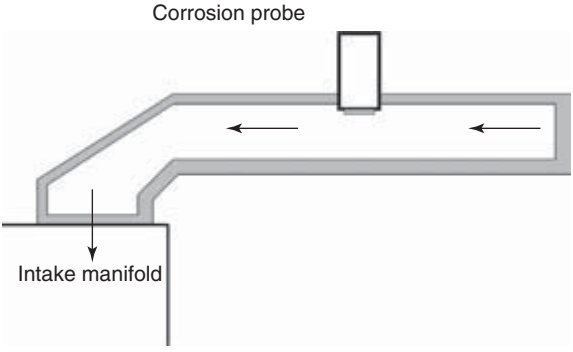

22.5 Schematic showing vertical mounting of the corrosion probe within the airhorn section of a heavy-duty diesel engine.

for transient analysis and is therefore limited to steady-state evaluation only. Future probe designs may be fast enough to compensate for transient operation but none as of yet are on the horizon.

The location and arrangement of the probe in the exhaust system is an important consideration. Previous studies have shown that an optimal consideration is to locate the probe in a vertical arrangement pointing down as shown in Fig. 22.5. The advantage of this orientation is that it prevents condensate from accumulating and stagnating on the probe elements. Also if the probe is located on the bottom with the tip facing upward, the probe elements may be placed in a non-uniform distribution of moving condensate. In other words, the condensate may pool along the bottom surface and travel as irregular rivulets which have the potential to eliminate the uniformity of the measurement. However, this effect, while suspected, has not been tested experimentally.

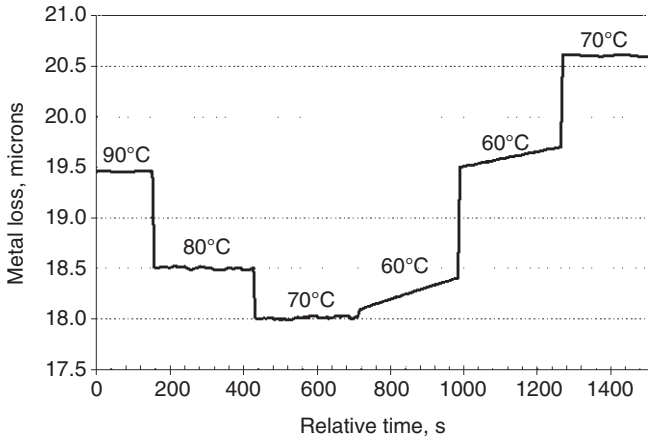

22.6 Plot of the mass loss as a function of engine exhaust temperature to demonstrate the performance of an ER probe to measure corrosion rate in diesel exhaust under steady-state operation. Note that the probe expresses mass loss in units of length (in microns) lost during corrosion (assuming uniform corrosion).

Performance and operation

In the Kass *et al.* study,[16] the engine was held at a fixed operating mode (speed and load) and EGR fraction. An example of the performance of the probe over time as a function of exhaust temperature is shown in Fig. 22.6. For the first three conditions, the mass loss is lowered with decreasing temperature; however, the resulting change in mass loss for these points is negligible (the slope or rate of corrosion is ~0). In contrast, the mass loss is observed to increase with time for the following 60 °C test points. It is important to note that the exhaust dewpoint for these conditions is ~65 °C, and hence corrosion does not occur significantly until conditions promoting condensation occur. Also note that the response of the probe is shown to be stable over the engine test conditions after about five minutes of exposure. However, the probe response is dependent on the stability and uniformity of the exhaust environment and does not reflect the performance to be achieved from other test conditions. Other studies have shown that 30 to 45 minutes of probe operation were necessary to achieve reliable and stable readings form which to determine corrosion rates.

Application of ER probe to assess corrosivity with key engine variables

ER probe measurements have proven useful in assessing the exhaust corrosivity associated with fuel sulfur level, water condensation, and EGR

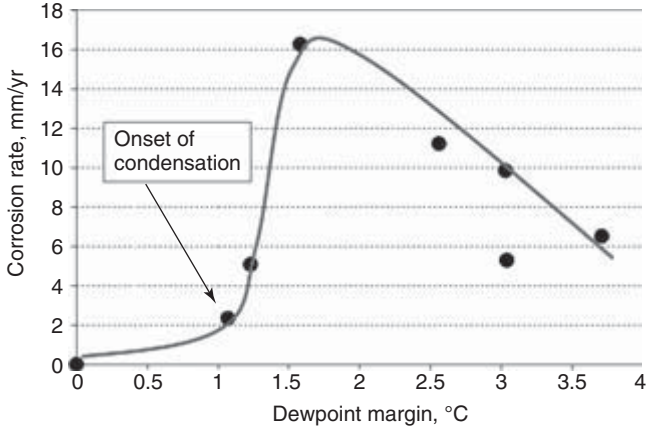

22.7 Corrosion rate results associated with the onset of condensation as measured using an ER probe in a heavy-duty diesel engine fueled by 350 ppm sulfur-bearing fuel.

fraction. This method has shown that mild steel probe elements only reported significant corrosion with the onset of condensation as shown in Fig. 22.7, where dewpoint margin is defined as the difference between the actual temperature and the theoretical dewpoint temperature of water. In this figure, corrosion does not occur until the exhaust temperature drops below the dewpoint temperature. As the exhaust temperature begins to decrease below the dewpoint temperature, the corrosion rate suddenly jumps to a high value and then begins to decrease with increasing dewpoint margin. This effect is expected since the acid concentration of the condensate would be highest at the point of onset as the dewpoint margin increases and the quantity of condensed water increases; the acid concentration of the condensate would decrease accordingly, assuming that the exhaust gas chemistry is unchanged. For this experiment the fuel used to operate the engine contained ~350 ppm sulfur. An ultra low sulfur diesel fuel (<15 ppm) was also evaluated and showed no evidence of noticeable corrosion, thereby indicating that sulfuric acid is the primary corrosive agent.[16]

22.4.3 Wet chemical analysis techniques

Wet chemistry methods have been utilized to assess the chemistry and acidity of exhaust condensate. To do so, it is necessary first to collect the condensate prior to analysis. A simple method to collect condensate in the exhaust is to attach a sampling tube to the exhaust component of interest. In one successful arrangement, a clear plastic tube was attached to a port valve connected to the intake airhorn where recirculated exhaust mixed

with incoming air prior to entering the combustion chamber. The port was located on the bottom of the airhorn, and during conditions in which condensation was observed, the top valve was opened while the release valve was kept closed. When the tube was filled up, the top valve was closed and the bottom one opened to allow the condensate to be poured into a container for subsequent analysis. Studies showed that condensation commences rapidly once the dewpoint temperature for the exhaust environment is reached.

Unfortunately, pH-based methods have not been reliable since the suspended particulate matter formed in the exhaust has been known to interfere with probe operation. However ion chromatography has been successfully employed to measure the dissolved levels of acetate, formate, nitrite, nitrate and sulfate in the collected condensate. During one study, the exhaust condensate was collected for two different fuel sulfur concentrations; 350 and 15 ppm, and analyzed using ion chromatography. Analysis of the data revealed that negligible amounts of acetate, formate, and nitrate were measured in the condensate samples. However, appreciable levels of both nitrate and sulfate were detected in the condensate samples for both fuel types. The results indicated that, for the 15 ppm sulfur fuel, the relative concentrations of sulfate and nitrate are similar. In contrast, the sulfate concentrations for 350 ppm sulfur fuel are around ten times higher than the 15 ppm sulfur fuel while the nitrate concentrations are similar to the 15 ppm sulfur fuel levels. When the sulfur concentrations (as measured via ion chromatography) are compared with the ER probe corrosion rate (see Fig. 22.8), a positive correlation was observed. The data shown in Fig. 22.8 also demonstrate the advantage of combining ER probe results with a more conventional wet chemistry method to further elucidate the corrosive behavior.[16]

22.5 Current issues and future needs

Because corrosion monitoring of engine exhaust is a relatively new area of study, there are a wide ranges of issues that need to be determined for conventional engine operation. One of the more immediate needs is to elucidate the condensation chemistry especially as a function of engine type, fuel chemistry and operating conditions. This information is critical in order to adequately model engine exhaust corrosion and to guide controlled bench-scale studies. Other areas needing further research include corrosion monitoring during transient operation and the influence of catalysts on condensate chemistry. Measurement during transient operation will necessitate the development of faster monitoring methodologies and novel applications of in-situ probes.

Currently, a dynamic area of research involves the application of very high levels of recirculated exhaust (up to 50%) to the combustion process.

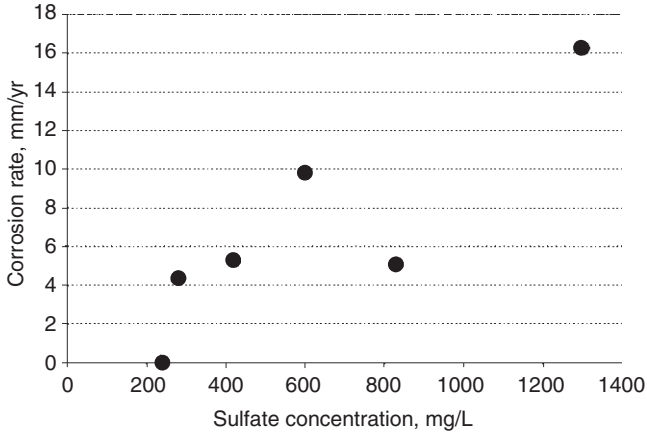

22.8 Correlation of corrosion rate (determined using an ER probe) with the sulfate concentration of the collected sulfate.

High EGR rates allow the engine to operate in unconventional combustion regimes that are characterized by low NOx and PM emissions. However, these regimes produce high levels of unburned hydrocarbons and CO in the exhaust, and, therefore, increase the potential of carboxylic acid formation. The effects of high levels of hydrocarbons and CO in the exhaust on system components have not been well studied. However, it is known that unburned hydrocarbons will coalesce and accumulate on cooled surfaces inside the exhaust. The effect of this buildup on material durability has not been evaluated but undoubtedly will be a future concern with the development of newer engines, gasoline and diesel.

22.6 References

1 Jamie Lincoln Kitman, 'The Secret History of Lead', *The Nation*, 20 March 2000 and Jane Armstrong, 'US Experience with Lead Phase-out', USEPA Office of Transportation and Air Quality, www.unep.org/pcfv/Documents/SADCJArmstrongPres.ppt.
2 Zoltan Fargo, 'Fuel Sulfur Content, Sulfur-Oxide Emission and Corrosion in Oil-Heated Plants', *Combustion Science and Technology*, 79: 73–96, 1991.
3 J. Uruchurtu, J. M. Malo, E. M. Garcia, U. Cano, L. Mariaca and A. Martinez, 'Corrosion Assessment of Regenerative Preheaters in Oil-Fired Power Plants', *Corrosion* 51 (11): 872–879, 1996.
4 R. T. Squires, 'The Kinetics of SO_3 Formation in Oil-fired Boilers', *Journal of the Institute of Energy* 55 (422): 41–46, 1982.
5 A. M. Kresco, J. H. Johnson, L. D. Gratz, S. T. Bagley and D. G. Leddy, 'A Study of the Vapor- and Particle-Phase Sulfur Species in the Heavy-Duty Diesel Engine EGR Cooler', SAE Paper No. 981423, 1998.

6 T. L. McKinley, 'Modeling Sulfuric Acid Condensation in Diesel Engine EGR Coolers', SAE Paper No. 970636, 1998.
7 P. K. Engle, R. E. Thompson and R. Silvestrini, 'Corrosion and Fouling Potential in Diesel Exhausts', Transactions of the ASME Series A: *Journal of Engineering for Power* 101 (4): 589–606, 1979.
8 EGR Systems & Components, *DieselNet Technology Guide*, www.DieselNet.com. Copyright Econopoint Inc. Revision 2004.12.
9 Richard Stone, *Introduction to Internal Combustion Engines*, second edition, Warrendale, PA: Society of Automotive Engineers, Inc. 400 Commonwealth Drive, 15096-001, 1995. Note: has a couple of words on EGR.
10 Horst Bauer (editor in chief), *Diesel Engine Management*, second edition, Stuttgart, Germany: Robert Bosch GmbH, 1999. Decent EGR section.
11 US EPA Emission Standards for Heavy Truck and Bus, http://www.dieselnet.com/standards/us/hd.html.
12 John B. Heywood, *Internal Combustion Engine Fundamentals*, New York: McGraw-Hill, Inc.
13 T. Land, 'The Theory of Acid Deposition and its Application to the Dew-Point Meter', *Journal of the Institute of Fuel* 50 (403): 68–75, 1997.
14 J. Uruchurtu, J. M. Malo, E. M. Garcia, U. Cano, L. Mariaca and A. Martinez, 'Corrosion Assessment of Regenerative Preheaters in Oil-Fired Power Plants', *Corrosion* 52 (11): 872–879, 1996.
15 E. S. Lisle and J. D. Sensenbaugh, 'The Determination of Sulfur Trioxide and Acid Dew Point in Flue Gases', *Combustion* 36: 12–16, January 1965.
16 M. D. Kass, J. F. Thomas, D. F. Wilson, S. A. Lewis, Sr. and A. Sarles, 'Assessment of Corrosivity Associated with Exhaust Gas Recirculation in a Heavy-Duty Diesel Engine', SAE Paper No. 2005-01-0657. 2005.
17 M. D. Kass and D. F. Wilson, DOE Report on EGR Corrosion of Heavy-Duty Diesel Engines, 2001.
18 *Cormon News*, www.cormon.com/cormon/news.aspx, August 2004.

23

Corrosion monitoring in cooling water systems using differential flow cell technique

BO YANG, Honeywell, Ridgefield, Connecticut, USA

23.1 Introduction

In this chapter, examples of laboratory and field applications of the differential flow cell technique for corrosion monitoring in cooling water systems are described. The differential flow cell technique is an on-line measurement method capable of real-time determination of localized and general corrosion rates of metals in aqueous solutions. The principles of the method, typical designs of the monitors, and guidance on data interpretation are described in Chapter 6.

23.2 Corrosion inhibition program selection and optimization

This study was conducted in a two-unit pressurized water reactor (PWR) nuclear power plant in the Midwest of the United States.[1] The plant uses water from an impounded lake for once-through cooling. Water from the lake is made-up and blown-down from a river. Condenser circulating water design flow is 720 000 gpm (2730 m^3/min) per unit (with three circulating water pumps running). The total essential service water flow is 24 000 gpm (90.8 m^3/min) and the total non-essential service water flow is 70 000 gpm (265 m^3/min). The service water systems were experiencing an increasing trend in corrosion rates based on corrosion coupon results (about 12 mpy (305 µm/y) for carbon steel coupons with >90 day exposure) and pipe inspection/repair frequency. Considering the large volumes of water to be treated (for this reason, no corrosion inhibitor was used), it was recognized that economics and environmental concerns would be major drivers in the development of a corrosion control program. Traditional treatments known to be effective would cost about $3 million per year to implement. Research was conducted in the laboratory to develop a treatment program that could deliver the desired results. Based on lab results, a combination of blended

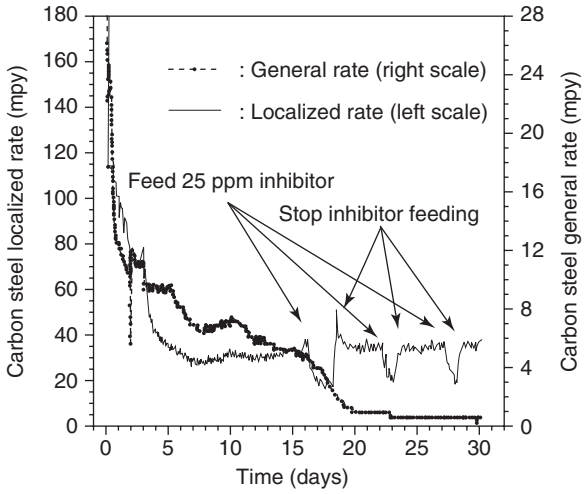

Note: Nuclear station lake water, once-through service water system
Continuous NaOCl feed. 1 mpy = 25.4 μm/y

23.1 Effect of intermittent inhibitor feed on carbon steel corrosion in a once-through cooling water system.

deposition corrosion inhibitors and a novel feed approach showed the greatest promise. A side-stream system was developed to model the cooling water system at the plant.

Several trials were run with varying degrees of success. Results from the treatment program that yielded the greatest potential are shown in Fig. 23.1. Analysis results of the lake water used as the once-through cooling water in the studied period is shown in Table 23.1. In this situation, it was shown that intermittently feeding a relatively high dosage of inhibitors provided the greatest overall corrosion control. This was compared to continuous feed of inhibitors at a medium dosage, which resulted in higher corrosion rates.[1] Not only did the continuous corrosion inhibitor feed give poorer results, it delivered more total amount of chemicals to the system, resulting in a higher costing program.

In Fig. 23.1, the general corrosion rate was shown to drop steadily and stay low following the first slug of inhibitor. The localized corrosion rate initially decreased by about half the original value after the first slug of inhibitor, but shortly thereafter the rates leveled off at a minimum value. At this point, inhibitor feed was discontinued and the localized corrosion rates rapidly increased to their original level. This cycle was twice repeated, showing similar responses in the localized corrosion rate when the corrosion inhibitor was intermittently fed.

Table 23.1 Midwest Nuclear Power Plant – once through cooling lake water

Date	26 Feb	12 Mar	13 May	18 Jun	28 Jul
Water analysis ICP or IC results, ppm	Total	Total	Total	Total	Total
Ca^{2+} ($CaCO_3$)	210	190	190	150	160
Mg^{2+} ($CaCO_3$)	330	310	310	290	330
Iron (Fe)	0.2	0.3	1.9	0.7	0.3
Sr^{2+} (Sr)	0.3	0.3	0.3	0.3	0.3
Na^{+} ($CaCO_3$)	100	99	92	84	98
K^{+} (K)	7.8	7.1	7.2	6.8	8.1
Aluminum (Al)		0.1	0.1	0.3	0.2
Phosphorus (PO_4)	<0.3	0.5	0.5	<0.3	<0.3
Silica (SiO_2)	3.1	1.5	1.5	3.9	9.8
Sulfur (SO_4)	260	260	270	250	290
Boron	0.2	0.2	0.2	0.2	0.5
Cl^{-} ($CaCO_3$)	110	110	110	85	120
Sulfate ($CaCO_3$)	230		260	230	270
M-alkalinity ($CaCO_3$)	238	217			
Nitrite (NO_2)		<2.9	<2.9	<2.9	<2.9
Nitrate ($CaCO_3$)		4.8	5.7	4.3	<2.9
Other					
Conductivity, µS/cm	1130	1140			
pH	7.5	8.6			

Note: ICP – Inductively Coupled Plasma Atomic Emission Spectroscopy. IC – Ion Chromatography.

From this case study, it is important to note that it is the area under the curve that relates to the total corrosion in the system. In this case, the general corrosion was maintained and the localized corrosion level was intermittently reduced, giving an overall performance better than could be achieved with a continuous feed approach. Thus, *the sensitivity of the LCM allowed for close monitoring of system corrosivity changes, resulting in a novel intermittent inhibitor dosage strategy*. Also, during this evaluation, it was shown that temperature and make-up water chemistry have a great impact on corrosion rates. These factors are intuitive to most water treatment professionals. However, given the sensitivity of the LCM it is possible to adjust the treatment program based on these clearly identifiable effects.

It should be noted that good correlation between LCM time average rate readings and coupon general rate and pitting rate results are obtained in the same exposure periods in this study.[1]

23.3 Program optimization at a chemical processing plant

This case study was conducted in the chlor-alkali cooling water system (system capacity: ~650 000 gallons or 2460 m^3) of a large integrated plastics producer in the Southwest of the United States.[2] The cooling water system had a very long holding time index (HTI up to 6–9 days; 5 to 15 cycles of concentration) with variable calcium ions (150 to 300 mg/L as $CaCO_3$ or 1.5 to 3 mM in the tower) and used condensate water as partial cooling water make-up. Other challenging conditions in the system included:

- Frequent leakage of 30 and 50% sodium hydroxide from the nickel plate and frame exchangers to the cooling water due to pitting corrosion, crevice corrosion, plastic deformation at the plate and frame contact points
- Low flow rates in certain shell-side carbon steel heat exchangers due to process demand variations (one shell-side carbon steel column condenser with double segment baffle design experienced a localized corrosion related failure after 2 years of service, indicating a time averaged penetration rate of 40 mpy or 1 mm/y)
- Low flow rate in the ethylene dichloride reactor jackets, resulting in high corrosion rates and plugging with corrosion products and other deposits (consisting of mostly iron oxides and hydroxides)
- Desire to operate at even higher cycles of concentration to conserve water

The system used an Alkaline Stabilized Phosphate program and chlorine gas at the start of the study. A Stabilized Phosphate program was used before, with unsatisfactory results. High carbon steel general corrosion rates were obtained in the bulk cooling water by coupons and LPR general corrosion rate measurements. Severe fouling occurred at the ethylene dichloride reactor requiring acid cleaning once per year.

A newly developed Alkaline Stabilized Phosphate treatment program containing a new stable cathodic localized corrosion inhibitor was judged to be especially suitable for this system.[3] The LCM was used to conduct on-line optimization of this new treatment program to minimize localized corrosion, the most critical concern at this plant. Several combinations of inhibitors, dispersants and biocides were used and an excellent program was developed. The results are shown in Fig. 23.2. Chemical analysis of several key parameters of the cooling water in the system (return water after flowing through all the heat exchangers) is shown in Table 23.2.

Over the four months period of this study, the cycles of concentration were steadily increased due to the need for reducing make-up water usage, ultimately rising by a factor of 4 at the end of the study. By taking a

Table 23.2 Chemical processing plant cooling water return analysis – stabilized alkaline phosphate treatment + Cl

Date	Conductivity µS/cm	Total hardness ppm $CaCO_3$	Ca^{2+} ppm $CaCO_3$	M-alk ppm $CaCO_3$	pH
3/9/1998		212	190		
3/19/1998	1170		203	136	8.4
4/14/1998	1820		205	135	8
4/15/1998	1880	220	166	132	8.41
4/16/1998	2040	250	194	148	8.47
4/17/1998	2230	266	212	156	8.46
4/18/1998	2390	280	220	164	8.33
4/20/1998	2220	248	204	148	8.57
4/21/1998	2250	244	208	156	8.42
4/22/1998	2150	260	188	144	8.22
4/23/1998	2100	270	200	140	8.42
4/24/1998	1910	270	210	132	8.37
4/25/1998	1808	285	220	152	8.4
4/27/1998	1910	350	280	140	8.53
4/28/1998	1970	370	300	150	8.49
4/29/1998	2090	412	324	160	8.47
4/30/1998	2130	460	360	168	8.44
5/1/1998	2140				8.5
5/4/1998	2120	448	400	136	8.33
5/5/1998	2140	470	390	126	8.37
5/6/1998	2100	480	410	140	8.43
5/7/1998	2135	500	412	144	8.5
5/8/1998	2180				8.5
5/11/1998	2360	600	488	144	8.37
5/12/1998	2402	620	500	140	8.4
5/14/1998	2410	624	508	148	8.43
5/16/1998	2620	628	510	148	8.32
5/18/1998	2643	680	552	160	8.5
5/19/1998	2730	710	600	160	8.48
5/20/1998	2930	716	600	140	8.33
5/21/1998	3093	728	608	140	8.34
5/22/1998	2917	716	600	120	8.38
5/23/1998	2990	712	600	120	8.4
5/24/1998	2940			120	8.4
5/25/1998	3040			126	8.46
5/26/1998	3070	736	612	122	8.41
5/27/1998	3091	736	614	168	8.59
5/29/1998	3190	832	692	172	8.57
6/1/1998	3790	824	712	188	8.61
6/2/1998	3850	820	732	204	8.64
6/3/1998	3910	1000	780	200	8.6
6/4/1998	3910	880	760	200	8.46
6/5/1998	3670	1120	810	160	8.48

Table 23.2 Continued

Date	Conductivity µS/cm	Total hardness ppm $CaCO_3$	Ca^{2+} ppm $CaCO_3$	M-alk ppm $CaCO_3$	pH
6/6/1998		380	340	180	8.4
6/7/1998		820	760	180	8.4
6/8/1998	2710	970	568	180	8.51
6/9/1998	2730	920	552	180	8.57
6/10/1998	2650	870	588	160	8.59
6/11/1998	2770	860	640	180	8.5
6/12/1998	2810	690	580	180	8.69
6/13/1998	2810	680	640	180	8.4
6/14/1998	2870	660	640	180	8.5
6/15/1998	2840	700	668	184	8.58
6/16/1998	2961	720	688	188	8.63
6/17/1998	3090	768	724	196	8.64
6/18/1998	3100	760	640	172	8.6
6/19/1998	3160	920	850	180	8.54
6/20/1998	3200	880	860	180	8.4
6/21/1998	3140	950	880	184	8.4
6/22/1998	3190	860	850	184	8.57
6/23/1998	3260	910	860	180	8.65
6/24/1998	2790	830	720	196	8.5
6/25/1998	3120	900	770	192	8.4
6/26/1998	3310	830	740	180	8.63
6/27/1998	3040	870	750	170	8.62
6/28/1998	3220	810	730	170	8.64
6/29/1998	3120	820	620	176	8.8
6/30/1998	3210	820	640	186	8.5
7/1/1998	3310	840	710	176	8.4
7/2/1998	3420	880	800	168	8.4
7/3/1998	3520	950	850	164	8.45
7/4/1998	3480	850	800	176	8.5
7/5/1998	3550	860	850	160	8.42
7/6/1998	4440	830	640	160	8.51
7/7/1998	4560	860	780	168	8.53
7/8/1998	4880	820	730	185	8.36
7/10/1998	4370	920	800	148	8.46
7/11/1998	4360	880	800	144	8.41
7/12/1998	3960	840	720	266	8.69
7/13/1998	3790	860	820	185	8.5
7/14/1998	3570	720	600	152	8.45
7/15/1998	3560	620	600	160	8.35
7/16/1998	3550	754	612	160	8.49
7/17/1998	3290	670	660	152	8.4
7/18/1998	3680	810	650	160	8.4

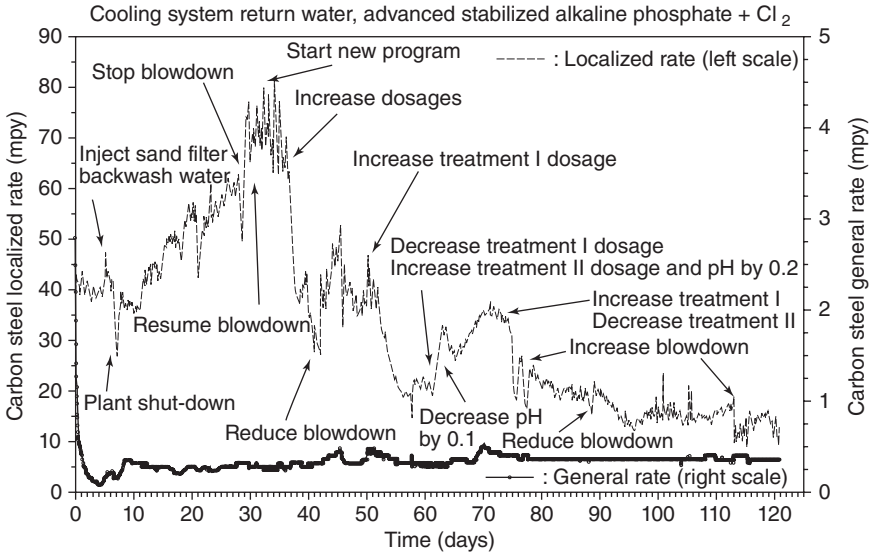

Note: Data shown: 19 March 1998 15:08 to 18 July 1998, 9:24. 1 mpy = 25.4 μm/y
March 1998: Ca = 150 – 200 ppm; July 1998: Ca = 600 – 1000 ppm as $CaCO_3$

23.2 Chemical process plant: chemical treatment optimization using the LCM.

macroscopic view of Fig. 23.2, one can see that the LCM was proven to be extremely useful in optimizing treatment performance for localized corrosion, decreasing the localized corrosion rate from 70–80 to 10–15 mpy (1780–2030 to 250–380 μm/y).

At the beginning of the study, the localized corrosion rate was increasing with time after the initial 13 days. Since the direction of the changes is opposite to the expected reduction of corrosion rate with time (see the previous example in Fig. 23.1), this indicates that the treatment performance against localized corrosion in the system is worsening. Application and optimization of the new program resulted in steadily decreasing localized corrosion rates, despite the approximately four-fold increase in cycles (conductivity changed from ~1200 μS/cm to 4000–5000 μS/cm and calcium concentration changed from 150–200 mg/L to 600–1000 mg/L as $CaCO_3$) during the study. A more microscopic view of the data shows that the LCM identified upset or non-ideal operating conditions and treatment program changes. The following are some of the specific results obtained:

Identified upset or changes in operating condition:

- Injection of sand filter backwash water to the cooling tower at about the fourth day
- A plant shut-down started at about the seventh day

- Stopped blowdown at about the 29th day and resumed blowdown at about the 32nd day
- Slug dose of new inhibitor treatment at about the 33rd day.

Treatment optimization:

- Increase product feed rates at about the 37th day
- Increase polymer feed rate at about the 50th day
- pH was raised, polymer feed rate was decreased, and inhibitor feed rate was increased at about the 62nd day
- pH was decreased at about the 63rd day
- Polymer feed rate was increased and inhibitor feed rate was decreased at about the 77th day
- Final blowdown rate adjustments through the end of the test.

The results from this study show that increasing the dosage of dispersant polymer under the plant conditions was the most effective way to reduce the carbon steel localized corrosion rate. Additionally, increasing the pH and pyrophosphate (corrosion inhibitor) feed at the high calcium conditions and at the same time reducing dispersant polymer feed rate resulted in an increase in localized corrosion rate. *This case study demonstrates the detrimental effect on localized corrosion by an excess dosage of deposition corrosion inhibitor and an insufficient dosage of dispersant polymer.* The polymer is needed to optimize the interaction of the phosphate and phosphonate corrosion inhibitors with the metal surface for optimum passive film formation. In this case, it is likely that the insufficient polymer dosage resulted in a porous, non-passive film of phosphate salts on the surface, promoting under-deposit (localized) corrosion. It also should be noted that the averaged localized corrosion rate detected by the LCM before the start of the new treatment program was consistent with the carbon steel shell-side heat exchanger failure frequency observed in the plant (i.e., failed after two years in service due to corrosion).

The new optimized treatment showed much better performance in controlling localized corrosion than the old Alkaline Stabilized Phosphate program, despite operating under a much more stressful scale and corrosion environment (higher cycles). Note that the general corrosion rate was much less sensitive to the corrosivity changes in the system, and could not have been used to achieve this program optimization. The improved localized corrosion results were confirmed by plant inspection results showing that no unacceptable carbon steel corrosion problems were found on the plant equipment inspected. The customer had since used the LCM to optimize the treatment programs in two different cooling water systems in the plant.[3] Thus, the LCM provided valuable information for developing a successful new treatment program in this customer application.

23.4 Program optimization using pilot cooling tower tests

To further optimize the chemical treatment program for the Southwest chemical processing plant described in the previous case history, a laboratory pilot cooling tower study was performed.[4–5] Over the course of several months, many scale and corrosion control programs were used and the program was optimized under long holding time conditions to a localized corrosion level of 10–20 mpy (254–508 µm/y). At one point during the test, the localized corrosion rate increased significantly. Figure 23.3 shows this increase. Adjustments in the scale and corrosion treatment programs had little effect on the increasing localized corrosion rate. It was also noted that a biofilm had developed on the heat exchanger surface and on the LCM anodes. Continuous bleach feed (maintaining 0.1 ppm free chlorine residual) was used throughout the test.

It is well known that hypochlorous acid is not as effective a biocide as hypobromous acid at pH values above 7.5. The pH of this test was approximately 8.4, therefore the observed results suggested that the current

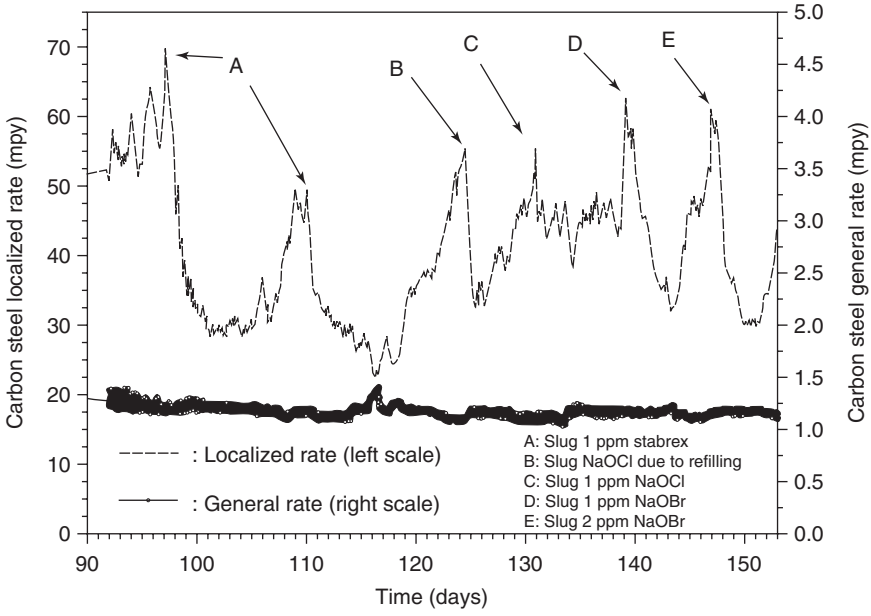

Note: Cooling system return water, advanced stabilized alkaline phosphate + NaOCl
HTI = 8 days, 260 ppm Ca^{2+}, pH = 8.4, 57.2°C. 1 mpy = 25.4 µm/y
Continuous NaOCl feed. Free Cl_2 = – 0.1 ppm, Total Cl_2 = – 0.35 ppm
Total aerobic bacteria in the bulk water: < 10^3 cfu/ml

23.3 Effect of oxidizing biocides on MIC control.

program was probably not sufficiently effective in controlling microbial growth. Following a slug dose of a stabilized liquid bromine biocide (STA•BR•EX™) (1 ppm TRO (total residual oxidant) as Cl_2), the localized corrosion rates dropped more than half (Fig. 23.3). (STA•BR•EX™ is the trade name used by Nalco, IL, USA.) Localized corrosion rates remained low for approximately one week before they started to increase. A second dose of stabilized liquid bromine (STA•BR•EX™) again quickly lowered localized corrosion rates for a period of about one week. When localized corrosion rates increased again, a batch of chlorinated water was added to the tower to refill the basin (dosage not recorded). This also showed a beneficial effect on reducing the localized corrosion rate. However the effects were not longstanding. After allowing time for the excess bleach to be depleted, a 1 ppm slug of bleach was applied, showing little or no effect. Subsequent doses of unstabilized bromine at 1 and 2 ppm TRO as Cl_2 were also effective at decreasing localized corrosion rates by half. Since stabilized bromine (STA•BR•EX™) and the unstabilized bromine are strong oxidants, they would normally be expected to increase corrosion rates. This effect was noticed immediately following the addition of the biocide. However, shortly thereafter, the localized corrosion rate dropped substantially. The corrosion monitor was found to be functioning properly during this test. Furthermore, sulfate reducing bacteria (100 colony-forming units per square centimeter (cfu/cm^2)) and aerobic bacteria (three orders of magnitude higher than elsewhere in the system) were measured on the corrosion monitor anode, at the end of the test.[4–5] A likely explanation for these observations is that the high localized corrosion rates were a result of microbial processes. Second, bromine based biocides were very effective at lowering the localized corrosion rate. Bromine chemistry most likely worked better than chlorine as result of the pH of the cooling water used in the tests. Localized corrosion rates remained low for a longer period following stabilized bromine (STA•BR•EX™) application as compared to un-stabilized bromine treatments (Fig. 23.3), suggesting that stabilized bromine may be more effective at reducing this type of corrosion under test conditions.

Microbial control monitoring during this test was primarily done on bulk water samples. Throughout the experiment, bulk water counts of aerobic bacteria did not exceed 10^3 cfu/mL. These results suggest that while the low-level continuous bleach feed (0.1 ppm as Cl_2) may be effective in controlling microbial growth in the bulk water, it may not be sufficient to control bacterial activity at all the corrosion sites. Surface microbial populations were not monitored regularly during this test. The reason for periodic monitoring is not to measure specific microorganisms, which may be contributing to the increased corrosion, but rather to determine how effective biocide treatments are in reducing the general surface population viability.

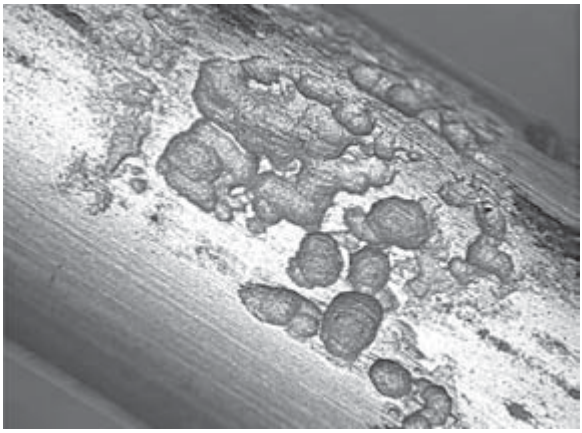

23.4 Typical MIC attack morphology identified on the carbon steel tube. Photo of a section of the CS tube (diameter = 1.27 cm) used as the cathode in the LCM to obtain the results shown in Fig. 23.3.

Rarely does presence, or for that matter absence, of specific groups of microorganisms correlate with localized corrosion rates. This test demonstrates that different biocides have distinguishable effects on the localized corrosion rate and can be measured using the Localized Corrosion Monitor. Post-test metallurgical examination of the carbon steel cathode tube concluded[4] that the corrosion attack was consistent with MIC, most likely by acid-producing bacteria (see Fig. 23.4). The test results were also confirmed in a second pilot cooling tower test, as described elsewhere.[5]

It is generally known that microbiologically influenced corrosion is difficult to detect and measure. This is because presence of species commonly associated with MIC may not be contributing substantially to the corrosion. Conversely, observation of high corrosion rates may not necessarily indicate that the corrosion is a result of MIC. The results obtained here indicate that the Localized Corrosion Monitor may be a useful tool to monitor and control MIC.

23.5 Refinery hydrocarbon leak detection and control

A corrosion study was performed in a large US Midwest refinery with no known carbon steel heat exchanger failures in the past five to six years before the study.[2,6] The plant has six cooling towers. No. 2, 4 and 5 towers normally use the blow-down water from the largest tower (No. 3) as make-up water. Thus, tower No. 3 usually runs at a lower cycle of concentration than the other towers. The carbon steel heat exchangers cooled by the No.

Table 23.3 Midwest Refinery Tower No. 3 cooling water return analysis results: low Zn + bleach

Date	11/10/97	1/6/1998
Water analysis ICP and IC results	Filtered (0.45 μm) (ppm)	Filtered (0.45 μm) (ppm)
Ca^{2+}	69	172
Mg^{2+}	24	48
Zn^{2+}	0.1	0.7
Iron	0.2	0.7
Cu^{2+}		
Sr^{2+}	0.2	1.4
Na^{+}	120	782
K^{+}	2.7	23
Phosphorus	1.9	2.3
Silica (SiO_2)	2.5	22
Boron		0.5
Mn^{2+}		0.1
Cl^{-}	230	994
Sulfate	110	682
M-alkalinity ($CaCO_3$)	144	243
Nitrate ($CaCO_3$) & Nitrite (NO_2)	<2.9	<2.9
Other		
Unf. Org. Phosphate (PO_4)	1.4	0.6
Ortho-PO_4 (PO_4)	5.1	1.4
Conductivity, μS/cm	1090	4280
pH	7.6	8.3

3 tower are all tube-side exchangers (water in the tube side). The system has excess cooling capacity. Hence some of the exchangers may be idle (i.e., no water flow) in the winter. A low Zn treatment and bleach were used as the cooling water treatment in the system. Some water analytical results of the tower water are shown in Table 23.3. The major concerns of the refinery before the study were:

- Admiralty exchanger stress corrosion cracking due to high NH_3 and SO_4^{2-}
- Carbon steel exchanger fouling
- Effect of a make-up water change in the winter (from lake water, which would freeze in the winter, to a more aggressive plant waste water)
- Possible options to minimize the potentially damaging effects associated with the increased corrosivity

The LCM was installed in a side stream of a tower return line for the purpose of treatment optimization and control, and to help manage prob-

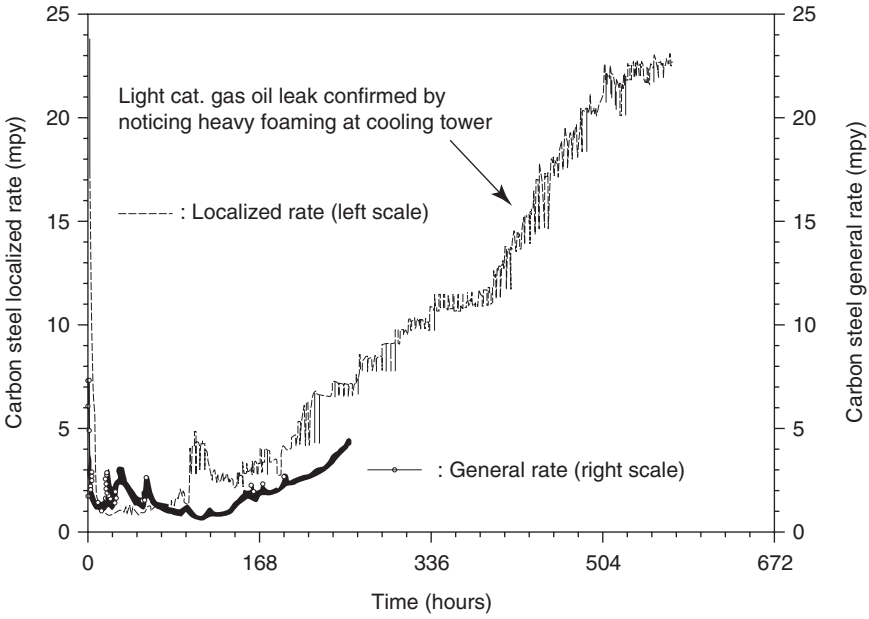

Note: Refinery return water, Low Zn treatment + NaOCl. 1 mpy = 25.4 μm/y

23.5 Effect of hydrocarbon leak on carbon steel corrosion.

lems that may arise due to the make-up water change in the winter. The results obtained from three weeks in the winter are shown in Fig. 23.5. Upon immersion, the localized corrosion was initially very high and then the rate decreased drastically (one to two days). This effect is due to the initial flash corrosion that any fresh metal experiences when exposed to corrosive waters. The localized corrosion rate stabilized for a short period and then rose throughout the remainder of this test. Note that the general rate obtained by the LCM's LPR probe also shows a similar pattern, i.e., it was first reduced to a low value upon immersion, followed by a steady increase. However, the increase in general rate occurred two to three days after the corresponding increase in the localized corrosion rate, showing the increased sensitivity of the localized rate over that of the general rate. One week later, the LCM's LPR probe failed due to short-circuiting by biofilm deposits. This occurs because the LPR probe tips are in close proximity. Thus, no general corrosion rate information was obtained after that time. About two weeks into the test, a leak in a carbon steel heat exchanger served by this tower was reported. The leakage was confirmed by noticing hydrocarbon foaming in the tower. The leaking exchanger was identified and isolated. It was not determined whether the failure was from the waterside or the process side. However, it is known that the heat

exchanger had been idled for some time during the previous winter (stagnant water can be very corrosive). It should be noted that after the Light Cat. Gas Oil leak was confirmed, the leaking heat exchanger was identified and isolated from the system. Blow-down from Tower No. 3 to other towers was stopped. Tower no. 3 was blown down and then allowed to cycle up. The chemical analysis of the cooling water under this operating condition (i.e., sampled on 1/6/98) is shown in Table 23.3. Since there was excess cooling capacity in the refinery, there is no need to stop production.

The results in Fig. 23.5 show that the LCM was able to provide a warning on the heat exchanger failure with the sudden increase in localized corrosion rate two to three days before LPR responded, and more than two weeks before being confirmed by other methods (cooling tower hydrocarbon foaming). In addition, the LCM electrodes did not short-circuit under heavily fouled conditions, unlike the LPR electrodes. This is due to the physical separation of the LCM anodes into their respective wells, while the LPR electrodes are very close to each other with no barrier in between. It should be noted that the LCM uses a ZRA to measure the galvanically coupled current between the electrodes. Thus, even in cases where there is low electrical resistance bridging between the electrodes, the LCM instrument would still be likely to be able to detect a major portion of the galvanically coupled corrosion current flowing between the anodes and cathode. The same LCM study continued for several more months without the LPR general corrosion rate information and is shown in Fig. 23.6.

The spike at about the 24th day was due to a change of LCM anode configuration to better simulate different operating conditions encountered in the plant. However, the localized corrosion rate continued to rise steadily after the 'electrode change' spike had receded. Due to a dramatic localized corrosion increase started at about the 55th day, it was suspected that the LCM was malfunctioning. However, at the 80th day, a complete flow and electronics inspection found that the LCM was working normally. A light oily odor in the return water and the cooling tower water was noted after the inspection (make-up water had no hydrocarbon odor and the basin only had a very small amount of foaming). Thus, a new hydrocarbon leak was suspected. Indeed, another exchanger leak was confirmed on a different carbon steel heat exchanger later on the same day. Analyzing the biofilm from the tower showed very high aerobic bacteria and sulfate reducing bacteria (SRB) counts (2.9×10^8 cfu/mL total aerobic bacteria and 3.9×10^5 cfu/mL SRB in the biofilm sample), suggesting that the high pitting rate observed may have been due to MIC. Thus, the LCM had detected the effects of a second heat exchanger leakage more than three weeks before being confirmed by other methods. Since the second leak was very likely a

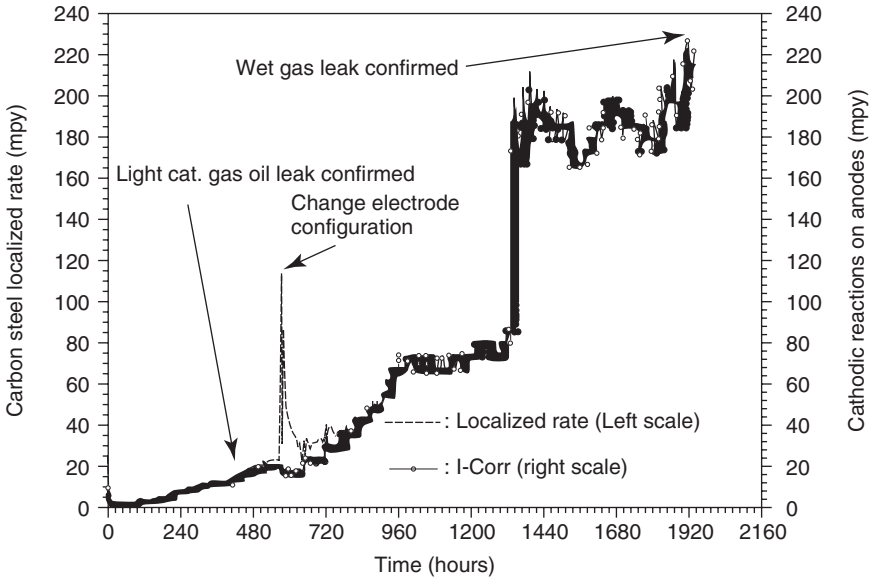

Note: Refinery return water, Low Zn treatment + NaOCl. 1 mpy = 25.4 μm/y
General rate was not available due to short-circuiting of
the probes by biofilm shortly after the first leak

23.6 Effect of hydrocarbon leaks on cooling water corrosion.

direct result of the damaging cascading effect of the corrosive contaminants from the first leak, the ability to provide an early warning to these conditions could be very useful in minimizing further damage to the refinery system.

After the confirmation of the second hydrocarbon leak, various standard damage control measures were taken, including isolating the leak, increasing blowdown rate, and increasing the bleach feed to oxidize the hydrocarbon and sulfide species. However, recommendations for use of more effective corrosion control treatments were not accepted by the refinery, due to concerns about treatment cost. Subsequently, the third heat exchanger leaked one month later (detected by LCM, confirmed soon afterwards). A carbon steel localized corrosion rate as high as 400 mpy (10.2 mm/y) was detected by the LCM. The general corrosion rate detected by the LCM was 10–12 mpy (250–305 μm/y) during the same period. Multiple heat exchanger leaks occurred within the next two months before the refinery was shut down for repair.

It should be noted that the heat exchanger leakage frequency observed in this case study was consistent with the localized corrosion rate results obtained from the LCM. When the localized rate is as high as 300 to 400 mpy (7.6–10.2 mm/y), leakage of carbon steel exchanger tubes (even for

new tubes, typical thickness of 2.08 mm) is predicted to occur in two to three months. Higher pressure in the process side would tend to lead to an earlier leakage of the exchanger.

23.6 Refinery leak detection and program optimization

This case study was conducted in a large US West Coast refinery.[2,6–7] In this case, the refinery wished to use California Title 22 Water (treated reclaimed wastewater) as make-up water for two of its cooling water systems. Information about the cooling water system, water chemistry conditions and typical LCM and other corrosion measurement results before and after the introduction of Title 22 water as make-up water can be found elsewhere.[7] The effects of daily temperature fluctuation, due to sunlight and weather conditions, and the introduction of the more corrosive Title 22 water on the localized and general corrosion rates can also be observed in Fig. 23.7. The fact that the localized corrosion rates increased due to the introduction of Title 22 water (initial peak at the beginning of the Figure) while the general rate did not, demonstrates the excellent sensitivity of the LCM toward corrosivity changes in the system.

At about the 18th day into the study the LCM showed a dramatic increase in the localized corrosion rate. The general corrosion rate also showed an

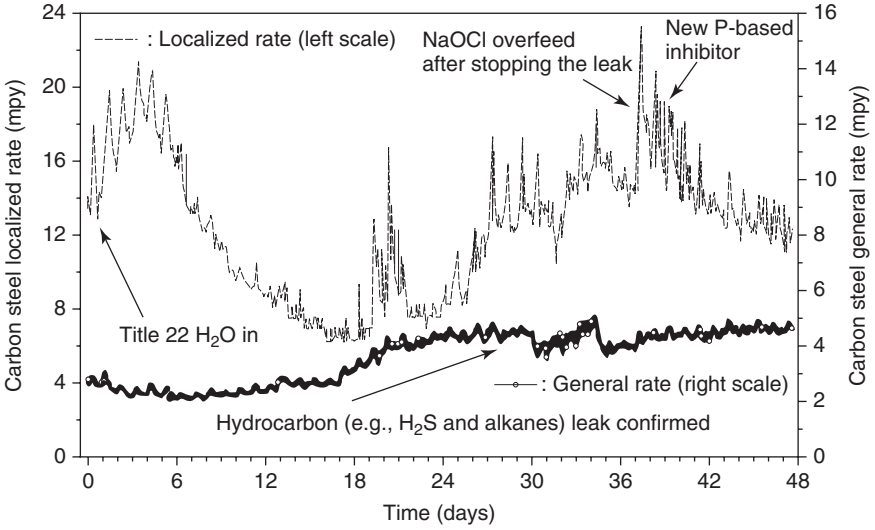

Note: Data shown: 14 July 1998, 7:46am to 30 August 1998, 23:36. 1 mpy = 25.4 μm/y
Refinery return water, stabilized phosphate + Acti-Brom

23.7 Hydrocarbon leak control.

increase. A hydrocarbon leak was confirmed about nine days later (at about the 27th day) by operators noticing a temperature rise in the cooling water outlet. The leak was further verified by using a leak detection bubbler pot. After discovering the leak, bleach feed was increased to oxidize the H_2S in the leaked hydrocarbon and regain microbial control. The bleach overfeed after stopping the leak (due to less demand by H_2S) was detected by the LCM at about the 37th day. The subsequent effective control of localized corrosion after the leakage situation was corrected is also clearly demonstrated by the LCM results.

Results obtained in this study demonstrate that the damaging effects of a hydrocarbon leak (overhead gases from a column containing H_2S, CH_4, C_3H_8, C_4H_{10}, etc.) can be controlled quite well with timely identification and stoppage of the leak, followed by appropriate chemical treatment procedures, in this case using an optimized Stabilized Phosphate program. The mitigation procedure entailed additional bleach feed to oxidize H_2S and control microbial growth, switching to a more effective cathodic inhibitor, and stopping the leak in a timely manner. The polymer dose and blowdown rates remained constant during the hydrocarbon leak. Comparing these results with those obtained from the Midwest refinery case study and considering the similar nature of the leaks, it is reasonable to assume that this West Coast refinery was able to maintain its acceptable level of operation because of the way it responded to the initially identified leak. On the other hand, the Midwest refinery was unable to maintain effective cooling tower operation because it did not effectively respond to the initially identified leaking exchanger. This led to subsequent leaks and, ultimately, an unscheduled unit shut-down.

From another viewpoint, the early response to the hydrocarbon leak also had a great impact on the corrosion performance of the treatment program. The West Coast Refinery was able to address the hydrocarbon leak earlier (about one week) than the Midwest Refinery described in the previous case history (two to three weeks). This earlier response could be the reason that the West Coast Refinery could bring corrosion under control while maintaining blowdown rates, while the Midwest Refinery could not. In addition, it is difficult to say whether the nature of the hydrocarbon in one cooling system was more corrosive than in the other. Certainly, the types and quantities of corrosive contaminants present in different hydrocarbon process streams can vary greatly.

23.7 Admiralty brass corrosion control in cooling water system using brackish water as make-up

This study was conducted in a two unit 180 MW conventional power plant located in Southwestern United States.[6] One unit (# 6, 100 MW) of the

power plant started operation in 1968–1969 and the other unit (# 5) started operation in the mid-1950s. Each unit is cooled with a five-cell cooling tower using well water as make-up water. The cooling system volume for unit #6 is 515 550 gallons (1951.6 m^3) with a holding time index of about 30 hours. The cooling treatment programs used before 1995 consisted of tolytriazole, sodium hexametaphosphate, chlorine and bromine. Since August 1995, a cooling water treatment program consisting of: zinc, phosphate and tolytriazole as corrosion inhibitors, a phosphonate scale inhibitor, and polymeric dispersants had been used in the system. The biocide treatment consisting of activated bromine (mixing bleach and NaBr at 1:1 mole ratio) had also been used since 1995. Biocide was normally fed for a maximum total time of one hour per every two days due to discharge permit restriction. The goal was to maintain a ~0.2 ppm as Cl_2 free halogen residual at the condenser outlet during the slug feed of the biocide. The feed dosage of corrosion and scale treatment was controlled via on-line measurement of an inert fluorescence tracer. The residual concentration of tolytriazole (yellow metal corrosion inhibitor) in the cooling water was controlled separately at 1.5 ppm by an on-line fluorescence monitor/controller. The chemical treatment programs and the state-of-the-art chemical feed control technology were selected to address the high admiralty brass heat exchanger pitting corrosion rate (e.g., frequent admiralty condenser leaks due to cooling water side corrosion; ~3% of the #6 unit condenser tubes were plugged at the start of the study, see Fig. 23.8), and excessive $CaSO_4$ scale formation on the condenser surfaces and tower fill encountered previously in the system.

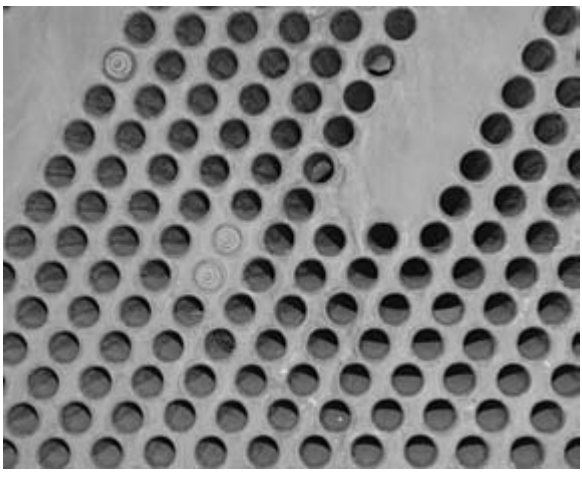

23.8 A photo of unit #6 condenser tubes showing the presence of tube plugging and debris blockage in several tubes.

Typical water analysis results of tower #6 using the new chemical treatments are shown in Table 23.4. The corresponding results obtained from corrosion coupon measurements in tower #6 are shown in Table 5. These results appear to show that the chemical treatments employed in the system are providing very good corrosion and scale control performance in spite of using a brackish well water as the make-up water in the system. Coupon corrosion rates were very low and well within the acceptable limits. Water analysis results showed that the corrosion product ion concentrations were also very low. In addition, water analysis results also showed that the cycle of concentrations of the deposit-prone ionic species and the non-deposit forming ionic species were the same in the system, indicating there was little scale formation in the system. Indeed, the good scale and corrosion control performance of the new treatments was confirmed by borescope inspection of the heat exchangers. In addition, admiralty brass (UNS number C44300) heat exchanger leakage had been stopped after the start of new treatment for about three years. Admiralty brass corrosion coupon results were also improved from 0.4 to 0.1–0.2 mpy (10.2 to 2.5–5.1 μm/y). However, leakage of admiralty brass exchangers re-appeared in 1999 (six leaks occurred in the first seven months of 1999). The condenser leaks occurred at an increasing frequency (one leak occurred in January 2000). The power plant had little confidence on the reliability of the results obtained from corrosion coupons since they did not simulate the actual corrosion conditions in the plant.

Metallographic analysis of condenser tube section removed from unit #6 in April 2000 shows that the internal surface of the condenser tubing suffered from numerous pitting corrosion under a layer of deposits consisting of mostly calcium, copper, iron and zinc phosphates and calcium carbonate (see Figs 23.9–23.12, and Table 23.6). The external surface (i.e., steam side) of the condenser tubes was covered by a thin layer of black oxide. No localized attack on the external surface was observed.

The metallographic analysis suggests that under-deposit corrosion in the water side may be the cause of the recent condenser leakages. It also revealed that the calculated time average maximum localized corrosion would be less than 1 mpy (25.4 μm/y) since the condenser was put into service ~31 years ago. However, the metallographic analysis did not provide information on the propagating under-deposit corrosion rate under the current operating conditions. Since operating conditions and treatment chemicals had been changed drastically in the long exposure period, one would not expect that the corrosion rates would be constant during that period.

To gain a better understanding of the effects of current operating conditions on condenser tube under-deposit localized corrosion and to optimize the chemical treatment to minimize the localized corrosion rate, a localized

Table 23.4 Southwestern US conventional power plant #6 unit cooling water analysis results

Date	2/17/00				5/7/99		12/1/98
	Filtered (0.45 μm)		Total (Un-filtered)		Filtered (0.45 μm)	Total	Total
Water Analysis ICP and IC Results, ppm	Make-up	Tower #6	Make-up	Tower #6	Tower #6	Tower #6	Tower #6
Ca^{2+}	260	1300	270	1300	1300	1300	1400
Mg^{2+}	60	300	61	300	300	300	336
Zn^{2+}	<0.01	0.47	<0.01	0.47	0.7	0.86	0.2
Iron	0.04	0.4	0.21	0.78	<0.25	0.66	1.2
Cu^{2+}	<0.01	<0.1	<0.01	<0.1	<0.25	<0.25	<0.1
Sr^{2+}	4.4	22	4.5	22	23	23	24
Na^{+}	190	1000	190	1000	900	900	1012
K^{+}	7	38	7.3	38	43	43	50
Phosphorus	<0.1	1.7	<0.1	1.6	<2.5	<2.5	3.2
Silica (SiO_2)	12	62	13	62	50	50	70
Boron	0.3	1.6	0.3	1.6	<2.5	<2.5	1.6
Li^{+}	0.08	0.37	0.08	0.37	0.51	0.53	0.5
Cl^{-}			330	1700		1600	1917
Sulfate			620	4300		4100	4512
M-alkalinity ($CaCO_3$)			210	110		74	
Br^{-}			<2.9	13		7.8	12
Nitrate ($CaCO_3$) & Nitrite (NO_2)			<2.9	<2.9		<2.9	<2.9
Other							
Phosphate (PO_4)	0.2	4.4	0.2	4.7	3.5	3.7	
Ing. Phosphate (PO_4)	0.2	2.1			1.9	1.9	
Ortho-PO_4 (PO_4)			<0.1	2.1	1.4		
Conductivity, μS/cm			2400	10000		9600	
pH			8.0	8.0		7.34	
Turbidity, NTU							0.2

Table 23.5 Southwestern US power plant – tower #6 corrosion coupon results

Corrosion coupon	Exposure	General rate	Pitting	Exposure length
Admiralty brass	9/23/99 to 12/21/99	0.1 mpy	N.D.	89 days
Admiralty brass	1/5/99 to 3/3/99	0.1 mpy	N.D.	57 days
Admiralty brass	10/14/98 to 1/5/99	<0.1 mpy	N.D.	83 days
Admiralty brass	5/6/98 to 7/30/98	0.2 mpy	N.D.	85 days
Admiralty brass	2/16/98 to 5/6/98	<0.1 mpy	N.D.	79 days
Carbon steel (C1010)	9/23/99 to 12/21/99	0.7 mpy	12.7 mpy	89 days
Carbon steel (C1010)	1/5/99 to 3/3/99	2.0 mpy	N.D.	57 days
Carbon steel (C1010)	10/14/98 to 1/5/99	2.8 mpy	N.D.	57 days

Note: N.D. denotes not determined.

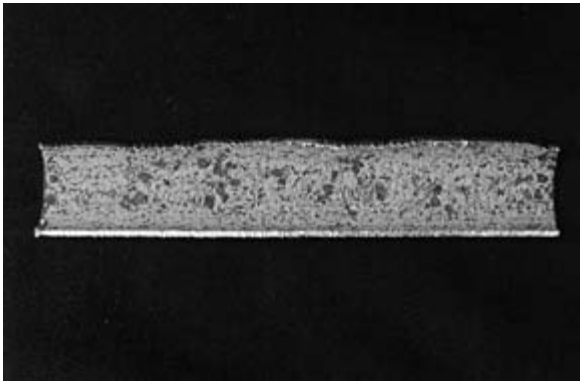

23.9 A section of condenser tube (outer diameter = 7/8 in. or 2.22 cm, thickness = 0.0046 in. or 116.8 μm) removed from unit #6 in April 2000.

corrosion monitor based on the DFC method was installed in a side-stream of the outlet of unit # 6 condenser. A tube-side heat exchanger flow set-up (see Fig. 6.2 in Chapter 6) was used. Admiralty brass (UNS C44300) was used for both the anodes and cathode. The flow rate was 2.3 gpm (8.7 L/min) or a flow velocity of 0.91 m/s near the cathode tube surface. To simulate the under-deposit corrosion conditions shown in Figs 23.11 and 23.12, the anodes were occluded (or pulled down) by 3 cm from the flow channel glass tube surface. The exposed anode surface (0.317 cm^2) was pre-corroded in the plant cooling water containing >100 ppm NaOCl for ~1 h before immersion. Laboratory tests (both bench-top and pilot cooling tower) showed that the electrode pre-treatment method and the flow cell set-up would simulate realistically the under-deposit corrosion attack observed on the plant condenser tube.

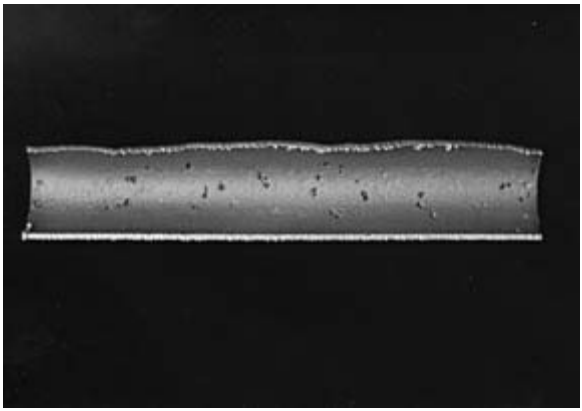

23.10 Section of the condenser tube shown in Fig. 23.9 after cleaning via bead blasting, revealing under-deposit corrosion attack sites. The deepest observed attack site penetrated as much as 0.026 in. or 66 μm into the tube wall.

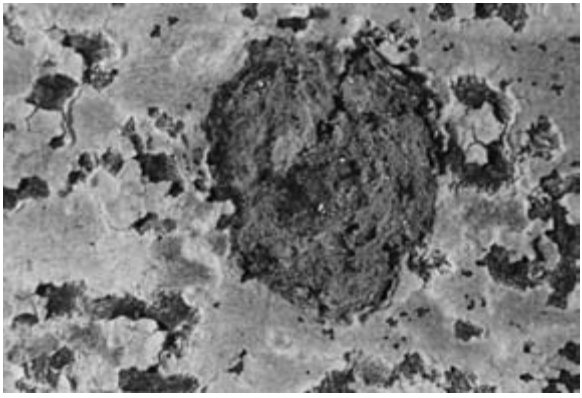

23.11 Closed up view of a corrosion site on the condenser tube before cleaning. Magnification: 12×.

The field study lasted nearly two years. Many useful results were obtained. Fig. 23.13 shows the LCM results obtained from 12 September 2000 to 31 October 2000. Based on laboratory and field studies, the scale inhibitor feed dosage was increased before 12 September 2000 to reduce the potential $CaSO_4$ scaling problem on the tower fill (a test tower fill unit installed on-site showed some $CaSO_4$ scaling in early 2000). As shown in Fig. 23.13, the admiralty brass localized corrosion rate was generally quite high in the two weeks of immersion (time average localized rate = 3.3 mpy or 83.8 μm/y in the first two weeks in Fig. 23.13). The localized corrosion rate also changed

23.12 Bowl-shape depressions (i.e., under-deposit corrosion sites) beneath the red deposit layers on the condenser tube internal surface. Magnification: 50×.

Table 23.6 EDS analysis of material on internal surfaces of the unit #6 condenser tube section

Element	Tan deposit	Green nodule	Corrosion site interior
Copper (as CuO)	24.0	15.2	83.8
Zinc (as ZnO)	5.3	5.5	4.1
Calcium (as CaO)	37.3	38.5	0.6
Phosphorous (as P_2O_5)	17.3	17.0	0.8
Iron (as Fe_2O_3)	7.2	9.9	0.2
Silicon (as SiO_2)	2.9	5.3	0.9
Magnesium (as MgO)	2.2	2.3	0.1
Aluminum (as Al_2O_3)	1.2	2.0	1.0
Chloride (as Cl)	0.4	0.4	7.0
Sulfur (as SO_3)	2.2	4.1	1.6

Note: EDS – Energy dispersive X-ray spectroscopy. Values are in weight percent as oxides unless specified otherwise.

with water temperature, showing daily fluctuations in response to the daily water temperature fluctuations associated with weather and operating heat load conditions. These results are similar to the ones observed from LCM field applications using carbon steel as the anodes and cathode. They demonstrate that admiralty brass LCM localized corrosion rate readings are very sensitive to corrosivity changes in the system. It should be noted that due to a data-logger wiring error, the water temperature readings in the initial 17 days of the test were not recorded. The time average general corrosion rate obtained from the LCM during the same time period was

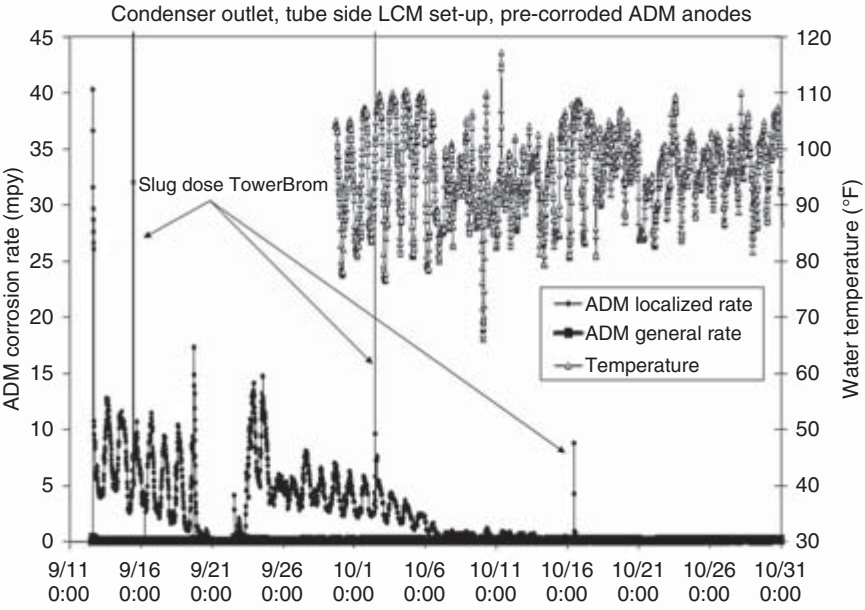

23.13 Effect of oxidizing biocide feed on admiralty brass under-deposit corrosion in a conventional power plant cooling water system using brackish water as make-up. 1 mpy = 25.4 μm/y, °C = 5/9 ∗ (°F − 32).

very low, i.e., 0.10 mpy (2.5 μm/y), in agreement with the mass loss results obtained from corrosion coupons. The LCM results show that although the admiralty brass general corrosion had been under excellent control by using the selected modern cooling water chemical treatments and the state-of-the-art active and inert fluorescent tracer based monitor and feed control instruments, the localized corrosion control had a substantial room for improvement.

On-site investigation suggested that microbiological fouling control had substantial room for improvement. Tower basin water was turbid and had a substantial amount of algae growth, especially during the summer months. High surface aerobic bacteria counts were detected on corrosion coupon swap samples (total count of 1.3×10^8 cfu/swab on both carbon steel and admiralty brass coupons) and on tower fill samples (total count of 500 000 cfu/gram) in February 2000. Significant sulfate reducing bacterial activity was also detected in both the tower fill sample (200 cfu/gram) and in a cooling tower water sample. In addition, analysis of the dried deposit sample from the condenser in #6 unit showed a high organic content (i.e., 34 weight % loss at 925 °C), indicating the possibility of fouling by biofilm. Thus, a once every two weeks slug dose (i.e., ~50 lb or ~22.7 kg) of high concentration of TowerBrom 60M™ (Occidental Chemical Corporation, TX, USA) (i.e.,

sodium dichloroisocyanurate + NaBr) was initiated in September 2000. In Fig. 23.13, the slug dosing of TowerBrom 60M™ was detected on 15 September 2000 [150.2 mpy (3815 µm/y) at 11:06 a.m.], 2 October 2000 [99.5 mpy (2530 µm/y) at 11:21 a.m.] and 16 October 2000 [8.8 mpy (224 µm/y) at 11:06 a.m.] as sudden spikes of admiralty brass localized corrosion rate. The general rates were only increased slightly, e.g., 0.04–0.05 mpy (1.0–1.3 µm/y), during the same time periods and the increases were not visible in Fig. 23.13. As shown in Fig. 23.13, the additional slug dose feed TowerBrom 60M™ was very effective in reducing the admiralty brass under-deposit localized corrosion rate rapidly, especially noticeable after the slug dose on 2 October 2000. By 15 October 2000, the admiralty brass localized corrosion rate was reduced to less than 0.2 mpy (5 µm/y). Inspection of the tower basin indicated that the additional TowerBrom 60M™ biocide slug dose had cleaned up the biomass in the system. The tower water had also become clearer. Furthermore, the feed dosage of tolytriazole to maintain the residual concentration of 1.5 ppm via on-line monitor/controller was reduced significantly. Roughly the same localized corrosion rate was observed up to December 2000. The admiralty brass general corrosion rate detected by the LCM remained largely constant during the same period. Results obtained later at the site confirmed that the optimized cooling water treatments (i.e., corrosion and scale inhibitors, biocides) via the help of the LCM were very effective in reducing the high admiralty brass localized corrosion rate problem in the system.

The results obtained in this study suggest that high microbial activity in the system may be one of the major factors in having high under-deposit localized corrosion rates being observed on the condensers. Once every two weeks slug dose of the bromine based biocide in the summer months, and the continued use of existing corrosion, scale inhibitors and biocide treatments, and the associated modern feed control technology could be used effectively to meet the needs of the cooling water system.

23.8 References

1 E. Hale and B. Yang, ‘Evaluation of Various Application Regimes to Control Mild Steel Corrosion in a Nuclear Power Service Water System Using a Localized Corrosion Monitor’, EPRI Service Water System Reliability Improvement Seminar, 13 July, (1999), Biloxi, MS.
2 Bo Yang, ‘Minimizing Localized Corrosion via New Chemical Treatments and Performance Based Treatment Optimization and Control’, *NACE Corrosion/99*, Paper no. 307 (1999).
3 D.A. Meier, E.B. Smyk and B. Yang, ‘Advances in Zinc Free Alkaline Cooling Water Treatment’, *Corrosion/99*, paper no. 304, Houston, TX: NACE (1999).
4 B. Yang, ‘Advances in Localized Corrosion Control in Cooling Water Systems’, *PowerPlant Chemistry*, 2 (6), 321 (2000).

5 M. Enzien and B. Yang, 'Effective Use of Monitoring Techniques for Use in Detecting and Controlling MIC in Cooling Water Systems', *Biofouling*, 17 (1) 47 (2001).
6 B. Yang, 'Corrosion Control in Industrial Water Systems', Presented at NACE Central Area Conference, Corpus Christi, TX, 7–10 October 2001.
7 B. Yang, 'Real-time Localized Corrosion Monitoring in Industrial Cooling Water Systems', *Corrosion*, 56, 743 (2000).

24

Corrosion monitoring in the pulp and paper industry

F. ALMERAYA-CALDERÓN, C. V. OROZCO, C. GAONA-TIBURCIO, T. A. BORUNDA, J. CHACÓN-NAVA and A. MARTÍNEZ-VILLAFAÑE,
Advanced Materials Research Center, CIMAV, Mexico

24.1 Introduction

In the pulp and paper industry, the equipment used in the pulping process includes pressure vessels (digesters), rotary drum washers, multiple-effect liquor evaporators, storage tanks, recovery boilers, liquor clarifiers, etc. Most of the equipment used in the pulping mill is fabricated from carbon steel (CS). Tubes in high-temperature multiple effect evaporators are routinely fabricated from stainless steel (SS) because of rapid attack in CS. However SS are susceptible to corrosion in this environment (McDonald, 1969).

Nowadays, the development of corrosion sensors represents a powerful tool in the monitoring and diagnosis of corrosion rates and mechanisms. Besides, with the proper procedures, it would be possible to establish correlations between corrosion rates and mechanisms with operational variables (such as temperature, load, relative humidity, pH, etc.) (Hines *et al.*, 1978). Thus, in corrosion monitoring an important goal is to ascertain the conditions leading to materials degradation in order to prevent forced outages, and the improvement of maintenance programs (Mansfeld, 1976).

The present work deals with corrosion monitoring in the pulp and paper industry at two main areas of work, i.e. the paper machine, and the multiple-effect liquor evaporators section (Figure 24.1). In the first case, general and localized corrosion problems in the paper machine structure were related with paint failure caused in the first place by a high humidity level in the environment coupled with the influence of various chemical additives added at the beginning of the process. Thus, corrosion probes designed to use electrochemical noise were installed in different areas on the paper machine. In order to identify possible corrosive agents from the environment further analysis on probe surfaces was carried out after the monitoring period. In this case, potential noise and current noise fluctuations as a function of time were obtained and analyzed. At the same time, the relative humidity conditions (%) and temperature were recorded.

(a)

(b)

24.1 General view: (a) paper machine and (b) multiple-effect evaporation system.

Regarding the multiple-effect evaporation system, the spent liquor extracted from the pulp is concentrated to increase the solids content. After being exposed to temperatures greater than boiling point, the concentration of aggressive compounds in the black liquor increases, and this may cause corrosion of the evaporator tubes (Casey, 1990). Subsequently, the heavy black liquor is burned in a chemical recovery boiler. In the multiple-effect evaporation system, newly designed *in-situ* corrosion probes were installed to determine the corrosion rate of type 304 SS specimens located at three selected evaporators. A monitoring probe type was specially designed and tested *in situ* for this purpose during three separate time intervals. To ascertain the influence of the electrolyte composition, black liquors of three different compositions were used. Linear polarization resistance (LPR) and Tafel extrapolation were used throughout the monitoring. SEM/EDX

(Scanning Electron Microscope/Energy Dispersive X-Ray Analysis) was used to characterize and evaluate the extent of surface damage on selected specimens (Orozco *et al.*, 2001).

24.2 Experimental procedures

24.2.1 Paper machine corrosion

Visual inspection

First, a visual inspection was carried out with the aim of determining the most convenient zones for probe installation and monitoring. At selected zones in the press room (Figure 24.2), temperature and relative humidity measurements were also recorded. The material tested was 1018 carbon steel (CS), since this is a common construction material in the paper machine structure.

Monitoring probe

The corrosion sensors used here consisted of three 1018 CS electrodes of the same size, all separated embedded for a dielectric material (Figure 24.3) (Cox *et al.*, 1985). In order to achieve an adequate response, an ionic activa-

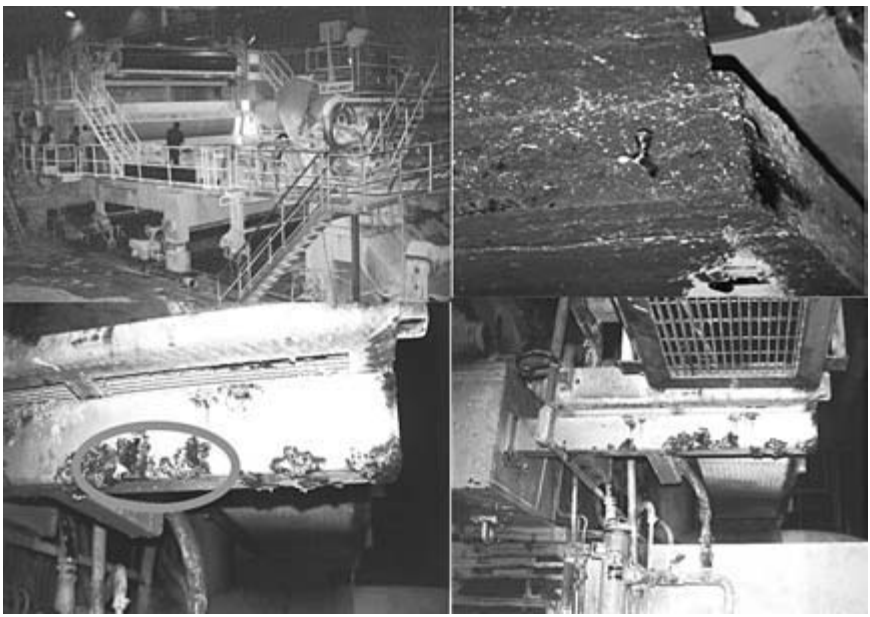

24.2 Visual inspections on the paper machine showing areas of materials deterioration.

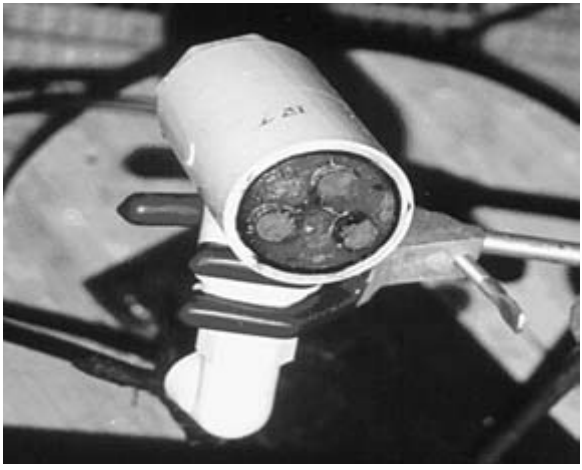

24.3 Corrosion sensor.

tion process on the corrosion probes was made as follows: the sensor was immersed in potassium hydroxide for one hour at 80 °C. After this, the sensor was rinsed with distilled water, dried and treated in hydrochloric acid for 30 s at 60 °C to remove any iron oxides remaining on the surface. Finally, it was rinsed again with distilled water and dried under a stream of hot air (Jasinski, 1986; Jasinski and Efird, 1987).

Electrochemical techniques

Here, the electrochemical noise (ECN) technique was used. Current noise and potential noise measurements were monitored simultaneously at a sampling interval of 1 s. Signals were collected at sampling intervals of 1800 s (Hladky *et al*., 1988; Cottis and Turgoose, 1999; Newman, 1986).

Experimental set-up

The corrosion monitoring involved the application of electrochemical noise measurements using a potentiostat/galvanostat/ZRA (Zero Resistance Ammeter) in an arrangement of three identical electrodes (working, reference and counter electrode) made of 1018 CS, which were placed inside the probe.

Temperature and relative humidity level

During a programmed outage, temperature and percent relative humidity measurements were taken as reference values by using commercial hygrom-

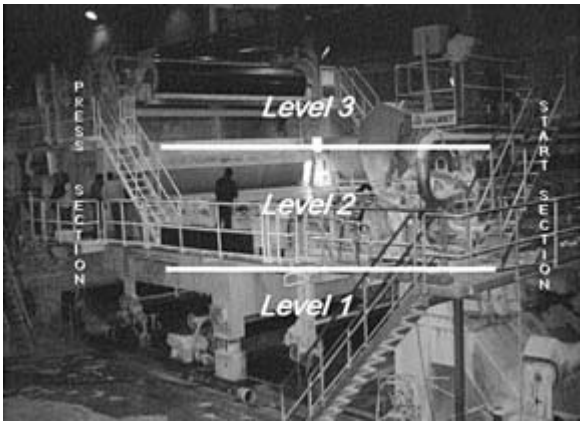

24.4 Location sites (white arrows) for corrosion probes and measurements of temperature and relative humidity in the paper machine.

eter/thermometer units (Scientific Instruments, USA) adjacent to the corrosion sensors. In addition, on the basis of visual inspection results and plant statistics, the various locations for the probes and measurements of temperature and relative humidity were defined through the three levels of the paper machine (Figure 24.4). Figure 24.5 shows a flow diagram of the machine paper indicating with more clarity the location of the corrosion probes in their respective sections. The sensors in the operations area were identified as 1-O, 2-O, 3-O and 4-O, and those at the transmission area as 1-T, 2-T, 3-T and 4-T.

24.2.2 Multiple-evaporator system

Material

The material tested was 304 stainless steel (UNS30400), since this is a common construction material of evaporator tubes in the black liquor process.

Electrolytes

The black liquors evaporated during the test periods were used as electrolytes. For each type of black liquor a descaling agent was added as follows:

- oak pine with descaling compound A (or agent A)
- pine with descaling compound B (or agent B)
- oak pine with descaling compound C (or agent C).

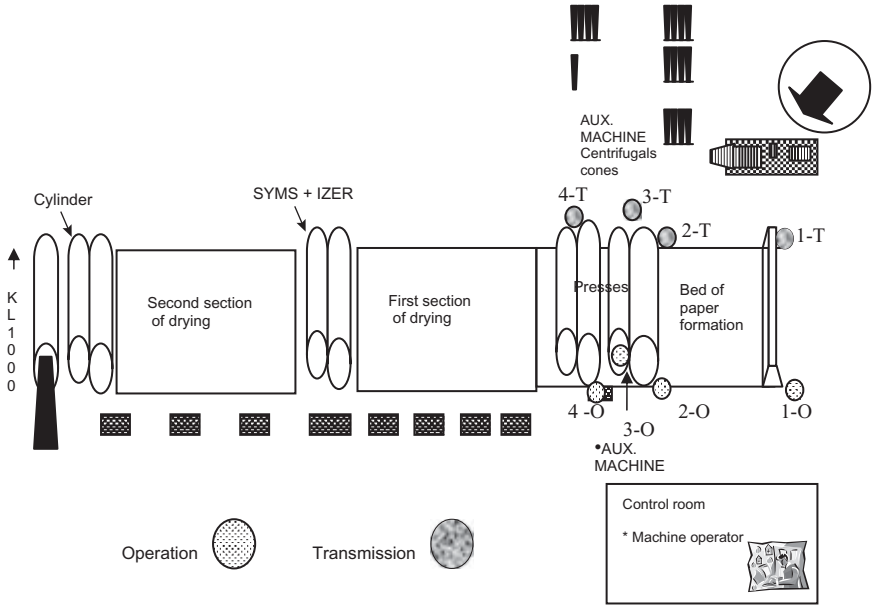

24.5 Flow diagram of the paper machine showing the location of corrosion sensors 1-O, 2-O, 3-O, 4-O and 1-T, 2-T, 3-T, 4-T in the operation and transmission areas, respectively.

Electrochemical techniques

In order to obtain instantaneous information on corrosion rates, linear polarization resistance and Tafel extrapolation techniques (see Chapter 3) were used (Uruchurtu *et al.*, 1990; Almeraya *et al.*, 2005).

Experimental arrangement

In this case, corrosion monitoring involved the application of electrochemical techniques using a potentiostat/galvanostat/ZRA in a system of three identical electrodes made of 304 SS, which were placed inside the probe.

Monitoring probe

Three similar monitoring probes were constructed, each one for a previously selected evaporator. Figure 24.6 shows a schematic diagram of a typical monitoring probe. Through the design and preparation of the monitoring probe (Almeraya *et al.*, 2005), the following activities were carried out:

1. Probe design: the design should withstand the operation conditions of the evaporators.

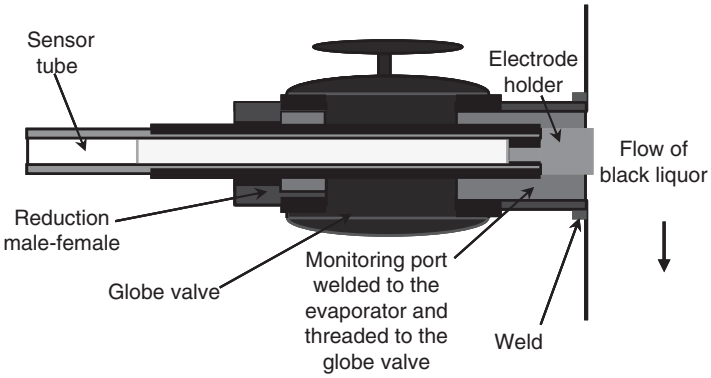

24.6 Schematic diagram of the monitoring probe, showing the main components.

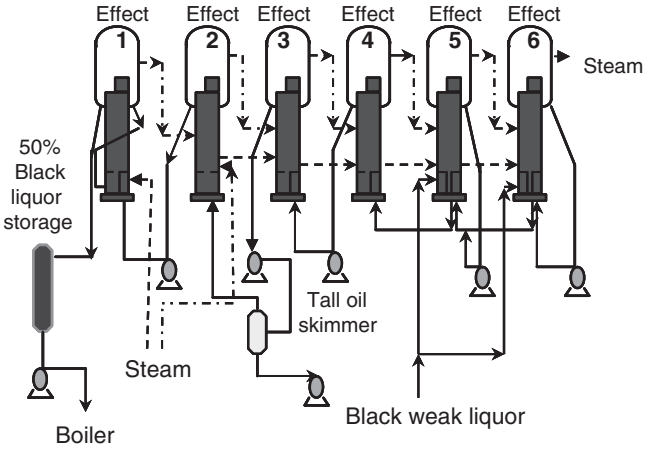

24.7 Schematic diagram of the evaporator distribution in the multiple-evaporator system.

2. Monitoring port design: the avoidance of leaks and the fulfillment of security standards were of paramount importance.
3. Operation characteristic of the probe: it should be free to move in the radial direction.
4. Corrosion sensor: it was made of three 304 SS metallic elements of the same size, all embedded for a dielectric material. A similar ionic activation process as the one previously described for the mild steel probe was carried out.

A schematic diagram of the evaporators distribution is shown in Figure 24.7. The selection of evaporators number 2, 3 and 6 as monitoring zones

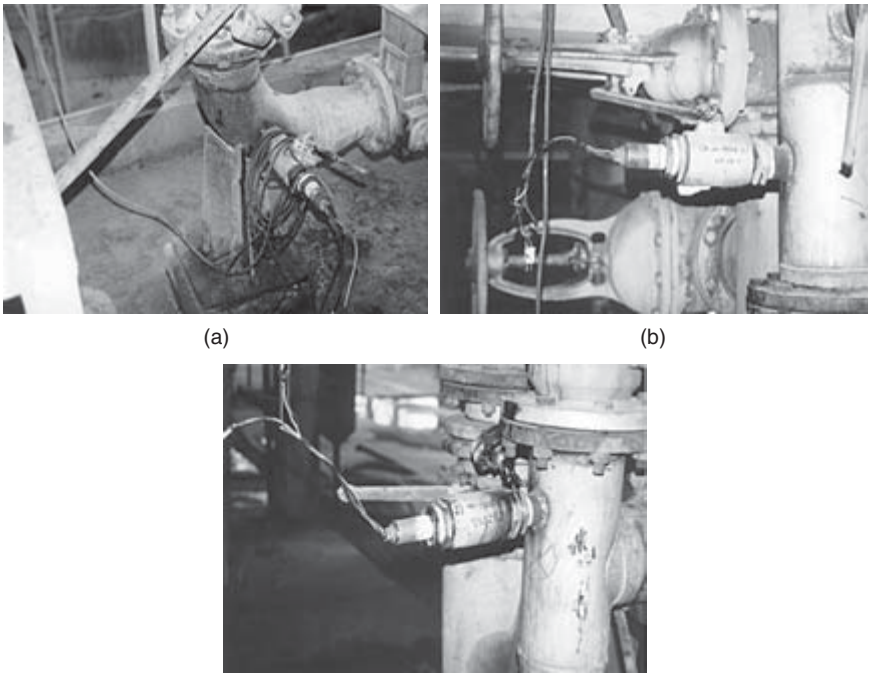

24.8 Monitoring sensors installed in: (a) evaporator 6, (b) evaporator 3, (c) evaporator 2.

was based on maintenance records given by the plant. Figure 24.8 presents a general view of the monitoring sensors located at the various evaporators.

24.3 Results and analysis

24.3.1 Paper machine corrosion

The visual inspection coupled with photographic records revealed that corrosion deterioration at the metallic structures was basically caused by paint failure. A principal source of this problem is related to the very high levels of humidity under operational conditions, particularly at the first steps of the paper manufacturing process.

Relative humidity and temperature measurements

Table 24.1 shows the results of relative humidity and temperatures recorded during a programmed machine outage. With these values as reference, it is

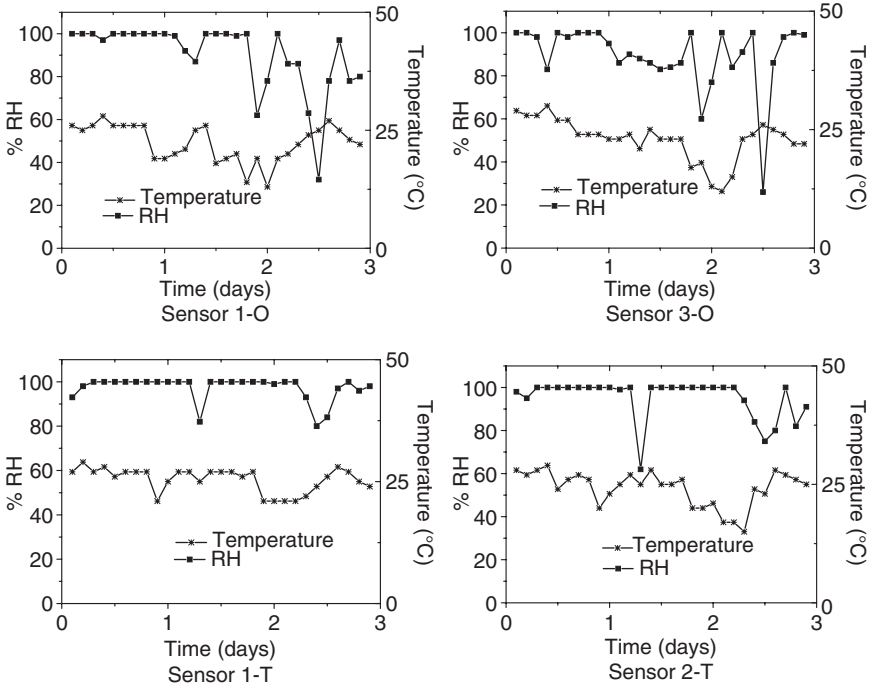

24.9 Relative humidity and temperature trends obtained with the probes 1-O and 3-O (operation area) and 1-T and 2-T (transmission area) under operation conditions.

important to note that, under operational conditions, the relative humidity is normally well above 80% in the paper machine area. Without any doubt, this is an important factor which could lead to paint failure. Thereafter, at places where the coating fails, corrosion of the underlying metal can be expected to occur as a natural process.

Figure 24.9 (a–d) shows the relative humidity and temperature trends obtained with the probes 1-O and 3-O and 1-T and 2-T during approximately three days of monitoring under operational conditions. The relative humidity values are somewhat higher in the transmission area than in the operational area. The RH (%) values in the transmission area were above 90% according to the data obtained for the various probes located in this area. If the coating fails, high humidity levels provide optimal conditions for steel corrosion. The temperature data obtained in the probes under operational conditions ranged from 25 to 30 °C, being somewhat higher than those recorded under shutdown conditions, see Table 24.1.

ECN measurements were performed during approximately three days. The potential noise time series obtained for the various sensors indicated

Table 24.1 Relative humidity (%) and temperature measurements in the paper machine during a programmed outage

	Percentage of relative humidity (% RH)						
	Level 1		Level 2		Level 3		Temp.
Zones	Oper.*	Trans.**	Oper.	Trans.	Oper.	Trans.	°C
Bed of paper formation	31	38	35	45	–	–	20
Press section	30	47	30	48	28	40	24
Press section	28	55	31	–	37	68	21

Notes: * Operation section; ** Transmission section

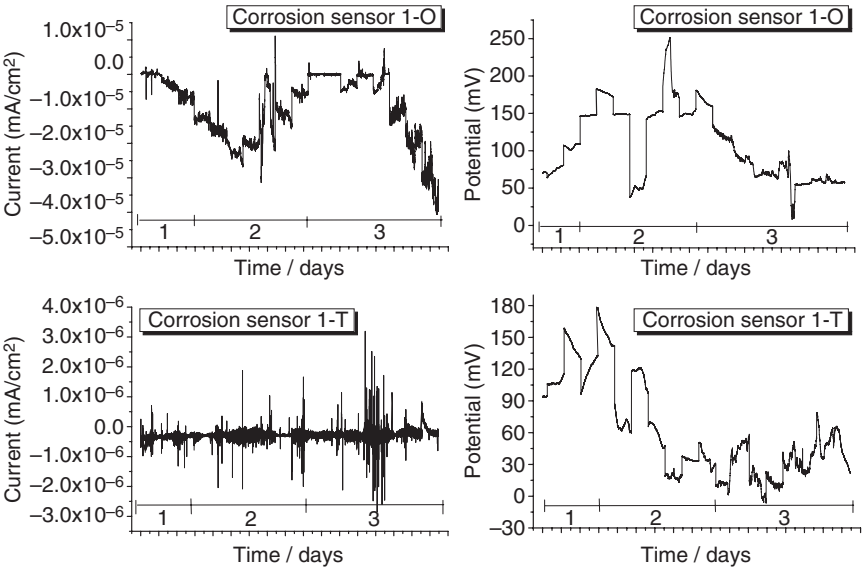

24.10 Current noise and potential noise time series obtained by the corrosion sensors 1-O (operation area) and 1-T (transmission area) during a three day monitoring trial.

that most of the potential values recorded are active, whereas the current noise shows some fluctuations over time. Thus, two corrosion probes 1-O and 1-T (at operation and transmission areas, respectively) were chosen as representatives of the general behavior.

Figure 24.10 shows the current and potential noise time series obtained for the aforementioned probes. For the one located at the operation area, the current noise fluctuations were higher than those recorded at

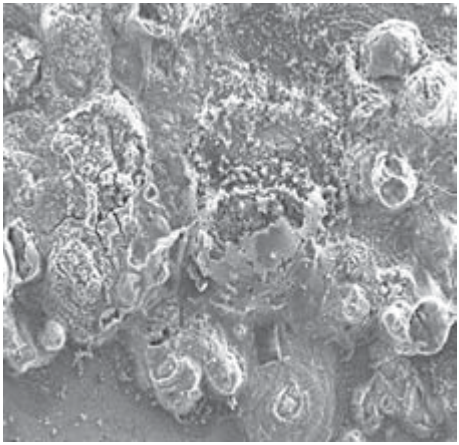

(a)

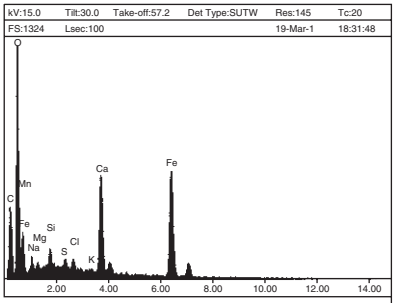

EDAX ZAF Quantification (Standardless)
Element Normalized

Element	Wt %	At %	K-Ratio	Z	A	F
C K	9.14	20.14	0.0348	1.1097	0.3423	1.0006
O K	27.83	46.02	0.1422	1.0884	0.4688	1.0013
Mab	9.10	4.38	0.0400	0.9007	0.4871	1.0014
NaK	0.99	1.13	0.0043	1.0149	0.4342	1.0003
MgK	0.38	0.41	0.0023	1.0393	0.5743	1.0006
Si K	1.09	1.03	0.0090	1.0413	0.7940	1.0022
S K	0.77	0.64	0.0072	1.0267	0.9084	1.0072
Cl K	0.03	0.02	0.0078	0.9806	0.9393	1.0119
K K	0.31	0.21	0.0031	0.9834	0.9756	1.0345
CaK	10.48	6.92	0.1064	1.0048	0.9853	1.0256
FeK	39.07	18.51	0.3549	0.9093	0.9990	1.0000
Total	100.00	100.00				

(b)

24.11 (a) SEM morphology at the surface of sensor 1-O (1200×) and (b) chemical analyses (EDX) on (a) after three days of exposure.

the transmission area. To some extent, this behavior might indicate that a localized corrosion process is more likely to occur here. It is known that a localized corrosion process is frequently associated with current transients as pits nucleate, propagate and die. Thus, the simplest approach to data analysis and probably one of the most powerful is to examine the time records for features that are characteristics of particular types of corrosion. Pitting corrosion exhibits larger current transient peaks as compared with the ones found in a more stable system, i.e. uniform corrosion (Cottis and Turgoose, 1999, Zielinsky *et al.*, 2002, A-Zanki *et al.*, 1988). Again, the potential noise time series obtained shows a general trend falling into more active (less positive) values. Since the relative humidity level is high, we could expect the potential to shift towards more active values. Therefore, the likelihood of corrosion increases.

At the end of the monitoring period, i.e. three days, the exposed surface of the sensors was examined by SEM/EDX. Figure 24.11 shows the surface morphology of sensor 1-O. Elements such as silicon, iron, manganese (from the steel) and chlorine, potassium, calcium and carbon (the last two from calcium carbonate added as additive in the process) were identified. In a similar manner, the analysis at the surface of sensor 1-T shows that only iron and oxygen peaks were identified, Figure 24.12 (a and b). Thus, the high moisture content in the environment coupled with chlorine develops an aggressive atmosphere in the paper machine structure.

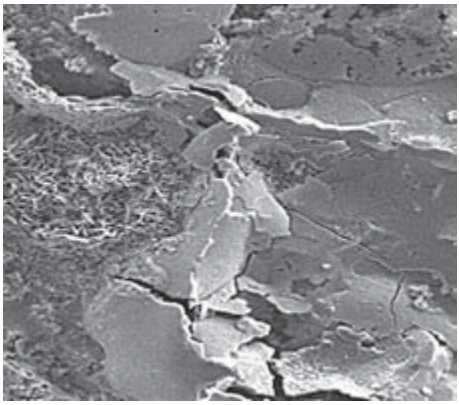

(a)

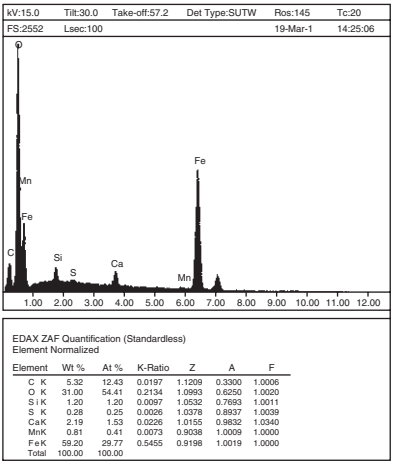

(b)

24.12 (a) SEM morphology at the surface of sensor 1-T, and (b) chemical analyses (EDX) on (a) after three days of exposure.

24.3.2 Evaporator corrosion

Corrosion monitoring

The corrosion monitoring of evaporators 2, 3 and 6 was carried out during three periods of time, which were selected according to the liquor of interest. The periods of work and their conditions were as follows

- Period A: Here, the black liquor is extracted from an 80%–20% mixture of oak–pine respectively, plus a descaling agent A.
- Period B: The black liquor extracted from pine, plus descaling agent B.
- Period C: The black liquor extracted from an 80%–20% mixture of oak–pine plus descaling agent C.

Figure 24.13 shows the condensed results of corrosion rates (CR) obtained by Tafel extrapolation as a function of the electrolyte in evaporators 2, 3 and 6. Figure 24.14 shows the results obtained by linear polarization resistance (LPR).

These results show that, in general, the corrosion rates were higher for evaporator 2 compared with the ones measured on evaporators 3 and 6, where lower corrosion rates were recorded. To explain this result, the following arguments are proposed: first, the black liquors from Oak-Agent A and Oak-Agent C caused more corrosion than that obtained with the Pine-Agent B liquor. This could be due to differences in chemical composition of the two oak-based black liquors and the pine-based black liquor. Second,

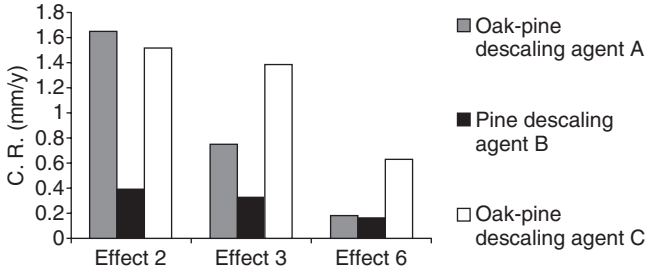

24.13 Corrosion rates obtained by Tafel extrapolation on evaporators 2, 3 and 6 with the various electrolytes.

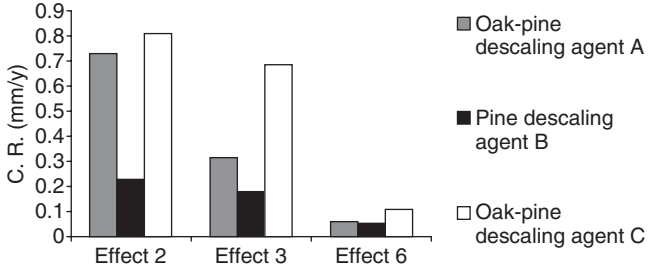

24.14 Corrosion rates obtained by linear polarization resistance on evaporators 2, 3 and 6 with the various electrolytes.

the operation temperature and percentage of dry solids in evaporator 2 was higher compared with the other two evaporators.

Overall, the recorded data indicate corrosion rate values somewhat higher than those usually found in the industry. This is attributed to the fact that Tafel and LPR measurements assume that only a single anodic and cathodic reaction is occurring on the metal surface. Because black liquor contains many organic and inorganic electroactive species, oxidation and reduction reactions other than those involved in the corrosion process may not be measured. The descaling agent may modify some reactions without changing the corrosion rate (Almeraya *et al.*, 2005).

On evaporator 3, the recorded corrosion rates indicate that the Oak-Agent A and Pine-Agent B based black liquors were less aggressive than Oak-Agent C. A similar behavior was observed on evaporator 6, where the evaporation process begins (Salais, 1977). Although the corrosion trends were similar irrespective of the technique used, differences and limitations can be expected. Thus, in a full evaluation exercise, it will be worth correlating the results with weight loss data or physical measurements and inspection of tubes for the sake of comparison.

Scanning electron microscopy

After exposure to the flow environment on each evaporator, some specimens from the monitoring probes were analyzed by SEM/EDX to characterize and evaluate the extent of damage. Figures 24.15 to 24.17 show the results. The morphology found on specimens exposed on evaporator 2

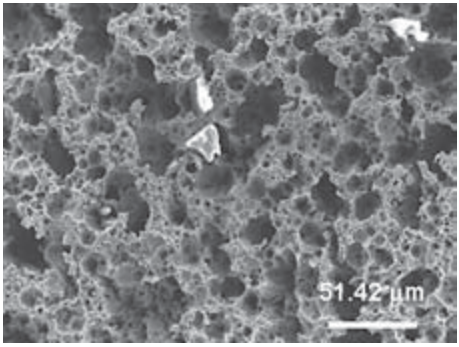

(a)

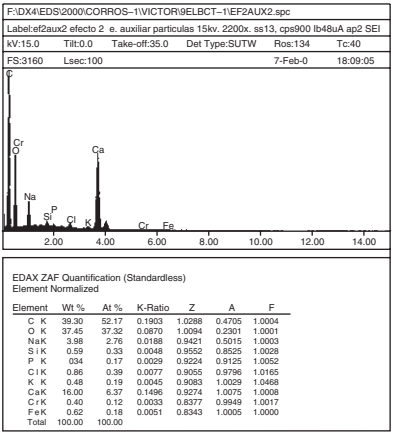

(b)

24.15 Morphology of the 304 steel, after being exposed for three days on the evaporator 2; and EDX analysis of the white particles.

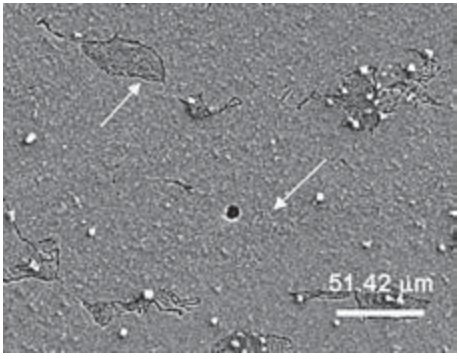

(a)

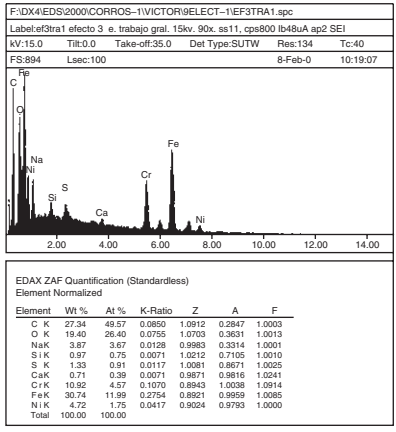

(b)

24.16 Morphology of the 304 steel, after being exposed for three days on the evaporator 3; and EDX analysis at the surface of the working electrode.

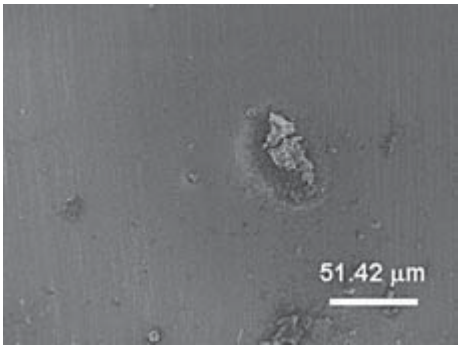

(a)

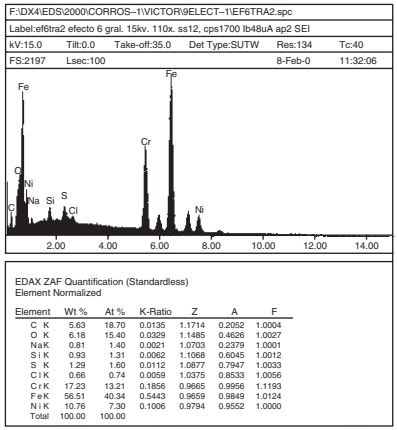

(b)

24.17 Morphology of the 304 steel, after being exposed for three days on the evaporator 6; and EDX analysis at the surface of the working electrode.

clearly shows the extent of the attack, see Fig. 24.15. In this case, large areas on the specimen were affected. Specimens from evaporator 3 showed less surface damage, as can be noted in Fig. 24.16. Overall, the specimens exposed on evaporator 6 were less affected, as can be seen in Fig. 24.17. The morphologies observed confirm and support the corrosion rate results obtained by the electrochemical techniques on each evaporator. In general, high contents of carbon, oxygen, sodium, sulfur and, to a lesser degree, chlorine, were found on the affected areas. Thus, possible compounds such as sodium carbonate, sodium sulfate or sodium thiosulfate, among others, formed by these elements could be responsible for the corrosion observed (Orozco *et al.*, 1999). On the whole, the monitoring probe discussed here has been shown to be helpful in evaluating the corrosion performance of materials exposed under the conditions of the present study.

24.4 Conclusions

24.4.1 Paper machine corrosion

The paper machine disclosed areas of preferential corrosion, being larger at the transmission area, as determined by visual inspection. The corrosion damage on the steel structure was primarily associated with failure of the protective coating. The corrosion monitoring through the sensors implemented here gave a reasonable response. Overall, at the operation area, current noise fluctuations were higher than those recorded in the transmission area. To some extent, this behavior might indicate that a localized

corrosion process is more likely to occur in the former (where chlorine was detected by EDX analyses), whereas in the latter a uniform corrosion process could be expected.

The high level of humidity (about 100% most of the time) recorded during operation conditions develops proper conditions for steel corrosion if the coating fails. Potential monitoring at two sections on the paper machine indicates a trend toward more active values. According with this, it can be expected that the likelihood of corrosion increases. This behavior was related with the high humidity levels found (about 100% RH) most of the time during operation conditions.

SEM/EDX analyses indicated the presence of elements such as chlorine, calcium and potassium on the 1-O sensor surface, whereas for sensor 1-T basically ion oxide was identified.

24.4.2 Evaporator corrosion

A corrosion monitoring probe was designed and tested *in situ* under conditions pertinent to the black liquor evaporation process in the pulp and paper plant. Overall, the corrosion rates recorded for evaporator 2 were higher than those measured on evaporators 3 and 6. It is thought that this behavior could be greatly influenced by the temperature conditions and changes in the composition of the black liquors on each evaporator during the various periods of monitoring. For a given evaporator, the trends in corrosion rates measured by Tafel extrapolation and LPR were similar and correlate well with the morphological features observed by SEM.

24.5 Acknowledgements

The authors are grateful to Consejo Nacional de Ciencia y Tecnología (Mexico), through project 35378-U, for economic support and the facilities granted for the realization of this work. The technical assistance of Jair Lugo, Gregorio Vazquez and Carlos Barrios is gratefully acknowledged.

24.6 References

Almeraya-Calderon F., Orozco C.V., Gaona-Tiburco, C.C., Borunda-Terrazas, A., Nava, J.C., Martinez-Villafane, A. and Mendoza, D.N. (2005) Corrosion Monitoring of Type 304 Stainless Steel in a Black Liquor Evaporation Process, *Materials Performance*, 44 (7), 34–37.

A-Zanky I.A., Gill J.S. and Dawson J.L. (1988) *Mat. Sci. Forum* 8, 463.

Casey James P. (1990) *Pulp and Paper: Chemistry and Chemical Technology*, Volume 1, New York, Wiley Interscience.

Cottis R. and Turgoose S. (1999) *Electrochemical Impedance and Noise*, Houston, TX: NACE Internacional.

Cox W.M., Farrell D.M. and Dawson J.L. (1985) Corrosion Monitoring for Process Control, in *Dewpoint Corrosion*, D.R. Holmes (ed.), Chichester: Ellis Horwood/ Institution of Corrosion Science and Technology, 191–217.

Hines J.G., Moreland P.J., Rothwell G.P., Rowlands J.C. and Morgan W.R. (1978) *Industrial Corrosion Monitoring, Department of Industry Committee on Corrosion*, London, UK: HMSO.

Hladky H., Lomas J.P., John D.G. Eden D.A. and Dawson J.L. (1988) *Corrosion by Electrochemical Noise: Theory and Practice*, Corrosion and Protection Center Industrial UMIST, England,

Jasinski R.J. (1986) *European Patent Application* EP-174468, March 1986, CA105: 81994P.

Jasinski R.J. and Efird K.D. (1987) Electrochemical Corrosion Measurements in Crude Oil, *Corrosion*, 43 (8), 476–478.

MacDonald R.G and Franklin J.N. (1969) *The Pulping of Wood, USA*, New York: MacGraw-Hill, Chapter 1.

Mansfeld B.F. (1976) Effect of uncompensated IR drop on polarization resistance measurements, *Corrosion*, 32 (4), 143–145.

Newman J. J. (1986) *Electrochemical Society Proceedings*, 86 (7), 139.

Orozco C.V., Almeraya-Calderon F., Gaona-Tiburcio C., Chacon-Nava J.G., Borunda-Terrazas A. and Martinez-Villafane A. (2001) Electrochemical Behaviour of Stainless Steel 304 in Black Liquor Evaporation Process, 10th International Symposium on Corrosion in the Pulp and Paper Industry. Helsinki, Finland VTT Manufacturing Technology.

Orozco C.V., Almeraya F., Gaona C. and Martínez A. (1999) *Evaluación del Deterioro por Corrosión en los Tubos de un Evaporador en la Industria del Papel*, XXI CIMM, Saltillo, Coah, México.

Uruchurtu Ch. J., Malo M.J. and García O.E. (1990) *Técnicas Electroquímicas Aplicadas Al Control y Seguimiento de le Corrosión*, IMICORR. México, D.F.

Salais V. (1977) Critical Components of the Paper Machine: Damage Caused by Metallic Corrosion in Pulp and Paper Industry, *Corrosion Problems*, 2, Houston, TX: NACE, USA.

Zielinsky A., Smulko J., Krakowiak A. and Darowicki K. (2002) The stationarity characteristics of electrochemical current noise, *Anti-Corrosion Methods and Materials*, 49 (1), 27–32.

25

Advanced corrosion control at chemical plants using a new corrosion monitoring technique

MASAZUMI MIYAZAWA, Mitsubishi Chemical Corporation, Japan

25.1 Introduction

Chemical plants manufacture products by the chemical reaction of raw materials. The substances used at chemical plants can be combustible, toxic and corrosive. Due to these factors, corrosion of facilities is a constant challenge for chemical plant operators. To help solve this serious problem, it is necessary first to learn the cause-and-effect relationship between corrosion damage and how the plant is run, and then to take preventive measures that are consistent with this relationship. A possible solution is the combination of monitoring chronological data for plant operations while evaluating simultaneously the progress of corrosion, then subsequently analyzing the complex interactions observed using these measurements. However, in order to accomplish this, a device is necessary that can measure simultaneously the plant operation and corrosion data corresponding to the target fault condition. For this reason, there has been a requirement for monitoring devices that can measure real-time corrosion in chemical plant facilities used for production. Chemical plant corrosion damage has been ascribed to raw material quality, operational conditions, and to other process factors, so in the past it has been difficult to propose changes to the operational conditions or other measures to prevent corrosion, unless the causes of corrosion were identified. This holds true even with changes of the service conditions, which have become increasingly sophisticated.

As discussed in Chapter 4, one method to identify the causes of corrosion and formulate preventive measures is the use of electrochemical noise (EN) measurements to measure general corrosion. Recently developed electrochemical noise measurements are gaining attention as a means to measure real-time corrosion of facilities. This chapter focuses on the issues and countermeasures involved in applying the measurement method to actual plants. Also reported is an example where a combination of laboratory tests and corrosion monitoring was applied to an actual chemical plant, in order to identify the causes of corrosion, and to consider and verify measures for the prevention of corrosion.

25.2 Investigation

25.2.1 Principles of the tri-electrode electrochemical noise measurement

The development history and principles of electrochemical noise methods has been described in detail in Chapter 4. This section presents a summary of the working principle for the electrochemical noise (EN) measurement methodology, which has been applied to investigate general corrosion using a sensor with three electrodes. Mansfeld and Xiao examined this electrochemical noise method. Eden *et al.*[2] proposed methodologies for the measurement of electrochemical noise using three electrodes, calculating the corrosion rate, and identifying the type of corrosion. Based on this research, the present author and co-workers at Mitsubishi Chemical Corporation (Japan) conducted experiments and analyzed data obtained from experimental observations. These efforts allowed the measurement methodology to be improved after reconsidering the issues that previous research had failed to clarify or explain.

Figure 25.1 is a schematic representation of the devices used for the tri-electrode electrochemical noise measurement. Three metal electrodes of the same material were used with a zero-resistant ammeter installed between two of them and an electrometer connected to the remaining electrode, which was used for comparison.

One of the features of this measurement method is that there is no need to apply an external electric current to the electrodes while measuring. In short, this method measures the corrosion occurring at the electrodes, and under natural conditions so that it should not disturb the electrochemical interface on the working surface of the sensor.

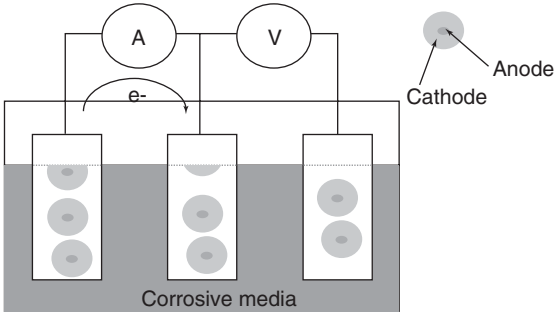

A: Zero resistance ammeter V: Electrometer

25.1 A schematic representation of the devices used for the tri-electrode electrochemical noise measurement.

On the electrodes, multiple anodes and cathodes work together during corrosion activity. Generally, it is impossible to measure externally what is occurring at the individual anodes and cathodes under natural conditions. However, when the two electrodes are connected by the ammeter, some of the electrons generated by corrosive reactions, which occur at the anodes and cathodes in the proximity of the connection, interact with the impedance of the electrochemical double layer, thereby causing the corrosion potential to fluctuate and this perturbation is monitored by the electrometer. The electrode connected by the electrometer on the right-hand side of Fig. 25.1 functions as the reference electrode. Figure 25.2 shows an example of measurement data obtained with this method.

Examination of the chronological changes in corrosive reactions at an anode and cathode pair, at a microscopic level, reveals subtle variations in the rate of the corrosive reactions depending on factors that include the supply rate of the oxidizer within the solution, and the speed of mobile ions. These microscopic changes within a tiny fraction of time are called fluctuations of corrosion. It was supposed that, within a very short period of time, the ratio of the changes in the electric current to that in the potential remains the same, unaffected by the changes in corrosive reactions occurring at the anode and cathode. The tri-electrode electrochemical noise measurement of uniform corrosion rates originated with consideration of such fluctuations of corrosion. While corrosion progresses on the macro scale, measurement and collection of data at very short time intervals should result in measurements unaffected by the corrosion cycle at the anode/cathode pair.

Based on this basic concept, and in an analogy to Ohm's Law, the ratio of change in the current, δI, and the corresponding change in the potential, δE, can be used to calculate the noise resistance, R_n, relevant to the corrosive reaction rate:

$$R_n = \delta E / \delta I \qquad [25.1]$$

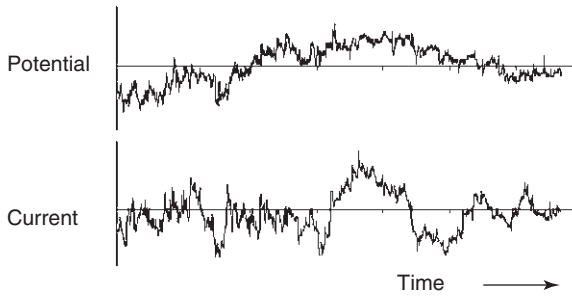

25.2 An example of measurement data obtained with electrochemical noise method.

However, during actual measurement, the R_n differs significantly among different measurements taken. Therefore, the standard deviations of the data measured during a specified measurement time (ΔI: standard deviation of the current, ΔE: standard deviation of the potential) were computed and used to obtain an average value for R_n. Different time periods of measurement were investigated in order to find one with the fewest fluctuations in the measurement.

$$R_n = \Delta E/\Delta I \qquad [25.2]$$

The current indication from the zero resistance ammeter should be a representative sample of the electron flow rate between the anodes and the cathodes, generated in the proximity of the two electrodes. However, since the actual areas occupied by the anodes and the cathodes are unknown, in addition to the ratio of the anode to the cathode divided between the electrodes, we are unable to evaluate the values related to the measured current in terms of corrosion current density.

For this reason, we introduced the coefficient of corrosion, G, as a constant of proportion between the corrosion rate (CR) and $1/R_n$:

$$CR = G/R_n \qquad [25.3]$$

where CR is the corrosion rate (mm/y), G is the coefficient of corrosion, and R_n is the noise resistance. The corrosion coefficient is not the same across all the areas of measurement. Even within a solution containing the same substances, if the density of the solution and/or other factors change and alter how the corrosion proceeds, the corrosion coefficient also must be altered. Eden *et al.*[2] employed a constant of proportion, obtained from the Tafel gradient, as the constant of proportion between CR and R_n. This was somewhat similar to the common polarization resistance method as described in Chapter 3. Still, as mentioned above, the area occupied by the anode may not be constant and therefore the use of such a constant of proportion cannot be considered appropriate.

Figure 25.3 summarizes the measurement device that was developed in accordance with the principles of the tri-electrode electrochemical noise measurement. This measurement device consisted of a data analyzer, a measurement section, and a tank containing the test solution into which the sensor was introduced. The data analyzer has two functions; one that outputs analysis results of chronological changes in the electrode potential and current measured, and a second that sets the data collection interval, a crucial feature of the tri-electrode electrochemical noise measurement methodology. The measurement section had a zero resistance ammeter (A) between two of the three electrodes and an electrometer (V) connecting the remaining electrode. The electrodes were placed within the solution while measurements were taken.

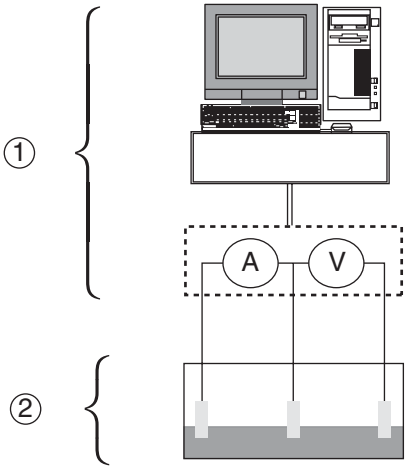

① Data analysis system and measurement equipment
② Test cell

25.3 The principles of the tri-electrode electrochemical noise measurement system.

25.2.2 Verification of the tri-electrode electrochemical noise measurement

Tests were conducted to verify whether the tri-electrode electrochemical noise measurement is applicable to the evaluation of uniform corrosion behavior. In these tests, we attempted to confirm that a correlation existed between the corrosion rate obtained by the weight loss method and the R_n value obtained by the tri-electrode electrochemical noise measurement. We employed solutions of the same substances, but with different concentrations.

The measuring device was a S11280B manufactured by Solartron of the UK, and the measurement specifications were as follows:

- number of cell electrodes: compatible with 2, 3 and 4 terminals
- range of current measurement resistance: 0.1 Ω to 1 MΩ
- range of current: 200 nA to 2 A
- maximum resolution: 1 pA.

The test sample, made from stainless steel (SUS304: UNS S30400), was a cylinder of 10 mm in diameter and 32 mm in length. The solutions used were four different concentrations of HCl solutions, each containing 100 cm^3 of distilled water and HCl concentrations of 10.0%, 5.0%, 1.0%, and 0.5%.

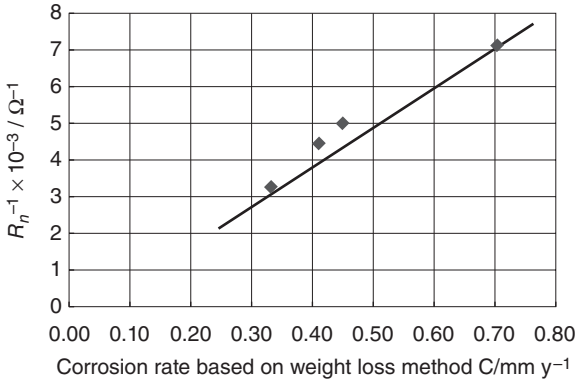

25.4 The values of the corrosion rate calculated using the weight loss method, and the *R*n calculated with the tri-electrode electrochemical noise measurement.

Figure 25.4 shows the values of the corrosion rate calculated using the weight loss method, and the R_n calculated with the tri-electrode electrochemical noise measurement. The Figure indicates a proportionality relationship between the corrosion rate from the weight loss method and the inverse of the R_n value from the tri-electrode electrochemical noise measurement. Thus, these tests confirmed that the tri-electrode electrochemical noise measurement was able to measure uniform corrosion, so long as an appropriate coefficient of corrosion was obtained from laboratory tests.

25.3 Monitoring and corrosion control

25.3.1 Outline description of the example chemical process plant and the corrosion damage sustained by it

The case of a corrosion monitor used to measure corrosion of heat exchangers at a chemical plant is presented. Figure 25.5 shows the process flow at the chemical plant. In the process, organic solution and organic gas were fed into a reactor, where they reacted to generate the intended product and its byproducts. The product then was refined in processes that followed. The organic solution was made from a solid substance, which was dissolved in an agitator tank and then fed into the reactor. Solution feeding must be performed at a constant temperature so as to stabilize the reaction. For this reason, part of the feed solution was branched into a heat exchanger and then fed back into the dissolving tank, in order to adjust the solution temperature. The heat exchanger generated steam for control of the solution temperature. This heat exchanger, which controlled the solution temperature, was the equipment that had corroded and the inside of its tube was

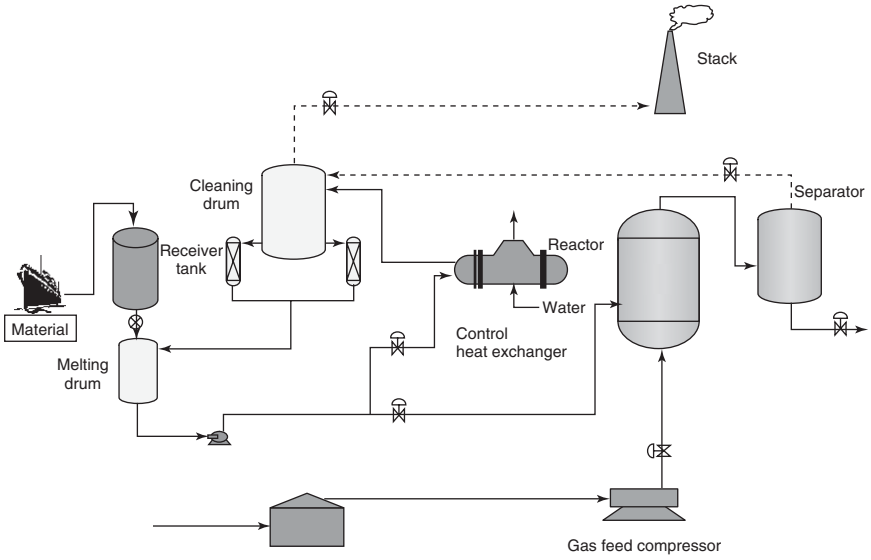

25.5 The process flow at the chemical plant.

especially damaged. The raw material solution is fed into the tube while some boiler water is fed into the exchanger's shell and comes out as steam. The tube is designed to allow the solution to flow at approximately 1.0 m/s. The raw material melting point is 140 °C and the exchanger is kept at approximately 150 °C when operating. The tube is made of SUS321 (UNS S32100).

Although the exchanger had been used for almost 20 years since installation, the tube damage had only become apparent three to four years ago. The operational information showed that there had not been a change in the raw material or the exchanger operating conditions. Figure 25.6 shows a photograph of the corroded heat exchanger and the extent to which the tube was damaged. The damage to the tube shows signs of erosion corrosion. To solve this corrosion problem, measurements were performed using an electrochemical noise corrosion monitor and the results considered to establish how to prevent the corrosion.

25.3.2 Preparations for the measurements

In order to measure the corrosion with the monitor, it was first necessary to obtain a coefficient of corrosion that fitted the relevant materials and environment. Thus, the laboratory test equipment was configured for use with the same solution and materials as were used in the plant heat exchanger. A preparatory measurement was then made using the tri-

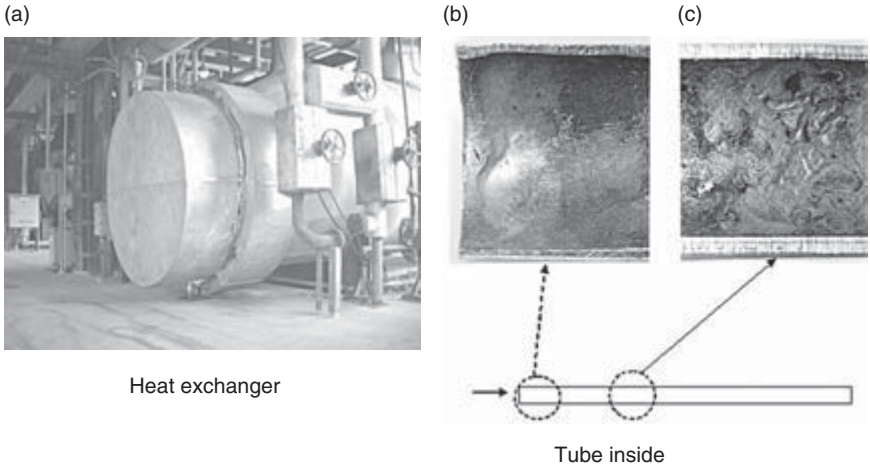

25.6 A photograph of the corroded heat exchanger and the extent to which the tube was damaged.

electrode electrochemical noise system to determine example data, and thence to calculate the coefficient of corrosion. During these measurements, special attention was given to observation of the surface of the electrodes, so that it could be confirmed that their condition was similar to damage observed in the actual heat exchanger. Additionally, it was confirmed that there was a correlation between the corrosion phenomena on the surface of the electrodes and the noise resistance patterns in the current and potential data collected. These observations were crucial to confirm that the correct measurements were being made to reflect conditions in the actual (plant) heat exchanger.

The coefficient of corrosion was obtained from R_n value determined with the tri-electrode electrochemical noise measurement and the physical corrosion rate determined from the weight loss values. A preparatory test was conducted within the sample solution using SUS321 electrodes. The measurement results enabled a corrosion coefficient of 103.9 to be calculated, which was used to calibrate the corrosion monitor. This coefficient was entered into the corrosion monitor software program. Subsequently, the coefficient value was fine tuned at the end of the test to better reflect plant conditions after measuring the weight loss of the sensor electrode at an overhaul inspection.

25.3.3 Installing the measurement equipment

The actual measurement equipment consisted of a data analyzer, a data-measuring device and a sensor. The data analyzer evaluates the data col-

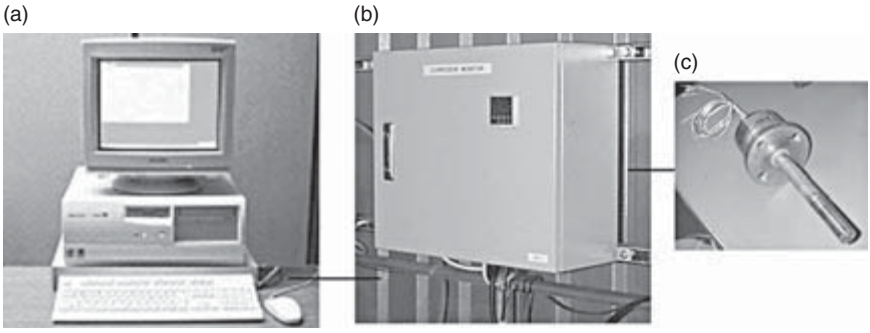

25.7 A photograph of the measurement devices installed in the meter room.

lected and outputs the rate of corrosion. The data measurement device measures changes in the corrosive reactions occurring at the sensor electrode. The structure of the measurement equipment is such that this sensor was inserted through an access nozzle in the exchanger and held in place with a flange. The sensor and the data measurement device were connected with a shielded cable because they measure a very subtle current and voltage signals and this requires protection from outside interference. With regard to attenuation of electrical signals, tests were performed with a cable actually installed, confirming that the influence of extraneous signals was negligible so long as the probe cable was less that 200 m in length. For the actual measurement with the corrosion monitor, the data analyzer and the data measurement device were placed in a meter room and the sensor was located at the nozzle of the heat exchanger, the subject of the measurement. Figure 25.7 shows a photograph of the measurement devices installed in the meter room. The measurement devices used for the actual measurement of the heat exchanger were developed from devices manufactured by Mitsubishi Chemical Corporation (Japan), and the data output format could be changed as desired. Measurement in an actual chemical plant can be affected by stray currents and other factors, and counteracting these types of interference is a very important issue. Corrosion was successfully measured without disturbance from such factors, even though the actual measurement was made beside a power station.

Analysis of the corrosion data was performed without any major problems. Currently, some 20 corrosion measurement units are in operation at Mitsubishi Chemical Corporation and its affiliates. Of these, the oldest unit has been taking measurements since 1997 and is still operational.

25.3.4 Monitoring and its results

The corrosion monitoring measurement on the heat exchanger installation began in June 1999, and the data obtained are shown in Fig. 25.8. The measurement results show a corrosion rate (approximately 1.0 mm/y), which is lower than that calculated from the actual corrosion loss measured at the initial overhaul inspection. Therefore, the change in the operation of the heat exchanger was evaluated over time. It was discovered that raw materials from two different manufacturers (Corporations A and B) were being used alternately. The damage was particularly marked when material from Corporation A was employed.

Since April 1999, materials from the two corporations had been used alternately. It was assumed, therefore, that while material from either of these two suppliers was fed for a certain period of time, the material from the other supplier was then fed to the heat exchanger before there was a complete replacement of the materials within the heat exchanger. It was supposed that this coexistence of materials from both suppliers lowered the actual corrosion rate.

For monitoring purposes, the division responsible for operation of the heat exchanger and its production line was asked to feed only the material from Corporation A for a period of time. Figure 25.9 shows the results of corrosion monitoring while only the material from Corporation A was fed.

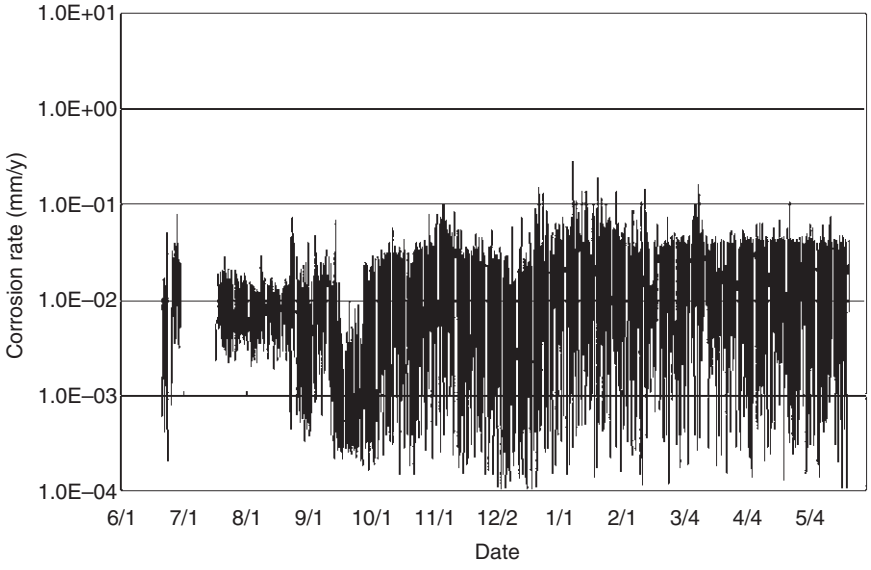

25.8 The corrosion monitoring measurement data on the heat exchanger installation began in June 1999.

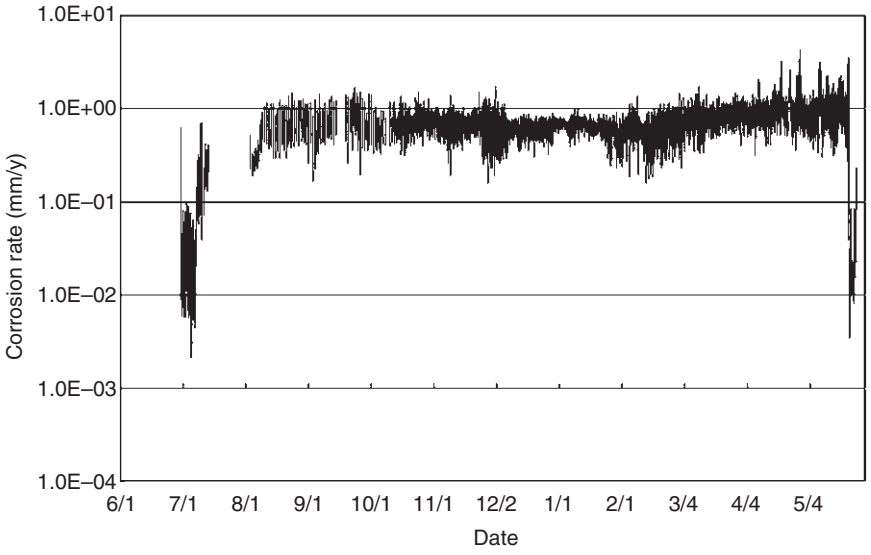

25.9 The corrosion monitoring measurement data on the heat exchanger installation began in June 2000.

It was observed that the corrosion rate obtained from the data actually measured was very close to that (approximately 1.0 mm/y) calculated for the corrosion loss at the initial overhaul inspection. This indicated that using only the material from Corporation A worsened the extent of corrosion.

To reveal what was in the material that caused this increased corrosion, the solution within the heat exchanger was sampled and its composition was analyzed. It was found that the difference was in the sulfur content. Therefore, a laboratory test was conducted to determine the relationship between the sulfur content and the corrosion rate. The test results are shown in Fig. 25.10, and they showed that sulfur added to the material drastically aggravated the corrosion rate. The cause of the corrosion was confirmed to be sulfur content in the material feed.

The way in which sulfur entered the material was then investigated and it was found that the contamination with sulfur occurred while the material, a solid substance, was moved on a belt conveyor that also was used to carry other substances. Thus, the sulfur content in the other material entered the feedstock under investigation. Because the mixing of sulfur was inconsistent, the analyses performed at the time had not identified sulfur in the material.

In June 2000, the plant staff improved quality control of the raw materials, and as Fig. 25.11 shows, the corrosion rate decreased to 0.05 mm/y or

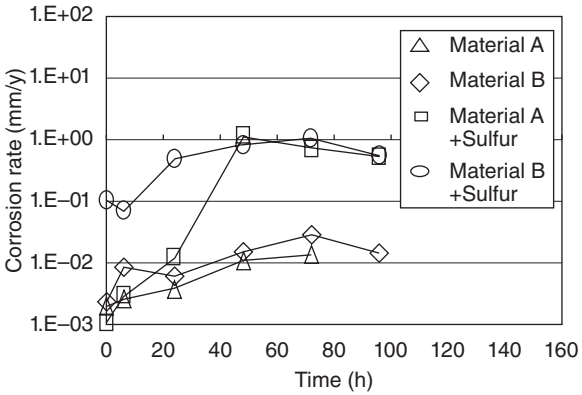

25.10 The corrosion measurement data at the laboratory.

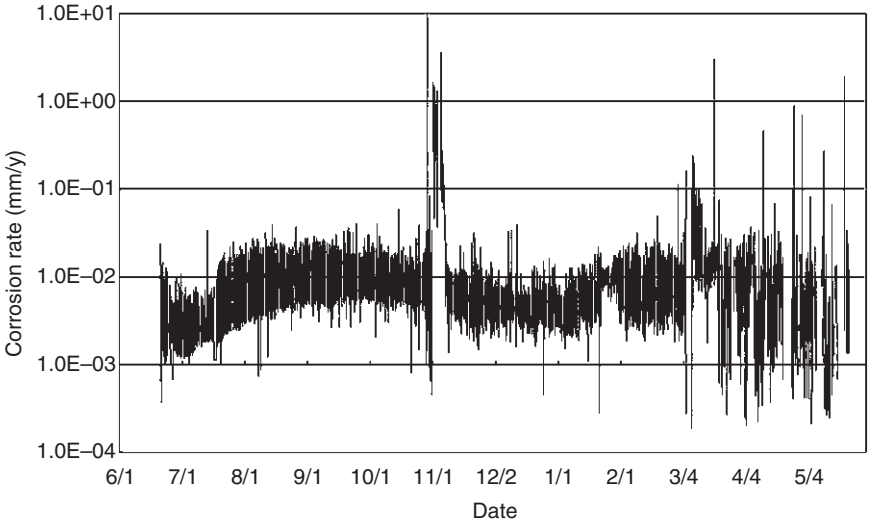

25.11 The corrosion monitoring measurement data on the heat exchanger installation begun in June 2001.

less. In this study, we achieved the effective combination of on-site facility monitoring and laboratory tests, identified the cause of corrosion, and even verified the effectiveness of a proposed measure by conducting corrosion monitoring. These findings illustrate well the importance of on-site monitoring, as many different factors typically combine to cause corrosion at chemical plants.

25.4 Conclusion

At Mitsubishi Chemical Corporation, corrosion was monitored and controlled at an operating chemical plant using tri-electrode electrochemical noise measurements. It was confirmed that the tri-electrode measurement is an effective method for the measurement of uniform corrosion in actual sites at a chemical plant.

25.5 References

1 M. Mansfeld and H. Xiao, *J. Electrochem. Soc.*, 140, 2205, (1993).
2 D. A. Eden, D. G. John and J. L. Dawson, European Patent 0 302 703 B1 (1992).

26

Corrosion monitoring under cathodic protection conditions using multielectrode array sensors

XIAODONG SUN, Corr Instruments LLC,
San Antonio, Texas, USA

26.1 Introduction

Cathodic protection (CP) is widely used to protect metallic structures and components in many industries, including infrastructure, transportation, oil and gas transmission and chemical processes. According to a recent NACE report,[1] the total estimated cost for cathodic and anodic protection in the United States alone in 1998 was $2.22 billion, of which the majority cost was associated with the CP. The protection provided by the CP depends on the distribution of the cathodic current density. Due to the variations in geometry of protected structures or components, or to the location of anodes, certain areas of the protected structure or component may not receive the minimum cathodic current density that is required to provide sufficient protection. Corrosion may take place in these areas and cause catastrophic failures, if not identified and mitigated at an early stage. Because corrosion in these areas is not easily detected, an effective monitoring technique is required to identify the problem at an early stage, in order to alleviate the problem in a timely manner. An online monitoring tool placed near these hard-to-protect and critical locations may provide a real-time indication of the effectiveness of the CP system. Often, the protection potential or current density is set at overly conservative values. An online monitoring tool may make it possible to automate the CP system, to enable the protection current or potential to be set at a value that is just sufficient to protect the critical areas and that, at the same time, can reduce the cost involved in the process. In addition, the values of conservative potentials or current densities for different applications are often determined on the basis of past experiences or tests conducted under only selected conditions. These values may be either insufficient or excessive, when the conditions in the field change. Therefore, an online corrosion monitor that works under cathodic protection conditions is an ideal tool for both the real-time monitoring of the effectiveness of the CP system and for minimizing the cost of the process.

Coupled multielectrode array sensors (CMAS) have been extensively used as *in situ* and online monitors for corrosion, especially localized corrosion, in laboratories and industry applications.[2–15] In this chapter, the use of coupled multielectrode corrosion sensors as online monitors under cathodic protection conditions was reviewed. The experimental results of corrosion rates of several cathodically protected metals in simulated seawater, soil, concrete and drinking water are presented.

26.2 Corrosion rate measurements for cathodically protected systems using CMAS probes

The principle of the CMAS probes has been described in Chapter 8. A nanoCorr™ CMAS analyzer (Model A-50) is shown in Figure 26.1 (nanoCorr is a trade mark of Corr Instruments, LLC., USA). This CMAS analyzer has a current resolution of 10^{-12} A and allows the measurement of coupling currents up to 50 electrodes in up to six separate probes at the same time. Figure 26.2 shows the wiring diagram between a CMAS probe and the CMAS analyzer when the probe was used to measure corrosion under cathodic protection conditions. In a CMAS analyzer, the coupling joint is essentially at the same potential of the CMAS probe. Therefore, the cathodically protected system (the metal block in Figure 26.2) was

26.1 Typical coupled multielectrode array sensor analyzers for corrosion monitoring of cathodically protected systems, courtesy of Corr Instruments LLC.

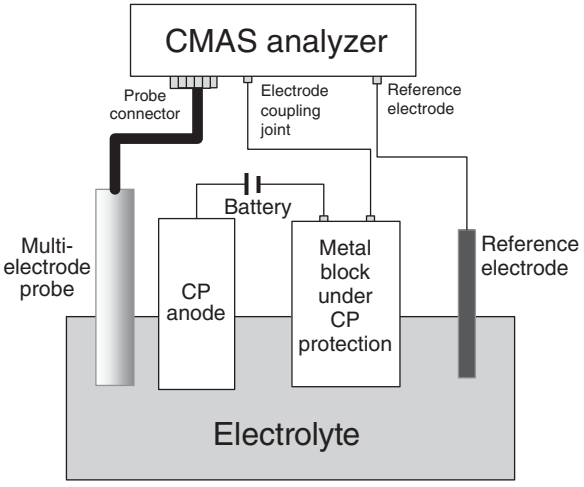

26.2 Connections of probes and the cathodically protected systems to the CMAS analyzers during the measurement of corrosion of cathodically protected systems.

connected to the coupling joint of the CMAS analyzer so that the sensing elements (the multiple electrodes) of the CMAS probe would have the same degree of protection as the cathodically protected metal block. In Fig. 26.2, the cathodic protection was provided by a power source (battery). This power source is not needed if the anode is a sacrificial anode. The electrolyte was either a liquid such as seawater, or a wet solid-water mixture such as concrete or soil. The reference electrode was used to indicate the protection potential. It should be noted that the reference electrode was not required for the measurements of the corrosion rate by the CMAS probe; it was used to gain information to understand how the cathodic protection systems functioned.

The CMAS analyzer was interfaced with a notebook computer and the factory-supplied software, CorrVisual™, was used for data acquisition (CorrVisual is a trade mark of Corr Instruments, LLC, USA). The currents from each electrode of a CMAS probe, the electrochemical potential of each probe, and the temperature were logged at a pre-determined interval (usually 1 to 5 minutes) and saved in a computer file. Processed signals, such as the maximum localized corrosion current, the cumulative charge for each sensor, and the corrosion rate and cumulative corrosion damage (or penetration depth) for each sensor were also saved in one or more separate data files. During the measurements, all the directly measured currents and the processed results (such as the minimum current, maximum current, mean current, current densities, corrosion rates, cumulative charges,

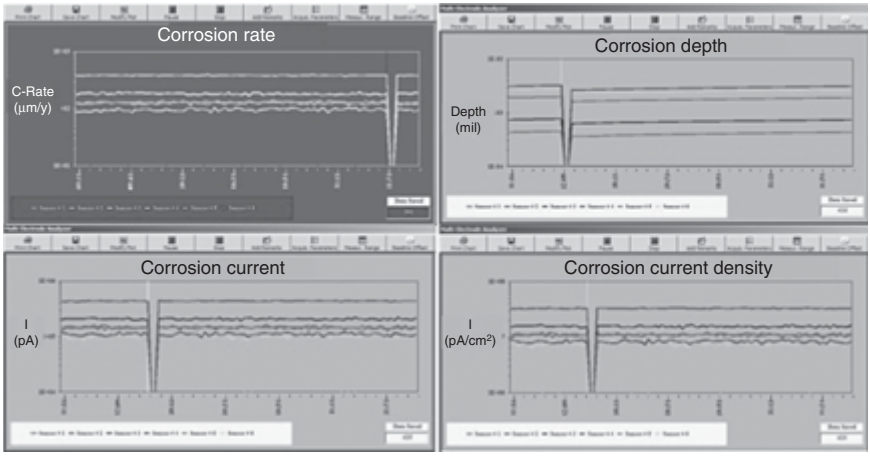

26.3 Typical real-time displayed parameters by CMAS analyzer software during the measurement of corrosion rate for cathodically protected systems.

penetration depth and electrochemical potentials), as well as the set-up parameters for data acquisition, were also dynamically available from the computer screen in both numerical and graphical forms. Figure 26.3 shows some of the typically displayed parameters.

26.3 Measurements of localized corrosion rates of carbon steel in simulated seawater

The maximum localized corrosion rate of carbon steel was measured in simulated seawater under different cathodic protection potentials.[10] The sensing electrodes of the coupled multielectrode sensor probes were made from an annealed mild carbon steel wire (concrete rebar wire), 1.5 mm in diameter and 1.77 mm^2 in electrode surface area. Each probe had 16 electrodes flush-mounted in epoxy. Typical probes that were used in the experiment are shown in Fig. 26.4. Prior to the test, the surfaces of sensing electrodes for each multielectrode probe were polished to 320 Grit and rinsed with distilled water and acetone. The experiments were conducted at 27 °C. Typical maximum localized corrosion rates from two carbon steel probes and the cathodic protection potential are shown in Fig. 26.5. The maximum localized corrosion current density signal for each probe was automatically calculated by the factory-supplied software based on the current from the most corroding or the most active electrode in the probe (see Chapter 8).[2]

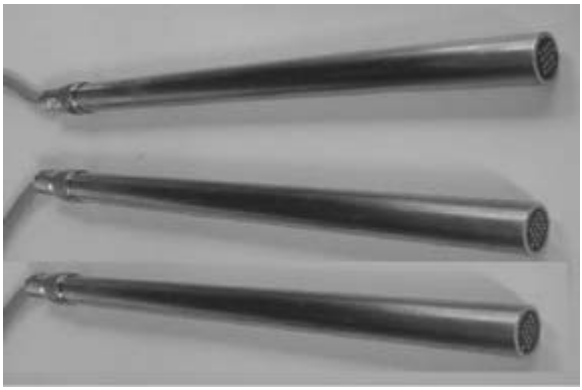

26.4 Typical coupled multielectrode array sensor probes used in the experiments.

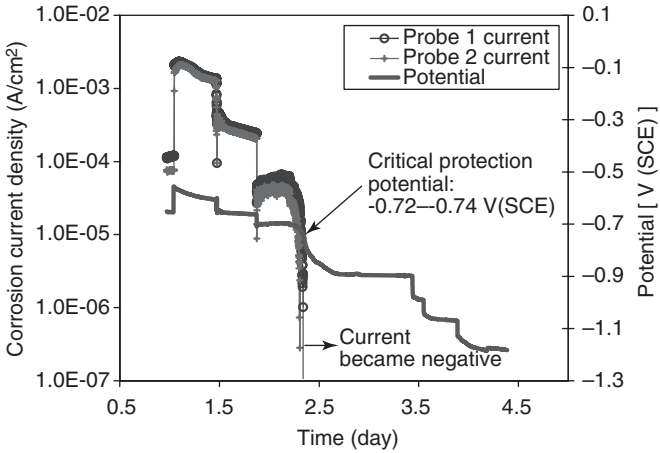

26.5 Responses of the maximum localized corrosion current density of two carbon steel probes to the changes of the CP potential in simulated seawater.

As can be seen from Figure 26.5, at the start of the test, the cathodic protection potential was controlled near the free open-circuit potential, by connecting the common joints of the probes to a separate large carbon steel coil that was made from the same wire as the sensing electrodes. The signal was 8×10^{-5} to 1.2×10^{-4} A/cm^2 (corresponding to approximately 1 mm/y) at the free open-circuit potential, which is consistent with the result measured in the same solution.[8] The corrosion signals increased to approximately 2×10^{-3} A/cm^2 (corresponding to approximately 30 mm/y), when the potential was increased by approximately 0.08 V. The increase in the

potential was to simulate the scenario when an operator incorrectly connected the polarity of the cathodic protection power source. The high corrosion current for the CMAS probes effectively indicated the adverse effect of an incorrectly connected cathodic protection system.

After the short-term anodic polarization which simulated the reversed polarity of the cathodic protection, the potential was slowly changed in the cathodic direction. The maximum localized corrosion current density gradually decreased with the decrease of the potential, and sharply dropped to near zero when the potential was near a critical potential and remained below zero (not shown in Fig. 26.5) when the cathodic protection potential was below this critical potential.

26.3.1 Measurement of critical protection potential

As described in the above section, the maximum localized corrosion current became near-zero and the sensing element of the probe was fully protected when the cathodic protection potential was near or close to a critical potential. In this chapter, such a critical potential is defined as the critical protection potential (CPP) which is the highest potential at which all the probe electrodes are fully protected (or the most anodic electrode is fully protected).

Figure 26.6 depicts the responses of the absolute values of the probe maximum localized corrosion current densities near the critical protection potential. The corrosion current densities stabilized at -4×10^{-5} A/cm^2 for Probe #2, at -3×10^{-6} A/cm^2 for Probe #1, and were relatively independent of the potential, when the cathodic protection potential was changed between the value slightly below the critical protection potential and $-1.18 V_{SCE}$. In Fig. 26.6, the corrosion signals were the current densities measured from the most corroding or most active electrode among all the sensing electrodes in the probes. The negative corrosion signal suggests that the most active electrode in the probe was actually a cathode (equivalent to the most active site in a metal piece being a cathodic site) and was effectively protected, when the potential was below the critical protection potential. This implies that all the electrodes in the probe (equivalent to all areas of the metal piece) were effectively protected by the cathodic protection, when the potential was below the critical protection potential.

26.3.2 Measurement of corrosion rate under cathodic protection conditions

Three probes (Probes #1, #2 and #3) were used in the measurements. Probe #1 was cathodically polarized to approximately $-0.9 V_{SCE}$, which is well below the critical protection potential. Probe #2 was slightly anodically

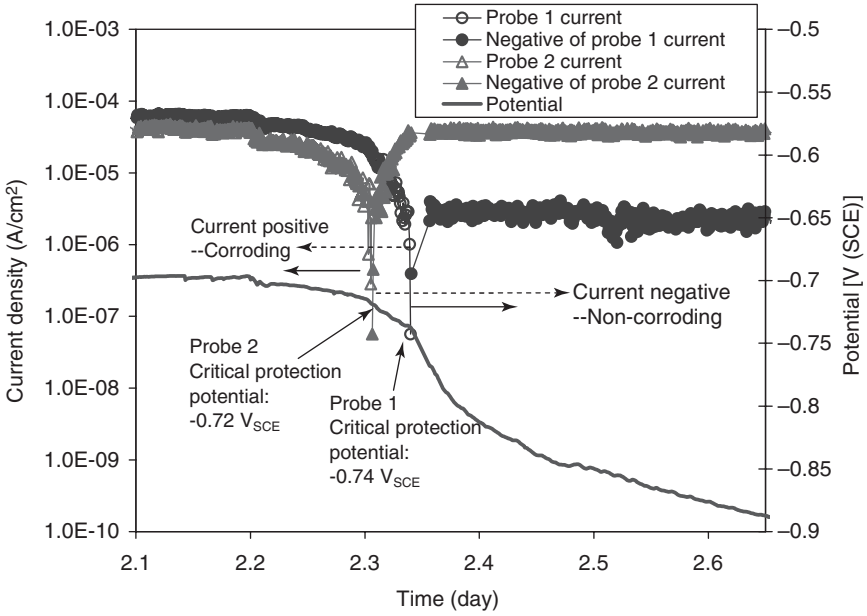

26.6 Responses of the absolute values of the sensor corrosion signals to the changes of the cathodic protection potential near the critical protection potential. The sensor corrosion signals became negative upon reaching the critical protection potential, indicating there was no corrosion on the sensing electrodes when the potential was below the critical protection potential.

polarized, to simulate a faulty polarity connection in the cathodic protection system. Probe #3 was left at the free corrosion potential, to simulate an inefficient protection from the cathodic protection system or the unprotected condition. Figure 26.7 shows the measured corrosion current density signals and the potentials of the three probes during the monitoring period. In Figure 26.7, the corrosion current density signal for each probe was automatically calculated by the software based on the most anodic electrode[2] during the measurement. The corrosion current from Probe #1 was negative throughout the monitoring period, indicating that there was no corrosion on the sensing electrodes of Probe #1. The corrosion current of Probe #3 was approximately 10^{-4} A/cm^2 during the first four days of monitoring and decreased to approximately 10^{-5} A/cm^2 on the fifth day. The corrosion current signal from Probe #2 was approximately 10^{-3} A/cm^2 throughout the monitoring period, indicating that the corrosion increased by more than one order of magnitude, when the potential was raised by approximately 0.07 V from the free corrosion potential. The slight decrease of the free corrosion potential of Probe #3 over the monitoring period was

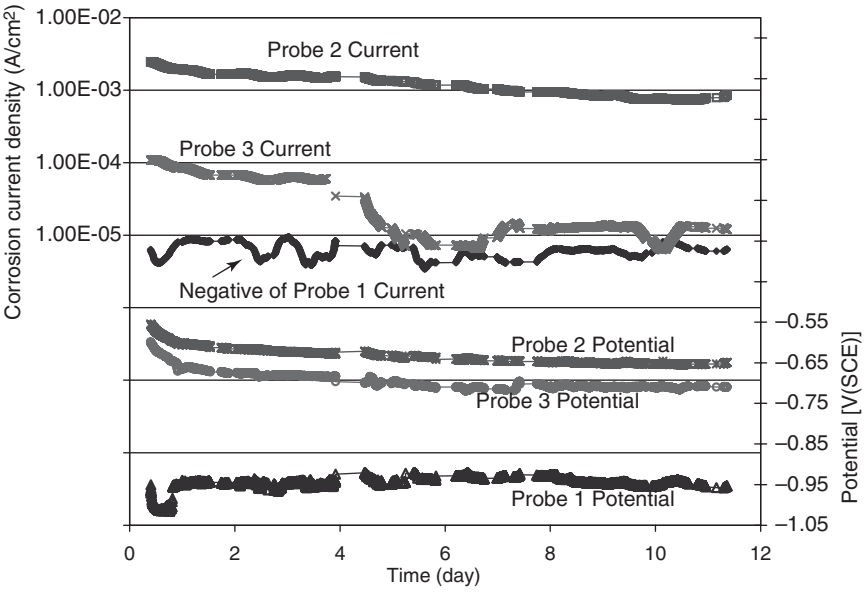

26.7 Corrosion current signals and the potentials of the sensors during the monitoring period. The corrosion signal from sensor #1 was negative (-6×10^{-6} to -1×10^{-5} A/cm^2), indicating no corrosion was taking place on sensor #1 electrodes.

probably due to the pH increase caused by the relatively large cathodic reaction of oxygen on the stainless steel counter electrode used to anodically polarize Probe #2. At the end of the test, a large amount of rust deposit was observed in the electrochemical cell, suggesting a high pH solution.

The maximum localized corrosion rates for the three probes were also available from the software during the measurement (Figure 26.8). The maximum localized corrosion rate of the unprotected probe – Probe #2 – in the first four days was approximately the same as the value measured in the previous measurements, which were conducted with similar probes in the simulated seawater. However, the rate was slightly lower after the fifth day. The difference between the values measured in the first four days and the values measured after the fifth day (Fig. 26.8) is within the expected range of variations for maximum localized corrosion rates in a given environment. The maximum localized corrosion rate for Probe #1 was automatically set to the lower detection limit of the instrument by the software because its corrosion current signal was negative, indicating that there was no corrosion.

Figure 26.9 shows the appearance of the probe electrodes after the monitoring period. Clearly, all the electrodes of Probe #2 (except the one with a faulty connection at the location of row 3 and column 2) were severely

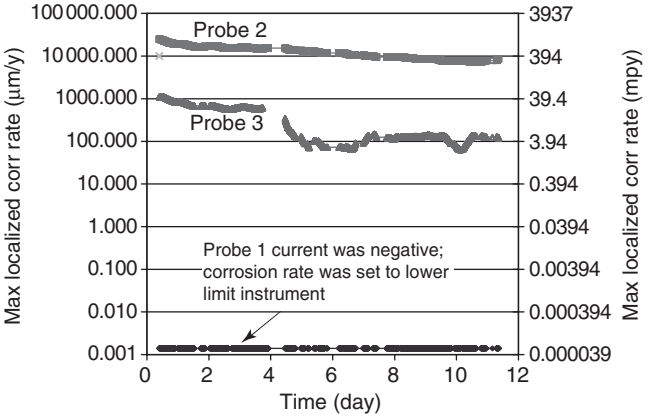

26.8 Measured corrosion rate during the monitoring period. Sensor 1 corrosion rate was set to the lower detection limit (1.4 nm/year) by the instrument, because its current was negative, indicating there was no corrosion on the sensing electrodes.

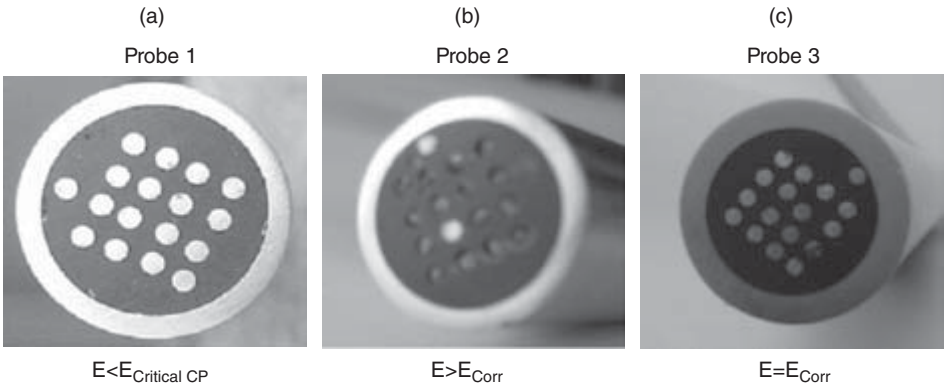

26.9 Appearances of the electrodes of sensors after the monitoring period. Sensor #-1 electrodes were cathodically protected. Sensor #-2 electrodes were anodically polarized except the shiny one that had a faulty connection (at row 3 and column 2). Sensor #-3 electrodes were maintained near the free corrosion potential. The electrode outside the 4 by 4 matrix in each sensor was used as a position locator and was not part of the sensing electrodes.

corroded. Slight pitting corrosion can be noticed on some of the electrodes of Probe #3. No significant pitting corrosion was observed on the electrodes of Probe #1. The result, as shown in Fig. 26.9, is in agreement with the measured corrosion rate shown in Fig. 26.8. In addition, Fig. 26.8 shows that, on average, the maximum localized corrosion rate for Probe #2 was

12.7 mm/y. Hence, the total penetration depth for the most corroded electrode on Pensor #2 should be 0.38 mm, after the 11 days of exposure. The measured depth of the most corroded electrode on Probe #2, as shown in Fig. 26.9, was approximately 0.4 mm, which is in excellent agreement with the depth estimated by the coupled multielectrode probe.

26.3.3 Summary

It was demonstrated that coupled multielectrode array sensor probes are effective tools for real-time measurement of the critical protection potential for cathodic protection. The probes can also be used as online tools to measure the localized corrosion rate under given cathodic protection potentials. If placed near the critical locations of engineering components, they can be used to detect either the effectiveness or faulty conditions of the cathodic protection system in real-time.

26.4 Measurements of localized corrosion rates of carbon steel in concrete

Steel reinforcements in concrete structures exposed to aggressive conditions, such as marine environments and de-icing salts, are subject to corrosion degradation and significant reductions in their service lives. This section presents the real-time measurements of localized corrosion rates for carbon steel in concrete with and without cathodic protections.[11] This measurement was conducted in an effort to understand the corrosion behavior of the carbon steel reinforcement rebars in concrete.

Figure 26.10 shows the experimental setup during the measurements. Two CMAS probes were vertically buried into a commercial grade concrete-sand mixture, which was initially mixed with distilled water. The concrete was formed in a plastic container with a dimension of 37 cm (length) × 25 cm (width) × 16 cm (height) and cured while it was submerged in distilled water. Corrosion rate measurements were taken shortly before the probes were buried into the concrete and then continued for approximately seven days, while the concrete was continuously submerged in distilled water. On the seventh day, the concrete was removed from the plastic container and partially immersed in a shallow bath filled with simulated seawater.

At the end of the first month of the test, cathodic protection was applied by connecting the aluminum wire electrodes that acted as the sacrificial anode to the common coupling joint of the CMAS system (see Figs 26.1 and 26.2). These aluminum wires were vertically buried near the probes.

A saturated calomel electrode (SCE) was dipped into a hole in the concrete, formed during the curing, between the two CMAS probes and was

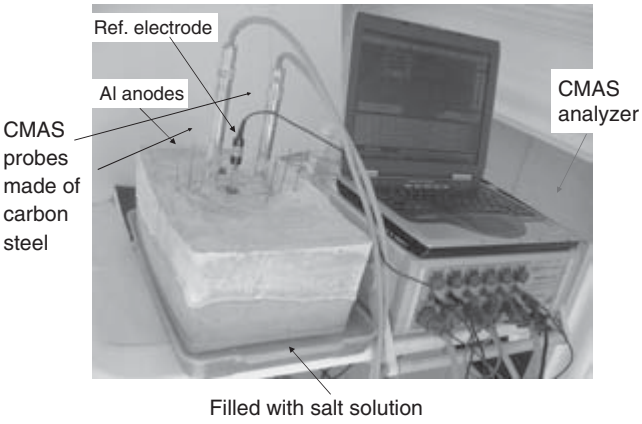

26.10 Experimental setup for the measurement of localized corrosion rate in concrete.
Note: The aluminum anodes were used for cathodic protection during the test.

used as the reference electrode for the measurement of the cathodic protection potential of the probes. Distilled water was added to the hole periodically to maintain the conducting path between the reference electrode and the two probes. The sensing electrodes were made from carbon steel concrete rebar wire (1.5 mm in diameter and 1.77 mm^2 in electrode surface area). Each probe had 16 electrodes flush-mounted in epoxy. Prior to the test, the surfaces of the sensing electrodes for each multielectrode array sensor probe were polished to 600 Grit and rinsed first with distilled water and then with acetone. The experiment was conducted at about 27 °C.

26.4.1 Localized corrosion of carbon steel in freshly mixed concrete

The maximum localized corrosion rates from the two CMAS steel probes in the first month of the test (with no cathodic protection) are shown in Fig. 26.11. The maximum localized corrosion rates were calculated by the software using the current from the most corroding (also called the most active electrode) among all the sensing electrodes on a probe. Upon placing the probes into the freshly mixed concrete (with distilled water initially), the corrosion rate from the two probes instantaneously increased to approximately 70 µm/y* (2.8 mil/y (or mpy)). The corrosion rate decreased rapidly to about 4 µm/y in the first 20 hours and slowly to 3 µm/y in the first seven days while the concrete was submerged in distilled water. This decrease in corrosion rate indicates that the carbon steel was passivated by the alkaline

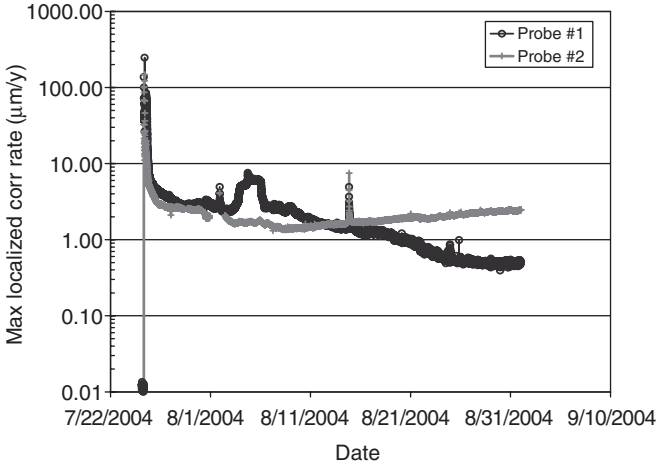

26.11 Maximum localized corrosion rates from two independent coupled multielectrode array sensor probes made of rebar material in concrete submerged in distilled water in the first week, and partially immersed in simulated seawater in the remaining test.

environment generated by the concrete. The corrosion rate stayed at about 2 µm/y for Probe #2, and continued to decrease for Probe #1 after the concrete was taken out of the distilled water bath and partially immersed in a shallow simulated seawater bath. The corrosion rate of Probe #1 reached 0.85 µm/y at the end of the first month of the measurements.

26.4.2 Localized corrosion rate during cathodic protection

Figure 26.12 shows the response of the corrosion rates and the potentials from the two probes to cathodic protection. Upon the connection between the common joints of the CMAS analyzer to the sacrificial aluminum anodes, the electrochemical potential of Probe #1 decreased from –0.735 V(SCE) to –1.27 V(SCE), and the corrosion rates of both probes dropped to 1.3 nm/y, which is below the lower detection limit of the CMAS analyzer (10 nm/y), suggesting that the carbon steel material in the two probes was adequately protected. When the cathodic protection was removed, the potential returned to –1.0 V(SCE), which is significantly lower than the previous value. However, the corrosion rates from both of the probes were significantly higher than those of the previous value. The lower potential and the higher corrosion rate immediately after removing the cathodic protection suggest that the concentrations were low for the corrosion products during the cathodic protection.

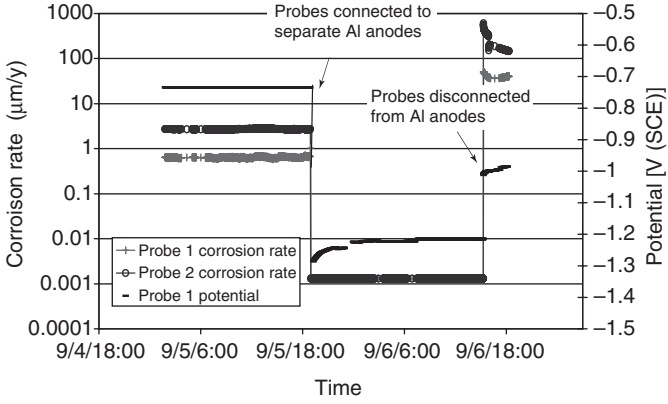

26.12 Maximum localized corrosion rates and electrochemical potential of rebar material measured from two coupled multielectrode array sensor probes before, during and after the probes were cathodically protected by sacrificial anodes.

26.4.3 Summaries

The steady-state corrosion rates measured in the concrete partially immersed in simulated seawater were 0.5 to 2.4 μm/y. When the carbon steel electrodes of the probe were connected to sacrificial aluminum anodes, the corrosion rate decreased instantaneously to a value that is below the lower detection limit of the instruments (10 nm/y). Coupled multielectrode array sensor probes can be used as a real-time tool to measure the effectiveness of cathodic protection for steel reinforcements in concrete.

26.5 Measurements of localized corrosion rates of cathodically protected carbon steel in soil

Corrosion of metallic components in soil has been a concern in many fields, including the pipeline industry and nuclear waste disposal programs. Metal loss corrosion probes based on electrical resistance methods have been used as online tools for corrosion monitoring in soil.[12] However, these probes are not sensitive enough for localized corrosions, such as pitting or crevice corrosion.[5] This section describes the application of the coupled multielectrode array probe as an on-line and real time tool for measuring the localized corrosion rate of carbon steel material in soil under cathodic protection conditions.

Figure 26.13 shows the experimental setup for the measurements of maximum localized corrosion in soil contained in a plastic container

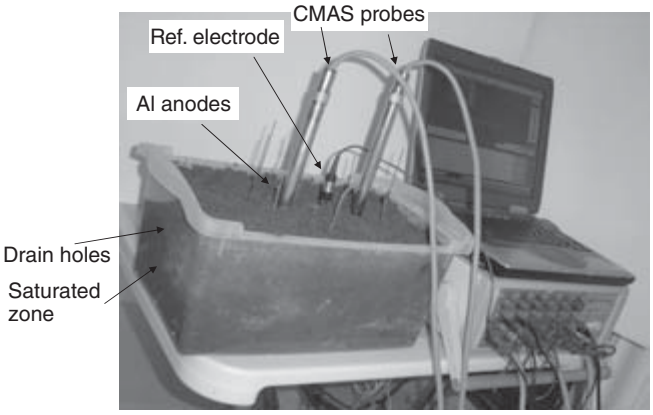

26.13 Experimental setup for the measurement of localized corrosion rate in soil.
Note: The aluminum anodes were used for cathodic protection during the test.

(35 cm long × 25 cm wide × 17.5 cm high) which was perforated at a height of 13.5 cm from the bottom to provide drain holes.[12] The coupled multielectrode probes were initially vertically placed in freshly prepared soil that was loose and relatively dry (unsaturated with water). After some initial measurements of the corrosion rate, simulated seawater was added to the container to flood the section below the drain hole. The flooded section is also called the saturated zone. The soil in this saturated zone was sticky and muddy. After the seawater was added, the probe was pushed into the bottom of the soil so that the sensing surface of the probe was in close contact with the sticky and densely compacted soil during the remainder of the test. Distilled water was frequently added from the top to make up for the evaporation loss.

The sensing electrodes of the coupled multielectrode probes were made from annealed mild carbon steel concrete rebar wire (1.5 mm in diameter and 1.77 mm^2 in electrode surface area). Each probe had 16 electrodes flush-mounted in epoxy. Prior to the test, surfaces of sensing electrodes for each multielectrode probe were polished to 600 Grit and rinsed with distilled water and then with acetone. The aluminum wires shown in Fig. 26.13 were also vertically buried near the probes and were used as sacrificial anodes during the cathodic protection test. A saturated calomel electrode (SCE) was dipped into the saturated zone near the probes and used as the reference electrode for electrochemical potential measurements.

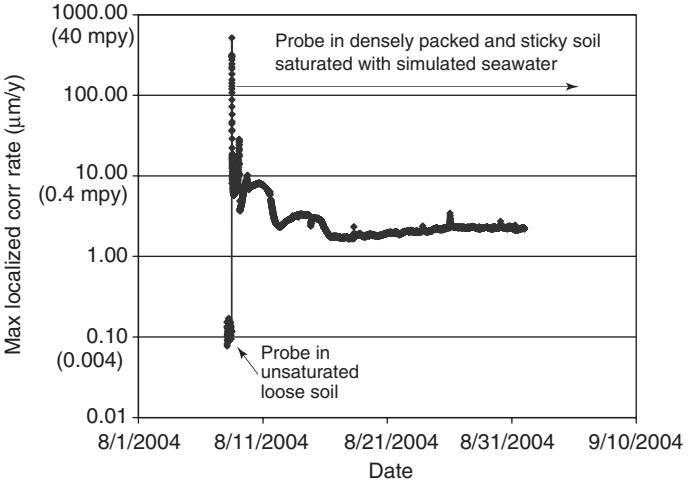

26.14 Maximum localized corrosion rates from a coupled multielectrode array sensor probe made of carbon steel in soil soaked with simulated seawater.

26.5.1 Corrosion rate in soil saturated with simulated seawater

Figure 26.14 shows the maximum localized corrosion rate from the carbon steel CMAS probe in soil before and after the addition of the simulated seawater, but prior to the application of cathodic protection. The corrosion rate was low (0.1 to 0.2 µm/y) when the simulated seawater was not added and the probe's sensing tip was in the relatively dry and loose soil. This low corrosion rate is expected because the probe was freshly polished (cleaned) and no significant liquid condensate was formed on the sensing surface of the CMAS probe.

After the addition of simulated seawater and the probe was pushed down to the flooded section of the soil, the maximum localized corrosion rate increased to about 600 µm/y, which is close to the corrosion rate of carbon steel in air-saturated simulated seawater.[8] However, a few minutes after the probe was pushed into the densely packed soil saturated with simulated seawater, the rate dropped rapidly, and reached 10 µm/y in about one hour. The rapid decrease in maximum localized corrosion rate was probably an indication that the corrosion process was under mass-transfer control. The migration of the corrosion products (such as metal ions) away from the corroding sites and the reactants (such as O_2) to the corroding sites are limited by the low diffusion rates of these species in the soil which was densely packed when the probe was pushed into the wet and sticky soil.

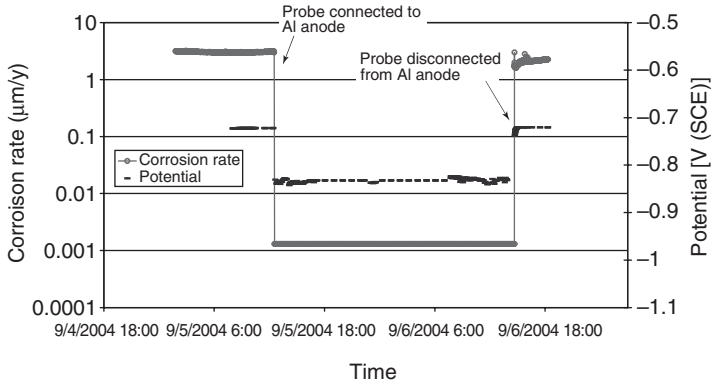

26.15 Maximum localized corrosion rates and potential of rebar material measured from two coupled multielectrode array probes before, during and after the probes were cathodically protected by sacrificial anodes.

The maximum localized corrosion rate was about 4 µm/y after three weeks in the densely packed soil.

26.5.2 Corrosion rate under cathodic protection conditions

After about three weeks in the densely packed and wet soil soaked with the simulated seawater, the carbon steel electrodes of the probe were connected to the aluminum sacrificial anodes (according to Fig. 26.2) to cathodically protect the electrodes. Figure 26.15 shows the measured corrosion rate and the electrochemical potential of the carbon steel electrodes before, during, and after cathodic protection. As soon as the carbon steel electrodes were cathodically protected, the electrochemical potential decreased from –0.72 V(SCE) to –0.83 V(SCE), and the maximum localized corrosion rate dropped from 3 µm/y to 1.3 nm/y, which is below the lower detection limit of the corrosion analyzer (10 nm/y). This suggests that the carbon steel material was adequately protected. When the cathodic protection was removed, the potential returned to –0.72 V(SCE) and the maximum localized corrosion current returned to approximately 2.2 µm/y.

26.5.3 Summary

Coupled multielectrode array sensor probes were used for real-time monitoring the corrosion rate of carbon steel material in soil with and without cathodic protection. The steady-state corrosion rate measured in the densely packed soil saturated with simulated seawater was found to be

approximately 2 to 15 μm/y. When the carbon steel electrodes of the probe were connected to sacrificial aluminum anodes, the corrosion rate decreased instantaneously to a value that is below the lower detection limit of instrument (10 nm/y), suggesting that the coupled multielectrode array sensor probe is an effective real-time tool to measure the effectiveness of cathodic protection in soil.

26.6 Measurements of localized corrosion rates of cathodically protected carbon steel in drinking water

Corrosion of metallic components in drinking water systems has been an ongoing concern. According to a recent report,[1] the total estimated cost of corrosion for drinking water systems is $19.26 billion per year, in the United States alone. To effectively control and mitigate corrosion, it is important to measure the real-time rate of corrosion – especially the rate of localized corrosion – taking place in the system. This section describes the application of coupled multielectrode array sensor probes as an online tool for measuring the general and maximum localized corrosion rates of three metals in drinking water systems with and without cathodic protections. These metals include low carbon steel, stainless steel and brass which are commonly used in drinking water systems.

A nanoCorr™ model S-50 CMAS analyzer was used in this measurement. In addition to the functions described for the Model A-50 CMAS analyzer, model S-50 also measures the general corrosion rate based on the average anodic currents from the CMAS probe.[8] The experiment was conducted in a beaker filled with natural drinking water (spring water). All coupled multielectrode probes (one carbon steel, one stainless steel and one brass) and a reference electrode were vertically immersed in water. Prior to the tests, drinking water was placed in the open air to enable saturation with the gases in the atmosphere (e.g. O_2 and CO_2). The water was not agitated during the experiments. One 1-mm-diameter aluminum wire was used as a sacrificial anode for each probe during the cathodic protection test. The reference electrode was a calomel electrode (SCE). The experiments were conducted at a temperature range from 17 to 23 °C. Other parameters such as oxidation and reduction potential (ORP), temperature, pH are also measured by the CMAS analyzer. These parameters are beyond the scope of this section and users are encouraged to consult the original publication[9] for additional information.

The sensing electrodes of the carbon steel multielectrode probe were made from annealed Type 1008 carbon steel (UNS G10080) wire (1.5 mm in diameter and 1.77 mm^2 in electrode surface area). The sensing electrodes of the brass multielectrode probe were made from Type 260 brass (UNS

C26000) wire (1 mm in diameter and 0.785 mm^2 in electrode surface area). The sensing electrodes of the stainless steel multielectrode probe were made from Type 316L (UNS S31603) wire (1 mm in diameter and 0.785 mm^2 in electrode surface area). Each probe had 16 electrodes flush-mounted in epoxy. Prior to the test, the surfaces of the sensing electrodes for each multielectrode probe were polished to 600 Grit and rinsed with distilled water and then with acetone.

26.6.1 Maximum localized corrosion rates

The maximum localized corrosion rates from the three CMAS probes are presented in Fig. 26.16. The maximum localized corrosion rates from the probes were calculated using the anodic current density from the most corroding electrode of the probe. The maximum localized corrosion rate of the carbon steel probe was initially low (90 µm/y or 3.5 mpy) and increased slowly to 330 µm/y (13 mpy) in two hours prior to cathodic protection. The maximum localized corrosion rates for the stainless steel and brass were 0.17 and 7.0 µm/y (0.0067 and 0.28 mpy), respectively, in the drinking water and remained unchanged during the two-hour exposure to the water prior to the application of the cathodic protection. When the electrodes of the three probes were connected to their respective sacrificial aluminum anodes, the maximum localized corrosion rates of the Type 316L stainless steel and the Type 260 brass immediately dropped below the detection limit of the instruments (10 nm/y or 0.0004 mpy), suggesting that these two probes were

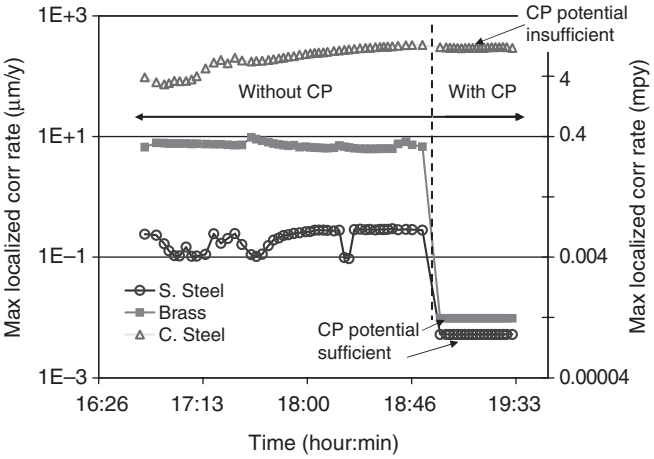

26.16 Maximum localized corrosion rates from three CMAS probes in drinking water before and after they were connected to their sacrificial CP anodes.

sufficiently cathodically protected by the potential (see Section 26.6.3) supplied by their sacrificial anodes. The maximum localized corrosion rate of the carbon steel probe, however, only decreased slightly (from 330 to 290 μm/y), when the probe was connected to the aluminum anode, indicating an insufficient cathodic protection. The insufficient protection by the aluminum anode is consistent with the relatively high potential (see Section 26.6.3) supplied by the sacrificial anode, because of its limited surface area.

26.6.2 General corrosion rates

The general corrosion rates from the three probes are presented in Fig. 26.17. The general corrosion rate was calculated using the average anodic current density, which is the total anodic current from all the electrodes of the probe divided by the total surface areas of all the electrodes of the probe. Because this average corrosion rate is similar to the general corrosion rate obtained by weight loss methods or by other electrochemical methods using large electrodes, the use of the average corrosion rate to approximate the general corrosion rate is a reasonable approach. Compared with Fig. 26.16, the average/general corrosion rates from these three metals have similar trends with the maximum localized corrosion rates, but the values are much smaller.

The maximum localized corrosion rates were 7.5 to 8 times higher than their general corrosion rates for the Type 260 brass and low carbon steel

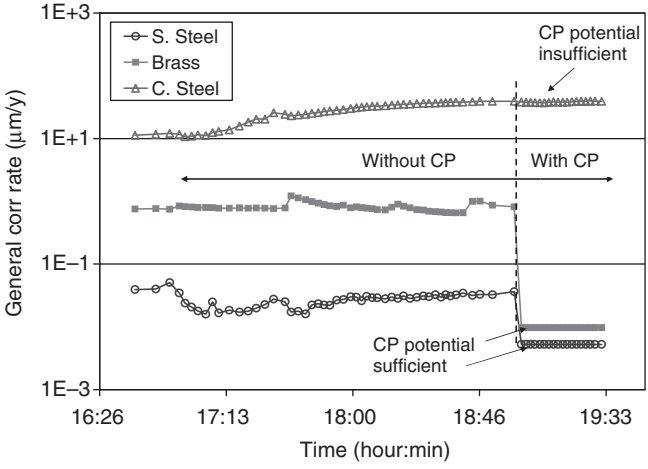

26.17 General corrosion rates from three CMAS probes in drinking water before and after they were connected to their sacrificial CP anodes.

during the test. The ratio of the maximum localized corrosion rate to the general corrosion rate for the Type 316L stainless steel was approximately 9 at the end of the test. These ratios are also called localized corrosion rate factors (see Chapter 8).

26.6.3 Probe potentials

The corrosion potentials of the Type 316L stainless steel, Type 260 brass in the drinking water prior to the cathodic protection were –20 and –100 mV (SCE), respectively (Figure 26.18). The corrosion potential of the Type 1008 carbon steel probe was –320 mV (SCE) initially and decreased to –374 mV (SCE) at the time the cathodic protection was about to be applied, indicating that the carbon steel electrode became more and more active, which is consistent with the measured steadily increased maximum localized corrosion rate from the carbon steel probe as shown in Figure 26.16. When the electrodes of the three probes were connected to their sacrificial aluminum anodes, the potentials of the Type 316L stainless steel and the Type 260 brass probes immediately dropped by more than 400 mV and 100 mV, respectively; the potential of the carbon steel electrode, however, dropped only by 10 mV. The variations in the drops of the potentials, during the cathodic protection, were due to the size of the aluminum anodes used as the sacrificial anodes. The surface areas of the aluminum anodes were sufficiently large to lower the potentials of the less active stainless steel and brass probes, but not enough to lower the potential of

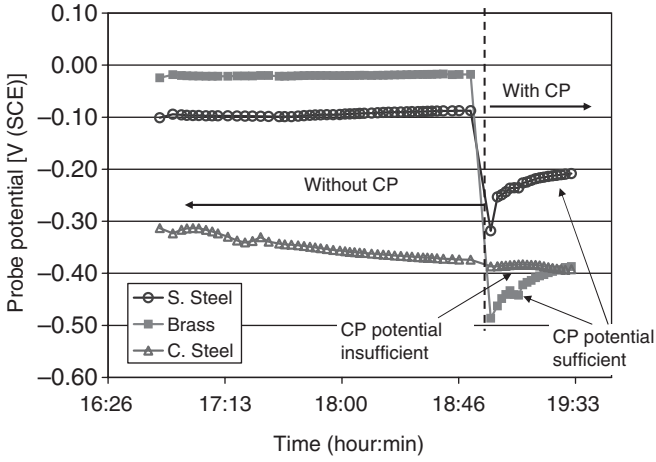

26.18 Corrosion potentials from three CMAS probes in drinking water before and after they were connected to their sacrificial cathodic protection (CP) anodes.

the more active carbon steel probe. Because of the significant drop in potentials, the stainless steel and brass probes were effectively protected and their corrosion rates were essentially zero (see Figure 26.16), while the slight drop in potential for the carbon steel probe proved to be insufficient for the carbon steel to be cathodically protected and its maximum localized corrosion rate remained essentially unchanged (from 330 to 290 µm/y) (Fig. 26.16). This underscores the significance of using the coupled multielectrode array sensor to monitor the effectiveness of the cathodic protection.

26.6.4 Post-test visual examination of the probes

Figure 26.19 shows the appearance of the 260 brass and 316L stainless steel probe electrodes after an eight-day exposure to the drinking water without cathodic protection. No localized corrosion was seen in the two probes, even though a slight discoloration was observed on some of the electrodes of the Type 260 brass probe, which is consistent with the low maximum localized corrosion rates, as shown in Figure 26.16.

Figure 26.20 shows the appearance of the carbon steel probe after the same eight-day exposure to the drinking water without cathodic protection. It is apparent that a few of the electrodes (#5 and #14) were covered by deposits (corrosion products), and most of others were clean. After cleaning off the corrosion products (bottom picture in Figure 26.20), pitting was observed on the electrodes covered by the deposits. No pitting corrosion was observed on the electrodes that did not have deposits. Therefore, the deposit-covered electrode served as the anodes and the clean electrodes served as the cathode, during the exposure. The pitting corrosion on the

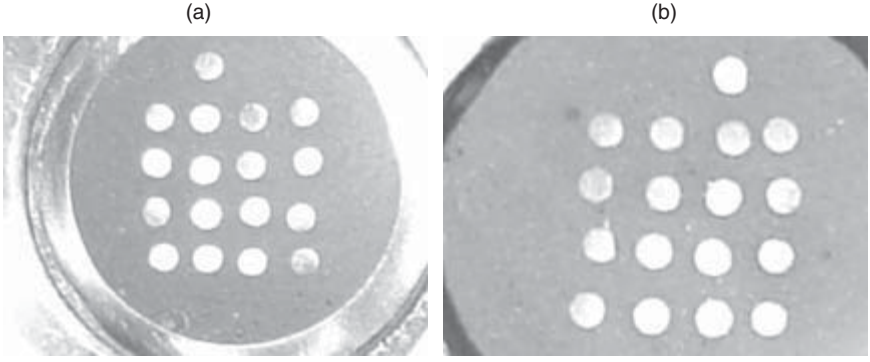

26.19 The appearances of the stainless steel and brass probes after eight-day immersion in drinking water without cathodic protection.

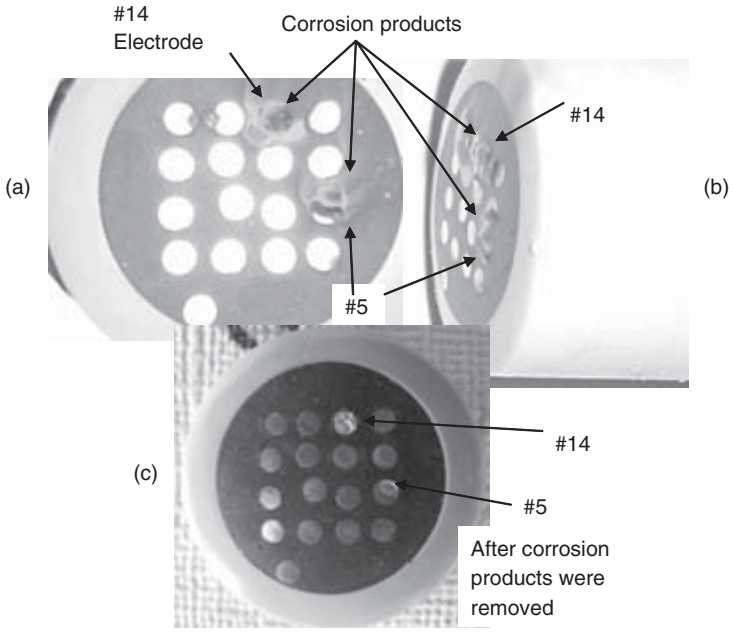

26.20 The appearances of the carbon steel probe after eight-day immersion in drinking water without cathodic protection.

carbon steel probe is consistent with the high maximum localized corrosion rate as shown in Figure 26.16.

It is worth mentioning that no significant corrosion between the electrodes and the surrounding epoxy was observed. The good bonding between the epoxy and the electrode side surface prevented the development of crevice corrosion, which may complicate the calculation of the localized corrosion rate by altering the true surface area.

26.6.5 Summary

Real-time coupled multielectrode array sensor probes were used to measure the maximum localized corrosion rates of Type 316L stainless steel, Type 260 brass and Type 1008 carbon steel materials in drinking water with and without cathodic protection. The maximum localized corrosion rates in the drinking water were approximately 0.3 µm/y (0.012 mpy) for stainless steel and 7 µm/y (0.28 mpy) for brass with no cathodic protection at ambient temperatures. The steady-state maximum localized corrosion rate for the carbon steel in the drinking water was found to be 300 µm/y (12 mpy). When cathodic protection was applied to the stainless steel and brass probes, the corrosion rate from these probes dropped below the lower detection limit

of the CMAS instruments (10 nm/y). However, the maximum localized corrosion rate and the general corrosion rate from the carbon steel probe remained the same after cathodic protection was applied. The potential measurements indicate that the potentials of the stainless steel and the brass probes were significantly lowered by their sacrificial anodes, but the potential of the carbon steel probe was lowered by only 10 mV. The insignificant lowering of the potential of the carbon steel probe indicates that the surface area of the sacrificial anode for the cathodic protection of the carbon steel probe was not large enough to provide the required cathodic protection potential for the carbon steel. The unchanged corrosion rates from the carbon steel probe after the application of the cathodic protection underscores the significance of the use of the CMAS probes for monitoring the effectiveness of cathodic protection systems.

26.7 References

1 G.H. Koch, M.P.H. Brongers, N.H. Thompson, Y.P. Virmani and J.H. Payer, 'Corrosion Cost and Preventive Strategies in the United States,' NACE Report, FHWA-RD-01-156 (Houston, TX: NACE, 2001).
2 L. Yang, N. Sridhar, O. Pensado and D.S. Dunn, *Corrosion*, 58 (2002), 1004.
3 X. Sun 'Online Monitoring of Undercoating Corrosions Utilizing Coupled Multielectrode Sensors', *CORROSION/2004*, paper no. 04033 (Houston, TX: NACE International, 2004).
4 A. Anderko, N. Sridhar1, L. Yang, S.L. Grise, B.J. Saldanha and M.H. Dorsey, 'Validation of a Localized Corrosion Model Using Real-Time Corrosion Monitoring in a Chemical Plant', *Corrosion Engineering, Science and Technology* (formerly *British Corrosion J.*), 40, 33–42, August, 2005.
5 L. Yang, N. Sridhar, C.S. Brossia and D.S. Dunn, 'Evaluation of the Coupled Multielectrode Array Sensor as a Real Time Corrosion Monitor', *Corrosion Science*, 47, 1794–1809 (2005).
6 L. Yang and N. Sridhar, 'Coupled Multielectrode Array Systems and Sensors for Real-Time Corrosion Monitoring – A Review', *CORROSION/2006*, paper no. 06681 (Houston, TX: NACE, 2006).
7 X. Sun and L. Yang, 'Real-time Measurement of Crevice Corrosion with Coupled Multielectrode Array Sensors', *CORROSION/2006*, paper no. 06679 (Houston, TX: NACE, 2006).
8 X. Sun and L. Yang, 'Real-Time Monitoring of Localized and General Corrosion Rates in Simulated Marine Environments Using Coupled Multielectrode Array Sensors', *CORROSION/2006*, paper no. 06284 (Houston, TX: NACE, 2006).
9 X. Sun and L. Yang, 'Real-Time Monitoring of Localized and General Corrosion Rates in Drinking Water Utilizing Coupled Multielectrode Array Sensors', *CORROSION/2006*, paper no. 06094 (Houston, TX: NACE, 2006).
10 X. Sun, 'Online Monitoring of Corrosion under Cathodic Protection Conditions Utilizing Coupled Multielectrode Sensors', *CORROSION/2004*, paper no. 04094 (Houston, TX: NACE International, 2004).

11 X. Sun, 'Online and Real-Time Monitoring of Carbon Steel Corrosion in Concrete, Using Coupled Multielectrode Sensors', *CORROSION/2005*, paper no. 05267 (Houston, TX: NACE International, 2005).
12 X. Sun, 'Real-Time Corrosion Monitoring in Soil with Coupled Multielectrode Sensors' *CORROSION/2005*, paper no. 05381 (Houston, TX: NACE, 2005).
13 L. Yang, R.T. Pabalan, L. Browning and G.C. Cragnolino, 'Measurement of Corrosion in Saturated Solutions under Salt Deposits Using Coupled Multielectrode Array Sensors', *CORROSION/2003*, paper no. 426 (Houston, TX: NACE, 2003).
14 C.S. Brossia and L. Yang, 'Studies of Microbiologically Induced Corrosion Using a Coupled Multielectrode Array Sensor', *CORROSION/2003*, paper no. 575 (Houston, TX: NACE, 2003).
15 X. Sun, 'Online Monitoring of Undercoating Corrosions Utilizing Coupled Multielectrode Sensors', *CORROSION/2004*, paper no. 04033 (Houston, TX: NACE, 2004).

27

Corrosion measurements with wire beam electrodes under temporarily protective oil coatings

QINGDONG ZHONG, Shanghai University, People's Republic of China

27.1 Introduction

Organic coatings, such as organic polymer coating (OPC) and temporarily protective oil coating (TPOC), are an effective way to prevent metals from corrosion. In general, organic coatings consist of vehicle, pigments and additives such as dryers, hardening agents, stabilising agents, surfactant, dispersion agents, etc. However, for temporarily protective oil coating, its major components are base oil (mineral machine oil) and oil soluble inhibitors (such as barium sulfonate, lanolin, benzotriazole, etc.).

Many electrical and electrochemical methods have been used to study and evaluate the protective nature of organic coatings. Measurements such as potential, DC resistance, polarisation resistance, electrochemical impedance spectroscopy (EIS), etc., have been used for the laboratory evaluation of organic coating (OPC[1–7] and TPOC[8–16]) for many years. Some of the methods of investigating polymer coatings on metals and corrosion of painted metal are reviewed in the literature.[17–21] Although these electrical and electrochemical methods are powerful tools for better understanding the fundamental processes of corrosion underneath coatings, there are some unsolved problems of corrosion protection by organic coatings that require further study.[22]

Since the 1980s, many in-situ electrochemical methods have been developed for detecting local defects of organic coatings, such as scanning electrode techniques (SET),[23–26] scanning vibrating electrode techniques (SVET),[27–31] the Kelvin method,[32–37] localised impedance spectroscopy (LEIS), etc.[38–44] Researchers of organic coating gradually realised that the electrochemical inhomogeneity of organic coatings was essential for the electrochemical study of organic coatings. The effectiveness of the coating depended on the conduction processes taking place in the coating material. If coating inhomogeneities (such as pore, pinhole, etc.) were present, the experimental results could be influenced significantly.[45–47]

Mayne and his coworkers studied the ionic conduction of detached coatings and concluded that polymer films were heterogeneous and contained fine areas of locally high conductivities.[48–49] The high conductivity was considered in the case of cross-linked polymer films to be due to a lower degree of cross-linking. Leidheiser and Kendig attributed impedance changes in coatings to the penetration of electrolytes.[50]

On the basis of microelectrode technique, integrated microelectrode array (interdigitated array microelectrodes or microarray electrodes) have been widely utilised in analytical chemistry, electroanalytical chemistry, and electrochemistry.[51–66] Unlike big square metal and one single metal electrode, integrated microelectrode array consists of many microelectrodes. The difference of electrochemical states at the coating/metal interface can be measured sequentially and results obtained this way are statistical results. The reproducibility of electrochemical measurements may be improved, making it possible to study the degradation process of coatings directly and quantitatively. Although the above-mentioned methods are powerful tools for studying the fundamental processes of corrosion underneath organic coatings, further work is required in the following areas.

First, in general, organic coating is a poor electronic conductor, i.e. an insulator. There is a need to understand: (a) why people could utilise electrical and electrochemical methods to study and evaluate the protective nature of organic coatings; (b) the conducting mechanism of organic coatings during their electrical and electrochemical testing in corrosive media; and (c) organic coating behaviour during its degradation in the metal/coating/solution system. Second, the simplest and non-destructive electrochemical test is the measurement of the electrode potential of the painted metal as a function of immersion time. The most useful and exacting study of this technique was achieved by Wormwell and Brasher in 1949.[67] A thorough review of this method has been made by Wolstenholme.[68] In Wormwell and Brasher's study, they found that the potential/time curve of painted steel samples immersed in artificial seawater was composed of three distinct sections: an initial falling potential, followed by a rise, and then a final decline.

Third, it is obvious that organic coatings (OPC and TPOC) are electronic insulators; they have very low electronic conductivity compared with an electronic conductor, and usually act as a barrier between the corrosive medium and the metal. Theoretical studies for the mechanism of these kinds of insulating films have been conducted based on the classic theory of solid state physics. Electron transport through such film can be effected by two mechanisms: first, if the film is highly doped with electron donors or acceptors, the electrons are transported via the conduction or the valence band; and second in heavily disordered films, which have a high concentra-

tion of localized electronic states in the band gap, electron transfer through the film can occur by a series of hops between such states, the so-called hopping conductivity mechanism. It is easy to see that the hopping conductivity mechanism is suitable for interpretation of conductivity for organic coatings. Many models have been used to study and describe these disordered systems such as ion implantation,[69–70] passive film[71,74] and polymer films with localized electronic states, etc.[72] Hopping conductivity in disordered systems is also well documented in the literature.[73]

According to the hopping conductivity mechanism, when the metal is coated with organic coatings, and placed in salt solution, conductivity of organic coating is controlled by the electron hopping conductivity mechanism. At this time, it is not possible for corrosive media to diffuse through the organic coating and transmit to the metal/coating interface. With increasing immersion time, along with penetration of corrosive media in organic coating, it is obvious that electronic hopping conductivity of organic coating may transform to ionic conductivity. However, previous studies omitted this obvious conductivity transformation.

In fact, the conducting behaviour of organic coating in the metal/coating/solution system is the same as that of passive film on the surface of metal.

27.2 Mechanism of organic coatings

Although passive film has attracted the interest of corrosion and electrochemistry researchers for about 150 years,[75] conduction behaviour and its model of passive film on the metal are still hot topics.[76–89] Bojinov *et al.* presented a quantitative kinetic model, which so called heavily doped *n*-type semiconductor-insulator-*p*-type semiconductor injunction, for steady-state passive films on Fe, Cr and Fe-Cr alloys.[86] For positive charge conduction, they proposed that at low potentials in the passive state, the positive defects injected at the metal/film interface played the role of electron donors; at high positive potentials, the negative defects injected at the film/solution interface played the role of electron acceptor.

Different from a semiconductor, according to the classic hopping conductivity mechanism in solid state physics, conductivity of organic coating could be achieved by continuous electron hopping through a disordered localised electronic state in the coating. On the basis of classic hopping conductivity mechanism in solid state physics, it is clear that, as an insulating film, temporarily protective oil coating has a certain conductivity, and this is also important for electrochemical analysis of the temporarily protective oil coating in salt solution.

In general, according to the theory of classic physics, temporary protective oil coating is taken as an insulating film in the vacuum. However, when the metal is coated with oil and placed in the electrolyte solution, the situ-

ation might change. Although oil coating has very low electronic conductivity compared with an electronic conductor, according to the hopping conductivity mechanism, electron transfer through the oil coating can occur by a series of hops between localized electronic states in the bandgap. At this time, the oil coating behaved as a bipolar film like the passive film formed on stainless steel (SS). Conducting behavior of TPOC could be interpreted as a hopping conductivity mechanism; it is the same as that of passive film forming on the surface of SS. It is obvious that the passive film on SS is the semiconductor, but whether or not the conducting mechanism of oil coating is semiconducting, and how the charge is transported in the oil coating, remain to be questioned.

27.2.1 Ionic-electronic conducting behaviour of TPOC in salt solution

As was first realized by Hoar and Price, an oxidizing metal could be thought of as a self-driving electrochemical cell.[90] Bailey and Ritchie presented a general electrochemical theory for the oxidation of metals: the oxidizing metal was viewed as a self-driving electrochemical cell in which the oxide acts as both ionic and electronic conductor.[91] However, the conductivity mechanism of temporarily protective oil coating (polymer film)[72] was different from the mechanism of oxide film (passive film).[71,76–89] Overall electrochemical processes in the metal/coating system are shown in Fig. 27.1.[92]

As a special electrochemical system, the metal/coating/electrolyte system is different from the metal/electrolyte system. In the metal/electrolyte system, anodic and cathodic reactions of corrosion cells take place at the metal/electrolyte interface simultaneously. However, anodic and cathodic reactions of corrosion cell in the metal/coating/electrolyte system take place simultaneously at metal/coating and coating/electrolyte interface respectively. When a metal specimen coated with oil is placed in the electrolyte

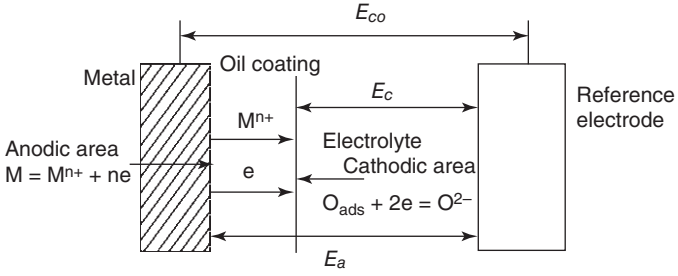

27.1 Overall electrochemical processes in the metal/coating system.

Table 27.1 Possible nine electrochemical steps in the overall reaction

Step No. (*s*)	Step
1	Cation transfer through metal/coating interface
2	Cation transfer in the oil coating
3	Cation transfer through coating/electrolyte interface
4	Electron transfer through metal/coating interface
5	Electron transfer in the oil coating
6	Electron transfer through coating/electrolyte interface
7	$M \rightarrow M^{n+} + ne^{-}$ at metal/coating interface
8	Oxygen reduction at coating/electrolyte interface
9	M^{n+} and anion form corrosive products at metal/coating, coating/electrolyte interface or in the coating

for potential measurement, metal, oil coating, electrolyte and reference electrode form a multi-electrode system, there are nine possible electrochemical steps in the overall reaction for potential measurement (Table 27.1).

As in Bailey and Ritchie's general electrochemical theory,[91] there are three electrochemical cells which have direct relationship for the potential measurement of an oil-coated metal electrode. A metal/coating/electrolyte cell connects with a reference electrode, whose equilibrium potential can be defined as E_{co}^{eq}. The anodic reaction of corrosion cell at the metal/coating interface connecting with the reference electrode, has an equilibrium potential that can be defined as E_a^{eq}. The cathodic reaction of the corrosion cell at the coating/electrolyte interface connecting with the reference electrode, has an equilibrium potential that can be defined as E_c^{eq}. So the potential of oil-coated metal electrode could be expressed as Equations [27.1] and [27.2]:

$$E = E_a^{eq} + \sum_{s=1}^{3} |\eta|_{t,s} - \left(\frac{1}{nF}\right)\gamma_7 \Delta G_7 \qquad [27.1]$$

$$E = E_c^{eq} - \sum_{s=4}^{6} |\eta|_{t,s} + \left(\frac{1}{nF}\right)\gamma_8 \Delta G_8 \qquad [27.2]$$

where $\eta_{t,s}$ is over the potential of each charge transfer step s, n is the total number of electrons transferred in the overall electrochemical reaction, F is the Faraday constant, γ is the stoichiometric number of the step s, and ΔGs is the Gibbs free-energy change of the step s.

Before the analysis, several simplifying assumptions will be made and are listed below:

1. The electrochemical reaction on the surface of reference electrode is in equilibrium.
2. Step 9 is at equilibrium and could not be a rate-determining step.
3. Only one step could be rate-determining, and other steps are at equilibrium at the same time.

Other assumptions are the same as those of Bailey and Ritchie's,[71] which could also be suitable for analysis in the organic coating system. On the basis of these assumptions, the over potential of the reference electrode is zero, and ΔG_9 is zero. At the early stage of immersion of the oil-coated metal specimen, electrochemical reactions in the metal/coating/electrolyte system are very small, the amount of metal cation produced at the metal/coating interface is ultrasmall, and the amount of corresponding anion pro-duced at the coating/electrolyte is very small. These ions could not diffuse through the coating and constructed steady-state diffusion pathway in the oil coating. At this time, only electrons could transfer through the coatings by electrons hopping the localised electronic states in organic coatings. The electrochemical reaction in the metal/coating/electrolyte system is determined by any one of the first, second, third and seventh steps, which directly relate to metal cation formation and transmission in the metal/coating/electrolyte system. Other steps listed in Table 27.1 are in equilibrium, i.e.

$$|\eta|_{t,s} = \begin{cases} E_{co}^{eq} & (s = 1, 2, 3) \\ 0 & (s = 4, 5, 6) \end{cases} \quad [27.3]$$

$$\text{or} \quad -\left(\frac{1}{nF}\right)\gamma_s \Delta G_s = \begin{cases} E_{co}^{eq} & (s = 7) \\ 0 & (s = 8) \end{cases} \quad [27.4]$$

Equations [27.1] and [27.2] can be simplified as Equation [27.5].

$$E = E_a^{eq} + E_{co}^{eq} = E_c^{eq} \quad [27.5]$$

At this time, potential value measured is equal to equilibrium potential of oxidant in salt solution reducing at coating/electrolyte interface, and it has most positive value. Considering that the steps of electron transmission in the oil coating are in equilibrium, in order to keep charge equilibrium in the oil coating and prevent charge accumulation in the metal/coating/electrolyte system, the amount of electrons produced at the metal/coating interface and transmitted through the coating is equal to amount of electrons consumed by the cathodic reaction (oxygen reduction, $O_2 + 2H_2O + 4e^- \rightarrow 4OH^-$) at the coating/electrolyte interface.

From the above analysis, it is clear that the anodic process in the metal/coating/electrolyte system is predominant, whereas the cathodic process is in equilibrium. Thus, the anodic reaction may lead to potential of oil-coated electrode shifting positively.

With increasing of immersion, ions in the electrolyte begin to diffuse in the oil coating, and gradually construct the steady diffusion layer in the coating. At this time, the electrochemical reaction in the metal/coating/electrolyte system is determined by any step concerned with electron transmission in the overall reaction of the metal/coating/electrolyte system (e.g. step 4, 5 or 6 or oxygen reduction step 8). Other steps are in equilibrium, i.e.

$$|\eta|_{t,s} = \begin{cases} 0 & (s = 1, 2, 3) \\ E_{co}^{eq} & (s = 4, 5, 6) \end{cases} \quad [27.6]$$

$$\text{or} \quad -\left(\frac{1}{nF}\right)\gamma_s \Delta G_s = \begin{cases} E_{co}^{eq} & (s = 8) \\ 0 & (s = 7) \end{cases} \quad [27.7]$$

So Equations [27.6] and [27.7] can be simplified as Equation [27.8].

$$E = E_a^{eq} = E_c^{eq} - E_{co}^{eq} \quad [27.8]$$

At this time, the potential measured is equal to the equilibrium potential of metal cation formation at the metal/coating interface, and it has the lowest negative value, and the oil coating shows obvious ionic conducting characteristics. The steps of cation production and transmission in the oil coating are considered to be in equilibrium. In order to keep the charge equilibrium in the oil coating and prevent charge accumulation in the metal/coating/electrolyte system, the amount of cations produced at the metal/coating interface and transmitting through the coating is equal to the amount of anion production of the cathodic reaction (oxygen reduction, $O_2 + 2H_2O + 4e^- \rightarrow 4OH^-$) at the coating/electrolyte interface.

From the above analysis, it is clear that the cathodic process concerned with electron production, electron transmission in coating and electron consumption at the coating/electrolyte interface is predominant, whereas the anodic process in the metal/coating/electrolyte is in equilibrium. Thus, the cathodic reaction may lead to the potential of oil-coated electrode shifting negatively. Wormwell and Brasher's results also verify this analysis.[67]

27.2.2 Semiconducting transformation of TPOC in salt solution during its degradation

On the basis of the abovementioned theory analysis of conducting behaviour of TPOC in the electrochemical testing system, it is suggested that, as an insulator, TPOC could transform from an insulator to a conductor during its degradation. During this two type conducting behaviour of the insulator and the conductor, there must be a semiconducting state of the TPOC

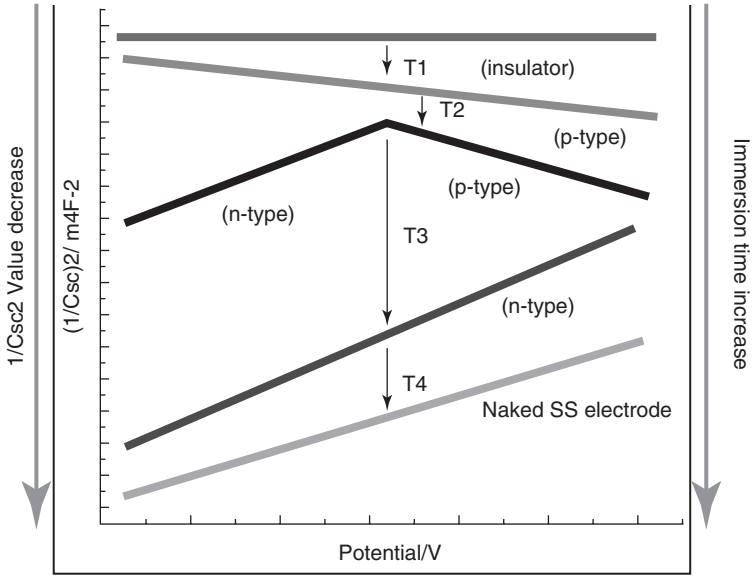

27.2 Mott–Schottky plots of TPOC in 5% Na_2SO_4 solution with immersion time (coated and naked SS electrode).

during its degradation in salt solution. As an effective semiconducting behaviour research method, the potential-capacitance method and Mott–Schottky analysis have been utilized to study the semiconducting behaviour of passive film comprehensively.

In Zhong *et al.*'s paper [93], the semiconducting behaviour of a temporarily protective oil coating on the surface of AISI 304 Stainless Steel in 5% Na_2SO_4 solution under corrosion potential was studied by utilizing the potential-capacitance method and Mott-Schottky analysis.

Results showed that there existed semiconducting behaviour of a temporarily protective oil coating during its degradation. With the increasing immersion time, temporarily protective oil coating transformed from the *p*-type semiconductor at an early stage of immersion to an *n*-type semiconductor. N_D and N_A of oil coating in different transition processes were also calculated.

Results also showed that at the early stage of immersion of an oil-coated metal specimen, electrochemical reactions in the metal/coating/electrolyte system are very small, the amount of metal cation produced at the metal/coating interface is ultra small, and the amount of corresponding anion produced at the coating/electrolyte is very small. These ions could not diffuse through the coating and constructed a steady diffusion passway in the oil

coating. At this time, only the electron could transfer through the coatings by electron hopping the localised electronic states in the organic coatings. The electrochemical reaction in the metal/coating/electrolyte system is determined by any single step, which directly relates to metal cation formation and transmission in the metal/coating/electrolyte system. At this time, oil coating behaves as a *p*-type semiconductor. However, the density of N_A is very small.

With increasing immersion, ions in the electrolyte begin to diffuse in the oil coating, and gradually construct the steady diffusion layer in the coating. At this time, the electrochemical reaction in the metal/coating/electrolyte system is determined by any single step concerned with electron transmission in the overall reaction of the metal/coating/electrolyte system. Steps of cation production and transmission in the oil coating are considered to be in equilibrium. In order to keep the charge equilibrium in the oil coating and prevent charge accumulation in the metal/coating/electrolyte system, the amount of cations produced at the metal/coating interface and transmission through the coating is equal to the amount of anions produced in the cathodic reaction (oxygen reduction, $O_2 + 2H_2O + 4e^- \rightarrow 4OH^-$) at the coating/electrolyte interface.

From the above analysis, it is clear that the cathodic process concerning electron production, electron transmission in the coating and electron consumption at the coating/electrolyte interface is predominant, whereas the anodic process in the metal/coating/electrolyte is in equilibrium. At this time, the oil coating behaves as an *n*-type semiconductor, and the density of N_D is more than that of the oil coating at an early stage of immersion.

27.3 Wire beam electrode and its working mechanism

Wire beam electrode (WBE) is a system that has multiple wire electrodes embedded in an insulator. The active electrodes are the exposed cross-sections of the wires arranged in certain patterns or arrays. Wire beam electrodes are also called multielectrode arrays by other researchers (see Chapter 8). The wire beam electrode is an effective method for studying the electrochemical inhomogeneity of organic coatings. Through the use of the wire beam electrode, both reproducibility and reliability in the study and evaluation of organic coatings may be improved significantly.[94–96] For undercoating studies, the wire beam electrode was typically made of mild steel (containing 0.18% C) wires regularly arranged. All wires were embedded in an epoxy resin and insulated from each other at 2 mm intervals. The diameter of each wire was 0.7 mm and the active electrode surface acted as the substrate for the oil coating.

By utilizing the wire beam electrode, electrochemical parameters such as potential, polarization resistance, etc., and their distribution could be meas-

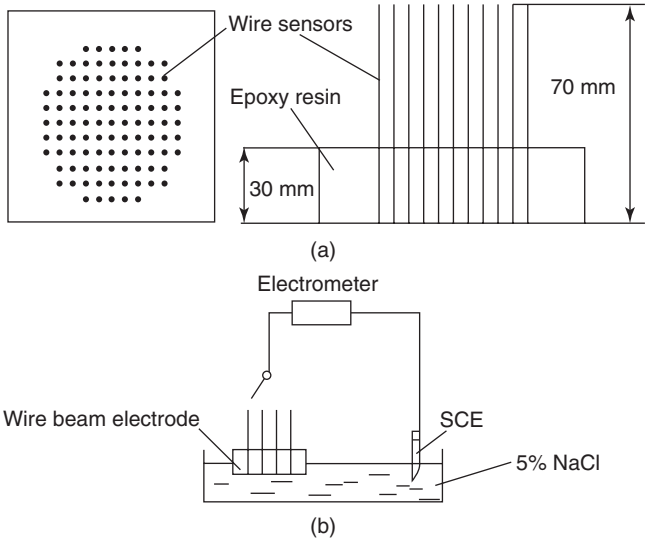

27.3 Schematic diagram of the wire beam electrode and experimental apparatus.[92]

ured. For potential measurements, high input impedance (>10^{12} Ω) voltmeters which prevent any electrical loading to the measurement circuit must be used. During the study, the electrochemical values of each mini-electrode are statistically analysed in order to improve the reproducibility and reliability of the potential measurement. The average of the electrochemical value of whole mini-electrodes and the standard deviation of the potential could also be calculated.

A wire beam electrode using mild steel wires has been developed and used to study temporarily preventive oil coatings in terms of the heterogeneous electrochemical states after immersion in a salt solution. The electrochemical states on the surface of the wire-beam electrode are homogeneous compared with an oil-painted electrode. The distribution of potential on oil-painted wire beam electrodes was heterogeneous and follows a discontinuous binomial probability distribution. Polarization resistance of each oil-coated wire sensor is randomly distributed over a given range of resistance and follows a lognormal probability distribution. The distribution of corrosion potential over a high potential range can be increased, distribution of polarization resistance over a low resistance range can be decreased and eliminated by adding an oil-soluble inhibitor.[97]

The feasibility of using a wire beam electrode for understanding the electrochemical inhomogeneity of temporarily protective oil coating was also studied.[98] Structure parameters of wire beam electrodes such as the

central distance (1.5 mm ~ 4 mm) of the adjacent wire pair, the diameter of the wires (0.7 mm ~ 1.2 mm), the number of wires (37 ~ 101), etc., and their effect on the study of electrochemical inhomogeneity of temporarily protective oil coatings are discussed in the following sections of this chapter.

27.4 Application of wire beam electrode

27.4.1 Potential variation of temporarily protective oil coating before its degradation

As mentioned in Section 27.1, the measurements of potential/time curves for painted steel are non-destructive and the simplest of all the electrochemical tests and can produce many interesting results. However, previous potential measurements utilized a single big square metal electrode. A big square metal electrode could only detect mixed or average potential data over the whole electrode surface and could not measure the potential value from chosen areas of the electrode surface. Considering the electrochemical inhomogeneity of organic coatings, it was difficult for the potential method to get precise results by using a single big square metal electrode.

A wire beam electrode using mild steel wires has been developed and used to study the potential variation of temporarily preventive oil coating before its degradation. It has been found that the distribution of corrosion potential on the surface of oil-coated wire beam electrodes is heterogeneous before the degradation of temporarily protective oil coating. At the early stage of immersion, the distribution of corrosion potential gradually shifts to a higher potential range with increasing immersion time. When the distribution of corrosion potential reaches the highest potential range, it begins to shift negatively to a lower potential range. It is suggested that this situation may be due to metal corrosion taking place at the metal/coating interface.

The distribution of corrosion potential on an oil-painted wire beam electrode follows a normal probability distribution before the degradation of the oil coating. With increasing immersion time, the distribution of corrosion potential on the oil-painted wire beam electrode may change from normal probability distribution before the degradation of oil coating to discontinuous binomial distribution after the degradation of oil coating. Further consideration showed that the potential variation of TPOC is due to the self-repairing ability of TPOC. Inhibited oil coatings had the ability of self-repairing, and oil-soluble inhibitors had a direct effect on the self-repairing ability of oil coating. The degradation processes that were related to the underfilm corrosion of oil coating could also be realized by investigating the self-repairing ability of the oil coating.[99]

27.4.2 Investigation of the underfilm corrosion of temporarily protective oil coating

Underfilm corrosion can be investigated by some classic methods, such as weight loss measurements, visual examination after long term exposure, etc. However, these methods are time consuming and not readily quantifiable because of day-to-day variations in environmental conditions. Several electrochemical techniques have been developed to obtain a more rapid assessment of underfilm corrosion and its mechanisms.

Previous methods usually utilized a big square metal electrode and depended greatly upon the integrity of the coatings. If the coating inhomogeneities are present, the experimental results obtained are the average result of the total specimen, so it is hard to investigate the process of underfilm corrosion. Unlike the big square metal electrode, the wire beam electrode consists of many mini-electrodes. The difference in electrochemical states at the coating/metal interface can be measured sequentially and results obtained this way are statistical. The reproducibility of electrochemical measurements may be improved, making it possible to study the degradation process of coatings directly and quantitatively.[100–102] This made it possible to measure electrochemical parameters that were related to underfilm corrosion of the organic coatings directly so as to study the mechanism of underfilm corrosion. Corrosion currents of micro-corrosion cells were measured, anodic and cathodic areas of underfilm corrosion cell were also documented. Results showed that underfilm corrosion taking place at the coating/metal interface is heterogeneous with respect to the corrosion current values and direction. It is suggested that this method is helpful in investigating the mechanism of underfilm corrosion and in studying the degradation process of oil coatings.[103]

27.4.3 Study of anti-contamination performance of temporarily protective oil coatings

It is well known that for the metal/coating system, corrosion usually takes place at the metal/coating interface. When metal articles are coated with oil coatings for temporary protection, it is necessary to avoid contamination residue on the surface of the metal substrate in practical applications. Contamination on the metal substrate may block the conjunction of oil coating and metal substrate, act as active corrosive media, and directly influence the protective effects of oil coatings. So the anti-corrosion performance of a temporary protective oil coating is an important criterion in practical use. In a study to understand anti-corrosion performance, the working surface of a wire beam electrode was contaminated with 5%(w/w) NaCl solution for different contamination area ratios of 0%, 25%, 50%, 75% and 100%

respectively before coating with TPOC. The results showed that the salt contamination on the metal substrate had an influence on the heterogeneous distributions of corrosion potential, polarisation resistance and their regularities. With an increasing degree of salt contamination, the distribution of the corrosion potential of oil coatings followed a discontinuous binomial probability distribution, whereas the anodic polarization resistance (Ra) distribution of oil coatings transformed from a lognormal probability distribution to an exponential probability distribution and then to a discontinuous binomial probability distribution, the cathodic polarization resistance (Rc) distribution of oil coatings followed a lognormal probability distribution. The influence of salt contamination on Ra and Rc of oil coatings was different. It was suggested that the wire beam electrode is a helpful tool to study the process of underfilm corrosion, and evaluate the performance of contamination resistance of oil coatings.

27.4.4 Study of the lubricant and its effect on the corrosion behaviour of TPOC

In steel plants, cold-rolled steel plates are usually manufactured by the following procedures: slab, hot tandem mill, pickling, cold tandem mill, annealing, skin pass, coating, shearing and packaging. Before the steel coils are coated with the temporary protective oil coatings, a skin pass line is needed to make the steel plate smoother after annealing, since annealing might deform the steel plate.

During the skinning pass, lubricants are sprayed on the surface of the steel plate to prevent any scratches. In fact, the water-soluble inhibitor has a direct effect on the lubricant's performance. Many kinds of water-soluble inhibitor, such as sodium nitrite, sodium sulfate (anhydrous), sodium phosphate, sodium chromate, sodium dichromate, sodium silicate, sodium benzoate, triethanolamine, hexamethylenetetramine, urea, etc., have been introduced into a variety of lubricant products. But sodium nitrite is still verified as the most effective one, though it is indirectly carcinogenic.

In steel plants, lubricants are required to have no adverse effect on the anti-corrosion ability as temporarily protective oil coatings. However, currently there is no such appropriate method in the steel plants to measure and evaluate the mutual interaction of the lubricant and the temporary protective oil coatings. There is no a practical method for the evaluation of the lubricant and its effect on the anti-corrosion performance as temporary protective oil coatings. Wire beam electrodes composed of mild steel wires were developed and used to study the lubricant and its effect on the corrosion behaviour of a temporarily protective oil coating.[105] Three types of lubricants, which contain 5% sodium silicate, triethanolamine and sodium nitrite respectively, were studied. The influence of a lubricant on the anti-

corrosion ability of a temporarily protective oil coating could be studied and evaluated by using a wire beam electrode to measure the change of corrosion potential and its standard deviations varying with immersion time. Two criteria were used to evaluate the characteristics of the lubricant, one was whether or not the lubricant might change the distribution of corrosion potentials of an oil-coated electrode, the other was whether or not the lubricant was beneficial to the homogeneous distribution of corrosion potentials of an oil-coated electrode.

27.5 References

1 Leidheiser Jr H (1979), 'Electrical and electrochemical measurements as predictors of corrosion at the metal-organic coating interface', *Prog Org Coat*, 7(1), 79–104.
2 Leidheiser Jr H, Standish J V (1980), 'Electrical properties of organic coatings on a local scale-relationship to corrosion', *Corrosion*, 36(8), 390–395.
3 Mansfeld F, Kendig M W, Tsai S (1982), 'Evaluation of corrosion behavior of coated metals with AC impedance measurements', *Corrosion*, 38(9), 478–485.
4 Szauer T (1982), 'Electrical and electrochemical resistances for the evaluation of protective nonmetallic coatings', *Prog Org Coat*, 10(2), 157–170.
5 Szauer T (1982), 'Impedance measurements for the evaluation of protective nonmetallic coatings', *Prog Org Coat*, 10(2), 171–183.
6 Mayne J E O, Mills D J (1982), 'Structural changes in polymer films part 1. The influence of the transition temperature on the electrolytic resistance and water uptake', *J Oil Col Chem Assoc*, 65(4), 138–142.
7 Mills D J (1986), 'DC electrical measurement on painted steel in relation to corrosion prevention mechanisms', *J Oil Col Chem Assoc*, 69(8), 203–206.
8 Szauer T, Klenowicz Z, Szklarska-Smialowska Z (1980), 'Inhibition by oleates of various amines in temporary protective coatings on mild steel. Part 1. Electrochemical and electrical investigations', *Corrosion*, 36(8), 400–404.
9 Szauer T, Klenowicz Z, Szklarska-Smialowska Z (1980), 'Inhibition by oleates of various amines in temporary protective coatings on mild steel Part 2. Chemical investigations', *Corrosion*, 36(9), 482–487.
10 Nowosz-Arkuszewska I (1981), 'Electrochemical studies of carbon steel coated with inhibiting oil films containing nitrated petroleum products', *Corros Sci*, 21(1), 41–48.
11 Nowosz-Arkuszewska I (1983), 'Nitrated petroleum product and some aspects of the mechanism of its action in an oil coating on steel – i. The characteristics of the petroleum product', *Corros Sci*, 23(12), 1259–1271.
12 Nowosz-Arkuszewska I (1983), 'Nitrated petroleum product and some aspects of the mechanism of its action in an oil coating on steel – ii. The investigation of surface layers on steel', *Corros Sci*, 23(12), 1273–1283.
13 Nowosz-Arkuszewska I (1983), 'Studies of the effect of some fatty acids on the inhibiting properties of nitrated petroleum products', *Corros Sci*, 23(1), 75–90.

14 Peny A Y M, Lyon S B, Thompson G E, Johnson J B, Wood G C, Ferguson J M (1989), 'Corrosion testing and appearance of grease coated galvanised steel', *Bri Corros J*, 24(4), 257–263.
15 Kennedy P J, Ruzansky M S, Agarwala V S (1989), 'New technique for determining corrosion behavior of lubricant systems', *Corrosion*, 45(2), 160–165.
16 Nowosz-Arkuszewska I, Krawczyk M (1992), 'Electrode impedance studies of steel in neutral sulfate solutions, covered with an oil coating containing a nitrated petroleum product', *Corros Sci*, 33(6), 861–871.
17 Leidheiser Jr H (1983), 'Towards a better understanding of corrosion beneath organic coatings', *Corrosion*, 39(5), 189–201.
18 Leidheiser Jr H (1982), 'Corrosion of painted metals – a review', *Corrosion*, 38(7), 374–383.
19 Leidheiser Jr H (1979), *Corrosion Control by Organic Coatings*, Princeton, NJ: Science Press.
20 Leidheiser Jr H (1981), *Corrosion Control by Organic Coatings*, Houston, TX: NACE.
21 Kendig M W, Leidheiser Jr H (1987), *Corrosion Protection by Organic Coatings*, Princeton, NJ: The Electrochemical Society.
22 Funke W, Leidheiser Jr H, Dickie R A, *et al.* (1986), 'Unsolved problems of corrosion protection by organic coatings: a discussion', *J Coat Tech*, 58(741), 79–86.
23 Isaacs H S, Vyas B (1979), 'ASTM Symposium on Progress in Electrochemical Corrosion Testing', San Francisco.
24 Isaacs H S, Kendig M W (1980), 'Determination of surface inhomogeneities using a scanning probe impedance technique', *Corrosion*, 36(6), 269–274.
25 Nyffenegger R, Ammann E, Siegenthaler H, Kotz R, Haas O (1995), 'In-situ scanning probe microscopy for the measurement of thickness changes in an electroactive polymer', *Electrochim Acta*, 40(10), 1411–1415.
26 Nichols R J, Schroer D, Meyer H (1995), 'In situ scanning probe microscopy study of copper electrode position on conductive polypyrrole', *Electrochim Acta*, 40(10), 1479–1485.
27 Isaacs H S (1988), 'Measurement of the galvanic corrosion of soldered copper using the scanning vibrating electrode technique', *Corros Sci*, 28(6), 547–558.
28 Isaacs H S (1991), 'Effect of height on the current distribution measured with a vibrating electrode probe', *J Electrochem Soc*, 138(3), 723–728.
29 Zou F, Barreau C, Hellouin R, Quantin D, Thierry D (1998), 'Application of scanning vibrating electrode techniques to study the degradation of coil-coated steel at edges', *Mater Sci Forum*, 289–292, 83–92.
30 He J, Gelling V J, Tallman D E, Bierwagen G P (2000), 'Scanning vibrating electrode study of chromated-epoxy primer on steel and aluminum', *J Electrochem Soc*, 147(10), 3661–3666.
31 He J, Gelling V J, Tallman D E, Bierwagen G P, Wallace G G (2000), 'Conducting polymers and corrosion III. A scanning vibrating electrode study of poly(3-octyl pyrrole) on steel and aluminum', *J Electrochem Soc*, 147(10), 3667–3672.
32 Stratmann M (1987), 'Investigation of the corrosion properties of metals, covered with adsorbed electrolyte layers – a new experimental technique', *Corros Sci*, 27(8), 869–872.

33 Oriani R A, Yee S, Stratmann M (1991), 'Application of a kelvin microprobe to the corrosion of metals in humid atmospheres', *J Electrochem Soc*, 138(1), 55–61.
34 Huang S M, Atanasoki R, Oriani R A (1993), 'Detection of effects of low electric fields with the Kelvin probe', *J Electrochem Soc*, 140(4), 1065–1067.
35 Leng A, Streckel H, Stratmann M (1999), 'The delamination of polymeric coatings from steel Part 1: Calibration of the Kelvinprobe and basic delamination mechanism', *Corros Sci*, 41(3), 547–578.
36 Leng A, Streckel H, Stratmann M (1999), 'Delamination of polymeric coatings from steel. Part 2: First stage of delamination, effect of type and concentration of cations on delamination, chemical analysis of the interface', *Corros Sci*, 41(3), 579–597.
37 Leng A, Streckel H, Hofmann K, Stratmann M (1999), 'Delamination of polymeric coatings from steel. Part 3: Effect of the oxygen partial pressure on the delamination reaction and current distribution at the metal/polymer interface', *Corros Sci*, 41(3), 599–620.
38 Lillard R S, Moran P J, Isaacs H S (1992), 'Novel method for generating quantitative local electrochemical impedance spectroscopy', *J Electrochem Soc*, 139(4), 1007–1012.
39 Zou F, Thierry D (1997), 'Localized electrochemical impedance spectroscopy for studying the degradation of organic coatings', *Electrochim Acta*, 42(20–22), 3293–3301.
40 Bayet E, Huet F, Keddam M, Ogle K, Takenouti H (1997), 'Novel way of measuring local electrochemical impedance using a single vibrating probe', *J Electrochem Soc*, 144(4), L87–L90.
41 Zou F, Thierry D, Isaacs H S (1997), 'High-resolution probe for localized electrochemical impedance spectroscopy measurements', *J Electrochem Soc*, 144(6), 1957–1965.
42 Bayet E, Huet F, Keddam M, Ogle K, Takenouti H (1999), 'Local electrochemical impedance measurement: Scanning vibrating electrode technique in ac mode', *Electrochim Acta*, 44(24), 4117–4127.
43 Zou F, Thierry D (1999), 'Diffusion effects in localized electrochemical impedance measurements by probe methods', *J Electrochem Soc*, 146(8), 2940–2947.
44 Wittmann M W, Leggat R B, Taylor S R (1999), 'Detection and mapping of defects in organic coatings using local electrochemical impedance methods', *J Electrochem Soc*, 146(11), 4071–4075.
45 Manegold E, Kalauch K (1939), 'Die Neutralitätsstörungen an stromdurchflossenen Membranen', *Kolloid Zeitschrift*, 86(3), 313–339.
46 Wirth J K, Machu W (1952), 'A new electroosmotic method for the investigation of the structure of pigments and other ultrathin layers', *Werkst Korros*, 3, 444–453.
47 Kittelberger W W, Elm A C (1947), 'Water-immersion testing of metal-protective paints–electroendosmosis in water absorption and blistering', *Ind Eng Chem*, 39, 876–881.
48 Kinsella E M, Mayne J E O (1969), 'Ionic conduction in polymer films', *Polym Br J*, 1(4), 173–6.

49 Mayne J E O, Mills D J (1975), 'Effect of the substrate on the electrical resistance polymer films', *J Oil Colour Chem Assoc*, 58(5), 155–159.

50 Leidheiser Jr H, Kendig M W (1967), 'The mechanism of corrosion of polybutadiene-coated steel in aerated sodium chloride', *Corrosion*, 32, 69–75.

51 Rieke P C, Vanderborgh N E (1987), 'Thin film electrode arrays for mapping the current-voltage distributions in proton-exchange-membrane fuel cells', *J Electrochem Soc*, 134(5), 1099–1104.

52 Cervera-March S, Smotkin E S, Bard A J, Campion A, Fox M A, Malouk T E, Webber S L E, White J M (1988), 'Modeling of bipolar semiconductor photoelectrode arrays for electrolytic processes', *J Electrochem Soc*, 135(3), 567–573.

53 Bartelt J E, Drew S M, Wightman R M (1992), 'Electrochemiluminescence at band array electrodes', *J Electrochem Soc*, 139(1), 70–74.

54 Shimizu Y, Morita K I (1992), 'Fabrication of microhole array electrodes', *J Electrochem Soc*, 139(5), 1240–1243.

55 Madigan N A, Hagan C R S, Coury Jr L A (1994), 'Preparation of microarray electrodes by sonochemical ablation of polymer films', *J Electrochem Soc*, 141(3), L23–L24.

56 He L, Franzen H F, Vitt J E, Johnson D C (1994), 'Synthesis and characterization of Ru-Ti_4O_7 microelectrode arrays', *J Electrochem Soc*, 141(4), 1014–1020.

57 de Lyon T J, Johnson S M, Cockrum C A, Wu O K, Hamilton W J, Kamath G S (1994), 'CdZnTe on Si(001) and Si(112): direct MBE growth for large-area HgCdTe infrared focal-plane array applications', *J Electrochem Soc*, 141(10), 2888–2893.

58 Horiuchi T, Niwa O, Morita M (1995), 'Fabrication and photoelectrochemical properties of interdigitated array microelectrodes consisting of optically transparent and nontransparent band electrodes', *J Electrochem Soc*, 142(9), L146–L149.

59 Datta M (1995), 'Fabrication of an array of precision nozzles by through-mask electrochemical micromachining', *J Electrochem Soc*, 142(11), 3801–3805.

60 Liang M, Lackey N, Carter S, Norton M L (1996), 'Electrodeposited silver array fabricated utilizing self-assembled alkanethiolate monolayer photoresist', *J Electrochem Soc*, 143(10), 3117–3121.

61 Shibuya M, Nishina T, Matsue T, Uchida I (1996), 'In situ conductivity measurements of $LiCoO_2$ film during lithium insertion/extraction by using interdigitated microarray electrodes', *J Electrochem Soc*, 143(10), 3157–3160.

62 Morita M, Niwa O, Horiuchi T (1997), 'Interdigitated array microelectrodes as electrochemical sensors', *Electrochim Acta*, 42(20–22), 3177–3183.

63 Matsuzaki K, Uematsu T, Ryokai Y, Amano A (1997), 'Characteristics of silicon-field emitter arrays fabricated by using wafers separated by implantation of oxygen', *J Electrochem Soc*, 144(7), 2538–2541.

64 Leventis N, Chen M, Liapis A I, Johnson J W, Jain A (1998), 'Characterization of 3 × 3 matrix arrays of solution-phase electrochromic cells', *J Electrochem Soc*, 145(4), L55–L58.

65 Eastman M P, Hughes R C, Yelton G, Ricco A J, Patel S V, Jenkins M W (1999), 'Application of the solubility parameter concept to the design of chemiresistor arrays', *J Electrochem Soc*, 146(10), 3907–3913.

66 Liu S Q, Wang B X, Liu B F, Dong S J (2000), 'Electrochemical behavior of redox species at carbon fibre microdisk array electrode modified with mixed-valent molybdenum(VI, V) oxide', *Electrochim Acta*, 45(10), 1683–1690.
67 Wormwell F, Brasher D M (1949), 'Electrochemical studies of protective coatings on metals I. electrode-potential measurements on painted steel', *J Iron Steel Inst*, 162, 129–135.
68 Wolstenholme J (1973), 'Electrochemical methods of assessing the corrosion of painted metals – review', *Corros Sci*, 13, 521–530.
69 Bartels C, Danzfuss B, Schultze J W (1983), *Passivity of Metals and Semiconductors* (ed. M. Froment), Amsterdam: Elsevier.
70 Schultze J W, Elfenthal L, Leitner K (1988), 'Modification of oxide films by ion implantation: tio2-films modified example', *Electrochimica Acta*, 33(7), 911–925.
71 Leiva E, Meyer P, Schmickler W (1988), 'Simulation of percolation processes in electrochemical systems', *J Electrochem Soc*, 135(8), 1993–1996.
72 Doblhofer K, Nölte D, Ulstrup J (1978), 'Polymer-film covered electrodes of stable electrochemical performance', *Berichte der Bunsengesellschaft fuer Physikalische Chemie*, 82(4), 403–408.
73 Ambegaokar V, Halperin B I, Langer J S (1971), 'Hopping conductivity in disordered systems', *Phys Rev B*, 4, 2612–2620.
74 Leiva E, Meyer P, Schmickler W (1989), 'Electron transfer through passive films: role of localized electronic states', *Corr Sci*, 29(2–3), 225–236.
75 Kruger J, Frankenthal R P (1978), *Passivity of Metals, The Electrochemical Society Corrosion Monograph Series*, Princeton, NJ: The Electrochemical Society.
76 Zhang L, Macdonald D D (1998), 'Segregation of alloying elements in passive systems – I. XPS studies on the Ni-W system', *Electrochim Acta*, 43(18), 2661–2671.
77 Zhang L, Macdonald D D (1998), 'Segregation of alloying elements in passive systems – II. Numerical simulation', *Electrochim Acta*, 43(18), 2673–2685.
78 Hakiki N E, Da Cunha Belo M, Simoes A M P, Ferreira M G S (1998), 'Semiconducting properties of passive films formed on stainless steels. Influence of the alloying elements', *J Electrochem Soc*, 145(11), 3821–3829.
79 Macdonald D D, Ismail K M, Sikora E (1998), 'Characterization of the passive state on zinc', *J Electrochem Soc*, 145(9), 3141–3149.
80 Cheng Y F, Luo J L (1999), 'Electronic structure and pitting susceptibility of passive film on carbon steel', *Electrochim Acta*, 44(17), 2947–2957.
81 Yang M Z, Luo J L, Yang Q, Qiao L J, Qin Z Q, Norton P R (1999), 'Effects of hydrogen on semiconductivity of passive films and corrosion behavior of 310 stainless steel', *J Electrochem Soc*, 146(6), 2107–2112.
82 Yang M Z, Luo J L, Patchet B M (1999), 'Correlation of hydrogen-facilitated pitting of AISI 304 stainless steel to semiconductivity of passive films', *Thin Solid Films*, 354(1–2), 142–147.
83 Li W S, Luo J L (1999), 'Electric properties and pitting susceptibility of passive films formed on iron in chromate solution', *Electrochemistry Communications*, 1(8), 349–353.
84 Sikora J, Sikora E, Macdonald D D (2000), 'Electronic structure of the passive film on tungsten', *Electrochim Acta*, 45(12), 1875–1883.

85 Cho E A, Kim C K, Kim J S, Kwon H S (2000), 'Quantitative analysis of repassivation kinetics of ferritic stainless steels based on the high field ion conduction model', *Electrochim Acta*, 45(12), 1933–1942.
86 Bojinov M, Fabricius G, Laitinen T, Mäkelä K, Saario T, Sundholm G (2000), 'Coupling between ionic defect structure and electronic conduction in passive films on iron, chromium and iron-chromium alloys', *Electrochim Acta*, 45(13), 2029.
87 Schultze J W, Lohrengel M M (2000), 'Stability, reactivity and breakdown of passive films. Problems of recent and future research', *Electrochim Acta*, 45(15–16), 2499–2513.
88 Santamaria M, Huerta D, Piazza S, Sunseri C, Di Quarto F (2000), 'Influence of the electronic properties of passive films on the corrosion resistance of Mo-Ta alloys – a photoelectrochemical study', *J Electrochem Soc*, 147(4), 1366–1375.
89 Davenport A J, Oblonsky L J, Ryan M P, Toney M F (2000), 'Structure of the passive film that forms on iron in aqueous environments', *J Electrochem Soc*, 147(6) (2000) 2162–2173.
90 Hoar T P, Price L E (1938), 'Elektrochemische Deutung der Wagnerschen Theorie der Anlaufvorgänge', *Trans Faraday Soc*, 34, 867–873.
91 Bailey J M, Ritchie I M (1988), 'Metal oxidation: an electrochemical perspective', *Oxid Met*, 30(5/6), 405–418.
92 Zhong Q D, Xu N X, Zhou G D, Rohwerder M (2003), 'Electronic-ionic conducting transition of temporarily protective oil coating in salt solution', *Werkstoffe und Korrosion*, 54(2), 97–105.
93 Zhong Q D, Rohwerder M, Zhang Z, Zheng J (2004), 'Semiconducting behavior of temporarily protective oil coating on the surface of AISI 304 Stainless Steel in 5% Na_2SO_4 solution during its degradation', *J Electrochem Soc*, 151(7), B446–B452.
94 Tan Y J (1991), 'Effects of inhomogeneity in organic coatings on electrochemical measurements using a wire beam electrode. Part I', *Prog Org Coat*, 19(1), 89–94.
95 Tan Y J, Yu S T (1991), 'Effects of inhomogeneity in organic coatings on electrochemical measurements using a wire beam electrode. Part II', *Prog Org Coat*, 19(3), 257–263.
96 Wu C L, Zhou X J, Tan Y J (1995), 'Study on the electrochemical inhomogeneity of organic coatings', *Prog Org Coat*, 25(4), 379–389.
97 Zhong Q D (1997), 'Electrochemical technique for investigating temporarily protective oil coatings', *Prog Org Coat*, 30(4), 213–218.
98 Zhong Q D (1997), 'Wire-beam electrode: A new tool for investigating electrochemical inhomogeneity of oil coatings', *Prog Org Coat*, 30(4), 279–285.
99 Zhong Q D (2001), 'Potential variation of a temporarily protective oil coating before its degradation', *Corr Sci*, 43(2), 317–324.
100 Tan Y J (1994), 'New crevice corrosion testing method and its use in the investigation of oil stain', *Corrosion*, 50(4), 266–269.
101 Tan Y J (1999), 'Monitoring localized corrosion processes and estimating localized corrosion rates using a wire-beam electrode', *Corrosion*, 54(5), 403–413.

102 Tan Y J (1999), 'Wire beam electrode: A new tool for studying localised corrosion and other heterogeneous electrochemical processes', *Corros Sci*, 41(2), 229–247.
103 Qingdong Z (2000), 'A novel electrochemical testing method and its use in the investigation of underfilm corrosion of temporarily protective oil coating', *Corrosion*, 56(7), 722–726.
104 Zhong Q D, Zhang Z (2002), 'Study of anti-contamination performance of temporarily protective oil coatings using wire beam electrode', *Corrosion Science*, 44(12), 2777–2787
105 Zhong Q D, Rohwerder M, Zhang Z (2004), 'Study of lubricants and their effect on the anti-corrosion performance as temporarily protective oil coatings', *Surface & Coatings Technology*, 185, 234–239.

28

Corrosion monitoring using the field signature method inspection tool (FSM-IT)

NGUYEN N. BICH, P. Eng,
Pangea Solutions Inc, Canada

28.1 Introduction

An effective corrosion control program for a pipeline should contain the following four components[1]:

- Understand the corrosion mechanisms prevailing during various phases of operations including startup, steady-state operations, shut-in, etc.
- Formulate and implement mitigation measures according to the appropriate corrosion mechanisms.
- Validate the effectiveness of the corrosion mitigation measures by monitoring corrosion at strategic locations.
- Verify the physical integrity of the pipeline by suitable inspection activities.

This chapter describes several case studies where the use of the field signature method inspection tool has led to early warnings of the lack of performance of the mitigation measures which, if left unchecked, could result in more severe corrosion and eventually, failure.

28.1.1 Field signature method inspection tool (FSM-IT)

The FSM-IT technology is a non-intrusive corrosion monitoring tool consisting of a geometric matrix of sensing pins (3 mm diameter) that are permanently attached to the outer pipe wall by spot welding (Figures 28.1 and 28.2). During measurements, by passing a controlled current through the sensing matrix, an electrical field signature is established. The first signature is unique to the geometry of the object. With the occurrence of internal corrosion or erosion, the electrical field is changed. This change is detected by the FSM-IT as a 'potential drop' across the matrix. Computer software then compares new measurements against the original signature to produce the metal loss value. The software can trend the metal loss over time, calculate corrosion rates and create three-dimensional plots to illustrate accumulated wall loss over the whole matrix.

28.1 Pin matrix layout.

28.2 An FSM-IT installation with protective cover.

To compensate for the effects of temperature on the conductivity of the steel, the pin matrix measurements are compared to parallel readings taken on a reference plate. This plate is made from the same material as the pipeline and is thermally coupled to the external surface. By comparing the reference plate and matrix readings, it is determined whether actual metal loss or just a change due to temperature or both causes the detected shift in electrical potential.

In terms of operating principles, FSM-IT is analogous to ER as FSM-IT uses the structure as the sensing element. For that reason, this method should be referred to as Electrical Resistance Matrix (ERM). FSM-IT

monitors internal corrosion over a large area and can differentiate between general corrosion and isolated pitting thanks to the matrix design where general corrosion affects all pin pair responses and pitting corrosion only affects nearby pin pairs.

28.1.2 Typical challenges for wet sour gas pipeline corrosion monitoring

The most common form of corrosion encountered in wet sour gas is pitting. The pitting growth, in many cases, starts with small or insignificant rate for a prolonged period of time, then suddenly due to various reasons, unexpectedly jumps to a very high value leading to failures. Pitting rates in the order of 50 mm/y have been reported in several wet sour gas pipelines. In many cases, the pits are very isolated. It is quite common to find pit depths of several millimeters and the pits are separated meters away from each other. In between, the pipeline surface is covered with protective iron sulfide scales and suffers no corrosion. A single point device such as a corrosion coupon or an electrical resistance (ER) probe (see Chapter 11) will have to be placed in a precise location to detect such isolated pits. Quite often, the coupon or ER probe shows very little or no corrosion, but a leak can develop just centimeters away. Due to the high toxicity of H_2S, non-intrusive devices are preferred. In the author's experience, FSM-IT is most suitable and efficient for sour gas pipeline corrosion monitoring.

28.2 Case studies

Six case studies[2–8] where the results from corrosion monitoring by FSM-IT have been beneficial to maintaining pipeline integrity and timely in preventing failure are presented in this chapter. FSM-IT data acquisition covers all pin pairs but in most applications, typical reports show the deepest metal loss readings and the most active pin pairs. Positions of the pits can be identified by the corresponding pin pair numbers.

28.2.1 Case study 1: 6 inch sour gas pipeline

The pipeline configuration and conditions are:

(a) pipeline particulars: 6 in (168.3 mm) in diameter and 12 km long
(b) fluid effluents: 15% H_2S, 2% CO_2, 100 000 ppm Cl^- and elemental sulfur deposition
(c) corrosion mechanisms: wet sour gas. Corrosion morphology: isolated pits mainly at the 6:00 o'clock position
(d) mitigation: continuous injection as there was no launcher/receiver facility.

28.3 An FSM-IT installation before earth filling.

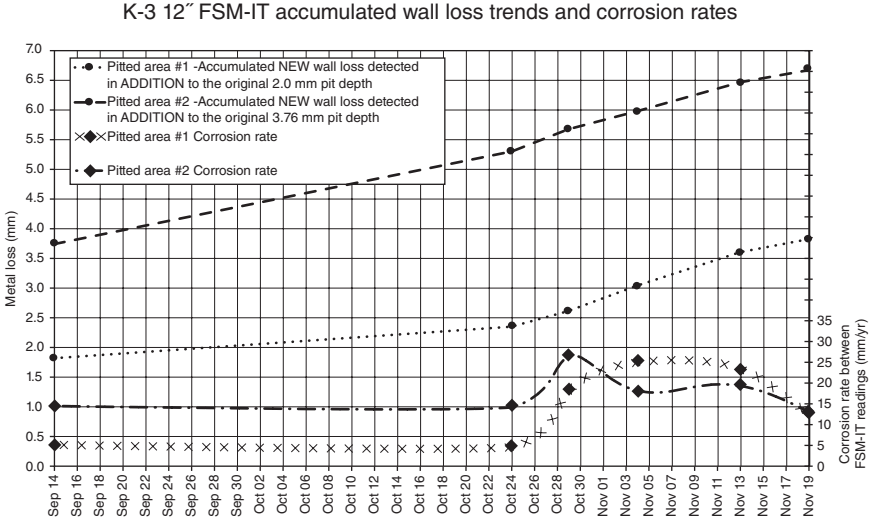

28.4 Case study 1: corrosion monitoring responses.

The line was shut down and FSM-IT device was installed 'over' existing pits. The monitoring was started in September 2004.

Results

Figure 28.4 shows the monitoring results. Area 1 had an original pit depth of 2.0 mm and was growing at a maximum rate of over 25 mm/y as detected by FSM-IT. Area 2 had an original pit depth of 3.8 mm and was growing at

a maximum rate of 28 mm/y as detected by FSM-IT. Up to 70% wall loss was detected.

Benefits

Because of the timely detection of high corrosion rate by the FSM-IT device, action was taken to cut out the section of the corroded pipe. In adjacent areas not covered by the device, corrosion rate as high as 75 mm/y was observed at the deepest pits. It was learned that it was difficult to mitigate deep pits with continuous-injection inhibitors. This FSM-IT monitoring program effectively prevented sour gas leak under river.

28.2.2 Case study 2: 4 inch sour gas pipeline

The pipeline configuration and conditions are:

(a) pipeline particulars: 4 in (114.3 mm) in diameter and 4 km long
(b) fluid effluents: 24% H_2S, 9% CO_2, 42 000 ppm Cl^- and elemental sulfur deposition
(c) corrosion mechanisms: wet sour gas. Corrosion morphology: isolated pits mainly at the 6:00 o'clock position
(d) mitigation: continuous injection and pigging/batching.

The previously corroded line was cut out and FSM-IT device was installed. The monitoring was started in January 2001.

Results

Figure 28.5 shows the monitoring results. Significant corrosion was detected from June 2002 with indicated wall loss of 87% as of January 2003.

Benefits

Because of the timely detection of high corrosion rate by the FSM-IT device, action was taken to cut out the section of the corroded pipe (Figure 28.6). It was learned that changing operations (plunger lift) resulted in more severe corrosivity/fluid flows. Actual wall loss was 44% and actual corrosion rate of 5 mm/y allowed re-calibration of software. The second sour gas leak was prevented.

28.2.3 Case study 3: 30 inch process water line

The pipeline configuration and conditions are:

(a) pipeline particulars: 30 in (762 mm) in diameter and 30 km long
(b) fluid effluents: process water

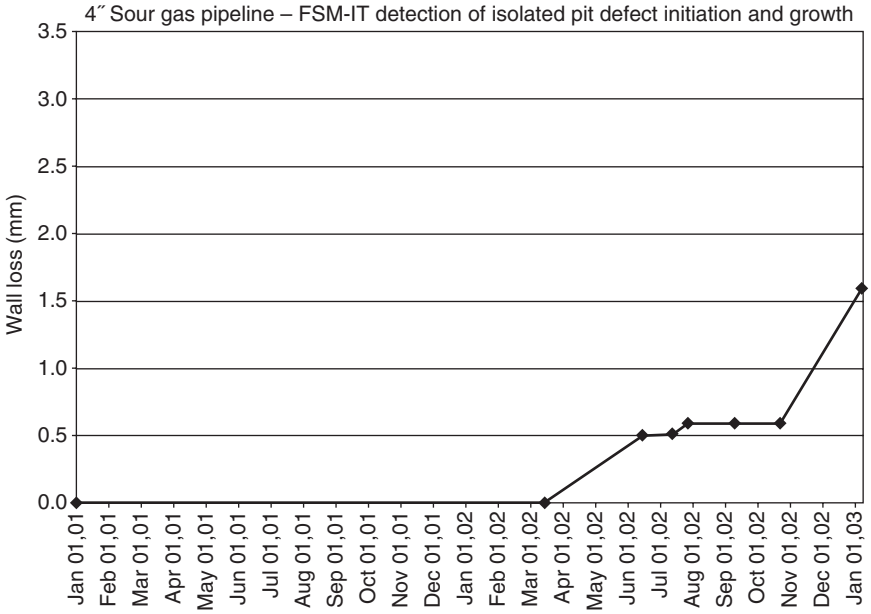

28.5 Case study 2: corrosion monitoring responses.

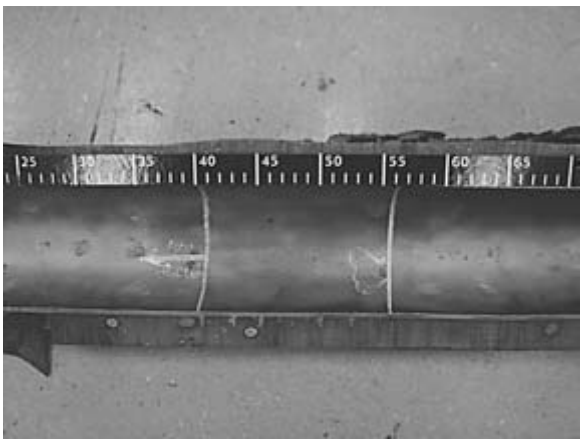

28.6 Case study 2: actual cut-out from monitored area.

(c) corrosion mechanisms: oxygen corrosion. Corrosion morphology: numerous pits occurring around the entire circumference of the pipe
(d) mitigation: continuous injection and pigging.

The line was shut down and one section was replaced with new pipe adjacent to an old section with 35% wall loss left in place. Two FSM-IT's were

28.7 Case study 3: two FSM-IT matrices installed on adjacent new/old pipes.

installed on the two adjacent old/new pipes (Fig. 28.7) and another one on one elbow. Corrosion monitoring was started in June 2002.

Results

Figures 28.8 and 28.9 show the monitoring results: 70% wall loss on old pipe, 52% on new one as of November 2002. On-going corrosion rate was in good trending agreement with LPR and ER (located in the plant further upstream) probe readings.

Benefits

Because of the timely detection of high corrosion rate by the FSM-IT devices, action was taken to cut out both new/old sections of the corroded pipe (Figure 28.10). It was learned that there was a slight difference in new/old pipe corrosion. The data was useful in evaluating further mitigation strategy.

28.2.4 Case study 4: 6 inch sour gas pipeline

The pipeline configuration and conditions are:

(a) pipeline particulars: 6 in (168.3 mm) in diameter and 15 km long
(b) fluid effluents: 18% H_2S, 5% CO_2, 30 000 ppm Cl^-
(c) corrosion mechanisms: wet sour gas. Corrosion morphology: isolated pits mainly at the 6:00 o'clock position
(d) mitigation: continuous-injection and pigging/batching.

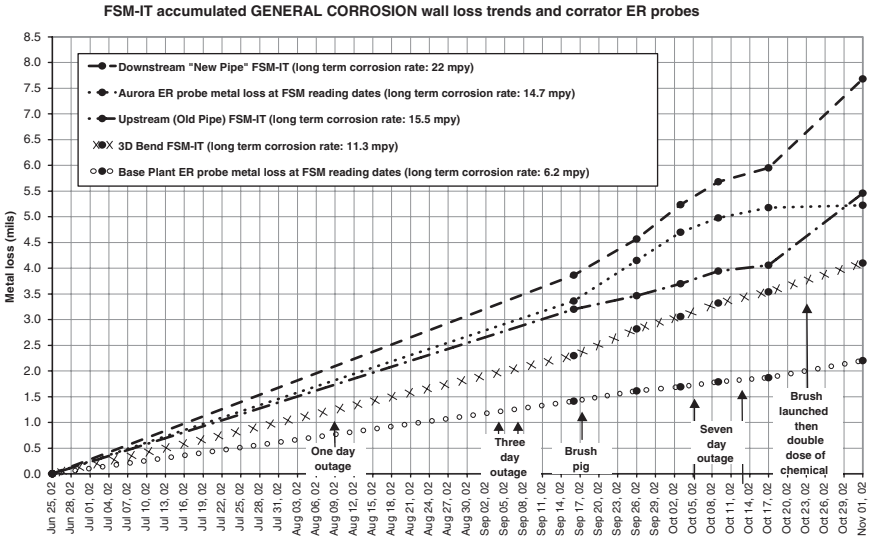

28.8 Case study 3: corrosion monitoring responses from FSM-IT and ER probes.

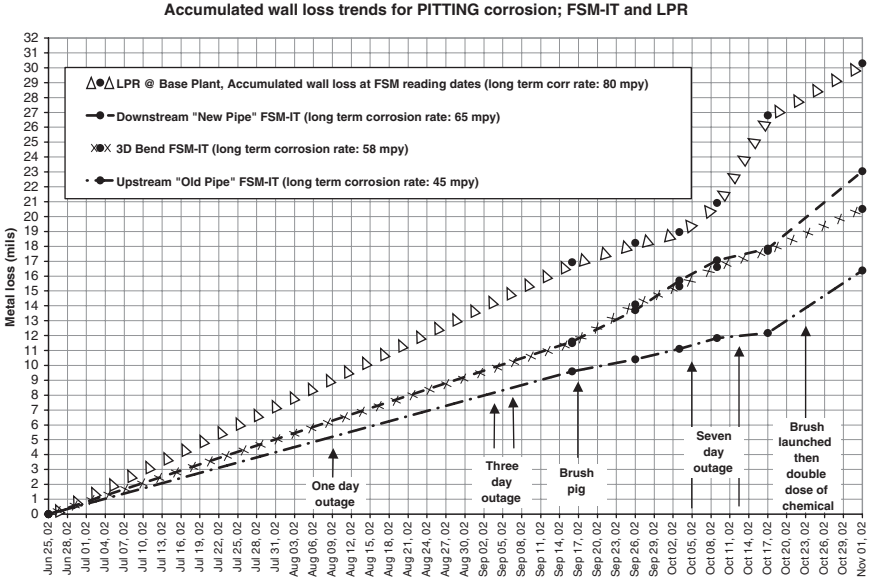

28.9 Case study 3: corrosion monitoring responses from FSM-IT and LPR probes.

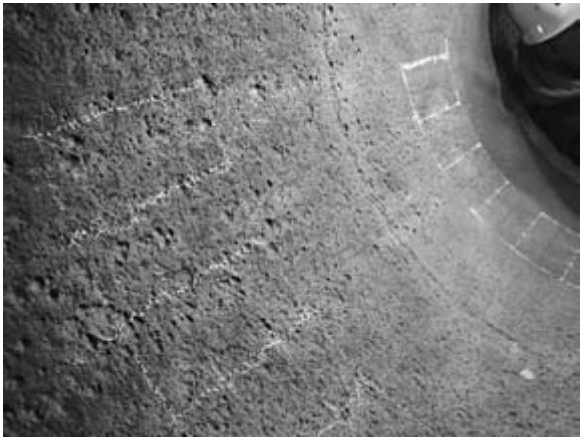

28.10 Case study 3: actual cut-out from the monitored old/new pipe section.

The previously corroded line was cut out and FSM-IT device was installed. The monitoring was started in October 2002.

Results

Figure 28.11 shows the monitoring results: an alarm of 66% wall loss and 19 mm/y corrosion rate.

Benefits

Because of the timely detection of high corrosion rate by the FSM-IT device, action was taken to shut down the pipeline, cut out the corroded pipe (Fig. 28.12) and in-line inspection of the remaining line. Actual wall loss was measured at 41%. The current inhibition program was not effective. A sour gas leak was prevented.

28.2.5 Case study 5: 48 inch oil transmission pipeline

The pipeline configuration and conditions are:

(a) pipeline particulars: 48 in (1220 mm) in diameter and 40 km long
(b) fluid effluents: low water-cut crude containing less than 1% H_2S, 5% CO_2, and sand deposits
(c) corrosion mechanisms: sour water corrosion. Corrosion morphology: pits at 6:00 o'clock where water drops out
(d) mitigation: batching.

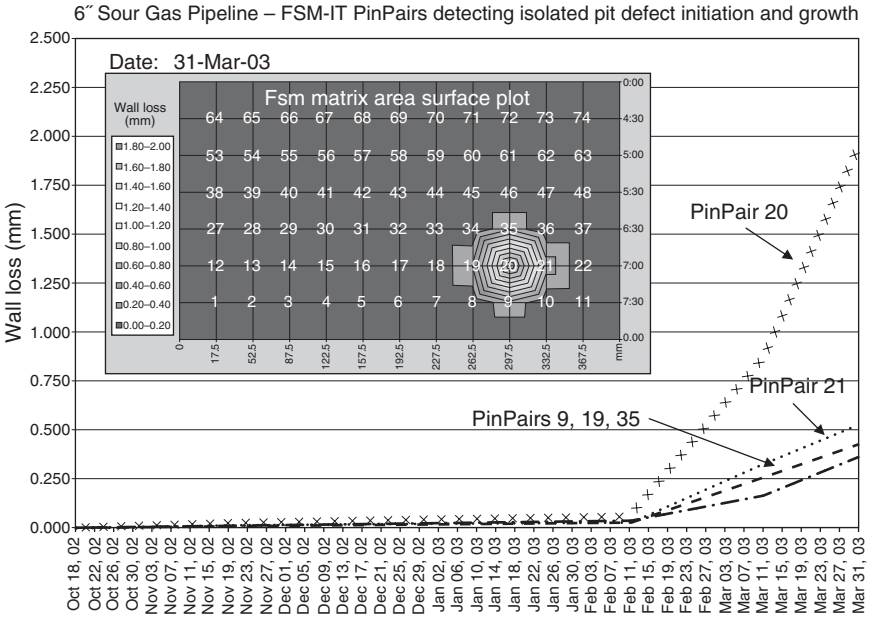

28.11 Case study 4: corrosion monitoring responses.

28.12 Case study 4: actual cut-out (rectangular area was covered by FSM-IT on the external side).

An FSM-IT was installed at a location where a previous in-line inspection indicated significant metal loss.

Results

Figure 28.13 shows the monitoring results. A maximum corrosion rate of 3.5 mm/y was indicated. The monitoring results will be validated in future in-line or UT inspection.

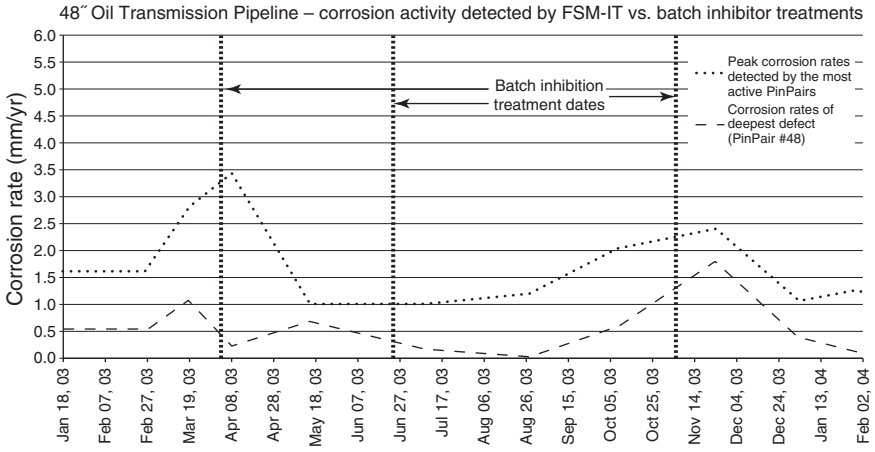

28.13 Case study 5: corrosion monitoring responses.

Benefits

Batching activities were found to be correlated to corrosion readings and hence could be optimized using FSM-IT results. The line will continue to operate until an alarm level is reached.

28.2.6 Case study 6: 8 inch sour gas process piping

The pipeline configuration and conditions are:

(a) pipeline particulars: 8 in (219.08 mm) and 300 m long
(b) fluid effluents: high-velocity gas containing 0.53% H_2S, 21% CO_2, 115 000 ppm Cl^- at 90°C and 19 000 kPa
(c) corrosion mechanisms: mixed H_2S/CO_2 corrosion/erosion. Corrosion morphology: general wall loss around whole circumference
(d) mitigation: continuous injection inhibition.

An FSM-IT was installed on a new pipe and the monitoring was started in October 2001.

Results

Figure 28.14 shows monitoring results. From October 2001 to June 2002, average corrosion of 2 mm/y (80 mpy) was detected. After October 2002, average corrosion of 5 mm/y (200 mpy) was detected.

Benefits

Because of the timely detection of high corrosion rate by FSM-IT, the line was shut down and a weld overlay was installed as the inhibition was not

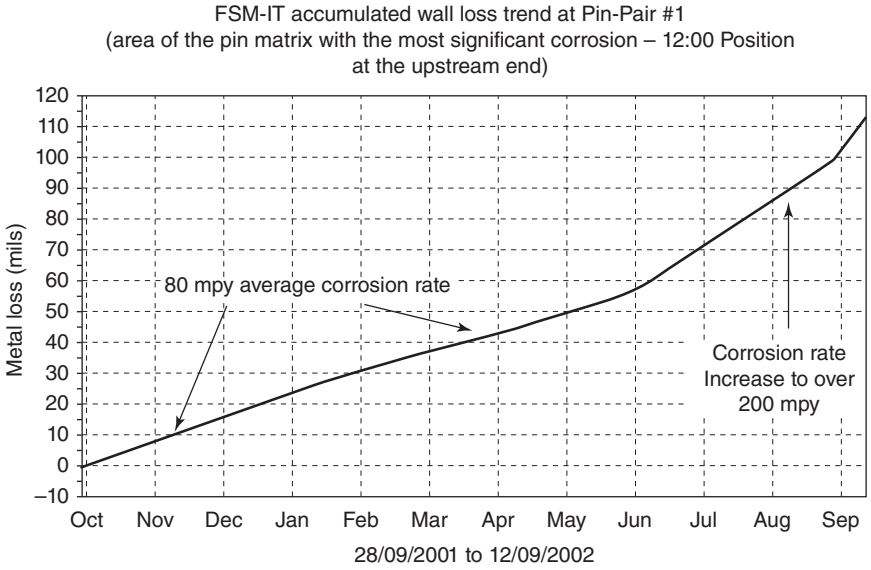

28.14 Case study 6: corrosion monitoring responses.

effective for the given high velocity/turbulent operating conditions. A sour gas leak was prevented.

28.2.7 Summary

In the six case studies, FSM-IT as a corrosion monitoring tool has been successfully used in monitoring the mitigation effectiveness and has been found beneficial in preventing sour gas leaks in four cases, and in providing useful data for further evaluation in the other two.

28.3 Acknowledgments

The sharing of corrosion experience and monitoring information by Ray Goodfellow and Jason Thomas of Chevron Texaco Canada, Harley Fear of Shell Canada, Ben Kitt and Dave Webster on behalf of Syncrude, Mike Johnson of Talisman and Tanis Elm and Joe Boivin of/on behalf of Enbridge is acknowledged and greatly appreciated.

28.4 References

1 Nguyen N. Bich, 'An Approach to Corrosion Mitigation for Wet Gas Pipelines', 4th International Pipeline Conference, 29 September–3 October 2002, Calgary, Canada, Paper IPC02-27417.

2 Nguyen N. Bich and Eric Kubian, 'Corrosion Monitoring as an Integral Component of an Effective Corrosion Management Program', 5th International Pipeline Conference, 4–8 October 2004, Calgary, Canada, Paper IPC04-0582.
3 Daryl Baxandall, Eric Kubian and Ray Goodfellow, 'Corrosion Assessment using Alternate Monitoring Tools for High Pressure and High Temperature Gas Wells', NACE Northern Area Western Conference, 3–6 February 2003, Calgary, Canada.
4 Jason Thomas, 'Corrosion Monitoring Using the Field Signature Method Inspection Tool', Upstream Pipeline Integrity Management Association, FSM-IT Workshop, 24 February 2004, Calgary, Canada.
5 Harley Fear, 'FSM Corrosion Monitoring Experiences on a 4-in Sour Gas Pipeline', Upstream Pipeline Integrity Management Association, FSM-IT Workshop, 24 February 2004, Calgary, Canada.
6 Ben Kitt, Dave Webster and Eric Kubian, 'Corrosion Monitoring Experiences on a 30-in Process Water Pipeline', Upstream Pipeline Integrity Management Association, FSM-IT Workshop, 24 February 2004, Calgary, Canada.
7 Mike Johnson and Eric Kubian, 'FSM Corrosion Monitoring Experiences on a 6-in Sour Gas Pipeline', Upstream Pipeline Integrity Management Association, FSM-IT Workshop, 24 February 2004, Calgary, Canada.
8 Tanis Elm, Joe Boivin and Eric Kubian, 'Summary of Initial Corrosion Monitoring Experiences on a 48-in Oil Transmission Pipeline', Upstream Pipeline Integrity Management Association, FSM-IT Workshop, 24 February 2004, Calgary, Canada.